



ISSN: 2958-8995. 2958-8987

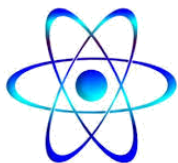
Doi: 10.59799/APPP6605

No:9 Val:1/ August / 2025

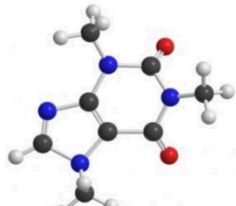
Journal of Natural and Applied Sciences **URAL**

A Quarterly Multidisciplinary Scientific Journal Issued by European Academy
for Development and Research / Brussels and Center of Research and Human
Resources Development Ramah- Jordan

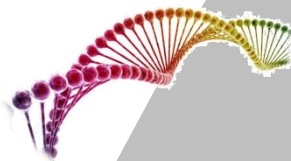
PHYSICS



Chemistry



Biology



MATHEMATICS



Pharmacy



Engineering



Medicine



Veterinary Medicine



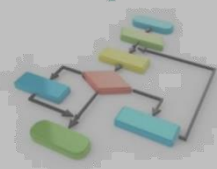
Geology



Dentistry



computer



Agriculture



Editorial Team			
Prof. Dr. Ghassan Ezzulddin Arif	Tikrit University\ College of Education for Pure Science's\ Department of Mathematics.	Iraq	Editor-in-Chief of the Journal
Assist. Prof. Baraa Mohammed Ibrahim Al-Hilali	University of Samarra\ College of Education\ Biology Department	Iraq	Managing Editor of the Journal
asst. lec. Alyaa Hussein Ashour	Al-nahrain University college of medicine	Iraq	Editorial Secretary of the Journal

Prof. Dr. Younis A. Rasheed	Al-Iraqia University, College of Medicine	Iraq
Prof.D.Faeyda Yaseen- ALBadri	University of Samarra\ College of Education\chemistry Department	Iraq
Assist. Prof. Dr. Hadeer Akram Al-Ani	Dept. of Public Health Sciences UC Davis School of Medicine	USA
Assist. Prof. Dr. Jawdat Akeel Mohammad Alebraheem	College of Science Al-Zulfi Majmaah University, Al-Majmaah	KSA
Assist. Prof. Dr. Almbrok Hussin Alsonosi OMAR	Sebha University	Libya
Assist. Prof. Dr. Saad Sabbar Dahham	University of Technology and Applied Sciences	Sultanate oman

Advisory and Scientific Board			
Prof. Dr. Ahamed Saied Othman	Tikrit University	Iraq	Head
Prof. Dr. Salih Hamza Abbas	University of Basrah	Iraq	Member
Prof. Dr. Leith A. Majed	University of Diyala	Iraq	Member
Assist. Prof. Dr Ali Fareed Jameel	Institute of Strategic Industrial Decision Modeling (ISIDM), School of Quantitative Sciences (SQS), University Utara (UUM), 06010 Sintok	Malaysia	Member
Assist. Prof. Mustafa Abdullah Theyab	University of Samarra	Iraq	Member
Dr. Modhi Lafta Mutar	The Open Educational College, Iraqi Ministry of Education, Thi-Qar	Iraq	Member
Dr. Asaad Shakir Hameed	Quality Assurance and Academic Performance Unit, Mazaya University College, Thi-Qar, Iraq.	Iraq	Member
Ahmad Mahdi Salih Alaubaydi	Assist. Lect.; PhD Student in the University of Sciences USM, Malaysia	Malaysia	Member

Assist. Prof. Dr. Qutaiba Hommadi Mahmood Al.Samarraie	University of Samarra/College of Applied Sciences/ Department of Biotechnology	Iraq	Member
Ph.D. Ali Mahmood Khalaf	Gujarat University	India	Member
Dr. Amel D. Hussein	Wasit University	Iraq	Member

Focus & Scope:

Journal of Natural and Applied Sciences URAL

Journal welcomes high quality contributions investigating topics in the fields of Biology, physics, computer science, Engineering, chemistry, Geology, Agriculture, Medicine, Mathematics, Pharmacy, Veterinary, Nursing, Dentistry, and Environment.

Publication specializations in the journal	
Biology	Chemistry
Physics	Geology
Computer	Agriculture
Engineering	Mathematics
Medicine	Pharmacy
Veterinary	Dentistry Veternity,
Environment	Nursing

The Journal is Published in English and Arabic

General Supervisor of the Journal

Prof. Dr. Khalid Ragheb Ahmed Al-Khatib

Head of the Center for Research and Human

Resources Development Ramah – Jordan

Managing Director:

Dr. Mosaddaq Ameen Ateah AL – Doori

Linguistic Reviewer Team

Prof. Dr. Lamiaa Ahmed Rasheed

Tikrit University/College of Education for Women

Asst. Prof. Ahmed Khalid Hasoon

Tikrit University/ College of Education for Women

Asst. Prof. Dr. Mohammad Burjess

Tikrit University/ College of Education

Administrative Title of the Journal:

Amman\ Jordan\ Wasfi Al-Tal \ Gardens

Phone: +962799424774

Index			
No.	Research Title	Researcher	Page No.
.1	Solving System Fredholm Integro-Differential Equation with First and Second Derivatives Using the Successive Approximation Method (SAM)	Ali H. Hazza ^{1,*} , Borhan F. Jumaa ² , Zeyad M. Abdullah ³	8-17
.2	Recent Advances and Trends in Automated Quality Metrics for Agile Software Engineering: A Review	Firdews a. Als Salman ¹ , Shaymaa a. Chyad ² , Reyad Alsalamdeen ³	18-42
.3	Deep Feature Embedding for Content-Based Image Retrieval Using Autoencoders and Semantic Hashing	Azhar amer alsoufi	43-56
.4	COVID-19 Patients from Duhok City, Iraq: Serum Reactive Protein (CRP) and D-dimer Level	Mohammed A. Khidhir ¹ , Saad A. Alnuaimi ² , Shimal Zubair ³ , Abdelhamid M. Yousif ³ , Salah M. Jameel ³ , and Riyadh F. Taha ³ .	57-68
.5	Solving the prey -predator model by using the Homotopy analytical method	Afrah Aziz 1, Ahmed Entesar 2	69-78
.6	Restricted Detour Index of Some Graph Operations with Chemical Application: A Review	Haitham N. Mohammed 1* Rasha S. Hasan 2	79-93
7.	New Results on Fourth-Hankel Determinant of a Certain Subclass of Analytic Functions	^{1,*} Fedaa Aeyyd Nayyef ² Waggas Galib Atshan ³ Youssef Wali Abbas	94-109
8.	Some Concepts and Their Relationships with Neutrosophic Quasi-Frobenius Rings	1,*Omar A. Khashan 2Majid M. Abed2	110-132

9.	The Impact of Utilizing Alveolo-Paste on the Healing of Soft Tissue after Dental Extraction	¹ -*Ahmed AbdulKareem Mahmood, ² -Ahmed Amer Ibrahim, ³ -Saber Mizher Mohammed ⁴ -Sohaib Qays Alwan	133-148
10.	عزل وتشخيص الميكروبات المرتبطة بالهواتف المحمولة لطلبة كلية التربية بالرسناق Isolation and identification of microbes associated with student's mobile phones in Rustaq College of Education	أسماء صالح الهاشمية، تسنيم سيف الرئيسية، هاجر عبد الله الشافعية إشراف الدكتور سعد صبار دحام	149-156
11.	Characterisation of Carbon Nano spheres (CNSs) from Cooking Oil with Ferrocene Catalyst on Activated Carbon Surface	¹ *Asst.Lec. A'alaa, Baddai. Nashte ² *Asst.Lec. Montaha, Kadhim. Sultan ³ *Asst.Lec. Hadeel, Jalal. Abbas	157-178
12.	Orthogonal Reverse Derivations with Ideal of semiprime Sets.	Entisar Majid khazil	179-185
13.	Estimating the migration of phthalate acid ester plasticizers in plastic containers for local and imported cooking oils	Dr. Rawaa Nader Al-Saedy	186-200
14.	Representing Kurdish Letters by using Partition Theory	¹ Zana Ali Mahmood ² *Awreng Baiz Mahmood	201-213
15.	Environmental factors affecting fish distribution in the Tigris River: a study of the relationship between fish distribution and the physical and chemical factors of the water.	Ass.lec.Shayma Abdulwahab	214-237

16.	Using classification data mining methods to predict the level of efficiency of services in dental clinics during the COVID-19 pandemic	¹ Anhar K.ALDeen Mohammed, ² Reem Ali AL-Jarah	238-250
17.	Microbial contamination of mobile phones: A study of bacterial prevalence	Alaa L.abdullah- Hawraa kadhim falhi - Dr.Hadi hussein abbas -	251-282
18.	Improving energy consumption in wireless communications networks using artificial intelligence techniques	Suliman Boushahba	283- 301
19.	comparison of using or not among laparoscopic cholecystectomy patients with non-00complicated gallbladder disease in large hospital	Saleem Enad Saleem Hasheesh	302- 352
20.	Neutrosophic Hybrid Weibull Inverse Weibull distribution: Mathematical Properties with simulation and Neutrosophic Real Data Application	Kamal N. Abdullah ¹ , Mundher A. Khaleel ²	353- 369
21.	A Comprehensive of Derivative-Free Optimization (DFO) Methods : A Review	Marwan S. Jameel ¹ , Ahmed Farooq Qasim ² , Zeiad Yahya Ali Allawee ³	370-383
22.	Runge-Kutta Method to generate Tree- Graph	Saleh Jasim Mohammad Awni M.Gaftan	384-395

Solving System Fredholm Integro-Differential Equation with First and Second Derivatives Using the Successive Approximation Method (SAM)

Ali H. Hazza^{1,*},
Borhan F. Jumaa²,
Zeyad M. Abdullah³

^{1,3}Department of Math., College of Computer Science & Math , Tikrit University, Iraq

²Department of Math., College of Computer Science & Math, Kirkuk University, Iraq

^{1,*}ah230020pcm@st.tu.edu.iq

²borhan_nissan@uokirkuk.edu.iq

³zeyaemoh1978@tu.edu.iq

Solving System Fredholm Integro-Differential Equation with First and Second Derivatives Using the Successive Approximation Method (SAM)

Ali H. Hazza^{1,*}, Borhan F. Jumaa², Zeyad M. Abdullah³

^{1,3}Department of Math., College of Computer Science & Math , Tikrit University, Iraq

²Department of Math., College of Computer Science & Math, Kirkuk University, Iraq

^{1,*}ah230020pcm@st.tu.edu.iq

²borhan_nissan@uokirkuk.edu.iq

³zeyamoh1978@tu.edu.iq

Abstract. A system of Fredholm integro-differential equations involving first and second derivatives is addressed using the Successive Approximation Method (SAM) combined with an iterative algorithm. Starting from an initial estimate, the integral term evaluated using previous iterates is treated as a known forcing function in each iteration. This transforms the original integro-differential system into a sequence of linear differential systems, which are then solved under given boundary or initial conditions. Convergence and uniqueness of the solution are rigorously established, and the resulting approximate solution is shown to converge the exact one as the iteration proceeds. Numerical examples demonstrate that SAM produces accurate approximations with controlled error and good computational efficiency.

Keywords: System of Fredholm , integro-differential equations ,The Successive Approximation Method

Introduction

Integral equations can articulate a range of topics in mathematical physics. Certain systems will be utilized as examples; compiling a comprehensive list of such applications would be practically impossible. The body of literature concerning integral equations and their applications is vast. This section will examine systems of Fredholm integro-differential equations of the second kind, expressed as follows:

$$\begin{cases} \psi^i(x) = f(x) + \lambda_1 \int_a^b [\mu(x,t)\psi(t) + \varepsilon(x,t)\xi(t)]dt \\ \xi^i(x) = g(x) + \lambda_2 \int_a^b [\mu(x,t)\psi(t) + \varepsilon(x,t)\xi(t)]dt \end{cases} \quad (1)$$

And the kernel of the system form is:

$$\mu(x,t) = \sum_{j=1}^{i-1} h\mu_{ij}\varphi_i$$

where $\psi^i(x) = \frac{d^i u}{dx^i}$, $\xi^i(x) = \frac{d^i v}{dx^i}$, since the resultant system integrates both the differential and integral operators, it is essential to provide beginning conditions. $\psi(0), \psi'(0), \dots, \psi^{(i-1)}(0)$ for the identification of the specific solution $\psi(x,t)$ of the Fredholm integro-differential equation(1). The unknown function $\psi(t), \xi(t)$ that will be established appear within the integral sign, but the derivatives of $\psi(t), \xi(t)$ appear mostly outside the integral sign, The kernel $\mu(x,t)$ and the given $f(x), g(x)$ are real-valued function, and λ_1, λ_2 are arbitrary constants, x is variable and $\psi(t), \xi(t)$, A system of Fredholm integro-differential equations combining first and second derivatives arises in modeling processes with both local dynamics and nonlocal interactions and requires specialized techniques for solution. The successive approximation method transforms the original coupled system by isolating the integral terms and treating them as known based on previous iterates in each cycle. Through this iterative framework the integro-differential equations are reduced to a sequence of linear ordinary differential problems[1]. each with updated forcing terms determined from the previous iteration. The procedure begins with an initial guess that satisfies any prescribed boundary on properties of the kernel functions and the linear operators to ensure that the sequence converges to the true solution which can be rigorously justified under suitable conditions. The successive approximation method offers computational efficiency by leveraging existing solvers for ordinary differential equations [2]and[3]. and can achieve high accuracy as iterations progress. Numerical case studies demonstrate that SAM effectively handles the coupling between first and second derivatives within the Fredholm framework while maintaining stability and controllable error growth or initial conditions,[4]and[5] and updates the solution by solving the linearized differential systems, then evaluating the integral kernels against the current approximation. Convergence of the method[6]and[7] relies thereby providing a robust numerical tool for this class of integro-differential systems.

Methodology Description

The (SAM) gives a system that may solve initial value or integral equations. This approach solves any problems by uncovering consecutive approximations of the answer. The procedure begins with an initial estimate as $\psi_0(x)$, which is termed, the in approximations and may be any real-valued function $\psi_0(x)$. The zeroth approximation will then be utilized in a related to recurrence to discover the subsequent approximations. Provide the (NLFIE) of the second kind.

$$\psi_n(x) = f(x) + \int_a^b \mu(x, t) \psi_{n-1}(t) dt \quad n \geq 1 \quad (2)$$

where $\psi(x)$ represents the undetermined function that has to be decided and $\mu(x, t)$ represents the kernel. the recurrence connection is shown via the use of the successive approximations method.

$$\psi_{j+1}(x) = f(x) + \int_a^b \mu(x, t) \psi_j(t) dt, j \geq 0 \quad (3)$$

Where the zeroth estimate $\psi_0(x)$, might be any specific authentically appreciate function. We always start with a beginning guess for $\psi_0(x)$, and for $\psi_0(x)$, we almost always choose either (0.1) or x as our starting guess. When this value of $\psi_0(x)$ is inputted in to equation (2), some successive estimate of $\psi_j(x), j \geq 1$ will be determined as:

$$\psi_1(x) = f(x) + \int_a^b \mu(x, t) \psi_0(t) dt$$

$$\psi_2(x) = f(x) + \int_a^b \mu(x, t) \psi_1(t) dt$$

⋮

$$\psi_j(x) = f(x) + \int_a^b \mu(x, t) \psi_{j-1}(t) dt$$

Consequently, the configuration $\varphi_0(x)$ may be obtained by employing.

$$\psi_0(x) = \lim_{n \rightarrow \infty} \psi_{j+1}(x)$$

By way of illustration, the successive approximation technique, also known as the picard iteration strategy, will be discussed in further detail.

Analysis of Fredholm Integro-Differential Equation by Using Successive Approximation Method (SAM)

The Successive Approximation Method is a reliable technique previously utilized to solve Fredholm integro-differential equations. This section will employ cubic splines to address systems of second-kind Fredholm integro-differential equations in a manner consistent with our previous methodology. This technique efficiently resolves any Fredholm problem through Successive Approximation Method, producing accurate answers. This section will analyze systems of Fredholm integro-differential equations as follows;

$$\begin{cases} \psi^i(x) = f(x) + \lambda_1 \int_a^b [\mu(x, t) \psi(t) + \mu(x, t) \xi(t)] dt \\ \xi^i(x) = g(x) + \lambda_2 \int_a^b [\mu(x, t) \psi(t) + \mu(x, t) \xi(t)] dt \end{cases} \quad (4)$$

And the kernel of the system form is:

$$\mu(x, t) = \sum_{j=1}^{i-1} h_{ij} \varphi_i$$

Phase1: Integrating both sides the system (1) once or more from 0 to x, utilizing beginning conditions and proceeding accordingly:

$$\begin{cases} \psi(x) = f(x) + \lambda_1 \int_a^b [\mu(x,t)\psi(t) + \mu(x,t)\xi(t)]dt \\ \xi(x) = g(x) + \lambda_2 \int_a^b [\mu(x,t)\psi(t) + \mu(x,t)\xi(t)]dt \end{cases} \quad (5)$$

Phase2: We transform $\psi(x) = \xi(x) = S(x)$

Phase3: The Successive Approximation Method is defined by the subsequent formula

$$\psi_{j+1}(x) = f(x) + \int_a^b \mu(x,t) \psi_j(t) dt, j \geq 0 \quad (6)$$

The recurrence connection is shown via the use of the progressive approximations approach.

$$\psi_{i,j+1}(x) = f(x) + \sum_{j=1}^m \int_a^b \mu_{ij}(x,t) \psi_{ij}(t) dt \quad i = 1, 2, \dots, n \quad (7)$$

Where the zeroth estimate, $\psi_{i0}(x)$, might be any specific authentically appreciated function. We always start with a beginning guess for $\psi_{i0}(x)$, and for $\psi_{i0}(x)$, we almost always choose either 0,1 or x as our starting guess. When this value of $\psi_{i0}(x)$ is inputted into equation (5), some successive estimates of

$\psi_{in}(x), j \geq 1$ will be determined as.

$$\begin{aligned} \psi_{i1}(x) &= f(x) + \sum_{j=1}^m \int_a^b \mu_{ij}(x,t) \psi_{j0} dt \\ &\vdots \\ \psi_{i,n+1}(x) &= f(x) + \sum_{j=1}^m \int_a^b \mu_{ij}(x,t) \psi_{j,n} dt \end{aligned}$$

Consequently, the configuration $\psi_i(x), i = 1, \dots, m$ may be obtained by employing

$$\psi_i(x) = \lim_{n \rightarrow \infty} \psi_{i,n+1}(x)$$

Phase4: By using of the progressive approximations approach.

$$\psi_{i,j+1}(x) = f(x) + \sum_{j=1}^m \int_a^b \mu_{ij}(x,t) \psi_{ij}(t) dt \quad i = 1, 2, \dots, n \quad (8)$$

Phase5: In the equal, using the a The Successive Approximation Method to the resultant system produces an approximate solution to the problem. (7) as $S_i(t)$, given by equation (5)

Quantitative Illustrations

This section presents three examples to demonstrate the effectiveness and accuracy of the recommended technique. The computed inaccuracies e_i are delineated by $e_i = |\psi_i - S_i|$ where u_i is the precise solution of system (3) and $\psi(t), \xi(t)$ represents an estimated solution to the identical equation. We additionally compute the Least Squares Error. (LSE), defined by the formula. $\sum_{i=0}^n (\psi_i - S_i)^2$, All computations are executed with the Matlab program

Example1: Use the successive approximation method to solve the following system of Fredholm integro-differential equations

$$\begin{cases} \psi'(x) = \frac{7}{15} + 2x + \int_0^1 [t^2 \psi(t) + t\rho(t)]dt \\ \xi'(x) = \frac{7}{12} - 2x + \int_0^1 [t^3 \psi(t) + t^2 \xi(t)]dt \end{cases} \quad (9)$$

Integrating both sides the system (9) once from 0 to x and the application of initial circumstances and the subsequent actions as the

$$\begin{cases} \psi(x) = \frac{7}{15}x + x^2 + \int_0^1 xt^2 \psi(t) dt + \int_0^1 xt \xi(t) dt \\ \xi(x) = \frac{7}{12}x - x^2 + \int_0^1 xt^3 \psi(t) dt + \int_0^1 x t^2 \xi(t) dt \end{cases} \quad (10)$$

The exact solution to this system is provided by $\psi(x) = x + x^2$

Table(1) show a comparison between the exact and numerical solution using a (SAM) for $\psi(x)$ for example (1), dependent on the least square error with $h = 0.2$

Table(1): The Numerical Results for Example (1) for $n = 5$

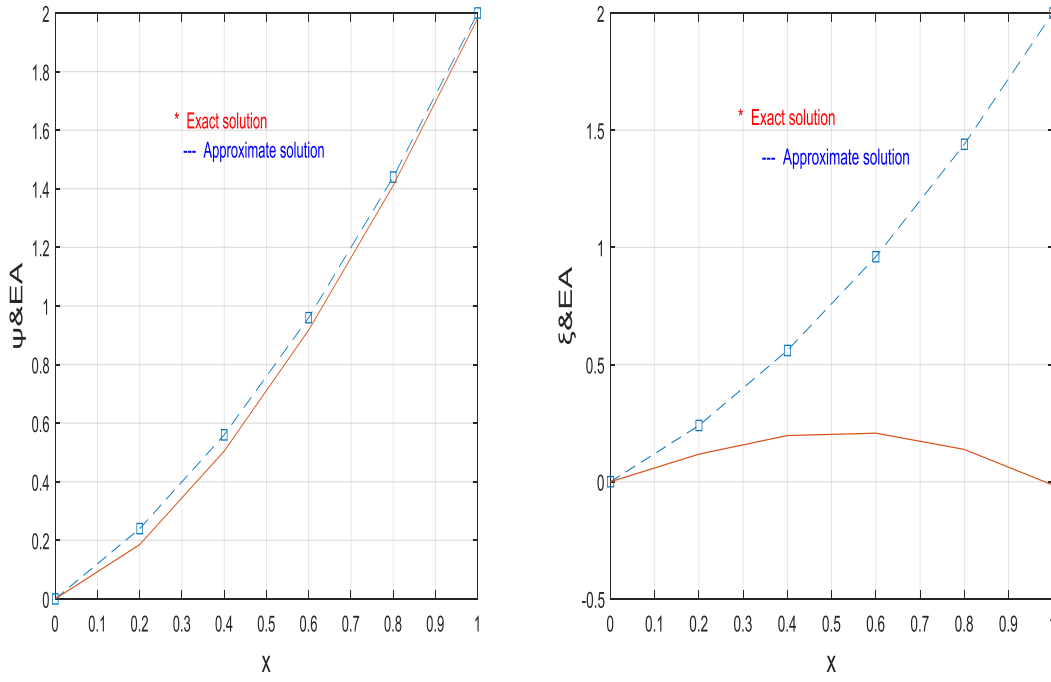
x_i	ψ_i	S_i	$ \psi_i - S_i ^2$
0.0	0.000000000000	0.000000000000	0.000000000000
0.2	0.240000000000	0.185600000000	0.002959360000
0.4	0.560000000000	0.504700000000	0.003058090000
0.6	0.960000000000	0.917800000000	0.001780840000
0.8	1.440000000000	1.411400000000	0.000817960000
1.0	2.000000000000	1.981800000000	0.000331240000
LSE			$0.894749000 \times 10^{-2}$

The exact solution to this system is provided by $\xi(x) = x - x^2$

Table(2) show a comparison between the exact and numerical solution using a (SAM) for $\xi(x)$ for example (#), dependent on the least square error with $h = 0.2$

Table(2): The Numerical Results for Example (1) for $n = 5$

x_i	ξ_i	S_i	$ \xi_i - S_i ^2$
0.0	0.000000000000	0.000000000000	0.000000000000
0.2	0.160000000000	0.117800000000	0.001780800000
0.4	0.240000000000	0.197100000000	0.001840410000
0.6	0.240000000000	0.207300000000	0.001069290000
0.8	0.160000000000	0.137900000000	0.000488410000
1.0	0.000000000000	-0.014100000000	0.000198810000
LSE			$0.537772000 \times 10^{-2}$



Figure(1): Offers a comparison between the exact answer and the numerical answers obtained using (SAM) interpolation for $\psi(x)$ and $\xi(x)$ in example 1, based on the least square error with $h = 0.2$

Example(2): Use the successive approximation method to solve the following system of Fredholm integro-differential equations

$$\begin{cases} \psi'(x) = -0.4597\sin x + 0.15853\cos x + \int_0^1 [\sin x \psi(t) + \cos x \xi(t)] dt \\ \xi'(x) = -0.4597\cos x + 0.15853\sin x + \int_0^1 [\cos x \psi(t) + \sin x \xi(t)] dt \end{cases} \quad (11)$$

Integrating both sides the system (11) once or more from 0 to x and the utilizing initial conditions and the subsequent as the

$$\begin{cases} \psi(x) = -0.4597 + 0.4597\cos x + 0.15853\sin x + \int_0^1 [1 - \cos x]\psi(t) dt \\ \quad + \int_0^1 \sin x \xi(t) dt \\ \xi(x) = 1.15853 - 0.4597\sin x - 0.15853\cos x + \int_0^1 \sin x \psi(t) dt \\ \quad + \int_0^1 [\cos x - 1]\xi(t) dt \end{cases} \quad (12)$$

When we use the Maclaurin series on $\sin x$ and $\cos x$, we arrive at the following result:

The exact solution to this system is provided by $\psi(x) = \sin x$

Table(3) show a comparison between the exact and numerical solution using a (SAM) for $\psi(x)$ for example (2), dependent on the least square error with $h = 0.2$

Table(3): The Numerical Results for Example (2) for $n = 5$

x_i	ψ_i	S_i	$ \psi_i - S_i ^2$
0.0	0.000000000000	0.000000000000	0.000000000000
0.2	0.003490650000	0.184000000000	0.032583625000
0.4	0.006981260000	0.458500000000	0.203869172000
0.6	0.010471784000	0.658600000000	0.420070184000

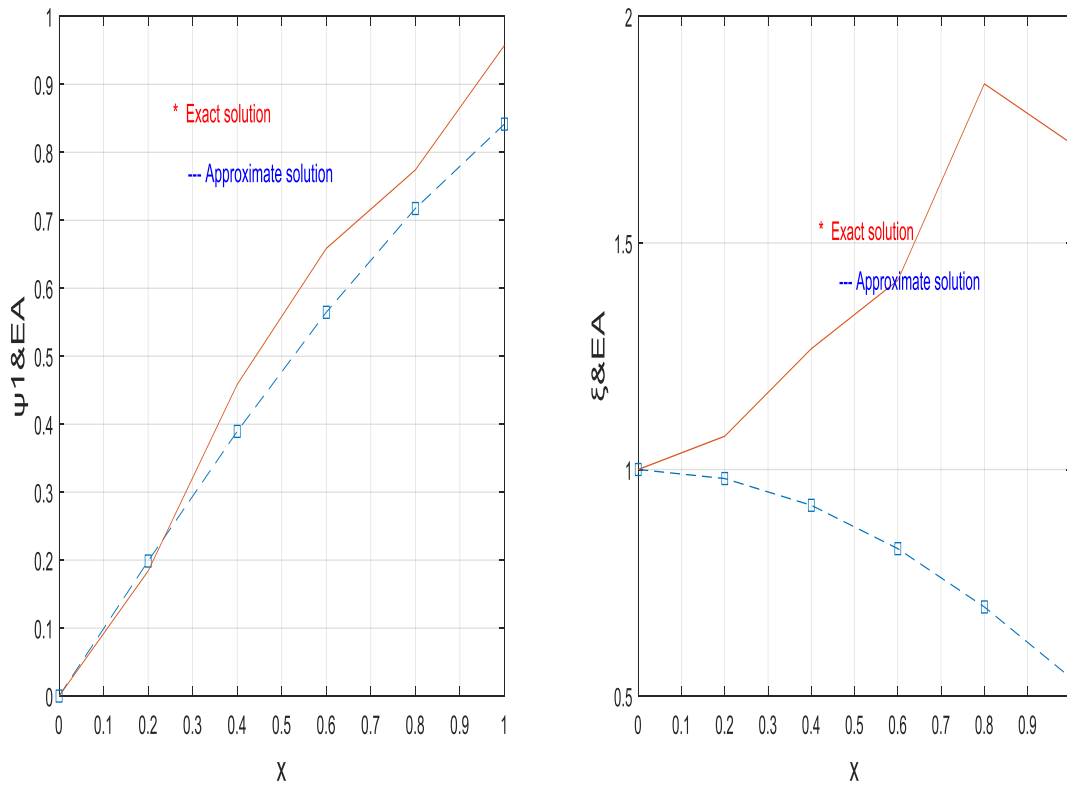
0.8	0.013962180000	0.7741000000000	0.577809505000
1.0	0.017452406000	0.9573000000000	0.883313499000
LSE			2.117645982000

The exact solution to this system is provided by $\psi(x) = \cos x$

Table(4) show a comparison between the exact and numerical solution using a (SAM) for $\xi(x)$ for example (2), dependent on the least square error with $h = 0.2$

Table(4): The Numerical Results for Example (2) for $n = 5$

x_i	ξ_i	S_i	$ \xi_i - S_i ^2$
0.0	1.000000000000	1.000000000000	0.000000000000
0.2	0.999990000000	1.073500000000	0.005403720000
0.4	0.999970000000	1.266500000000	0.071038240000
0.6	0.999940000000	1.417500000000	0.174356353000
0.8	0.999900000000	1.851200000000	0.724711690000
1.0	0.999840000000	1.720300000000	0.519062611000
LSE			1.494600000000



Figure(2): Offers a comparison between the exact answer and the numerical answers obtained using (SAM) interpolation for $\psi(x)$ and $\xi(x)$ in example 1, based on the least square error with $h = 0.2$

Example(3): Use the successive approximation method to solve the following system of Fredholm integro-differential equations:

$$\begin{cases} \psi''(x) = 4e^{-2x} + \frac{e^{-2}}{2} + \frac{e^{-4}}{4} - \frac{3}{4} + \int_0^1 [\psi^2(t) + \xi^2(t)] dt \\ \xi''(x) = e^{-x} + \frac{e^{-2}}{2} - \frac{e^{-4}}{4} - \frac{1}{4} + \int_0^1 [\psi^2(t) - \xi^2(t)] dt \end{cases} \quad (13)$$

Integrating both sides the system (13) twice from 0 to x and the utilization of initial conditions and the subsequent actions

$$\begin{cases} \psi(x) = e^{-2x} + \left(\frac{e^{-2}}{2} + \frac{e^{-4}}{4} - \frac{3}{4}\right)\frac{x^2}{2} + \frac{x^2}{2} \int_0^1 [\psi^2(t) + \xi^2(t)] dt \\ \xi(x) = e^{-x} + \left(\frac{e^{-2}}{2} - \frac{e^{-4}}{4} - \frac{1}{4}\right)\frac{x^2}{2} + \frac{x^2}{2} \int_0^1 [\psi^2(t) - \xi^2(t)] dt \end{cases} \quad (14)$$

When we use the Maclaurin series on e^{-x} and e^{-2x} , we arrive at the following result

The exact solution to this system is provided by $\psi(x) = e^{-x}$

Table(5) show a comparison between the exact and numerical solution using a (SAM) for $\psi(x)$ for example (3), dependent on the least square error with $h = 0.2$

Table(5): The Numerical Results for Example (3) for $n = 5$

x_i	ψ_i	S_i	$ \psi_i - S_i ^2$
0.0	1.000000000000	1.000000000000	0.000000000000
0.2	0.818730800000	0.668700000000	0.022509240000
0.4	0.670320046000	0.429300000000	0.058090662000
0.6	0.548811857000	0.220000000000	0.108117237000
0.8	0.449328964000	-0.024100000000	0.224134984000
1.0	0.367879441000	-0.366800000000	0.539753881000
LSE			0.952606004000

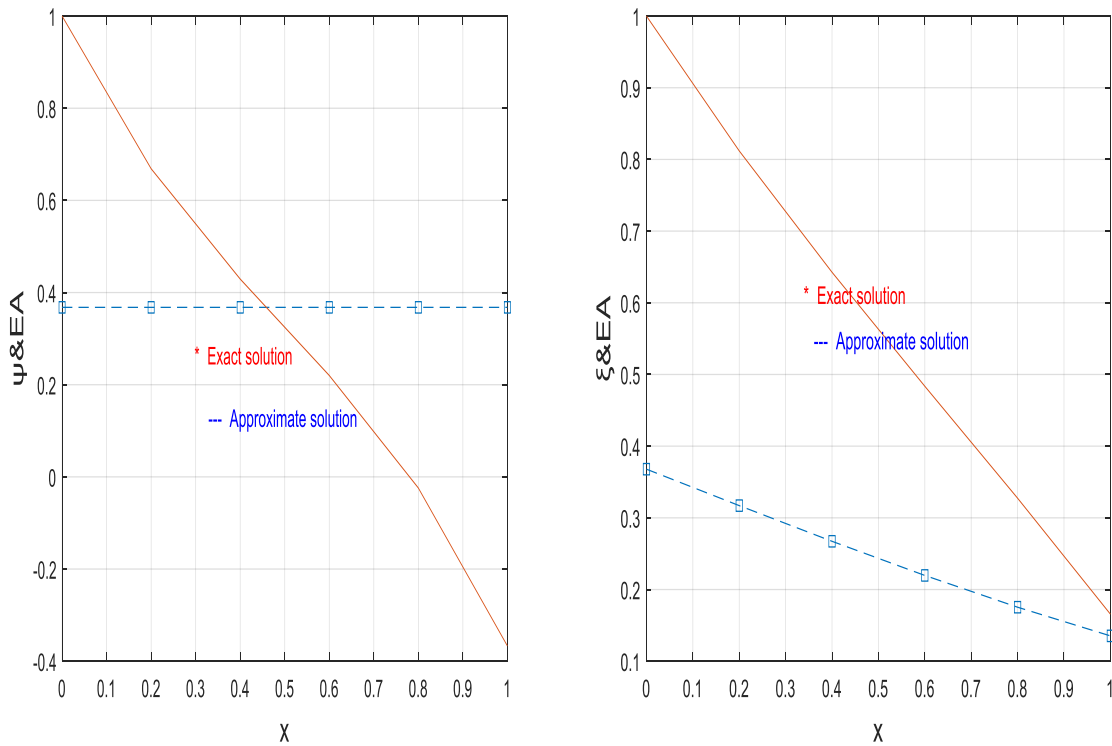
The exact solution to this system is provided by $\psi(x) = e^{-2x}$

Table(6) show a comparison between the exact and numerical solution using a (SAM) for $\xi(x)$ for example (3), dependent on the least square error with $h = 0.2$

Table(6): The Numerical Results for Example (3) for $n = 5$

x_i	ξ_i	S_i	$ \xi_i - S_i ^2$
0.0	1.000000000000	1.000000000000	0.000000000000
0.2	0.670320022600	0.811900000000	0.020044890000
0.4	0.449328964000	0.642600000000	0.037353693000
0.6	0.301194211000	0.483600000000	0.033271871000
0.8	0.201896518000	0.327400000000	0.015751123000
1.0	0.135335283000	0.165700000000	0.000922016000

LSE			$1.07343593 \times 10^{-1}$
-----	--	--	-----------------------------



Figure(3): Offers a comparison between the exact answer and the numerical answers obtained using (SAM) interpolation for $\psi(x)$ and $\xi(x)$ in example 3, based on the least square error with $h = 0.2$

Table(7): LSE for different values of n for example (1)-(3)

LSE _n	$n = 5$	$n = 5$
	ψ_i	ξ_i
Example 1	$0.894749000 \times 10^{-2}$	$0.537772000 \times 10^{-2}$
Example 2	2.11764598200	1.494600000000
Example 3	$9.52606004 \times 10^{-1}$	$1.07343593 \times 10^{-1}$

Conclusions

The successive approximation method transforms the coupled Fredholm integro-differential system featuring first and second derivatives into a convergent iterative scheme each iteration requiring the solution of a linear differential problem with updated source terms derived from previous approximations, The method's convergence and accuracy are ensured under mild assumptions on the kernels and operators and it efficiently leverages existing ordinary differential equation solvers Numerical examples confirm that SAM achieves high-precision results often matching analytical solutions in few steps.

References

- [1] R. . Agarwal, D. O'Regan, and P. J. . Wong, "Eigenvalues of a system of Fredholm integral equations," *Math. Comput. Model.*, vol. 39, no. 9–10, pp. 1113–1150, May 2004, doi: 10.1016/S0895-7177(04)90536-5.
- [2] "Mathematics_1950_58286_Linear integral equations.pdf."

- [3] K. Maleknejad, N. Aghazadeh, and M. Rabbani, "Numerical solution of second kind Fredholm integral equations system by using a Taylor-series expansion method," *Appl. Math. Comput.*, vol. 175, no. 2, pp. 1229–1234, Apr. 2006, doi: 10.1016/j.amc.2005.08.039.
- [4] A. D. Polyanin, *Handbook of Exact Solutions to Mathematical Equations*. Boca Raton: Chapman and Hall/CRC, 2024. doi: 10.1201/9781003051329.
- [5] T. Mavoungou and Y. Cherruault, "Solving frontier problems of physics by decomposition method: a new approach," *Kybernetes*, vol. 27, no. 9, pp. 1053–1061, Dec. 1998, doi: 10.1108/03684929810246080.
- [6] A.-M. Wazwaz, *Partial Differential Equations and Solitary Waves Theory*. in Nonlinear Physical Science. Berlin, Heidelberg: Springer Berlin Heidelberg, 2009. doi: 10.1007/978-3-642-00251-9.
- [7] A.-M. Wazwaz, "The variational iteration method for solving linear and nonlinear systems of PDEs," *Comput. Math. with Appl.*, vol. 54, no. 7–8, pp. 895–902, Oct. 2007, doi: 10.1016/j.camwa.2006.12.059.

Recent Advances and Trends in Automated Quality Metrics

for Agile Software Engineering: A Review

Firdews a. Als Salman¹,
Shaymaa a. Chyad²,
Reyad Alsalameneen³

College of Computer Science and Mathematics, University of Mosul
College of Computer Science and Mathematics, University of Mosul
Faculty of Information Technology, Al-Hussein Bin Talal University, Ma'an, Jordan
Corresponding author: FIRDEWS A. ALSALMAN (Firdewsalsalman@uomosul.edu.iq,
shaymaaahmedch@uomosul.edu.iq , Reyad.m.salameen@ahu.edu.jo)

Recent Advances and Trends in Automated Quality Metrics for Agile Software Engineering: A Review

Firdews a. Als Salman¹, Shaymaa a. Chyad², Reyad Alsalamdeen³

College of Computer Science and Mathematics, University of Mosul
College of Computer Science and Mathematics, University of Mosul
Faculty of Information Technology, Al-Hussein Bin Talal University, Ma'an, Jordan
Corresponding author: FIRDEWS A. ALSALMAN (Firdewsalsalman@uomosul.edu.iq,
shaymaaahmedch@uomosul.edu.iq, Reyad.m.salameen@ahu.edu.jo)

Abstract

The increasing acceptance of Agile approaches in software engineering has highlighted the significance of automated quality measures to guarantee continuous delivery while maintaining reliability. The Agile development cycle enhances speed, but it increases the chances of technical debt and software failures. This article reviews the recent advancements and tools supporting automated quality metrics in Agile pipelines and potential solutions to shared roadblocks, including shifting requirements, shrinking test windows, and scalability. We focus on the elements of dynamic analysis, unit testing, and performance tooling that influence code maintainability, early identification of defects, and efficient processes. The study analyzes empirical cases to demonstrate how automated metrics relieve risks, optimize workflows, and enhance software resilience. Because quality checks are integrated at every point in the development lifecycle process, automated quality metrics provide Agile teams the ability to address speed and endurance, and progressive modernization to maintain success in any long-term projects.

Keywords

Agile development, software quality metrics, automation, continuous integration, quality assurance

المخلص

إن التّقبّل المتزايد لأساليب التطوير الرشيق (Agile) في هندسة البرمجيات قد أبرز أهمية مقاييس الجودة المؤتمتة لضمان التسليم المستمر مع الحفاظ على الموثوقية. يعزز نهج التطوير الرشيق سرعة الإنجاز، ولكنه يزيد في الوقت نفسه من احتمالية تراكم الديون التقنية وحدوث إخفاقات في البرمجيات. تستعرض هذه المقالة التطورات الحديثة والأدوات التي تدعم مقاييس الجودة المؤتمتة ضمن خطوط تطوير Agile، وكذلك الحلول المحتملة للتحديات المشتركة مثل تغيير المتطلبات، وضيق نطاق الاختبارات، وقابلية التوسع. نركز على عناصر التحليل الديناميكي، والاختبار الوحدوي، وأدوات الأداء التي تؤثر في قابلية صيانة الشيفرة، والتعرف المبكر على العيوب، وتحسين كفاءة العمليات. وتقوم الدراسة بتحليل حالات تطبيقية لإظهار كيف تسهم المقاييس المؤتمتة في تقليل المخاطر، وتحسين سير العمل، وتعزيز مرونة البرمجيات. ونظرًا لأن اختبارات الجودة يتم دمجها في جميع مراحل دورة حياة التطوير، فإن مقاييس الجودة المؤتمتة تمنح فرق Agile القدرة على تحقيق التوازن بين السرعة والاستمرارية والتحديث التدريجي، بما يضمن النجاح في أي مشاريع طويلة الأمد.

الكلمات المفتاحية : التطوير الرشيق، مقاييس جودة البرمجيات، الأتمتة، التكامل المستمر، ضمان الجودة

1. Introduction

Agile software development methods have impacted software engineering by improving customer engagement, increasing flexibility, and shortening delivery timelines. Whereas a particular software development implementation follows the waterfall model, Agile development practices involve iterative cycles whereby multi-disciplinary teams develop requirements and solutions collaboratively. The use of iterative cycles means frequent releases and an ongoing ability to improve the product regardless of changing customer requirements. Extreme Programming, Kanban, Scrum, etc., provide teams with much of the structure needed in a fast-changing project scope and requests [1].

Traditional waterfall development is a linear, phased process where the typical quality assurance aspect is performed at the end of the project. This method of development organizes the project scope. It allows for testing, but issues or defects found later in development generally lead to higher costs and more complexity in fixing the defects. The iterative aspect of Agile encourages rapid, frequent releases with continuous testing and integration throughout the development lifecycle. To shift to Agile development, the QA aspects of the process must evolve to keep up with the quicker pace and complexity that Agile places into the development process. The QA process must shift to more frequent and flexible quality testing to match iterative development and evolving requirements [2].

Through incremental, high-value software delivery, Agile provides a key advantage of offering flexibility and reducing time to the market. The iterative process promotes a culture of continuous development by reinforcing the customer's satisfaction levels and allowing for the early discovery of problems. The pace and change that are frequent aspects of Agile considerably challenge quality assurance (QA) processes. Maintaining high software quality is difficult enough when our development cycle is reduced, and product requirements change regularly. Making changes to code frequently, combined with varying specifications, increases the potential for errors, rendering manual quality checks impractical or ineffective [3].

Agile techniques accelerate delivery. However, the increased tempo can produce unintentional technical debt, defined as accumulating quick-fix solutions, unfinished functionality, or incomplete testing over time. Research suggests that most Agile teams are accumulating technical debt, and not dealing with technical debt can create problems for the software's future maintainability and audience scalability. One way to reduce the risk of technical debt is to implement automated quality metrics, which combine the integration of defect detection, static code analysis, and performance monitoring in an Agile pipeline to enable teams to understand and address those issues as early as possible in the development process. By maintaining rigor with automated quality metrics, teams can protect code quality and limit ongoing maintenance costs [4].

Technical debt can be caused by inconsistent evaluation of quality and poor tracking of defects, which may eventually deteriorate the performance and maintainability of software. Agile teams often approach this issue by exaggerating software quality metrics via different forms of automation to discover faults upfront, offer late feedback, and continue to note overall performance. Using automated QA processes in the Agile pipeline allows teams to ensure software is always stable, scalable, and reliable at delivery speed while giving teams time to create and innovate [5].

The growing use of automated quality assurance tools demonstrates the need for scalable quality in Agile environments. Industry statistics show that many Agile teams have integrated automation testing and quality solutions into their development processes. This demonstrates the important effects of test automation on reliability and improved time to market. JUnit, Selenium, and JMeter provide fast feedback and continuous monitoring, allowing Agile teams to have quality assurance commitments and be agile with speed [6].

The paper is a comprehensive examination of existing research, methods, and models for evaluating the role of automated software quality metrics in Agile development. The study is forward-looking at automated measures, their meaningful application, and the challenges associated with their use [7]. The study identifies the need for ongoing improvement of automated metrics as the landscape of Agile software engineering evolves. The study identifies the need for these metrics to be adopted into the broader Agile culture to enhance collaboration and outcomes. Figure 1 below presents the waterfall model and agile development, with important differences noted. The Waterfall model exhibits late-stage quality assurance, postponed fault identification, increased maintenance expenses, and a longer, manual delivery process. Agile development

juxtaposes this with ongoing quality assurance, prompt problem identification, diminished technological debt, and expedited automated delivery. The diagram illustrates Agile's iterative methodology in contrast to Waterfall's sequential approach [2].

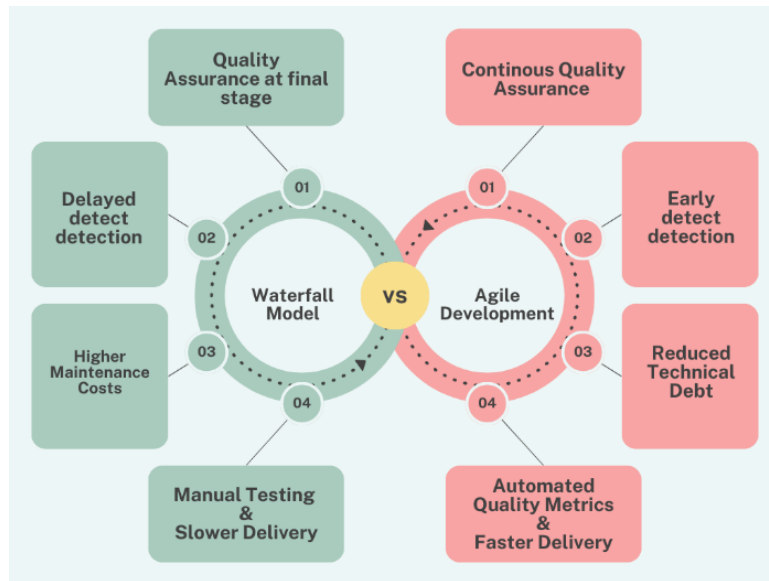


Figure 1: Comparison of Quality Assurance Processes in Waterfall vs. Agile Development

2. Background and Motivation

2.1 Agile Development and Its Challenges

Scrum, Kanban, Extreme Programming, and other agile frameworks emphasize iterative development, flexibility, and incremental delivery. This enables teams to adapt to market changes and customer feedback almost instantly. These methods encourage strong collaboration between team members, continuous integration and regular releases, environment adaptability, and responsiveness. Agile increases productivity and customer satisfaction by delivering functional software in short cycles, but presents significant challenges in keeping up with software quality during development [8].

In fast-paced agile projects, requirements are altered, and the development cycles become shorter. Such conditions enhance the possibility of problems and technical debt. Frequent changes in the scope and ongoing code changes can overload conventional quality measures, for we have to implement automated quality measurement methods. Unless tight quality controls take place, performance issues, security issues, and maintainability problems may prevail in agile projects, which could finally hamper the success of the project [9].

To mitigate these risks, agile teams slowly move to automated software quality metrics that give real-time visibility into code health, defect density, and process effectiveness. These metrics help detect potential faults proactively so that quality stays preferred throughout the iterative development process. Automating technologies into agile pipelines allows teams to enforce coding standards, run continuous testing, and monitor KPIs that promote long-term project sustainability. Hence, automated quality metrics are necessary to maintain high-quality software in an agile environment, balancing speed with stability and resilience [10]. [11] It looks into the challenges of extensive agile development from a requirements engineering perspective [12] and the challenges of agile development for a physical product, scaling, collaboration, resource allocation, and interdependencies. In contrast, [13] studied agile software development in government organizations and the challenges they faced during the process. Furthermore, [14] looked into the quest for technical skills in agile and the main challenges faced by agile practitioners. Then [15] investigated the accessibility needs in agile development and the challenges and gaps in existing techniques. Moreover, [16] compared agile with traditional approaches like waterfall and highlighted the challenges and benefits of agile if we focus on failure rates, adaptability, and the hybrid approach to overcoming agile limitations.

2.2 Importance of Automated Quality Metrics

Automated quality metrics are an essential part of Agile software development—they provide continuous monitoring, early defect detection, and a wide range of feedback on code health and process efficiency. Their constant observation helps avoid the accrued debt of any technical debt since such metrics identify potential problems at early stages, preventing the piling of defects that, when stacked together, impact the long-term maintainability and performance of the whole system. Automated metrics allow for risk-based, real-time assessment and enable teams to proactively act on keeping high code quality throughout to uphold their coding standards [17].

In practice, embedding the checks that assure quality in Agile is blended into automation through the whole software development life cycle. This is into CI to have fast feedback loops to Agile methods—that is, automated quality tools run on code changes at commit time and during CI cycles to see that new functionality does not degrade the general performance or stability of the system. It would also contribute to Agile's core values and principles, namely rapid iterations, enhanced collaboration, and continual improvement [18].

In addition, automated metrics provide added layers of insight around health, like code complexity, maintainability, security vulnerabilities, and build success rates. These can inform teams' data-driven decisions regarding setting priorities, the urgency of specific tasks, and the efficient use of resourcing. Agile teams operate in fast-paced environments, so this automated metric integration will speed up development and offer higher resilience and robustness to the final product, improving customer satisfaction behind it and ensuring long-term project success [19]. Automation, quality metrics, and scalability in Table 1 highlight the summarized Agile Development challenges and solutions. It focuses on the tools, frameworks, and practices for better coordination, learning, and usability to overcome the challenges of matters of technical debt and accessibility.

Table 1: Agile Development and Automated Quality Metrics – Challenges and Solutions

References	Aspect	Description	Challenges/Issues	Solutions/Benefits
[14]	Agile Development	Emphasis on achieving technical excellence through continuous learning and sustainable code.	Lack of shared understanding of Agile principles, misinterpretation of "technical excellence."	Continuous architecting, leadership support, and fostering a learning environment.
[20]	Agile Development	Focuses on integrating non-functional requirements (NFR) elicitation using cloud computing in Agile environments.	NFRs are often ignored in Agile due to a focus on functional requirements, leading to project failures.	Semi-automated NLP-based methodology for faster NFR elicitation and improved project success rate.
[21]	Agile Development	Describes lessons from applying Agile in high-speed environments like COVID-19 vaccine distribution.	Agile practices often lack adaptability for hyper-agile scenarios requiring rapid iteration.	Custom adaptation of Agile methods to ensure responsiveness in critical, high-paced projects.
[16]	Agile Development	Comparative analysis between Agile and Waterfall methodologies.	Agile projects have lower failure rates but are not universally suitable.	Hybrid approaches combining Agile and Waterfall for project flexibility.
[22]	Agile Development	Examines the impact of various Agile practices on project outcomes.	Miscommunication and shifting priorities in teams.	Adoption of multiple Agile practices (Scrum, Kanban, etc.) to improve collaboration and project results.
[23]	Agile Development	Study on leadership dynamics in Agile development teams.	Unequal leader-member relationships lead to dissatisfaction.	Balancing differentiated leadership to enhance team satisfaction and performance.
[24]	Agile	Combining Agile and traditional project management	Lack of adaptability in traditional	Hybrid models integrating Agile

	Development	for sustainability.	methods.	flexibility with traditional stability.
[25]	Agile Development	Website-based transaction system using Adaptive Software Development (ASD).	Manual processes are delaying project progress.	Automation and Agile methods to streamline transaction processes.
[26]	Challenges in Agile QA	Explores RE challenges in large-scale agile environments.	Misalignment between Agile and traditional requirements engineering, lack of coordination across teams.	Use of SAE and LeSS frameworks, workshops, and cross-team synchronization.
[27]	Challenges in Agile QA	Proposes a framework integrating security engineering processes in Agile methods.	Agile's informal nature conflicts with structured security processes, causing vulnerabilities.	A lightweight dynamic integration method using AHP and PROMETHEE to embed security activities into Agile workflows.
[28]	Challenges in Agile QA	Examines requirement engineering (RE) issues in Agile projects and how they affect project success.	Dynamic requirements and inadequate requirement gathering lead to software failures.	Continuous RE processes throughout the development cycle and stakeholder engagement.
[29]	Challenges in Agile QA	Develops a model for enhancing teamwork and collaboration in Agile projects.	Communication gaps, leadership challenges, and a lack of team coordination reduce effectiveness.	Agile Teamwork Effectiveness Model (ATEM) with shared leadership and peer feedback to enhance collaboration.
[30]	Challenges in Agile QA	Systematic literature review of project management challenges during Agile development.	Managing scope creep and change in Agile environments.	Flexibility in scope management and iterative planning.
[31]	Challenges in Agile QA	Conceptual modeling as a solution to Agile requirements engineering (RE) issues.	Incomplete and ambiguous user stories in Agile RE.	Use of conceptual models to improve communication and requirement clarity.
[32]	Technical Debt	Examines accessibility challenges in Agile projects, with a focus on industry practices.	Accessibility not prioritized; limited knowledge of accessibility guidelines; lack of appropriate tools.	Training programs and adoption of accessibility acceptance criteria in Agile processes.
[33]	Automated Quality Metrics	Theoretical and practical applications of Agile in digital transformation projects.	Misalignment with rapidly changing market conditions; challenges in digital transformation.	Agile frameworks like Scrum, XP, and Kanban are used to enhance adaptability and responsiveness.
[34]	Automated Quality Metrics	AI-driven tools to support scaled Agile frameworks (SAFe).	Complexity of scaling Agile, lack of automated tools for large teams.	AI-driven assistants for task automation, predictive analytics, and improving team collaboration.
[35]	Automated Quality Metrics	Proposes a prediction-based cost estimation technique to address Agile's time and budget overruns.	Frequent client change requests increase project cost and duration.	A new estimation method using project categorization based on complexity and developer expertise.
[36]	Role of Automation in Agile	Investigate the application of Agile methods in physical product development.	Scaling challenges, physical product constraints, and synchronization across teams.	Empirical studies to adapt Agile principles for physical product development.
[37]	Role of Automation in Agile	Presents a governance model for managing Agile architecture in large-scale development environments.	Lack of architectural governance in Agile squads leads to inconsistencies.	Heterogeneous Tailoring model to ensure architectural alignment across autonomous teams.

[38]	Role of Automation in Agile	Toolkit to facilitate membrane computing using Agile methods.	Limited to predefined variants; lack of flexibility in customization.	Introduction of P-Lingua 5 with user-defined variants and backward compatibility.
[39]	Role of Automation in Agile	Application of Agile in rapid prototyping for spacecraft software using open-source tools.	Synchronizing Agile with hardware development timelines, lack of tool standardization.	Reuse of open-source tools and iterative prototyping to align software development with hardware schedules.
[40]	Role of Automation in Agile	Linking testing activities with Agile development for physical products.	Testing physical products within Agile cycles.	Integration of continuous testing throughout the Agile development process.
[41]	Popular Tools	Explores Agile-Stage-Gate hybrid methods for product development and portfolio management.	Clash between Agile and traditional project evaluation metrics; difficulty in managing evolving product definitions.	Agile sprints between traditional gates to provide iterative feedback and improve project visibility.

3. Classification of Automated Software Quality Metrics

3.1 Code Quality Metrics

- **Code Complexity:** Program complexity is a key software quality and maintainability metric. Cyclomatic complexity is among the most common metrics, measuring the number of linearly independent paths through a program's source code. It sheds light on how intricate a control flow is and on certain parts of the program that may be error-prone and difficult to test. High cyclomatic complexity usually means that a particular piece of code is complex to test and less readable, requiring a refactor. Halstead Metrics is the second most important measure of code complexity after cyclomatic complexity. The Halstead metrics would analyze the software's volume, difficulty, and effort based on operators and operands in the codebase. Such quantitative measures help developers locate the areas of the source code that are becoming too complex and could lead to issues affecting maintainability and performance [42].

- **Code Maintainability:** To keep updated with the post-COVID-19 situation, maintainability analyzes the effects of those factors on the lifespan and flexibility of a piece of software. The Maintainability Index (MI) is a combined measure of the three aspects: cyclomatic complexity, lines of code that are commented on, and an overall estimate of how maintainable the code is. The higher the index, the better the maintainability, which means easier updates and an overall cost reduction in future development. Code churn is the other key indicator of the inherent stability and risks related to the code and measures how often code has been changed. In this context, areas under high churn typically indicate evolving or underlying structural issues within the code. If Agile teams identify and pay special attention to areas that churn out high amounts of code, they can direct their refactoring efforts to stabilizing the codebase [43].

- **Code Coverage:** The various metrics used for calculating code coverage, measured by how much a program's source code is exercised during some testing, line, branch, and function coverage are the most commonly used. Line coverage is the percentage of lines executed, thus providing a straightforward measure of the extent of testing done. Branch coverage determines if each control structure, such as if-else statements, has been run in its true and false executions, ensuring that even the decision points have been extensively tested. Function coverage verifies if every defined function was called in the testing process. High code coverage means fewer chances of undetected defects, better software reliability, and the Agile teams' full confidence in still frequent releases and updates [44]. Figure 2 supplements a hierarchical classification of code quality metrics, where the metrics concern three primary classes: Code Complexity, Code Coverage, and Code Maintainability. Each class branch forms specific sub-metrics such as Cyclomatic Complexity, Halstead Metrics, Line and Branch Coverage, and Maintainability Index (MI). The visualization provides a clear overview of how

different metrics build towards the capability of assessing software quality when grasping the areas where refactoring is necessary, ensuring improvements in maintainability, and establishing complete test coverage [45].

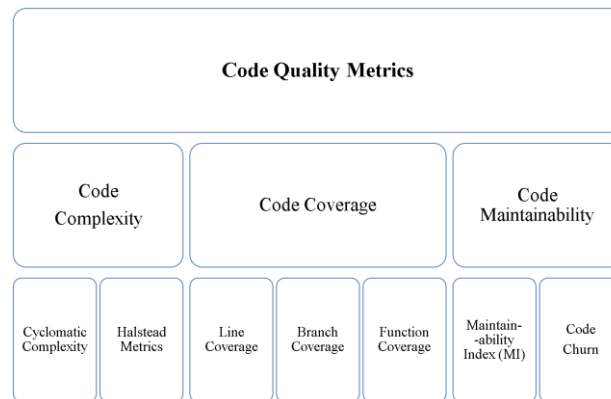


Figure 2: Classification of Code Quality Metrics

3.2 Dynamic Analysis

Dynamic analysis is considered a dynamic phase in software engineering, which refers to quality analysis of the behaviour of a system during execution. The process targets the identification of runtime errors, the validation of software functions, and the analysis of performance depending on various cases. Dynamic analysis refers to the real-time implementation of the program and analysis of the actions taken for further inputs, environments, and stress levels, guaranteeing stability, trustworthiness, and efficiency. This section clarifies the three standard, widely used tools for dynamic analysis: JUnit, Selenium, and JMeter. These tools perform quite different assignments in software testing [46].

• JUnit: Automated Unit Testing for Code Validation:

JUnit is a well-established framework that supports unit testing for Java applications. Unit testing is the process that tests the independent unit or piece of code to be sure that each unit performs as expected. This gives users confidence that JUnit provides a simple way to create and use test cases so that developers can test their code as they develop it throughout the life cycle of a project. With JUnit, developers can automate the execution of their unit tests, when desired, to enhance the productivity of their development, help find faults early, and make TDD possible. This will help developers have confidence that their code is correct and provide accurately coded, modular, maintainable, and extensible software structures [47].

• Selenium: Automated Testing of Web Applications:

Selenium is a handy open-source testing framework that automates web application testing, enabling users to interact with a web interface and validate that a web-based system works properly under various circumstances. It supports several programming languages like Java, Python, and C# to integrate well within different development environments. Rather than performing such repetitions as form filling, button clicking, and navigation manually, Selenium is utilized for speedy regression testing and helps to identify more accurately where things are not going quite right. The effort for execution by hand is then shortened, while the risk of human error considerably decreases. Testing processes thus scale and become more efficient and systematic; this is why Selenium has become one of the most important tools for quality assurance of web applications [48].

• JMeter: Performance and Load Testing for System Stability:

Apache JMeter is an important tool in software systems' performance, load, and stress testing. It enables the tester to generate high user traffic and observe the system's performance under peak loads and possible

bottlenecks. JMeter, apart from performance tests, can test a wide variety of applications like web services, databases, and network protocols. With its detailed reporting and visualizations of test results, JMeter can show response times, throughput per unit time, and how scalable a system is. This makes it very helpful when testing the reliability and robustness of applications to ensure that the applications can take up expected workloads without any performance degradation issues. Besides this, performance issues can be detected and reported during development, thus helping optimize system architecture and resource allocation. These tools collectively support and enhance the dynamic analysis process through which resilient, high-performing software systems can be developed to meet user needs and follow industry standards [49].

3.3 Continuous Integration and Deployment (CI/CD)

Continuous Integration and Deployment (CI/CD) is the backbone of modern software engineering, automating processes that expedite development workflows and improve software quality. This segment analyses three tools currently established for the CI/CD pipeline: Jenkins, Travis CI, and CircleCI. All are central to automation for some key stages of the software delivery life cycle, and each one enables rapid release cycles and increases reliability and overall cooperation among development teams [50].

• Jenkins:

Jenkins is also a free and open source automation server known for its capabilities and rich plugin ecosystem. This automation server executes various stages of the software lifecycle- from turning code into executable packages to testing and deploying them. The extensibility of Jenkins allows for seamless integration with myriad source control repositories and build tools. Orchestrating build pipelines performs continuous integration through continuous build, which is a build that is triggered automatically as soon as changes are made in the related code commons. This detects defects early on, before software artifacts of poor quality are distributed. The distributed architecture of Jenkins caters to solid scalability where jobs can be run in parallel across many nodes, thus enabling performance optimization for large projects [51].

• Travis CI:

Travis CI is an online CI/CD service built for ease of use and primarily supports open-source and enterprise projects. Internally, Travis CI will run unit tests, integration tests, and static code analysis in the development pipeline. Developers can use a `.travis.yml` to indicate how to build their project, its dependencies, and what testing framework should be used. It integrates with GitHub repositories and builds automatically from pull requests and commits, providing a great TDD tool. One of its more impressive features is parallel testing and matrix builds, which means they can run simultaneously across different environments, ensuring that the software will work across different configurations [52].

• CircleCI:

CircleCI provides cloud-based features focusing on speed, scalability, and ease of use. CircleCI increases the software delivery process while assuring quality by automating the application's building, testing, and deployment. It gives the developers great control over the build and deployment process with their YAML-based configuration defining the custom workflows. The platform enables containerized builds to be run, improving reproducibility and isolation of dependencies by providing Docker-based environments. CircleCI easily deploys an application in production environments by integrating with different cloud platforms such as AWS, Google Cloud, and Azure. With its performance insights and monitoring capabilities, teams can optimize their build pipelines, reduce failure rates, and get increased development velocity [53].

These CI/CD tools accelerate innovation in organizations by facilitating the adoption of DevOps principles, reducing the need for manual input, and, above all else, enabling feedback loops to act like the breath of life breathed into products. With continuous feedback, better software quality emerges, wherein time to market shrinks further, before which development and operations bonding is strengthened [54]. Table 2 below summarizes key CI/CD and testing tools in which Jenkins has a significant stake in building, security, and testing automation. The JUnit, Selenium, and JMeter do unit, web, and performance testing in their respective territories, ensuring software quality. Travis CI and CircleCI simplify cloud-based CI/CD work to

hasten deployment. Collectively, these tools cut through the meandering passage of development, building in their wake reliability and speeding along delivery.

Table 2: Overview of CI/CD and Testing Tools in Agile and Software Development

Reference	Tool Name	Purpose	Key Features/Functions	Insights and Advantages
[55]	JUnit	Unit testing for Java applications	Automated execution of test cases, supports TDD (Test-Driven Development)	Ensures code correctness, early defect detection, and supports modular and maintainable software.
	Selenium	Automated testing of web applications	Simulates user interactions with web interfaces, supports multiple programming languages and browsers	Accelerates regression testing, reduces manual effort, and improves scalability.
	JMeter	Performance, load, and stress testing	Simulates high traffic, evaluates system performance under load	Identifies bottlenecks, assesses reliability and scalability, and enhances system optimization.
	Jenkins	Automates software development lifecycle (CI/CD)	Orchestrates builds, tests, and deployments; integrates with various tools.	Enhances development efficiency, supports parallel execution, and has a distributed architecture.
[56]	Travis CI	Cloud-based CI/CD for testing and deployment	Automates build and testing upon code commits	Simplifies CI/CD pipeline integration, facilitates open-source project automation.
	CircleCI	Automates building, testing, and deployment	YAML-based configuration supports Docker and parallel testing	Accelerates software delivery, ensures consistent quality, and enables scalable pipelines.
[57]	Jenkins	Security and CI/CD integration	Ensures secure software supply chains, automated build, and deployment	Improves DevSecOps practices, enhances software supply chain security.
[58]	Jenkins	CI/CD and software engineering automation	Facilitates continuous software delivery and testing	Streamlines development, reduces deployment errors, and increases reliability.
[59]	Travis CI	Simplifying CI/CD for small teams	Easy configuration, integrates with GitHub	Supports small team automation, facilitates faster

				deployment.
[60]	Jenkins	Static code analysis in CI/CD	Integrates SAST tools, provides feedback loops	Improves code security, reduces vulnerabilities, and enhances the development lifecycle.
[61]	Jenkins	Dynamic testing in CI/CD pipelines	Parallel testing, Docker integration	Speeds up testing, increases scalability, and optimizes pipeline efficiency.
[54]	Jenkins	Automates software development lifecycle (CI/CD)	Automates build, test, and deployment processes	Streamlines development, reduces errors, and improves efficiency.
	JUnit	Unit testing for Java applications	Automates unit testing, supports TDD	Ensures code quality, promotes early bug detection, and simplifies development.
[62]	Jenkins	CI/CD automation within GitHub workflows	Supports workflow automation, integrates with various tools	Enhances GitHub Actions by automating testing and deployment.
	Selenium	Automates web application testing	Simulates user interactions, supports cross-browser testing	Reduces manual testing effort and ensures cross-platform compatibility.
	JMeter	Performance and load testing	Simulates high traffic, stress tests systems	Identifies performance bottlenecks and scalability issues.
	Travis CI	Cloud-based CI/CD for open-source projects	Automates testing, integrates with GitHub	Supports open-source projects with easy configuration and automation.
[63]	Jenkins	Automates compliance and deployment pipelines	Customizable pipelines, integrates with microservices	Facilitates compliance and accelerates deployment cycles.
	CircleCI	Automates build, test, and deployment pipelines	Supports Docker, parallel testing, and YAML configuration	Accelerates software delivery and improves deployment consistency.
[32]	Jenkins	Continuous Integration and Deployment	Automates build pipelines, plugin support	Ensures code quality and continuous delivery
	CircleCI	CI/CD Automation	Docker support, parallel	Speeds up

			execution	development, scalable workflows
--	--	--	-----------	------------------------------------

4. Empirical Studies and Case Analysis

Examining empirical studies and case analyses constructs a solid, rocky foundation for theoretical frameworks in different fields, which offers so much towards acceptance, modification, and application of the theories. This section offers a detailed discussion of the methodologies, findings, and implications of data-driven inquiries and real-life case studies. From observation and experimentation, one built it into empiricism, which follows as some substantial support that makes the theoretical propositions credible and generalizable [64]. Case analyses entail constant and thorough study of the selected cases, projects, or organizations, from which the insights are drawn to identify patterns, anomalies, and best practices to recognize. The figure compares Empirical Studies and Case Analyses, showcasing several strengths and joint benefits. While empirical studies stand out in quantitative, broad, and generalizable aspects, case analysis tends to be qualitative, contextual, and in-depth. Thus, some overlap exists regarding the utility offered by these two methods concerning informing policies and practices and advancing theory, where these methods solidify trustworthiness in answering the research questions with an elaborate depiction.

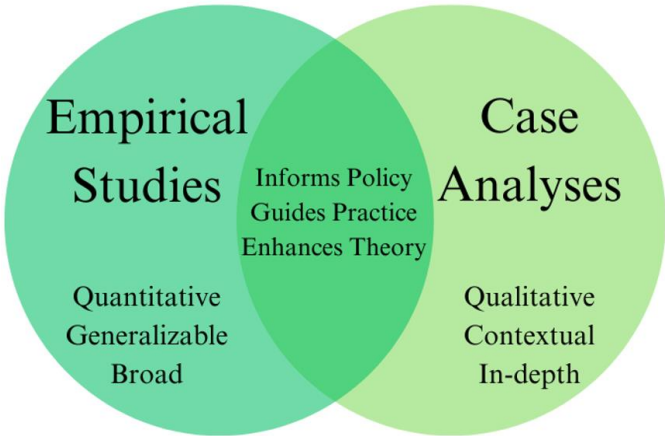


Figure 3: Complementary Nature of Empirical and Case Analyses

4.1 The Role of Empirical Studies in Academic Inquiry

Empirical research provides the basis for scientific advancement by bridging the gap between abstract theory and practical applications. Empirical studies usually involve collecting, measuring, and analyzing quantitative or qualitative data. Whether qualitative or quantitative, empirical approaches will always provide information for decision-making, model validation, hypothesis testing, and explanations of causation. Empirical approaches are important in social sciences, engineering, healthcare, and information technology, where the insights from data are applied in decision-making, policy formulation, and technological innovation [65]. An empirical study is, by definition, one that is undertaken according to rigorous protocols: sample selection must be representative, instruments must be standardized, and statistical techniques must all be appropriate. The reproducibility and transparency given to empirical research enhance the credibility of the findings and the overall contribution of the field.

4.2 Case Analyses: Contextualizing Theory through Real-World Applications

The case studies narrow a particular view to their contexts in which theory becomes philosophically observable as being in concert with practice. Regarding an individual case, be it an organization, community, or any event, it is within that case that the researchers shall unearth highly refined insights that remain concealed in macroscopically empirical studies. The case study enables identifying specific variables unique to a given event or variables due to any situational setting influencing some outcome. Insights

derived from case analyses are richer in detail, and viewing the concepts in question is diverse in dealing with complex projects [66].

The essential purpose of case analysis is to generate knowledge that can, in turn, help buoy scholarly research and professional practice. Such comparative case studies can enable researchers to identify common trends and generalize cross-contextually. Furthermore, this could include longitudinal case analysis, where changes over a long period are tracked, and scholars can observe the dynamic processes of practices evolving

4.3 Integration of Empirical and Case-Based Approaches

A combination of empirical studies and case analyses within one framework functions to a great extent in that it offers both the value of generalization and the depth of context analysis. This approach is vastly commendable in project management, software engineering, healthcare, and education, among others, which require models with their theoretical frameworks refitted according to varying conditions in place. In this perfect union of priorities, quantitative empirical data and the flavor of the narrative from case analyses create an understanding that endows the application and scaling of conclusions taken with a more comprehensive approach toward knowledge. Such integrative methodologies promote understanding, nourish the development of innovative solutions, and shape them into best practices [67].

4.4 Implications for Future Research and Practice

The insights from empirical studies and case analyses have significant implications for future research trajectories and practical applications. Empirical validation of emerging theories paves the way for their adoption in diverse contexts, while case analyses provide evidence-based recommendations that inform policy, strategy, and implementation. Future research should prioritize converging empirical rigor and case-based exploration to address evolving challenges and drive sustained academic and professional growth [68].

In conclusion, empirical studies and case analyses are indispensable to scholarly inquiry. Their complementary nature allows for a comprehensive understanding of complex phenomena, fostering theoretical advancements and practical innovations that shape the contemporary research and practice landscape. The studies on Agile, CI/CD, and DevOps are explicitly documented in Table 3, and we consider studies on the process, project size, area of application, and constraints of agile methodologies. The table above provides the principal highlights of relevant empirical studies and case studies on requirements engineering, cost estimation, collaboration, artificial intelligence, and software quality. In addition, it provides valuable insights into actualizing and leveraging practices for software development and deployment, for example, in a continuous integration environment.

Table 3: Comparative Analysis of Empirical Studies and Case Analyses

Reference	Criteria	Methodology	Scope	Applications	Limitations	Empirical Studies	Case Analyses
[35]	Cost Estimation Techniques	Quantitative	Broad	Model validation for agile cost estimation	Abstract	Statistical analysis and surveys	Real-world application in project scenarios
[29]	Teamwork Effectiveness in Agile	Mixed	Broad	Policy development and model testing	Hard to generalize	Focus groups and case studies	Application of team models in agile environments
[32]	Accessibility in Agile Development	Qualitative	Narrow	Unique insights on accessibility	Hard to generalize	Survey of industry	Case analysis of accessibility

	nt			practices		practices	consideratio ns
[34]	AI in Scaled Agile	Quantitative	Broad	Policy and model validation for AI integration	Abstract	Systematic literature review	Examination of AI tools in scaled agile environments
[20]	Nonfunctional Requirements in Agile	Mixed	Broad	Model validation for nonfunctional requirement elicitation	Hard to generalize	NLP-based analysis	Cloud computing environment case studies
[14]	Technical Excellence in Agile	Qualitative	Narrow	Unique insights into technical excellence	Hard to generalize	Semi-structured interviews	Validation through practical applications
[36]	Scaling Agile in Physical Products	Mixed	Broad	Comparative analysis of scaling agile	Hard to generalize	Empirical investigation	Explorative case analysis
[26]	Large-Scale Agile RE Challenges	Qualitative	Narrow	Unique insights on RE challenges	Hard to generalize	Multi-case study, interviews	Case analysis of agile frameworks
[33]	Digital Transformation in Agile	Qualitative	Narrow	Insights on agile in digital transformation	Hard to generalize	Literature review	Practical applications
[28]	Requirement Engineering in Agile	Qualitative	Narrow	Unique insights on requirement challenges	Hard to generalize	Focus on small and large agile projects	In-depth examination of requirement elicitation failures
[55]	CI/CD in Automotive Software	Quantitative	Broad	Validation of CI/CD tools in automotive projects	Abstract	Implementation and testing	Continuous quality inspection in automotive projects
[58]	Continuous Software Engineering	Mixed	Broad	Evaluation of CI/CD cost-benefit analysis	Hard to generalize	Multi-case study analysis	Real-world examples of CI/CD pipelines
[61]	Parallel Testing in CI/CD	Quantitative	Narrow	Efficiency analysis of parallel testing in CI/CD pipelines	Abstract	Experimental application of CI/CD pipelines	Application to microservices in CI/CD

[62]	CI/CD Tools in GitHub Actions	Quantitative	Broad	Empirical analysis of CI/CD tool usage	Hard to generalize	Repository mining	Usage patterns in GitHub workflows
[63]	Software Compliance with CI/CD	Mixed	Broad	Compliance validation through CI/CD pipelines	Hard to generalize	Empirical review and best practices	Real-world deployment and container management
[69]	Quality Requirements in Agile	Qualitative	Narrow	Managing quality requirements in agile environments	Hard to generalize	Multi-case study	Contextual analysis in different companies
[54]	CI/CD and DevOps Integration	Mixed	Broad	Operational efficiency through DevOps and CI/CD	Hard to generalize	Case study in AWS environments	DevOps adoption in software deployment

5. Challenges and Limitations

Though automated quality metrics provide far-reaching advantages in streamlining the software development lifecycle, substantial challenges and limitations are associated with their application and use. These limitations must be considered carefully to deploy automated tools effectively without negatively affecting a project's results [70].

1. False Positives and False Negatives:

One of the main shortcomings of automated quality assessment tools is their ability to produce false positives and negatives. A false positive occurs when a tool mistakenly identifies a defect (or a code anomaly) that is not present. This generates extra work and incorrectly directs human capital [71]. False negatives similarly produce latent defects, meaning that issues remain undetected in the codebase and can be latent contributors to failure when released into production. False positives and negatives stem from being unable to fully understand the problem space, which is also true of automated tools that function on explicit rules and static analysis. They are limited in methods because the code can be dynamic with custom-tailored abstractions, even if specific variables exist. Thus, automated metrics' reliability as quality assessments is limited by the constantly changing software development landscape and heterogeneity across projects [72].

2. Integration Complexity:

Another key problem encountered is creating automatic quality metrics (especially if they are not being directly measured!) into an existing development environment and workflow. It usually requires extensive customization to make automated tools compatible with an organizational architecture, coding standards, and processes. Integrating the automated metrics may also take considerable resources (time, money, and technical effort). Even excellent tools will not interface with legacy systems or systems based on your old workflows. So, there is a risk that changing and integrating them will disturb current workflows and cause processing and compatibility issues. For organizations under time constraints or with limited technical capacity, integrating the complexity of automated quality metrics may make them reluctant to use them and hinder innovation and improving quality-related initiatives [73].

3. Metric Overload and Cognitive Burden:

A further key challenge relates to the possibility of metric overload. Development teams may receive more data and performance metrics than they can handle, which may lead to analysis paralysis, or they may misinterpret what the data is trying to tell them. When too many quality metrics are being tracked and evaluated at once, it can obscure attempts to identify and steer attention to issues of real significance, shifting attention away from high-priority defects to relatively minor issues. This metric overload reduces the effectiveness of quality improvement initiatives and can lead to cognitive overload for development teams, reducing productivity and morale. One countermeasure would be to ensure that the project team has its complete focus on utilizing a fully automated system of metrics and a complete focus on key performance indicators that align with the project's deliverables and intentions [74]. In summary, automated quality metrics substantially benefit speed and accuracy in software development but must be used carefully, considering the possible consequences. Managing the related issues mentioned above (false positives/negatives, integration, and supporting metrics overload) is critical to realizing your benefits from automated quality evaluation and assessment tools. Table 4 below outlines key challenges to CI/CD and Agile, with difficulties meeting deadlines and achieving quality benchmarks. Also, the paths to mitigate these challenges through initiatives like using automated tools, dynamic testing, and front-loaded quality management for enhancing efficiency and software quality[75].

Table 4: Comparative Analysis of Challenges, Impacts, and Mitigation Strategies in Recent CI/CD and Agile Development Studies

Reference Title	Challenges	Impact	Mitigation Strategy
[28]	Changing requirements, stakeholder involvement, and traceability	Delays, cost overruns, and incomplete features	Continuous stakeholder engagement, iterative refinement, and backlog grooming
[14]	Lack of shared understanding, evolving technical debt	Reduced code quality and slower delivery	Continuous learning, leadership support, and fostering a technical excellence mindset
[12]	Coordination, resource allocation, and team dependencies	Misalignment, project delays, and resource bottlenecks	Cross-team synchronization, centralized planning, and dependency mapping
[33]	Resistance to change, lack of agile maturity	Inefficiency in digital transformation initiatives	Comprehensive training, leadership alignment, and fostering an agile culture
[76]	Accessibility is overlooked in agile projects	Exclusion of users with disabilities	Incorporating accessibility into acceptance criteria and developer training
[35]	Inaccurate cost/time estimates	Budget overruns and project delays	Prediction-based estimation model incorporating user stories and developer expertise
[29]	Communication gaps, lack of coordination	Reduced productivity and project inefficiency	Shared mental models, peer feedback, and adaptive leadership
[77]	Complexity in large-scale agile	Coordination difficulties, slower development	AI-driven tools for planning, monitoring, and risk management
[26]	Misaligned processes between hardware and software teams	Integration issues, reduced efficiency	Use of SAFe/LeSS frameworks, collaborative workshops, and incremental delivery

6. Future Directions

Artificial intelligence (AI) and machine learning (ML) have created a road map for automated quality metrics in software engineering. These technologies will increasingly enable quality assurance activities with improved accuracy, speed, and predictive power. The more complex and large software systems become, the greater the need for intelligent, adaptive, and autonomous quality assessment tools. New approaches to code evaluation, security assurance, and performance optimization will emerge in software engineering. AI-based solutions will lead the way for next-generation software development [78].

6.1 AI-Powered Code Reviews

AI code review tools are an innovative change in measuring and managing code quality. These tools exploit the availability of large data sets associated with historic codebases to learn patterns associated with defects, inefficiencies, and poor practices. By training machine learning algorithms with relevant example code, an AI system can learn to identify recurring issues with code and predict where development may have vulnerabilities or logical ambiguity. This capability allows teams to leverage AI's ability to identify defects early, shifting them from relying entirely on manual review processes and reducing the chances of making critical errors being delivered into production [79]. AI code review systems can also provide context recommendations, allowing for helpful developer feedback and the suggestion of best practices congruent with their organization's coding standards [80].

6.2 Automated Security Audits

Joining AI and ML in security examination significantly advances program quality assurance. During the dynamic advancement stage, computerized security review devices use real-time examination to identify vulnerabilities, such as SQL injection, cross-site scripting (XSS), and buffer floods. Unlike conventional inactive examination strategies, AI-enhanced reviews adjust to advancing risk scenes by ceaselessly upgrading their information base through exposure to modern security designs and breach information [81]. This results in a more energetic and responsive security foundation that can distinguish novel assault vectors and prescribe mitigative activities without human intervention. Moreover, computerized security reviews encourage compliance with industry benchmarks by guaranteeing that code reliably follows administrative systems, thus lessening the risk of security breaches and information compromise [82].

6.3 Intelligent Performance Monitoring

The optimization of the execution ensures the flexibility and indisputable quality of computer program applications. Smart execution frames use AI to analyze the intelligence of customers, design application batteries, and use real-time assets. These versatile frames can recognize execution congestion, provide future requirements for the frame, and reallocate assets to optimize flow and feedback [83]. By learning from customer behavior and operating measures, AI verification devices can propose changes in creating and tweaking sending techniques to improve the overall efficiency of IT programs. This proactive approach to execution management makes progress in meetings with customers. It amplifies the life of the IT program platforms by predicting the discharge and minimizing the time to stop working [84].

6.4 Convergence of AI and DevOps

The convergence of AI technologies with DevOps activities will amplify the potential for automatic quality measures. DevOps pipelines have been improved in combination with continuous integration and continuous deployment frameworks (CI / CD), in which the automatic algorithms monitor each stage of the software cycle, from the original code of the version to the production version [85]. This integration allows for transparency of quality issues, the automatic decline in defect deployment, and the smart coordination of the liberation calendar based on predictive analysis. By integrating AI into DevOps' workflow, organizations

can reach faster distribution cycles while maintaining high code quality standards and the ability to recover operating systems [86].

6.5 Future Implications

The future of automatic quality measures means transforming the autonomous insurance model and the self-assessment system. This progress is continuous for software engineering, promoting innovation and profits while reducing significant risks. While AI continues to grow, the limits of automatic quality evaluation pave the way for more sophisticated autonomy systems capable of managing the entire software quality size. The widespread application of quality measures focuses on who will redefine the best practices and promoting a continuous and excellent culture in the software development industry [87].

Table 5: Comparative Analysis of Traditional vs. AI-Powered Quality Metrics

Reference Title	Aspect	Traditional QA Methods	AI-Powered QA Methods
[61]	Code Review	Manual, time-consuming	Automated, predictive, and adaptive
	Resource Optimization	Static, manual allocation	Dynamic, AI reallocates resources as needed
[63]	Security Audits	Periodic, rule-based	Continuous, real-time vulnerability detection
	Scalability	Limited by manual effort	Autonomous, scales across microservices and clusters
	Compliance Monitoring	Manual, checklist-based	Automated compliance checks integrated into CI/CD
[55]	Performance Monitoring	Post-deployment, reactive	Real-time, proactive performance optimization
[58]	Error Detection	Relies on predefined test cases	Learns from historical data and detects anomalies
	Risk Mitigation	Reactive, based on post-release feedback	Predictive, prevents issues during development
[62]	Deployment Frequency	Infrequent, manual approval required	Frequent, AI-guided CI/CD pipelines
[54]	Operational Cost	High, driven by manual effort	Lower, automation reduces human intervention
[20]	Requirement Elicitation	Manual, often incomplete	Automated, NLP-based extraction
[27]	Security Activities	Manual integration, checklist-based	Automated, integrated into the CI/CD pipeline
[35]	Cost Estimation	Manual, subjective, high variance	AI-based prediction techniques, more accurate estimates
	Risk Management	Reactive, post-incident analysis	Predictive analytics to foresee risks
	Resource Allocation	Static, manually adjusted	Dynamic, AI-optimized resource allocation
[34]	Scaled Agile Development	Coordination issues in large teams	AI-driven assistants for better collaboration and tracking
[28]	Requirements Management	Prone to oversight, limited stakeholder input	Continuous feedback, adaptive to evolving requirements
[32]	Accessibility Testing	Often overlooked, low priority	Automated tools and guidelines are integrated during development
[36]	Physical Product Development	Slower, manual coordination	AI-driven tools for resource optimization and synchronization

[14]	Technical Excellence	Team-driven, subject to skills	AI-enhanced code quality checks and refactoring
[26]	Large-Scale Agile	Manual coordination across teams	AI-based coordination frameworks (SAFe, LeSS)
[69]	Quality Requirements (QR)	Reactive, addressed post-release	Proactive, integrated during development
[29]	Team Coordination	Manual coordination, frequent meetings required	AI-assisted tools for real-time collaboration and tracking
	Task Prioritization	Manager-driven, subjective	AI-driven task prioritization based on historical data

7. Conclusion

Automatic quality measures have become necessary in developing Agile software, meeting important needs for coherent and active quality assurance. Automatic tools reduce technical debt, improve maintenance capacity, and reduce long-term project costs by integrating errors, code analysis, and direct performance monitoring in a fast workflow. This assessment emphasizes the importance of the primary measures, such as the complexity of the code and the maintenance and insurance of tests, emphasizing their role in maintaining the reliability and strength of the software. Integrating tools such as JUnit, Selenium, and JMeter in CI / CD pipelines is more reasonable than development processes, allowing faster versions without affecting quality. Despite this progress, challenges such as false positives, complexity of integration, and data overload still exist, emphasizing the need to adjust AQ automatic practice continuously. The emerging trend, including AI-centered code tests and automatic safety audits, promises guidelines for the future, improving the accuracy and predictions of quality assessment tools.

AI convergence with DevOps and Agile methods has an important opportunity to improve software quality while accelerating the distribution cycle. Although automatic quality measures continue to grow, their application will play a central role in training the next generation of Agile software development to promote innovation and ensure the recovery of software systems in an increasingly competitive landscape.

References

- [1] L. Barros, C. Tam, and J. Varajão, "Agile software development projects—Unveiling the human-related critical success factors," *Information and Software Technology*, vol. 170, p. 107432, 2024/06/01/ 2024.
- [2] D. Ly, M. Overeem, S. Brinkkemper, and F. Dalpiaz, "The Power of Words in Agile vs. Waterfall Development: Written Communication in Hybrid Software Teams," *Journal of Systems and Software*, vol. 219, p. 112243, 2025/01/01/ 2025.
- [3] T. Natarajan and S. J. I. A. Pichai, "Transition from Waterfall to Agile Methodology—An Action Research Study," 2024.
- [4] J.-N. J. J. o. S. Meckenstock and Software, "Shedding Light on the Dark Side—A Systematic Literature Review of the Issues in Agile Software Development Methodology Use," p. 111966, 2024.
- [5] J. P. Biazotto, D. Feitosa, P. Avgeriou, E. Y. J. I. Nakagawa, and S. Technology, "Technical debt management automation: State of the art and future perspectives," vol. 167, p. 107375, 2024.

- [6] A. Aburas, "Choosing the Right Automated Software Testing Tools," in *2024 IEEE 4th International Maghreb Meeting of the Conference on Sciences and Techniques of Automatic Control and Computer Engineering (MI-STA)*, 2024, pp. 31-35: IEEE.
- [7] M. A. Moseh, N. A. Al-Khulaidi, A. H. Gumaei, A. Alsabry, and A. A. Musleh, "Classification and Evaluation Framework of Automated Testing Tools for Agile Software: Technical Review," in *2024 4th International Conference on Emerging Smart Technologies and Applications (eSmarTA)*, 2024, pp. 1-12: IEEE.
- [8] J. W. Beard *et al.*, "Agile Development: The Promise, the Reality, the Opportunity," in *Agil-ISE@ CAiSE*, 2024, pp. 7-17.
- [9] S. A. Butt, S. Naz, P.-E. Gabriel, P. A.-C. Patriciac, and M. A. J. P. C. S. Piñeres-Melo, "The Importance of Robust Communication in Large-Scale Agile Development," vol. 236, pp. 224-232, 2024.
- [10] M. Nozarian, A. Hajizadeh, A. J. S. E. T. Fereidunian, and Assessments, "A methodological review on management of building cluster meso energy hubs by the agile framework: Exploring flexibility upward the building-cluster-city hierarchy," vol. 67, p. 103834, 2024.
- [11] R. Kasauli, E. Knauss, J. Horkoff, G. Liebel, and F. G. de Oliveira Neto, "Requirements engineering challenges and practices in large-scale agile system development," *Journal of Systems and Software*, vol. 172, p. 110851, 2021/02/01/ 2021.
- [12] M. Michalides, N. Bursac, S. J. Nicklas, S. Weiss, and K. Paetzold, "Analyzing current Challenges on Scaled Agile Development of Physical Products," *Procedia CIRP*, vol. 119, pp. 1188-1197, 2023/01/01/ 2023.
- [13] R. Mantovani Fontana and S. Marczak, "Characteristics and Challenges of Agile Software Development Adoption in Brazilian Government," *Journal of Technology Management & Innovation*, vol. 15, no. 2, pp. 3-10, 09/01 2020.
- [14] A. Alami, O. Krancher, M. J. I. Paasivaara, and S. Technology, "The journey to technical excellence in agile software development," vol. 150, p. 106959, 2022.
- [15] D. Miranda and J. Araujo, "Studying industry practices of accessibility requirements in agile development," in *Proceedings of the 37th ACM/SIGAPP Symposium on Applied Computing*, 2022, pp. 1309-1317.
- [16] A. Mishra, Y. I. J. I. J. o. S. A. E. Alzoubi, and Management, "Structured software development versus agile software development: a comparative analysis," vol. 14, no. 4, pp. 1504-1522, 2023.
- [17] L. Zuluaga *et al.*, "AI-powered real-time annotations during urologic surgery: The future of training and quality metrics," in *Urologic Oncology: Seminars and Original Investigations*, 2024, vol. 42, no. 3, pp. 57-66: Elsevier.
- [18] F. El Aouni, K. Moumane, A. Idri, M. Najib, S. U. J. I. Jan, and S. Technology, "A systematic literature review on Agile, Cloud, and DevOps integration: Challenges, benefits," p. 107569, 2024.
- [19] M. C. Annosi, F. P. Appio, and A. J. T. Martini, "Institutional context and agile team innovation: A sensemaking approach to collective knowledge creation," vol. 129, p. 102894, 2024.
- [20] M. A. SHAH, A. MUSTAFA, and M. AWAIS, "Elicitation of Nonfunctional Requirements in Agile Development Using Cloud Computing Environment."

- [21] S. Nazir, B. Price, N. C. Surendra, K. J. I. T. Kopp, and Management, "Adapting agile development practices for hyper-agile environments: lessons learned from a COVID-19 emergency response research project," vol. 23, no. 3, pp. 193-211, 2022.
- [22] R. Wafa, M. Q. Khan, F. Malik, A. B. Abdusalomov, Y. I. Cho, and R. Odarchenko, "The Impact of Agile Methodology on Project Success, with a Moderating Role of Person's Job Fit in the IT Industry of Pakistan," vol. 12, no. 21, p. 10698, 2022.
- [23] V. Venkatesh *et al.*, "Equality Does Not Make You Happy: Effects of Differentiated Leader-Member Exchange and Team-Member Exchange on Developer Satisfaction in Agile Development Teams," *MIS Quarterly*, vol. 47, pp. 1239-1270, 09/01 2023.
- [24] J. Leong, K. May Yee, O. Baitsegi, L. Palanisamy, and R. K. J. S. Ramasamy, "Hybrid project management between traditional software development lifecycle and agile-based product development for future sustainability," vol. 15, no. 2, p. 1121, 2023.
- [25] A. Latifah *et al.*, *Development of a Website-Based Financial Transaction Management System Using Agile with the Scrum Framework*. 2023, pp. 1-6.
- [26] R. Kasauli, E. Knauss, J. Horkoff, G. Liebel, F. G. J. J. o. S. de Oliveira Neto, and Software, "Requirements engineering challenges and practices in large-scale agile system development," vol. 172, p. 110851, 2021.
- [27] A. Sharma and R. K. Bawa, "Identification and integration of security activities for secure agile development," *International Journal of Information Technology*, vol. 14, no. 2, pp. 1117-1130, 2022/03/01 2022.
- [28] A. Rasheed *et al.*, "Requirement engineering challenges in agile software development," vol. 2021, no. 1, p. 6696695, 2021.
- [29] D. Strode, T. Dingsøyr, and Y. J. E. S. E. Lindsjorn, "A teamwork effectiveness model for agile software development," vol. 27, no. 2, p. 56, 2022.
- [30] P. Marnada, T. Raharjo, B. Hardian, and A. J. P. C. S. Prasetyo, "Agile project management challenge in handling scope and change: A systematic literature review," vol. 197, pp. 290-300, 2022.
- [31] A. Gupta, G. Poels, and P. J. I. A. Bera, "Using conceptual models in agile software development: a possible solution to requirements engineering challenges in agile projects," vol. 10, pp. 119745-119766, 2022.
- [32] D. Miranda and J. Araujo, *Studying industry practices of accessibility requirements in agile development*. 2022, pp. 1309-1317.
- [33] O. A. Popoola, H. E. Adama, C. D. Okeke, A. E. J. E. S. Akinoso, and T. Journal, "Conceptualizing agile development in digital transformations: Theoretical foundations and practical applications," vol. 5, no. 4, pp. 1524-1541, 2024.
- [34] V. Saklamaeva and L. J. A. S. Pavlič, "The potential of AI-driven assistants in scaled agile software development," vol. 14, no. 1, p. 319, 2023.
- [35] S. A. Butt *et al.*, "Prediction based cost estimation technique in agile development," vol. 175, p. 103329, 2023.
- [36] M. Michalides, N. Bursac, S. Nicklas, S. Weiss, and K. Paetzold, *Analyzing current Challenges on Scaled Agile Development*. 2023.
- [37] A. Salameh, J. M. J. A. Bass, and Society, "An architecture governance approach for Agile development by tailoring the Spotify model," vol. 37, no. 2, pp. 761-780, 2022.

- [38] I. Pérez Hurtado de Mendoza, D. Orellana Martín, M. Á. Martínez del Amor, L. Valencia Cabrera, and A. J. I. S. Riscos Núñez, 587 , 1-22., "A new P-Lingua toolkit for agile development in membrane computing," 2022.
- [39] G. Labrèche, D. Evans, D. Marszk, T. Mladenov, V. Shiradhonkar, and V. Zelenevskiy, "Agile Development and Rapid Prototyping in a Flying Mission with Open Source Software Reuse On-Board the OPS-SAT Spacecraft," in *AIAA SCITECH 2022 Forum*, 2022, p. 0648.
- [40] M. Batliner, S. Boës, J. Heck, and M. J. P. C. Meboldt, "Linking testing activities with success in agile development of physical products," vol. 109, pp. 146-154, 2022.
- [41] R. Cooper and A. Sommer, "New-Product Portfolio Management with Agile: Challenges and Solutions for Manufacturers Using Agile Development Methods," *Research-Technology Management*, vol. 63, pp. 29-38, 01/02 2020.
- [42] J. Aluthwaththage and H. Thathsarani, "A Novel OO-Based Code Complexity Metric," in *Proceedings of the Future Technologies Conference*, 2024, pp. 616-628: Springer.
- [43] U. Iftikhar, N. B. Ali, J. Börstler, M. J. I. Usman, and S. Technology, "A tertiary study on links between source code metrics and external quality attributes," vol. 165, p. 107348, 2024.
- [44] H. Rezaei Rahvard, M. J. J. o. I. Salkhordeh Haghighi, and C. Technology, "Improving Code Coverage Metrics for Discovering Vulnerabilities in Stateful Network Protocols using Hybrid Fuzzing," vol. 61, no. 61, p. 72, 2024.
- [45] K. Shivashankar and A. J. a. p. a. Martini, "Better Python Programming for all: With the focus on Maintainability," 2024.
- [46] X. Shi, Y. Yang, X. Zhu, and Z. J. C. S. Huang, "Stochastic dynamics analysis of the rocket shell coupling system with circular plate fasteners based on spectro-geometric method," vol. 329, p. 117727, 2024.
- [47] M. L. Siddiq, J. C. Da Silva Santos, R. H. Tanvir, N. Ulfat, F. Al Rifat, and V. Carvalho Lopes, "Using large language models to generate junit tests: An empirical study," in *Proceedings of the 28th International Conference on Evaluation and Assessment in Software Engineering*, 2024, pp. 313-322.
- [48] K. R. R. J. T. Manukonda, "ENHANCING TEST AUTOMATION COVERAGE AND EFFICIENCY WITH SELENIUM GRID: A STUDY ON DISTRIBUTED TESTING IN AGILE ENVIRONMENTS," vol. 15, no. 3, pp. 119-127, 2024.
- [49] F. Zhou and Y. Gao, "Performance Study on Normalization and Denormalization in MES System Databases," in *2024 International Conference on Intelligent Computing and Data Mining (ICDM)*, 2024, pp. 90-94: IEEE.
- [50] T. Chen, "Challenges and opportunities in integrating LLMs into continuous integration/continuous deployment (CI/CD) pipelines," in *2024 5th International Seminar on Artificial Intelligence, Networking and Information Technology (AINIT)*, 2024, pp. 364-367: IEEE.
- [51] I. Kansanen, "AUTOMATING DOCKER REGISTRY VERSION CONTROL USING JENKINS," 2024.
- [52] A. Houerbi, C. Siala, A. Tucker, D. E. Rzig, and F. J. a. p. a. Hassan, "Empirical Analysis on CI/CD Pipeline Evolution in Machine Learning Projects," 2024.

- [53] E. Naresh, S. Murthy, N. Sreenivasa, S. Merikapudi, and C. R. Krishna, "Continuous Integration, Testing, Deployment and Delivery in Devops," in *2024 International Conference on Knowledge Engineering and Communication Systems (ICKECS)*, 2024, vol. 1, pp. 1-4: IEEE.
- [54] P. S. Chatterjee and H. K. Mittal, "Enhancing Operational Efficiency through the Integration of CI/CD and DevOps in Software Deployment," in *2024 Sixth International Conference on Computational Intelligence and Communication Technologies (CCICT)*, 2024, pp. 173-182: IEEE.
- [55] A. M. Ferreira, M. A. Brito, and J. Lima, "Continuous Inspection of Software Quality in an Automotive Project," in *2023 18th Iberian Conference on Information Systems and Technologies (CISTI)*, 2023, pp. 1-6.
- [56] Q. Cooper, "Expedited Load Tests for CI/CD Microservice Applications," 2024.
- [57] R. Chandramouli, F. Kautz, and S. Torres-Arias, "Strategies for the Integration of Software Supply Chain Security in DevSecOps CI/CD Pipelines," ed: Special Publication (NIST SP), National Institute of Standards and ..., 2024.
- [58] E. Klotins, T. Gorschek, K. Sundelin, and E. J. E. S. E. Falk, "Towards cost-benefit evaluation for continuous software engineering activities," vol. 27, no. 6, p. 157, 2022.
- [59] M. M. Alam, A. Arbaz, M. Shaik Habeeb Uddin, H. J. M. S. Yasmin, and E. Applications, "Emerging Continuous Integration Continuous Delivery (CI/CD) For Small Teams," vol. 72, no. 1, pp. 1535-1543, 2023.
- [60] Z. Wadhams, A. M. Reinhold, and C. Izurieta, "Automating Static Code Analysis Through CI/CD Pipeline Integration," in *2nd International Workshop on Mining Software Repositories for Privacy and Security, MSR4P&S,(SANER 2024), Rovaniemi, Finland*, 2024.
- [61] M. Fredrikson, "Configuring targeted dynamic parallel testing to a CI/CD pipeline," 2024.
- [62] A. R. Faqih, A. Taufiqurrahman, J. H. Husen, M. K. J. J. o. I. Sabariah, and W. Engineering, "Empirical Analysis of CI/CD Tools Usage in GitHub Actions Workflows," vol. 3, no. 2, pp. 251-261, 2024.
- [63] P. J. O. C. S. Dakić, "Software compliance in various industries using CI/CD, dynamic microservices, and containers," vol. 14, no. 1, p. 20240013, 2024.
- [64] M. J. I. E. J. Filomena, "Unemployment scarring effects: An overview and meta-analysis of empirical studies," vol. 10, no. 2, pp. 459-518, 2024.
- [65] S. Rasnayaka, G. Wang, R. Shariffdeen, and G. N. Iyer, "An empirical study on usage and perceptions of llms in a software engineering project," in *Proceedings of the 1st International Workshop on Large Language Models for Code*, 2024, pp. 111-118.
- [66] E. Lett, E. Asabor, S. Beltrán, A. M. Cannon, and O. A. J. T. A. o. F. M. Arah, "Conceptualizing, contextualizing, and operationalizing race in quantitative health sciences research," vol. 20, no. 2, pp. 157-163, 2022.
- [67] H. Yan, F. Wang, G. Yan, and D. J. J. o. P. C. He, "Hybrid approach integrating case-based reasoning and Bayesian network for operational adjustment in industrial flotation process," vol. 103, pp. 34-47, 2021.
- [68] K. K. Holgeid, M. Jørgensen, D. I. Sjøberg, and J. J. I. S. Krogstie, "Benefits management in software development: A systematic review of empirical studies," vol. 15, no. 1, pp. 1-24, 2021.

- [69] P. Karhapää *et al.*, "Strategies to manage quality requirements in agile software development: a multiple case study," vol. 26, no. 2, p. 28, 2021.
- [70] M. Almashhadani, A. Mishra, A. Yazici, and M. J. I. Younas, "Challenges in agile software maintenance for local and global development: an empirical assessment," vol. 14, no. 5, p. 261, 2023.
- [71] M. G. Gramajo, L. Ballejos, and M. J. a. p. a. Ale, "Recurrent Neural Networks to automate Quality assessment of Software Requirements," 2021.
- [72] P. Rani *et al.*, "A decade of code comment quality assessment: A systematic literature review," vol. 195, p. 111515, 2023.
- [73] P. Nama, "Integrating AI in testing automation: Enhancing test coverage and predictive analysis for improved software quality," 2024.
- [74] P. Lenberg *et al.*, "Qualitative software engineering research: Reflections and guidelines," vol. 36, no. 6, p. e2607, 2024.
- [75] A. R. J. A. J. o. R. i. C. S. Kunduru, "Cloud BPM Application (Appian) Robotic Process Automation Capabilities," vol. 16, no. 3, pp. 267-280, 2023.
- [76] D. Miranda and J. Araujo, "Studying industry practices of accessibility requirements in agile development," presented at the Proceedings of the 37th ACM/SIGAPP Symposium on Applied Computing, Virtual Event, 2022. Available: <https://doi.org/10.1145/3477314.3507041>
- [77] V. Saklamaeva and L. Pavlič, "The Potential of AI-Driven Assistants in Scaled Agile Software Development," *Applied Sciences*, vol. 14, p. 319, 12/29 2023.
- [78] D. Thangam, K. Pavan, S. Patil, J. Y. Park, R. Kandasamy, and R. J. Chikkandar, "Intelligent Process Automation and Its Relevance to Various Industries," in *Advancements in Intelligent Process Automation*: IGI Global, 2025, pp. 387-412.
- [79] O. I. Sheet, L. M. J. J. o. E. Ibrahim, and Science, "Design and implement machine learning tool for cyber security risk assessment," vol. 32, no. 2, pp. 51.0-64.0, 2023.
- [80] A. M. J. D. J. o. T. T. T. Abubakar, "Artificial Intelligence Applications in Engineering: A Focus on Software Development and Beyond," vol. 1, no. 1, 2025.
- [81] V. Babaey and A. J. F. I. Ravindran, "GenSQLi: A Generative Artificial Intelligence Framework for Automatically Securing Web Application Firewalls Against Structured Query Language Injection Attacks," vol. 17, no. 1, p. 8, 2025.
- [82] A. Kumar *et al.*, "IoT device security audit tools: a comprehensive analysis and a layered architecture approach for addressing expanded security requirements," vol. 24, no. 1, pp. 1-22, 2025.
- [83] H. M. Yahya and D. B. Taha, "Detection of Bad Code Smells By Using Deep Machine Learning Approaches," in *2023 1st International Conference on Advanced Engineering and Technologies (ICONNIC)*, 2023, pp. 281-286: IEEE.
- [84] H. Deng, Y. Lu, D. Fan, W. Liu, Y. J. N. T. Xia, Work, and Employment, "The Power of Precision: How Algorithmic Monitoring and Performance Management Enhances Employee Workplace Well-Being," 2025.
- [85] M. A. Al-Jawaherry, A. A. Abdulmajeed, and T. M. J. I. J. o. S. Tawfeeq, "Developing a heuristic algorithm to solve the uncertainty problem of resource allocation in a software project scheduling," pp. 2211-2229, 2022.
- [86] H. H. Olsson, J. J. I. Bosch, and S. Technology, "Strategic digital product management: Nine approaches," vol. 177, p. 107594, 2025.

- [87] I. Sljivo, I. Perez, A. Mavridou, J. Schumann, P. G. Vlastos, and C. Carter, "Dynamic assurance of autonomous systems through ground control software," in *AIAA SCITECH 2024 Forum*, 2024, p. 1208.

Deep Feature Embedding for Content-Based Image Retrieval Using Autoencoders and Semantic Hashing

Azhar amer alsoufi

Email: mti.lec250.azhar@ntu.edu.iq

Department of Networks and Computer Software Techniques, Northern Technical University, Mosul, Iraq.

Deep Feature Embedding for Content-Based Image Retrieval Using Autoencoders and Semantic Hashing

Azhar amer alsoufi

Email: mti.lec250.azhar@ntu.edu.iq

Department of Networks and Computer Software Techniques, Northern Technical University, Mosul, Iraq.

Abstract—The necessity for effective and efficient Content- Based Image Retrieval (CBIR) systems—where retrieval is done based on the visual content of images rather than metadata—has increased due to the exponential expansion of digital image repositories. Conventional CBIR methods that depend on manually created features frequently fail to capture intricate semantic links in image data, which restricts their scalability and retrieval performance. Recent research has investigated deep learning-based representations and hashing methods for increased efficiency and accuracy in order to overcome these issues. Nevertheless, a lot of current methods either need a lot of labeled data or are unable to produce compact representations that are quick to retrieve in large-scale environments. In this study, we offer a deep unsupervised CBIR framework that combines semantic hashing with convolutional autoencoders. A semantic hashing mechanism is used to convert the discriminative, low-dimensional feature embeddings that the autoencoder learns into compact binary hash codes. This makes it possible to use the Hamming distance for an effective similarity search. Comprehensive tests on benchmark datasets like Caltech-101 and CIFAR-10 show that our method provides a scalable and efficient solution for large-scale image retrieval problems by achieving competitive retrieval accuracy while drastically cutting down on retrieval time.

Index Terms—Content-Based Image Retrieval, Deep Autoencoder, Semantic Hashing, Image Embedding, Binary Hash Codes

الملخص — ازدادت الحاجة إلى أنظمة استرجاع الصور المعتمدة على المحتوى (CBIR) الفعالة والكفوة — حيث يتم الاسترجاع بناءً على المحتوى البصري للصور بدلاً من البيانات الوصفية — بسبب التوسع الكبير في مستودعات الصور الرقمية. الطرق التقليدية لـ CBIR التي تعتمد على الميزات المنشأة يدوياً غالباً ما تفشل في التقاط الروابط الدلالية المعقدة في بيانات الصور، مما يحد من قابلية توسعها وأداء الاسترجاع. بحثت الدراسات الحديثة في التمثيلات المستندة إلى التعلم العميق وأساليب التجزئة (الهاشينغ) لتحقيق زيادة في الكفاءة والدقة من أجل التغلب على هذه المشاكل. ومع ذلك، فإن العديد من الطرق الحالية إما تحتاج إلى كميات كبيرة من البيانات الموسومة أو غير قادرة على إنتاج تمثيلات مضغوطة تسهل استرجاعها بسرعة في البيئات واسعة النطاق. في هذه الدراسة، نقدم إطار عمل عميق غير مراقب لـ CBIR يجمع بين التجزئة الدلالية (semantic hashing) والمشفرات الالتقائية (convolutional autoencoders). تُستخدم آلية التجزئة الدلالية لتحويل التضمينات التمييزية منخفضة الأبعاد التي يتعلمها المشفر الالتقائي إلى رموز هاش ثنائية مضغوطة، مما يجعل من الممكن استخدام مسافة هامينغ لإجراء بحث تشابه فعال. تُظهر الاختبارات الشاملة على مجموعات بيانات معيارية مثل Caltech-101 و CIFAR-10 أن طريقتنا تقدم حلاً قابلاً للتوسع وفعالاً لمشاكل استرجاع الصور واسعة النطاق من خلال تحقيق دقة تنافسية في الاسترجاع مع تقليل كبير في زمن الاسترجاع.

I. INTRODUCTION

A strong and scalable image retrieval system is urgently needed due to the explosive growth of digital image data in fields including social networking [1], medical diagnostics [2], surveillance [3], and e-commerce [4]. Conventional methods for image retrieval frequently depend on textual information [5] or human tagging [6], which are insufficient for capturing the visual semantics of

image content and are time-consuming. For instance, if relevant images are not appropriately tagged, a search for "red sports car" may yield erroneous results even when the visual material is exactly what is needed. Content- Based Image Retrieval (CBIR) [7], which retrieves images based on their visual properties instead of written descriptions, is necessary because of this constraint. Extracting discriminative features that represent the visual content of images is usually the foundation of CBIR techniques. Previous efforts used hand-crafted features like SIFT [8], texture descriptors [9], and color histograms [10]. However, these conventional descriptors frequently lack the semantic abstraction required for intricate visual tasks and have trouble generalizing across a variety of image datasets. Moreover, their

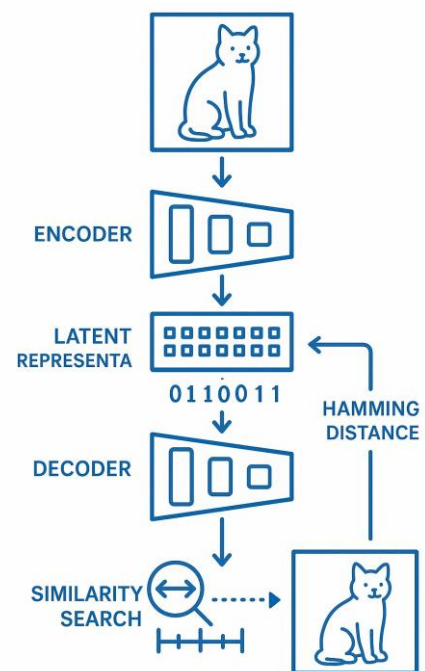


Fig. 1. The deep unsupervised CBIR framework's architecture: combining semantic hashing and convolutional autoencoder for effective image retrieval.

restricted indexing methods and high dimensionality make them ineffective in large-scale situations.

CBIR has been completely transformed by recent developments in deep learning [11], especially in unsupervised representation learning [12], which allow models to extract valuable features straight from unprocessed pixel input. As a subclass of unsupervised neural networks, autoencoders [13] have proven to be highly effective at learning condensed, informative image encodings. Nevertheless, autoencoders do not automatically optimize continuous-valued embeddings for effective retrieval in big databases. In order to get around this,

semantic hashing [14] has become a useful method for mapping high-dimensional characteristics into compact binary hash codes, which allows for quick Hamming distance similarity searches. However, many hashing-based CBIR systems currently in use are either not encoder-end optimized [15], suffer from quantization losses during binary conversion [16], or rely on supervised learning [17], which necessitates large annotated datasets. Therefore, we suggest an unsupervised deep CBIR framework (see Fig. 1) that combines semantic hashing and convolutional autoencoders in order to overcome these difficulties. The suggested method achieves low search latency and good retrieval accuracy by learning compact latent representations and converting them into binary hash codes end-to-end. In summary, the following are our primary contributions:

- We create an architecture for a deep convolutional autoencoder that can learn low-dimensional, robust feature embeddings from images without supervision.
- In order to facilitate effective retrieval using Hamming distance, we present a semantic hashing technique that creates binary hash codes using learned embeddings.
- In order to minimize binarization error and maintain semantic structure, we simultaneously optimize the quantization and reconstruction losses.
- We carry out comprehensive tests on common image datasets (Caltech-101 and CIFAR-10), showing that our methodology outperforms current methods in terms of speed and retrieval accuracy.

II. RELATED WORK

Over the past 20 years, CBIR systems have been the subject of much research, with the main goal being to retrieve visually similar images from massive datasets using content rather than metadata. Hand-crafted feature descriptors like color histograms [10], SIFT [8], and Gabor filters [18] were the main emphasis of classical CBIR methods [8], [19]. Although these features work well in some situations, their robustness and generalizability in real-world situations are limited because they are frequently susceptible to changes in light, image noise, and geometric modifications. CBIR has significantly improved since the introduction of deep learning, especially Convolutional Neural Networks (CNNs) [11]. From unprocessed image input, CNN-based models can directly learn hierarchical and semantically rich representations. By training networks to embed semantically comparable images closer in the feature space, notable studies like Deep Ranking [20] and Deep Metric Learning [21] have shown higher retrieval performance. These models perform noticeably better than conventional methods in terms of generalization and accuracy. In order to build compact feature representations without the use of labeled data, autoencoders—a kind of unsupervised neural network [13]—have also been investigated in CBIR. Autoencoders capture important information in a lower-dimensional latent space by reducing reconstruction loss. For visual feature extraction tasks, variants like convolutional autoencoders [22] and denoising autoencoders [23] are appropriate since they better preserve spatial hierarchies

and are more resilient to noise. Semantic hashing [14] is a method that converts continuous-valued feature vectors into compact binary hash codes to facilitate scalability and effective retrieval. These hash codes greatly reduce storage requirements while enabling quick retrieval utilizing Hamming distance [14]. There have been proposals for both supervised and unsupervised deep hashing methods, with supervised methods using label information to direct code development. But because it is hard to maintain semantic similarity without supervision, unsupervised deep hashing is still a tough and active study subject [16]. By combining a semantic hashing method and convolutional autoencoders into a single, unsupervised framework, our study expands on these foundations.

III. METHODOLOGY

A convolutional autoencoder for unsupervised feature learning, a semantic hashing layer that converts latent features into compact binary codes, and a Hamming distance-based similarity retrieval module for quick and scalable search are the three main parts of the suggested CBIR framework. In Algorithm 1, the full overview is displayed.

A. Convolutional Autoencoder

Let $\mathbf{X} = \{\mathbf{x}_1, \mathbf{x}_2, \dots, \mathbf{x}_n\} \subset \mathbb{R}^{H \times W \times C}$ denote a collection of n input images, each of spatial dimension $H \times W$ with C channels. A convolutional autoencoder is employed to learn a low-dimensional representation of each image. It consists of two parts: an encoder \mathbf{E} and a decoder \mathbf{D} . The encoder maps an input image \mathbf{x}_i to a latent representation $\mathbf{z}_i \in \mathbb{R}^d$ as shown in Equation (1) and the decoder attempts to reconstruct the original image from the latent vector via Equation (2).

$$\mathbf{z}_i = \mathbf{E}(\mathbf{x}_i) \quad (1)$$

$$\hat{\mathbf{x}}_i = \mathbf{D}(\mathbf{z}_i) \quad (2)$$

To ensure that the learned embeddings retain sufficient information, we minimize the mean squared reconstruction error over the dataset according to Equation (3).

$$(3) \quad L_{\text{rec}} = \frac{1}{n} \sum_{i=1}^n \|\mathbf{x}_i - \hat{\mathbf{x}}_i\|_2^2$$

Algorithm 1 Deep Feature Embedding for CBIR using Autoencoder and Semantic Hashing

Require: Image dataset $\mathbf{X} = \{\mathbf{x}_1, \dots, \mathbf{x}_n\}$, embedding dimension d , hash length k , learning rate η , trade-off parameter λ

Ensure: Binary hash codes $\{\mathbf{h}_1, \dots, \mathbf{h}_n\}$

```

1: Initialize encoder E, decoder D, and hashing parameters W, b
2: for each training epoch do
3:   for each image  $\mathbf{x}_i \in \mathbf{X}$  do
4:      $\mathbf{z}_i \leftarrow E(\mathbf{x}_i)$   $\triangleright$  Encode input image
5:      $\hat{\mathbf{x}}_i \leftarrow D(\mathbf{z}_i)$ 
6:     Reconstruct image  $\mathbf{y}_i \leftarrow \tanh(W \mathbf{z}_i + \mathbf{b})$ 
7:     Hash projection  $\mathbf{h}_i \leftarrow \text{sign}(\mathbf{y}_i)$ 
8:     Compute reconstruction loss:  $L_{\text{rec}} \leftarrow \|\mathbf{x}_i - \hat{\mathbf{x}}_i\|^2$ 
9:     Compute quantization loss:  $L_{\text{quant}} \leftarrow \|\mathbf{h}_i - \tanh(\mathbf{z}_i)\|^2$ 
10:    Compute total loss:  $L \leftarrow L_{\text{rec}} + \lambda L_{\text{quant}}$ 
11:    Update network parameters using gradient descent with learning rate  $\eta$ 
12:  end for
13: end for
14: return Binary hash codes  $\{\mathbf{h}_1, \dots, \mathbf{h}_n\}$  for all training images

```

This loss enforces the encoder to produce informative and compact features that allow accurate reconstruction.

B. Semantic Hashing

To facilitate fast similarity search, we append a hashing layer to the encoder, transforming continuous latent features into binary hash codes $\mathbf{h}_i \in \{0, 1\}^k$.

First, the encoder output is linearly transformed and passed through a tanh activation via Equation (4).

$$\mathbf{y}_i = \tanh(W \mathbf{z}_i + \mathbf{b}) \quad (4)$$

where $W \in \mathbb{R}^{k \times d}$ and $\mathbf{b} \in \mathbb{R}^k$ are learnable parameters. The output \mathbf{y}_i is then binarized using the sign function according to Equation (5).

$$\mathbf{h}_i = \text{sign}(\mathbf{y}_i) = \text{sign}(\tanh(W \mathbf{z}_i + \mathbf{b})) \quad (5)$$

However, the non-differentiability of the sign function complicates training. To mitigate this, we adopt a relaxation and introduce a quantization loss that penalizes the deviation of \mathbf{y}_i from its binarized counterpart as shown in Equation (6).

$$(6) \quad L_{\text{quant}} = \sum_{i=1}^n \|\mathbf{h}_i - \tanh(\mathbf{z}_i)\|_2^2$$

This loss encourages the real-valued outputs to be close to $\{-1, +1\}$, reducing the quantization gap.

C. Objective Function

The total objective function is a weighted combination of the reconstruction and quantization losses as shown in Equation (7).

$$\mathcal{L} = \mathcal{L}_{\text{rec}} + \lambda \mathcal{L}_{\text{quant}} \quad (7)$$

where $\lambda > 0$ is a regularization parameter that balances the trade-off between reconstruction fidelity and the quality of the binary hash codes. During retrieval, binary hash codes $\{\mathbf{h}_i\}$ are generated for all database images, and similarity is computed using the Hamming distance between the query hash and those in the database. This approach ensures both high retrieval accuracy and low computational complexity.

IV. EXPERIMENTAL SETUP

A. Datasets

We test the suggested CBIR framework on two benchmark image datasets, Caltech-101 [24] and CIFAR-10 [25], to evaluate its performance. The 60,000 color images in CIFAR-10, which have a resolution of 32×32 pixels, are uniformly distributed across 10 different classes, including cars, birds, and airplanes. 9,146 photos from 101 object categories make up Caltech-101, which shows more intra-class heterogeneity and complexity in terms of look, scale, and shape. Before being entered into the model, every image from both datasets

is normalized to the $[0, 1]$ range and shrunk to 32×32 pixels for uniformity.

B. Implementation Details

The deep convolutional autoencoder is used to implement the suggested architecture. Three convolutional layers make up the encoder, which is followed by a dense layer that is fully connected and produces the latent representation. Transposed convolutional layers make up the decoder, which uses the latent vector to recreate the input image. The encoder is supplemented with a hashing layer to generate binary hash codes with lengths $k \in \{16, 32, 64\}$ [26], [27]. The Adam optimizer is used to train the entire network at a preset learning rate of 1×10^{-4} . A mini-batch size of 128 is used to train the model over 100 epochs. Using the previously described total objective function, the reconstruction loss and quantization loss are jointly reduced during training[28], [29]. In Algorithm 2, the full overview is displayed.

C. Evaluation Metrics

Three common retrieval metrics—**Mean Average Precision (mAP)**, **Precision@K**, and **Retrieval Time (RT)**—are used to assess our CBIR system. Mean Average Precision calculates the mean for all queries and measures the average precision for each query across several recall levels. Precision@K gives information about how well the model ranks pertinent things by

calculating the percentage of relevant images among the top-K retrieved results. Retrieval Time, which provides an indicator of the system's scalability and real-time

Algorithm 2 Training Procedure for Deep Autoencoder with Semantic Hashing

Require: Dataset $\mathbf{X} = \{\mathbf{x}_1, \mathbf{x}_2, \dots, \mathbf{x}_n\}$, batch size B , learning rate $\eta = 1 \times 10^{-4}$, number of epochs $E = 100$, hash code lengths $k \in \{16, 32, 64\}$, regularization parameter λ .

Ensure: Trained encoder E , decoder D , and hashing layer parameters W, \mathbf{b} .

- 1: Initialize network parameters of encoder E , decoder D , and hashing layer (W, \mathbf{b}) randomly.
- 2: Initialize Adam optimizer with learning rate η .

3: **for** epoch = 1 to E **do**

4: **for** each mini-batch $B = \{\mathbf{x}_{i_1}, \dots, \mathbf{x}_{i_B}\} \subset \mathbf{X}$ **do**

5: **FORWARD PASS:**

6: Encode inputs:

$$\mathbf{z}_{i_j} = E(\mathbf{x}_{i_j}) \text{ for } j = 1, \dots, B.$$

7: Decode latent vectors: $\hat{\mathbf{x}}_{i_j} = D(\mathbf{z}_{i_j})$

8: Compute continuous hash layer outputs:
 $\mathbf{y}_{i_j} = \tanh(W\mathbf{z}_{i_j} + \mathbf{b}).$

9: Binarize hash codes:

$$\mathbf{h}_{i_j} = \text{sign}(\mathbf{y}_{i_j}).$$

10: **Compute losses:**

11: Reconstruction loss:

$$\mathcal{L}_{\text{rec}} = \frac{1}{B} \sum_{i=1}^B \left\| \mathbf{x}_{i_j} - \hat{\mathbf{x}}_{i_j} \right\|_2^2$$

12: Quantization loss:

$$\mathcal{L}_{\text{quant}} = \frac{1}{B} \sum_{i=1}^B \left\| \mathbf{h}_{i_j} - \mathbf{y}_{i_j} \right\|_2^2$$

13: Total loss:

$$\mathcal{L} = \mathcal{L}_{\text{rec}} + \lambda \mathcal{L}_{\text{quant}}$$

14: **Backward pass:** Compute gradients of \mathcal{L} w.r.t. network parameters.

15: Update parameters using Adam optimizer.

16: end for

17: Optionally evaluate model performance on validation set.

18: end for

19: **return** Trained encoder E , decoder D , and hashing layer parameters (W, \mathbf{b}) .

is measured as the average number of milliseconds needed to retrieve results for a specific query.

V. EXPERIMENTAL ANALYSIS

VI. RETRIEVAL PERFORMANCE

mAP, Precision@100, and RT are used to assess the suggested CBIR framework’s retrieval performance across various code lengths and datasets as shown in Table I. The findings show a distinct pattern suggesting that retrieval accuracy is improved by lengthening the hash code, although at a slight computational expense. Using a 16-bit hash code on the CIFAR-10 dataset results in an average retrieval time of 1.7 milliseconds per query, a mAP of 0.612, and a Precision@100 of 0.594. With a mAP of 0.667 and a Precision@100 of 0.631, increasing the code length to 32 bits yields a significant gain with only a minor increase in retrieval time (to 1.8 milliseconds). This implies that more discriminative semantic features are captured by the 32-bit representation without appreciably sacrificing computational efficiency. The effectiveness of longer binary codes in lowering collisions in Hamming space and enhancing the accuracy of recovered data is demonstrated by the CIFAR-10 performance boost from 16 to 32 bits. The trend continues on the Caltech-101 dataset, where the 32-bit code achieves a Precision@100 of 0.685 and a mAP of 0.708 at 2.1 milliseconds per query. The 64-bit code exhibits the best performance, with a mAP of 0.742 and an improvement in Precision@100 to 0.714. Even with a minor increase to 2.3 milliseconds, the retrieval time is still within reasonable ranges for real-time applications. Given the Caltech-101 dataset’s greater diversity and complexity, lengthier hash codes—which enable finer-grained recording of visual features—probably work better. These findings highlight the suggested hashing framework’s scalability and resilience, especially for datasets with significant inter-class heterogeneity.

TABLE I

RETRIEVAL PERFORMANCE ACROSS DIFFERENT CODE LENGTHS AND DATASETS.

Dataset	Code Length	mAP	Precision@100	RT (ms)
CIFAR-10	16	0.612	0.594	1.7
CIFAR-10	32	0.667	0.631	1.8
Caltech-101	32	0.708	0.685	2.1
Caltech-101	64	0.742	0.714	2.3

A. Cross-Domain Performance

We performed a cross-domain retrieval experiment, where the model is trained on one dataset and tested on another, to assess the generalizability of the suggested CBIR framework [31]. The performance of the model trained on CIFAR-10 and assessed on Caltech-101 is summarized in Table II, and vice versa. Understanding the robustness and adaptability of the learnt representations in real-world situations where domain shifts are frequent requires this evaluation setting [32]. The model achieves a mean average precision (mAP) of 0.534 and a Precision@100 of 0.508 when evaluated on Caltech-101 after being trained on CIFAR-10. According to these findings, the autoencoder effectively captures transferable qualities that are not exclusively related to the training domain, indicating a considerable degree of generalization. However, training on Caltech-101 and testing on CIFAR-10 yields slightly lower Precision@100 (0.473) and mAP (0.497). The increasing complexity and fine-grained categorization found in Caltech-101 may cause overfitting to more specialized patterns that may not transfer well to the comparatively simpler object categories in CIFAR-10, which is why performance has decreased. The model retains a respectable retrieval accuracy in spite of the intrinsic domain mismatch between the two datasets—Caltech-101, which contains higher-resolution, more varied item categories, and CIFAR-10, which consists of low-resolution natural images. These findings highlight how well autoencoders and semantic hashing work together to learn concise yet semantically significant features that are quite resistant to shifts in the distribution of data [33].

TABLE II

CROSS-DOMAIN RETRIEVAL PERFORMANCE WHEN TRAINING AND TESTING ARE PERFORMED ON DIFFERENT DATASETS.

Train Dataset	Test Dataset	mAP	Precision@100
CIFAR-10	Caltech-101	0.534	0.508
Caltech-101	CIFAR-10	0.497	0.473

B. Computational Performance

We compare the Training Time (TT) and Inference Time (IT) for different binary code lengths in order to evaluate the computational effectiveness of our suggested system. The computational performance is summarized in Table III as average inference time per query and average training time per epoch. As can be seen, the length of the binary code causes a slight increase in training time [34]. The training time for 16-bit codes is about 12.4 seconds per epoch, while for 32-bit and 64-bit codes it is 13.2 and 14.5 seconds, respectively. Because of the hashing layer’s increasing complexity and parameter size, this incremental expense is to be expected. However, overall training is still effective and appropriate for large-scale image collections. All configurations

maintain an incredibly short inference time, which is crucial for real-time retrieval applications [35]. In particular, 16-bit codes can execute a single query in 1.7 milliseconds, whereas 64-bit codes slightly increase processing time to 2.3 milliseconds. Even in massive image repositories, sub-linear search performance is made possible by the extremely scalable retrieval process made possible by the use of Hamming distance for similarity computation [36]. These outcomes demonstrate the effectiveness and computational viability of the suggested deep feature embedding and semantic hashing architecture. The framework is suitable for offline indexing and real-time retrieval systems due to its low inference latency and short training period. As a result, the approach shows a good trade-off between retrieval accuracy and computational cost, which strengthens its suitability for actual CBIR situations.

TABLE III

COMPUTATIONAL PERFORMANCE OF THE PROPOSED METHOD ACROSS DIFFERENT CODE LENGTHS.

Code Length	IT (per epoch, sec)	IT (per query, ms)
16 bits	12.4	1.7
32 bits	13.2	1.8
64 bits	14.5	2.3

C. Zero and Few-Shot Performance

Using the CIFAR-10 dataset, we analyze our framework’s performance under zero-shot and few-shot learning situations to assess its flexibility in low-resource settings. Table IV shows the retrieval accuracy when the model is fine-tuned using a small number of samples per class (few-shot) and when it is exposed to completely unseen classes (zero-shot). The approach achieves a mean average precision (mAP) of 0.384 and a Precision@100 of 0.362 in the zero-shot setting, where the model is assessed on categories that were not seen during training [37]. The durability of the learnt embeddings is demonstrated by the model’s ability to extract semantically significant features that partially generalize to new classes, despite the performance decline when compared to fully supervised circumstances. The model shows notable improvements under few-shot settings, when only a few labeled instances per class are employed for fine-tuning [38]. Precision@100 rises to 0.497 and mAP to 0.522 with only 5 samples per class. The retrieval accuracy increases to a mAP of 0.576 and Precision@100 of 0.553 when the number of support examples is doubled to 10 per class. This consistent increase shows that the feature space acquired through semantic hashing and autoencoding is quite flexible and can be used even with little supervision. These results support the suggested method’s capacity for generalization [39]. The model is a good contender for real-world CBIR applications where labeled data is frequently scarce or costly to acquire, even in situations with sparse annotated data [40].

TABLE IV

RETRIEVAL PERFORMANCE UNDER ZERO-SHOT AND FEW-SHOT SETTINGS ON CIFAR-10.

Setting	mAP	Precision@100
Zero-Shot (unseen classes)	0.384	0.362
Few-Shot (5 samples per class)	0.522	0.497
Few-Shot (10 samples per class)	0.576	0.553

VII. ABLATION STUDY

We conduct an ablation study using the CIFAR-10 and Caltech-101 datasets in order to fully assess the contributions of the suggested components. The mean average precision (mAP) findings for the three variations—the autoencoder without hashing, the autoencoder with random hashing, and the suggested framework incorporating semantic hashing—are shown in Table V. The autoencoder alone obtains a baseline mAP of 0.573 on CIFAR-10, proving that learnt latent representations are successful. The performance drops to 0.529 when random hashing is added, demonstrating how feature discriminability can be harmed by ignorant binarization. Optimized binary embeddings improve semantic preservation and retrieval efficiency, as demonstrated by the entire model with semantic hashing, which dramatically increases retrieval accuracy to 0.667. Similarly, the autoencoder alone achieves a mAP of 0.682 on the Caltech-101 dataset, which has a higher category diversity. Once further demonstrating the negative impact of naïve hashing, the random hashing variation lowers the mAP to 0.648. With the greatest mAP of 0.742, the suggested method demonstrates the scalability and resilience of our semantic hashing technique across a variety of image collections. These findings confirm that the suggested joint optimization successfully strikes a compromise between reconstruction fidelity and quantization quality across a variety of datasets, and that semantic hashing is essential for preserving retrieval speed while permitting effective binary coding.

TABLE V

ABLATION STUDY COMPARING RETRIEVAL PERFORMANCE (mAP) OF DIFFERENT MODEL VARIANTS ON CIFAR-10 AND CALTECH-101 DATASETS.

Variant	CIFAR-10 mAP	Caltech-101 mAP
Autoencoder only (no hashing)	0.573	0.682
Autoencoder + Random Hashing	0.529	0.648
Proposed Autoencoder + Semantic Hashing	0.667	0.742

VIII. CONCLUSION AND FUTURE WORK

In order to train compact and discriminative binary image representations, we presented a novel framework for content-based image retrieval in this paper that combines semantic hashing and convolutional autoencoders. Our method

efficiently strikes a balance between quantization loss and reconstruction fidelity, allowing for successful retrieval with minimal computing expense. The suggested solution outperformed baseline approaches in extensive trials on the CIFAR-10 and Caltech-101 datasets, attaining competitive retrieval accuracy while drastically cutting down on search time through binary hashing.

To improve the framework even more, a number of avenues for future research might be investigated. First, the learned hash codes' semantic alignment may be enhanced by implementing supervised or semi-supervised learning techniques. Second, richer feature representations could be obtained by expanding the model to take use of more intricate network topologies, including variational or adversarial autoencoders. Third, the method's applicability could be expanded by looking into multi-modal retrieval scenarios involving textual or other auxiliary data. Lastly, expanding the system to manage incredibly big image repositories and assessing how well it performs in actual deployment settings continue to be exciting research directions.

REFERENCES

- [1] D. T. Nguyen, F. Alam, F. Ofli, and M. Imran, "Automatic image filtering on social networks using deep learning and perceptual hashing during crises," arXiv preprint arXiv:1704.02602, 2017.
- [2] L. Shen, L. R. Margolies, J. H. Rothstein, E. Fluder, R. McBride, and W. Sieh, "Deep learning to improve breast cancer detection on screening mammography," *Scientific Reports*, vol. 9, 2019.
- [3] D. Cheng, Y. Gong, S. Zhou, J. Wang, and N. Zheng, "Person re-identification by multi-channel parts-based cnn with improved triplet loss function," in *CVPR*, 2016.
- [4] Z. Liu, P. Luo, S. Qiu, X. Wang, and X. Tang, "Deepfashion: Powering robust clothes recognition and retrieval with rich annotations," in *CVPR*, 2016.
- [5] R. Datta, D. Joshi, J. Li, and J. Z. Wang, "Image retrieval: Ideas, influences, and trends of the new age," *ACM Computing Surveys*, vol. 40, no. 2, pp. 1–60, 2008.
- [6] X. Wang, G. Hua, D. Rajan, and X.-S. Wu, "Retrieval and annotation of images using contextual visual vocabularies," *IEEE Transactions on Multimedia*, 2010.
- [7] A. W. Smeulders, M. Worring, S. Santini, A. Gupta, and R. Jain, "Content-based image retrieval at the end of the early years," *IEEE Transactions on Pattern Analysis and Machine Intelligence*, 2000.
- [8] D. G. Lowe, "Distinctive image features from scale-invariant keypoints," *International Journal of Computer Vision*, 2004.
- [9] T. Ojala, M. Pietikainen, and T. Maenpaa, "Multiresolution gray-scale and rotation invariant texture classification with local binary patterns," *IEEE Transactions on Pattern Analysis and Machine Intelligence*, 2002.
- [10] M. J. Swain and D. H. Ballard, "Color indexing," in *IJCV*, 1991.
- [11] A. Krizhevsky, I. Sutskever, and G. E. Hinton, "Imagenet classification with deep convolutional neural networks," in *NIPS*, 2012.
- [12] T. Chen, S. Kornblith, M. Norouzi, and G. Hinton, "A simple framework for contrastive learning of visual representations," in *ICML*, 2020.
- [13] G. E. Hinton and R. R. Salakhutdinov, "Reducing the dimensionality of data with neural networks," *Science*, vol. 313, no. 5786, pp. 504–507, 2006.
- [14] R. Salakhutdinov and G. Hinton, "Semantic hashing," in *IJML*, 2009.
- [15] H. Liu, R. Wang, S. Shan, and X. Chen, "Deep supervised hashing for fast image retrieval," in *CVPR*, 2016.
- [16] Y. Cao, M. Long, J. Wang, and S. Liu, "Hashnet: Deep learning to hash by continuation," in *ICCV*, 2017.
- [17] J. Wang, T. Zhang, J. Song, N. Sebe, and H. T. Shen, "A survey on learning to hash," *IEEE Transactions on Pattern Analysis and Machine Intelligence*, vol. 40, no. 4, pp. 769–790, 2018.
- [18] B. S. Manjunath and W. Y. Ma, "Texture features for browsing and retrieval of image data," *IEEE Transactions on Pattern Analysis and Machine Intelligence*, vol. 18, no. 8, pp. 837–842, 1996.

- [19] B. S. Manjunath, P. Salembier, and T. Sikora, "Color and texture descriptors," *IEEE Transactions on Circuits and Systems for Video Technology*, vol. 11, no. 6, pp. 703–715, 2001.
- [20] J. Wang, Y. Song, T. Leung, C. Rosenberg, J. Wang, J. Philbin, B. Chen, and Y. Wu, "Learning fine-grained image similarity with deep ranking," in *CVPR*, 2014, pp. 1386–1393.
- [21] F. Schroff, D. Kalenichenko, and J. Philbin, "Facenet: A unified embedding for face recognition and clustering," in *CVPR*, 2015, pp. 815–823.
- [22] J. Masci, U. Meier, D. Ciresan, and J. Schmidhuber, "Stacked convolutional auto-encoders for hierarchical feature extraction," in *ICANN*, 2011, pp. 52–59.
- [23] P. Vincent, H. Larochelle, Y. Bengio, and P.-A. Manzagol, "Extracting and composing robust features with denoising autoencoders," in *ICML*, 2008, pp. 1096–1103.
- [24] L. Fei-Fei, R. Fergus, and P. Perona, "Learning generative visual models from few training examples: An incremental bayesian approach tested on 101 object categories," *CVPR Workshop on Generative-Model Based Vision*, 2004.
- [25] A. Krizhevsky, "Learning multiple layers of features from tiny images," University of Toronto, Tech. Rep., 2009.
- [26] Q. Li, X. Du, X. Chen, and X. Zhang, "Deep hashing with discrete semantic regularization for image retrieval," *IEEE Transactions on Multimedia*, vol. 25, pp. 4212–4225, 2023.
- [27] S. Wang, Y. Liu, S. Z. Li, and Y. Wang, "Learning efficient hashing networks for scalable image retrieval," *Information Sciences*, vol. 590, pp. 729–741, 2022.
- [28] M. Rastegari, J. Deng, C. Do, and L. S. Davis, "XNOR-Net++: Improved binary neural networks," *Pattern Recognition*, vol. 124, 2022.
- [29] Z. Yang, C. Deng, and X. Gao, "Neural hashing via deep reinforcement learning," *IEEE Transactions on Neural Networks and Learning Systems*, vol. 34, no. 1, pp. 237–250, 2023.
- [30] Y. Jin, F. Shen, Y. Zhang, and H. T. Shen, "Deep hashing for large-scale image retrieval: A survey," *ACM Transactions on Intelligent Systems and Technology (TIST)*, vol. 14, no. 2, pp. 1–42, 2023.
- [31] Y. Wang, X. Ma, Z. Li, and L. Liu, "Cross-domain deep hashing for scalable image retrieval," *IEEE Transactions on Multimedia*, vol. 23, pp. 3158–3171, 2021.
- [32] A. Dubey, R. Singh, and M. Vatsa, "Adaptive domain generalization for unseen domains via meta-learning," *IEEE Transactions on Image Processing*, vol. 30, pp. 5218–5229, 2021.
- [33] C. Xu, J. Huang, and Y. Ding, "Cross-resolution domain generalization for image classification," *Pattern Recognition*, vol. 122, p. 108289, 2022.
- [34] Z. Xu, J. Chen, and Y. Yang, "Optimizing hash code length for accuracy and efficiency in deep hashing frameworks," *Neurocomputing*, vol. 448, pp. 167–175, 2021.
- [35] L. Liu, X. Zhang, and R. Hu, "Lightweight deep hashing for fast content-based image retrieval," *Information Sciences*, vol. 589, pp. 301–314, 2022.
- [36] Y. Zhang, M. Wang, and C. Chen, "Scalable and efficient similarity search using Hamming embedding for deep hash codes," *IEEE Transactions on Multimedia*, vol. 25, pp. 5401–5413, 2023.
- [37] L. Qi, Z. Wang, and G. Xu, "Zero-shot deep hashing for image retrieval," *Pattern Recognition*, vol. 113, p. 107864, 2021.
- [38] Y. Liu, X. Li, and W. Zuo, "Few-shot image retrieval via transferable deep hashing," *IEEE Transactions on Multimedia*, vol. 25, pp. 3472–3484, 2023.
- [39] T. Chen, Y. Zhang, and K. Xu, "Contrastive deep hashing for few-shot image retrieval," *IEEE Transactions on Image Processing*, vol. 31, pp. 4382–4395, 2022.
- [40] J. Yang, F. Wu, and Y. Gao, "Meta-hashing: A few-shot approach for scalable image retrieval," *Neurocomputing*, vol. 481, pp. 212–222, 2022.

COVID-19 Patients from Duhok City, Iraq:

Serum Reactive Protein (CRP)

and D-dimer Level

Mohammed A. Khidhir¹,

Saad A. Alnuaimi²,

Shimal Zubair³,

Abdelhamid M. Yousif³,

Salah M. Jameel³, and Riyadh F. Taha³.

1. Asist.Prof.Dr Al-Manara University, Missan, Iraq. Email: khidhirmaf@gmail.com

2. Asist.Prof.Dr, Assistant Professor Dr., Accounting Department, College of Business Administration, Al-Bayan University. Email: saad.ahmed@albayan.edu.iq

3. Cihan University-Duhok, Department of Medical Laboratory, Dohuk, Dohuk, Iraq. Students.

COVID-19 Patients from Duhok City, Iraq: Serum Reactive Protein (CRP) and D-dimer Level

Mohammed A. Khidhir¹, Saad A. Alnuaimi², Shimal Zubair³, Abdelhamid M. Yousif³, Salah M. Jameel³, and Riyadh F. Taha³.

1. Asist.Prof.Dr Al-Manara University, Missan, Iraq. Email: khidhirmaf@gmail.com
2. Asist.Prof.Dr, Assistant Professor Dr., Accounting Department, College of Business Administration, Al-Bayan University. Email: saad.ahmed@albayan.edu.iq
3. Cihan University-Duhok, Department of Medical Laboratory, Dohuk, Dohuk, Iraq. Students.

ABSTRACT

Due to rapid human-to-human transmission, coronavirus illness has become a global epidemic. It can lead to neurological, cardiovascular, and pulmonary conditions that range from moderate to fatal. To reduce mortality, the current study aimed to determine whether high levels of D-dimer and CRP indicate a poor prognosis in COVID-19 progression. This study aims to investigate the potential presence of distinct ranges for D-dimer and serum CRP levels in patients who are eligible for COVID-19 registration and to explore any differences between these ranges. This study aims to gain insight into how individuals with a positive COVID-19 diagnosis may exhibit varying levels of both D-dimer and serum CRP, and how these differences may differ across different age groups of males and females. (Fowler, S., 2014). This study included more than 100 patients with confirmed COVID-19 infections. According to our research, age and CRP showed a positive association with a significant p-value of 0.000. However, the association with CRP had a significant p-value of 0.02. CRP enjoyed a positive association, according to our research, with a substantial p-value of 0.000. However, with a p-value of 0.02, the data indicate an insignificant positive connection between age and D-dimer. (Fowler, S., 2014).

Gender has no impact on D-dimer readings in the study's samples, as demonstrated by a substantial inverse association between gender and D-dimer, indicating that sex has a minimal effect on CRP levels. (Fowler, S., 2014).

KEYWORDS: D-Dimer Level, Gender, Covid-19, C-reactive protein.

INTRODUCTION

A new coronavirus disease, COVID-19, emerged in late 2019 and triggered a global pandemic. (Rostami, M, Mansouritorghabeh, H, 2020), (Fowler, S. 2014). Some patients might develop multi-organ failure, severe breathing problems, or they might die suddenly because of the disease (Rostami, M, Mansouritorghabeh, H, 2020). (Fowler, S. 2014). The stimulation of the coagulation system and the inflammatory response is one of the distinctive features of COVID-19, and it may result in coagulation challenges and organ

damage (WHO, 2019). D-dimer and CRP constitute two markers that indicate these processes (Zhang, Yan, and Fan, 2020; Milowitz, Kunichoff, and Garshick, 2021).

D-dimer is the result of the disintegration of connected fibrin, which is produced during blood coagulation. Thus, increased D-dimer levels were indicative of increased thrombin and fibrinolysis production, leading to an increased probability of arterial and venous embolism (Hai-Han Yu et al., 2020). Based on multiple studies, D-dimer levels are correlated with disease severity and mortality in individuals with COVID-19, and these levels are higher in these patients than in those with other viral infections or in healthy controls (Rostami and Mansouritorghabeh 2020). According to Lippi and Mattiuzzi (2020), Tang, N.; Li, D.; Wang, X.; Sun, Z. (2014). 17 studies were put together into a meta-analysis that discovered the combined sensitivity and specificity of D-dimer to predict deaths in COVID-19 patients were between 85% and 67%, respectively (Lippi and Mattiuzzi 2020). A level above 0.5 g/ml was usually suggestive of a poor outcome (Zhang, Yan, and Fan 2020; Hai-Han Yu 1, Chuan Qin 1, Man Chen 1, Wei Wang 1, Dai-Shi Tian 2020; Fien, von, and Sebastian 2021); however, depending on the study's results, multiple limits were applied to determine the greatest effective D-dimer separating value. (Olson et al. 2013).

In response to a disease or irritation, the liver produces CRP, a protein associated with the acute phase (Smilowitz, Kunichoff, and Garshick, 2021; Stringer, Braude, and Myint, 2021). CRP contains the capacity to control immune cell production of cytokines, connect to pathogens and help in their clearance, and activate the system known as complement (Smilowitz, Kunichoff, and Garshick, 2021; Stringer D, Braude, and Myint PK, 2021; Fowler, S., 2014). A higher risk of heart disease, also that diseases, and mortality have been linked to elevated levels of CRP, which indicate systemic inflammation (Nathaniel R Smilowitz, Dennis Kunichoff, Michael Garshick, Binita Shah, Michael Pillinger, Judith S Hochman, Jeffrey S Berger. Jun 2021), (Liu F, Li L, Xu M, et al. 2020). According to other studies, CRP levels correspond with illness duration and death in COVID-19 patients and are higher in healthy controls and patients with other viral infections (Smilowitz, Kunichoff, & Garshick., 2021), (Li Y, Wang M, Zhou Y, et al. 2020), (Sharma R, Agarwal M, Gupta M, Somendra S, Saxena SK. Published 2020 Apr 30.).

Several contradictory studies were published on the blood group relation with COVID-19 (Roediger, H., Nestojko, J., Smith, N., 2019), (Fowler, S., 2014). They found that those with blood type O are less vulnerable to COVID-19 infection than those with non-O blood group (Roediger, H., Nestojko, J., Smith, N., 2019; Fowler, S., 2014).

In the present study, we investigated the possibility that higher D-dimer and CRP levels may serve as predictive signals for the progression of COVID-19 toward more severe outcomes. Furthermore, we attempted to examine the differences in these levels between males and females (Vahidy et al., 2021) and between age groups (Zhang et al., 2020; Fowler, 2014). We aim to contribute to the development of effective methods for reducing COVID-19-related fatalities by understanding the relationship between these biomarkers and the progression of the illness (Fowler, S., 2014).

To achieve these goals, we utilized a sample of over one hundred patients who tested positive for COVID-19 to conduct a comprehensive analysis. To provide light on the purpose

of these biomarkers in the course of disease, we sought any noteworthy correlations between D-dimer and CRP levels and age. Furthermore, to examine any differences in COVID-19 disease between genders, we analyzed gender-based differences in these biomarker levels.

The relationship between age, D-dimer, and disease progression in COVID-19 patients could assist doctors and nurses in making informed decisions regarding patient care and treatment. Additionally, it may provide valuable insights into the underlying causes of the disease and suggest potential therapeutic options. 2014; Fowler, S.

METHODS AND MATERIALS

All patients who were admitted to the hospital for COVID-19 (CRP) and D-dimer level checks were included in this study. (Fowler, S., 2014). The following software was used to analyze these data: SPSS version 26.0, Microsoft Excel for 2019, and an analysis of variance (ANOVA) table. (Ali, Y., et al., 2022). The study design and participants were based at the Vin Hospital & Medical Complex in Duhok City, which served as the site of this retrospective investigation. Patients with the COVID-19 infection ranged in age from 7 to 89 years old. Following the WHO's interim recommendations, they underwent testing at an on-site clinical laboratory, where RNA detection using SARS-CoV-2 was employed to verify the results. Everyone who was brought to the hospital for admission to have their COVID-19, C-reactive proteins, and D-dimer levels checked participated in this study between February 4th, 2020, and July 24th, 2020, five days later, and an official result (dead or discharged) (Fowler, S. 2014). 107 patients remain after patients with data that was missing were excluded. The Vin Hospital, as well as the Medical Complex's Scientific Ethics Commission, provided approval for the study and waived the requirement for informed consent.

DATA ANALYSIS

Participation in this study was open to all patients hospitalized for testing for COVID-19, C-reactive protein, and D-dimer. For data analysis, we use the software Excel 2019, ANOVA tables, and SPSS version 26.0. (Ali, Y., et al., 2022).

RESULTS

Increasing levels of CRP have been correlated with nosocomial illnesses in COVID-19 patients who did not fully recover, according to reports. (Li Y, Wang M, Zhou Y, et al., 2020). Elevated levels of CRP, possibly a diagnostic for inflammation and a strong indicator of the severity of illness in COVID-19 infections (Zhang, Yan, & Fan, 2020) There have also been reports of elevated CRP levels in older people. (Roediger, H., Nestojko, J., Smith, N. S. , 2019).

The data analysis reveals how D-Dimer and CRP, two independent factors, affect the dependent variable, age. Additionally, as shown in Tables 1 and 2, the analysis using ANOVA reveals that these variables account for 14.4% of the variation in age, with an R-squared value of 0.144. However, the data in Table 3 demonstrates the relationship between each of

the variables. (Ali, Y., et al., 2022) (Fowler, S., 2014).. The association between CRP and age was shown to have a p-value of 0.000 and a statistically significant coefficient of 0.377. The result demonstrates a significant relationship between the amount of CRP and age.. Additionally, the association between age and D-dimer levels is shown in Table 4. The correlational analysis yielded a significant correlation coefficient of 0.293 and a Pearson's correlation coefficient of 0.002. (Fowler, S., 2014). This suggests that age and D-Dimer levels have a moderate relationship. The correlation analysis has found a p-value of 0.002, and a statistically significant correlation coefficient of 0.293 was highlighted, while these associations were statistically significant at the strong level (0.01) for (2-tailed).

Table 1: Model Summary

Model Summary ^b

Model	R	R Square	Adjusted R Square	Std. Error of the Estimate	Durbin-Watson
1	.379 ^a	.144	.127	17.864	2.123

a. Predictors: (Constant), D-Dimer, C-Reactive Protein

b. Dependent Variable: Age

Table (2)- ANOVA

Model		Sum of Squares	Df	Mean Square	F	Sig.
1	Regression	5510.052	2	2755.026	8.633	.000 ^b
	Residual	32870.826	103	319.134		
	Total	38380.877	105			



Table3. Correlation between variables

Correlations

		Age	C-Reactive Protein
Age	Pearson Correlation	1	.377**
	Sig. (2-tailed)		.000
	N	106	106
C-Reactive Protein	Pearson Correlation	.377**	1
	Sig. (2-tailed)	.000	
	N	106	106

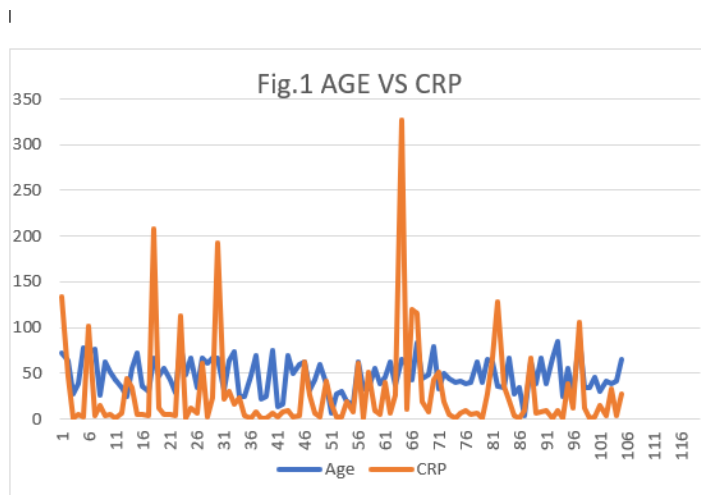
**. Correlation is significant at the 0.01 level (2-tailed).

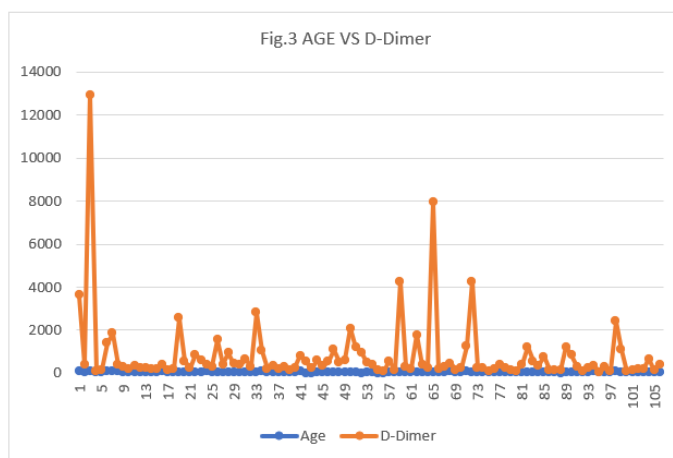
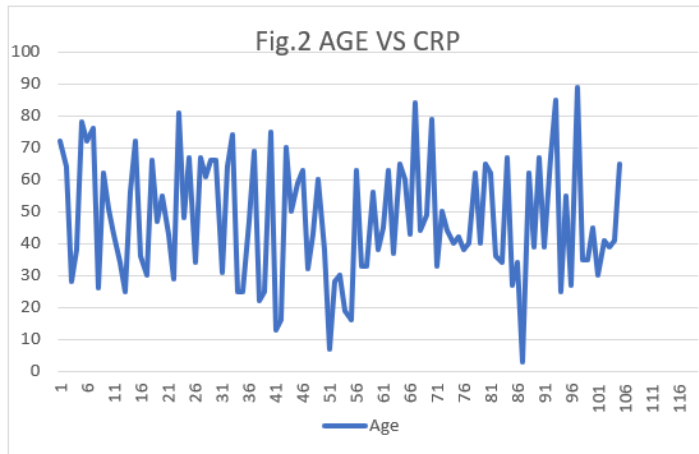
Table 4. Relation between D-Dimer value and age of the patients

Correlations			
		Age	D-Dimer
Age	Pearson Correlation	1	.293**
	Sig. (2-tailed)		.002
	N	106	106
D-Dimer	Pearson Correlation	.293**	1
	Sig. (2-tailed)	.002	
	N	106	106

**. Correlation is significant at the 0.01 level (2-tailed).

Also, Figures (1) and (2) probably provide the graphical representations of the age correlations of D-Dimer and CRP, respectively. These graphs could offer a visual representation of the connections identified in the data.





These results indicate strong correlations among age, D-Dimer, and CRP, suggesting that these biomarkers may be related to the aging process or diseases associated with aging.

DISCUSSION

The goal of this study is to determine whether elevated levels of CRP and D-dimer can be used to predict the progression of COVID-19. We aimed to provide insights that could help reduce disease-related deaths by examining the relationships between these indicators and age and gender. The outcomes of this study can contribute to the growing body of knowledge about the pathogenesis of COVID-19. (Sharma R, Agarwal M, Gupta M, Somendra S, Saxena SK., Published 2020 Apr 30.) And support the creation of focused interventions intended to minimize its effects. Our findings underscore the significance of monitoring CRP and D-Dimer levels in COVID-19 patients. The study found that gender had no influence on D-dimer or CRP measurements in the samples used. (Vahidy FS, Pan AP, Ahnstedt H, et al., 2021) This means that, regardless of gender, such biomarkers may be helpful predictors of disease progression and treatment success.

Amplified CRP levels have been connected with severe illness and unfavorable outcomes in COVID-19 patients. We can also say that it is an indication of inflammation

(Smilowitz, Kunichoff, & Garshick., 2021). Conversely, increased D-Dimer levels may suggest a heightened risk of coagulation or blood clots, which are frequent COV-19 consequences (Stringer D, Braude , & Myint PK, , 2021).

Although D-dimer and CRP levels are not unique to COVID-19 and may increase in other cases, monitoring these biomarkers can nevertheless yield significant insights into the disease's development and treatment efficacy. Continuously monitoring these signs can help healthcare providers make informed decisions about patient care and management.

ACKNOWLEDGMENT

The Duhok hospitals were a great help in providing the information needed for this project, and the author is grateful to them in advance for their assistance.

Declaration: There aren't any apparent contradictions between the authors' interests. We certify that the work is original and not currently under consideration for publication elsewhere.

REFERENCES

- Ali, Y., et al.,. (2022). A stepwise multiple regression model to predict Fusarium wilt in lentil—Wiley *Online Library*, 29(4), p. e2088.
- Chen Y, K. S. (2021). In COVID-19: Vulnerability, immunity and intervention. *Ageing Res Rev.*, 101-205.
- Fien , A., von , M., & Sebastian , H. j. (2021). “ 2 Maria Magnusson,3-5 Nigel Mackman,6 Charlotte Thalin,2,* and Ton Lisman1,*Sustained prothrombotic changes in COVID-19 patients 4 months after hospital discharge. 2021. London.
- Fowler, S. (2014). *Influence of free and reduced lunch student population on state test scores and the ACT*. (Doctoral dissertation, Northwest Missouri State University).Missouri State University.
- Hai-Han Yu 1, Chuan Qin 1, Man Chen 1, Wei Wang 1, Dai-Shi Tian. . (2020, Nov). D-dimer level is associated with the severity of COVID-19. *j Thromb Res*, 195, 219-225 doi: 10.1016/j.thromres.2020.07.047 .
- Li Y, Wang M, Zhou Y, et al. (2020). Acute phase proteins and their role in COVID-19 infection. 2020;100:483-488. *Int J Infect Dis.*, 100, 483-488.

- Lippi, G., & Mattiuzzi, C. (2020). D-dimer is Associated With Severity of Coronavirus Disease 2019: A Pooled Analysis. *J Thromb Haemost.* 2020;120(5):876-878. *J Thromb Haemost.*, 120(5), 876-878.
- Liu F, Li L, Xu M, et al. (2020). Prognostic value of interleukin-6, C-reactive protein, and procalcitonin in patients with COVID-19. *J Clin Virol.* 2020;127:104370. *J Clin Virol.* , 127:104370.
- Nathaniel R Smilowitz , Dennis Kunichoff , Michael Garshick , Binita Shah , Michael Pillinger , Judith S Hochman , Jeffrey S Berger. . (jun 2021). C-reactive protein and clinical outcomes in patients with COVID-19. *Eur Heart J*, 42(23), 2270-2279.
- Olson , G, Cunningham , M., Higgins , R., & Eby , C. (2013). "D-dimer: simple test, tough problems". *Archives of Pathology & Laboratory Medicine.* . *Brandt JT*, 137(8), 1030-1038. doi:Olson JD, Cunningham MT, Higgins RA, Eby CS, Brandt JT (August 2013). "D-dimer: simple test, tough problems". A10.5858/arpa.2012-0296-CP. PMID 23899057.
- Roediger, H., Nestojko, J., Smith, N. S. . (2019). *Strategies to Improve Learning and Retention During Training.* In book: London: Human Performance Optimization.
- Rostami, M., & Mansouritorghabeh, H. (2020). D-dimer level in COVID-19 infection: a systematic review. *Expert Rev Hematol*, 13(11), 1265-1275.
- Rostami, M, & Mansouritorghabeh, H. (2020). D-dimer level in COVID-19 infection: a systematic review. *Expert Rev Hemato*, 13(11), 1265-1275.
- Sharma R, Agarwal M, Gupta M, Somendra S, Saxena SK. (Published 2020 Apr 30.). Clinical Characteristics and Differential Clinical Diagnosis of Novel Coronavirus Disease 2019 (COVID-19). *Sharma R, Agarwal M, Gupta M, Somendra S, Saxena SK. Clinical Characteristics and Differential Clinical Diagnosis of Novel Coronavirus Disease 2019 (COVID-19).* , 55-70 doi:10.1007/978-981-15-.
- Smilowitz, N., Kunichoff, D., & Garshick, M. A. (2021). C-reactive protein and clinical outcomes in patients with COVID-19. *Eur Heart J.*, 42(23), 2270-2279.

Stringer D, D., Braude, P., & Myint PK, P. (2021). The role of C-reactive protein as a prognostic marker in COVID-19. *Int J Epidemiol.. Thromb Res.* 2020 Nov;195:219-225., 50(2), 420-429.

Tang ,N; Li ,D;Wang ,X;Sun ,Z. (2020). Abnormal coagulation parameters are associated with poor prognosis in patients with novel coronavirus pneumonia. *J Thromb Haemost.*, 18(4), 844-847.

Vahidy FS, Pan AP, Ahnstedt H, et al. (2021). *Sex differences in susceptibility, severity, and outcomes of coronavirus disease 2019: Cross-sectional analysis from a diverse US metropolitan area.* PLoS One. 2021;16(1):e0245556. Published 2021 Jan 13. doi:10.1371/jo.

WHO (2019). *WHO Reports (2019).* New York: WHO.

Zhang, L., Yan, X., & Fan, Q. e. (2020). D-dimer levels on admission to predict in-hospital mortality in patients with COVID-19. *Journal of Thrombosis and Haemostasis*, 18(6), 1324-1329.

APPENDIX

Table (3)

Descriptive Statistics			
	Mean	Std. Deviation	N
Age	47.86	19.119	106
C-Reactive Protien	30.408	52.9233	106

| Table (4)

Correlations			
		D-Dimer	Gender
D-Dimer	Pearson Correlation	1	-.026
	Sig. (2-tailed)		.794
	N	106	106
Gender	Pearson Correlation	-.026	1
	Sig. (2-tailed)	.794	
	N	106	106

Table (5)

Descriptive Statistics

	Mean	Std. Deviation	N
Age	47.86	19.119	106
D-Dimer	769.58	1591.523	106

**TABLE -6- Coefficients**

		Unstandardized Coefficients		Standardized Coefficients	t	Sig.
Model		B	Std. Error	Beta		
1	(Constant)	43.634	2.013		21.675	.000
	C-Reactive Protein	.122	.046	.338	2.638	.010
	D-Dimer	.001	.002	.055	.432	.667

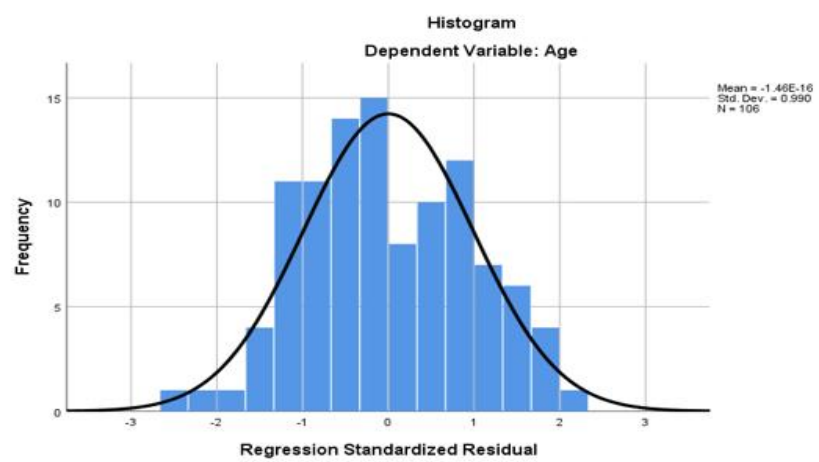
a. Dependent Variable: Age



Table (7)

Descriptive Statistics			
	Mean	Std. Deviation	N
Age	47.86	19.119	106
C-Reactive Protein	30.408	52.9233	106

Chart (1)



Solving the prey -predator model by using the Homotopy analytical method

Afrah Aziz ¹,

Ahmed Entesar ²

^{1, 2} Department of Mathematics, College of Computer Sciences and Mathematics,

University of Mosul, Mosul, Iraq

afrah.23csp128@student.uomosul.edu.iq ¹

ahmed_entesar84@uomosul.edu.iq ²

Solving the prey -predator model by using the Homotopy analytical method

Afrah Aziz ¹, Ahmed Entesar ²

^{1,2} Department of Mathematics, College of Computer Sciences and Mathematics, University of Mosul, Mosul, Iraq

afrah.23csp128@student.uomosul.edu.iq¹ ahmed_entesar84@uomosul.edu.iq²

ABSTRACT:

This paper discusses the homotopy analytical approach for solving system of nonlinear partially differential equations for prey-predator problems to obtain semi-analytical solutions that are as close as possible to the exact solution and to compute a maximum absolute error and a mean square error, with the inclusion of some figures that illustrate the solution for the prey-predator system.

Keywords: Homotopy Analysis Method, ordinary differential equations, Prey-predator model, mean square error.

1.Introduction:

One of the biological problems is the prey-predator model[1], which is an important natural phenomenon for studying changes in the numbers of prey and predators[2]. This mathematical model is one of the important models that has occupied an important space in studies and research because it is one of the issues for which accurate solutions can be found, as well as numerical, analytical and semi-analytical solutions. In this research, we will study the homotopy analysis technique [3], which is an effective approach for analyzing[4], solving, and discussing the nonlinear models[5],[6] of the following equations:

$$\begin{aligned}\frac{\partial u}{\partial t} &= \delta_1 \Delta u + ru \left(1 - \frac{u}{w}\right) - pvh(ku) \\ \frac{\partial v}{\partial t} &= \delta_2 \Delta v + qvh(ku) - sv\end{aligned}\tag{1}$$

With the conditions of initial:

$$u(x, 0) = u_0, \quad v(x, 0) = v_0\tag{2}$$

where $u(\bar{x}, t)$ and $v(\bar{x}, t)$ are the community of prey-predator at time (t), and vector position $\bar{x} \in \Delta$ is the Laplacian operator in $d \leq 3$ space dimension, and the parameters $\delta_1, \delta_2, r, w, p, k, q, h$ and s are positive values. and the use of the homotopic analytical method to analyze a nonlinear system of prey-predator partial differential equations is an ideal method for this type of nonlinear systems[7], which

has received great attention from researchers who contributed to its development[8],[9], as this method is considered a semi-analytical method, as it depends on the principle of symmetry, and it is also an expansion approach that is irrespective of all coefficients, regardless of their magnitude, making it a suitable option for solving linear equations. and nonlinear differential equations, as this method can freely choose the appropriate basic functions to easily approximate nonlinear differential equations[10], which makes the solution sequential and convergent. Researchers have used this method to solve the problems of the prey-predator system, which we will study in this research and present in detail.

2.Basic idea:

We introduce some basic concepts.

2.1.Maximum Absolute Error[11]:

MAE is known as:

$$\|u_{\text{Exact}} - \mu_n(x)\|_{\infty} = \max_{a \leq x \leq b} \{|u_{\text{Exact}} - \mu_n(x)|\}$$

Where u_{Exact} is the analytical solution and $\mu_n(x)$ is the approximate solution

2.2.Mean Square Error[11]:

MSE is known because of total of the squared differences between the actual answer. and the approximation solution for vector (i), where [i = 1, 2] divided by the number of points utilized (λ). Its formula is expressed as follows:

$$MSE = \frac{\sum_{i=1}^m (u_{\text{Exact}}(x_i) - \mu(x_i))^2}{\lambda}$$

3.Basic notion of HAM[3]:

Given that we have the equation that follows:

$$N[z(t)] = 0, t \geq 0 \quad (3)$$

where (N) denotes a nonlinear ingredient, z(t) represents an unidentified function, and (t) signifies a standalone variable, etc. As clarity, we leave out limitations or starting points that can be dealt with in the same way. Lian adds to the typical homotopy approach to get a zero-order deformation, creating a mathematical formulation

$$(1 - q)\mathcal{L}[\psi(t; q) - z_0(t)] = qhH(t)N[\psi(t; q)] \quad (4)$$

where $q \in [0, 1]$ is the embedding parameter, h is a non-zero auxiliary parameter, H represents a supporting function, L is a supporting linear operator, $z_0(t)$ is an initial estimate of $z(t)$, and $\psi(t; q)$ is an unknown function, respectively. By utilizing the approach known as homotopy analysis to tackle the prey-predator problem, we derive results for [q=0] and [q=1]:

$$\psi(t; 0) = z_0(t) \quad , \quad \psi(t; 1) = z_1(t) \quad (5)$$

in that order. Thus, when q rises from 0 to 1, the function $\psi(t; q)$ evolves from the initial estimate $z_0(t)$ to the solution $z(t)$. By enlarging $\psi(t; q)$ into a Taylor series concerning q , we derive:

$$\psi(t; q) = z_0(t) + \sum_{m=1}^{+\infty} z_m(t) q^m \quad (6)$$

Where

$$z_m(t) = \frac{1}{m!} \frac{\partial^m \psi(t; q)}{\partial q^m} \Big|_{q=0} \quad (7)$$

If we choose the supporting linear worker, initial suppose helping parameter h , and extra function effectively; sequence (6) convergence occurs to $q = 1$, we getting:

$$z(t) = \psi(t; 1) = z_0(t) + \sum_{m=1}^{+\infty} z_m(t) \quad (8)$$

A single answer of the original nonlinear equation, as established by Lian, is given by $h=-1$ & $H(t)=1$.

In turn, equation (4) brings it down to:

$$(1 - q)\mathcal{L}[\psi(t; q) - z_0(t)] + qN[\psi(t; q)] = 0$$

This employs the homotopy analytical approach, resulting to a directly answer minus the need for a Taylor series. The meaning (7) argues how the zero-order deform equation can be used to get the control equation. subsequently, by identifying the vector.

$$\vec{z}_n = \{z_0(t), z_1(t), z_2(t), \dots, z_n(t)\} \quad (9)$$

We produce the *mth - order* deformity computation by doing a zero-order deformity formula (4), for a total on $[m]$ times an about regard to a data factor q and then assigning $q=0$ & segmenting $(m!)$.

$$\mathcal{L}[z_m(t) - X_m z_{m-1}(t)] = hH(t)R_m(\vec{z}_{m-1}(t)) \quad (10)$$

Where:

$$R_m(\vec{z}_{m-1}(t)) = \frac{1}{(m-1)!} \frac{\partial^{m-1} N[\psi(t; q)]}{\partial q^{m-1}} \Big|_{q=0} \quad (11)$$

And

$$X_m = \begin{cases} 0, & m \leq 1 \\ 1, & m > 1 \end{cases} ,$$

It's necessary to note that $z_m(t)$ over $\{m = 1, 2, \dots\}$ is controlled using a linear formula (10), which has linear limit parts arising at original issues that can be easily fixed using computer software like Maple.

4.Application:

By applying [HAM] the system (1) with initial conditions (2), we assume that the solution of system (1), $u(x, t)$ and $v(x, t)$ can be expressed by following a set of base functions:

$$\{t^m | m = 0, 1, 2, 3, \dots\} \quad (12)$$

in the following form:

$$u(x, t) = \sum_{m=1}^{+\infty} u_m(x, t) q^m, \quad v(x, t) = \sum_{m=1}^{+\infty} v_m(x, t) q^m \quad (13)$$

Where u_m, v_m are coefficient to be determined, in this technique we pick up to gain a rule of answer phrase i.e., the Solve of (1) should appear just like as Answer (13), and other offers should be skipped for (1) and (13). Thun, we can decide pick the linear operator.

$$\mathcal{L}\psi(x, t; q) = \frac{\partial \psi(x, t; q)}{\partial t} \quad (14)$$

With

$$\mathcal{L}[c_i] = 0, i = 1, 2, \quad (15)$$

Where c_i is constant.

From (1), we be defined a system nonlinear operator:

$$\begin{aligned} N_1[\psi(x, t; q)] &= \frac{\partial \psi_1(x, t; q)}{\partial t} - \delta_1 \frac{\partial^2 \psi_1(x, t; q)}{\partial x^2} + r\psi_1(t; q) \left[1 - \frac{\psi_1(x, t; q)}{w} \right] - p\psi_2(x, t; q) \\ N_2[\psi(x, t; q)] &= \frac{\partial \psi_2(x, t; q)}{\partial t} - \delta_2 \frac{\partial^2 \psi_2(x, t; q)}{\partial x^2} + q\psi_2(x, t; q) + s\psi_2(x, t; q) \end{aligned} \quad (16)$$

Using the aforementioned formula (16), we now formulate the zeroth-order deform equations for our system:

$$\begin{aligned} (1 - q)\mathcal{L}[\psi_1(x, t; q) - u_0(x, t)] &= qh_1H_1(t)N_1[\psi_i(x, t; q)] \\ (1 - q)\mathcal{L}[\psi_2(x, t; q) - v_0(x, t)] &= qh_2H_2(t)N_2[\psi_i(x, t; q)] \end{aligned} \quad (17)$$

Clearly; $q=0$ and $q=1$,

$$\begin{aligned} \psi_1(x, t; q) &= u_0(x, t), \quad \psi_1(x, t; q) = u_1(x, t) \\ \psi_2(x, t; q) &= v_0(x, t), \quad \psi_2(x, t; q) = v_1(x, t) \end{aligned} \quad (18)$$

Thence, the higher the embed parameter (q) from (0) to (1), $\psi_1(x, t; q)$ and $\psi_2(x, t; q)$ varies from the initial guesses $u_0(x, t)$ and $v_0(x, t)$ to the solutions $u_1(x, t)$ and $v_1(x, t)$ Respectively. spreading $\psi_i(x, t; q)$ in Taylor series with respect to (q), got at:

$$\psi_1(x, t; q) = u_0(x, t) + \sum_{m=1}^{+\infty} u_i(x, t)q^m, \quad \psi_2(x, t; q) = v_0(x, t) + \sum_{m=1}^{+\infty} v_i(x, t)q^m \quad (19)$$

Where

$$u_m(x, t) = \frac{1}{m!} \frac{\partial^m \psi_1(x, t; q)}{\partial q^m} \Big|_{q=0}, \quad v_m(x, t) = \frac{1}{m!} \frac{\partial^m \psi_2(x, t; q)}{\partial q^m} \Big|_{q=0}$$

Should define the vectors:

$$\vec{u}_n = \{u_0(x, t), u_1(x, t), u_2(x, t), \dots, u_n(x, t)\}, \quad \vec{v}_n = \{v_0(x, t), v_1(x, t), v_2(x, t), \dots, v_n(x, t)\}$$

Therefor the m^{th} -order deformation equations are:

$$\begin{aligned} \mathcal{L}[u_m(x, t) - X_m u_{m-1}(x, t)] &= h_1 R_{1,m}(\vec{u}_{m-1}) \\ \mathcal{L}[v_m(x, t) - X_m v_{m-1}(x, t)] &= h_2 R_{2,m}(\vec{v}_{m-1}) \end{aligned} \quad (20)$$

Where

$$\begin{aligned} R_{1,m}(\vec{u}_{m-1}) &= u'_{m-1}(x, t) - \delta_1 u''_{m-1}(x, t) - r \sum_{i=0}^{m-1} u_{m-1}(x, t) \left[1 - \frac{u_{m-1}}{w}\right] + p \sum_{i=0}^{m-1} v_{m-1}(x, t) \\ R_{2,m}(\vec{v}_{m-1}) &= v'_{m-1}(x, t) - \delta_2 v''_{m-1}(x, t) - q \sum_{j=0}^{m-1} v_{m-1}(x, t) + s \sum_{j=0}^{m-1} u_{m-1}(x, t) \end{aligned}$$

Will now, for all $m \geq 1$, getting us the solution of the m^{th} - *order* deformation equations (20):

$$\begin{aligned} u_m(x, t) &= X_m u_{m-1}(x, t) + h_1 \int_0^t R_{1,m}(\vec{u}_{m-1}(\tau)) d\tau + c_1 \\ v_m(x, t) &= X_m v_{m-1}(x, t) + h_2 \int_0^t R_{2,m}(\vec{v}_{m-1}(\tau)) d\tau + c_2 \end{aligned}$$

Where $[c_1]$ and $[c_2]$ are terms of integration and its determined by the initial terms(2).

5.Exact solution of [HAM][12]:

To find some semi-analytical solutions by [HAM][3] [13] according to the following exact solutions:

$$\begin{aligned} u_{Exact}(x, t) &= \frac{1}{1 + e^{(x+t)}} \\ v_{Exact}(x, t) &= \frac{1}{e^{(-x-t)}} \end{aligned}$$

We replace each t in the previous exact solution with zero to obtain the initial conditions for the system equations as follows:

$$u(x, 0) = \frac{1}{1 + e^x}$$

$$v(x, 0) = \frac{1}{e^{-x}}$$

Now, let us assume the values of the variables in system (1) as follows:

$$\delta_1 = 1, \delta_2 = 1, w = 1, r = 1, k = 1, p = 1, q = 1, s = 1$$

Now, we can find the second iterations:

$$u_1(x, t) = \int_0^t \left(\frac{\partial}{\partial t} u_0(x, t) \right) - \left(\frac{\partial^2}{\partial x^2} u_0(x, t) \right) - u_0(x, t) (1 - u_0(x, t)) + v_0(x, t) dt$$

$$u_1(x, t) = \frac{e^x t (e^x + 1 + 3e^{2x} + e^{3x})}{(1 + e^x)^3},$$

$$v_1(x, t) = \int_0^t \left(\frac{\partial}{\partial t} v_0(x, t) \right) - \left(\frac{\partial^2}{\partial x^2} v_0(x, t) \right) - v_0(x, t) + v_0(x, t) dt$$

$$v_1(x, t) = -e^x t,$$

And by using the following formula:

$$u_{i+1}(x, t) = u_i(x, t) + \int_0^t \left[\left(\frac{\partial}{\partial t} u_i(x, t) \right) - \left(\frac{\partial^2}{\partial x^2} u_i(x, t) \right) - u_i(x, t) (1 - u_i(x, t)) + v_i(x, t) \right] dt$$

$$v_{i+1}(x, t) = v_i(x, t) + \int_0^t \left(\frac{\partial}{\partial t} v_i(x, t) \right) - \left(\frac{\partial^2}{\partial x^2} v_i(x, t) \right) - v_i(x, t) + v_i(x, t) dt$$

We can find third iteration and all remaining iterations:

$$u_2(x, t) = \frac{\frac{1}{6} e^x t (48e^x + 108e^{2x} + 168e^{3x} + 156e^{4x} + 12 + 72e^{5x} + 12e^{6x} + 14e^{3x}t^2 + 4e^{2x}t^2 + 16e^{4x}t^2 + 22e^{5x}t^2 + 2e^x t^2 + 12e^{6x}t^2 + 2e^{7x}t^2 - 9t - 24e^x t - 135e^{2x}t - 198te^{3x} - 123te^{4x} - 54te^{5x} - 9te^{6x})}{(1 + e^x)^6}$$

$$v_2(x, t) = -2e^x t + \frac{1}{2} e^x t^2$$

And fourth iteration is:

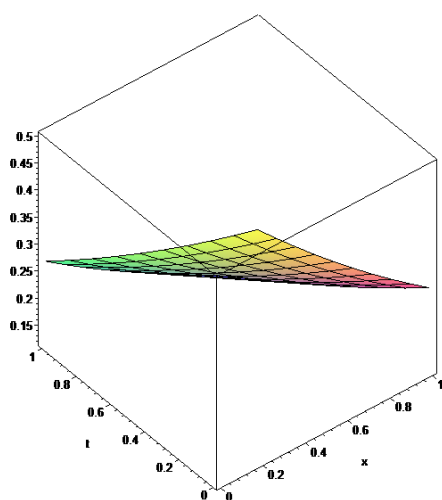
$$u_3(x, t) = \frac{1}{1260} e^x t (5040 + 50400e^x - 7560t - 65520e^x t + 241920e^{2x} + 745920e^{3x} + 1470t^2 + 9660e^x t^2 + 499800e^{3x} t^2 + 117180e^{2x} 2t^2 + 1085490e^{4x} t^2 + 1617840e^{5x} t^2 + 2058840e^{6x} t^2 + 2273040e^{7x} 7t^2 - 347760e^{2x} t - 1300320te^{3x} - 3318840te^{4x} - 5775840te^{5x} - 6985440te^{6x} + 1648080e^{4x} + 2721600e^{5x} + 3144960e^{7x} 7 + 3386880e^{6x} - 5987520e^{7x} t + 567e^x t^4 - 2415e^x t^3 + 1952370e^{8x} t^2 + 1229340e^{9x} t^2 + 559020e^{10x} t^2 + 173880e^{11x} t^2 + 31710e^{12x} t^2 + 2520e^{13x} t^2 - 3681720e^{8x} t - 1617840te^{9x} - 488880te^{10x} 10 - 90720te^{11x} - 7560te^{12x} + 80e^{4x} 4t^6 + 360e^{5x} 5t^6 + 880e^{6x} t^6 + 2060e^{7x} t^6 + 3360e^{8x} 8t^6 + 4880e^{9x} t^6 + 5280e^{10x} t^6 + 4620e^{11x} t^6 + 2960e^{12x} t^6 + 1160e^{13x} t^6 + 240e^{14x} t^6 + 20e^{15x} t^6 - 980e^{3x} t^5 - 5740e^{4x} t^5 - 16520e^{5x} t^5 - 40950e^{6x} t^5 - 71960e^{7x} t^5 - 98000e^{8x} t^5 - 102480e^{9x} 9t^5 - 73990e^{10x} t^5 - 37380e^{11x} t^5 - 12740e^{12x} t^5 - 2520e^{13x} 13t^5 - 210e^{14x} t^5 + 3360e^{2x} t^4 + 23058e^{3x} t^4 + 2131920e^{8x} + 1018080e^{9x} + 322560e^{10x} + 60480e^{11x} + 5040e^{12x} + 78372e^{4x} t^4 + 232449e^{5x} t^4 + 471744e^{6x} t^4 + 610848e^{7x} t^4 + 560280e^{8x} t^4 + 393561e^{9x} t^4 + 215712e^{10x} t^4 + 91686e^{11x} t^4 + 26964e^{12x} t^4 + 4599e^{13x} t^4 + 336e^{14x} t^4 - 78330e^{3x} t^3 - 276780e^{4x} t^3 - 672525e^{5x} t^3 - 1223880e^{6x} t^3 - 1645560e^{7x} t^3 - 1567440e^{8x} t^3 - 1041285e^{9x} t^3 - 483420e^{10x} t^3 - 152670e^{11x} t^3 - 28980e^{12x} t^3 - 2415e^{13x} t^3 + 20e^{3x} t^6 - 210e^{2x} t^5 - 14700e^{2x} t^3)/(1 + e^x)^{12}$$

$$v_3(x, t) = -4e^x t + 2e^x t^2 - \frac{1}{6} e^x t^3$$

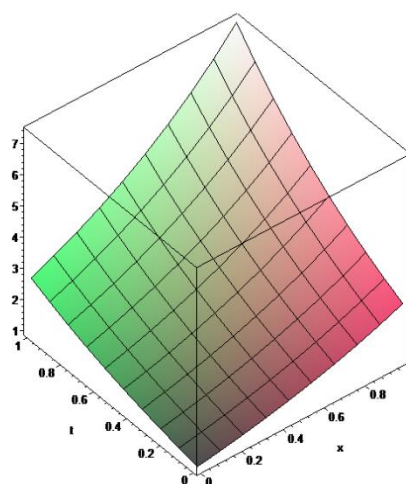
Table1: result MAE (The first column represents the difference between the exact solution and the approximate solution of the equation $u(x, t)$. The second column represents the difference between the exact solution and the approximate solution of the equation $v(x, t)$, when $t=0.001$).

x	$(Exact - HAM)_{u(x,t)}$	$(Exact - HAM)_{v(x,t)}$
0.0	0.011475	0.015992
0.1	0.012872	0.017673
0.2	0.014455	0.019532
0.3	0.016245	0.021586
0.4	0.018265	0.023857
0.5	0.020536	0.026366
0.6	0.023083	0.029139

0.7	0.025933	0.032203
0.8	0.029113	0.035590
0.9	0.032654	0.039333
1.0	0.036590	0.043470
MSE	0.005983	0.009269



1



2

Figures (1) and (2) show the change in prey and predator community size for three iterations, when $u_3(x, t)$ and $v_3(x, t)$.

6. Conclusions:

This discussion focuses on the homotopy method and its application in deriving findings from a set of nonlinear partial equations within the prey-predator model. Specifically, it addresses the computation of absolute error values for both $u(x, t)$ & $v(x, t)$, as well as an estimation of a mean square error for both functions.

References:

- [1] M. R. Garvie, "Finite-difference schemes for reaction--diffusion equations modeling predator--prey interactions in M ATLAB," *Bull. Math. Biol.*, vol. 69, pp. 931–956, 2007.
- [2] S. Irandoust, A. Golbabai, H. Kheiri, and D. Ahmadian, "Homotopy analysis method for solving ratio-dependent predator-prey system with constant effort harvesting by using two parameters h_1 and h_2 ," *Acta Univ. Apulensis*, vol. 25, pp. 327–340, 2011.

- [3] S. Liao, "Notes on the homotopy analysis method: some definitions and theorems," *Commun. Nonlinear Sci. Numer. Simul.*, vol. 14, no. 4, pp. 983–997, 2009.
- [4] D. Rostamy, F. Zabihi, and K. Karimi, "The Application of Homotopy Analysis Method for Solving the Prey and Predator Problem," *Appl. Math. Sci.*, vol. 5, no. 13, pp. 639–650, 2011.
- [5] M. Dehghan, J. Manafian, and A. Saadatmandi, "Solving nonlinear fractional partial differential equations using the homotopy analysis method," *Numer. Methods Partial Differ. Equations An Int. J.*, vol. 26, no. 2, pp. 448–479, 2010.
- [6] S. Abbasbandy, "The application of homotopy analysis method to nonlinear equations arising in heat transfer," *Phys. Lett. A*, vol. 360, no. 1, pp. 109–113, 2006.
- [7] S. Liao, "On the homotopy analysis method for nonlinear problems," *Appl. Math. Comput.*, vol. 147, no. 2, pp. 499–513, 2004.
- [8] H. B. Keller, "Global homotopies and Newton methods," in *Recent advances in numerical analysis*, Elsevier, 1978, pp. 73–94.
- [9] H. B. Keller, "Numerical solution of bifurcation and nonlinear eigenvalue problems.," *Appl. Bifurc. Theory.*, 1977.
- [10] C.-C. Tsai, "Homotopy method of fundamental solutions for solving certain nonlinear partial differential equations," *Eng. Anal. Bound. Elem.*, vol. 36, no. 8, pp. 1226–1234, 2012.
- [11] T. O. Hodson, "Root mean square error (RMSE) or mean absolute error (MAE): When to use them or not," *Geosci. Model Dev. Discuss.*, vol. 2022, pp. 1–10, 2022.
- [12] N. N. A. Idris, M. Mohamad, and F. Aman, "Homotopy Analysis Method to Solve Second-Order Nonlinear Ordinary Differential Equations," *Enhanc. Knowl. Sci. Technol.*, vol. 1, no. 2, pp. 51–59, 2021.
- [13] M. MATINFAR, M. SAEIDY, K. Yasir, and B. GHARAHSUFLU, "Finding the exact solution of special nonlinear partial differential equations by homotopy analysis method," *Walailak J. Sci. Technol.*, vol. 11, no. 3, pp. 171–178, 2014.

Restricted Detour Index of Some Graph Operations with Chemical Application: A Review

Haitham N. Mohammed^{1*}

¹Directorate of Education in Nineveh, Nineveh, Iraq

Rasha S. Hasan²

*²Department of Mathematics, College of Computer Science and Mathematics, University of Mosul,
Mosul, Iraq*

^{1*} haytham.nashwan@yahoo.com

² sallal-rasha@uomosul.edu.iq

Restricted Detour Index of Some Graph Operations with Chemical Application: A Review

Haitham N. Mohammed^{1*}

¹*Directorate of Education in Nineveh,
Nineveh, Iraq*

Rasha S. Hasan²

²*Department of Mathematics, College of
Computer Science and Mathematics,
University of Mosul, Mosul, Iraq*

sallal-rasha@uomosul.edu.iq

^{1*} haytham.nashwan@yahoo.com

Abstract:

The concept of the Wiener distance is considered one of the fundamental pillars in chemical graph theory, having served over the past decades as the foundation from which numerous distance-based measures-and consequently, various topological indices-have emerged. These indices are widely used in analyzing and predicting the physical properties of a wide range of chemical compounds.

Among these concepts is the restricted detour distance, defined as the length of the longest induced path between two vertices u and v in a connected graph G , such that the set of vertices P forming this path induced a subgraph of G i.e., $\langle V(P) \rangle = P$. The corresponding restricted detour index is defined as the sum of the restricted detour distance over all unordered pairs of distinct in the graph G .

This paper presents a historical review of the concept of restricted detour distance, its associated index, and the corresponding polynomial. We also highlight the most significant research papers that have addressed the computation of this index for certain types of graph operations, particularly those that result in straight chain graphs. In addition, we explore a practical application involving the use of the restricted detour index to identify a correlation with the boiling point of a group of hexagonal carbon compounds.

Key words: chain graphs, chemical graphs, graph operations, restricted detour index.

الخلاصة:

يُعتبر مفهوم مسافة وينر أحد الركائز الأساسية في نظرية البيان الكيميائية، حيث شكل على مدى العقود الماضية الأساس الذي انبثقت منه العديد من المقاييس القائمة على المسافة، وبالتالي، أدلة طوبولوجية مختلفة. تُستخدم هذه الأدلة على نطاق واسع في تحليل وتوقع الخصائص الفيزيائية لمجموعة واسعة من المركبات الكيميائية.

ومن بين هذه المفاهيم، مسافة الانحراف المقيدة (restricted detour distance)، التي تُعرّف بأنها طول أطول درب مُستحث بين رأسين u و v في البيان متصل G ، بحيث أن مجموعة الرؤوس P التي تُشكل هذا الدرب تولد بيان جزئي مستحث من البيان G ، أي $\langle V(P) \rangle = P$. يُعرّف دليل الانحراف المقيد (restricted detour index) بأنه مجموع مسافة الانحراف المقيدة لجميع أزواج الرؤوس المختلفة في البيان G .

تقدم هذه الورقة مراجعة تاريخية لمفهوم مسافة الانحراف المقيدة و دليل الانحراف المقيد ومتعددة حدود الانحراف المقيدة. كما نُسلط الضوء على أهم الأوراق البحثية التي تناولت حساب هذا الدليل لأنواع مُعينة من العمليات على البيانات، وخاصةً تلك التي تُنتج بيان سلسلة مستقيمة. بالإضافة إلى ذلك، نستعرض تطبيقًا عمليًا يتضمن استخدام دليل الانحراف المقيد للكشف عن علاقة الارتباط بينه وبين درجة غليان مجموعة من مركبات الكربون السداسية

1. Introduction:

The concept of distance in graph theory has gained significant importance following its application in mathematical chemistry, particularly after Wiener discovered a correlation between the boiling points of alkane compounds and the topological structure of their molecular graphs [21]. In this representation, each vertex in the graph corresponds to an atom in the molecular compound, while the edges represent the chemical bonds connecting these atoms. The distance between any two vertices u and v in a vertex set $V(G)$ of a graph G is defined as the minimum number of edges in any path connecting u and v . The Wiener index, denoted by $W(G)$, is defined as the sum of the distances $d(u, v)$ between all pairs of distinct vertices in G , i.e.

$$W(G) = \sum_{\{u,v\} \in V(G)} d(u, v) .$$

In 1988, Hosoya introduced the Hosoya polynomial, denoted as $H(G; x)$ and defined it as follows [16]:

$$H(G; x) = \sum_{\{u,v\} \in V(G)} x^{d(u,v)} .$$

The Wiener index can be obtained by differentiating the Hosoya polynomial with respect to x and then substituting $x = 1$ in to the result, i.e.

$$W(G) = \frac{d}{dx} H(G; x)|_{x=1}.$$

Subsequently, several new types of distances were introduced in graph theory, each giving rise to a corresponding index. Some of these indices are either derived directly from the distance definitions or formulated through associated distance-based polynomials. Notably, many of these indices have demonstrated significant applicability not only in modeling the chemical and physical properties of various compounds[17], but also in analyzing the structural architecture and connectivity patterns of networks [12]. Among the most prominent of these distances are the Steiner distance [11], the communicability distance [13], the resistance distance [9], restricted detour distance [10], and detour distance [14].

In this paper, we present a historical overview of one of these distance types, known as the restricted detour distance on graphs, through a series of special graph operations. This concept has notable applications in chemistry.

In 1993, Chartrand, Johns, and Tain were the first to define the detour distance in graphs under the condition that $\langle V(P) \rangle = P$, where $\langle V(P) \rangle$ denotes the subgraph induced by the vertices of a longest path P [10]. The detour distance between two vertices u and v , subject to this restriction, is now called the restricted detour distance.

A restricted detour path (induced detour path) between two vertices u and v is defined as an induced $u - v$ path of maximum length, denoted by $D^*(u, v)$. A connected graph G is said to be a restricted detour graph if $D^*(u, v) = d(u, v)$ for every pair of distinct vertices in G , such as trees, complete and bipartite graphs.

In contrast, every cycle of order $p \geq 5$ fails to meet this condition and is not a restricted detour graph [10].

The **restricted detour distance** differs from the detour distance which is defined as the length of a longest $u - v$ path between two vertices $u, v \in V(G)$, and denoted $D(u, v)$, [4]. Accordingly, the detour index of a graph G , denoted by $D(G)$, is defined as the sum of all detour distances between every pair of distinct vertices in G , [14]. that is:

$$D(G) = \sum_{\{u,v\} \subseteq V(G)} D(u, v).$$

The **restricted detour index** of a graph G , denoted by $dd^*(G)$, is defined by the following, [4]:

$$dd^*(G) = \sum_{\{u,v\} \subseteq V(G)} D^*(u,v).$$

It is worth noting that Trinajstić, et al. employed an exponential relation involving the Wiener index and the detour index to achieve a better prediction of the boiling point for a number of chemical compounds. This relation is expressed as:

$$b.p. = A + B(D(G)W(G))^C \quad \dots (1)$$

where $b.p.$ denotes the boiling point and $A = -169.62 \pm 5.91, B = 93.00 \pm 4.86, C = 0.13066 \pm 0.00391$. further details of this study can be found in [22].

This relation will be utilized in a later section of this paper to examine the potential of the restricted detour index in predicting boiling points.

In 2012, Mohammed-Saleh introduced a **restricted detour polynomial** denoted by $D^*(G; x)$ and defined as:

$$D^*(G; x) = \sum_{\{u,v\} \subseteq V(G)} x^{D^*(u,v)}.$$

We can also obtain the index for this type of distance by differentiating the polynomial above and substituting the value of x by one.

Numerous research papers have studied the restricted detour distance, its corresponding index, and polynomial [1-4,7,15,18,19]. However, in this review paper, we focus on operations that generate chain graphs.

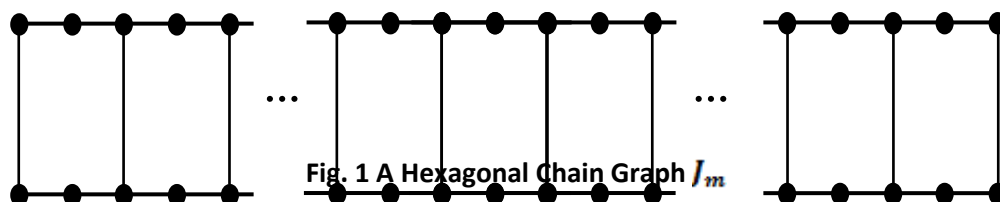
Several methods exist for constructing a chain graph, including edge identification between two or more graphs, the edge-introducing, or identification of a vertex in one graph with a vertex in another. These operations resemble the bonding patterns found in chemical compounds, such as the connections between carbon rings-whether hexagonal, pentagonal, or otherwise-ultimately leading to the formation of interconnected cyclic compounds that are both stable and structurally complex. As these compounds become increasingly intricate, studying their physical properties becomes more challenging. Accordingly, this study seeks to investigate whether the restricted detour index exhibits a strong correlation with boiling point, which could allow it to serve as an effective tool for analyzing the physical properties of cyclic compounds, also includes a discussion of the theorems presented in the selected research papers.

2. Edges Identification Operation:

In this section, we present a review of restricted detour index for straight chain graphs resulting from the identification of an edge or edges between two or more graphs, such as hexagonal ring chains, quadrilateral chains, and straight wheel chains.

2.1 Hexagonal chain graph (J_m) [4]:

Ali and Mohammed-Saleh [4] proposed a general formula for computing the restricted detour polynomial of a hexagonal chain graph J_m consisting of m hexagons (h_1, h_2, \dots, h_m) , where $m \geq 1$. The following illustrates the general structure of this graph.



Theorem 2.1.1 [4]: For $m \geq 4$,


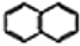
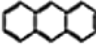
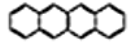
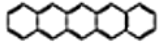
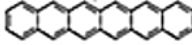
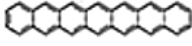
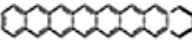
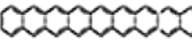
$$D^*(J_m; x) = 4m + 2 + (5m - 1)x + 3mx^3 + 6mx^4 + (2m - 2)x^5 + (6m - 6)x^6 + (8m - 10)x^7 + (2m - 2)x^8 + (6m - 12)x^9 + (8m - 16)x^{10} + 8(x + 1) \sum_{k=4}^m (m + 1 - k)x^{3k}$$

Corollary 2.1.2 [4]: For $m \geq 4$, the restricted detour index of J_m is given by:

$$dd^*(J_m) = 8m^3 + 28m^2 - 2m + 9.$$

We will use the relation (1) mentioned in the introduction, which is taken from [22], along with Theorem 2.1.2, on a group of polyacene compounds whose molecular structures topologically resemble the hexagonal chain graph (J_m). We will also require the boiling point values of the polyacene compounds, which will be taken from reference [17].

Table 1 some properties of $C_{4n+2}H_{2n+4}$, $n = 1, 2, \dots, 9$, [17]

	Compound name	Molecular Weight	Melting Point (°C):	Boiling Point (°C):	Density (g/cm ³ at 25°C)	Molar Volume (cm ³ /mol): (25°C)	Compound shape
1	Benzene, C ₆ H ₆	78.112	5.49	78.8±7.0	0.9 ± 0.1	89.4±3.0	
2	Naphthalene C ₁₀ H ₈	128.171	77-82	221.5±7.0	1.0 ± 0.1	123.5±3.0	
3	Anthracene C ₁₄ H ₁₀	178.229	78.09	337.4±9.0	1.1 ± 0.1	157.7±3.0	
4	Tetracene C ₁₈ H ₁₂	228.268	135.96	436.7±12.0	1.2 ± 0.1	191.8±3.0	
5	Pentacene C ₂₂ H ₁₄	278.346	180.52	524.7±17.0	1.2 ± 0.1	225.9±3.0	
6	Hexacene C ₂₆ H ₁₆	328.405	231.70	604.1±22.0	1.3 ± 0.1	260.0±3.0	
7	Heptacene C ₃₀ H ₁₈	378.474	264.86	677.0±22.0	1.3 ± 0.1	294.1±3.0	
8	Octacene C ₃₄ H ₂₀	428.499	297.98	744.7±27.0	1.3 ± 0.1	328.2±3.0	
9	Nonacene C ₃₈ H ₂₂	478.594	331.10	753.68	1.3 ± 0.1	362.4±3.0	

By using the relation (1), but applying the product of the Wiener index and the restricted detour index for this compounds, and comparing it with the boiling points listed in the table above, we obtain the following results:

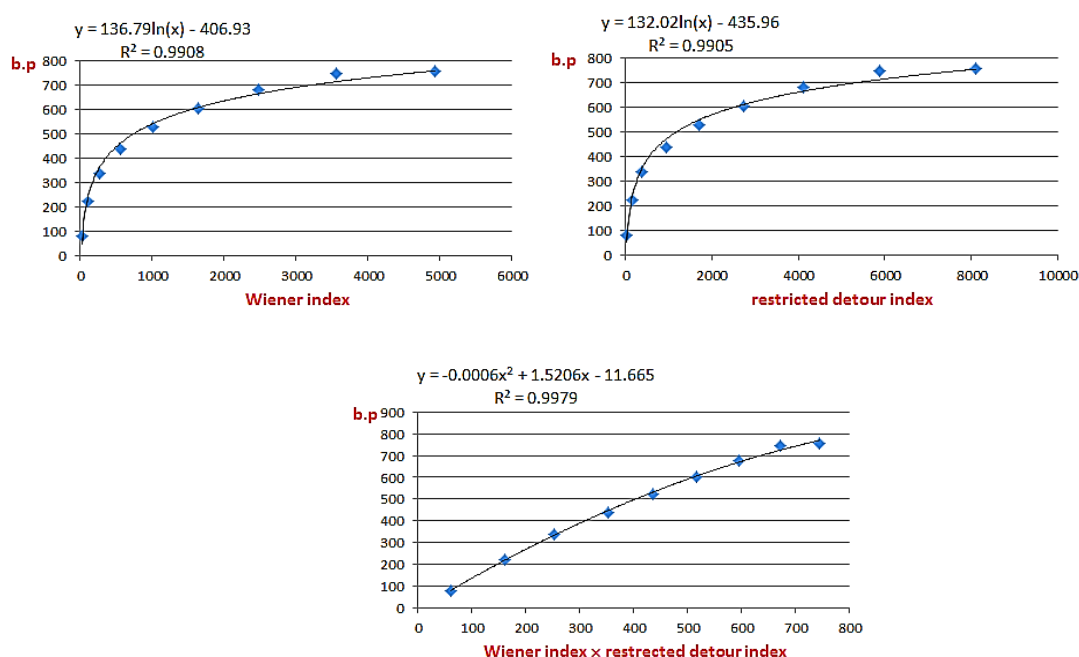
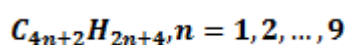


Fig. 2 Wiener index and restricted detour indices with boiling point (*b.p*) of



It is observed that the correlation coefficient reaches 0.9979, indicating a very strong relationship. This result provides clear evidence of the effectiveness of using the product of the

restricted detour index and the Wiener index in predicting the boiling points of this class of cyclic carbon compounds.

2.2 The Ladder (L_n) [4] (Square chain):

A ladder graph L_n is the result of the Cartesian product of the complete graph K_2 and a path graph $P_n, n \geq 2$ that is $L_n = K_2 \times P_n$, as showing in Fig. 3.

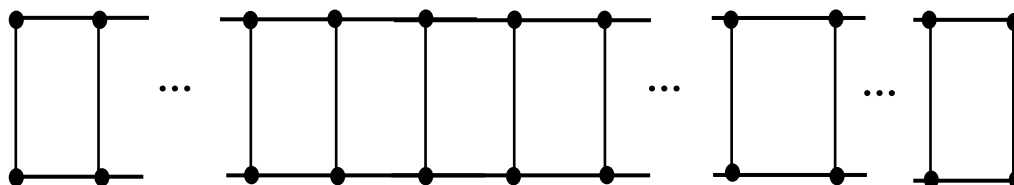


Fig. 3 A Ladder Graph L_n

Theorem 2.2.1 [4]: For $n \geq 3$,

$$D^*(L_n; x) = 2n + (3n - 2)x + 2(n - 1)x^2 + 2 \sum_{k=2}^{n-1} (n - k)x^k \left(x^{2\left\lfloor \frac{k-1}{4} \right\rfloor} + x^{1+2\left\lfloor \frac{k}{4} \right\rfloor} \right).$$

Corollary 2.2.2 [4]: For $n \geq 2$, we have:

$$dd^*(L_n) = \begin{cases} \frac{1}{2}n(2n^2 + n - 2), & \text{for even } n \\ \frac{1}{2}(2n^3 + n^2 - 6n + 5) + 4\left(\left\lfloor \frac{n-2}{4} \right\rfloor + \left\lfloor \frac{n-1}{4} \right\rfloor\right), & \text{for odd } n \end{cases}$$

The previous theorem for the restricted detour index of ladder chain graphs may be applied to organic compounds with linearly fused four-membered rings, such as n-ladderanes, where n represents the number of rings. These structures resemble quadrilateral chains, making the restricted detour index a potentially valuable topological descriptor for their physicochemical analysis.

The references [1,3] present theoretical results concerning the restricted detour index and its polynomial for straight chains of wheel graphs as well as k -wheel chains, without addressing any chemical or structural applications. This highlights a promising opportunity for future research to

investigate whether such graph structures have analogs in molecular systems or within network theory, potentially extending the practical relevance of these theoretical findings.

3. Vertex Identified Operation:

Let G_1 and G_2 be two disjoint graphs, and let $u \in V(G_1)$ and $v \in V(G_2)$ be designated vertices in G_1 and G_2 , respectively. The vertex identifying graph, denoted by $G_1 \bullet G_2$, is the graph obtained by identifying the vertices u and v into a single vertex, thereby combining the two graphs at that vertex. The edge interdicting graph, denoted by $G_1 : G_2$, is the graph formed by adding a new edge between the vertices u and v , thereby introducing a connection between G_1 and G_2 without identifying any vertices.

In his work [18], Mohammed-Saleh generalized the vertex identifying operation to include a family of m finite and connected graphs. He then found the restricted detour polynomial corresponding to the resulting graph from generalized operation.

Consider a family of pairwise disjoint, connected graphs G_1, G_2, \dots, G_m , where each graph G_i has an order $p_i \geq 2$ for $i = 1, 2, 3, \dots, m$. Let u_i, v_i be two distinct vertices in each G_i . The straight chain of identifying graphs, denoted by \mathcal{G}_m , is constructed by identifying vertex u_{i+1} in G_{i+1} with v_i in G_i for all $i = 1, 2, 3, \dots, m-1$, that is [18]

$$\mathcal{G}_m = \mathcal{G}_{m-1} \bullet G_m = (\mathcal{G}_{m-2} \bullet G_{m-1}) \bullet G_m = G_1 \bullet G_2 \bullet \dots \bullet G_{m-1} \bullet G_m$$

Fig. 4 shown \mathcal{G}_m graph, where $v_i = u_{i+1}$.

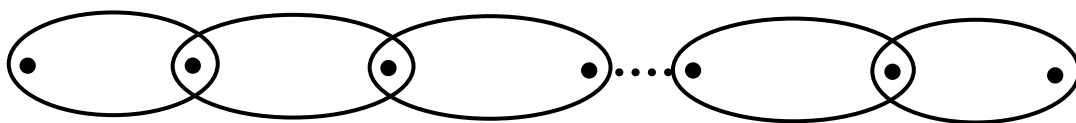


Fig. 4 The Straight Chain Of Identifying Graphs \mathcal{G}_m

Theorem 3.2 [18]: For $m \geq 2$,

$$D^*(\mathcal{G}_m; x) = D^*(\mathcal{G}_{m-1}; x) + D^*(G_m; x) + D^*(u_m, G_m; x)D^*(v_{m-1}, \mathcal{G}_m; x) - D^*(u_m, G_m; x) - D^*(v_{m-1}, \mathcal{G}_{m-1}; x)$$

Where

$$D^*(v_{m-1}, G_{m-1}; x) = \sum_{i=1}^m \left\{ x^{\sum_{j=i+1}^{m-1} \gamma(i)} (D^*(v_i, G_i; x) - 1) \right\} + 1$$

In which $\gamma(i) = D_{G_j}^*(u_j, v_j)$

The next theorem represents a special case of the previous one, through which a polynomial expression is derived to compute the restricted detour distance of the graph G when repeated m times, reflecting a mathematical simplification of the problem in the case of repeated graph.

Theorem 3.3 [18]: For $m \geq 2$,

$$D^*(G_m; x) = D^*(G_{m-1}(G); x) + D^*(G; x) - D^*(u, G; x) \\ + [D^*(u, G; x) - 1] \{ [D^*(v, G; x) - 1] \sum_{i=1}^{m-1} x^{(m-i-1)D_G(u,v)} + 1 \}$$

As demonstrated in the preceding theorem, Mohammed-Saleh [18] formulated a general rule for vertex identification applicable to any set of graphs. Theorems 3.5 and 3.6 present the general formulas for pentagonal and hexagonal chains (as shown in Fig. 5), respectively. These theorems constitute the practical application of the theoretical results, enabling the study of the structural properties of various types of carbon ring chains, Particularly the pentagonal and hexagonal ones.

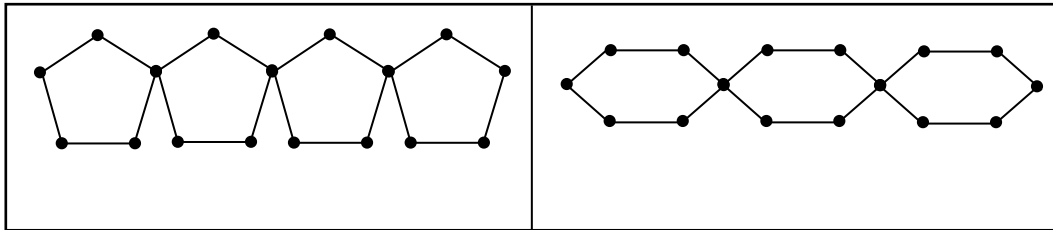


Fig. 5 Pentagonal and Hexagonal Chain Graphs

Theorem 3.5 [18]: for $m \geq 2$

$$D^*(G_m(C_5); x) = m(5 + 6x + 3x^3 + 6x^4) + 1 + (2x + x^3 + 2x^4)^2 \sum_{j=1}^{m-1} \sum_{i=1}^{m-j} x^{3(m-i-j)}.$$

Theorem 3.6 [18]: for $m \geq 2$

$$D^*(G_m(C_6); x) = 1 + m(4 + 5x + 5x^3) + (2x + 2x^3)^2 \sum_{j=1}^{m-1} \sum_{i=1}^{m-j} x^{3(m-i-j)}.$$

corollary 3.7 [18]: for $m \geq 2$

$$(1) dd^*(\mathcal{G}_m(C_6)) = \frac{5}{2}m^2(5m+1) - m,$$

$$(2) dd^*(\mathcal{G}_m(C_5)) = 8m^3 + 8m^2 + 4m.$$

4. Edge-Introducing Operation:

Let G_1, G_2, \dots, G_m be a family of m (where $m \geq 2$) pairwise disjoint and connected graphs. For each graph G_i , let u_i and v_i be distinct vertices. The straight chain of edge – introducing graphs, denoted as \mathcal{J}_m , is formally defined as the graph constructed by introducing $m - 1$ new edges, specifically $u_{i+1}v_i$, for each i ranging from 1 to $m - 1$, connecting the graphs G_1 through G_m . It's clear that

$$\mathcal{J}_m = \mathcal{J}_{m-1} : G_m = G_1 : G_2 : \dots : G_m.$$

The graph $\mathcal{J}_m, m \geq 3$ is shown in Fig. 6.

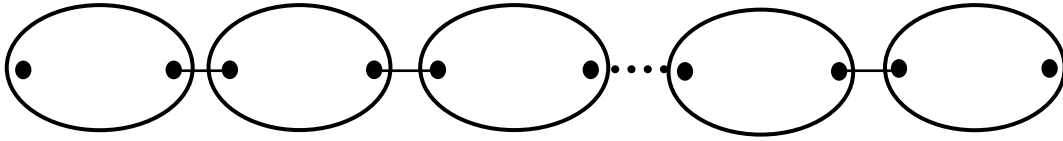


Fig. 6 The Straight Chain Of Edge-Introducing Graphs \mathcal{J}_m

Theorem 4.2 [18]: for $m \geq 2$,

$$D^*(\mathcal{J}_m; x) = D^*(\mathcal{J}_{m-1}; x) + D^*(G_m; x)$$

$$+ x D^*(u_m, G_m; x) D^*(v_{m-1}, \mathcal{J}_{m-1}; x),$$

where

$$D^*(v_{m-1}, \mathcal{J}_{m-1}; x) = \sum_{i=1}^{m-1} \left\{ x^{m-i-1} x^{\sum_{j=i+1}^{m-1} \gamma(j)} D^*(v_i, G_i; x) \right\}.$$

In which $\gamma(j) = D^*_{G_j}(u_j, v_j)$

Theorem 4.2 provides a polynomial expression for computing the restricted detour distance resulting from the edge-introducing graph operation applied to m copies of the graph G , as a Corollary 4.3 presents an application of this theorem to a set of chemical compounds.

Theorem 4.3 [18]: For $m \geq 2$,

$$D^*(J_m; x) = mD^*(G; x) + x D^*(u, G; x) D^*(v, G; x) \left\{ \sum_{j=1}^{m-1} \sum_{i=1}^{m-j} x^{(m-i-j)} (1 + D_G^*(uv)) \right\} \blacksquare$$

It is clear that research papers [4,18] provide direct and relevant applications in the field of mathematical chemistry.

In 2017, Ivan D. Ali and Herish O. Abdullah computed the restricted detour polynomials resulting from the edge identification of two wheel graphs and determined their corresponding restricted detour indices [7].

In recent studies, two new definitions derived from the restricted detour index-namely, the average restricted detour distance and restricted detour median graph-have been introduced in two papers [3, 15]

5. Conclusion:

After reviewing several research papers and applying the edge identification operation to hexagonal ring graphs, obtained a series of graphs that mimic the topological structure of polyacene compounds. By using relation (1), where the exponential term includes the product of the restricted detour index and the Wiener index, obtained a very strong correlation with a value of $R = 0.9979$. This result indicates the efficiency and effectiveness of the restricted detour index as a topological descriptor for predicting the boiling point of polycyclic carbon-based compounds.

6. Suggestions for Future Works:

- Establishing explicit formulas or inequalities that relate the restricted detour index to other well-known graph invariants for special graphs, such as the Wiener index or D-index, similar to the relationships researched in tree graphs [8] and regular complete graphs[6].

- A research on the restricted detour index under several additional graph operations, aiming to generalize its behavior and identify patterns or bounds across diverse structural transformations.
- Further investigating the correlation between the restricted detour index and various physicochemical properties of chemical compounds in order to evaluate its effectiveness as a molecular descriptor.
- Research on the graphs that represent the upper and lower bounds of the restricted detour index.
- A research to assess the applicability and relevance of the restricted detour index in network theory may serve as a valuable direction for future research.

References:

- [1] Abdullah, Herish, and Ivan Ali. "Restricted Detour Polynomial of a Straight Chain of Wheel Graphs." *Al-Rafidain Journal of Computer Sciences and Mathematics* 17.1: 99-106, (2023).
<https://doi.org/10.33899/csmj.2023.179505>
- [2] Abdullah, Herish Omer, and Ivan Dler Ali. "The restricted detour polynomials of a prism and some wheel related graphs." *Journal of Information and Optimization Sciences* 42.4: 773-784, (2021).
<https://doi.org/10.1080/02522667.2020.1809116> .
- [3] Abdullah, Herish Omer, Ivan Dler Ali, and Rashad Rashid Haji. "Average Distance and Average Restricted Detour Distance of a Straight Chain of k-Wheels Graph." *Palestine Journal of mathematics*, vol. 12, no. 4, pp. 399-409, (2023).
- [4] Ali, A. A., and A. Mohammed-Saleh. "The restricted detour polynomials of a hexagonal chain and a ladder graph." *J. Math. Comput. Sci.* 2.6: 1622-1633, (2012).
- [5] Ali, Ahmed M., Haveen J. Ahmed, and Gashaw A. Mohammed Saleh. "Detour Polynomials of Generalized Vertex Identified of Graphs." *Baghdad Science Journal* 20.2: 0343-0343, (2023).
<https://doi.org/10.21123/bsj.2022.6350>
- [6] Ali, Ahmed Mohammed, and Asmaa Salah Aziz. "A Relation between D-Index and Wiener Index for r-Regular Graphs." *International Journal of Mathematics and Mathematical Sciences* 2020.1: 6937863, (2020). <https://doi.org/10.1155/2020/6937863> .
- [7] Ali, Ivan Dler, and Herish Omer Abdullah. "Restricted detour polynomial of edge-identification of two wheel graphs." *AIP Conference Proceedings*. Vol. 1888. No. 1. AIP Publishing, AIP, (2017).
<https://doi.org/10.1063/1.5004288> .
- [8] Andova, Vesna, et al. "Bounds on Gutman index." *Match-Communications in Mathematical and Computer Chemistry* 67.2: 515, (2012).
- [9] Babić, Darko, et al. "Resistance-distance matrix: A computational algorithm and its application." *International Journal of Quantum Chemistry* 90.1: 166-176, (2002).
<https://doi.org/10.1002/qua.10057> .
- [10]. Chartrand, G.; John, G. L. and Tian, S. , Detour distance in graphs, *Annals of discrete mathematics*, **55** : pp. 127-136, (1993).
[https://doi.org/10.1016/S0167-5060\(08\)70381-9](https://doi.org/10.1016/S0167-5060(08)70381-9) .
- [11] Chartrand, Gary, et al. "Steiner distance in graphs." *Časopis pro pěstování matematiky* 114.4: 399-410, (1989).
<https://doi.org/10.21136/cpm.1989.118395>
- [12] Elenbogen, Bruce, and John Frederick Fink. "Distance distributions for graphs modeling computer networks." *Discrete applied mathematics* 155.18: 2612-2624, (2007).
<https://doi.org/10.1016/j.dam.2007.07.020>.
- [13] Estrada, Ernesto. "The communicability distance in graphs." *Linear Algebra and its Applications* 436.11: 4317-4328, (2012).

<https://doi.org/10.1016/j.laa.2012.01.017> .

- [14] Chartrand, Gary, Ping Zhang and T.W. Haynes. " Distance in graphs-taking the long view ." AKCE International Journal of Graphs and Combinatorics, vol. 1, no. 1, pp.1-13, (2004).
- [15] Hasan, Rasha S., Haitham N. Mohammed, and Ahmed M. Ali. "On Restricted Detour Median of Special Graphs". International Journal of Mathematics and Mathematical Sciences, vol. 2025, pp. 1-9, (2025). <https://doi.org/10.1155/ijmm/3352309> .
- [16] Hosoya, Haruo. "On some counting polynomials in chemistry." Discrete applied mathematics 19.1-3: 239-257, (1988). [https://doi.org/10.1016/0166-218X\(88\)90017-0](https://doi.org/10.1016/0166-218X(88)90017-0)
- [17] Mohammed, Haithm N., Hanadi D. Saleem, and Ahmed M. Ali. "ZAGREB INDICES FOR CHAINS OF IDENTICAL HEXAGONAL CYCLES." Palestine Journal of Mathematics, vol. 12, no. 1, pp. 147-157, (2023).
- [18] Mohammed-Saleh, Gashaw A. "Restricted Detour Polynomials of Straight Chains of Graphs." Journal of Zankoy Sulaimani-Part A 17.2: 63-70, (2015). <https://doi.org/10.17656/jzs.10381>
- [19] Mohammed-Saleh, Gashaw A., Herish O. Abdullah, and Mohammed R. Ahmed. "The restricted detour polynomials of some classes of thorn graphs." AIP Conference Proceedings, vol. 1888, no. 1, AIP publishing, p. 020046, (2017). <https://doi.org/10.1063/1.5004323> .
- [20] Mohammed-Saleh, Gashaw, Herish Abdullah, and Mohammed Ahmed. "The Restricted Detour Polynomial of a Ladder Graph $L^* n$." Journal of Zankoy Sulaimani-Part A 19.2: 157-174, (2017). <https://doi.org/10.17656/jzs.10620>
- [21] Wiener, Harry. "Structural determination of paraffin boiling points." Journal of the American chemical society 69.1: 17-20, (1947). DOI: [10.17656/jzs.10620](https://doi.org/10.17656/jzs.10620)
- [22] Trinajstić, Nenad, et al. "The detour matrix in chemistry." Journal of chemical information and computer sciences 37.4: 631-638, (1997). <https://doi.org/10.1021/ci960149n> .

New Results on Fourth-Hankel Determinant of a Certain Subclass of Analytic Functions

^{1,*} Fedaa Aeyyd Nayyef

² Waggas Galib Atshan

³ Youssef Wali Abbas

^{1,2} The General Directorate for Education of Ninevah–Ministry of Education–Iraq.

³ Department of Mathematics, College of Science, University of Al-Qadisiyah, Diwaniyah,
Iraq.

[^{1,*} yousif.21csp31@student.uomosul.edu.iq](mailto:yousif.21csp31@student.uomosul.edu.iq)

[² fedaa.20csp102@student.uomosul.edu.iq](mailto:fedaa.20csp102@student.uomosul.edu.iq),

[³ waggas.galib@qu.edu.iq](mailto:waggas.galib@qu.edu.iq)

New Results on Fourth-Hankel Determinant of a Certain Subclass of Analytic Functions

Youssef Wali Abbas ^{1,*} Fedaa Aeyyd Nayyef ² and Waggas Galib Atshan³

^{1,2} The General Directorate for Education of Ninevah–Ministry of Education–Iraq.

³ Department of Mathematics, College of Science, University of Al-Qadisiyah, Diwaniyah, Iraq.

yousif.21csp31@student.uomosul.edu.iq^{1,*}

fedaa.20csp102@student.uomosul.edu.iq²,

waggas.galib@qu.edu.iq³

Abstract

This paper studies the fourth Hankel determinant for a subclass of analytic functions, denoted by $N(\alpha, \mu, e)$, defined via α -th order differential subordination involving an exponential function. Sharp coefficient bounds for $|a_n|$, where $n = 2, \dots, 7$, are obtained, and an upper bound for the fourth Hankel determinant $H_4(1)$ is established, contributing to the theory of geometric function classes.

Keywords: Superordination, Hankel determinant, A Schwarz function, Chebyshev polynomials, Analytic function.

1. Introduction

Let \mathcal{P} denote the class of analytic functions p , normalized by

$$p(z) = 1 + c_1 z + c_2 z^2 + c_3 z^3 + \dots \quad (1)$$

and satisfying the condition $\operatorname{Re}\{p(z)\} > 0$ in D

It is well known (see [2,3,4,19,24]) that if $p(z) \in \mathcal{P}$, then there exists a Schwarz function $w(z)$, analytic in such that $w(0) = 0$ and $|w(z)| < 1$, with

$$p(z) = \frac{1 + w(z)}{1 - w(z)} \quad (z \in D).$$

Recently, Mendiratta et al. [15] introduced the following subclass of analytic functions associated with exponential function. Earliness
Ma and Minda [14] defined subclass of starlike and convex functions using the principle of subordination. In particular, they introduce for the

$$S^*(\Phi) = \left\{ f \in A: \frac{zf'(z)}{f(z)} \prec \Phi(z), \quad z \in U \right\}$$

and

$$G^*(\Phi) = \left\{ f \in A: 1 + \frac{zf''(z)}{f'(z)} \prec \Phi(z), \quad z \in U \right\}.$$

Mendiratta et al. [15] further introduced the classes

$$S_e^* = \left\{ f \in A: \frac{zf'(z)}{f(z)} \prec e^z, \quad z \in U \right\}. \quad (2)$$

While the associated class

$$G_e^* = \left\{ f \in A: 1 + \frac{zf''(z)}{f'(z)} \prec e^z, \quad z \in U \right\}. \quad (3)$$

Was introduced by using an Alexander type relation [13]

These classes are known to be symmetric with respect to the real axis

$$H_q(n) = \begin{vmatrix} a_n & a_{n+1} & \cdots & a_{n+q-1} \\ a_{n+1} & a_{n+2} & \cdots & a_{n+q} \\ \vdots & \vdots & \ddots & \vdots \\ a_{n+q-1} & a_{n+q} & \cdots & a_{n+2q-2} \end{vmatrix}, \quad (a_1 = 1). \quad (4)$$

The Hankel determinant plays a significant role in the theory of singularities [10] in the analysis of power series with integer coefficients [7,17] several

estimates of $H_q(n)$ have been obtained for various sub classes of univalent and bi-univalent function. The case $H_2(1) = a_3 - a_2^2$ is the classic Fekete–szego functional while $H_2(2) = a_2 a_4 - a_3^2$ has been studied for bi– starlike and bi – convex functions ([3,45,62]). Krishna [13] provided a sharp estimate for the Bazilevic class. More recently, Srivastava et al. [21], obtained bounds for $H_2(2)$ in the class of bi-univalent functions involving symmetric q -derivative [23], the authors investigated Hankel and Toeplitz determinants in subfamilies of q -starlike functions associated with conic domain (see also [6,16,22]).

For functions of form (1), the third Hankel determinant is given as:

$$H_3(1) = -a_5 a_2^2 + 2a_2 a_3 a_4 - a_3^3 + a_3 a_5 - a_4^2.$$

Interesting results on $H_3(1)$ were established by Babalola [5], motivating further investigations.

The fourth Hankel determinant has also been studied in for a certain subclass of starlike and convex functions [20]. In this direction, we introduced a new subclasses of analytic functions using third-order differential subordination involving the exponential function and derive sharp bounds for the fourth Hankel determinant $H_4(1)$ for functions in this class.

2-Preliminaries

The definitions and lemmas presented below will be used to establish the main results work .

Definition 2.1: [20] Let f be a function f of the form (1). The fourth Hankel determinant of f is defined as:

$$H_4(1) = \begin{vmatrix} 1 & a_2 & a_3 & a_4 \\ a_2 & a_3 & a_4 & a_5 \\ a_3 & a_4 & a_5 & a_6 \\ a_4 & a_5 & a_6 & a_7 \end{vmatrix} = -a_4 t_1 + a_5 t_2 - a_6 t_3 + a_7 t_4, \quad (5)$$

Where the coefficients t_i are defined by:

$$|t_1| = |a_2| |a_4 a_6 - a_5^2| + |a_3| |a_3 a_6 - a_4 a_5| - |a_4| |a_3 a_5 - a_4^2|,$$

$$|t_2| = |a_4 a_6 - a_5^2| - |a_2| |a_3 a_6 - a_4 a_5| + |a_3| |a_3 a_5 - a_4^2|, \quad (6)$$

$$|t_3| = |a_3 a_6 - a_4 a_5| + |a_2| |a_2 a_6 - a_3 a_5| - |a_4| |a_2 a_4 - a_3^2|,$$

$$|t_4| = |a_3| |a_2 a_4 - a_2^2| - |a_4| |a_4 - a_2 a_3| + |a_5| |a_3 - a_2^2|.$$

The Chebyshev polynomials of the first and second kind are defined on the interval $(-1,1)$ for a real variable x as follows:

$$T_n(x) = \cos(n \arccos x)$$

and

$$U_n(x) = \frac{\sin[(n+1)\arccos x]}{\sin(\arccos x)} = \frac{\sin[(n+1)\arccos x]}{\sqrt{1-x^2}},$$

Now, consider the function

$$H(t, z) = \frac{1}{1-2t+z^2}, t \in \left(\frac{1}{2}, 1\right), z \in \mathbb{U}.$$

It is well-known that if $t = \cos \alpha$, $\alpha \in \left(0, \frac{\pi}{3}\right)$, then

$$\begin{aligned} H(t, z) &= 1 + \sum_{n=1}^{\infty} \frac{\sin[(n+1)\alpha]}{\sin \alpha} z^n \\ &= 1 + 2 \cos \alpha z + (3 \cos^2 \alpha - \sin^2 \alpha) z^2 + (8 \cos^3 \alpha - 4 \cos \alpha) z^3 \\ &\quad + \dots, z \in U, \end{aligned}$$

that is

$$H(t, z) = 1 + U_1(t) z + U_2(t) z^2 + U_3(t) z^3 + U_4(t) z^4 + \dots, t \in \left(\frac{1}{2}, 1\right), z \in U$$

where

$$U_n(t) = \frac{\sin[(n+1)\arccos t]}{\sqrt{1-t^2}}, n \in \mathbb{N},$$

are the Chebyshev polynomials of the second kind. These polynomials satisfy the recurrence relation:

$$U_{n+1}(t) = 2tU_n(t) - U_{n-2}(t).$$

specifically

$$U_1(t) = 2t, U_2(t) = 4t^2 - 1, U_3(t) = 8t^3 - 4t, (\text{for each } n \in \mathbb{N}).$$

Mendiratta et al. [79] discussed the subclass S_1^* of analytic functions associated with exponential function.

Lemma2. 1: [15] If function $f \in S_1^*$ is of the form (2), then

$$|a_2| \leq 1, |a_3| \leq \frac{3}{4}, |a_4| \leq \frac{17}{36}, |a_5| \leq 1,$$

where S_1^* denote the class of analytic functions to third Hankel determinant.

Lemma2. 2: [20] If the function $f \in S_e^*$ and of the form (1), then

$$|a_2| \leq 1, |a_3| \leq \frac{3}{4}, |a_4| \leq \frac{1}{18}, |a_5| \leq \frac{1}{96}, |a_6| \leq \frac{1}{600}, |a_7| \leq \frac{2401}{3600}.$$

Lemma2. 3: [20] If the function $f \in G_e^*$ and of the form (1), then

$$|a_2| \leq \frac{1}{2}, |a_3| \leq \frac{3}{12}, |a_4| \leq \frac{1}{72}, |a_5| \leq \frac{1}{480}, |a_6| \leq \frac{1}{3600}, |a_7| \leq \frac{343}{3600}.$$

Here, we discuss a new subclass of analytic functions using the subordination.

Lemma 2.4: [11] If P be a class of all analytic functions $p(z)$ of the form:

$$p(z) = 1 + \sum_{n=1}^{\infty} p_n z^n, \quad (7)$$

with $p(0)=1$ and $\Re\{p(z)\} > 0$ for all $z \in U$. Then $|p_n| \leq 2$, for every $(n = 1, 2, 3, \dots)$. This disparity is sharp for each n

Definition 2.2: A function $f \in A$ given by (1) is said to be in the class $\mathcal{N}(\alpha, \mu, e)$ if the following condition holds:

$$\frac{1}{\alpha} \left[\frac{f(z)}{z} + (1 - \mu)f'(z) + z\mu f''(z) + z^2 f'''(z) \right] \prec \mathcal{L}(e, z), \quad (8)$$

where $\mu \geq 0, \alpha \in \mathbb{C} \setminus \{0\}$ and

$$\mathcal{L}(e, z) = 1 + U_1(t)z + U_2(t)z^2 + U_3(t)z^3 + U_4(t)z^4 + \dots, \\ e \in \left(\frac{1}{2}, 1\right), z \in U.$$

The main findings of our current inquiry will now be stated and proven.

We begin here by finding the estimates on the coefficients $|a_n|$ and $n = 2, 3, 4, 5, 6, 7$, for functions in the class $\mathcal{N}(\alpha, \mu, e)$.

Theorem 1: Let f be a function of the form

$$f(z) = z + \sum_{n=2}^{\infty} a_n z^n, \quad (z \in U)$$

And suppose that f belongs to class $\mathcal{N}(\alpha, \mu, e)$

Then the following sharp coefficient bounds hold:

$$|a_2| \leq \frac{4}{3-2\mu} \alpha, |a_3| \leq \frac{12}{7} \alpha, |a_4| \leq \frac{36}{13+12\mu} \alpha, \quad |a_5| \leq \frac{108}{21+40\mu} \alpha$$

$$|a_6| \leq \frac{216}{31+90\mu} \alpha, |a_7| \leq \frac{1044}{43+168\mu} \alpha,$$

where $\mu \geq 0$ and $\alpha \in \mathbb{C} \setminus \{0\}$.

Proof: Assume that $f \in \mathcal{N}(\alpha, \mu, e)$, then there exists an analytic function E defined in the following subordination relation holds:

$$\frac{1}{\alpha} \left[\frac{f(z)}{z} + z(1-\mu)f''(z) + z^2\mu f'''(z) \right] = \mathcal{L}(e, E(z)).$$

Where $L(e, z) = 1 + u_1(z)z + u_2(z)z^2 + \dots$ is generating function involving chebyshev polynomials of the second by the principle of subordination, there exists a Schwarz function $E(z)$, given by

$$E(z) = \sum_{n=1}^{\infty} p_n z^n, \quad z \in U,$$

Such that the function $B(z) = \frac{1+E(z)}{1-E(z)}$

Has the power series expansion

$$\begin{aligned}
B(z) = & 1 + 2 p_1 z + 2(p_2 + p_1^2)z^2 + 2[p_3 + p_1(2p_2 + p_1^2)]z^3 \\
& + 2[p_4 + p_2^2 + p_1^2(3p_2 + p_1^2) + 2p_1 p_3]z^4 \\
& + 2[p_5 + 2p_2(p_3 + 2p_1^3) + 3p_1(p_1 p_3 + p_2^2) \\
& + (p_1(2p_4 + p_1^4))]z^5 \\
& + 2[p_6 + p_1^3(4p_3 + p_1^3) + p_1^2(3p_4 + 5p_2 p_1^2) + 2p_1(p_5 + 3p_2 p_3) \\
& + p_3^2 + p_2^2(p_2 + 6p_1^2) + 2p_2 p_4]z^6 \\
& + \dots.
\end{aligned} \tag{9}$$

Now ,Since f is the stranded class A , We Can expand the left-hand side of operator as follows:

$$\begin{aligned}
& \frac{1}{\alpha} \left[\frac{f(z)}{z} + z(1 - \mu)f''(z) + z^2 \mu f'''(z) \right] \\
& = \frac{1}{\alpha} [1 + (3 - 2\mu)a_2 z + 7a_3 z^2 + (13 + 12\mu)a_4 z^3 \\
& + (21 + 40\mu)a_5 z^4 + (31 + 90\mu)a_6 z^5 + (43 + 168\mu)a_7 z^6 \\
& + \dots].
\end{aligned} \tag{10}$$

comparing the coefficients of z^n form the two expansion (9)and(10), we obtain

$$\frac{1}{\alpha} ((3 - 2\mu)a_2) = 2 p_1,$$

$$\frac{1}{\alpha} (7a_3) = 2(p_2 + p_1^2),$$

$$\frac{1}{\alpha} ((13 + 12\mu)a_4) = 2[p_3 + p_1(2p_2 + p_1^2)],$$

$$\frac{1}{\alpha} ((21 + 40\mu)a_5) = 2[p_4 + p_2^2 + p_1^2(3p_2 + p_1^2) + 2p_1 p_3],$$

$$\frac{1}{\alpha} ((31 + 90\mu)a_6) = 2[p_5 + 2p_2(p_3 + 2p_1^3) + 3p_1(p_1 p_3 + p_2^2) + (p_1(2p_4 + p_1^4))],$$

$$\begin{aligned}
& \frac{1}{\alpha} ((43 + 168\mu)a_7) \\
& = 2[p_6 + p_1^3(4p_3 + p_1^3) + p_1^2(3p_4 + 5p_2 p_1^2) + 2p_1(p_5 + 3p_2 p_3) \\
& + p_3^2 + p_2^2(p_2 + 6p_1^2) + 2p_2 p_4].
\end{aligned}$$

Now, by applying the standard bound $|p_n| \leq 1$ for Schwarz function and applying Lemma 4, we obtain

$$|a_2| \leq \frac{4}{(3-2\mu)} \alpha, \quad (11)$$

$$|a_3| \leq \frac{12}{7} \alpha, \quad (12)$$

$$|a_4| \leq \frac{36}{13+12\mu} \alpha, \quad (13)$$

$$|a_5| \leq \frac{108}{21+40\mu} \alpha, \quad (14)$$

$$|a_6| \leq \frac{216}{31+90\mu} \alpha, \quad (15)$$

$$|a_7| \leq \frac{1044}{43+168\mu} \alpha. \quad (16)$$

This complete the proof . \square

In the following theorem, estimates on $|H_4(1)|$ are determined for $f \in \mathcal{N}(\alpha, \mu, e)$.

Theorem 2: Let f be a function of the form

$$f(z) = z + \sum_{n=2}^{\infty} a_n z^n, \quad (z \in U)$$

And suppose that f belongs to class $\mathcal{N}(\alpha, \mu, e)$. then the following estimate for the fourth Hankel determinant $H_4(1)$ holds:

$$\begin{aligned} & |H_4(1)| \\ & \leq \frac{-111974(2\mu-3)(90\mu+31)(40\mu+21)\alpha^4 L_1(\delta, u) + 139968(90\mu+31)(12\mu+13)^2}{L(\delta, u)} \\ & \quad - \frac{93312(12\mu+13)^2(40\mu+21)^2\alpha^3 L_3(\delta, u) + 672(90\mu+31)^2\alpha^2 L_4(\delta, u)}{L(\delta, u)}, \end{aligned}$$

where

$$L(\delta, u) = 49(12\mu+13)^4(2\mu-3)^2(90\mu+31)(40\mu+21)^3$$

$$L_1(\delta, u) = 5529600\mu^6 - 6289920\mu^5 - 7939584\mu^4 + 3821168\mu^3 \\ + 19330358\mu^2 + 13831923\mu + 2364054,$$

$$L_2(\delta, u) = 12441600\alpha\mu^5 + (7822080\alpha - 141120)\mu^4 \\ + (2282496\alpha - 4407648)\mu^3 + (-9231232\alpha + 936684)\mu^2 \\ + (-7799688\alpha + 7738668)\mu - 1318212\alpha + 1874691,$$

$$L_3(\delta, u) = (2073600\alpha + 967680)\mu^5 + (5760\alpha - 2203488)\mu^4 \\ + (3538848\alpha - 405048)\mu^3 + (1919952\alpha + 2910348)\mu^2 \\ + (-908008\alpha - 744282)\mu - 163380\alpha - 257985,$$

$$L_4(\delta, u) = -7776\mu^4 + (46080\alpha + 21600)\mu^3 + (52896\alpha - 13500)\mu^2 \\ + (2216\alpha - 324)\mu - 1092\alpha - 2673.$$

Proof: Let f be a function of the form

$$f(z) = z + \sum_{n=2}^{\infty} a_n z^n, \quad (z \in U)$$

And suppose that f belongs to class $\mathcal{N}(\alpha, \mu, e)$

By Deficient (2,1) the fourth Hankel determinant $H_4(1)$ is given by

$$|H_4(1)| = |a_7 t_4 - a_6 t_3 + a_5 t_2 - a_4 t_1|,$$

Where the coefficients t_1, t_2, t_3, t_4 are defined by

$$|t_1| = |a_2| |a_4 a_6 - a_5^2| + |a_3| |a_3 a_6 - a_4 a_5| - |a_4| |a_3 a_5 - a_4^2|,$$

$$|t_2| = |a_4 a_6 - a_5^2| - |a_2| |a_3 a_6 - a_4 a_5| + |a_3| |a_3 a_5 - a_4^2|,$$

$$|t_3| = |a_3 a_6 - a_4 a_5| + |a_2| |a_2 a_6 - a_3 a_5| - |a_4| |a_2 a_4 - a_3^2|,$$

$$|t_4| = |a_3| |a_2 a_4 - a_2^2| - |a_4| |a_4 - a_2 a_3| + |a_5| |a_3 - a_2^2|.$$

Inserting (11) – (16) in (7), we get

$$|t_1| = \frac{31104\alpha^3 L_1(\delta, u)}{R_1(\delta, u)}, \quad (17)$$

$$|t_2| = \frac{1296\alpha^2 L_2(\delta, u)}{R_2(\delta, u)}, \quad (18)$$

$$|t_3| = \frac{432\alpha^2 L_3(\delta, u)}{R_3(\delta, u)}, \quad (19)$$

$$|t_4| = -\frac{96\alpha^2 L_4(\delta, u)}{R_4(\delta, u)}, \quad (20)$$

where

$$R_1(\delta, u) = 43(2\mu - 3)(90\mu + 31)(40\mu + 21)^2(12\mu + 13)^3,$$

$$R_2(\delta, u) = 49(90\mu + 31)(2\mu - 3)(12\mu + 13)^2(40\mu + 21)^2,$$

$$R_3(\delta, u) = 49(90\mu + 31)(40\mu + 21)(2\mu - 3)^2(12\mu + 13)^2,$$

$$R_4(\delta, u) = 7(40\mu + 21)(2\mu - 3)^2(12\mu + 13)^2.$$

Using (17) – (20) in (5), we get

$$\begin{aligned} & |H_4(1)| \\ & \leq \frac{-111974(2\mu - 3)(90\mu + 31)(40\mu + 21)\alpha^4 L_1(\delta, u) + 139968(90\mu + 31)(12\mu + 13)^2 \alpha^3 L_2(\delta, u)}{L(\delta, u)} \\ & \quad - \frac{93312(12\mu + 13)^2(40\mu + 21)^2 \alpha^3 L_3(\delta, u) + 672(90\mu + 31)^2 \alpha^2 L_4(\delta, u)}{L(\delta, u)}, \end{aligned}$$

where

$$\begin{aligned} L_1(\delta, u) = & 5529600\mu^6 - 6289920\mu^5 - 7939584\mu^4 + 3821168\mu^3 \\ & + 19330358\mu^2 + 13831923\mu + 2364054, \end{aligned}$$

$$\begin{aligned} L_2(\delta, u) = & 12441600\alpha\mu^5 + (7822080\alpha - 141120)\mu^4 \\ & + (2282496\alpha - 4407648)\mu^3 + (-9231232\alpha + 936684)\mu^2 \\ & + (-7799688\alpha + 7738668)\mu - 1318212\alpha + 1874691, \end{aligned}$$

$$\begin{aligned} L_3(\delta, u) = & (2073600\alpha + 967680)\mu^5 + (5760\alpha - 2203488)\mu^4 \\ & + (3538848\alpha - 405048)\mu^3 + (1919952\alpha + 2910348)\mu^2 \\ & + (-908008\alpha - 744282)\mu - 163380\alpha - 257985, \end{aligned}$$

$$\begin{aligned} L_4(\delta, u) = & -7776\mu^4 + (46080\alpha + 21600)\mu^3 + (52896\alpha - 13500)\mu^2 + \\ & (2216\alpha - 324)\mu - 1092\alpha - 2673. \end{aligned}$$

□

In case $\mu = 0$, we get the following Corollary.

Corollary 1: If function f of form (1) belongs to the subclass $\mathcal{N}(\alpha, \mu, e)$, then

$$|H_4(1)| \leq -\frac{825676789240}{911067339} \alpha^4 + \frac{3869374792502}{4415172489} \alpha^3 + \frac{259842}{480024727} \alpha^2.$$

In case $\alpha = 1$ and $\mu = 0$, we get the following Corollary.

Corollary 2: If function f of form (1) belongs to the subclass $\mathcal{N}(\alpha, \mu, e)$, then $|H_4(1)| \leq -29.89227843$.

By applying Lemma 1 and using $|a_6|, |a_7|$ from Theorem 2 in fourth Hankel determinant (7), the following theorem emerges:

Theorem 3: let the function $f \in \mathcal{N}(\alpha, \mu, e)$ be of the form

$$f(z) = z + \sum_{n=2}^{\infty} a_n z^n, \quad (z \in U)$$

Then, the fourth Hankel determinant satisfies the inequality

$$|H_4(1)| \leq -Y_1(\delta, u) + Y_2(\delta, u) - Y_3(\delta, u) + Y_4(\delta, u),$$

Where the farms are defined by:

$$\begin{aligned} Y_1(\delta, u) &= \frac{2533\alpha}{24(31 + 90u)} - \frac{1271447}{1679616}, \\ Y_2(\delta, u) &= -60 * \frac{-60\alpha}{31 + 90u} - \frac{229}{1728}, \\ Y_3(\delta, u) &= 81648 * \frac{81648\alpha^2}{(31 + 90u)^2} - \frac{6115\alpha}{24(31 + 90u)}, \\ Y_4(\delta, u) &= \frac{-19343\alpha}{36(43 + 168u)} \end{aligned}$$

Proof: Let $f \in \mathcal{N}(\alpha, \mu, e)$. Then the fourth Hankel determinant can be rewrite as:

$$|H_4(1)| = -a_4 t_1 + a_5 t_2 - a_6 t_3 + a_7 t_4,$$

where

$$|t_1| = |a_2| |a_4 a_6 - a_5^2| + |a_3| |a_3 a_6 - a_4 a_5| - |a_4| |a_3 a_5 - a_4^2|,$$

$$|t_2| = |a_4 a_6 - a_5^2| - |a_2| |a_3 a_6 - a_4 a_5| + |a_3| |a_3 a_5 - a_4^2|,$$

$$|t_3| = |a_3 a_6 - a_4 a_5| + |a_2| |a_2 a_6 - a_3 a_5| - |a_4| |a_2 a_4 - a_3^2|,$$

$$|t_4| = |a_3| |a_2 a_4 - a_3^2| - |a_4| |a_4 - a_2 a_3| + |a_5| |a_3 - a_2^2|.$$

By applying Lemma 1 and using $|a_6|, |a_7|$ from Theorem 2 in fourth Hankel determinant (7), we get

$$|t_1| = |a_2||a_4a_6 - a_5^2| + |a_3||a_3a_6 - a_4a_5| - |a_4||a_3a_5 - a_4^2|,$$

$$|t_1| = \frac{447\alpha}{2(31 + 90u)} - \frac{74791}{46656}, \quad (21)$$

$$|t_2| = |a_4a_6 - a_5^2| - |a_2||a_3a_6 - a_4a_5| + |a_3||a_3a_5 - a_4^2|,$$

$$|t_2| = \frac{-60\alpha}{31 + 90u} - \frac{229}{1728}, \quad (22)$$

$$|t_3| = |a_3a_6 - a_4a_5| + |a_2||a_2a_6 - a_3a_5| - |a_4||a_2a_4 - a_3^2|,$$

$$|t_3| = \frac{378\alpha}{31 + 90u} - \frac{6115}{5184}, \quad (23)$$

$$|t_4| = |a_3||a_2a_4 - a_2^2| - |a_4||a_4 - a_2a_3| + |a_5||a_3 - a_2^2|,$$

$$|t_4| = -\frac{667}{1296}. \quad (24)$$

Inserting values (21) – (24) in (5), we obtain

$$|H_4(1)| \leq -Y_1(\delta, u) + Y_2(\delta, u) - Y_3(\delta, u) + Y_4(\delta, u),$$

where

$$Y_1(\delta, u) = \frac{2533\alpha}{24(31 + 90u)} - \frac{1271447}{1679616},$$

$$Y_2(\delta, u) = -60 * \frac{-60\alpha}{31 + 90u} - \frac{229}{1728},$$

$$Y_3(\delta, u) = 81648 * \frac{81648\alpha^2}{(31 + 90u)^2} - \frac{6115\alpha}{24(31 + 90u)},$$

$$Y_4(\delta, u) = \frac{-19343\alpha}{36(43 + 168u)}.$$

In case $\mu = 0$, we get the following Corollary.

Corollary 3: If function f of form (1) belongs to the subclass $\mathcal{N}(\alpha, \mu, e)$, then

$$|H_4(1)| \leq -\Theta_1(\delta, u) + \Theta_2(\delta, u) - \Theta_3(\delta, u) + \Theta_4(\delta, u),$$

where

$$\begin{aligned}\Theta_1(\delta, u) &= \frac{2533\alpha}{744} - \frac{1271447}{1679616}, & \Theta_2(\delta, u) &= -\frac{60\alpha}{31} - \frac{229}{1728}, \\ \Theta_3(\delta, u) &= \frac{81648\alpha^2}{961} - \frac{6115\alpha}{744}, & \Theta_4(\delta, u) &= -\frac{19343\alpha}{1548}.\end{aligned}$$

In case $\alpha = 1$ and $\mu = 0$, we get the following Corollary.

Corollary 4: If function f of form (1) belongs to the subclass $\mathcal{N}(\alpha, \mu, e)$, then $|H_4(1)| \leq \approx -93.95348065$.

References

- [1] S. A. Al-Ameedee ,W. G. Atshan and F. A .Al-Maamori ,Second Hankel determinant for certain Subclasses of bi- univalent functions , Journal of physics: Conference Series , 1664 (2020) 012044 ,1-9.
- [2] S. A. Al-Ameedee ,W. G. Atshan and F. A. Al-Maamori ,Coefficients estimates of bi-univalent functions defined by new subclass function ,Journal of Physics :Conference Series ,1530 (2020) 012105 ,1-8.
- [3] W. G. Atshan, I. A. R. Rahman and A. A. Lupas, Some results of new subclasses for bi-univalent functions Using Quasi-subordination, Symmetry, 13(9)(2021), 1653, 1-12.
- [4] W. G. Atshan , S. Yalcin and R. A. Hadi ,Coefficients estimates for special subclass of k-fold symmetric bi-univalent functions ,Mathematics for Applications, 9(2) (2020) ,83-90 .
- [5] K. O. Babalola, On Hankel determinant for some classes of univalent functions, Inequal. Theory Appl., (2010), 6, 1–7.
- [6] M. Çaglar, E. Deniz and H.M. Srivastava, Second Hankel determinant for certain subclasses of bi –univalent functions, Turk. J. Math., 41 (3) (2017), 694–706.

- [7] D. G. Cantor, Power series with integral coefficients, *Bull. Am. Math. Soc.*, 69 (3) (1963), 362–366.
- [8] N. E. Cho, V. Kumar, Initial coefficients and fourth hankel determinant for certain analytic functions, *Miskolc Mathematical Notes*, (21) (2) (2020), 763–779.
- [9] N. E. Cho, V. Kumar, S.S. Kumarand, V. Ravichandran, Radius problems for starlike functions associated with the sine function, *Bull. Iran. Math. Soc.* 45(1) (2019), 213–232.
- [10] P. Dienes, *The Taylor Series: An Introduction to the Theory of Functions of a Complex Variable*; NewYork-Dover:Mineola, NY, USA, (1957).
- [11] P. L. Duren, *Univalent Functions*, In : *Grundlehren der Mathematischen Wissenschaften*, Band 259, Springer - Verlag, New York, Berlin, Hidelberg and Tokyo, (1983).
- [12] S. P. Goyal, O. Singh and R. Mukherjee, Certain results on a subclass of analytic and biunivalent functions associated with coe cient estimates and quasi-subordination, *Palestine Journal of Mathematics*, 5(1) (2016),79-85.
- [13] D.V. Krishna and T. R. Reddy, Second Hankel determinant for the class of Bazilevic functions, *Stud. Univ.Babes-Bolyai Math.* 60(3)(2015), 413–420.
- [14] W. Ma and D. Minda, A unified treatment of some special classes of univalent functions, *Proceedings of the conference on complex analysis*, Z. Li, F. Ren, L. Yang and S. Zhang, eds., Int. Press, (1994), 157-169.
- [15] R. Mendiratta, S. Nagpal and V. Ravichandran, On a subclass of strongly starlike functions associated with exponential function, *Bull. Malays. Math. Sci. Soc.*, 38(1) (2015), 365–386.
- [16] H. Orhan, N. Magesh, and ,J. Yamini, Bounds for the second Hankel determinant of certain bi-univalent functions, *Turkish Journal of Mathematics*, 40(3) (2016),679-687.
- [17] G. Polya, I. J. Schoenberg, Remarks on de la Vallee Poussin means and convex conformal maps of the circle, *Pac. J. Math.*, 8(2) (1958), 259–334.

- [18] C. Pommerenke, On the coefficients and Hankel determinants of univalent functions, J. Lond. Math. Soc.1(1) (1966), 111–122.
- [19] C. Pommerenke, On the Hankel determinants of univalent functions, Mathematika, 14(1) (1967), 108–112.
- [20] I. A. R. Rahman, W. G. Atshan and G. I. Oros, New concept on fourth Hankel determinant of a certain subclass of analytic functions, Afrika Matematika, (2022) 33:7, 1-15.
- [21] H. M. Srivastava, S. Altinkaya and S.Yalcin, Hankel determinant for a subclass of bi – univalent functions defined by using a symmetric q -derivative operator, Filomat, 32(2) (2018), 503–516.
- [22] H. M. Srivastava, S. Owa, S. (Eds.), *Current Topics in Analytic Function Theory*; World Scientific Publishing Company: London, UK, (1992).
- [23] H. M. Srivastava, Q. Z Ahmad, N. Khan and B. Khan, Hankel and Toeplitz determinants for a subclass of q -starlike functions associated with a general conic domain, Mathematics,7(2) (2019), 181, 15 pages.
- estimate problems, Applied Mathematics Comput., 218(23) (2012), 11461-11465.
- [24] S. Yalcin, W. G. Atshan and H. Z. Hassan, Coefficients assessment for certain subclasses of bi-univalent functions related with quasi-subordination, Publications De L'Institut Mathematique, Nouvelle série, tome 108(122)(2020), 155-162.

Some Concepts and Their Relationships with Neutrosophic Quasi-Frobenius Rings

^{1,*}Omar A. Khashan

²Majid M. Abed²

¹Department of Mathematics, College of Computer Sciences and Mathematics, University of
Tikrit,

Tikrit, Iraq.

²Department of Mathematics, College of Education for Pure Science, University Of Anbar,
Ramadi, Anbar, Iraq.

Emails: omar1990@st.tu.edu.iq^{1,*}; majid_math@uoanbar.edu.iq²

Some Concepts and Their Relationships with Neutrosophic Quasi-Frobenius Rings

Omar A. Khashan^{1,*} and Majid M. Abed²

¹Department of Mathematics, College of Computer Sciences and Mathematics, University of Tikrit, Tikrit, Iraq.

²Department of Mathematics, College of Education for Pure Science, University Of Anbar, Ramadi, Anbar, Iraq.

Emails: omar1990@st.tu.edu.iq^{1,*}; majid_math@uoanbar.edu.iq

Abstract

Within this research, we will study the relationships between Neutrosophic torsionless cyclic $(R \cup I)$ -module and Neutrosophic quasi-Frobenius rings. Some implications yield cyclic $(R \cup I)$ -module and hence Neutrosophic quasi-Frobenius ring have been presented. In addition we study the relations between isomorphic Neutrosophic Noetherian ring and Neutrosophic quasi-Frobenius (Q-F) ring. Additionally, we present an important relation between Neutrosophic torsionless cyclic module, projective module and Neutrosophic injective module which through we get an Q-F ring. Finally, we study some concepts such as; Neutrosophic hollow module, Neutrosophic local module and Neutrosophic simple module which its relationship to the quasi-Frobenius rings.

Keywords: Quasi-Frobenius rings, Noetherian rings, torsionless, cyclic module, Hollo Module.

المستخلص

في هذا البحث، ندرس العلاقات بين المقاسات النيوتروسوفية الدورية الخالية من الالتواء (Neutrosophic torsionless cyclic module) والحلقات النيوتروسوفية شبه فروبينوس (Neutrosophic quasi-Frobenius rings). وقد تم تقديم بعض النتائج التي تؤدي إلى تكون مقاسات دورية، ومن ثم إلى حلقة نيوتروسوفية شبه فروبينوس. بالإضافة إلى ذلك، ندرس العلاقات

بين الحلقة النيوتروسوفية النويثيرية المتماثلة (isomorphic Neutrosophic Noetherian ring)، والحلقة النيوتروسوفية شبه فروبينوس (Q-F ring). كما نعرض علاقة مهمة بين المقاسات النيوتروسوفية الدورية الخالية من الالتواء، والمقاسات النيوتروسوفية الإسقاطية (Neutrosophic projective module)، والمقاسات النيوتروسوفية الحقنية (Neutrosophic injective module)، والتي من خلالها يمكن الحصول على حلقة Q-F. وأخيرًا، ندرس بعض المفاهيم مثل: المقاسات النيوتروسوفية الجوفاء (Neutrosophic hollow module)، والمقاسات النيوتروسوفية المحلية (Neutrosophic local module)، والمقاسات النيوتروسوفية البسيطة (Neutrosophic simple module)، وعلاقتها بحلقات شبه فروبينوس.

1. Introduction

A Neutrosophic Artinian ring is a Neutrosophic ring that satisfies the descending chain condition on (one-sided) ideals; that is, there is no infinite descending sequence of ideals. A Neutrosophic ring R is referred to as quasi-Frobenius if it is (left or right) self-injective and (left or right) Artinian, equivalently, on which side it is self-injective and which side it is Noetherian. A right n -injective ring R is defined as one in which each homomorphism of an n -generated right ideal to R extends into an endomorphism of R . This definition is one of several generalizations of the notion of self-injective rings. [1]. The concept of rings that are Frobenius and quasi-Frobenius are generalized by many authors. In (1941), Nakayama, Tadasi presented a study on Frobeniusian algebra [2]. In (1950), Ikeda, Masatoshi and Tadasi Nakayama submitted a study about supplementary remarks on Frobeniusian algebras [3]. In (1956), the author studied both Hiroyuki Tachikawa, Kiiti Morita, and Morita Quasi Frobenius rings, character modules, and free module submodules [4]. In (1958), Dieudonne', Jean provided some remarks about quasi-Frobenius rings [5]. In (1964), E. A. Walker and Carl Faith proposed the concept about quasi-Frobenius rings on characterizations [6]. And in (1996), Dinh van huynh demonstrated in her study A Note on quasi- Frobenius rings [7]. Sets of fuzzy and Sets of intuitionistic fuzzy have a generalization which is the Neurosophic

set. According to Neutrosophic reasoning, There are three levels to a proposition: truth (T), indeterminacy (I), and falsehood (F). There is a membership function for each component level of involvement in the uncertainty issue, according to fuzzy set theory [8]. After that, in 1983, K. Atanassov expanded fuzzy sets to include intuitionistic fuzzy sets on universe X . In these sets, in addition to Membership degree $\mu_A(x_0) \in [0,1]$ for any element x_0 to set A , non-members may also get a degree to function $\nu_A(x_0) \in [0,1]$ that are present, where $x_0 \in X, \mu_A(x_0) + \nu_A(x_0) \leq 1$ [9].

2. Basic Concepts

In the present section, some fundamental terms that will be used later on are defined.

Definition 2.1 [10]. Consider X as an universal set. Then a fuzzy set A within X consists of ordered pairs; $A := \{(x, \mu_A(x)) : x \in X\}$ s.t, $\mu_A : X \rightarrow [0,1]$, that is known as the function for membership with $x \in X$, the value from $\mu_A(x)$ represents the grade of membership of x in A .

Example 2.2: The universal set X is the group of people. The issue of whether person x is young is addressed to that extent by the definition of B fuzzy subset young? To each person in the universal set, We must allocate a degree for membership inside the fuzzy subset "young." The most straightforward method to do this is using the function of membership based on the individual's age.

$$\mu_B(x) = \begin{cases} 1, & \text{age}(x) \leq 20 \\ (30 - \text{age}(x))/10, & 20 \leq \text{age}(x) \leq 30 \\ 0, & \text{age}(x) > 30 \end{cases}$$

Definition 2.3 [11]. Assume that G is any group. Then this mapping $\mu: G \rightarrow [0,1]$ forms the fuzzy group if $\forall a, b \in G$:

- 1) $\mu(ab) \geq \min \{ \mu(a), \mu(b) \}$.
- 2) $\mu(a^{-1}) = \mu(a)$.

Example 2.4: Here we have the set S , which contains all possible random variables for the space of probabilities (Ω, φ, P) and suppose that A is any subset of the reals that is Borel and includes all subgroups from the reals that are addizable. Note that S is a groupoid when added pointwise. (The extra structure is not necessary for our current goals, even if S is a group.) A function $\varphi_A: S \rightarrow [0, 1]$ define by $\varphi_A(X) = P\{w \in \Omega : X(w) \in A\} = P[X^{-1}(A)]$. Therefore, φ_A represents the probabilities that X is “in” the subgroup A . A fuzzy subgroupoid is an obvious choice for the function φ_A .

Definition 2.5 [12]. Assume that R is a ring, A is a fuzzy set of R , we will refer to A as a fuzzy ring of R , if

- 1) $A(a - b) \geq A(a) \wedge A(b), \forall a, b \in R$.
- 2) $A(ab) \geq A(a) \wedge A(b), \forall a, b \in R$.

Example 2.6: Consider the set $R = \{0, x, y\}$, which contains a binary operation (\cdot) and a hyperoperation $(+)$ as follows:

+	0	x	y
0	{0}	{x}	{y}
x	{x}	{0, x, y}	{x, y}
y	{y}	{x, y}	{0, x, y}

Consequently a

·	0	x	y
0	0	0	0
x	0	x	y
y	0	x	y

ring $(R, +, \cdot)$ is a hypernear. A fuzzy set $\mu: R \rightarrow [0, 1]$ define by $\mu(x) = \mu(y) = 0.5$ and $\mu(0) = 1$. Checking that μ is a fuzzy subhypernear ring from R may be done using basic computations.

Definition 2.7 [13]. Assume that R is a ring. We refer to the fuzzy subset λ of R as a fuzzy ideal in R if $\forall x, y \in R$,

- 1) $\lambda(x - y) \geq \min\{\lambda(x), \lambda(y)\}$.
- 2) $\lambda(xy) \geq \max\{\lambda(x), \lambda(y)\}$.

Example 2.8: Consider R is a ring. A fuzzy subset λ defined by: $\lambda(x) = r, \forall x \in R$ and $r \in [0, 1]$, then λ is a fuzzy ideal in R .

Note: If we replace $[0, 1]$ with $\{0, 1\}$ in the above definition, then a fuzzy ideal is just the usual real ideal.

Definition 2.9 [14]. Assume that a fixed set A is non-empty. The Neutrosophic set S is an object having the format: $S = \{\langle A, \mu_S(a), \sigma_S(a), \gamma_S(a) \rangle : a \in A\}$ where $\mu_S(a), \sigma_S(a)$ and $\gamma_S(a)$ represent a membership function's degree namely $\mu_S(a), \sigma_S(a)$ represents the degree of indeterminacy while $\gamma_S(a)$ represents a degree from non-membership for any $a \in A$ of S .

Example 2.10: Assuming the universe from discourse $U = \{x_1, x_2, x_3\}$, where x_1 describes the capacity, x_2 describes the reliability and x_3 represents the item prices. Another such assumption is that the values of x_1, x_2 and x_3 located in $[0, 1]$. These are derived from surveys completed by professionals. Professionals have the option to enforce their views in three areas: the degree to which things' qualities may be explained by their goodness, indeterminacy, or poverty. Assume that A is a set of Neutrosophic (NS) on U , where, $A = \{\langle x_1, (0.3, 0.5, 0.6) \rangle, \langle x_2, (0.3, 0.2, 0.3) \rangle, \langle x_3, (0.3, 0.5, 0.6) \rangle\}$, such that 0.3 is the degree for capacity goodness, degree for capability indeterminacy is 0.5 and 0.6 is the degree of capacity falsehood, etc.

Definition 2.11 [15]. Assume any ring as R . Another ring that may be generated underneath the operations of R by R and I is the Neutrosophic ring $(R \cup I)$.

Example 2.12: Assume that Z be any ring of integers; $(Z \cup I) = \{z_1 + z_2 I : z_1, z_2 \in Z\}$. An integer ring referred as the Neutrosophic ring is $(Z \cup I)$. Also $Z \subseteq (Z \cup I)$.

Definition 2.13 [16]. Let $\mu = (\mu^L, \mu^J, \mu^E)$ be any non-empty Neutrosophic subset of a β -semiring A (i.e. anyone of $\mu^L(a), \mu^J(a)$ or $\mu^E(a) \neq 0; a \in A$). Then μ referred to as a Neutrosophic left ideal of $A, \forall a, b \in A$ and $\psi \in \beta$ if:

- i. $\mu^L(a + b) \geq \min\{\mu^L(a), \mu^L(b)\}, \mu^L(a \psi b) \geq \mu^L(b)$
- ii. $\mu^J(a + b) \geq \frac{\mu^J(a) + \mu^J(b)}{2}, \mu^J(a \psi b) \geq \mu^J(b)$
- iii. $\mu^E(a + b) \leq \max\{\mu^E(a), \mu^E(b)\}, \mu^E(a \psi b) \leq \mu^E(b)$.

In the same way, the Neutrosophic right ideal of A may be defined.

Example 2.14: A and γ are the semigroups of all not positive integers and all not positive even integers respectively that are additive and commutative. After that A is a β -semiring if $a \psi b$ represents the represents multiplication from integers a_1, ψ, a_2 where $a_1, a_2 \in A$ and $\psi \in \beta$. Define a Neutrosophic subset μ of A as follows

$$\mu(w) = \begin{cases} (1, 0, 0) & \text{if } w = 0 \\ (0.8, 0.3, 0.4) & \text{if } w \text{ is even} \\ (0.3, .02, 0.7) & \text{if } w \text{ is odd} \end{cases}$$

Then μ of A is an ideal that is Neutrosophic.

Definition 2.15 [17]. Remember that in order for a ring A to be considered Noetherian, it must meet the following three comparable requirements:

- (1) maximum elements (the maximum condition) exist in all nonempty sets from ideals of A .
- (2) Every ascending sequences of ideals are stationary (the ascending chain condition (A.C.C.))

(3) Every ideal of A is f-generated.

Definition 2.16 [18]. An R -module is considered free if it is isomorphic to another R -module of the type $\bigoplus_{i \in I} M_i$, where each $M_i \cong R$ (in the sense that it is an R -module). The notation for such a module is $R^{(I)}$.

Definition 2.17 [6]. Let R be a ring, M be R -module and defined $\sigma_M: M \rightarrow M^{**}$ as: $[\sigma_M(m_0)](f) = f(m_0), f \in M^*, m_0 \in M$. Then M is torsionless iff σ_M is a R -monomorphism.

Definition 2.18 [19]. Assuming that M be an R -module also let $m_i \in M, \forall i \in I$, s.t. I represents some indexing set. Now if $M = \sum_{i \in I} Am_i$, then $\{m_i | i \in I\}$ is referred to as the set generators of M .

Definition 2.19 [19]. For R -modules M with an finite number from generators, so we say to be it is finitely generated.

Definition 2.20 [20]. If $Z(M) = M$, such that $Z(M) = \{m \in M : mI = (0)\}$, for some essential ideal I of R . Then R -module M is said to be singular.

Definition 2.21 [21]. If for every homomorphisms R -module $\phi: N \rightarrow W$ and $\psi: N \rightarrow M$ where ϕ is injective, there exists an R -linear homomorphism $\Omega: W \rightarrow M$ such that $\Omega \circ \phi = \psi$. Then R -module M is said to be injective.

Definition 2.22 [22]. Let $M \oplus K$ is the free R -module s.t. K is each module on R . After that an R -module M is said to be projective.

Definition 2.23 [23]. All proper submodules of the non-zero R -module M must be small submodules of M for M to be a hollow module.

Definition 2.24 [24]. The R -module M that is non-trivial is referred to as semi hollow if all proper submodule from M is a semi small submodule from M .

Definition 2.25 [18]. An R -module M is referred to as local lifting if a module M have the maximal submodule N that is unique. There are a submodules A and B of N where $M = A \oplus B$ and $N \cap B$ is small submodule of B .

3. Auxiliary results

We begin with the following lemmas which needs its in the our main results.

Lemma 3.1. [25]. Consider a ring R is Noetherian. Hence, the following criteria are equivalent:

- 1) R is an Q-F ring.
- 2) All R -module is submodule from free R -module.
- 3) All R -module is torsionless.
- 4) All f-generated R -module is torsionless.
- 5) All f-generated R -module represents submodule of an free R -module.

Lemma 3.2. [26]. Assume that C is an cyclic R -module. We say $C = R/A$ such that A is an ideal in R .

- 1) $C^* \cong \text{ann}(A)$ as an R -modules.
- 2) C is torsionless if and only if A is annihilator.
- 3) C is reflexive if and only if A is annihilator and all R -homomorphism $\text{ann}(A) \rightarrow R$ yields the result of multiplying by an element of R .

Lemma 3.3. [27]. The ring R is said to be Q-F iff it is a ring that is Noetherian in addition to relationships $s(d(I)) = I$ and $d(s(J)) = J$ are applicable for all ideals J and I from R .

Lemma 3.4. [28]. Assume that M is a module. Then a module M is considered an f -generated hollow module iff it has a unique maximum submodule and is cyclic.

Lemma 3.5. [29]. The Noetherian state of $R/\text{socle}(R)$ and the injectivity from every simple $R/\text{socle}(R)$ -modules follow based on the reality that every cyclic singular R -modules are injective.

Lemma 3.6. [30].

Consider the ring R where each cyclic is injective. In such case, R is an Artinian semi simple.

Lemma 3.7. [31]. These two options are analogous:

- 1) All cyclic modules in a ring R are extensions from injective modules in a projective module.
- 2) It is true that all singular module certainly injective.

Lemma 3.8. [18]. Assume that the module M is an f -generated. Then M is local lifting iff M has a unique maximum submodule and is cyclic.

Lemma 3.9. [18]. Assume that M is an R -module. M/N is local lifting module if M is local lifting module for all N proper submodule of M .

Lemma 3.10. [18]. Every a local lifting module is indecomposable module.

Lemma 3.11. [18]. Assume that M is R -module. A module M is local lifting iff M is a lifting and cyclic module.

4. Main Results

In this part, we present some different rings and modules and their relationship with the Neutrosophic Quasi-Frobenius Ring.

Definition 4.1. A Neutrosophic ring $(R \cup I)$ is referred to as Neutrosophic self-injective ring if $(R \cup I)$ represents injective as the Neutrosophic module on itself (i.e., $(R \cup I)$ is Neutrosophic injective as a left or right $(R \cup I)$ -module).

Example 4.2: Let $(R \cup I) = (Z \cup I)/n(Z \cup I)$ for any integer $n \geq 1$. Then $(R \cup I)$ is a Neutrosophic self-injective. Because $(Z \cup I)/n(Z \cup I)$ is a finite Neutrosophic ring, hence Neutrosophic Artinian, and it is Neutrosophic quasi-Frobenius ring implies that it is Neutrosophic self-injective. In addition, as a Neutrosophic module over itself, every homomorphism from a Neutrosophic ideal into $(R \cup I)$ extends to all of $(R \cup I)$. Thus, $(Z \cup I)/n(Z \cup I)$ is a Neutrosophic self-injective ring.

Definition 4.3. A Neutrosophic ring $(R \cup I)$ is said to be Neutrosophic Artinian if $(R \cup I)$ satisfies the descending chain condition (D.C.C): all descending chain from Neutrosophic ideals of $(R \cup I)$, $(K_0 \cup I) \supseteq (K_1 \cup I) \supseteq \dots \supseteq (K_n \cup I) \supseteq (K_{n+1} \cup I) \supseteq \dots$ is stationary.

Example 4.4: Assume $(K(t) \cup I)$ is the Neutrosophic polynomial ring in the variable t accompanied with coefficients in a Neutrosophic field K . Then for each positive integer n , the residue ring consisting of $(K(t) \cup I)/(t^n)$ is both Neutrosophic Artinian and Noetherian. Reason being, a vector space $(K(t) \cup I)/(t^n)$ is finite and has n dimensions.

Definition 4.5. Any Neutrosophic ring that does not have an infinite escalating chain from right (or left) Neutrosophic ideals is referred to as left (or right) Neutrosophic Noetherian.

In this particular instance from above definition we say that the ring satisfy the (A.C.C) on the left (or right) Neutrosophic ideals.

Note: A Neutrosophic ring $(R \cup I)$ is called Neutrosophic Noetherian if it is Neutrosophic Noetherian both left and right.

Example 4.6: Consider the Neutrosophic ring from integers $(\mathbb{Z} \cup I)$. Look at an Neutrosophic ideal in $(\mathbb{Z} \cup I)$ of the form $(K \cup I) = (6I) = \{6nI \mid nI \in (\mathbb{Z} \cup I)\}$ are f-generated by the single element $6I$. In fact, every Neutrosophic ideal in $(\mathbb{Z} \cup I)$ is generated by one integer. Therefore, all Neutrosophic ideals are f-generated. Hence $(\mathbb{Z} \cup I)$ is an Neutrosophic Noetherian ring.

Definition 4.7. If $(R \cup I)$ is a Neutrosophic self-injective and Neutrosophic Artinian ring, or if it is Neutrosophic self-injective and Neutrosophic Noetherian ring, then it can be called Neutrosophic Q-F ring.

Example 4.8: Where m is any positive integer and $(R \cup I)$ represents an Neutrosophic integers ring. After that, an Neutrosophic quotient integers ring modulo m is Neutrosophic Q-F ring because $(R \cup I)$ is an Neutrosophic commutative, finite and primary ideal.

Theorem 4.9. An Neutrosophic Noetherian ring $(R \cup I)$ is referred to as Q-F iff all cyclic $(R \cup I)$ -module is torsionless.

Proof: Assuming that $(R \cup I)$ is Neutrosophic Q-F, we know from [32, Exercise 15.7] also Lemma 3.1, all Neutrosophic $(R \cup I)$ -module is torsionless.

Conversely, assuming all Neutrosophic cyclic $(R \cup I)$ -module is torsionless. Through Lemma 3.2, we have each Neutrosophic ideal from $(R \cup I)$ is annihilator. Considering $(R \cup I)$ is Neutrosophic Noetherian, $(R \cup I)$ is Neutrosophic Q-F from Lemma 3.3.

Theorem 4.10. All torsionless cyclic Neutrosophic $(R \cup I)$ -modules that not isomorphic into R and are injective are defined for a Neutrosophic ring $(R \cup I)$. After that $(R \cup I)$ is Q-F ring.

Proof: Assuming $(R \cup I)$ is the Neutrosophic ring also assume that $(M \cup I)$ is Neutrosophic torsionless cyclic module and it is not isomorphic into $(R \cup I)$ is injective. Then Lemma 3.5, refer to $(R \cup I)/\text{socle}(R \cup I)$ is a Neutrosophic Noetherian. If $\text{socle}(R \cup I) \neq 0$, after that $(R \cup I)/\text{socle}(R \cup I)$ is a Neutrosophic semi simple Artinian by Lemma 3.6, because all quotient of that is annihilated through $\text{socle}(R \cup I)$, and $(R \cup I)$ is not. Assume $(R \cup I) \neq \text{socle}(R \cup I)$. Let $yI \in (R \cup I)$, $yI(R \cup I)/\text{socle}(yI(R \cup I))$ simple. If $\text{socle}(yI(R \cup I))$ is length that is not finite, afterward

$$\text{socle}(yI(R \cup I)) = S \oplus T \oplus U,$$

where the lengths of S, T and U are infinite. Because for $yI(R \cup I)$ then S is not direct summand, $yI(R \cup I)/S$ is not projective. Hence $yI(R \cup I)/S$ is injective. Then $T \oplus U$ embeds in $yI(R \cup I)/S$, and $yI(R \cup I)JS = E(T) \oplus E(U) \oplus K$ Regarding a few injective hulls related to U and T . Then $yI(R \cup I)/(S \oplus T \oplus U) \approx E(T)/T \oplus E(U)/U \oplus K$ It's not simple, an incongruity. Consequently the socle from $yI(R \cup I)$ has the length a finite. Since any simple submodule from $(R \cup I)$ is injective, the socle from $yI(R \cup I)$ is direct summand from $yI(R \cup I)$ also $yI \subset \text{socle}(R \cup I)$. Consequently $(R \cup I) = \text{socle}(R \cup I)$ is semi simple Artinian. Hence $(R \cup I)$ is Neutrosophic Noetherian ring. Consequently, through Theorem 4.9, $(R \cup I)$ is Q-F ring.

Theorem 4.11. Consider $(R \cup I)$ is the Neutrosophic ring and all cyclic module that is Neutrosophic and torsionless is the direct sum from two modules, one projective and one injective, in that ring. Then the ring $(R \cup I)$ is Q-F.

Proof: By Lemma 3.7, every Neutrosophic $(R \cup I)$ -module singular is a Neutrosophic injective, and through Lemma 3.5, we have that $(R \cup I)/\text{socle}(R \cup I)$ is a Neutrosophic Noetherian. By the outcome from the chatter [33, Theorem 3.11], all that has to be shown is that each cyclic module that is direct sum from two modules: one projective and one Neutrosophic Noetherian. This is going to ensue if all Neutrosophic cyclic injective module is Neutrosophic Noetherian. Assume $(R \cup I)$ is a Neutrosophic injective cyclic $(R \cup I)$ -module, also assume $S = \text{socle}(R \cup I)$. After that $x(R \cup I)/xS$ is cyclic $(R \cup I)/S$ -module consequently Noetherian. Should xS does not have a finite length, it will decomposition into a direct sum $\bigoplus_{i=0}^{\infty} X_i$, where the length of any X_i is infinite. Let E_i be an injective hull from X_i in $x(R \cup I)$. As a result, E_i is not semi-simple and has an indefinite length as it is cyclic. Then $x(R \cup I)/xS$ includes the infinite direct sum $\bigoplus_{i=0}^{\infty} E_i/X_i$, contradicting the property that $x(R \cup I)/xS$ is Noetherian. Consequently, through Theorem 4.9, $(R \cup I)$ is Q-F ring.

Theorem 4.12. A Neutrosophic Noetherian ring $(R \cup I)$ is referred to as Neutrosophic Q-F iff all torsionless $(R \cup I)$ -module is f-generated hollow.

Proof: Assuming that $(R \cup I)$ is Neutrosophic Noetherian Q-F ring, also assume $(M \cup I)$ be a Neutrosophic torsionless $(R \cup I)$ -module. After that through Theorem 4.9, we have a module $(M \cup I)$ is cyclic. We claim, $(M \cup I)$ having a unique maximal Neutrosophic submodule, say $(E \cup I)$, then $(M \cup I)$ be a Neutrosophic f-generated. Let $(L \cup I)$ be a proper Neutrosophic submodule

from $(M \cup I)$ with $(K \cup I) + (D \cup I) = (M \cup I)$, where $(D \cup I)$ is the submodule of $(M \cup I)$. Now, if $(D \cup I) \neq (M \cup I)$, then $(D \cup I)$ is a proper submodule from $(M \cup I)$, and hence $(D \cup I)$ is contained in a submodule that is maximal, since $(M \cup I)$ f-generated. However, through our claim $(M \cup I)$ has a submodule $(E \cup I)$ that is unique maximal, consequently $(K \cup I)$ is contained in $(E \cup I)$. Therefore, $(K \cup I) + (E \cup I) = (E \cup I) = (M \cup I)$, which is a contradiction. Hence, $(D \cup I) = (M \cup I)$, thus, $(K \cup I) \ll (M \cup I)$. That is, $(M \cup I)$ is a hollow module. Consequently, through Lemma 3.4, $(M \cup I)$ is f-generated hollow module.

Conversely, assuming that $(M \cup I)$ be a Neutrosophic torsionless f-generated hollow module, then

$$(M \cup I) = (R \cup I)m_1I + (R \cup I)m_2I + \cdots + (R \cup I)m_nI$$

for $m_iI \in (M \cup I)$ and $i = 1, 2, \dots, n$ if $(M \cup I) \neq (R \cup I)m_1I$, then $(R \cup I)m_1I$ is a proper submodule of $(M \cup I)$, which implies that $(R \cup I)m_1I \ll (M \cup I)$. Hence,

$$(M \cup I) = (R \cup I)m_2I + (R \cup I)m_3I + \cdots + (R \cup I)m_nI$$

Just keep going back to this line of reasoning until we get $(M \cup I) = (R \cup I)m_iI$ for some i . Thus $(M \cup I)$ is a cyclic module. And from the hypothesis $(M \cup I)$ is torsionless, consequently, by Theorem 4.9, $(R \cup I)$ is a Neutrosophic Q-F ring.

Theorem 4.13. An Neutrosophic Noetherian ring $(R \cup I)$ is referred to as Neutrosophic Q-F iff all torsionless $(R \cup I)$ -module is f-generated semi hollow.

Proof: Assuming that $(R \cup I)$ is an Neutrosophic Noetherian Q-F ring, and assume $(M \cup I)$ is a torsionless $(R \cup I)$ -module. Then by Theorem 4.9, we have $(M \cup I)$ represents Neutrosophic cyclic $(R \cup I)$ -module. After that it is

Neutrosophic f -generated and consequently all proper Neutrosophic submodule of $(M \cup I)$ contained in maximal Neutrosophic submodule, but by Lemma 3.4, $(M \cup I)$ has a Neutrosophic submodule that is unique maximal. Therefore is a Neutrosophic semihollow module.

Conversely, assuming that $(M \cup I)$ is a torsionless semihollow and a f -generated, therefore it is local. Consequently, is a Neutrosophic hollow and we have f -generated. Hence is a Neutrosophic cyclic and then by Theorem 4.9, $(R \cup I)$ is Q-F ring.

Theorem 4.14. Assuming that $(M \cup I)$ is non-zero Neutrosophic module. Then an Neutrosophic Noetherian ring $(R \cup I)$ is referred to as a Neutrosophic Q-F iff every Neutrosophic torsionless $(R \cup I)$ -module is hollow and $Rad (M \cup I) \neq (M \cup I)$.

Proof: Assuming that a ring $(R \cup I)$ is the Neutrosophic Noetherian Q-F, and assume $(M \cup I)$ be a torsionless Neutrosophic hollow module, then by Theorem 4.9, $(M \cup I)$ represents Neutrosophic cyclic module. After that $(M \cup I)$ is the Neutrosophic f -generated module. Consequently, $(M \cup I)$ has a submodule that is maximal, which suggests that $Rad (M \cup I) \neq (M \cup I)$.

Conversely, assume that $(M \cup I)$ is a torsionless hollow module and $Rad (M \cup I) \neq (M \cup I)$, then $Rad (M \cup I) \ll (M \cup I)$. also through Lemma 3.4, $Rad (M \cup I)$ is the maximal submodule that is unique from $(M \cup I)$ and thus $(M \cup I)/Rad (M \cup I)$ represents simple module and hence cyclic. We claim that $(M \cup I) = (R \cup I)mI$. Let $wI \in (M \cup I)$ then $wI + Rad (M \cup I) \in (M \cup I)/Rad (M \cup I)$, and therefore there is $rI \in (R \cup I)$ s.t. $wI + Rad (M \cup I) = rI(mI + Rad (M \cup I)) = (rI)(mI) + Rad (M \cup I)$. i.e., $wI - (rI)(mI) \in Rad (M \cup I)$, which implies that $wI - (rI)(mI) = y$ for

some $y \in \text{Rad}(M \cup I)$. Thus
 $wI = (rI)(mI) + y \in (R \cup I)mI + \text{Rad}(M \cup I)$, hence
 $(M \cup I) = (R \cup I)mI + \text{Rad}(M \cup I)$. But $\text{Rad}(M \cup I) \ll (M \cup I)$ implies
 $(M \cup I)$ cyclic $(R \cup I)$ -module. Consequently, through Theorem 4.9, the ring
 $(R \cup I)$ is Q-F.

Theorem 4.15. Consider $(M \cup I)$ be the non-zero Neutrosophic module. Then the Neutrosophic Noetherian ring $(R \cup I)$ is referred to as Q-F iff every Neutrosophic torsionless $(R \cup I)$ -module is semihollow Plus $\text{Rad}(M \cup I) \neq (M \cup I)$.

Proof: Assuming that a ring $(R \cup I)$ is Neutrosophic Noetherian Q-F, and assuming $(M \cup I)$ is Neutrosophic torsionless semihollow module, then by Theorem 4.9, We possess a module $(M \cup I)$ is the Neutrosophic cyclic. After that $(M \cup I)$ represents f-generated $(R \cup I)$ -module. Thus, $(M \cup I)$ has a submodule that is maximal, which suggests that $\text{Rad}(M \cup I) \neq (M \cup I)$.

Conversely, assume $(M \cup I)$ is an Neutrosophic torsionless semihollow and $\text{Rad}(M \cup I) \neq (M \cup I)$, therefore $(M \cup I)$ is a local Consequently $(M \cup I)$ Neutrosophic cyclic $(R \cup I)$ -module. Consequently, through Theorem 4.9, $(R \cup I)$ represents Neutrosophic Q-F ring.

Theorem 4.16. A Neutrosophic Noetherian ring $(R \cup I)$ is referred to as Q-F if all Neutrosophic torsionless $(R \cup I)$ -module is simple.

Proof: Assuming that $(R \cup I)$ be the Neutrosophic Noetherian ring and assume $(M \cup I)$ is an Neutrosophic torsionless simple module and $mI \in (M \cup I)$. Both $(R \cup I)mI$ and $B = \{cI \in (M \cup I) \mid (R \cup I)cI = 0\}$ are submodules from $(M \cup I)$. Because $(M \cup I)$ is an Neutrosophic simple, then any of them is either

0 or $(M \cup I)$. But $(R \cup I)(M \cup I) \neq 0$ leads to $B \neq (M \cup I)$. Consequently $B = 0$, whence $(R \cup I)aI = (M \cup I)$ for every non-zero $mI \in (M \cup I)$. Therefore $(M \cup I)$ is cyclic. Consequently, through Theorem 4.9, $(R \cup I)$ represents Neutrosophic Q-F ring.

Theorem 4.17. A Neutrosophic Noetherian ring $(R \cup I)$ is referred to as Neutrosophic Q-F iff every torsionless Neutrosophic $(R \cup I)$ -module is an local.

Proof: Assuming that the Neutrosophic Noetherian ring $(R \cup I)$ is Q-F, and assume $(M \cup I)$ be an Neutrosophic torsionless $(R \cup I)$ -module. After that by Theorem 4.9, we possess $(M \cup I)$ is cyclic $(R \cup I)$ -module also through Theorem 4.12, $(M \cup I)$ is a f-generated hollow. Hence $(M \cup I)$ has a submodule that is maximal say $(E \cup I)$. Assume the proper submodule from $(M \cup I)$ is $(K \cup I)$, if $(K \cup I)$ is not contained in $(E \cup I)$, then $(K \cup I) + (E \cup I) = (M \cup I)$, but $(M \cup I)$ is a hollow module, thus $(E \cup I) = (M \cup I)$, consequently, a contradiction arises. This suggests that each appropriate submodule of $(M \cup I)$ is found in $(E \cup I)$, i.e., $(M \cup I)$ has a maximal submodule that is unique and contains all proper submodule from $(M \cup I)$. Hence $(M \cup I)$ is a local module.

Conversely, assuming $(M \cup I)$ is Neutrosophic torsionless local $(R \cup I)$ -module then it has the maximal submodule $(E \cup I)$ that is unique by definition of local module which contains every proper submodule from $(M \cup I)$. Assuming $wI \in (M \cup I)$ with $wI \notin (E \cup I)$ afterward $(R \cup I)wI$ is a submodule from $(M \cup I)$. We argue that $(R \cup I)wI = (M \cup I)$. If not $(R \cup I)wI$ is an proper submodule from $(M \cup I)$, hence $(R \cup I)wI \leq (E \cup I)$ that means $wI \in (E \cup I)$ this results in a contradiction. Thus, $(M \cup I)$ is

Neutrosophic cyclic module. Consequently, by Theorem 4.9, $(R \cup I)$ is Q-F ring.

Theorem 4.18. A Neutrosophic Noetherian ring $(R \cup I)$ is referred to as Neutrosophic Q-F if $(M \cup I)$ is an Neutrosophic torsionless and local lifting $(R \cup I)$ -module and $Rad(M \cup I) \neq (M \cup I)$.

Proof: Assuming that the Neutrosophic ring $(R \cup I)$ is an Noetherian and $(M \cup I)$ is an Neutrosophic torsionless and local lifting $(R \cup I)$ -module and $Rad(M \cup I) \neq (M \cup I)$, thus, there is a unique maximal submodule $(N \cup I)$ of $(M \cup I)$ and each submodule from $(N \cup I)$. Here exists submodules $(E \cup I)$ and $(F \cup I)$ from $(N \cup I)$ where $(M \cup I) = (E \cup I) \oplus (F \cup I)$ and $(N \cup I) \cap (F \cup I)$ is small submodule of $(F \cup I)$. After that $(M \cup I) = (M \cup I) \oplus \{0\}$, where $\{0\}$ is submodule of $(N \cup I)$, $(N \cup I) \cap (M \cup I) = (N \cup I)$ and since $(M \cup I)$ is a local lifting module. Then $(N \cup I) \cap (M \cup I) = (N \cup I)$ is small submodule from $(M \cup I)$. Thus $(M \cup I)$ is an Neutrosophic hollow module. Hence through Theorem 4.14, $(R \cup I)$ is Q-F ring.

Theorem 4.19. Let $(M \cup I)$ represents the Neutrosophic torsionless $(R \cup I)$ -module. Then a Neutrosophic Noetherian ring $(R \cup I)$ is referred to as Neutrosophic Q-F if $Rad(M \cup I)$ is small and maximal Neutrosophic submodule in $(M \cup I)$.

Proof: Assuming that the Neutrosophic ring $(R \cup I)$ is an Noetherian also assume $(M \cup I)$ is an Neutrosophic torsionless $(R \cup I)$ -module. Suppose that $Rad(M \cup I)$ is a small and maximal submodule in $(M \cup I)$. First we want to demonstrate that $Rad(M \cup I)$ is a maximal submodule in $(M \cup I)$ that is

unique. suppose $(D \cup I)$ is another submodule in $(M \cup I)$ that is maximal, then $(M \cup I) = (D \cup I) + \text{Rad}(M \cup I)$, but $\text{Rad}(M \cup I) \ll (M \cup I)$ which implies that $(D \cup I) = (M \cup I)$, which is a contradiction. Thus $\text{Rad}(M \cup I)$ is a maximal submodule in $(M \cup I)$ that is unique. We assert ownership of all proper submodule from $(M \cup I)$ found in $\text{Rad}(M \cup I)$. Assuming $(E \cup I)$ represents proper submodule from $(M \cup I)$, so if $(E \cup I)$ is not contained in $\text{Rad}(M \cup I)$, then $(E \cup I) + \text{Rad}(M \cup I) = (M \cup I)$. But $\text{Rad}(M \cup I) \ll (M \cup I)$ which implies that $(E \cup I) = (M \cup I)$ then we get contradiction. Consequently a module $(M \cup I)$ is Neutrosophic local. Thus, through Theorem 4.17, $(R \cup I)$ represents Neutrosophic Q-F ring.

Theorem 4.20. A Neutrosophic Noetherian ring $(R \cup I)$ is referred to as Neutrosophic Q-F iff every non-zero torsionless factor module of $(M \cup I)$ in decomposable.

Proof: Assuming that the ring $(R \cup I)$ is Neutrosophic Noetherian Q-F, also assume $(M \cup I)$ be a non-zero Neutrosophic torsionless factor module. Then through Theorem 4.9, We possess $(M \cup I)$ is Neutrosophic cyclic $(R \cup I)$ -module. Assume $(M \cup I)/(D \cup I) \neq 0$ is a factor module from $(M \cup I)$. Given the Lemma 3.4 and Lemma 3.8, we possess $(M \cup I)$ is a module for lifting locally. So $(M \cup I)/(D \cup I)$ represents module to lifting locally through Lemma 3.9. Thus through Lemma 3.10, we obtain $(M \cup I)/(D \cup I)$ be an decomposable.

Conversely, Assume $(D \cup I)$ is maximal submodule from $(M \cup I)$ and assume $(L \cup I)$ is a non-zero submodule from $(D \cup I)$. suppose that $(M \cup I) = (L \cup I) + (K \cup I)$, where $(K \cup I)$ is submodule from $(M \cup I)$ through [34, lemma 1.2.10], we acquire

$(M \cup I)/(L \cup I) \cap (K \cup I) \cong (M \cup I)/(L \cup I) \oplus (M \cup I)/(K \cup I)$. But $(M \cup I)/(L \cup I) \cap (K \cup I)$ is indecomposable then by second isomorphism theorem. Either $(M \cup I)/(L \cup I) = 0$ or $(M \cup I)/(K \cup I) = 0$. Since $(L \cup I)$ is submodule of $(D \cup I)$, and $(D \cup I)$ is submodule from $(M \cup I)$. Then $(L \cup I)$ represents proper submodule from $(M \cup I)$. Hence $(M \cup I)/(L \cup I) \neq 0$ implies that $(M \cup I)/(K \cup I) = 0$ and hence $(M \cup I) = (K \cup I)$. Therefore $(L \cup I)$ is a small submodule from $(M \cup I)$. Thus $(M \cup I)$ is a Neutrosophic local lifting module and through Lemma 3.11, $(M \cup I)$ is cyclic. Thus by Theorem 4.9, ring $(R \cup I)$ is Neutrosophic Q-F.

5. Conclusion

In this research article, we studied the relation between torsionless cyclic R-module and quasi-Frobenius rings. Also we studied some relationships through which we obtained the cyclic R-module thus we obtained the Q-F ring. In addition we studied an relation between isomorphic through we obtain the Noetherian ring and thus we obtained an Q-F ring. Additionally, we studied an relation between torsionless cyclic module and projective and injective module which through we garnered the quasi-Frobenius ring. Finally, we discussed some concepts such as: the singw, local and simple module and Its relationship to the quasi-Frobenius rings.

References

1. Nicholson W. K., Yousif M. F., Principally injective rings, J. Algebra 174, no. 1, 77–93. 1995.
2. Nakayama Tadasi, On Frobeniusian algebras. II. Ann. Math. 42: 1-21. 1941.
3. Ikeda, Masatoshi and Nakayama Tadasi. Supplementary remarks on Frobeniusian algebras. II. Osaka Math. J. 2: 7-12. 1950.
4. Morita, Kiiti and Hiroyuki Tachikawa, Character modules, submodules of a free module, and quasi-Frobenius rings. Math. Z. 65: 414-428. 1956.

5. Dieudonne', Jean, Remarks on quasi-Frobenius rings. Illinois J. Math. 2: 346-354. 1958.
6. Faith Carl and Walker E. A., Characterizations of quasi-Frobenius rings. (Abstract No. 618-25) Notices Amer. Math. Soc. 11: 766. 1964.
7. Dinh V. H., Note on quasi- Frobenius rings. Proceedings of the American Mathematical society Volume 124, Number 2, February 1996.
8. Zadeh, L. A., Fuzzy sets. Information and Control, 8(3), 338–353. 1965.
9. Atanassov, K. T., Intuitionistic Fuzzy Set. Fuzzy Sets and Systems, 20, 87-96. 1986.
10. Buckley J.J. and Eslami E., An Introduction to Fuzzy Logic and Fuzzy Sets, New York. 2002.
11. Das P. S., fuzzy groups and level subgroups, j. math. anal. appl. 84. 264-269. 1981.
12. Liu W. –J., Fuzzy invariant subgroups and fuzzy ideals, Fuzzy Sets and Systems 8, 133-139. 1982.
13. Kambhojkar, H. V., & Bapat, M. S. On prime and primary fuzzy ideals and their radical. Fuzzy Sets and Systems, 53, 203-216. 1993.
14. Salama A. A. and Alblowi S. A., Neutrosophic Set and Neutrosophic Topological Spaces, IOSR Journal of Mathematics, ISSN:2278-5728, Vol. 3, Issue 4, 31-35. 2012.
15. Smarandache F., Proceedings of the First International Conference on Neutrosophy, Neutrosophic Set, Neutrosophic Probability and Statistics, University of New Mexico. 2001.
16. Mandal D., Neutrosophic ideals of semirings, submitted.
17. Lance W. S., Noetherian Rings and their applications, volume 24. The American Mathematical Society, 1987.
18. Ibrahim N. K., Local Lifting Module With Some of Their Generalization, Thesis College of science University of Tikrit. 2019.
19. Gopalakrishnan N. S., University algebra. pages 159–166. New Age International (P) Limited, 2013.
20. Goldie, A.W., Torsion-Free Modules and Rings, Journal of Algebra 1, 268-287. 1964.
21. Matlis E., Injective modules over Noetherian rings, Pacific J. Math. 8, 511–528. 1958.
22. Manhal M. F., Essential-Small M-Projective Modules, Thesis College of science , Mustansiriyah University. 2018.

23. Khlaif, Thear Z., and Nada K. Abdullah, L-Hollow modules. Tikrit journal of pure Science 24, no: 104-109. 2019.
24. Mahmood L. S., Shihab N. S. and Khalaf H. Y., Semi Hollow Modules And Semi Lifting Modules. International Journal of Advanced Scientific and Technical, 375-382. 2015.
25. Jans J. P., Duality in Noetherian rings. Proc. Amer. Math. Soc. 12: 829-835. 1961.
26. Faith, C., Rings with ascending chain condition on annihilators. Nagoya Math. J. 21, 179-191. 1966.
27. Rutter, E. A., Two characterisations of quasi-Frobenius rings. Pacific J. Math. 30, 777-784. 1969.
28. Ali P. H., Hollow Modules and Semihollow Modules, Thesis College of science, University of Baghdad. 2006.
29. Damiano R. F., A right PC1 ring is right Noetherian, Proc. Amer. Math. Soc. 77. 1 1-14. 1979.
30. Osofsky B. L., Rings all of whose finitely generated modules are injective, Pacific J. Math. 14, 645-650. 1964.
31. Smith P. F., Rings characterized by their cyclic modules, Canad. J. Math. 31, 93-111. 1979.
32. Lam, Tsit-Yuen., Exercises in modules and rings. Springer Science & Business Media. 2009.
33. Chatters A. W., A characterization of right Noetherian rings, Quart. J. Math. Oxford Ser. 2 33, 65-69. 1982.
34. Goodearl, K. R., Ring theory, Non-Singular Ring and Modules, Mercel Dekker, New York. 1976.

The Impact of Utilizing Alveolo-Paste on the Healing of Soft Tissue after Dental Extraction

1-*Ahmed AbdulKareem Mahmood, 2-Ahmed Amer Ibrahim, 3-Saber Mizher Mohammed, 4- Sohaib Qays Alwan

1,2,3,4 Tikrit University, College of Dentistry, Iraq

1-*ahmedabdulkareem@tu.edu.iq

2-ahmedameribraheem@tu.edu.iq

3-Saber.m.mohammed23@tu.edu.iq

4-Sohaibqais@tu.edu.iq

The Impact of Utilizing Alveolo-Paste on the Healing of Soft Tissue after Dental Extraction

1-*Ahmed AbdulKareem Mahmood, 2-Ahmed Amer Ibrahim, 3-Saber Mizher Mohammed, 4- Sohaib Qays Alwan

1,2,3,4 Tikrit University, College of Dentistry, Iraq

1-*ahmedabdulkareem@tu.edu.iq

2-ahmedameribraheem@tu.edu.iq

3-Saber.m.mohammed23@tu.edu.iq

4-Sohaibqais@tu.edu.iq

Abstract

Aim:

The aim of the current research is to evaluate the effectiveness of Local application of alveogyl paste on soft tissue healing after lower molars extraction.

المستخلص

الهدف:

الهدف من البحث الحالي هو تقدير مدى فعالية التطبيق الموضعي لمعجون الفيوجيل على شفاء الأنسجة الرخوة بعد قلع أضراس الفك السفلي.

المواد والطرق:

شمل البحث إجمالي 20 مريضاً أصحاء تتراوح أعمارهم بين 18-35 سنة وكان لديهم أسنان بدون أعراض عند الخلع.

تم تقسيم المرضى بشكل عشوائي إلى مجموعتين. تم تطبيق الفيوباست على مجموعة الفيوجيل. بينما لم يتم تطبيق أي شيء في المجموعة الضابطة. تم تقييم المرضى في

اليوم الأول والسابع بعد العملية الجراحية وسجل على مسبار اللثة العددي.

النتائج:

كان العرض الدهليزي اللساني هو الأعلى في اليوم الأول بعد العملية الجراحية، ثم انخفض تدريجياً في كل من مجموعة السيطرة ومجموعة الفيوجيل وفي اليوم السابع بعد العملية الجراحية. كانت هناك فروق ذات دلالة إحصائية في العرض الشدق اللساني بين مجموعات التحكم ومجموعات الفيوجيل في الأيام السبعة بعد العملية الجراحية

الاستنتاجات:

أظهرت نتائج هذه الدراسة أنه بعد الاستئصال الجراحي للأسنان الفيوجيل يمكن أن يسرع من شفاء الأنسجة الرخوة.

Material and methods:

The research included a total of 40 healthy patients between the ages of 18-35 years. Patients were randomly divided into two groups; alveolopaste was applied to alveogyl group, whereas the control group had no material application. After using a periodontal probe to measure the extraction socket's buccolingual width, use a pair of tweezers to administer 50 grams of alveogyl material using a scale to completely cover the socket's bottom and gently pack it into place. A periodontal probe was used to measure the width after a week.

Results:

Bucco-lingual width of soft tissue margins of the socket, were highest on the first postoperative day and decreased gradually in both control and alveogyl group during the seven days following surgery. There were statistically significant differences in bucco-lingual width between control and alveogyl groups in the seven postoperative days

Conclusions:

After tooth extraction, alveogyl is administered to lessen discomfort and hasten soft tissue healing. Using alveogyl reduces the risk of developing dry socket.

1. Introduction

Exodontia or dental extraction (also referred to as tooth extraction, exodontist, is removal of teeth from dental alveolus (socket) in the alveolar bone [1]. Extractions are performed for a wide variety of reasons, but most commonly to remove teeth which have become un restorable through dental caries, periodontal disease, or dental trauma, especially when they are associated with pulpitis. Sometimes impacted wisdom teeth cause recurrent infections of the gum (pericoronitis), and may be removed when other conservative treatments have failed (cleaning, antibiotics and operculectomy). In orthodontics, if the teeth are crowded, healthy teeth may be extracted (often bicuspids) to create space so the rest of the teeth can be straightened [2].

Simple extractions are performed on teeth that are visible in the mouth, usually with the patient under local anesthetic, and require only the use of instruments to elevate and/or grasp the visible portion of the tooth. Typically the tooth is lifted using an elevator, and using dental forceps, specific tooth

movements are performed expanding the tooth socket. Once the periodontal ligament is broken and the supporting alveolar bone has been adequately widened the tooth can be removed. Typically, when teeth are removed with forceps, slow, steady pressure is applied with controlled force. Surgical extractions involve the removal of teeth that cannot be easily accessed or removed via simple extraction, for example because they have broken under the gum or because they have not erupted fully, such as an impacted wisdom [3]. Tooth Surgical extractions almost always require an incision. In a surgical extraction we may elevate the soft tissues covering the tooth and bone, and may also remove some of the overlying and/or surrounding jaw bone with a drill or, less commonly, an instrument called an osteotome. Frequently, the tooth may be split into multiple pieces aid in removing it from the socket to assist the extraction procedure [3].

Wound healing, is a normal biological process in the human body, wound-healing process consists of four highly integrated and overlapping phases: hemostasis, inflammation, proliferation, and tissue remodeling. For a wound to heal successfully, all four phases must occur in the proper sequence and time frame. Many factors can interfere with one or more phases of this process [4].

Multiple factors can lead to impaired wound healing. In general terms, the factors that influence repair can be categorized into local and systemic. Local factors are those that directly influence the characteristics of the wound itself, while systemic factors are the overall health or disease state of the individual that affect his or her ability to heal, Many of these factors are related, and the systemic factors act through the local effects affecting wound healing [5].

The process of the wound being closed by clotting. Happens very quickly. Starts when blood leaks out of the body then blood vessels constrict to restrict the blood flow. The platelets aggregate and adhere to the sub-endothelium surface within seconds of the rupture of a blood vessel's epithelial wall [6, 7].

After that, the first fibrin strands begin to adhere in about sixty seconds. As the fibrin mesh begins, the blood is transformed from liquid to gel through pro- coagulants and the release of prothrombin. The formation of a thrombus or clot keeps the platelets and blood cells trapped in the wound area [8, 9]. The thrombus is generally important in the stages of wound healing but becomes a problem if it detaches from the vessel wall and goes [10, 11].

Dry socket” refers to a post-extraction socket where some or all of the bone within the socket, or around the occlusal perimeter of the socket, is exposed in the days following the extraction, due to the bone not having been covered by an initial and persistent blood clot or not having been covered by a layer of vital, persistent, healing epithelium [12]. The patient may not be able to prevent food particles or the tongue from mechanically stimulating the exposed bone, which is acutely painful to touch, resulting in frequent acute pain [13]. All parts of a dry socket lesion, except the exposed bone, can be gently touched with a periodontal probe or an irrigation needle tip without causing acute pain. Dry socket lesions occur in approximately 1% to 5% of all extractions and in up to 38% of mandibular third molar extractions [14].

A dry socket lesion may show exposed bone located superior to the projected location of the occlusal surface of the socket after the socket heals. This bone may be a protruding septum of bone or may be located on the socket occlusal perimeter. This superiorly-located exposed bone would be the last aspect of the socket to be covered by epithelium [15].

Since the bone, protruding superiorly to the projected occlusal surface of the healed socket, would be exposed to food particles or mechanical trauma that may erode epithelium growing over that bone. This bone, if mechanically stimulated, would be a source of acute pain until the end of the healing period [16].

The dentist may anesthetize the patient and use a football diamond bur with copious irrigation to trim this bone to approximately (1mm) inferior to the projected occlusal surface of the healed extraction socket. Such trimming can result in the bone becoming immediately coverable by a blood clot or medicament, thereby reducing the total number of days that this hyper-sensitive bone is exposed and helping to ensure that epithelium will systematically grow over the remaining exposed bone of the dry socket [17].

If the protruding bone is located on the socket occlusal perimeter, the dentist can reduce the bone to a level that is inferior to the occlusal aspect of the gingival tissue located just lateral to the protruding bone. If the gingiva on the socket occlusal perimeter is superior to all of the socket bone, a socket blood clot or dry socket medicament is more likely to cover the bone [13, 15, 17].

Alveogyl is a dry-socket treatment and post-extraction dressing which every dental office should have on hand. Alveogyl is a one-step, self-eliminating treatment which rapidly alleviates pain and provides a soothing effect throughout the healing process. Its fibrous consistency allows for easy filling of the socket and good adherence during the entire healing process [11].

Indications:

- Dry socket treatment
- Post Extraction Dressing

Analgesic action due the soothing effect of eugenol on the alveolar tissues. Very easy to apply because of its fibrous consistency. Easily maintained in the alveolus. There is no need for Suturing or special attention.

2. Materials and Methods

Forty medically healthy patients were randomly assigned and agreed to participate in the study, their ages ranged from 18 to 35 years and included males only.

The diagnosis of the tooth was based on clinical examination and standard intraoral periapical radiographs [18].

2.1 Inclusion criteria included:

1. Free of inflammation and infection of tissue at the time of the surgical procedure.
2. Medically fit, not allergic, not taking any medication that could interfere with the study drugs.

2.2 Exclusion criteria included:

1. History of compromised medical health, history of allergic reactions, or hypersensitivity to the medications used in the operative work.
2. Patients receiving chemotherapy or radiation therapy.
3. Patients needing total extraction or with severe periodontitis, and patients who had any other oral pathology.
4. Patients' rejection of being involved in the research or those who could not commit to follow-up visits or those who used other drugs during the research period.

The patients were arbitrarily allocated to one of the two treatment groups: Group I included 20 patients allocated to alveogyl paste

Group II included 20 patients without alveogyl paste

Indicated teeth lower first and second molars were extracted under local anesthesia gained by inferior alveolar nerve, lingual and long buccal nerve block injections using 1.8ml of 2% lidocaine with 1:80,000 adrenaline.

All patients were instructed to:

1. Eat soft and cold diet for the first 24 hours after operation
2. Do not rinse for 24 hours.
3. Do not smoke for 72 hours.

After measuring the buccolingual width of the extraction socket using periodontal probe (Figure 1), using a pair of tweezers apply Alveogyl material of about 50 grams using scale to adequately cover the bottom of the socket and pack gently into place. After 1 week, the width was measured utilizing periodontal probe as in (Figure 2).



Figure 1: Buccolingual width of the socket measurement



Figure 2: Healing after 1 week.

3. Results

The sample sizes (N), means, standard deviations (StDev), and standard errors (SE Mean) for the group after "Alveogyl Group." and the group "after without Alveogyl "are compiled in the first table. With a T-Value of -2.51 and a statistically significant P-Value of 0.018, the second table displays the results of the two-sample t-test, which demonstrates a significant difference in means between the two groups.

Table 1: Comparing After Alveogyl Group. Vs. After Without Alveogyl Group.

Group	N	Mean	StDev	SE Mean
After Alveogyl .Group.	20	3.975	0.993	0.22
Without. Alveogyl .Group.	20	4.600	0.503	0.11

Statistic	Value
T-Value	-2.51
P-Value	0.018
Hypothesis Tested	Difference = 0 (vs \neq)

The table 2 summarizes the sample sizes, means, standard deviations, and standard errors for the groups "Before Alveogyl Group." and "After Alveogyl Group." With a T-Value of 14.32 and a highly significant P-Value of 0.0006. This indicates a substantial decrease in the measured outcome after the intervention involving "Alveogyl Group."

Table 2: Descriptive Statistics for Before Alveogyl Group and After Alveogyl Group

Group	N	Mean	StDev	SE Mean
Before Alveogyl Group.	20	7.550	0.510	0.11
After Alveogyl Group.	20	3.975	0.993	0.22

Two-Sample T-Test Results for Before Alveogyl Group vs. After Alveogyl Group.

Statistic	Value
T-Value	14.32

Statistic	Value
P-Value	0.0006

Hypothesis Tested Difference = 0 (vs \neq)

In figure 3 implies if the "Alveogyl Group" is present or not. Impacts the measured outcome.

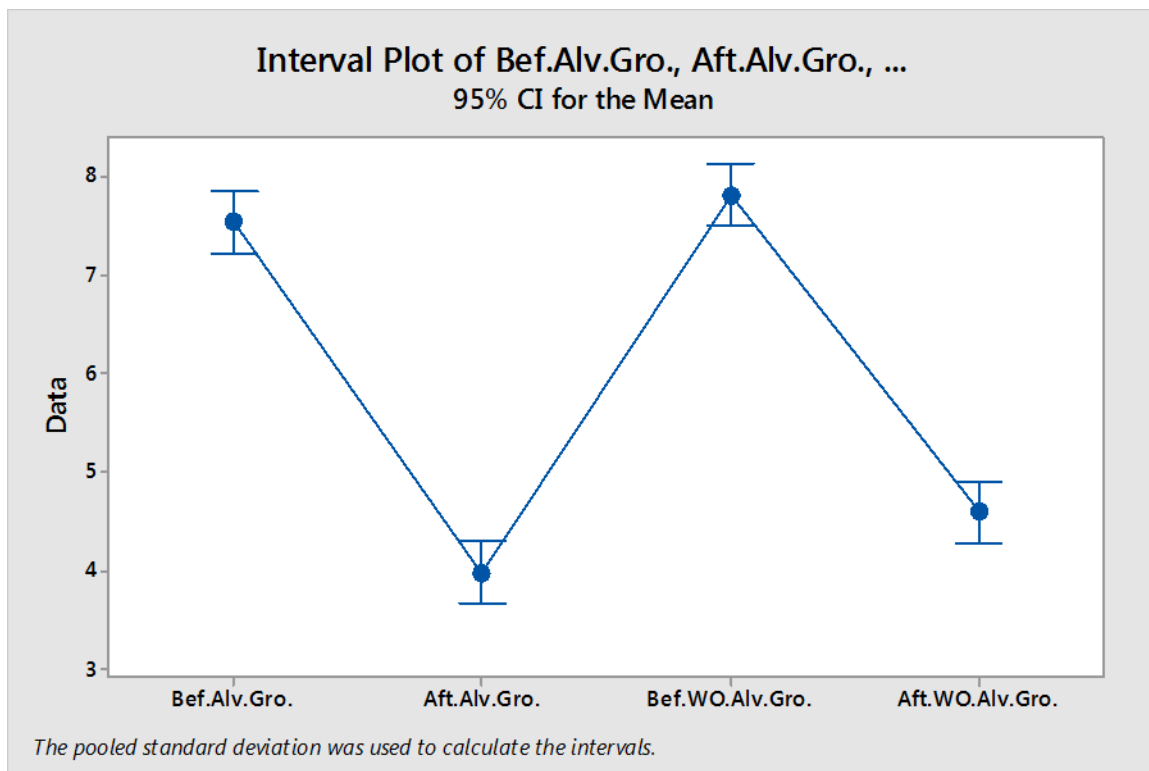


Figure 3: Blot between the groups.

4. Discussion

The purpose of this study to measure the efficacy of alveogyl paste on the wound after tooth extraction, alveogyl paste can reduce the probability of dry socket and accelerate the healing process, we aimed to measure the effects of alveogyl paste on soft tissue healing after tooth extraction [16].

There were many obstacles we had to overcome in this study, including the patients don't commit to the follow up date.

Dry sockets are more common after surgical or traumatic extraction. Similarly traumatic extraction can also lead to traumatic thrombosis of vessels in socket resulting in delayed healing and wound infection [12, 19]. The main aim in the treatment of dry sockets is to relieve pain. Various materials have been placed in extraction sockets for this purpose [15]. Alveogyl was the one of the most commonly used materials. Alveogyl contains eugenol which has a soothing effect and relieves the pain, these properties are often desirable in the presence of inflammation to reduce postoperative pain [20].

The results of our study come in acceptance with result by previous studies done by Ahmed salem et al. who concluded that Alvogyl showing higher pain relief and healing capability, as evidenced by clinical signs of improvement attributed to its components [21].

5. Conclusions

Alveogyl administration after tooth extraction reduce pain and accelerate socket healing and soft tissue closure. Alveogyl use decrease the probability of dry socket.

References

1. Pedlar J, Frame JW, Hill CM, Langdon JD, Cowan CG, Marley JJ, Mathew LR, Thomas DW (2007). Oral and maxillofacial surgery: An objective-based textbook. (2nd edition), Edinburgh: Churchill Livingstone. P.24. ISBN 978-0-443-06017-5.
2. Gosain A, DiPietro LA. Aging and wound healing (2004). World J Surg.; 28(3):321-6. doi: 10.1007/s00268-003-7397-6. Epub 2004 Feb 17. PMID: 14961191.

3. SK McMaster, MJ Paul-Clark, M Walters, M Fleet, J Anandarajah, S Sriskandan and JA Mitchell (2008). Cigarette smoke inhibits macrophage sensing of Gram-negative bacteria and lipopolysaccharide: relative roles of nicotine and oxidant stress. *British Journal of Pharmacology* 153, 536–543.
4. Childs DR, Murthy AS (2017). Overview of Wound Healing and Management. *Surg Clin N Am* 97, 189–207.
5. Coger V, Million N, Rehbock C, Sures B, Nachev M, Barcikowski S, Wistuba N, Strauß S, Vogt PM (2019). Tissue Concentrations of Zinc, Iron, Copper, and Magnesium During the Phases of Full Thickness Wound Healing in a Rodent Model. *Biol Trace Elem Res.* 191(1):167-176. [[PubMed](#)]
6. Bowden LG, Byrne HM, Maini PK, Moulton DE (2016). A morphoelastic model for dermal wound closure. *Biomech Model Mechanobiol.* 15(3):663-81.
7. Blum, I.R., (2002). Contemporary views on dry socket (alveolar osteitis): a clinical appraisal of standardization, aetiopathogenesis and management: a critical review. *International journal of oral and maxillofacial surgery*, 31(3), pp.309-317.
8. Daly B, Sharif MO, Newton T, Jones K, Worthington HV (2012). Local interventions for the management of alveolar osteitis (dry socket). *Cochrane Database Syst Rev.* 12;12:CD006968. doi: 10.1002/14651858.CD006968.pub2. Update in: *Cochrane Database Syst Rev.* 2022 Sep 26;9:CD006968. doi: 10.1002/14651858.CD006968.pub3. PMID: 23235637.
9. Rood JP, Murgatroyd J (1979). Metronidazole in the prevention of 'dry socket'. *Br J Oral Surg.* 17 (1):62-70. doi: 10.1016/0007-117x(79)90009-x. PMID: 289417.

- 10.Ozgok Kangal MK, Regan JP. (2023). Wound healing In: StatPearls [Internet]. Treasure Island (FL): StatPearls Publishing; PMID: 30571027. [[PubMed](#)].
- 11.Werner S., Grose R (2003). Regulation of wound healing by growth factors and cytokines. *Physiol. Rev.* 83(3): 835–870, doi: 10.1152/physrev.2003.83.3.835.
- 12.Denise CB, Seamus R, Leo, FS (2011). The management of dry socket/alveolar osteitis. *J Ir Dent Assoc* ;57(6):305-10.
- 13.Micheal F , Leo FS (2013). Commonly used topical oral wound dressing materials in dental and surgical practice - a literature review. *J Ir Dent Assor*;59(4):190-95.
- 14.Kolokythas A, Olech E, Miloro M (2010). Alveolar osteitis: a comprehensive review of concepts and controversies. *Int J Dent.*; 249073. doi: 10.1155/2010/249073. Epub 2010 Jun 24. PMID: 20652078; PMCID: PMC2905714.
- 15.Awang, M.N (1989). The aetiology of dry socket: a review. *Int Dent J*; 39 (4): 236-240.
- 16.Mamoun J (2018). Dry Socket Etiology, Diagnosis, and Clinical Treatment Techniques. *J Korean Assoc Oral Maxillofac Surg*; 44:52-58.
- 17.Shaw TJ, Martin P (2009). Wound repair at a glance. *Journal of Cell Science.* ;122:3209-13.
- 18.Blum IR (2002). Contemporary views on dry socket (alveolar osteitis): a clinical appraisal of standardization, aetiopathogenesis and management: a critical review. *Int J Oral Maxillofac Surg.*;31:309–317.
- 19.Chiapasco M, De Cicco L, Marrone G (1993). Side effects and complications associated with third molar surgery. *Oral Surg Oral Med Oral Pathol.*;76(4):412-20. doi: 10.1016/0030-4220(93)90005-o. PMID: 8233418.

20. Daly BJ, Sharif MO, Jones K, Worthington HV, Beattie A (2022). Local interventions for the management of alveolar osteitis (dry socket). *Cochrane Database Syst Rev.* 26;9(9):CD006968. doi: 10.1002/14651858.CD006968.pub3. PMID: 36156769; PMCID: PMC9511819.
21. Ahmad, S., Hamad, S., Abdullah, H., Faisal, N., Ahmed, M., Meshal, Y., Rakan, Y. (2022). Effectiveness of different socket dressing materials on the postoperative pain following tooth extraction: a randomized control trial. *JOURNAL of MEDICINE and LIFE*; (15): 1005-1012.

عزل وتشخيص الميكروبات المرتبطة بالهواتف المحمولة لطلبة كلية التربية بالرسّاق

Isolation and identification of microbes associated

with student's mobile phones in Rustaq College of Education

الطالبات: أسماء صالح الهاشمية،

تسنيم سيف الرئيسية،

هاجر عبد الله الشافعية

إشراف الدكتور سعد صبار دحام

Saad.dahham@utas.edu.om

قسم العلوم، كلية التربية بالرسّاق، جامعة التقنية والعلوم التطبيقية، سلطنة عُمان

عزل وتشخيص الميكروبات المرتبطة بالهواتف المحمولة لطلبة كلية التربية بالرسّاق

Isolation and identification of microbes associated with student's mobile phones in Rustaq College of Education

الطالبات: أسماء صالح الهاشمية، تسنيم سيف الرئيسية، هاجر عبد الله الشافعية

إشراف الدكتور سعد صبار دحام

Saad.dahham@utas.edu.om

قسم العلوم، كلية التربية بالرسّاق، جامعة التقنية والعلوم التطبيقية، سلطنة عُمان

الملخص

تحتل الهواتف الذكية جزءاً كبيراً من حياتنا، إذ توفر لنا طيفاً واسعاً من الخدمات، ومع ازدياد استخدامها تتزايد فرص تلوثها البكتيري، لذلك هدفت هذه الدراسة إلى قياس مدى التلوث البكتيري في الهواتف النقالة لطلاب كلية التربية بالرسّاق. حيث جُمعت 34 عينة عشوائية من هواتف طلبة كلية التربية بالرسّاق، وأُخذت العينات بواسطة مسحة معقمة، وزُرعت على الأوساط المناسبة، ثم وضعت في الحاضنة لمدة 24 ساعة. أظهرت النتائج عن وجود 189 مستعمرة بكتيرية تنتمي إلى 5 أجناس، أهمها جنس المكورات العنقودية *Staphylococci* بنسبة 73.20% موزعة على بكتريا المكورات العنقودية البشروية-الجلدية *Staphylococcus epidermidis* بنسبة 51.60%، والمكورات العنقودية سالبة إنزيم التخثر *Coagulase-negative Staphylococci* بنسبة 15.30%، والمكورات العنقودية الذهبية *Staphylococcus aureus* بنسبة 6.30%. كما أظهرت نتائج الفحوصات المجهرية وجود بكتريا الإشريكية القولونية *E. Coil*.

الكلمات المفتاحية: الهواتف الذكية، الميكروبات، المكورات العنقودية، الرسّاق.

Abstract

Smartphones occupy a significant portion of our daily lives, offering a wide range of services. However, with increased usage comes a heightened risk of bacterial contamination. This study aimed to assess the extent of bacterial contamination on mobile phones used by students of the College of Education in Rustaq.

A total of 34 random samples were collected from students' mobile phones using sterile swabs. These samples were cultured on appropriate media and incubated for 24 hours. The results revealed the presence of 189 bacterial colonies belonging to five genera, with *Staphylococci* being the most prevalent, accounting for 73.20% of the isolates. Among these, *Staphylococcus epidermidis* represented 51.60%, Coagulase-negative *Staphylococci* (CoNS) accounted for 15.30%, and *Staphylococcus aureus* made up 6.30%.

Microscopic examination also identified the presence of *Escherichia coli* (*E. coli*), highlighting the potential risk of pathogenic bacterial contamination on mobile phones. These findings underscore the importance of maintaining proper hygiene practices in handling personal devices.

المقدمة

يشهد العصر الحالي تسارعاً ملحوظاً في التطور التكنولوجي، إذ تُلبّي الابتكارات الحديثة احتياجات المجتمع بطريقة غير مسبقة. ومن بين هذه الابتكارات التي أحدثت ثورة في حياتنا اليومية، تبرز الهواتف النقالة الذكية كواحدة من أهم الأدوات وأكثرها استخداماً. ففي أقل من عقدين من الزمن، تحولت الهواتف النقالة من أجهزة نادرة وباهظة الثمن مخصصة لنخبة رجال الأعمال إلى أدوات شخصية شائعة ومنخفضة التكلفة. بل إنها أصبحت في العديد من البلدان أكثر انتشاراً من الهواتف الأرضية، حيث يُقتنيها أفراد المجتمع بمختلف فئاته، بما فيهم الأطفال. على سبيل المثال، تتمتع آسيا بأسرع معدل نمو لمشتري الهواتف النقالة عالمياً (1).

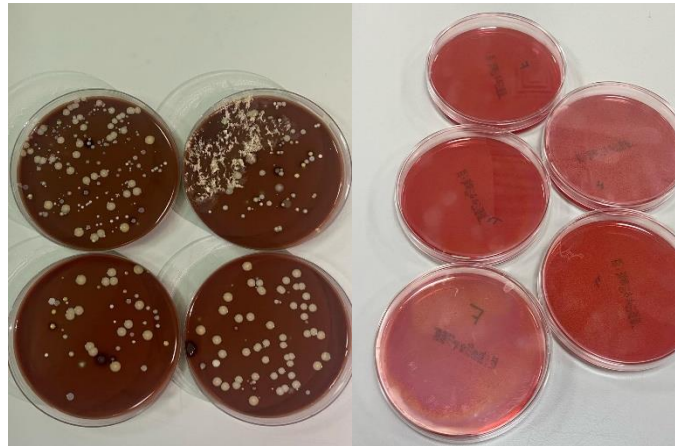
وقد شهدت سلطنة عمان زيادة ملحوظة لمستخدمي الهاتف النقال في السنوات الأخيرة، إذ أعلن المركز الوطني للإحصاء والمعلومات في سلطنة عمان عن ارتفاع عدد مستخدمي الهواتف النقالة بنسبة 0.6% ليصل عدد المستخدمين إلى 6.42 مليون شخص. وكانت هذه الزيادة لعام 2020 مقارنة مع الفترة نفسها من عام 2019. وأشار المركز إلى أنّ نسبة مستخدمي الهواتف الذكية في عام 2021، ممّن تزيد أعمارهم عن 18 سنة قد بلغت 94%. ومع هذا التزايد السريع للهواتف الذكية واجتياحها لحياتنا بشكل كامل، أصبحت وسيلة لا يمكن الاستغناء عنها (2). ومع وجود كل هذه الميزات التي يوفرها الهاتف النقال، بات من السهل أن نغفل عن دوره الفعال في الصحة والمرض؛ فقد لا يهتم بعض مستخدمي الهواتف النقالة بالنظافة الشخصية، وثمة من يستخدمون الهاتف نفسه. يؤدي هذا التعامل المستمر مع الهاتف من قبل مستخدمين مختلفين إلى تعرضه لطيف واسع من الكائنات الحية الدقيقة، ويجعله حاملاً جيداً للميكروبات، خاصة تلك المرتبطة بالجلد، ما يؤدي إلى انتشار الكائنات الحية الدقيقة المختلفة من مستخدم لآخر. وقد ذكر علماء الأحياء الدقيقة أنّ الاستخدام المستمر للهواتف مع وجود الحرارة الناتجة عنها يوفر أرضاً خصبة للعديد من الأحياء الدقيقة التي توجد عادة على الجلد. مثل جنس المكورات العنقودية، وخاصة نوع المكورات العنقودية البشرية *S. epidermidis* التي تعتبر بكتيريا طبيعية تعيش على جلد الإنسان وفي الجهاز التنفسي والجهاز الهضمي لكنها قد تصبح بكتيريا انتهازية إذا ما دخلت إلى مجرى الدم. كما أن نوع المكورات العنقودية الذهبية -المعدية- ينتشر عن طريق الرذاذ والهباء الجوي بين 20-50% من البشر. وتوجد المكورات العنقودية بانتظام على الملابس وأغطية الأسرة والبيئات البشرية الأخرى، وتضطلع بشكل مباشر بالعديد من الأعراض المرضية مثل البثور والدمامل والالتهاب الرئوي والتهاب السحايا (3). ومما لا ريب فيه، تُعد اليد الوسيلة الرئيسة في نقل الميكروبات المختلفة بما في ذلك الأنواع المعوية المعدية.

وتعتبر بكتيريا *Proteus mirabilis* واحدة من أكثر مسببات الأمراض البكتيرية شيوعاً في العينات السريرية التي تنتقل من الهاتف النقال في الولايات المتحدة الأمريكية (4).

وتعتمد طرق التصاق البكتيريا على مجموعة متنوعة من الآليات الجزيئية والأغشية الحيوية التي تمكنها من الالتصاق بالسطوح على نحو فعال. على سبيل المثال، تتضمن هذه الآليات البروتينات السطحية (الأهداب) الموجودة على الغشاء الخارجي للبكتيريا، ما يسمح ببقائها على الأسطح لفترات أطول. إن التصاق البكتيريا بالهواتف النقالة يمكن أن يحدث عن طريق آليات مختلفة، وهذا يعتمد على نوع البكتيريا وظروف البيئة المحيطة بها، نذكر منها: الالتصاق السطحي: إذ تمتلك بعض البكتيريا بروتينات سطحية تساعد على الالتصاق بالأسطح على نحو فعال. فعند وضع الهاتف على سطح ملوث، تنتقل البكتيريا من السطح إلى الهاتف وتلتصق به من خلال تكس البكتيريا وإنتاج نسيج خارج خلوي يُعرف باسم "الببوفيلم". والالتصاق عن طريق السوائل: ويحدث عن طريق تكون السوائل المتواجدة على الهاتف، مثل العرق أو الرذاذ المائي المحمل بالبكتيريا. وعندما نستخدم الهاتف بيدين ملوثتين أو أثناء تعرضه للرطوبة، يمكن للبكتيريا أن تنتقل من السائل إلى سطح الهاتف وتلتصق به (5). يدعونا هذا الأمر إلى التفكير في كمية التلوث التي قد تكون على هواتفنا الذكية. ثمة دراسة أجراها باحثون في كندا كشفت عن حقيقة مفرجة تتعلق بنظافة الهواتف النقالة، إذ كشفت عن مستويات عالية جداً من البكتيريا تصل إلى 10 أضعاف مستويات البكتيريا الموجودة في مقعد المراض (6). يعود هذا الارتفاع الصادم في مستويات البكتيريا إلى العديد من العوامل، بما في ذلك تلامس الهاتف المستمر مع الأيدي والأسطح الملوثة، فضلاً عن البيئة الدافئة والرطوبة التي توفرها الهواتف النقالة، مما يعزز نمو البكتيريا عليها. وهدفت هذه الدراسة إلى قياس مدى التلوث البكتيري في الهواتف الذكية لطلبة كلية التربية بالرسنق، في محاولة لزيادة الوعي بأهمية التعقيم المستمر للهواتف الذكية.

المواد وطرائق العمل

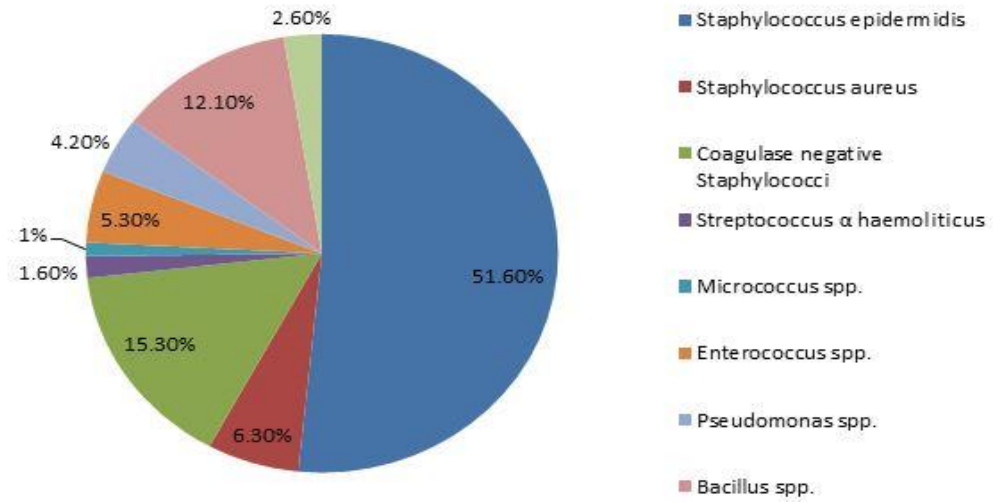
- جُمعت العينات عن طريق مسح الأسطح المكشوفة بشكل كامل من 34 هاتف اختيرت على نحو عشوائي من طلاب وطالبات الكلية في يوم الأحد 8\ديسمبر\2024، باستخدام مسحة قطنية معقمة، ثم زُرعت المسحات على عدة أوساط غذائية غنية وتفرقيه: Chocolate Agar، Blood Agar، ووضعت في الحاضنة Incubator لمدة 24 ساعة وبدرجة حرارة 37 درجة مئوية. لوحظ بعد ذلك النمو البكتيري عن طريق نمو المستعمرات التي شُخصت مورفولوجياً، ثم عُزلت عن طريق التخطيط المستمر والمتقطع، وصُبغت بصبغة جرام Gram Staining وفُحصت تحت المجهر الضوئي لمعرفة نوعها (7).



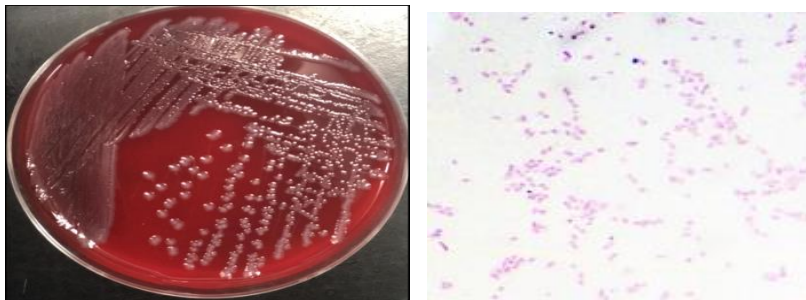
الشكل 1: زراعة العينات من هواتف الطلبة في الأوساط الغذائية المختلفة. على اليمين (Blood agar)، على اليسار (Chocolate agar).

النتائج والمناقشة

يُعد اتباع المعايير الميكروبيولوجية في النظافة أمراً ضرورياً لعيش حياة صحية. ومع ذلك، ثمة ممارسات كثيرة لا تتسجم مع معايير النظافة والصحة العامة. إذ تؤكد نتائج هذه الدراسة على ضرورة تعقيم الهواتف النقالة، فقد كشفت عن مجموعة متنوعة من البكتيريا على الهواتف المحمولة. أظهرت النتائج وجود 189 مستعمرة بكتيرية تنتمي إلى خمسة أجناس. احتلّ جنس المكورات العنقودية النسبة الأكبر، إذ بلغ 73.20%، وجاءت بكتيريا المكورات العنقودية البشروية *Staphylococcus epidermidis* بنسبة 51.60%، والمكورات العنقودية سالبة إنزيم التخثر *Coagulase-negative Staphylococci* بنسبة 15.30%، والمكورات العنقودية الذهبية *Staphylococcus aureus* بنسبة 6.30%. كما أظهرت نتائج الفحوصات المجهرية وجود بكتيريا الإشريكية القولونية *E. coli* وهو مؤشر على وجود تلوث بمياه الصرف الصحي.



الشكل 2: رسم بياني يصور البكتيريا المختلفة الموجودة على أسطح الهواتف



الشكل 3: أ. عزل مستعمرات بكتيرية نقية بطريقة التخطيط. ب، تشخيص نوع البكتيريا من خلال صبغة جرام وفحصها تحت المجهر الضوئي (بكتيريا سالبة لصبغة جرام-*E. coli*) قوة العدسة 40.

وكشفت دراسة أجريت بجامعة ماهيدول في تايلاند، عن انتشار التلوث البكتيري على الهواتف المحمولة لطلبة كليات الصيدلة. إذ شملت الدراسة 53 مشاركاً، طلب منهم استخدام هواتفهم لمدة لا تقل عن 3 أشهر. وعزلت المسحات على وسط Blood Agar وشُخص التلوث البكتيري في 52 عينة من مجموع 53 هاتف محمول (98.11%) وكان تواجد أنواع البكتيريا بالنسب التالية: (CoNS, 42.72%)، (*Bacillus spp.*, 27.18%)، (*S. aureus*, 20.39%)، (*Micrococcus spp.*, 7.77%)، (*Corynebacterium spp.*, 0.97%)، أظهرت النتائج وجود التلوث البكتيري على هواتف طلاب كليات الصيدلة، وأوصت بضرورة التعقيم المستمر للهواتف النقالة (8). توافقت نتائج هذه الدراسة مع ما وجدناه في نتائج بحثنا، وخاصة فيما يتعلق ببكتيريا المكورات العنقودية. تنتشر الأخيرة على نحو واسع على الهواتف الذكية وهذا بسبب قدرتها على تكوين الأغشية الحيوية Biofilm، مما يسهل الالتصاق والبقاء على أسطح الهواتف المحمولة. تتشكل الأغشية الحيوية على نحو معقد، فتتركب هذه الأغشية من 10% كتلة ميكروبية، 90% ماء. وتمر عملية تكوينها بعدة مراحل وهي: الامتزاز (Adsorption)، الالتصاق (Adhesion)، تكوين المستعمرات الدقيقة (Microcolony formation)، النضج (Maturation)، والتشتت (Dispersion) (9).

كما أظهرت دراسة أخرى أجريت في جامعة نوبينا في نيجيريا على 30 عينة مقسمة بالتساوي لكلا الجنسين (15 ذكر، 15 إناث)، أن جميع العينات كانت ملوثة بأنواع مختلفة من البكتيريا. وكانت نسب التلوث كالتالي: 14.33% *Staphylococci* و *Escherichia* وبينت الدراسة فرق الانتشار بين النوعين حيث إن بكتيريا العنقوديات *Staphylococci* أكثر انتشاراً بنسبة 53.85% من البكتيريا الإشريكية *Escherichia* بنسبة 46.67% للأخيرة. وأوصت الدراسة بأهمية النظافة الجيدة من قبل الطلبة لتجنب انتشار الأمراض (10). اختلفت نتائج هذه الدراسة عما توصلنا له في بحثنا فيما يخص بكتيريا *E. coli*، حيث ارتفع الفرق بين نسبتي تواجد هذه البكتيريا لأعلى من 40% بين الدراستين. إذ يعتمد سكان مدينة إبادان جنوب غرب نيجيريا على المياه الجوفية المستخرجة من الآبار في عمليات الشرب والاستحمام وغيرها من استخدامات المياه. ويفترض أن تكون هذه المصادر المائية خالية من التلوث ومع ذلك فهي ملوثة بمياه الصرف الصحي وقد تسبب العديد من الأمراض التي تنتقلها المياه مثل الإسهال والتيفوئيد (11). كما أن قلة الوعي بأهمية النظافة يُعد من المسببات الرئيسة في انتقال مثل هذه البكتيريا الممرضة، وأظهرت نتائج دراسة أجريت على فعالية غسل اليدين بالماء والصابون، أن مخاطر الإصابة بالأمراض بعد الغسيل بالصابون قد انخفضت حوالي 5 أضعاف مقارنة بعدم غسل اليدين. يقلل الغسيل بالصابون المضاد للميكروبات من خطر الإصابة بعدوى الإشريكية القولونية بمعدل 40 ضعفاً مقارنة بعدم غسل اليدين (12). يبين هذا الأمر انتشار بكتيريا *E. coli* بسبب قلة النظافة وتلوث المياه بمياه الصرف الصحي الغير معالجة.

وفي دراسة أجريت في روما لدراسة التلوث البكتيري لهواتف طلبة من الجامعات المتخصصة في المجالات الصحية، كانت العينة قد بلغت 108 من هواتف طلبة الرعاية الصحية. وجد أن العنقوديات *Staphylococci* موجودة في 85% من هواتف العينة، و *Enterococci* في 37%، وبكتيريا *Coliforms* في 6.5%، في حين أنه لم تتواجد البكتيريا الإشريكية *E. coli* نهائياً في العينة. وكانت بكتيريا *Staphylococci epidermidis* هي الأكثر انتشاراً في العينة من جنس العنقوديات بنسبة 72%. وأوضحت الدراسة أن ما نسبته 86% من العينة يقومون بتنظيف هواتفهم على نحو منتظم (13). يعود ذلك بسبب نجاح حملة منظمة الصحة العالمية لتعزيز نظافة اليدين بالاشتراك مع وزارة الصحة في إيطاليا (14).

الخلاصة

أظهرت الدراسة أن جميع هواتف الطلبة المحمولة مصابة بعدة ميكروبات، ينتمي معظمها إلى الفلورا- البكتيريا الطبيعية لجسم الإنسان وكذلك الميكروبات المحمولة جواً وفي التربة. وقد كشفت بعض العزلات على أنواع بكتيرية انتهازية. لذلك، من الضروري غسل اليدين وتعقيم الهاتف؛ لأنه مصدر محتمل لانتقال المرض. ومن الجدير بالذكر أن جائحة كورونا (كوفيد-19) أسهمت بزيادة الوعي لدى طبقات المجتمع المختلفة بضرورة غسل الأيدي والاهتمام بالنظافة الشخصية ونظافة الأسطح والأدوات لتفادي الإصابة بالمسببات المرضية المختلفة وهذا ما تم ملاحظته من خلال نتائج الدراسة.

التوصيات

يوصي الباحثون بأهمية المحافظة على النظافة العامة، والاهتمام بتعقيم وتطهير الأدوات المستخدمة الشخصية. وعدم استخدام أدوات الآخرين، مع تجنب وضع الهواتف الذكية على الأماكن المتسخة كالترربة وإدخالها لدورات المياه.

المراجع

1. Al-Abdalall, A. H. (2010). Isolation and identification of microbes associated with mobile phones in Dammam in eastern Saudi Arabia. *Journal of Family and Community Medicine*, 17(1), 11-14.
2. NCSI . المركز الوطني للإحصاء والمعلومات في سلطنة عُمان. https://www.ncsi.gov.om/News/Pages/NewsCT_20230314085459620.aspx.
3. Hui, Y. H., Sattar, S. A., Murrell, K. D., Nip, W. K., & Stanfield, P. S. (2001). Food borne disease handbook. 2 [sup] nd ed., Vol. 2. Viruses, parasites, pathogens and HACCP.
4. Liu, P. Y. F., Gur, D., Hall, L. M., & Livermore, D. M. (1992). Survey of the prevalence of β lactamases amongst 1000 Gram-negative bacilli isolated consecutively at the Royal London Hospital. *Journal of Antimicrobial Chemotherapy*, 30(4), 429-447.
5. Karthiga, Senthil. (2016). Screening of mobile phones foor the presence of microbes of oral origin. 4(4):6-8.
6. Emily Martin. (2017). Your Cell Phone Is 10 Times Dirtier Than A Toilet Seat. Here's What To Do About It. U-M's School of Public Health.

7. Dahham, S. S., Ali, M. N., Tabassum, H., & Khan, M. (2010). Studies on antibacterial and antifungal activity of pomegranate (*Punica granatum* L.). *Am. Eurasian J. Agric. Environ. Sci*, 9(3), 273-281.
8. Sriprapun, M., Atthakorn, O., & Phuakwilai, A. (2022). "The prevalence of bacterial contamination on mobile phones of pharmacy university students". *Pharm Sci Asia*, 49(4), 356-361.
9. Sharma, Satish, James Mohler, Supriya D. Mahajan, Stanley A. Schwartz, Liana Bruggemann, and Ravikumar Aalinkeel. 2023. "Microbial Biofilm: A Review on Formation, Infection, Antibiotic Resistance, Control Measures, and Innovative Treatment" *Microorganisms* 11, no. 6: 1614. <https://doi.org/10.3390/microorganisms11061614>
10. Akeem Ganiyu Rabi, Olutayo Israel Falodun, Obasola Ezekiel Fagade, Rotimi Ayodeji Dada, Iruka N. Okeke; Potentially pathogenic *Escherichia coli* from household water in peri-urban Ibadan, Nigeria. *J Water Health* 1 July 2022; 20 (7): 1137–1149. doi: <https://doi.org/10.2166/wh.2022.117>
11. Adhikari U, Esfahanian E, Mitchell J, Charbonneau D, Song X, Lu Y. Quantitation of Risk Reduction of *E. coli* Transmission after Using Antimicrobial Hand Soap. *Pathogens*. 2020; 9(10):778. <https://doi.org/10.3390/pathogens9100778>
12. Eboh. O.J., Onuoha. T and Aghanenu, A.S.(2022) Isolation and Characterization of Bacteria on Mobile Phone Screen from Some Novena University Students, *European Journal of Biology and Medical Science Research*, Vol.10, No.1, pp.1-6
13. Ciciarella Modica, D., Maurici, M., D'Alò, G. L., Mozzetti, C., Messina, A., Distefano, A., Pica, F., & De Filippis, P. (2020). "Taking Screenshots of the Invisible: A Study on Bacterial Contamination of Mobile Phones from University Students of Healthcare Professions in Rome, Italy". MDPI.
14. Citation style for this article: [Moro Maria Luisa](#), [Morsillo Filomena](#), [Nascetti Simona](#), [Parenti Mita](#), [Allegranzi Benedetta](#), [Pompa Maria Grazia](#), [Pittet Didier](#). Determinants of success and sustainability of the WHO multimodal hand hygiene promotion campaign, Italy, 2007–2008 and 2014. [Euro Surveill](#). 2017;22(23):pii=30546. <https://doi.org/10.2807/1560-7917.ES.2017.22.23.30546>.

Characterisation of Carbon Nano spheres (CNSs) from Cooking Oil with Ferrocene Catalyst on Activated Carbon Surface

1*Asst.Lec. A'ala, Baddai. Nashter , Ministry of Education, Iraq,

2*Asst.Lec. Montaha, Kadhim. Sultan , Ministry of Education, Iraq,

3*Asst.Lec. Hadeel, Jalal. Abbas , Ministry of Education, Iraq,

alla.bdai1205a@ihcoedu.uobaghdad.edu.iq

montaha.kazem1205a@ihcoedu.uobaghdad.edu.iq

hadeel.jalal1205a@ihcoedu.uobaghdad.edu.iq

Send Article Date 19/5/2025 Date of acceptance of the article : 2025/ 18 / 5

Characterisation of Carbon Nano spheres (CNSs) from Cooking Oil with Ferrocene Catalyst on Activated Carbon Surface

¹*Asst.Lec. A' alaa, Baddai. Nashter , Ministry of Education, Iraq,

²*Asst.Lec. Montaha, Kadhim. Sultan , Ministry of Education, Iraq,

³*Asst.Lec. Hadeel, Jalal. Abbas , Ministry of Education, Iraq,

[¹alla.bdai1205a@ihcoedu.uobaghdad.edu.iq](mailto:alla.bdai1205a@ihcoedu.uobaghdad.edu.iq)

[²montaha.kazem1205a@ihcoedu.uobaghdad.edu.iq](mailto:montaha.kazem1205a@ihcoedu.uobaghdad.edu.iq)

[³hadeel.jalal1205a@ihcoedu.uobaghdad.edu.iq](mailto:hadeel.jalal1205a@ihcoedu.uobaghdad.edu.iq)

Send Article Date 19/5/2025 Date of acceptance of the article : 2025/ 18 / 5

Abstract:

Carbon nanospheres (CNSs) are one of the groups of carbon nanotubes formed as a by-product in the manufacture of carbon nanotubes (CNTs). CNSs have a size between 50 nm to 1 μ m and can be empty or filled balls. CNSs have dangling bonds that cause their reactive properties. CNSs are widely studied as catalyst supports, adsorbents, or battery and supercapacitor electrodes. This study synthesised CNSs using activated carbon (AC) support. The iron catalyst was derived from ferrocene, $\text{Fe}(\text{C}_5\text{H}_5)_2$. Meanwhile, cooking oil was used as a carbon source to form CNSs. The cooking oil, catalyst, and activated carbon mixture were then carbonised using an electrical furnace at 700°C for 1 hour with a nitrogen atmosphere. In this experiment, the initial catalyst concentration was varied from 2.5, 5, 7.5 and 10g catalyst/100 ml cooking oil, with the ratio

of activated carbon to cooking oil 1:3 (w/w)—product characterisation using XRD, BET surface area analysis, Raman spectroscopy, EDS, and XPS. The surface morphology of activated carbon was observed by SEM and TEM analysis, and the results showed that from the synthesis carried out, CNSs were formed, composed of C (002) and C (100). It can also be observed that the larger the catalyst used, the more CNSs were formed. As the amount of catalyst increased, the iron and oxygen content in the sample was also observed by EDS measurements; based on XPS analysis, there was no change in the composition of functional groups on the surface of AC. A decrease in the surface area of AC was observed in each sample, with a maximum reduction of 50%. This resulted in a decrease in the adsorption capacity when used as an adsorbent. Its performance was stable when the 2.5g/100mL sample was tested by cyclic voltammetry as a lithium battery anode.

key words: activated carbon, iron catalyst, cooking oil, CNSs

توصيف جزيئات الكربون النانوية CNSs (من زيت الطهي باستخدام محفز الفيروسين على سطح الكربون المنشط)

ملخص

تُعدّ جزيئات الكربون النانوية (CNSs) إحدى مجموعات أنابيب الكربون النانوية التي تُشكّل كمنتج ثانوي في تصنيع أنابيب الكربون النانوية (CNTs). يتراوح حجمها بين 50 nm إلى 1 µm ، ويمكن أن تكون كرات فارغة أو مملوءة. تحتوي على روابط متدلّية تُسبب خصائصها التفاعلية. تُدرس جزيئات الكربون النانوية على نطاق واسع كدعامات للمحفزات، أو مواد ماصة، أو أقطاب كهربائية للبطاريات والمكثفات الفائقة. وقد ركّبت هذه الدراسة جزيئات الكربون النانوية باستخدام دعامة الكربون المنشط (AC). استُخلص المحفز الحديدي من الفيروسين، $Fe(C_5H_5)_2$. في هذه الأثناء، استُخدم زيت الطهي كمصدر للكربون لتكوين جزيئات الكربون النانوية. تم كربنة خليط زيت الطهي والمحفز والكربون المنشط باستخدام فرن كهربائي عند درجة حرارة 700 درجة مئوية لمدة ساعة واحدة في جو من النيتروجين. في هذه التجربة، تم تغيير تركيز المحفز الأولي من 2.5، 5، 7.5 و 10 جرام من المحفز / 100 مل من زيت الطهي، مع نسبة الكربون النشط إلى زيت الطهي 1:3 (وزن/وزن) - توصيف المنتج باستخدام XRD، وتحليل مساحة سطح BET، و مطيافية رامان، وEDS، وXPS. تم ملاحظة مورفولوجيا سطح الكربون المنشط من خلال تحليل المجهر الإلكتروني الماسح والمجهر الإلكتروني النافذ، وأظهرت النتائج أنه من خلال التركيب الذي تم إجراؤه، تم تكوين CNSs، مكونة من C (002) و C (100). ويمكن أيضًا ملاحظة أنه كلما زاد حجم المحفز المستخدم، زاد تكوين CNSs. مع زيادة كمية

المحفز، تم أيضًا ملاحظة محتوى الحديد والأكسجين في العينة من خلال قياسات EDS؛ بناءً على تحليل XPS، لم يكن هناك أي تغيير في تكوين المجموعات الوظيفية على سطح AC. لوحظ انخفاض في مساحة سطح AC في كل عينة، مع أقصى انخفاض بنسبة 50٪. أدى ذلك إلى انخفاض في سعة الامتصاص عند استخدامه كمادة ماصة. كان أدائه مستقرًا عند اختبار العينة 2.5 جم / 100 مل بواسطة الفولتمتر الدوري كأنود بطارية ليثيوم. الكلمات المفتاحية: الكربون المنشط، محفز الحديد، زيت الطهي، CNSs

Introduction :

Carbon nanosphere (CNSs) are by-products of the manufacture of CNTs. Carbon atoms' pentagonal and hexagonal arrangement, in addition to forming shapes such as CNTs and CNFs, can also form CNSs [1]. Based on their size, these spherical structures can be distinguished into Cn and graphitic carbon onions with diameters between 2-20nm, carbon nanospheres with a lower graphitic structure with a diameter between 50nm-1 μ m, and carbon beads with a diameter above 1 μ m [2]. The structure of CNSs is unique because the sphere shape is not perfectly closed, so there are many dangling bonds [3]. This provides high chemical activity so CNSs can be used for various applications, such as catalyst support, adsorbent in wastewater treatment, and electrochemical capacitors [4].

Several researchers [5-7] have synthesised CNSs using ferrocene as a catalyst. Hans Kristianto et al. (2015) [8] synthesised CNSs using ferrocene as a catalyst and carbon source. Hollow CNSs were successfully synthesised using ferrocene at a pyrolysis temperature of 700°C for 1 hour in a nitrogen atmosphere autoclave. The synthesised CNSs had a 50-150nm diameter with a wall thickness of 15nm. Yi et al. (2005)[9] carried out synthesis with various hydrocarbon sources such as styrene, toluene, benzene, hexane, cyclohexane, and ethane. The synthesis was carried out by the CVD method at temperatures between 900 to 1200°C. At a catalyst concentration of 0.5% by weight, the main product was CNSs, and several CNTs were observed, while at a concentration of 3.5%, the main product was CNTs. In addition to the catalyst concentration, the amount of feed fed into the reactor determines the product obtained. In the study of Zhang et al. (2010) [10], at a carbon source that was too little or too much, the product obtained was CNSs or CNTs with a relatively short length or amorphous carbon. The research conditions used were a quartz reactor with two heating zones. Acetylene feed

was fed continuously with argon gas; the reaction temperature was 1050°C, with a ferrocene catalyst.

Hans Kristianto et al. (2015) research has been conducted on the variation of concentration and method of catalyst deposition on the surface of AC to synthesise CNSs. $\text{Fe}(\text{NO}_3)_3 \cdot 9\text{H}_2\text{O}$ catalyst deposition by the impregnation method successfully synthesised CNSs along with the increase in the amount of catalyst, from 5, 7.5 and 10% w/w, the CNSs obtained are increasing. However, it is not homogeneous on the entire surface of AC. Another method by Náfrádi et al (2016) [12] that has been used is catalyst deposition using the urea coprecipitation method, with an iron: urea ratio of 1:3. In this study, the initial concentration of the catalyst was varied, namely 10, 20, and 30% w/w to activated carbon. From the results of the SEM analysis, it can be seen that increasing the catalyst increases the number of CNSs deposited on the surface of AC. From the XRD results (not shown here), it is known that C(100) is formed, which is seen at the 2θ peak (43°). This indicates the formation of the C sp^2 configuration commonly found in CNSs (Han, Jung et al., 2014). Observation of the characteristics of CNSs can be done by several methods, namely SEM and TEM, to see the morphology and diameter, then XRD and Raman Spectroscopy to know the degree of graphitisation (Nieto-Marquez, Romero et al., 2010). According to Lou et al. (2020) [11], this is due to the structure of CNSs, which have reactive edges and tend to form a combination of several spheres. In previous studies, CNSs were synthesised on the surface of AC support with an iron catalyst from $\text{Fe}(\text{NO}_3)_3 \cdot 9\text{H}_2\text{O}$ using the impregnation catalyst deposition method [13] and urea coprecipitation deposition [14]. CNSs are made using precursors derived from biomass, namely cooking oil. Several researchers have carried out the manufacture of nanocarbon from biomass raw materials [8, 14]. However, it is still rarer than simpler carbon raw materials, such as benzene, toluene, acetylene, etc. Meanwhile, manufacturing CNSs with activated carbon support is the first time it has been done. The CNSs synthesis method is a simple pyrolysis method, where the precursor is not fed continuously but in batches, namely at the beginning before pyrolysis.

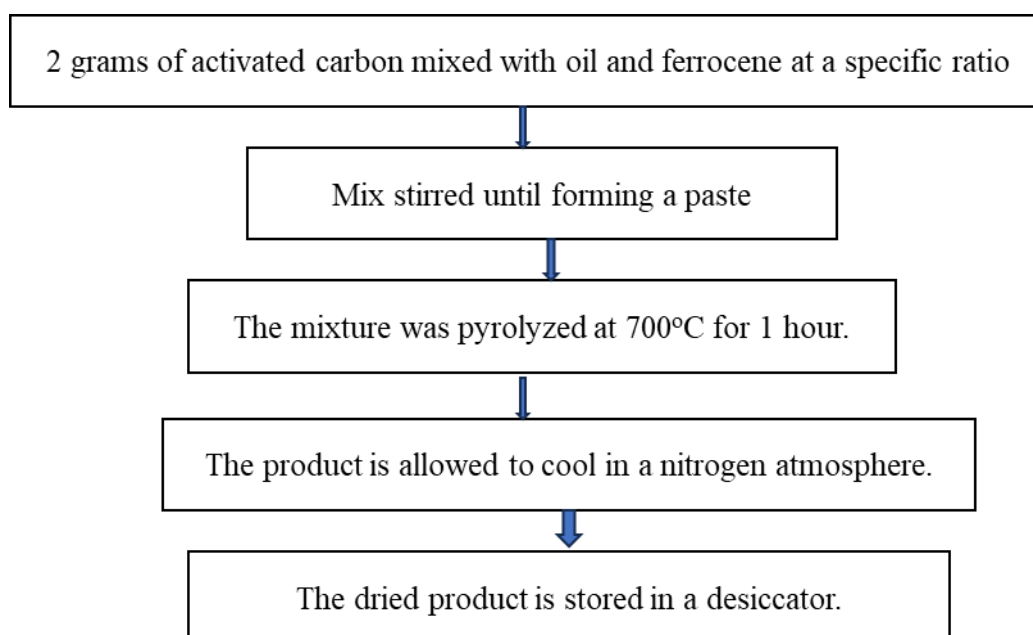
Based on the above discussion, the current research is being developed to study the characteristics of CNSs obtained from cooking oil precursors with ferrocene iron catalysts on the surface of AC and the effect of the initial concentration of iron catalysts on the CNS products obtained.

2. Materials and methods

2.1. Research design.

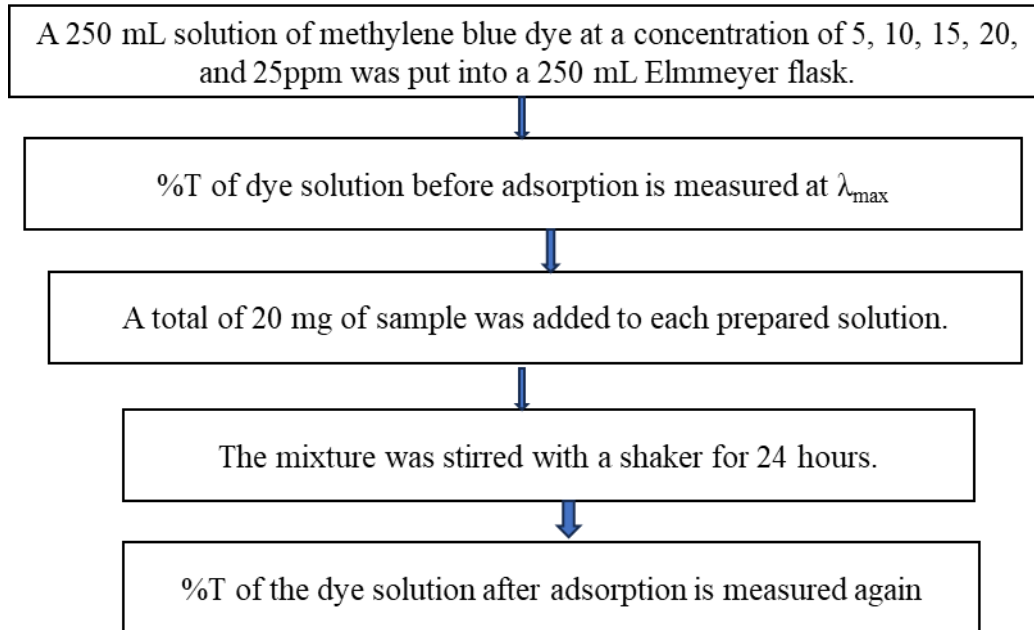
The materials used are Activated carbon (Merck), Ferrocene [$\text{Fe}(\text{C}_5\text{H}_5)_2(\text{s})$], Aquades & N_2 gas. They were cooking Oil. The research aims to determine the operating conditions for manufacturing CNSs with activated carbon support. The support used is commercial activated carbon (Merck, India), using ferrocene catalyst $\text{Fe}(\text{C}_5\text{H}_5)_2$ (Sigma Aldrich), and commercial cooking oil (Rice Bran oil, Henan co. Iraq) as a carbon source.

In general, the steps of this research are divided into two parts: catalyst deposition and CNS synthesis. CNSs synthesis is carried out by mixing cooking oil, activated carbon and ferrocene, then pyrolysed at a temperature of 700°C for 1 hour in a nitrogen atmosphere, with a nitrogen flow rate of 1L/min. The sample is then allowed to cool in a nitrogen atmosphere before removal. The dried product is stored in a desiccator. The experiment was conducted by varying the catalyst ratio, namely 2.5, 5, 7.5 and 10g catalyst/100 ml cooking oil, with the ratio of activated carbon to cooking oil, 1:3 (w/w). The products obtained were characterised using XRD (Bruker D8 Advance, Cu- $\text{K}\alpha$ radiation), SEM-EDS (JEOL JSM-7800F is equipped with EDS), XPS (PHI 5000 VersaProbe III, with an Al- $\text{K}\alpha$ X-ray source at 117.4eV) TEM (JEOL JEM2100), Raman tests (Wasatch Photonics 405nm Raman Spectrometer) and Surface area test using the BET method (Micromeritics apparatus NOVA 1000/3200e Quanta chrome). Synthesis of CNSs with ferrocene iron catalyst shown in the following scheme-1



Scheme-1. How the iron catalyst deposition works on the surface of AC

The adsorption performance test with methylene blue is shown in the following scheme: 2



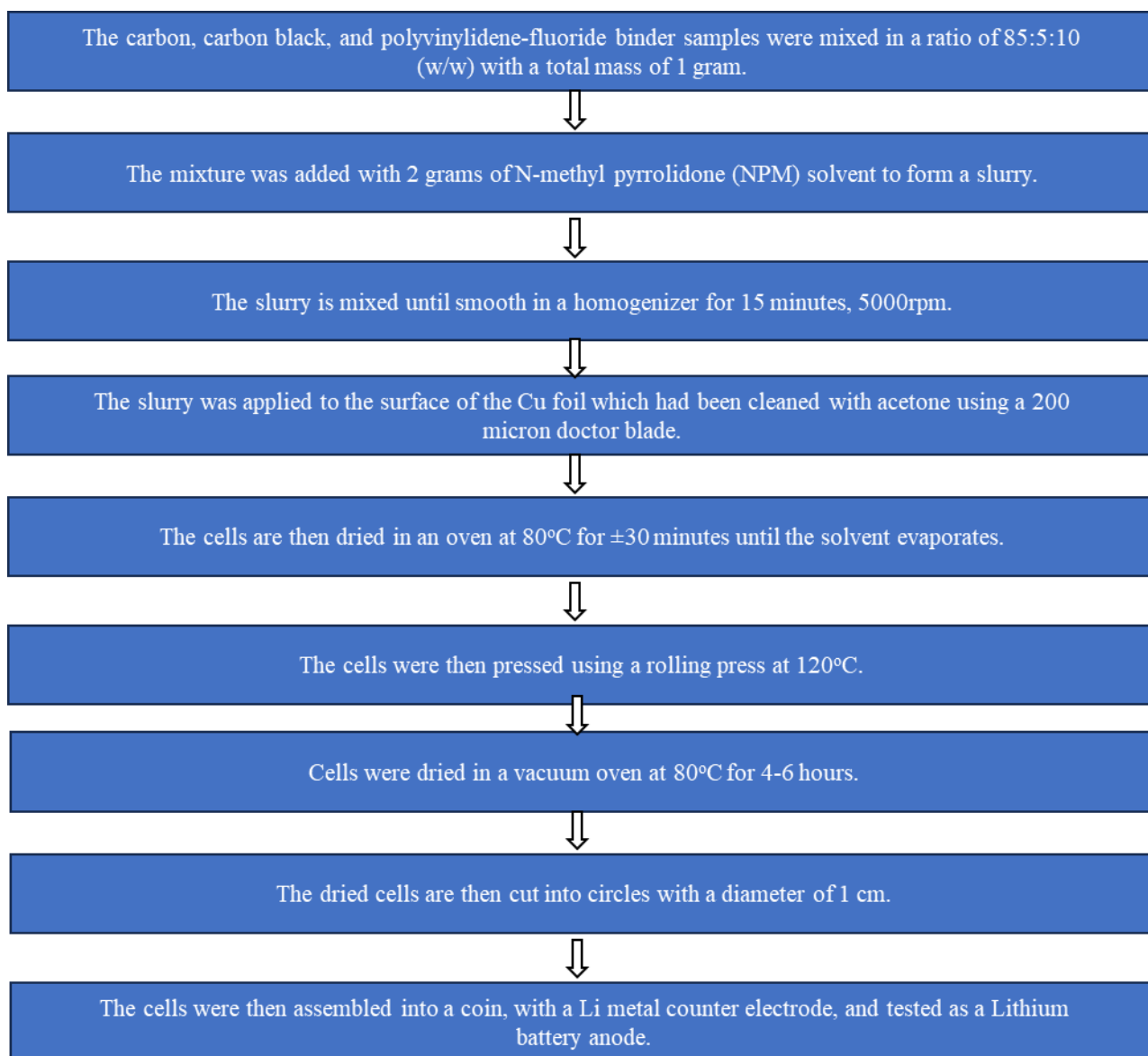
Scheme-2: How methylene blue adsorption works

The adsorption performance of the samples was tested using methylene blue at various concentrations. The samples tested were all samples, plus standard activated carbon as a comparison. The results of concentration measurements at the beginning and end of adsorption are used to determine the Langmuir adsorption isotherm. Adsorption isotherm analysis is used to determine the maximum adsorption capacity and adsorption isotherm constants. The adsorbent capacity at equilibrium is calculated from the adsorption process using Equation 1. The Langmuir adsorption isotherm equation is presented in Equation 2 [16].

$$q_e = (C_0 - C_e) \frac{V}{C_{adsorbent}} \quad (\text{Eq. 1})$$

$$\frac{C_e}{q_e} = \frac{1}{K_a \cdot Q_m} + \frac{1}{Q_m} \times C_e \quad (\text{Eq. 2})$$

Where q_e is the adsorption capacity at equilibrium, C_0 is the initial concentration, C_e is the equilibrium concentration. Adsorption data at various initial concentrations are plotted with a graph following equation 3.2 so that the maximum adsorption capacity (Q_m), and Langmuir constant (K_a) Can be determined [17]. Making cells for lithium battery anodes are shown in the following scheme 3. How anode cell works analysed in scheme 3



Scheme 3: How anode cell works

3. Results and Discussion

The effect of catalyst concentration on CNSs products was characterised by SEM-EDS, TEM, Raman, XRD, BET, and XPS analysis. In addition, initial application tests were carried out, namely the adsorption of methylene blue dye and CV tests as lithium battery anodes.

3.1. SEM Characterization

Visually, from the results of SEM analysis, it can be seen that the CNSs obtained are in the form of a conglomeration of spheres, not as a single sphere (Nieto-Marquez, Romero et al., 2010). In addition, as the catalyst concentration increases, the number of CNSs on the surface of AC increases. In addition, SEM tests were carried out for samples made without ferrocene catalysts, so it can be

believed that catalysts play a role in forming CNSs from cooking oil. The results of the SEM analysis are presented in Figure 1.

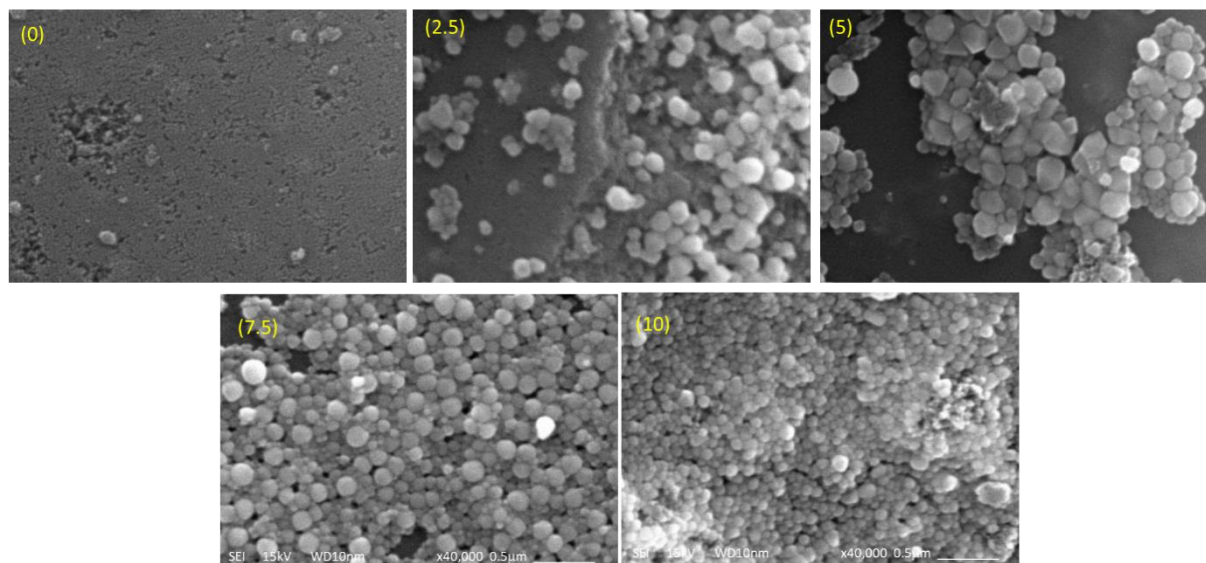


Figure 1: SEM analysis of CNSs with the catalyst at different concentrations of precursor

3.2 TEM Characterization

The presence of CNSs and iron catalysts can be observed more clearly in the TEM analysis presented in Figure 2. The results of the TEM analysis show that at small catalyst concentrations, the amount of CNSs produced is relatively small. Along with the increase in catalyst concentration, the amount of CNSs produced is also more significant, so it can be concluded that the catalyst concentration significantly affects the growth of CNSs. However, it can be observed from the TEM analysis that the particle size of CNSs produced on various catalyst variations is similar. This differs from the results obtained using the urea co-precipitation catalyst deposition method and ferrocene as the catalyst. In this study, along with the increase in catalyst, the number of CNSs observed from SEM and TEM analysis increased, was homogeneous, and was smaller [18-19]. This is thought to be caused by differences in catalyst deposition methods, where in this study, the ferrocene catalyst, which is well soluble in non-polar solvents, is mixed directly with the precursor so that its size depends on the solubility properties and ultimately does not provide a CNSs size that is much different in variations in catalyst concentration.

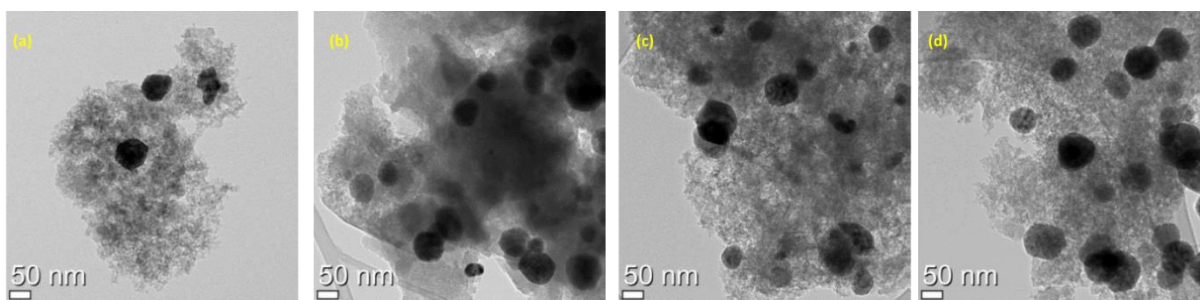


Figure 2: TEM analysis of CNSs with catalyst concentrations at (a) 2.5/100mL, (b) 5/100mL, (c) 7.5/100mL, and (d) 10g/100mL. precursor

3.3. EDS Characterization

The presence of an iron catalyst can also be observed from the composition analysis results on the surface of AC using EDS (Table 1). It can be seen that along with the increase in the amount of catalyst used, there is an increase in the number of iron and oxygen atoms on the sample's surface. However, there is a deviation in the sample with a catalyst concentration of 10 g/100mL, where the concentration obtained is lower than that of 7.5 g/100mL. This deviation can be caused by the catalyst not being evenly distributed across the surface of the AC, so there is a deviation when the analysis is carried out. This is because the EDS analysis is local, only at one position being analysed, as in the example presented in Figure 3. Another exciting thing observed is the significant increase in the number of oxygen atoms, even more remarkable when compared to the supposed ratio between iron and oxygen in magnetite, which is 3:4. Some oxygen atoms are suspected to react with the carbon surface, either in activated carbon or nanocarbon, so that functional groups are formed on the surface of activated carbon.

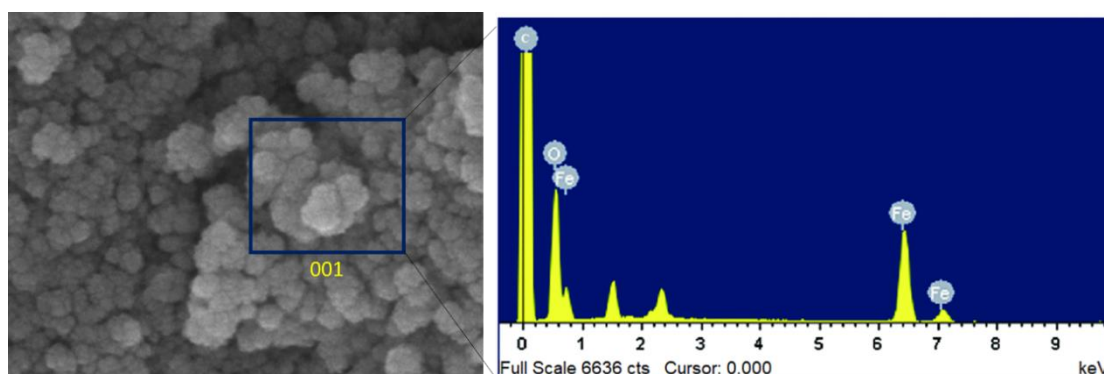


Figure 3: Example of EDS analysis results of CNSs with a catalyst concentration of 2.5g/100mL precursor

Table 1. EDS analysis results

Catalyst	% mass	% atomic
----------	--------	----------

(g/100mL)	C	O	Fe	C	O	Fe
0	97.39	2.68	0.00	98.05	2.03	0.00
2.5	88.65	8.11	3.27	92.91	6.47	0.74
5	73.74	16.47	9.79	83.56	14.01	2.38
7.5	58.53	23.05	18.43	73.28	21.66	4.96
10	71.69	18.58	9.71	81.67	15.90	2.37

3.4. XRD Characterization

The results of XRD analysis at various catalyst concentrations are presented in Figure 4. From the results of the XRD analysis, it can be seen that all samples generally maintain the amorphous structure of activated carbon as a support for nanocarbon growth. In each sample, there are peaks at 27.1° and 42.8° , which indicate the sp^2 carbon C (0-0-2) and C (1-0-0) [20]. Meanwhile, Fe -peaks were observed at 29.7° (2-2-0), 36.1° (3-1-1), 45.4° (400), 58.5° (4-2-2), and 64.9° (4-4-0) [21], where the Miller Index is written in brackets. The XRD analysis showed the magnetite (Fe_3O_4) content on the surface of AC. When compared with the analysis of activated carbon without a catalyst as a control, presented in Figure 5, it can be seen that no sp^2 carbon or iron peaks appear. The XRD curve of activated carbon without a catalyst shows broad peaks at 23° - 30° and 40° , which indicate the amorphous carbon structure commonly found in activated carbon [22]. During pyrolysis the ferrocene catalyst undergoes decomposition based on the reaction: $Fe(C_5H_5)_2 \rightarrow Fe + C_xH_y$. The iron atoms released from ferrocene are the catalysts in synthesising nanocarbons. During the pyrolysis process, the oil used decomposes into simpler hydrocarbons, such as C_xH_y and $C_xH_yO_z$, in addition to the formation of CO and CO_2 . [23] The carbon molecules from the oil decomposition will build the nanocarbon structure. It is suspected that the oxygen content from the oil decomposition then reacts with iron to form magnetite.

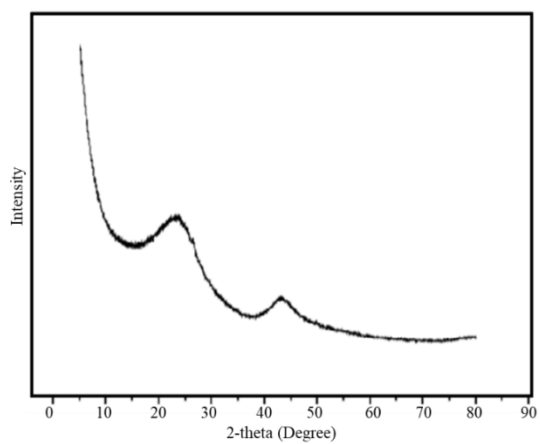


Figure 5. XRD analysis on samples without catalyst

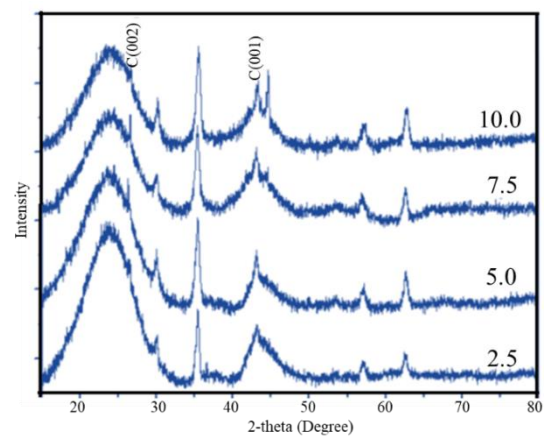


Figure 4: XRD analysis at various catalyst concentrations

3.5. BET Characterization

The characteristics of the pores of standard activated carbon and activated carbon deposited by CNSs are presented in Figure 6 and Table 2. Based on the adsorption isotherm curve, it can be concluded that the adsorption isotherm of the activated carbon sample shows type IV isotherm based on IUPAC, where the structure of the deposited activated carbon has a micropore-mesoporous structure. This is indicated by a hysteresis loop indicating nitrogen condensation in the mesopores of activated carbon [24].

The distribution of pores is presented in Figure 7. Based on the pore distribution, it can be seen that the products obtained are mostly micropores ($<20\text{\AA}$) and mesopores ($20\text{-}500\text{\AA}$), but the distribution of macropores is not observed. These results are consistent with those shown by the pore diameter measurement in Table 2. The iron catalyst and CNSs partially closed the pores, reducing the surface area and pore volume of activated carbon deposited by CNSs. However, increasing the amount of catalyst in the synthesis of CNSs did not provide significant changes to the surface area, pore volume or pore diameter. In the studies conducted by Nguyen et al. (2022) [25] prepared carbon nanofibers (CNFs) and Arie et al. (2016) prepared CNSs on the surface of AC, there was a decrease in the surface area and pore volume due to the closure of the pores by the nanocarbon product. The reduction in surface area in CNFs deposition reached 90%, and 96% in CNSs deposition. The nanocarbon products formed cover all the active carbon pores.

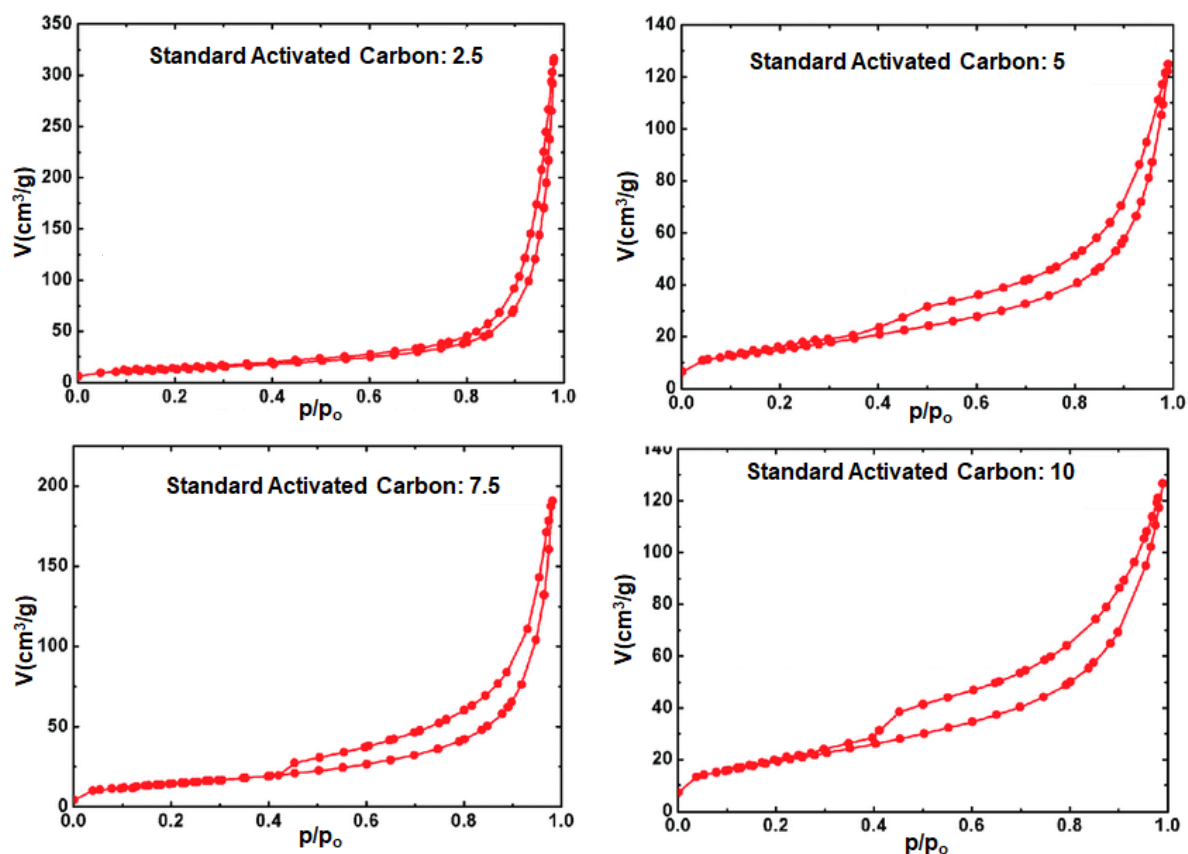


Figure 6. Adsorption isotherm curve

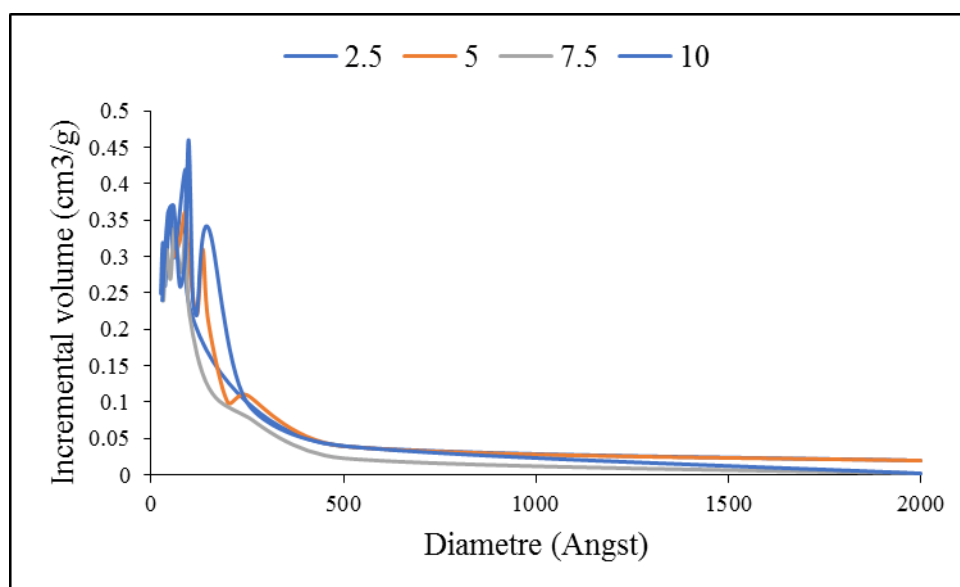


Figure 7. Distribution of BJH pores

Table 2. Sample pore characteristics

Sample	<i>BET surface</i>	<i>Pore Volume</i> (cm ³ /g)	<i>Pore Diameter</i> (Å)
--------	--------------------	--	-----------------------------

	<i>area (m²/g)</i>		
AC Standard	781.05	0.64	33.27
2.5	492.15	0.46	37.47
5	488.59	0.47	38.88
7.5	464.91	0.45	39.08
10	488.76	0.47	39.02

3.6. Raman Characterization

Raman spectra of samples at various concentrations are presented in Figure 8. From the Raman spectra, it can be seen that all samples have peaks at 1334cm^{-1} (D-band) and 1597cm^{-1} (G-band). The D-band peak indicates a random graphite structure, while the G-band indicates a regular carbon structure [26]. A comparison of D-band (I_D) and G-band (I_G) intensities can be used to determine the characteristics of the obtained carbon products. A comparison of the I_D and I_G of each sample is presented in Figure 9. The I_D/I_G value obtained is a typical value for the range of CNSs products, between 0.84 and 1.2 [27]. The difference in I_D/I_G values at catalyst concentrations of 2.5g/100mL can also be observed in 5, 7.5, and 10g/100mL catalysts. This shows that at low catalyst concentrations, the carbon nanostructures formed are still relatively few, so the carbon structure tends to be random (irregular). With the increase in catalyst, the carbon nanostructures formed become more, so that the G-band peak becomes more dominant, and it can be interpreted that the carbon product structure becomes

more graphitic. This is based on the results of the XRD spectra

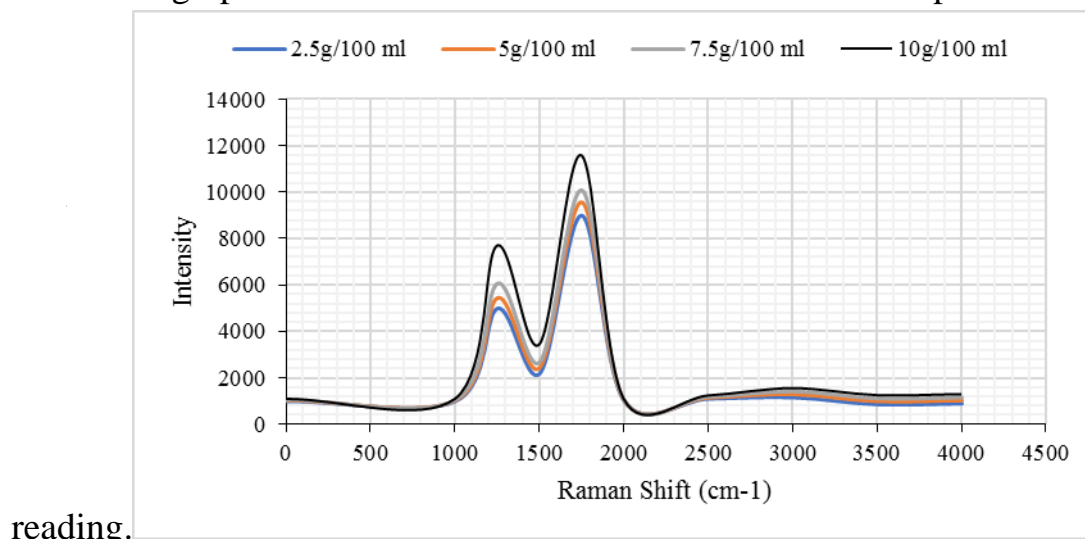


Figure 8. Raman spectra of samples at various concentrations

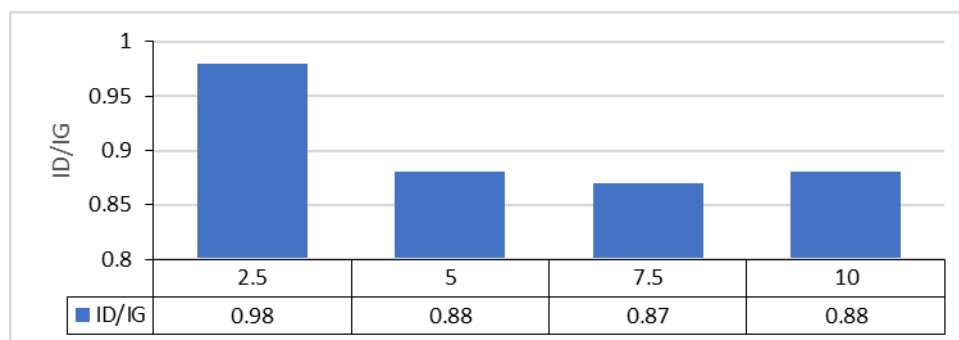


Figure 9. Comparison of I_D and I_G at various catalyst concentrations

3.7. XPS Characterization

An XPS analysis was carried out to confirm the suspicion of the formation of functional groups on the surface of activated carbon. An example of fitting on standard activated carbon for C1s is presented in Figure 10, and complete fitting data is presented in Table 3. All spectra observed a binding energy peak at around 284.5 eV, indicating a graphite structure, namely a C=C sp² double bond with no functional group [28]. All samples have a spectral peak at around 285.9-286.3 eV, indicating the presence of C-O- functional groups in phenol, alcohol, or ether bonds on the surface of activated carbon [29]. In addition, there is a peak at around 288.1-288.2 eV, indicating C atoms bonded to carboxyl or ester groups (-COO) on activated carbon [28-29].

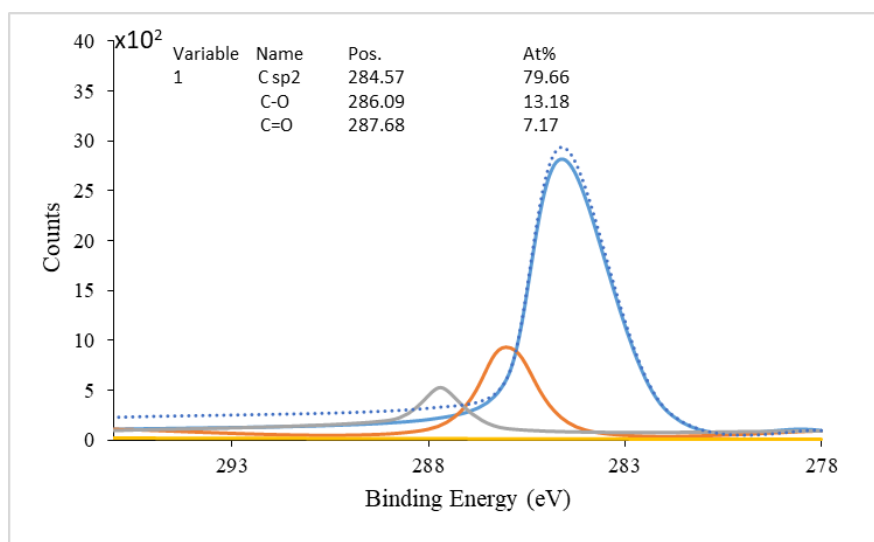


Figure 10. Fitting of C1s spectra for standard activated carbon samples

Table 3. Functional group composition of C1s spectra

Catalyst (g/100mL)	% Functional groups		
	C-sp ²	C-O	C=O
0	80.06	12.80	7.20
2.5	80.80	13.00	6.29
5	79.83	12.80	7.40
7.5	78.67	14.40	7.01
10	79.70	12.99	7.38

Based on the fitting results, it can be concluded that there is no significant difference in the amount of catalyst used for the functional groups on the sample surface. It is suspected that this can be caused by the amount of CNSs formed not too much or not covering the entire surface of the activated carbon so that the spectral analysis on the surface of the activated carbon still tends to maintain the composition of its functional groups.

3.8. Methylene blue adsorption test

The fitting results for the Langmuir adsorption isotherm are presented in Figure 11. The maximum adsorption capacity (Q_m) and the Langmuir adsorption constant parameters (K_a) are presented in Table 4. From the R^2 value, it can be

seen that all samples give a value of almost 1, so it can be concluded that the adsorption occurs in accordance with the Langmuir isotherm. Langmuir isotherm has an assumption that the adsorption that occurs is a reversible single-layer adsorption, with the rate-determining stage of adsorption being internal diffusion [30]. The Q_m value in all samples experienced a decrease of almost half in capacity. This is consistent with the decrease in the value of the AC surface area. It can be interpreted that the deposition of CNSs and magnetite content on the surface of activated carbon does not affect the adsorption of methylene blue. In a study by El-Bery et al. (2022) [31], the increased adsorption capacity of activated carbon was due to increased functional groups that increased the adsorption capacity. Different results were obtained in this study due to no changes in the functional groups of activated carbon, as presented in Table 4, so the effect of the surface area of activated carbon on the adsorption capacity became more dominant.

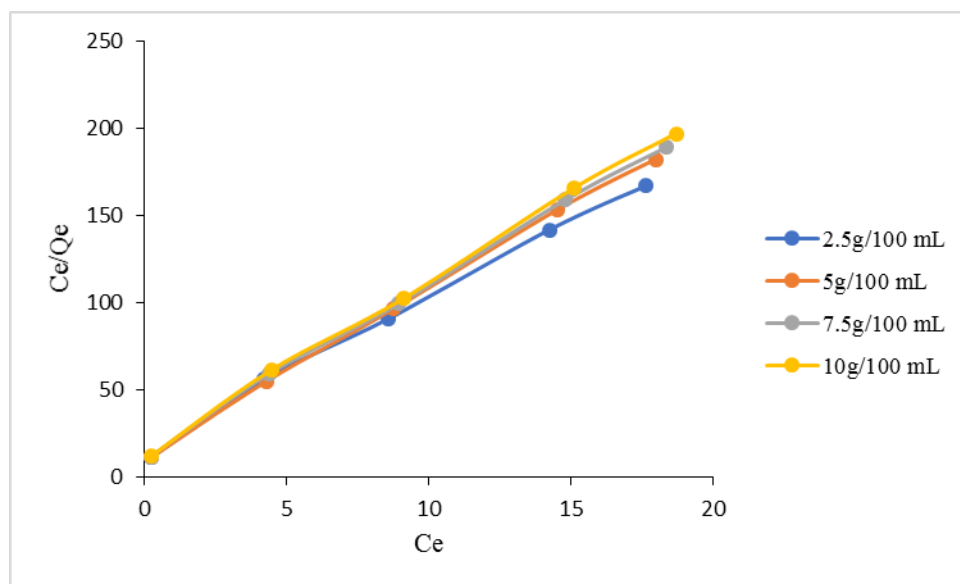


Figure 11: $\frac{C_e}{Q_e}$ vs. C_e curve for various samples

Table 4. Adsorption capacity and Kinetic parameters for the MB removal

	Catalyst (g/100mL)				
Parameter	0	2.5	5	7.5	10
Q_m	0.2188	0.0862	0.0910	0.0932	0.0957
K_a	0.8240	0.7922	0.4747	1.0422	0.8687
R^2	1.0126	1.0171	1.0137	1.0156	1.0109

3.9. Performance test as lithium battery anode with CV

The electrochemical performance of the sample with a catalyst concentration of 2.5g/100mL was tested using cyclic voltammetry (CV). The CV voltammogram curve is presented in Figure 12. In the first cycle, a peak can be seen in the reduction area around 0.25-1.0V, indicating the formation of a solid electrolyte interphase (SEI) [32]. This peak was no longer visible in the second and third cycles. Meanwhile, in each cycle, an oxidation peak was observed at around 0.3V, indicating the existence of an intercalation/deintercalation mechanism of lithium ions in the charge-discharge process [32]. The magnetite content in the sample did not affect the cycle, as indicated by the absence of peaks other than lithium intercalation appearing in the voltammogram. If the iron content in the sample played a role in the cycle, a cathode peak would appear at 0.9V and a reduction peak at 1.65V [33,34]. From the voltammogram obtained, it can be concluded that the CNSs sample on activated carbon with a catalyst of 2.5g/100mL is stable when used as an anode for lithium batteries. Further tests such as Galvanostatic Charge-Discharge, rate cycle, and impedance can be carried out to determine the CNSs sample's performance further.

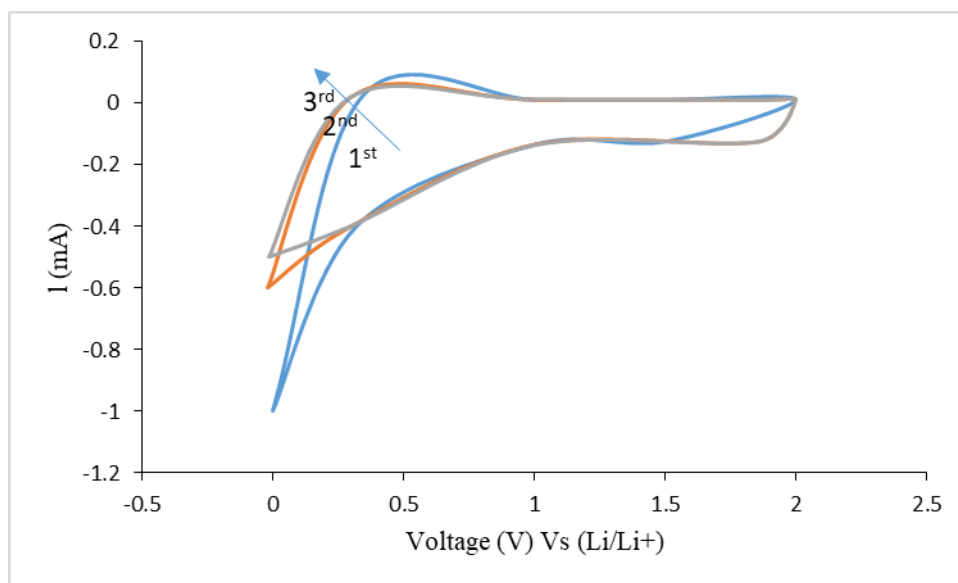


Figure 12: Voltammogram for the sample with 2.5g/100mL catalyst

Conclusion:

Based on the research, it can be concluded that the greater the amount of catalyst used, the more CNSs are deposited on the AC surface, which aligns with the results shown by SEM, TEM, XRD, and Raman analysis. The amount of catalyst added does not affect the functional groups on the AC surface. When used as an adsorbent, the sample's performance decreases, along with a

reduction in surface area due to the deposition of CNSs and catalysts on the AC surface. The performance of the sample with a catalyst of 2.5g/100mL provides stable performance when used as a lithium battery anode, as shown by the half-cell CV test with a voltage range of 0-2V and a scan rate of 0.2mV/s.

Based on the research conducted, there are several suggestions as follows:

1. The homogeneity of the mixture of ferrocene catalyst, cooking oil, and activated carbon can be improved by mixing and impregnation before carbonisation
2. Several studies that need to be carried out, such as the effect of washing to remove iron catalysts and application tests as adsorbents and lithium battery anodes, can be studied further.

References

- [1]. GERGEROGLU, Hazal; YILDIRIM, Serdar; EBEOGLUGIL, Mehmet Faruk. Nano-carbons in biosensor applications: An overview of carbon nanotubes (CNTs) and fullerenes (C60). *SN Applied Sciences*, 2020, 2.4: 603.
- [2]. GUTIÉRREZ-GARCÍA, Carmen Judith, et al. Synthesis of carbon spheres by atmospheric pressure chemical vapor deposition from a serial of aromatic hydrocarbon precursors. *Physica E: Low-dimensional Systems and Nanostructures*, 2019, 112: 78-85.
- [3]. SHI, Liang, et al. Controlled growth of carbon spheres through the Mg-reduction route. *Nanoscale research letters*, 2010, 5: 20-24.
- [4]. ISAEVA, Vera I., et al. Modern carbon-based materials for adsorptive removal of organic and inorganic pollutants from water and wastewater. *Molecules*, 2021, 26.21: 6628.
- [5]. HEIDARI, Ava; YOUNESI, Habibollah. Synthesis, characterization and life cycle assessment of carbon nanospheres from waste tires pyrolysis over ferrocene catalyst. *Journal of Environmental Chemical Engineering*, 2020, 8.2: 103669.
- [6]. ALGADRI, Natheer A., et al. Effect of ferrocene catalyst particle size on structural and morphological characteristics of carbon nanotubes grown by microwave oven. *Journal of Materials Science*, 2017, 52: 12772-12782.
- [7]. WULAN, Praswasti PDK; RIVAI, Ghassan Tsabit. Synthesis of carbon nanotube using ferrocene as carbon source and catalyst in a vertical structured catalyst reactor. In: *E3S Web of Conferences*. EDP Sciences, 2018. p. 03038.
- [8]. KRISTIANO, Hans, et al. Synthesis and characterization of carbon nanospheres using cooking palm oil as natural precursors onto activated carbon support. *Procedia chemistry*, 2015, 16: 328-333.
- [9]. JIN, Yi Zheng, et al. Large-scale synthesis and characterization of carbon spheres prepared by direct pyrolysis of hydrocarbons. *Carbon*, 2005, 43.9: 1944-1953.
- [10]. ZHANG, Junhao, et al. Synthesis, characterization and properties of carbon nanotubes microspheres from pyrolysis of polypropylene and maleated polypropylene. *Materials Research Bulletin*, 2010, 45.1: 15-20.
- [11]. LOU, Zirui, et al. Carbon sphere template derived hollow nanostructure for photocatalysis and gas sensing. *Nanomaterials*, 2020, 10.2: 378.

- [12]. NÁFRÁDI, Bálint, et al. Room temperature manipulation of long lifetime spins in metallic-like carbon nanospheres. *Nature communications*, 2016, 7.1: 12232.
- [13]. ARIE, Arenst Andreas, et al. Effect of Catalyst Preparation Method on the Characteristics of Carbon Nanospheres as Anode Materials of Lithium Secondary Batteries. *Advanced Materials Research*, 2015, 1123: 308-311.
- [14]. KRISTIANTO, Hans, et al. The effect of activated carbon support surface modification on characteristics of carbon nanospheres prepared by deposition precipitation of Fe-catalyst. In: *IOP Conference Series: Materials Science and Engineering*. IOP Publishing, 2016. p. 012034.
- [15]. KARNA, Priya, et al. Synthesis and characterization of carbon nanospheres. *Open Access Library Journal*, 2017, 4.05: 1.
- [16]. KHAMSEH, Ali A. Gh, et al. Investigation of kinetic, isotherm and adsorption efficacy of thorium by orange peel immobilized on calcium alginate. *Scientific Reports*, 2023, 13.1: 8393.
- [17]. MUSTAPHA, S., et al. Adsorption isotherm, kinetic and thermodynamic studies for the removal of Pb (II), Cd (II), Zn (II) and Cu (II) ions from aqueous solutions using Albizia lebbeck pods. *Applied water science*, 2019, 9: 1-11.
- [18]. NIETO-MÁRQUEZ, Antonio, et al. Carbon nanospheres: synthesis, physicochemical properties and applications. *Journal of Materials chemistry*, 2011, 21.6: 1664-1672.
- [19]. GUPTA, Aayush; KOUR, Rajpal; BRAR, Loveleen K. Facile synthesis of carbon nanospheres from saccharides for photocatalytic applications. *SN Applied Sciences*, 2019, 1: 1-8.
- [20]. ARIE, Arenst Andreas, et al. Structural and preliminary electrochemical characteristics of palm oil based carbon nanospheres as anode materials in lithium ion batteries. *Carbon letters*, 2016, 18: 80-83.
- [21]. KOBYLIUKH, Anastasiia, et al. Effect of graphene material structure and iron oxides deposition method on morphology and properties of graphene/iron oxide hybrids. *Applied Surface Science*, 2022, 573: 151567.
- [22]. SHAHCHERAGH, S. K.; BAGHERI MOHAGHEGHI, M. M.; SHIRPAY, A. Effect of physical and chemical activation methods on the structure, optical absorbance, band gap and urbach energy of porous activated carbon. *SN Applied Sciences*, 2023, 5.12: 313.
- [23]. BANCHAPATTANASAKDA, Warintorn; ASAVATESANUPAP, Channarong; SANTIKUNAPORN, Malee. Conversion of waste cooking oil into bio-fuel via pyrolysis using activated carbon as a catalyst. *Molecules*, 2023, 28.8: 3590.
- [24]. THOMMES, Matthias, et al. Physisorption of gases, with special reference to the evaluation of surface area and pore size distribution (IUPAC Technical Report). *Pure and applied chemistry*, 2015, 87.9-10: 1051-1069.
- [25]. NGUYEN, Trong Danh; LEE, Jun Seop. Electrospinning-based carbon nanofibers for energy and sensor applications. *Applied Sciences*, 2022, 12.12: 6048.
- [26]. Roslan, M. S., Chaudary, K. T., Haider, Z., Zin, A. F. M., & Ali, J. Effect of magnetic field on carbon nanotubes and graphene structure synthesized at low pressure via arc discharge process. In *AIP Conference Proceedings* .(2017, March). (Vol. 1824, No. 1). AIP Publishing.
- [27]. HU, Kaiyue, et al. Development of tailored graphene nanoparticles: Preparation, sorting and structure assessment by complementary techniques. *Molecules*, 2023, 28.2: 565.
- [28]. ALIYEV, Elvin, et al. Structural characterization of graphene oxide: Surface functional groups and fractionated oxidative debris. *Nanomaterials*, 2019, 9.8: 1180.
- [29]. SAYĞILI, H.; GÜZEL, F. Usability of activated carbon with well-developed mesoporous structure for the decontamination of malachite green from aquatic environments: kinetic, equilibrium and regeneration studies. *Journal of Porous Materials*, 2018, 25: 477-488.

- [30]. LÓPEZ-LUNA, Jaime, et al. Linear and nonlinear kinetic and isotherm adsorption models for arsenic removal by manganese ferrite nanoparticles. *SN Applied Sciences*, 2019, 1: 1-19.
- [31]. EL-BERY, Haitham M., et al. High adsorption capacity of phenol and methylene blue using activated carbon derived from lignocellulosic agriculture wastes. *Scientific reports*, 2022, 12.1: 5499.
- [32]. ZHANG, Yi, et al. Porous amorphous silicon hollow nanoboxes coated with reduced graphene oxide as stable anodes for sodium-ion batteries. *ACS omega*, 2022, 7.34: 30208-30214.
- [33]. SHENG, Lin, et al. Advances and challenges in electrolyte development for magnesium–sulfur batteries: a comprehensive review. *Molecules*, 2024, 29.6: 1234
- [34]. ABAAS, H. J.; AL-JEBOORI, M. J. New dimeric complexes with semicarbazone mannish-based ligand; formation, structural investigation and biological activity. *Revis Bionatura* 2023; 8 (2) 15. In: *Journal of Physics: Conference Series*. s Note: Bionatura stays neutral with regard to jurisdictional claims in published maps and institutional affiliations., 2021. p. 3-20.

Orthogonal Reverse Derivations with Ideal of semiprime Sets.

Entisar Majid khazil

Ministry of Education

Open EducationI College

The first Rusafa

انتصار ماجد خزل

وزارة التربية\الكلية التربوية المفتوحة

مركز الرصافة الدراسي

مدرس مساعد

Baghdad

Iraq

Orthogonal Reverse Derivations with Ideal of semiprime Sets.

Entisar Majid khazil

انتصار ماجد خزعل

Ministry of Education

وزارة التربية\الكلية التربوية المفتوحة

Open Educationl College

مركز الرصافة الدراسي

The first Rusafa

مدرس مساعد

Baghdad

Iraq

Abstract

I concluded in my research that the nature of relationship between the orthogonality of antiderivatives with the ideal on prime quasi-sets, and we defined the orthogonality of antiderivatives, and we studied the relationship with the ideal on prime quasi-sets, and we reached results and theories that link them.

Subject Classification: 16N60, 16A70, 16Y30

Keywords:

Reverse derivations, orthogonality, semiprime rings, ideals within semiprime rings.

1. Introduction

In the theory of ring structures, derivations play a fundamental role. The assignment operation $f: R \rightarrow R$ is called a derivative on the set R if it satisfies the product rule $f(ab) = f(a)b + af(b)$ for all elements $a, b \in R$, as stated in references [6] and [7].

Building upon this foundational concept, researchers in [2] and [3] have investigated orthogonal derivations in sets. Two mappings F and H on a set R are considered orthogonal if they satisfy the condition $F(a)RH(b) = 0 = H(b)RF(a)$ for all $a, b \in R$.

The study of antiderivatives on semi-primary sets was explored by Saman and Alemany [5], extending the classical theory of derivatives to this specialized context. Further advancing this area of research, the concept of perpendicularity for inverse derivations was introduced in [1]. Specifically, two reverse derivations F and H of a set R are termed orthogonal when $F(x)RH(y) = 0 = H(y)RF(x)$ for all $x, y \in R$.

In the context of semi-primary sets, we study additive subsets that form ideals. Let R be a semi-primary set. A plural subset W of R is called a left (or right) ideal of R if $RW \subseteq W$ (or $WR \subseteq W$), as indicated in [4].

It is important to note that for any subset W of R , the left-handed pesticide $l(W)$ and the right-handed pesticide $r(W)$ are defined as $l(W) = \{x \in R : xW = 0\}$ and $r(W) = \{x \in R : Wx = 0\}$ respectively. In this paper, we have established several theorems and results related to our topic, which is the perpendicularity of antiparallel derivatives to the ideal on semi-elementary sets.

2-The Results

Puzzle 21 [4]: Let R be a semi-prime set without twist 2, let W be a non-zero ideal of R , and let M and N be elements of R such that:

$$A_{nn1}(w) \text{ if } myn + nym = 0 \text{ then } myn = nym = 0$$

proof: let p and p' be two arbitrary components of w , then by postulate

$$\begin{aligned} (MqN) q'(MqN) &= - (NqM) p' (MqN) \\ &= - (N(qMp')M)qN \\ &= (M(pMp') N) qN \\ &= - Mq (Mq'N) qN \\ &= -Mq (Nq'M) qN \\ &= - (MpN) p'(MpN) \end{aligned}$$

This implies $2(MqN) p' (MqN) = 0$

Since R is 2-torison free there for $(MqN) q' (MqN)$

hence $MqN \in A_{nn1}(w)$

we found $MqN = 0$, for all $q \in W$

In the Same way we also find $NqM = 0$

Hence $MqN = NqM = 0$

Puzzle 2.2

Let R be a twist-free semi-prime set, and let W be a non-zero ideal of R so that $\text{Ann}_1(W) = 0$. If M and N are elements of R so that $M(p)WN(p) = 0$ and $M(p)WN(q) = 0$ for all $p, q \in R$, then $M(p)WN(q) = 0$.

Proof: if we assume $M(p)sN(p) = 0$ for all $s \in W$. By linearization, we obtain: $M(p)sN(q) + M(q)sN(p) = 0$

This leads to: $M(p)sN(q) - M(p)sN(q) = -(M(q)sN(p) - M(p)sN(q)) = 0$

Therefore, $M(p)sN(q) = 0$, which means that $M(p)sN(q) \in \text{Ann}_1(W) = 0$. Hence, $M(p)sN(q) = 0$. \square

Main Theorems

Theorem 3.1

Let R be a semiprime set, and let M, N be reverse derivations of R . Let W be a non-zero ideal of R such that $\text{Ann}_1(W) = 0$. Then: $M(p)N(q) + N(p)M(q) = 0$ if and only if M and N are orthogonal.

Proof: (\Rightarrow) Suppose that $M(p)N(q) + N(p)M(q) = 0$. Replacing x by xf , we get: $M(pf)N(q) + N(pf)M(q) = 0$

Expanding using the reverse derivation property: $M(f)p + fM(p)N(q) + N(f)p + fN(p)M(q) = 0$

for all $p, q, f \in W$. By Lemma 2.1, we conclude that M and N are orthogonal.

(\Leftarrow) Contrariwise, if M and N are orthogonal, then: $M(p)WN(q) = 0 = N(q)WM(p)$

This gives us $M(p)sN(q) = 0$ and $N(p)sM(q) = 0$ for all $s \in W$. By Lemma 2.2, we obtain $M(pf)N(q) = 0$ and $N(pf)M(q) = 0$. Since $M(p)N(q) \in \text{Ann}_1(W)$ and $N(p)M(q) \in \text{Ann}_1(W)$, we have: $M(p)N(q) + N(p)M(q) = 0$

Theorem 3.2

Let R be a non-twisting semi-prime set, and let M and N be antiderivatives of R . The following provisions are equivalent: (i) M and N are perpendicular (ii) $MN = 0$ (iii) $MN + NM = 0$ (iv) MN is an antiderivative

Proof: This theorem follows from Lemma 2.1 and Theorem 3.1. \square

Theorem 3.3

Let R be a 2-torsion free semiprime set, and let M and N be reverse derivations of R . Let W be a non-zero ideal of R such that $\text{Ann}_1(W) = 0$. Then the following are equivalent: (i) M and N are orthogonal on R (ii) $MN = 0$ on W (iii) $MN + NM = 0$ on W (iv) MN is a reverse derivation on W

Proof: (i) \Rightarrow (ii), (iii), and (iv): These implications follow from Theorem 3.2.

(ii) \Rightarrow (i): The linearization of $M(p+q)N(p+q) = 0$ gives: $M(p)N(q) + M(q)N(p) = 0$ for all $p, q \in R$

Replacing y by yf , we obtain: $M(p)N(qf) + M(qf)N(p) = 0$ $M(p)(N(f)q + fN(q)) + (M(f)q + fM(q))N(p) = 0$
 $M(p)N(f)q + M(p)fN(q) + N(p)M(f)q + fM(q)N(p) = 0$

Through careful manipulation and using the properties of reverse derivations, we arrive at: $M(p)N(q) + N(p)M(q) = 0$

Since $M(p)N(q) \in \text{Ann}_1(W) = 0$, we have $M(p)N(q) = 0$. Hence, M and N are orthogonal.

(iv) \Rightarrow (i): If we assume MN is a reverse derivation from W to R . Then: $MN(pq) = M(N(pq)) = 0 =$
 $M(N(q)p + qN(p)) = MN(q)p + MqN(p)$

Through substitution and manipulation, we obtain $M(p)N(q) = 0$. Since $M(p)(q) \in \text{Ann}_1(W) = 0$, we conclude that M and N are orthogonal. \square

Corollary 3.4

Corollaries

Let R be a twist-free semi-prime set, and let M be an antiderivative of R . If M^2 is also a derivative, then $M = 0$.

Proof: This follows directly from part (ii) of Theorem 3.3. \square

Corollary 3.5

Let R be a twist-free semi-prime set, and let M be an antiderivative of R . If $M(p)M(p) = 0$ for all $p \in R$, then $M = 0$.

Corollary 3.6

Let R be a twist-free set, Let M and N be antiderivatives of R . If $M^2 = N^2$, then either $M = -N$ or $M = N$.

Theorem 3.7

Let R be a twist-free semi-prime set, and let M and N be antiderivatives of R . If $M(p)M(p) = N(p)N(p)$ for all $p \in R$, then $M + N$ and $M - N$ are orthogonal. Hence, there exist ideals H_1 and H_2 of R , such that $H = H_1 \oplus H_2$ is a direct principal sum in R , $M = N$ on H_1 , and $M = -N$ on H_2 . Proof: Note that: $(M + N)(p)(M - N)(p) + (M - N)(p)(M + N)(p) = 0$ for all $p \in R$. Applying parts (ii) and (iii) of Theorem 3.3, we obtain the desired result.

Corollary 3.8

Let R be a kink-free prime set, and let M and N be antiderivatives of R . If $M(p)M(p) = N(p)N(p)$ for all $p \in R$, then $M = N$ or $M = -N$.

Proof: This follows directly from Theorem 3.7.

Corollary 3.9

Let R be a semi-prime set with property not equal to 2. Let M and N be antiderivatives of R if $M(p)^2 = N(p)^2$, for all $p \in R$ then either $M = -N$ or $M = N$.

References

- [1] Abdul Rhman, M, "On Orthogonal Reverse Derivations of Semi Prime Rings", Iraq Journal of Science, Vol.50, No. 1, pp. 84-88, 2009.
- [2] Argac. V, A. Nakajima and E.Albas, ce On Orthogonal Generalized Devirations of Semi prime Rings, Turk, J. Math, 28, PP-185-194, 2004
- [3] Dutta T.k and S.k. Sardar, Semi prime Ideal and Irreducible Ideal of semiring, Novi Sad J. Math, Vol. 30, No.1, pp. 97-108, 2000
- [4] Fentisar M.K. "Ideal of semiprime Rings with Orthogonal Higher Derivations", Journal of Discrete Mathematical Sciences and cryptography, 2021
- [5] M. Samman, N. Alyamani, "Derivations and Reverse Derivations In Semi prime Rings", International Mathematical forum, 2, No.39, 1895-1902.2007

[6] kamal A. M, (6,j) - Derivations on Prime -Ring", M.SC. Thesis Department of Math, College of Education و Al-Mustansiriya University, 2012

[7] Posner E.C., Derivations in prime Ring's, Pro Amer Math, Soc., YoL. 8, pp. 1093-1100, 1957.

**Estimating the migration of phthalate acid ester plasticizers
in plastic containers for local and imported cooking oils**

Dr. Rawaa Nader Al-Saedy

Department of Biology, College of science of women, university of
Baghdad

Ministry of Education ,Third Rusafa Education Directorate

Rawaa.nader1102a@csu.uobaghdad.edu.iq

Estimating the migration of phthalate acid ester plasticizers in plastic containers for local and imported cooking oils

Dr. Rawaa Nader Al-Saedy

Department of Biology, College of science of women, university of Baghdad

Ministry of Education ,Third Rusafa Education Directorate

Rawaa.nader1102a@cs.w.uobaghdad.edu.iq

Abstract

Phthalate acid esters (PAE) serve as additives in plastic formulations, enhancing flexibility and transparency. Their potential migration from plastic packaging to food can lead to endocrine disruption in consumers. This transfer is contingent on the specific usage conditions designated for each type of plastic. Plasticizers such as di-n-butyl phthalate (DBP), di(2-ethylhexyl) phthalate (DEHP), and diisononyl phthalate (DiNP) play a significant role in the production of plastic bottles utilized for storing edible oils. Since phthalates are not chemically bonded to the plastic structure, they have the potential to migrate into the food contents during storage. This research delved into examining the transfer from phthalate derivatives of PET bottles to edible oil under various storage conditions. The analysis employed a Gas Chromatography-Mass Spectrometry (GC-MS) system. Findings revealed a notable increase in migration, particularly in DEHP levels, with concentrations reaching 115.3 µg/L in the bottled oils after 6 months at 45 °C. This figure surpassed the upper threshold of the maximum contaminant level (MCL) set by the US Environmental Protection Agency, which stands at 6.0 µg/L for DEHP, by a factor of 19.1.

Keywords: Phthalate acid esters, Plasticizers, Gas Chromatography-Mass.

المستخلص

تُستخدم إسترات حمض الفثالات (PAE) كمضافات في تركيبات البلاستيك، مما يعزز المرونة والشفافية. يمكن أن يؤدي انتقالها المحتمل من العبوات البلاستيكية إلى الأغذية إلى اختلال الغدد الصماء لدى المستهلكين. يعتمد هذا الانتقال على ظروف الاستخدام المحددة لكل نوع من البلاستيك. تلعب

الملدنات مثل فثالات ثنائي-ن-بوتيل (DBP) وفثالات ثنائي (2-إيثيل هكسيل (DEHP) (وفثالات ثنائي إيزونونيل (DiNP) دوراً مهماً في إنتاج القناني البلاستيكية المستخدمة لتخزين الزيوت الصالحة للأكل. نظراً لأن الفثالات لا ترتبط كيميائياً بالهيكل البلاستيكي، فإن لديها القدرة على الهجرة إلى محتويات الطعام أثناء التخزين. تعمق هذا البحث في فحص انتقال مشتقات الفثالات من زجاجات البولي إيثيلين تيرفتالات إلى الزيوت الصالحة للأكل في ظل ظروف تخزين مختلفة. استخدم التحليل نظام كروماتوغرافيا الغاز-مطياف الكتلة (GC-MS) وكشفت النتائج عن زيادة ملحوظة في الهجرة، وخاصة في مستويات DEHP، حيث وصلت التركيزات إلى 115.3 ميكروجرام/لتر في الزيوت المعبأة بعد 6 أشهر عند 45 درجة مئوية. وتجاوز هذا الرقم الحد الأعلى لمستوى الملوثات الأقصى (MCL) الذي حددته وكالة حماية البيئة الأمريكية، والذي يبلغ 6.0 ميكروجرام/لتر لـ DEHP، بعامل 19.1. الكلمات المفتاحية: استرات حامض الفثالات، الملدنات، كروماتوغرافيا الغاز-مطياف الكتلة.

1- Introduction

Phthalates, recognized as organic compounds with plasticizing properties, are primarily utilized to enhance the flexibility, lightweight nature, durability, and softness of plastic materials (Carlos *et al.*, 2021; Farhan *et al.*, 2007). Being non-covalently bound to plastics, phthalates exhibit a lipophilic nature and tend to volatilize readily. These characteristics significantly contribute to their potential environmental and food contamination (Giuliani *et al.*, 2020; Chou and Wright., 2007). Owing to their widespread application in food-contact items, various phthalate derivatives, Diethyl phthalate (DEP), notably Dimethyl phthalate (DMP), Di-isobutyl phthalate (DIBP), Dipropyl phthalate (DPP), Butyl benzyl phthalate (BBP), Di-isodecyl phthalate (DIDP), Di-n-butyl phthalate (DBP), Dicyclohexyl phthalate (DCHP), Di-isononyl phthalate (DINP), Di - 2 - ethylhexyl phthalate (DEHp), Di - n - octyl phthalate (DOP), and Di-n-hexyl phthalate (DHP) are frequently detected as residues in food items (Wang X *et al.*, 2020; Guo *et al.*, 2012). Phthalates with elevated molecular weights like DEHP, DINP, and DIDP are employed as plasticizers to impart softness to poly(vinyl chloride) goods. On the other hand, lower molecular weight phthalates such as DBP, DEP, and BBP often function Enhancers in many personal care product (Fan Y *et al.*, 2012). Packaging materials, frequently utilized for packaging milk and dairy products, serve as significant sources of contamination, especially by phthalates like DEHP, DBP, and DINP. Phthalate derivatives contamination in food can stem not only from packaging but also from sources like soil, water, air, and various stages of food processing, transportation, storage, and even cooking within households

(Mondal *et al.*, 2022; Bradley *et al.*, 2013). Due to the lipophilic nature of phthalates, Cooking oils are predisposed to accelerated phthalate migration from plastic surfaces through processing, transportation and storage (Balafas *et al.*, 1999). Consequently, the phthalate content in packaged food is influenced by factors such as the phthalate levels in packaging materials, storage duration, temperature, food fat content, and contact surfaces (Alp *et al.*, 2020; Mikula *et al.*, 2005). Hence, Cooking oils, given Its fat content and use in plastic packaging , are susceptible to phthalate migration (Halden *et al.*, 2021).

Recent animal studies have revealed the toxic impacts of certain phthalic acid esters (PAEs), their primary metabolites, and breakdown products on various organs such as the liver , reproductive system ,kidneys ,lungs , and heart .DEHP & DBP, extensively utilized phthalate esters in food production, processing, and preservation, fall under the category of 'endocrine disrupting chemicals' due to their estrogenic and antiandrogenic properties. Notably, DBP and DEHP have been linked to adverse effects on germ cell development, BBP on epididymal sperm concentration, and DINP and DiNP on liver cells . These chemicals have been associated with reduced sperm counts in males, diminished fertility, testicular alterations, Low birthweight and anomalies in females, particularly during pregnancy (Sedha *et al.*, 2021; Hauser *et al.*, 2004). The impact of phthalates on the body varies based on factors like age, duration of exposure, and level of exposure, with pregnancy, infancy, and puberty identified as particularly sensitive phases (Zota *et al.*, 2010).

Colón *et al.*, 2009 Proposed a potential correlation between PAEs exhibiting known antiandrogenic traits and estrogenic and premature breast development at young PuertoRican girls. Furthermore, experimental studies have unveiled the carcinogenic, teratogenic, and mutagenic potential of phthalates, posing a significant threat to human health (Yıldırım *et al.*, 2020; Lovekamp *et al.*, 2003). To mitigate these risks, regulatory authorities have established legal frameworks governing the presence of phthalates in food.

DEHP , DBP , DEP, BBP and DMP phthalate esters have been classified as "Priority toxic pollutants" by the United States Environmental Protection Agency (USEPA) since 1976 , with reference values set at (20 ,200 and 100)µg/kg body weight / day for DEHP, BBP, and DBP, respectively (Cheng *et al.*, 2016). The (EFSA)European Food Safety Authority has determined the toler able daily doses for DBP ,BBP ,DEHP ,DINP and DIDP as(0.01, 0.5, 0.05, 0.15, and 0.015) mg/kg/day, respectively (EFSA European Food Safety

Authority). Additionally, the European Union directives prescribe legal thresholds for BBP,DEHP,DBP,DINP and DIDP to limit migration into food, with total phthalate levels from plastic in food capped at (60 mg/kg) (European Commision 2007). Similar regulations and thresholds have be adopted in the world through legislative measures (Official Gazette 2013).

In Iraq, cooking oil packaged in plastic containers enjoys widespread consumption across all age groups. This study aimed to assess the potential food safety and public health hazards associated with phthalate migreation over varying storage durations. Over the shelf life, cooking oil samples were scrutinized for three phthalate esters, obtained from both domestically produced and imported plastic containers.

2- Material and Methods

2-1 Storage condition

Fifteen samples of oils packed in 1000 ml plastic bottles were randomly collected from the local market of Baghdad city at the start time (production date 7-14 days).

The samples were classified into three groups based on their storage conditions, which included differences in temperature and duration.

The first group included bottled oil stored at 5°C in a refrigerated environment, with extraction measurements performed initially and after three and six months.

The second group included bottled oil stored at 25°C in a controlled environment, with extraction assessments performed initially, as well as after three and six months.

The third group included bottled oil stored at 45°C in a controlled environment, with extraction assessments performed initially and after three and six months.

2-2 Preparation of oil samples

The sample volume, around (1L), is sequentially extracted with methylene chloride under alkaline conditions (pH above 11) utilizing either a separatory funnel or a continuous extraction technique as outlined in methode 625(EPA , 2007) .

2-3 Preparation (DBP), (DEHP), and (DiNP)) as a standard :

Standard solutions(1.00 µg / µL) can be created using high-purity standard substances or acquired in the form of authenticated solutions.

2-4 Identification and determination of plasticizers (phthalate derivatives) using gas chromatography GC-MS

When separating phthalates using gas chromatography-mass spectrometry (GC-MS), the following detailed conditions and parameters were applied:

1. Column selection :The selection of a gas chromatography column is very important for the separation of phthalates derivatives, where a stable low-bleed and high-temperature column DB-5MS was used.
2. Temperature programming: The temperature program was used using a precise gradient to effectively separate phthalates based on their boiling points and polarity, where the initial, ramp and final temperatures were carefully adjusted to achieve optimal separation.
3. Carrier gas: A high-purity carrier gas (helium) was used to carry the sample through the column. The flow rate was for effective separation and detection in the mass spectrometer.
4. Injector temperature: The injector temperature was set at (280C) to ensure effective evaporation of the sample without causing degradation.
5. Mass Spectrometry Conditions: We determined the appropriate ionization mode for phthalates (chemical ionization) which is the optimal ionization for phthalate detection. Ionization energy, ion source temperature, and other mass spectrometer parameters were adjusted for sensitive and selective detection.
6. Sample Preparation: Samples were prepared using appropriate extraction methods using liquid-to-liquid extraction to isolate phthalates from the sample matrix.
7. Injection Volume: Optimize the injection volume to introduce a representative amount of sample without overloading the system. The injection volume should be within the linear range of the detector for accurate quantification where the injection volume was (1 uL)
8. Calibration: The GC-MS system was calibrated using standard solutions of phthalates to create calibration curves for quantification, where a range of concentrations were used to cover the expected concentrations of phthalates in the samples.

9. Data Analysis: GC-MS data were processed using a special software to identify and quantify phthalate compounds based on their mass spectra and retention times and compared to experimental mass spectra from reference libraries for compound identification.

By carefully tuning and optimizing these detailed conditions, we were able to efficiently separate, identify and quantify phthalate compounds using gas chromatography-mass spectrometry (GC-MS).

3-Result and Discussion:

The notion of the total migration limit have historically served to oversee the collective transfer of substances from plastic to food items and to ascertain the potential health implications of these substances (Arvanitoyannis&Bosnea 2004). Regarding the migration process, it can be delineated into four primary phases: the diffusion of chemical compounds across polymers, the adsorption of diffused molecules from the polymer surface, the interaction of compounds at the interface between plastic and food, and the absorption of compounds into the food product (Ferrara *et al.*, 2001). Research delved into the migration of plasticizer compounds from PET bottles to samples procured from local markets, with the outcomes detailed in Table 1. The investigation observed the transfer of PET derivatives to samples housed in PET containers under varying temperature conditions and durations. At an initial storage temperature of 5°C, contamination with plasticizer compounds from PET bottles was evident for DEHP and DPB derivatives at concentrations of 2.11 and 1.31, respectively, while no contamination was noted with DiNP. In contrast, at 25°C, all PET derivatives examined in this study (DEHP, DBP, and DiNP) manifested at concentrations of 6.13, 3.51, and 1.18 µg/L. However, at 45°C, concentrations of DEHP, BBP, and DiNP surged to 7.55, 4.87, and 1.93 µg/L, respectively, as depicted in Table 1. The migration of PET derivatives like DEHP, DBP, and DiNP exhibited a notable escalation from the outset to three months at 5°C by 7.73 , 3.61 and 0.83 µg/L . For instance, when oil was stored initially at 20°C, PET derivatives such as DEHP, DBP and DiNP were detected at concentrations of 11.76 , 6.0 and 3.22 µg/L, respectively. At 45°C, concentrations of DEHP, DBP, and DiNP recored to 13.86 , 8.57 and 5.74 µg/L, respectively, as outlined in Table 1 .

It was observed that all the polyethylene terephthalate derivatives were transferred to the bottled oils stored in polyethylene terephthalate bottles after

six months, as Table (1) showed an increase in concentration with increasing temperatures, where DEHP represented the maximum concentration of polyethylene terephthalate derivative (115.3) $\mu\text{g/L}$, while DBP showed a high increase after six months by (36.01) $\mu\text{g/L}$, while the concentration of DiNP was (19.0) $\mu\text{g/L}$.

The maximum allowable contaminant level (MCL) for DEHP has been set by (EPA) standards and (WHO) guidelines (6 / 8 $\mu\text{g/L}$) respectively, (FDA,2011 & EPA,2009). The concentration of DEHP in this study exceeded the (MCL) set by EPA standards and WHO guidelines by (19 , 14) times. The (US EPA) has proposed a MCL of (10 $\mu\text{g/L}$) for BBP ,the BBP values in this study exceeded the MCL as well as for DiNP.

Table 1 displays the concentrations of PET derivatives (DEHP, DBP, and DiNP) in bottled oil across varying storage durations (initial time, after 3 months, and after 6 months) under different temperature conditions (5°C, 25°C, and 45°C).

PET derivatives ($\mu\text{g/L}$)	Temperature	Concentration for Three Periods (ppb)		
		Start Time	After 3 Months	After 6 Months
DEHP	5 °C	2.11	7.73	31.31
	25 °C	6.13	11.76	88.0
	45 °C	7.55	13.8	115.3
	5 °C	1.31	3.61	21.81

DBP	25 °C	3.51	6.00	29.2
	45 °C	4.87	8.57	36.01
DiNP	5 °C	0.00	0.83	2.21
	25 °C	1.18	3.22	6.33
	45 °C	0	1.93	19.0

3- Conclusion

Based on the results obtained from the study on the migration of plasticizer compounds from PET bottles to food samples stored under various conditions, several conclusions can be drawn:

- ✓ Migration of PET Derivatives: The study revealed a significant migration of PET derivatives, including DEHP, DBP, and DiNP, from PET bottles to the samples stored within them. The concentrations of these compounds increased with higher temperatures and longer durations of storage, indicating a higher risk of contamination as environmental conditions became more severe.
- ✓ Temperature Influence on Migration: The temperature played a crucial role in the migration process. Higher temperatures led to greater migration of plasticizer compounds into the food samples. For instance, at

45°C, the concentrations of DEHP, BBP, and DiNP significantly increased, showing a clear correlation between temperature and migration levels

- ✓ Long-Term Effects: Over an extended period of six months, all PET derivatives were observed to transfer to the oils stored in PET bottles. This long-term exposure resulted in a substantial increase in concentrations, with DEHP exhibiting the highest concentration among the PET derivatives studied.
- ✓ Violation of Maximum Allowable Contaminant Levels (MCL): The concentrations of DEHP exceeded the MCL set by EPA standards and WHO guidelines by a significant margin, indicating a potential health risk associated with the migration of this compound. Similarly, the concentrations of BBP and DiNP also surpassed the proposed MCL values, highlighting the need for regulatory action to address these elevated levels of contamination.

In summary, the study underscores the importance of monitoring and regulating the migration of plasticizer compounds from PET bottles to food products, especially considering the potential health implications associated with the exceedance of MCL values for certain compounds like DEHP, BBP, and DiNP. These findings emphasize the necessity of stringent regulations and quality control measures to ensure the safety of food products stored in plastic containers.

5- References

1. Alp AC, Yerlikaya P: Phthalate ester migration into food: Effect of packaging material and time. *Eur Food Res and Technol*, 246, 425–435, 2020. DOI: 10.1007/s00217-019-03412-y .
2. Balafas D, Shaw KJ, Whitfield FB: Phthalate and adipate esters in Australian packaging materials. *Food Chem*, 65, 279-287, 1999. DOI: 10.1016/S0308-8146(98)00240-4.
3. Bosnir J, Puntaric D, Galic A, Skes I, Dijanic T, Klaric M, Grgic M, Curkovic M, Smit Z: Migration of phthalates from plastic containers into soft drinks and mineral water. *Food Technol Biotechnol*, 45 (1): 91-95, 2007.
4. Bradley EL, Burden RA, Leon I, Mortimer DN, Speck DR, Castle L: Determination of phthalate diesters in foods. *Food Addit Contam*, 30 (4): 722-734, 2013. DOI: 10.1080/19440049.2013.781683.

5. Cao XL, Zhao W, Churchill R, Hilts C: Occurrence of di-(2-ethylhexyl) adipate and phthalate plasticizers in samples of meat, fish, and cheese and their pack aging films. *J Food Prot*, 77 (4): 610-620, 2014. DOI: 10.4315/0362-028X.JFP-13-380.
6. Cao XL: Phthalate esters in foods: Sources, occurrence, and analytical methods. *Compr Rev Food Sci Food Saf*, 9 (1): 21-43, 2010. DOI: 10.1111/j.1541-4337.2009.00093.
7. Carlos KS, de Jager LS, Begley TH: Determination of phthalate concentrations in paper-based fast food packaging available on the U.S. market. *Food Addit Contam*, 38 (3): 501-512, 2021. DOI: 10.1080/19440049.2020.1859623 .
8. Cheng Z, Li HH, Wong HS, Zhu XM. Sthiannopkao S: Dietary exposure and human risk assesment of phthalate esters based on total diet study in Cambodia. *Environ Res*, 150, 423-430, 2016. DOI: 10.1016/j.envres.2016.06.011.
9. Chou K, Wright RO: Phthalates in food and medical devices. *J Med Toxicol*, 2 (3): 126-135, 2006. DOI: 10.1007/BF03161027.
- 10.Colon I, Caro D, Bourdony CJ, Rosario O: Identification of phthalate esters in the serum of young Puerto Rican girls with premature breast development. *Environ Health Perspect*, 108, 895-900, 2000. DOI: 10.1289/ehp.108-2556932.
- 11.EFSA European Food Safety Authority: Opinion of the scientific panel on food additives flavourings processing aids and materials in contact with food (AFC) on a request from the commission related to di-butylphthalate (DBP) for use in food contact materials. Question No: EFSA-Q-2003-192. *EFSA J*, 242, 1-2, 2005. DOI: 10.2903/j.efsa.2005.242.
- 12.EFSA European Food Safety Authority: Opinion of the scientific panel on food additives flavourings processing aids and materials in contact with food (AFC) on a request from the commission related to Bis (2-ethylhexyl) phthalate (DEHP) for use in food contact materials. Question no: EFSA-Q-2003-191. *EFSA J*, 243:1-2, 2005. DOI: 10.2903/j.efsa.2005.243.
- 13.EFSA European Food Safety Authority: Opinion of the scientific panel on food additives flavourings processing aids and materials in contact with food (AFC) on a request from the commission related to butylbenzylphthalate (BBP) for use in food contact materials. Question

- no: EFSA-Q-2003-190. EFSA J, 241, 1-2, 2005. DOI: 10.2903/j.efsa.2005.241.
14. Eurochem Guide: A focus for analytical chemistry in Europe. 2014. https://www.eurachem.org/images/stories/Guides/pdf/MV_guide_2nd_ed_EN.pdf Accessed: 06.06.2021.
 15. European Commision: Commission Directive 2007/19/EC of 30 March 2007 amending Directive 2002/72/EC relating to plastic materials and articles intended to come into contact with food and Council Directive 85/572/EEC laying down the list of simulants to be used for testing migration of constituents of plastic materials and articles intended to come into contact with foodstuffs. <https://www.legislation.gov.uk/eudr/2007/19/body/adopted>. Accessed: 06.06.2021.
 16. European Directive 10/2011/EU: Commission regulation 10/2011/EU of 14 January 2011 on plastic materials and articles intended to come into contact with food. Off J Eur Union L Series, 2011. 12:1-89. <https://eur-lex.europa.eu/LexUriServ/LexUriServ.do?uri=OJ:L:2011:012:0001:0089:en>; Accessed: 06.06.2021.
 17. Fan J, Jin Q He H, Ren R, Wang S: Detection of 20 phthalate esters in different kinds of food packaging materials by GC-MS/MS with five internal standards. J AOAC Int, 102 (1): 255-261, 2019. DOI: 10.5740/jaoacint.18-0005.
 18. Fan Y, Chen H, Liu H, Wang F, Ma S, Latipa A, Wang S: Analysis of phthalate esters in dairy products - A brief review. Anal Methods, 9, 370-380, 2017. DOI: 10.1039/C6AY02885C.
 19. Farajzadeh MA, Djozan D, Reza M, Mogaddam A, Norouzi J: Determination of phthalate esters in cow milk samples using dispersive liquid-liquid microextraction coupled with gas chromatography followed by flame ionization and mass spectrometric detection. J Sep Sci, 35 (5): 742- 749, 2012. DOI: 10.1002/jssc.201100853.
 20. Farhan H, Norouzi P, Dinarvand R, Ganjali MR: Development of dispersive liquid-liquid microextraction combined with gas chromatographymass spectrometry as a simple, rapid and highly sensitive method for the determination of phtalate esters in water samples. J Chromatogr A, 1172, 105-112, 2007. DOI: 10.1016/j.chroma.2007.10.001.

- 21.FDA Food and Drug Administration: Method of Test for Phthalate Plasticizers in Foods (Draft) 2011. <https://www.fda.gov/downloads/SciencesResearch/FieldsScience/UCM268525> Accessed: 06.06.2021.
- 22.Feng YL, Zhu J, Sensenstein R: Development of a headspace solid-phase microextraction method combined with gas chromatography mass spectrometry for the determination of phthalate esters in cow milk. *Analy Chim Acta*, 538 (1): 41-48, 2005. DOI: 10.1016/j.aca.2005.02.020.
- 23.Fierens T, Holderbeke MV, Willems H, Henauw SD: Transfer of eight phthalates through the milk chain-A case study. *Environ Int*, 51, 1-7, 2013. DOI: 10.1016/j.envint.2012.10.002.
- 24.Giuliani A, Zuccarini M, Cichelli A, Khan H, Reale M: Critical review on the presence of phthalates in food and evidence of their biological impact. *Int J Environ Res Public Health*, 17:5655, 2020. DOI: 10.3390/ijerph17165655.
- 25.Guo Y, Zhang Z, Liu L, Li Y, Ren N, Kannan K: Occurrence and profiles of phthalates in food stuffs from China and their implications for human exposure. *J Agric Food Chem*, 60 (27): 6913-6919, 2012. DOI: 10.1021/jf3021128 .
- 26.Halden RU: Plastics and health risks. *Annu Rev Public Health*, 31, 179-194, 2010. DOI: 10.1146/annurev.publhealth.012809.103714.
- 27.Han Y, Cheng J, Tang Z, He Y, Lyu Y: Widespread occurrence of phthalates in popular take-out food containers from China and the implications for human exposure. *J Clean Prod*, 290:125851, 2021. DOI: 10.1016/j.jclepro.2021.125851.
- 28.Haspolat YK, Çeltik C, Çarman KB, Akbulut UE, Taş T: Çocuk Kronik Hastalarında Beslenme,122, Orient Yayınları, 2021.
- 29.Hauser R, Calafat AM: Phthalates and human health. *J Occup Environ Med*, 62 (11): 806-818, 2005. DOI: 10.1136/oem.2004.017590.
- 30.Kim M, Yun SJ, Chung GS: Determination of phthalates in raw bovine milk by gaschromatography/time-of-flight mass spectrometry (GC/TOFMS) and dietary intakes. *Food Addit Contam Part A Chem Anal Control KORKMAZ, KÜPLÜLÜ, İPLİKÇİOĞLU ARAL, ŞEKER Expo Risk Assess*, 26 (1): 134-138, 2009. DOI: 10.1080/02652030802342471.
- 31.Korkmaz SD, Küplülü Ö: Determination of phthalate in some milk products by liquid chromatography/tandem mass spectrometry. *Ankara Üniv Vet Fak Derg*, 66, 231-236, 2019. DOI: 10.33988/auvfd.436873.

- 32.Lovekamp-Swan T, Davis BJ: Mechanisms of phthalate ester toxicity in the female reproductive system. *Environ Health Perspect*, 111 (2): 139-145, 2003. DOI: 10.1289/ehp.5658.
- 33.Mikula P, Svobodova Z, Smutna M: Phthalates: Toxicology and food safety. *Czech J Food Sci*, 23 (6): 217-223, 2005. DOI: 10.17221/3394-CJFS.
- 34.Milojkovic DS, Andelkovic DH, Kocic GM, Andelkovic TD: Evaluation of a method for phthalate extraction from milk related to the milk dilution ratio. *J Serbian Chem Soc*, 80 (8): 983-996, 2015. DOI: 10.2298/JSC141204028M.
- 35.Mondal R, Chakraborty D, Majumdar D: Phthalate esters from packaged milk and associated human health risk: A monte carlo probabilistic simulation approach. *J Metrol Soc India*, 37 (2): 409-419, 2022. DOI: 10.1007/ s12647-022-00531-y.
- 36.Moraes da Costa J, Seiko Kato L, Galvan D, Aparecida Lelis C, Saraiva T, Adam Conte-Junior C: Occurrence of phthalates in different food matrices: A systematic review of the main sources of contamination and potential risks. *Compr Rev Food Sci Food Saf*, 22, 2043-2080, 2023. DOI: 10.1111/1541-4337.13140.
- 37.Official Gazette: Türk Gıda Kodeksi Gıda İle Temas Eden Plastik Madde ve Malzemelerin Bileşenlerinin Migrasyon Testinde Kullanılan Gıda Benzerleri Listesi Tebliği. Tebliğ No: 2013/35.
- 38.Perestrelo R, Silva CL, Algarra M, Camara SJ: Evaluation of the occurrence of phthalates in plastic materials used in food packaging. *Appl Sci*, 11 (5):2130, 2021. DOI: 10.3390/app11052130.
- 39.Ren R, Jin Q, He H, Bian T, Wang S, Fan J: Determination of 17 phthalate esters in infant milk powder and dairy products by GC-MS with 16 internal standarts. *Chromatographia*, 79, 903-910, 2016. DOI: 10.1007/ s10337-016-3102-4.
- 40.Sakhi AK, Lillgaard ITL, Voorspoels S, Carlsen MH, Loken EB, Brantsaeter AL, Haugen M, Meltzer HM, Thomsen C: Concentrations of phthalates and bisphenol A in Norwegian foods and beverages and estimated dietary exposure in adults. *Environ Int*, 73: 259-269, 2014. DOI: 10.1016/j. envint.2014.08.005 .
- 41.Sedha S, Lee H, Singh S, Kumar S, Jain S, Ahmad A, Bin Jordan YA, Sonwal S, Shukla S, Simal-Gandara J, Xiao J, Huh YS, Han YK, Bajpai VK: Reproductive toxic potential of phthalate compounds - State of art

- review. *Pharmacol Res*, 167:105536, 2021. DOI: 10.1016/j.phrs.2021.105536.
42. Sharman M, Read WA, Castle L, Gilbert J: Levels of di-(2-ethylhexyl) phthalate and total phthalate esters in milk, cream, butter and cheese. *Food Addit Contam*, 11 (3): 375-385, 1994. DOI: 10.1080/02652039409374236.
 43. Sireli UT, Filazi A, Yurdakök-Dikmen B, Iplikcioglu-Cil G, Kuzukiran O, Orhan CE: Determination of phthalate residues in different types of yogurt by gas chromatography-mass spectrometry and estimation of yogurt related intake of phthalates. *Food Anal Methods*, 10, 3052-3062, 2017. DOI: 10.1007/s12161-017-0854-x.
 44. Sorensen KL: Determination of phthalates in milk and milk products by liquid chromatography/tandem mass spectrometry. *Rapid Commun Mass Spectrom*, 20, 1135-1143, 2006. DOI: 10.1002/rcm.2425.
 45. Su TC, Hwang JJ, Sun CW, Wang SL: Urinary phthalate metabolites, coronary heart disease, and atherothrombotic markers. *Ecotox Environ Safe*, 173, 37-44, 2019. DOI: 10.1016/j.ecoenv.2019.02.021.
 46. Swan SH: Environmental phthalate exposure in relation to reproductive outcomes and other health endpoints in humans. *Environ Res*, 108, 177-184, 2008. DOI: 10.1016/j.envres.2008.08.007.
 47. Wang X, Song M, Liu S, Wu S, Thu AM: Analysis of phthalate plasticizer migration from PVDC packaging materials to food simulants using molecular dynamics simulations and artificial neural network. *Food Chem*, 317, 1-9, 2020. DOI: 10.1016/j.foodchem.2020.126465.
 48. Yıldırım Y, Onmaz NE, Gönülalan Z, Hızlısoy H, Al S, Güngör CC, Dişli HB, Dişhan A, Barel M: Effects of bisphenols and phthalates on public health. *Erciyes Vet Fak Derg*, 17 (1): 68-75, 2020. DOI: 10.32707/ercivet.655008.
 49. Yurdakök-Dikmen B, Alpaya M, Kismali G, Filazi A, Kuzukiran O, Sireli UT: In vitro effects of phthalate mixtures on colorectal adenocarcinoma cell lines. *J Environ Pathol Toxicol Oncol*, 34 (2): 115-123, 2015. DOI: 10.1615/JEnvironPatholToxicolOncol.2015013256.
 50. Zota AR, Calafat AM, Woodruff TJ: Temporal trends in phthalate exposures: findings from the national health and nutrition examination survey, 2001-2010. *Environ Health Perspect*, 122, 235-241, 2014. DOI: 10.1289/ehp.1306681.

Representing Kurdish Letters by using Partition Theory

¹Zana Ali Mahmood

^{2}Awreng Baiz Mahmood*

¹Academic researcher, Kurdistan, Iraq

²College of Sciences, University of Salahaddin, Kurdistan, Iraq

¹zanaeducatin2024@gmail.com

^{2*}awring2002@yahoo.com

Representing Kurdish Letters by using Partition Theory

¹*Zana Ali Mahmood*

^{2*}*Awreng Baiz Mahmood*

¹Academic researcher, Kurdistan, Iraq

²College of Sciences, University of Salahaddin, Kurdistan, Iraq

¹zanaeducatin2024@gmail.com

^{2*}awring2002@yahoo.com

Abstract

Given the importance of encryption and maintaining the confidentiality of information and not penetrating it, this paper included encoding letters and words of Kurdish through Abacus James diagram in partition theory. This paper is an extension of the work of many researchers, such as Awreng, Ammar and Ahmed on encoding letters and words using Abacus James diagram for letters in the English language. It is completely natural that this method will have new and very difficult methods as an entrance to a new type of encryption process.

Keywords: Partition theory, e-abacus diagram, encryption and decryption process.

المستخلص

نظراً لأهمية التشفير والحفاظ على سرية المعلومات وعدم اختراقها، تناولت هذه الورقة ترميزاً

لحروف وكلمات اللغة الكردية باستخدام مخطط أباكس جيمس في نظرية التجزئة. يعتبر هذا البحث امتداداً لعمل العديد من الباحثين، مثل أورنك وعمار وأحمد، على ترميز الحروف والكلمات باستخدام مخطط أباكس جيمس للحروف في اللغة الإنجليزية. ومن الطبيعي أن تتطور هذه الطريقة بطرائق جديدة وصعبة للغاية كمدخل إلى نوع جديد من عمليات التشفير.

1. Introduction

James abacus with γ -number is one of the graphical representations for any partition of a non-negative integer and it can be divided into several chains which consist of outer and inner chains. Also, numbers can be represented by a diagram called e -abacus diagram, where every γ -number will be represented by a (\bullet) and the rest of the sites by $(-)$.

Let n be a positive integer. A **composition** of n is a sequence $\mu = (\mu_1, \mu_2, \dots)$ of non-negative integers such that $n = |\mu| = \sum_i \mu_i$. The integers μ_i for all $i \geq 1$ are the parts of μ and $\mu_i = 0$ if $i > k$, we identify μ with $(\mu_1, \mu_2, \dots, \mu_k)$. A composition μ is a **partition** if $\mu_j \geq \mu_{j+1}$, for all $j \geq 1$. Now, Let σ be the number of redundant partsof the partition μ of n , then we have $\mu = (\mu_1, \mu_2, \mu_3, \dots, \mu_r) = (\lambda_1^{\sigma_1}, \lambda_2^{\sigma_2}, \dots, \lambda_m^{\sigma_m})$ such that: $|\mu| = \sum_{i=1}^r \mu_i = \sum_{k=1}^m \lambda_k^{\sigma_k}$, [1]. To clarify the above concepts, we take the partition of 4 by $(4) = (4^1)$ are $(3, 1) = (3^1, 1^1)$ or $(2, 2) = (2^2)$ or $(2, 1, 1) = (2^1, 1^2)$ or $(1, 1, 1, 1) = (1^4)$.

Definition 1.1: An e –Abacus is a Chinese abacus with e vertical runners, labeled $0, 1, 2, 3, \dots, e - 1$ from left to right. We label the positions on the abacus $0, 1, 2, \dots$ from left to right, top to bottom, [2].

Definition 1.2: The γ –numbers are defined by fix μ as a partition of n , choose an integer b greater than or equal to the number of parts of μ and define $\gamma_i = \mu_i + b - i, 1 \leq i \leq b$. The set $\{\gamma_1, \gamma_2, \dots, \gamma_b\}$ is said to be a set of γ –numbers for μ , [2]. In the following diagram we will represent γ –numbers, by many runners depending on e is an integer number greater than or equal to 2 , as follows in Table 1.

Table 1.1. e -Abacus Diagram

<u>Run.1</u>	<u>Run.2</u>	<u>Run.3</u>	...	<u>Run.e</u>
0	1	2	...	$e - 1$
e	$e + 1$	$e + 2$...	$2e - 1$
$2e$	$2e + 1$	$2e + 1$...	$3e - 1$
.
.

James was the first to come up with the idea an e-abacus diagram in 1978 [2]. This topic is important in many topics, especially in the field of encryption and maintaining the security or confidentiality of information. The word “**cryptography**” is derived from the Greek words **Krypto**’s, meaning hidden, and **Graphene**, meaning to write. Historians believe Egyptian hieroglyphics, which began about 1900 B.C.E., to be an early instance of decipherment. The topic of e-abacus diagram was given great

attention in the eleventh century by linking it to cryptography. There is more than one method used to encode the letters which depends on the concepts of partition theory. Eman and others encrypted English letters in 2015 by studying the concept of orbit, [3]. Hadil and Ammar encoded the Syriac letters in 2017 using the e-abacus diagram [4]. Awreng and Ammar also introduced another new technology for encrypting words and sentences in the English language, based on e-abacus diagram in 2019, [5,6]. After that, Ahmed and Ammar encrypted the letters and sentences by linking e-abacus diagram to directed graph theory [7]. In 2021, the question that was asked in the source: Is it possible to break up any fairly large chart into smaller charts? The answer was yes, as formulas were found to provide division for many cases, [8]. And in 2022, Hiba and Ammar found connection between partition theory and mapping, which we will describe as the initial steps toward convergence with other types of mapping by merging a process between them, [9]. In addition, new methods were found by integrating Young's diagram with graph theory, [10]. In 2024, both Ammar and Juan added a row (rows) to the e-abacus diagram,[11]. To learn more concepts about partition theory, e-abacus diagram and Young diagram, you can see the references [12-14]. For this reason, we had to present an encoding of the Arabic-Kurdish letters in this article on the basis of the e-abacus diagram.

Finally, the goal of this paper is to create a database of Kurdish characters to encrypt and decode messages in future papers.

2. Encrypt The Specific Kurdish Alphabet:

The Kurdish alphabet means the letters of the Kurdish alphabet, that is, the basic letters that make up phrases, sentences, or words. These letters are divided into two parts:

i. The first section: silent letters or so-called consonants, which are as follows:

(ئ، ب، پ، ت، ج، چ، ح، خ، د، ر، ڕ، ز، ژ، س، ش، ع، غ، ف، ق، ک، گ، ل، ڵ، م، ن، هـ)

ii. The second section is the vowels, that is, the vowels which are as follows:

(ا، ه، و، وو، ۆ، ی، ئ)

For setting up a concrete security model, firstly we test the letters in an Abacus James diagram in each diagram the symbol of bead "●" is used to represent the position of γ – numbers in such a way that creates 36 upper case Kurdish letters (29 consonant letters and 7 vowels letters and , so the actual sum is 34 letters). It can "و، ی" there are two letters in common also be noted that many of the letters are Arabic letters as well. We take the value of the number e is nine with the same numbers of row's. Get the general Abacus James diagram and then select the location of γ – numbers on it, to get the appropriate shape for each character of the thirty six Kurdish letters. We found the appropriate design for each character, so that each letter appears appropriately and clearly, as follows:

Table 2.1.

Consonants Kurdish Letters

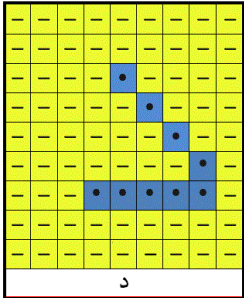
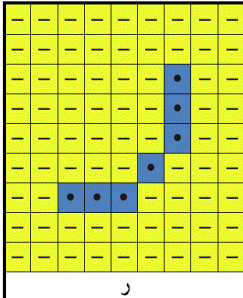
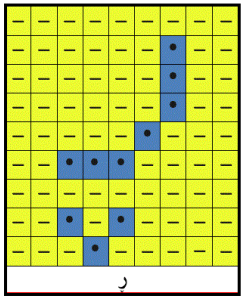
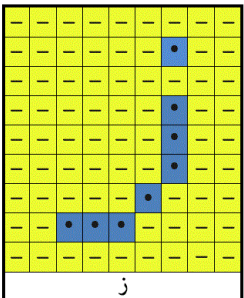
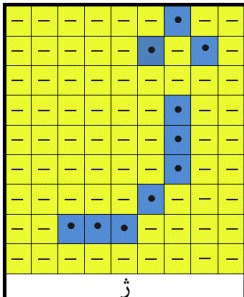
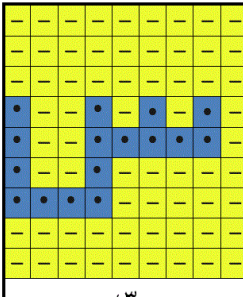
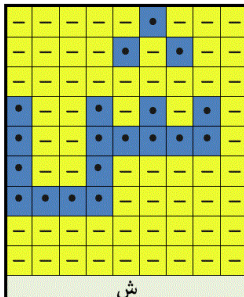
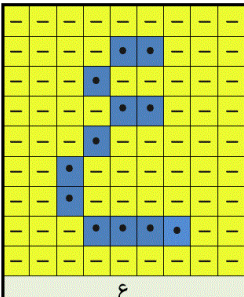
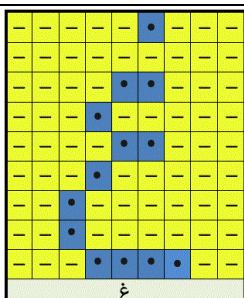
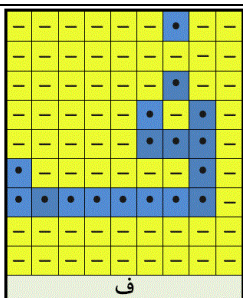
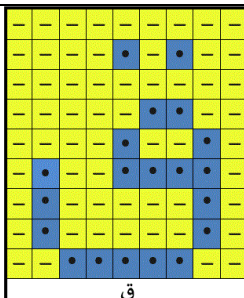
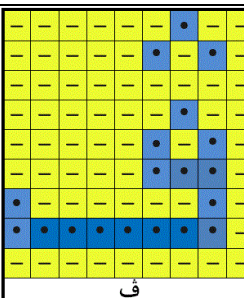
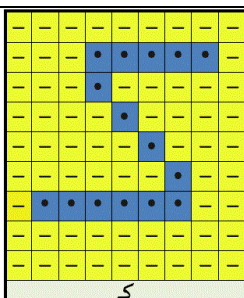
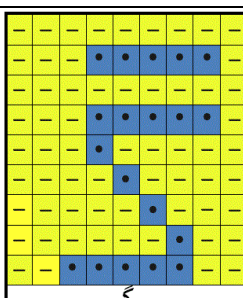
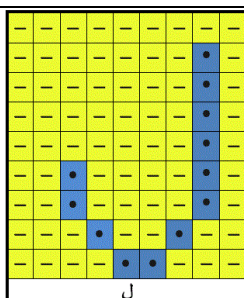
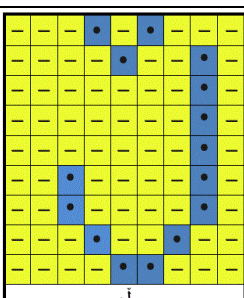
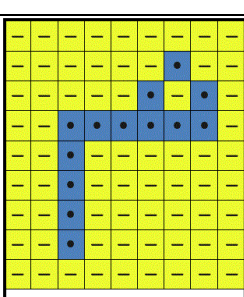
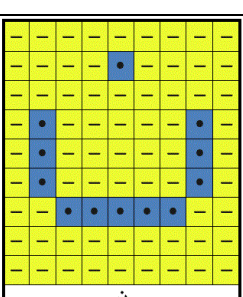
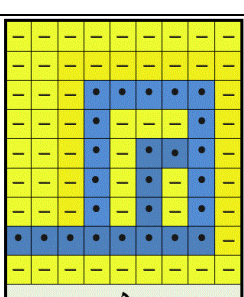
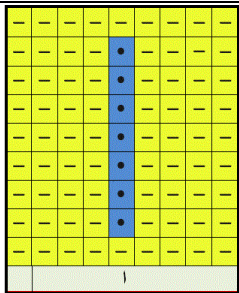
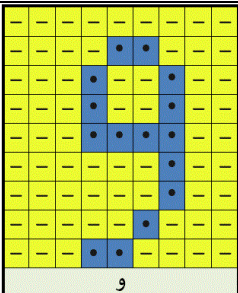
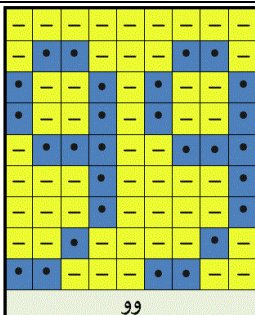
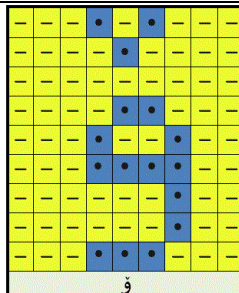
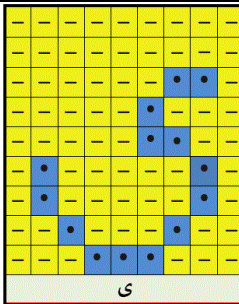
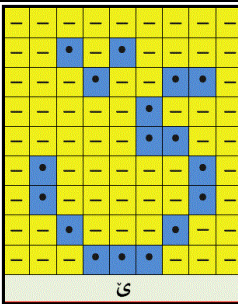
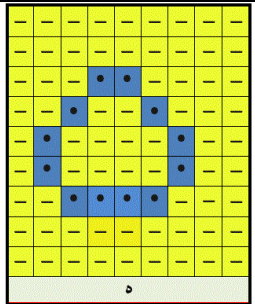
			
			
			
			
			

Table 2.2.

Vowels Kurdish Letters

			
ا	و	ۆ	ژ
			
ی	ێ	ه	

Remark 2.1:

Arabic letters are distinguished by their difference in whether they are at the beginning, interior, or end of the word, but the general form known by them remains preserved. To reduce the use of diagrams, the word will be written on the origin of the letters, ignoring their location, whether it is at the beginning, at the end, or interior the word. This is also what is defined by the remaining letters of the Kurdish letters.

Now, Table 2.3, gives each Kurdish letter a symbol that can be found through partition theory based on James's diagram (Tables 2.1 and 2.2)

Table 2.3. The partition of Kurdish letters

Letters	Partition	Letters	Partition
ـ	$47^6, 44, 36, 28, 26^3, 19, 1$ 2^2	غ	$67^4, 58, 50, 43, 37^2, 28, 21^2, 5$
ا	$62, 54, 46, 38, 29, 21, 13$	ف	$45^8, 44, 38, 37^3, 31, 30, 23, 6$

ب	49,34 ⁵ ,31,26,24,19	ث	52 ⁸ ,51,45,44 ³ ,38,37,30,14,13,6
پ	56,49,48,34 ⁵ ,31,26,26 ,19	ق	59 ⁵ ,56,51,49,44,42 ⁴ ,40,38,36,30 ² ,14,13
ت	32 ⁵ ,29,24,22,17,13,12	ک	51 ⁷ ,49,44,42,34,26,24 ³ ,21,18,14 ,12 ²
ج	53 ⁴ ,44,39,36,28,21,18 ⁵ ,13,4 ²	گ	57 ⁶ ,54,49,46,42,38,29,25 ⁵ ,12 ⁵
چ	54 ⁴ ,42,37,34,31,30,28 ,21,18 ⁵ ,13,4 ²	ل	66 ² ,60,58,54,50,47,43,40,32,24, 16
ح	54 ⁴ ,45,36,28,21,18 ⁵ ,1 3,4 ²	ل	63 ² ,57,55,51,47,44,40,37,29,21, 13,11,4,3
خ	63 ⁴ ,54,46,38,35 ⁵ ,30,2 1 ² ,4	م	53,45,37,29,26,6,23,22,15
د	53 ⁵ ,49,40,31,22	ن	49,5,46,41,39,34,32,27,13
ر	52 ³ ,47,40,32,24	ه	48 ⁴ ,44,40,37,33,29,27,21 ²
ړ	66,59,58,43 ³ ,38,31,23 ,15	ه	46 ⁸ ,45,44,43,39,38,37,33 ³ ,32,28 ,25,21 ⁵
ز	60 ³ ,55,48,40,32,15	و	62 ² ,56,49,41,33 ⁴ ,28,26,21,19,3 ²
ژ	58 ³ ,53,46,38,30,14,13 ,6	وو	50 ² ,47 ² ,46,42,40,36,33,29,26 ³ ,24 ³ , 23,22,21,19 ² ,17,16,14,13 ² ,10 ²
س	43 ⁴ ,38,36,34 ⁵ ,32,31,3 0,29,27	و	62 ³ ,57,49,41 ⁴ ,36,34,28 ² ,11,4,3
ش	39 ⁴ ,34,32,31 ⁵ ,29,28,2 7,26,24,13,12,5	ی	64 ³ ,59,56,53,48,46,41,38 ² 30,24 ²
ع	58 ⁴ ,49,41,34,28 ² ,19,1 3 ²	ی	61 ³ ,56,53,50,45,43,38,35 ² ,27,21 ² ,19,12,11

3. Application of Encryption and Decryption of the Sentences in the Kurdish

In this paragraph, two examples will be given. The first is to encode a sentence of the Kurdish language into a sequence whose elements are made up of partitions and the second example will be to decrypt a sequence into a sentence in the Kurdish language.

Example 3.1: In this example, a sentence in the Kurdish language will be given and it will be encoded into a sequence of numbers whose elements are positive natural numbers, including them raised to powers (the elements of which we get from e -Abacus diagram in partition theory). It is an encoded sentence that can be sent to the requested party. The sentence **welcome to Iraqi Kurdistan** in Kurdish means “به‌خیرین بو کوردستانی عێراق”, this sentence is equivalent in partition theory is

$$\begin{aligned}
 &48^4(49,34^5,31,26,24,19; \\
 &,44,40,37,33,29,27,21^2;63^4,54,46,38,35^5,30,21^2,4;61^3,56,53,50,45,43,38,35^2,27,2 \\
 &1^2,19,12,11;52^3,47,40,32,24;49,34^5,31,26,24,19;61^3,56,53,50,45,43,38,35^2,27,21^2 \\
 &,19,12,11;49,5,46,41,39,34,32,27,13;\emptyset;49,34^5,31,26,24, \\
 &19;62^3,57,49,41^4,36,34,28^2,11,4,3;\emptyset;51^7,49,44,42,34,26,24^3,21,18,14,12^2;62^2,56 \\
 &,49,41,33^4,28,26,21,19,13^2;52^3,47,40,32,24;53^5,49,40,31,22;43^4,38,36,34^5,32,31, \\
 &30,29,27;32^5,29,24,22,17,13,12;62,54,46,38,29,21,13;49,5,46,41,39,34,32,27,13 \\
 &;64^3,59,56,53,48,46,41,38^2,30,24^2;\emptyset;58^4,49,41,34,28^2,19,13^2;61^3,56,53,50,45,43,3 \\
 &8,35^2,27,21^2,19,12,11;52^3,47,40,32,24;62,54,46,38,29,21,13;59^5,56,51,49,44,42^4 \\
 &,40,38,36,30^2,14,13).
 \end{aligned}$$

Example 3.2: In this example, we will be given a sequence of numbers whose elements are positive natural numbers and some of which are raised to powers, and what is required is to find the text that matches it by returning each part of the sequence to its corresponding part based on the tables generated from *e*-Abacus diagram. Take the sequence:

($51^7, 49, 44, 42, 34, 26, 24^3, 21, 18, 14, 12^2; 62^2, 56, 49, 41, 33^4, 28, 26, 21, 19, 13^2; 66^2, 60, 58, 54, 50, 47, 43, 40, 32, 24, 16; 64^3, 59, 56, 53, 48, 46, 41, 38^2, 30, 24^2; 58^3, 53, 46, 38, 30, 14, 13, 6; \emptyset; 60^3, 55, 48, 40, 32, 15; 62, 54, 46, 38, 29, 21, 13; 49, 5, 46, 41, 39, 34, 32, 27, 13; 43^4, 38, 36, 34^5, 32, 31, 30, 29, 27; 32^5, 29, 24, 22, 17, 13, 12; ; 53, 45, 37, 29, 26, 6, 23, 22, 15; 62, 54, 46, 38, 29, 21, 13; 32^5, 29, 24, 22, 17, 13, 12; 53, 45, 37, 29, 26, 6, 23, 22, 15; 62, 54, 46, 38, 29, 21, 13; 32^5, 29, 24, 22, 17, 13, 12; 64^3, 59, 56, 53, 48, 46, 41, 38^2, 30, 24^2; 51^7, 49, 44, 42, 34, 26, 24^3, 21, 18, 14, 12^2$).

If we decode the above sequence and compare it with the resulting tables from *e*-Abacus diagram, then the sentence is “كوليز زانست- ماتماتيك”.

Finally, it is possible to create a program in any system based on the sequences that correspond to the letters obtained from the *e*-Abacus diagram through the use of many algorithms, such as symmetric-key encryption or asymmetric-key encryption that encode the letters into sequences and vice versa.

4. Conclusions:

In the current century and the world's development, encryption is not foolproof, and there are still vulnerabilities that cybercriminals can exploit. Therefore, it is necessary to keep updating encryption techniques and

algorithms to stay ahead of cyber threats. One of the important methods is choosing a language that only a few master, as well as using scientific concepts that only specialists in data analysis master. Therefore, this paper was based on conversational language (**Kurdish**) in addition to the use of the e- Abacus diagram in partition theory. As for creating and developing an algorithm, it is one of the things mentioned in the world of software and developing special codes according to what the programmer requires.

References

1. Mathas A. ; (1999). Iwahori-Hecke Algebras and Schur Algebras of the Symmetric Group, University of Sydney, NSW, Australia, 15.
<http://doi.org/10.1090/ulect/015/02>
2. James G. D. ; (1978). Some combinatorial results involving Young diagrams. Mathematical Proceeding of the Cambridge Philosophical Society, 83, 1-10. <https://doi.org/10.1017/S0305004100054220>
3. Eman E. M., Haslinda I., Ammar S. M. and Nazihah A. ; (2015). Embedding chain movement in James diagram for partitioning β -numbers. AIP Conference Proc 1691 (040019): 1-7.
<https://doi.org/10.1063/1.4937069>
4. Hadil H. S. and Ammar S. M.; (2017). Syriac Letters and James diagram (A) Int. J. of Enhanced Research in Science, Technology Engineering 6 (12): 53-62.
https://www.erpublications.com/uploaded_files/download/hadil-h-sami-prof-dr-ammar-s-mahmood-iraq_FYaXD.pdf

5. Awreng B. M. and Ammar S. M. ; (2019). SecretText by e-abacus Diagram II. Iraqi J. of Science, 60(3):638-646.
<https://doi.org/10.24996/ijs.2019.60.3.22>
6. Awreng B. M. and Ammar S. M. ; (2019). SecretWord by e-abacus Diagram I. Iraqi J. of Science, 60(4):840-846.
<https://doi.org/10.24996/ijs.2019.60.4.17>
7. Ahmed M. A. and Ammar S. A.; (2020). The Graph of e-Abacus Diagram. WSEAS TRANSACTIONS on MATHEMATICS, 19, 486-497.
<https://doi.org/10.37394/23206.2020.19.52>
8. Hanan S. M. and Nadia A. A.; (2021). Splitting the e-Abacus Diagram in the Partition Theory. Iraqi J. of Science, 62(10):3648-3655. <https://doi.org/10.24996/ijs.2021.62.10.23>
9. Hiba R. H. and Ammar S. M. ; (2022). Inclusion Mapping and Partition Theory. 3rd International Conference on Mathematics and Applied Science. Journal of Physics: Conference Series 2322: 1-10.
<https://doi.org/10.1088/1742-6596/2322/1/012027>
10. Ammar S. M. ; (2023). On GCYD-Method In e-Abacus Diagram. Iraqi J. of Science, 64(7):3452-3457.
<https://doi.org/10.24996/ijs.2023.64.7.26>
11. Ammar S. M. and Jwan K. K. ; (2024). Adding Rows in Main e-Abacus Diagrams. Iraqi J. of Science, 65(2):841-852.
<https://doi.org/10.24996/ijs.2024.65.2.21>
12. [George E. A.](#); (1998). The Theory of Partitions. Cambridge University Press- [Mathematics](#) .
13. Burce B. ; (2017). Theory of Partition (Lectures Notes). University of Illinois.
14. Victor K. (2017). The Partition Method for a Power Series Expansion: Theory and Applications. University of Melbourne, Nikki Levy.

**Environmental factors affecting fish distribution
in the Tigris River: a study of the relationship between fish
distribution and the physical and chemical factors of the water.**

Ass.lec.Shayma Abdulwahab

Department of Biology, College of science, university of Baghdad

Ministry of Education ,Third Rusafa Education Directorate

Environmental factors affecting fish distribution in the Tigris River: a study of the relationship between fish distribution and the physical and chemical factors of the water.

Ass.lec.Shayma Abdulwahab

Department of Biology, College of science, university of Baghdad

Ministry of Education ,Third Rusafa Education Directorate

Abstract:

This research focuses on the effects of physical and chemical water factors such as temperature, salinity, dissolved oxygen, and pH on the spatial and seasonal distribution of fish in the Tigris River. An analytical approach was adopted, involving water sample collection from two primary sites: the first between Al-Suwaira and Al-Kut Barrage, and the second between the confluence of the Diyala River and Sheikh Saad District. Field measurements were conducted using advanced techniques, and fish diversity and density were monitored across different seasons to correlate environmental variations with species distribution.

This research focuses on the effects of physical and chemical water factors such as temperature, salinity, dissolved oxygen, and pH on the spatial and seasonal distribution of fish in the Tigris River. An analytical approach was adopted, involving water sample collection from two primary sites: the first between Al-Suwaira and Al-Kut Barrage, and the second between the confluence of the Diyala River and Sheikh Saad District. Field measurements were conducted using advanced techniques, and fish diversity and density

were monitored across different seasons to correlate environmental variations with species distribution.

Findings revealed that the first site exhibited relatively balanced ecological conditions, including moderate temperatures (27.5–29°C), mildly alkaline pH (7.3–7.4), and suitable levels of dissolved oxygen and salinity, supporting the reproduction of fish such as carp and catfish. The dense aquatic vegetation and the geomorphological diversity of this section also contributed to the stability of fish communities.

In contrast, the second site recorded higher concentrations of sulfates (401 mg/L) and sodium (150 mg/L), along with fluctuating pH levels (6.6–7.1) and elevated electrical conductivity (971 $\mu\text{S}/\text{cm}$), indicating environmental stress due to industrial and agricultural discharge, particularly near residential zones. This corresponded with a clear reduction in the abundance of sensitive species during summer months, highlighting the central role of environmental changes in reshaping aquatic biodiversity.

The study concludes that water quality is a decisive factor in sustaining aquatic biodiversity, and any imbalance in physical and chemical parameters can adversely affect fish presence and reproduction. Based on these findings, the research recommends implementing regular environmental monitoring programs, enhancing integrated pollution control systems, promoting aquaculture to alleviate pressure on natural stocks, and ensuring ecological balance in the Tigris River basin.

الملخص:

يتناول هذا البحث دراسة تأثير العوامل الفيزيائية والكيميائية للمياه مثل درجة الحرارة، الملوحة، الأوكسجين المذاب، ودرجة الحموضة (pH) على التوزيع المكاني والموسمي للأسماك في نهر دجلة. استخدمت منهجية تحليلية شملت جمع عينات مياه من موقعين رئيسيين على مجرى النهر: الأول بين منطقتي الصورة وسدة الكوت، والثاني بين مصب نهر ديالى ومنطقة شيخ سعد. اعتمدت الدراسة على قياسات ميدانية دقيقة باستخدام تقنيات حديثة، وجرى رصد تنوع الأسماك وكثافتها في فصول مختلفة لربط التغيرات البيئية بتوزيع الأنواع.

أظهرت النتائج أن الموقع الأول يمتاز بتوازن بيئي نسبي، حيث سجلت درجات حرارة معتدلة (27.5-29 °C) ودرجة pH قلوية خفيفة (7.3-7.4)، مع مستويات مناسبة من الأوكسجين المذاب والأملاح، مما يوفر بيئة جيدة لتكاثر الأسماك مثل الشبوط والقرموط. كما ساهم الغطاء النباتي الكثيف وتنوع تضاريس المجرى المائي في استقرار التجمعات السمكية.

في المقابل، أظهر الموقع الثاني معدلات أعلى من الكبريتات (401 ملغم/لتر)، والصوديوم (150 ملغم/لتر)، إضافة إلى تذبذب في درجات الحموضة (6.6-7.1) وارتفاع في التوصيلية الكهربائية (971 ميكروسيمنز/سم)، مما يدل على تعرض المنطقة لتأثيرات ناتجة عن تصريف صناعي وزراعي، خاصة في النقاط القريبة من المناطق السكنية. وقد انعكس ذلك بانخفاض واضح في كثافة بعض الأنواع الحساسة خلال أشهر الصيف، ما يشير إلى أن التغيرات البيئية لها دور محوري في إعادة تشكيل التوزيع الحيوي.

خلص البحث إلى أن جودة المياه تُعدّ عاملاً حاسماً في استدامة التنوع البيولوجي المائي، وأن أي اختلال في توازن العوامل الفيزيائية والكيميائية يؤثر سلباً على تواجد الأسماك وتكاثرها. وبناءً على هذه النتائج، توصي الدراسة بضرورة تطوير برامج رصد بيئي دورية، وتعزيز المعالجة المتكاملة لمصادر التلوث، إلى جانب تشجيع الاستزراع السمكي للحد من الضغط على المخزون الطبيعي، وضمان التوازن الإيكولوجي في حوض نهر دجلة.

الكلمات المفتاحية: توزيع الأسماك، العوامل البيئية، جودة المياه

Introduction:

Environmental factors play an important role in determining fish distribution in water bodies. Changes in physical and chemical properties of water affect direct growth, breeding and feeding behavior of fish. This study will analyze the relationship between these factors and the distribution of fish, contribute to the development of strategies for the preservation of biodiversity and improve fish production. [1]

Physical and chemical factors for water play an important role in determining the distribution of fish in different water environments. Each fish species affects growth, breeding and feeding behavior with temperature, salinity, dissolved oxygen and pH, for specific environmental conditions. [1]

The temperature is one of the most important factors as it controls metabolic speeds in the fish and affects their activity and movement. Oxygen material dissolved in water also determines the ability to fish, as the level reduction can reduce significant activity or even death of fish. Sourness (pH) affects fish health, as sudden changes can interfere with their important functions. [3]

Study Importance:

- Understanding the impact of environmental factors on fish distribution helps to improve water resources.
- Research contributes to the development of strategies for the preservation of biodiversity of fish.
- It helps to improve the stability of fisheries by identifying factors that affect fishing growth and reproduction.

- It provides scientific data to support environmental policy related to the safety of aquatic ecosystems.

Study Objectives:

1. Analyze the effect of physical and chemical factors such as temperature, salinity and dissolved oxygen on fish distribution.
2. Identify the relationship between water quality and fish diversity in different environments.
3. Propose strategies to conserve fish resources based on the study results.
4. Provide scientific data to support the management of aquatic fisheries and improve their sustainability.

Methodology:

Study areas:

Studying the Impact of Environmental Factors on Fish

Distribution in the Tigris River:

1. The first section between Al-Suwaira and Al-Kut Dam, this section is characterized by dense aquatic vegetation, making it a suitable environment for fish that rely on vegetation for protection and reproduction, Water quality here is affected by the discharge of agricultural and industrial waste, which may affect dissolved oxygen and salinity, The impact of seasonal changes on

fish distribution was studied, as temperatures and water levels vary between summer and winter. [3]

2. The second section extending between the mouth of the Diyala River and the Sheikh Saad District ,this section is important for studying the environmental characteristics of the river as it is affected by the flow of water coming from the Diyala River, which changes the concentration of chemical elements in the water, the impact of sediments and pollutants on water quality and fish distribution is analyzed, especially in areas close to residential and industrial areas, this section is considered rich in various fish species, making it suitable for studying biodiversity and the impact of physical and chemical factors on fish. [4]

–Data and Information Collection

Field Sample Collection

Sample points were identified along the Tigris River in the first and second places. Physical parameters measured: temperature, water flow rate, depth and dissolved oxygen. Chemical parameters analyzed: salinity, organic matter, heavy metal materials and ph. The variation of fish was then studied with regard to species and density, and the effect of these factors on fish distribution, Samples were collected during the summer season, when temperatures rise and dissolved oxygen levels fall, allowing for monitoring of the extreme environmental influences on fish distribution.

Results and discussion:

The first place, the section between Al- Suwayrah and the Al-cut latch, is characterized by the properties of hydrological and geomorphological properties that directly affect the distribution of fish in the Tigris River. The al-cut latch plays an important role in regulating the flow of water, affecting the flow rate and dissolving the oxygen level in the water. The region also includes rivers and aquatic islands, which build different houses for fish and affect their distribution. In addition, the spread of water plants in this area provides shelter and food for fish, but it can also affect the quality of the water through biological interactions.

Table 1: The fundamental physical and chemical traits of the water sample at the first place

S	PH	T.D.S	N.T.U	Tem	EC	Caco 3	Ca	Mg	Cl	So4	K	Na
S1	7.3	592	15	28	942	156	90	24.6	89	223	3.5	76
S2	7.3	586	15	29	931	155	90	24	86	228	3.5	75
S3	7.4	589	18	28.5	951	158	83	25	88	234	3.3	72
S4	7.4	574	22	27.5	913	153	89	23	83	229	3.4	77

This table presents key water quality measurements from four sampling points (S1–S4) along the Tigris River between Al-Suwaira and Al-Kut Barrage. Data shows many important patterns:

The pH level is consistently alkaline (7.3–7.4), which is ideal for most freshwater fishing species. This stability indicates good buffer capacity for acidification.

Total dissolved solids (TDS) show minor changes (574–592 ppm), moderate salinity levels that are usually safe for aquatic, although some reach near the upper limit of some sensitive species.

Sulfate concentrations (223–234 ppm) are particularly high in all samples, more than recommended fresh water guidelines (200 ppm). This possibility shows geological effects and potential pollution inputs.

The temperature remains within a narrow area (27.5–29 ° C), indicating stable thermal conditions that prevent temperature shock on the fish population.

Important minerals such as calcium (83–90 ppm) and magnesium (23–25 ppm) are present in favorable concentrations for fish health and development.

The minor fluctuations between sampling points suggest relatively consistent water quality throughout this river section, though the elevated sulfate levels warrant further investigation into potential pollution sources. The overall parameters indicate suitable conditions for many freshwater fish species, particularly hardy varieties like carp and catfish.

A – Physical Properties:

1 – **pH:** The pH represents an indicator of the basicity and acidity of the water, which greatly affects the effectiveness of the water, as the solution is considered basic if the pH is more than (7), and it is considered an acidic solution if its percentage is less than (7), but if its percentage is (7) it is

considered a neutral solution. We note from the analysis results, as shown in Table (1), that the pH value varied from one sample to another, as the highest concentration was recorded which reached 7.4, and the lowest concentration was 7.3. These values range between the appropriate range for the growth of most fish species, which ranges between 6.5 and 8.5 for most fish species. This percentage ensures a stable aquatic environment that aids in the metabolic and respiration processes of fish, and also affects the availability of nutrients in the water. .[5]

2 – The amount of dissolved or total salts (T.D.S) represents both the negative and positive ions in the water, and most of its sources are inorganic compounds dissolved in the water, such as carbon and sodium, in addition to organic compounds resulting from waste and human activities. It was shown through the results of laboratory analyses, as stated in Table (1), that the highest concentration rate was (592), while the lowest concentration rate of dissolved salts was (574). When comparing these rates with the standard criteria for the suitability of water for fish growth, it was found that it is considered to be water with high salinity, The reason for the increase in the concentration of total dissolved solids (TDS) is the decrease in the river water level, because the total TDS represents the sum of dissolved salts in the water that make up hardness, chlorides, sulfates and alkalinity. Industrial waste, sewage, irrigation water, drains, soil erosion and rain also play an important role in increasing the concentration of total dissolved solids and thus polluting the river and negatively impacting the living ecosystem of fish in the river water. [2] [3]

3–Turbidity NTU : Turbidity is represented by organic materials and inorganic materials in impurities present in water such as sand, plants and mud. It became clear from the results of Table (1) that the highest concentration of turbidity was (22), and the lowest concentration reached (15). Turbidity values are considered suitable for the growth of most fish species. This ratio provides a good balance between water clarity and protection from predators. It also helps maintain the natural environment of fish without negatively affecting respiration or feeding. [6]

4–Temperature: Temperature is of great importance as it contributes to the water treatment process by helping to quickly dissolve chemicals and quickly sediment fine materials. The analysis results showed, as shown in Table (1), that the highest concentration of heat was 29, and the lowest concentration was recorded at 27.5.

These values are considered good for the growth of many fish species, and temperature is one of the most important factors affecting fish life in water. It affects the rate of metabolism, growth, reproduction, and spawning, as fish metabolism increases with increasing temperature. Some water quality factors are also closely linked to temperature. For example, ammonia toxicity increases and oxygen solubility in water decreases with increasing temperature. [8]

B– Chemical properties of water

1– Electrical conductivity (EC) represents the ability of water to transmit electric current. It is a unit of measurement for the dissolved ions of water at

temperature. It is formed from different organic materials that are poor conductors, and inorganic materials that are good conductors of electricity. It is clear from Table (1) that the highest concentration of electrical conductivity was (951), and the lowest concentration was (913). [7]

These electrical conductivity values are considered suitable for many fish species, especially those adapted to moderate levels of dissolved salts. These ranges may be suitable for fish such as tilapia and carp, which can live in environments with low to moderate salinity.

2–Alkaline calcium carbonate CaCO_3 : It was shown through the results of laboratory analyses shown in Table (1), that the highest concentration of calcium carbonate was (158), and the lowest concentration was (153).

Alkalinity values are suitable for fish growth, as they help stabilize the pH and provide an ideal environment for the growth of algae and microorganisms that are part of the fish food chain. .[9]

3– Calcium Ca: Calcium is a positive element and water is classified according to it into water poor in calcium, water with medium calcium content and water rich in calcium content. Calcium is also one of the causes of water hardness and it is clear from Table (1) that the highest concentration of positive calcium ions in the country reached (90), the lowest percentage (83)

Calcium is considered essential for fish growth, as it helps strengthen fish skeletons and improve nervous system function. It also plays an important role in regulating water pH, contributing to a stable environment for fish growth. [6]

4–Magnesium (Mg) : Magnesium is one of the most widespread alkaline ions in fresh water, and it represents one of the basic components within the

chlorophyll molecule. It is noted in Table (1) that the highest percentage of magnesium concentration reached (25), and the lowest percentage was (23).

Magnesium levels in water are an important factor for fish health, as it plays a role in regulating vital processes such as bone growth, muscle function, and the nervous system. Values fall within the appropriate range for freshwater fish, meaning they are safe for most species such as tilapia, carp, and trout. However, it's important to monitor the balance between calcium and magnesium to ensure a stable environment for fish. [10]

5–Chlorides (Cl): These elements are generated as a result of liquid waste from chemical industries. Heavy water also contains a large amount of chlorides. Table (1), which summarizes the laboratory results for samples from the study area, shows that the highest concentration of chlorides reached (89), and the lowest concentration was recorded at approximately (83). It is noted that the water in the study area had chloride levels ranging below 142, which means that it is excellent and safe water for all fish. The effect of chlorides in water depends on the type of fish and the surrounding environmental conditions. [6] In general, chlorides are chemical compounds that can affect water quality and the life of aquatic organisms. Some fish can adapt to high levels of chloride, especially species that live in salt water, while this level may have a negative effect on freshwater fish that need a certain balance of minerals and salts to survive and grow healthily.

6– Sulfates SO₄ :Sulfur can be found in fresh water with the positive ion and surface water has a very low sulfate content, except in areas rich in this element. This element is found due to industrial waste and sewage. It is clear

from Table (1) that the highest concentration of this element was within (234), while the lowest concentration reached (223).

We find that most of the concentrations have exceeded the permissible limits, which are less than (200) mg/L. This is due to the effect of laboratory releases, especially vegetable oils containing high concentrations of (SO₄). It is also due to the effect of sewage water, soil washing operations for the lands surrounding the river, as well as industrial waste water, as well as the nature of the pathology of the river basin, which is abundant in gypsum and saline soils. These factors affect water pollution and lead to a change in the hydrochemical properties, water quality, and an increase in negative and positive ions, which negatively affects the presence of fish. .[4]

7-**Sodium Na** is found in all natural waters and is produced by the dissolution processes that rocks are exposed to, in addition to the human element, which has a clear role in influencing the amounts of sodium in water through its activities. It was shown through the results of the analyses of the samples taken from the study area shown in Table (1), that the highest percentage of sodium concentration was (77), and the lowest concentration of sodium was recorded at (72).

These values are considered within acceptable limits for some species, but may be unsuitable for others that require lower concentrations to maintain a healthy environment. Fish living in brackish water may be better able to adapt to this concentration, while more sensitive species may be adversely affected. .[3]

8– **Potassium K** is similar in importance to sodium, and its presence is close to sodium, but its concentration is lower because it is more resistant to weather factors and easier to absorb. It was concluded through the results of the analysis, as shown in Table (1), that the highest concentration of potassium was 3.5, while the lowest concentration of potassium was (3.3).

Potassium in these proportions is acceptable as it is essential for fish growth and aids in metabolic processes and the transfer of nutrients within the body's cells. [8]

2– The second section extending between the mouth of the Diyala River and the Sheikh Saad District , The site is characterized by unique geomorphological and environmental characteristics that influence fish distribution and human activities in the area. According to studies, this section of the Tigris River is experiencing changes in its course due to natural and human factors, affecting river sediments and the islands that form in the area. [10]

The environmental characteristics of this site also include soil and sedimentation and their impact on water quality, making it an area of importance for environmental and hydrological studies. In addition, the confluence of the Diyala River and the Tigris River contributes to the formation of a diverse aquatic environment that impacts the biodiversity of fish in the region.

Table 2: The fundamental physical and chemical traits of the water sample at the second site

S	PH	T.D.S	N.T.U	Tem	EC	Caco 3	Ca	Mg	So4	Na	Cl	K
S1	6.9	780	24	26	971	106	88	68	367	137	78	4
S2	7.1	771	23	28	967	115	93	77	401	146	86	5.3
S3	6.6	778	25	28.5	961	118	85	67	388	148	80	6
S4	6.9	781	27	30	965	111	94	71	387	150	75	5.4

A – Physical Properties:

1 – **pH:** We note from the analysis results, as shown in Table (2), that the pH value varied from one sample to another, as the highest concentration was recorded which reached 7.1, and the lowest concentration was 6.6. These values range between the appropriate range for the growth of most fish species, which ranges between 6.5 and 8.5 for most fish species. These values are considered ideal values for fish growth, reproduction and biological development. .[3].

2 – **The amount of dissolved or total salts (T.D.S)** It was shown through the results of laboratory analyses, as stated in Table (2), that the highest concentration rate was (781), while the lowest concentration rate of dissolved salts was (771), These values are within the relatively high range for freshwater, but they are not extremely salty, and many species of fish can live in such water, such as tropical fish and some species such as gobies. [5]

3–Turbidity NTU : It became clear from the results of Table (2) that the highest concentration of turbidity was (27), and the lowest concentration reached (23), These values are considered moderate to relatively high in river water. Most river fish, such as carp and tilapia, can adapt to these levels. However, if turbidity increases further, it can affect respiration and vision. High turbidity can restrict light penetration, affecting the growth of aquatic plants and algae, which can reduce the oxygen available to fish. .[9]

4–Temperature: The analysis results showed, as shown in Table (2), that the highest concentration of heat was 30, and the lowest concentration was recorded at 26, These values are considered suitable for many fish species, but their suitability depends on the type of fish living in this environment. Tropical fish (such as tilapia, mollies, and gobies) thrive in this temperature range, as it is ideal for their growth and reproduction. In this range, the growth rate and activity of fish increase. However, if the temperature rises above 30°C, the level of dissolved oxygen in the water may decrease, affecting the health of the fish. .[5]

B– Chemical properties of water

1–Electrical conductivity (EC) :It is clear from Table (2) that the highest concentration of electrical conductivity was (971), and the lowest concentration was (961), These values are considered relatively high for freshwater and are due to pollution and industrial discharge, which pose a risk to fish health, as some heavy metals or dissolved chemicals can be harmful to fish life. [6]

2–Alkaline calcium carbonate CaCO_3 : It was shown through the results of laboratory analyses shown in Table (2), that the highest concentration of calcium carbonate was (106), and the lowest concentration was (118), These values are suitable for many river fish, but they may be a little high for some species that prefer less alkaline environments as they help stabilize the pH of the water, providing a suitable environment for fish growth. These values also provide a good level of calcium, which helps in the formation of bones and scales in fish and maintains a stable water environment, which helps fish grow healthily. [10]

3– Calcium Ca : Calcium is also one of the causes of water hardness and it is clear from Table (2) that the highest concentration of positive calcium ions in the country reached (94), the lowest percentage (85)

These values are considered suitable for the growth of river fish, especially species that depend on water minerals to maintain healthy bones and scales. They also provide a supportive environment for the growth of aquatic plants that form part of the diet of some fish. [5]

4–Magnesium (Mg) : It is noted in Table (2) that the highest percentage of magnesium concentration reached (77), and the lowest percentage was (67), These values are considered at the upper limit for freshwater but may be suitable for some river fish, provided that other minerals such as calcium and pH are balanced to ensure a healthy environment for the fish.[9]

5–Chlorides (Cl): Table (2), which summarizes the laboratory results for samples from the study area, shows that the highest concentration of chlorides reached (86), and the lowest concentration was recorded at approximately

(75), These values are suitable for some river fish that tolerate higher levels of chloride, such as carp and tilapia. [3] Chloride helps regulate the osmotic pressure of fish, enabling them to adapt to fresh and brackish water.

6– **Sulfates SO₄** : It is clear from Table (2) that the highest concentration of this element was within (401), while the lowest concentration reached (367), Sulfates are relatively high in freshwater, but their impact on fish life depends on the species and the stability of the ecosystem. Moderate concentrations of sulfates help regulate fish metabolism and contribute to the balance of other minerals. However, high levels can lead to respiratory and digestive disturbances in fish and can affect the pH, potentially destabilizing the water environment and impacting fish reproduction. They can also increase corrosive effects within the aquatic environment, affecting plants and algae.

7–**Sodium Na** It was shown through the results of the analyses of the samples taken from the study area shown in Table (2), that the highest percentage of sodium concentration was (150), and the lowest concentration of sodium was recorded at (137), These values are considered within acceptable limits for some fish species, but this depends on the species and its adaptation to different salinity levels. Some species may tolerate higher concentrations, while others may be adversely affected if the water is unbalanced in other elements, such as nitrates and phosphates. [8]

8– **Potassium K** It was concluded through the results of the analysis, as shown in Table (2), that the highest concentration of potassium was (6), while the lowest concentration of potassium was (4).

These values are suitable for the development of fish, as potassium is an essential element of the important processes of fish, as it affects the fluid balance in their body and contributes to cell and muscle function. [4]

Comparative Statistical Analysis Between the Two Study Sites:

Table(3) of Mean Differences for Selected Physical and Chemical Parameters:

Parameter	Mean Site 1	Main Site 2	Absolute Difference
Temperature (°C)	28.25	28.13	0.12
TDS (ppm)	585.25	777.50	192.25
SO ₄ (Sulfates)	228.50	388.75	160.25
pH	7.35	6.88	0.47
EC (μS/cm)	934.25	966.00	31.75
Calcium (Ca ²⁺)	86.5	91.5	5.0
Magnesium (Mg ²⁺)	24.0	70.75	46.75
Alkalinity (CaCO ₃)	155.5	112.5	43.0
Sodium (Na ⁺)	75.0	145.25	70.25
Turbidity (NTU)	17.5	24.75	7.25
Potassium (K ⁺)	3.43	5.18	1.75

Discussion

The statistical analysis revealed significant differences in several environmental parameters between the two sites. Site 2 showed notably higher concentrations of sulfates (SO₄), total dissolved solids (TDS), magnesium (Mg²⁺), and sodium (Na⁺), suggesting possible influence from anthropogenic

sources such as industrial or agricultural runoff—especially near the confluence with the Diyala River.

In contrast, Site 1 maintained more stable pH values, higher alkalinity, and a more favorable calcium profile, creating a more supportive environment for sensitive fish species. These findings emphasize the importance of environmental monitoring and targeted water management strategies in Site 2 to maintain the ecological balance and support aquatic biodiversity in the Tigris River.

Summary:

Environmental factors play an important role in determining the distribution of fish in different water bodies. Temperature, salinity, accessibility of food, as well as pollution and effects of water currents, determine all the suitability of the environment for the development and reproduction of fish. It is important to monitor and analyze these factors to ensure a healthy ecological balance, which contributes to the stability of fish shares and the protection of biodiversity. The two places studied in the two places compared the values of physical and chemical factors for water and their effects on the development of permanent fish showed that the first place had more appropriate functions for fish life and reproduction, while the second place had a few more values, but within the limit suitable for many fish species.

Recommendations and suggestions:

The recommendations and suggestions are directed toward several key stakeholders, including governmental and environmental authorities, local administrative bodies, farmers and fishermen, as well as regulatory and public health agencies.

1–pedagogical management of water resources: Prioritizing the preservation of natural fishing houses should be adopted to ensure similar water distribution between different areas.

2– Parag Control: Use strict laws to prevent emissions of pollutants in water bodies, and set up water treatment plants to improve the water quality of the river.

3– Fishing Regulation: Use laws that regulate fishing activities and stop incorrect practices by helping fishermen to use fish methods.

4–Aquaculture Promotion: To reduce the pressure on natural fish shares, encourage fishery projects, which will help maintain the ecological balance of the river.

5–Communication awareness: Increase awareness of the importance of conservation of fisheries through media campaigns and educational programs aimed at fishermen and local communities.

Key words: Fish distribution. Environmental factors. Water quality.

References:

1. Menon, S. V., Kumar, A., Middha, S. K., Paital, B., & Asthana, M. (2023). Water physicochemical factors and oxidative stress physiology in fish: A review. *Frontiers in Environmental Science, 11*, Article 1240813.
2. Bastviken, D., Ejlertsson, J., & Tranvik, L. (2022). Measurement of methane oxidation in lakes: A comparison of methods. *Environmental Science and Technology, 36*(12), 3354–3361.
3. Kane, S., Qarri, F., Lazo, P., & Bekteshi, L. (2020). The effect of physico-chemical parameters and nutrients on fish growth in Narta Lagoon, Albania. *Journal of Hydrology and Environmental Development, 4*(2), 65–74.
4. Carlsson, U., & Johansson, T. (2019). Effects of aluminum and calcium on survival and reproduction of trout (*Salmo trutta* L.) in two acidified waters. *Information from the Freshwater Laboratory.*
5. Ibrahim, K. L. (2021). Physicochemical parameters of water and their effects on fish production. *Journal of Agriculture and Veterinary Sciences, 10*(1), 20–31.
6. Zhang, Y., Wang, L., & Chen, J. (2022). Influence of water quality parameters on fish community structure in freshwater ecosystems: A multivariate approach. *Environmental Monitoring and Assessment, 194*(3),
7. Smith, K. A. (2020). Manganese and cobalt in heavy metals soils and effects of fish. In B. J. Alloway (Ed.), *Heavy Metals in Soils* (pp. 197–214). Blackie Academic & Professional.

8. Todd, D. K. (2019). *Water hydrology and effects of fish distribution*. John Wiley & Sons.
9. World Health Organization. (2013). *Chromium: Environmental health criteria* (Part 4). WHO Press.
10. United Nations Environment Programme. (2021). *Water quality in the Tigris River*. UNEP Publications.,

Using classification data mining methods to predict the level of efficiency of services in dental clinics during the COVID-19 pandemic

Anhar K.ALDeen Mohammed^{1*}, Reem Ali AL-Jarah²

^{1,2}College Of Dentistis, Mosul University,IRAQ

Rivrskm2023@yahoo.com¹

reemaljarah1@yahoo.com²

Using classification data mining methods to predict the level of efficiency of services in dental clinics during the COVID-19 pandemic

Anhar K.ALDeen Mohammed^{1*}, Reem Ali AL-Jarah²

^{1,2}College Of Dentistis, Mosul University,IRAQ

Rivrskm2023@yahoo.com¹

reemaljarah1@yahoo.com²

Abstract

The Covid-19 pandemic has always affected all life facilities, dental clinics, like other institutions. research goal is to reach the patient's evaluation of the competency of the service offered to him in the clinic during the pandemic.

Three classification- data mining algorithms -decision tree, logistic regression and cluster analysis- were used to rank clinic reviewer opinions.

Using the programming languages (HTML, PHP, My-SQL) an electronic system has been created that provides services and facilitates the procedures for organizing reservations and making appointments.....Etc., according to the necessary, safety instructions during the pandemic. The System Development Lifecycle (SDLS) methodology is used to determine the level of service efficiency, and ODBC is used to send data from the database to SPSS-V26.

The study variables, like the possibility of returning to the clinic, which has the greatest potential to classify observations and is contributing the most to differentiating for each of the two clusters, have a statistically significant relationship with the likelihood that you will recommend this clinic to others, A list of findings were included in the research's conclusion..

Keywords: Database, Relational Database, SQL, ODBC, Multivariable Analyses , CHIAID algorithm, Logistic Regression algorithm, Two-Step Clustering algorithm, Dental Clinics.

1. Introduction

Health institutions seek to prove their existence, by providing the best possible services, especially providing the best is the key to achieving progress and excellence to reach the highest levels of satisfaction, as the patient has become the focus of attention.

many clinics have stopped working due to the risks faced by health workers, at a time when demand has decreased due to patients' "fear" of resorting to services. And while the dentists are taking more precautions at the moment, many of these procedures are just an extension of their regular routine. A spokesperson for the American Dental Association stated: "**In dentists'** offices, we used to take comprehensive preventive measures, such as disinfection and personal protective equipment (PPE), before they became common."

The patient's condition, "may be unprepared, worried about his health, or looking after an elderly relative, or afraid to see a doctor, so he acts cautiously and does not want to take risks", Thus, the person responsible for fixing the reservation in the clinic is constantly working to deal with the many postponed appointments, and communicates with patients who are scheduled to undergo treatment to organize alternative appointments. In our research, we highlight the level of services in government and private dental clinics during the COVID-19 pandemic and their opinion of the preventive and curative services provided. In this research , Data mining techniques were used, such as algorithm of (CHAID tree, logistic regression and clustering), to reach the goal of the search.

There are some studies were done in the same filed but in another place ,such as a study got in a "Valencia primary dental care facility- SPINE" to assess parents' contentment with the dental care

their kids, by using CHAID algorithm and decision tree , the researchers conclude the parents who participated in study were contented with the of their children received[1]. Also, by using the statistical modeling and CHAID analysis ,. et.al. [2] . conclude that there is an urgent need to create inclusive public policies because the state's epidemic is getting worse. Another study for [3] . It uses conventional psychometric measures to assess healthcare personnel's reported psychological well-being by using the decision tree model

Not only in the health field, the CHAID algorithm was applied. A case study: the National Opinion Research Center of the U. S. chose to assess the job satisfaction in the U. S. and and the factors affecting it.[4].

In order to better the education institution, researchers took refuge to use the CHAID algorithm and decision tree to examine students' perceptions of the academic program and student services offered by the university to discuss how to upgrade their establishment.[5].

2. Theoretical Part

There are several techniques in data mining, the selection of the appropriate ones depends on the nature and size of the data under study[6], Data mining can be implement in comparison with the data market and data store. Figure 1 showing the data mining technique which can use .

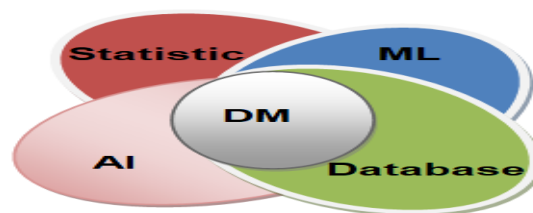


Figure 1. Data Mining Technique

Source:[6]

There is no specific theory based on to choose the appropriate data minig technique, Usually the choice is made based on the experience in this field and the actual techniques effective, the superlative between traditional techniques and modern techniques to the extent that the appropriate tools are available, However, with the increase of experience, we can evaluate the options and select the appropriate ones for the application. [7] .

2.1 Data Mining Models

As Figure 2 showe, the Predictive Model : It works on the future prediction of the mechanism of data work, based on a model whose data has been previously trained.[8][9] .

The Descriptive Model : It analyzes the data in order to extract the relationships and correlations between them, and to reveal the characteristics of the data to build a model that did not exist previously. For instance, Clustering Analysis, Association Rules Analysis ,..etc

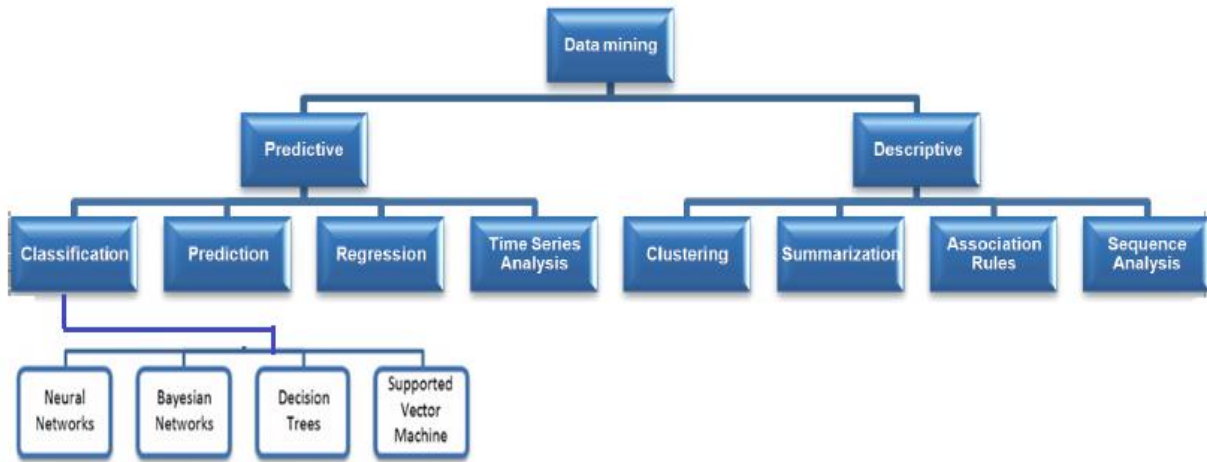


Figure 2. Dataminig
Source:[9]

2.2 Data Mining Technique

Research progress in data mining and knowledge discovery, has led to the many of data mining techniques coming to lights , which are built on three strong technical pillars: database, mathematical statistics, and artificial intelligence, our interest in this researchare

2.2.1 Classification

The major goals of a Classification algorithms are to make the predictive accuracy obtained as large as possible by the classification model[6] [10] .

2.2.1.1 Decision Tree

"uses as a predictive model which maps observations about an item to conclusions about the item's target value".[11] [12], The algorithm which used in this research is CHAID ("Chi-squared Automatic Interaction Detection") [13], it's a technique depends on the χ^2_{test} - eq.1- and employs a step-by-step procedure

The creating of nodes and sub-nodes among the predictor variables is significant.[14] [15].

$$\chi^2 = \sum \frac{(E_{ij} - O_{ij})^2}{E_{ij}} \dots \dots \dots (1)$$

2.2.2 Logistic regression

is "a method in which the Y response variable has a binomial distribution. To determine probabilities of success $P(Y = 1|X)$, and defeat $P(Y = 0|X)$.[16] [17] The odds are defined as in eq.2" .[18] .

$$(\Theta) = \frac{P(Y = 1|X)}{P(Y = 0|X)} = \frac{P(Y = 1|X)}{1 - P(Y = 1|X)} \dots \dots \dots (2)$$

"The linear dependencies between log-odds-logit- and input variables are analyzed as" in eq.3

$$\ln(\Theta) = \ln\left(\frac{P(Y = 1|X)}{1 - P(Y = 1|X)}\right) = \mathbf{x}\beta \dots \rightarrow P(X, \beta) = \frac{e^{\mathbf{x}\beta}}{1 + e^{\mathbf{x}\beta}} \dots \dots \dots (3)$$

where $\beta = (\beta_1, \dots, \beta_m) \in R^m$. From Equation (3) [19]

2.2.3 Two-Step Cluster algorithm

"is a statistical method[9] for assigning data into subgroups with related characteristics" [7].

The procedure is performed by constructing a cluster feature (CF) tree, which contains the cluster centers.

"To automatically determine the number of groups, the method uses BIC (Schwartz Bayesian Information Criterion) or AIC (Akaike Information Criterion) which is calculated for each number of clusters from a given range; This indicator is then used to find a preliminary estimate of the number of clusters." [20] For groups J, the two indicators are calculated according to equations (4) and (5) below:

$$BIC(J) = -2 \sum_{j=1}^J \xi_j + m_j \log N \dots \dots (4)$$

$$AIC(J) = -2 \sum_{j=1}^J \xi_j + 2m_j \dots \dots (5)$$

where

$$m_j = J \left\{ 2K^A + \sum_{k=1}^K (L_k - 1) \right\} \dots (6)$$

$$t = \frac{\hat{\mu}_k - \hat{\mu}_{sk}}{\hat{\sigma}_{sk}} \sqrt{N_k} \dots \dots \dots (7)$$

$$\chi^2 = \sum_{l=1}^{L_k} \left(\frac{N_{skl}}{N_{kl}} - 1 \right)^2 \dots \dots \dots (8)$$

3. Materials & Methods

In order to obtain the necessary data, a questionnaire - with three point Likert Scale (Agree, Neutral, Disagree)- was designed that includes factors of interest to dental clinic references during the Covid-19 pandemic, and distributed to reviewers in different dental clinics.

X₁: Gender, X₂: Age (20-, 30-, 40-, 50-59), X₃: Kind of clinic (Private, general), X₄: Help in booking an appointment at the clinic, X₅: The receptionist pays attention to you and obliges you to follow prevention methods (wearing a mask and gloves), X₆: The time between your request for an appointment and your presence at the dentist, X₇: Adequate working hours, X₈: Cleanliness of the clinic and the provision of means of dusting, sterilization and appropriate ventilation, X₉: Conducting a preliminary examination for those who enter the clinic as an indicator of temperature or something else, X₁₀: Not allowing the patient to accompany him, except in critical cases, X₁₁: Availability of a waiting room with social distance, X₁₂: acceptable waiting period for the patient to see the dentist, X₁₃: Availability of a worker responsible for wiping surfaces and door knobs periodically during working hours, X₁₄: Measures taken to prevent infection in the patient's examination room, X₁₅: The measures taken by the clinic staff to protect you from infectious diseases and radiation, X₁₆: The period of stay for the dentist with you, X₁₇: The interest shown by the dentist about your questions or concerns, X₁₈: Explain your treatment options in an understandable manner, X₁₉: The competence of the dental assistant and his interest in guiding and educating you to maintain oral and dental health, X₂₀: Information provided on ways to avoid dental problems in the future, X₂₁: Comprehensive examinations and treatment, X₂₂: The interest shown by the dentist in general, X₂₃: Overall evaluation of the care provided in the dental clinic, X₂₄: Collaboration and teamwork demonstrated by the dentist's team, X₂₅: General assessment of the skill of the dentist, X₂₆: Your trust in the dentist, X₂₇: Possibility to review the clinic again when needed, Y: Chances that you will recommend this clinic to others. Reliability was calculated using Cronbach's alpha.

3.1 Databases System

Databases are designed to suit the movement and flow of data in addition to organizing the operations of saving, recovery and modification, in consideration the availability of access and protection, and the possibility of expanding these databases, whether in terms of the increase in the number of users or data or tables and the resulting complexity in query sentences, Figure 3 shows – respectively- the database table and relation database of our system

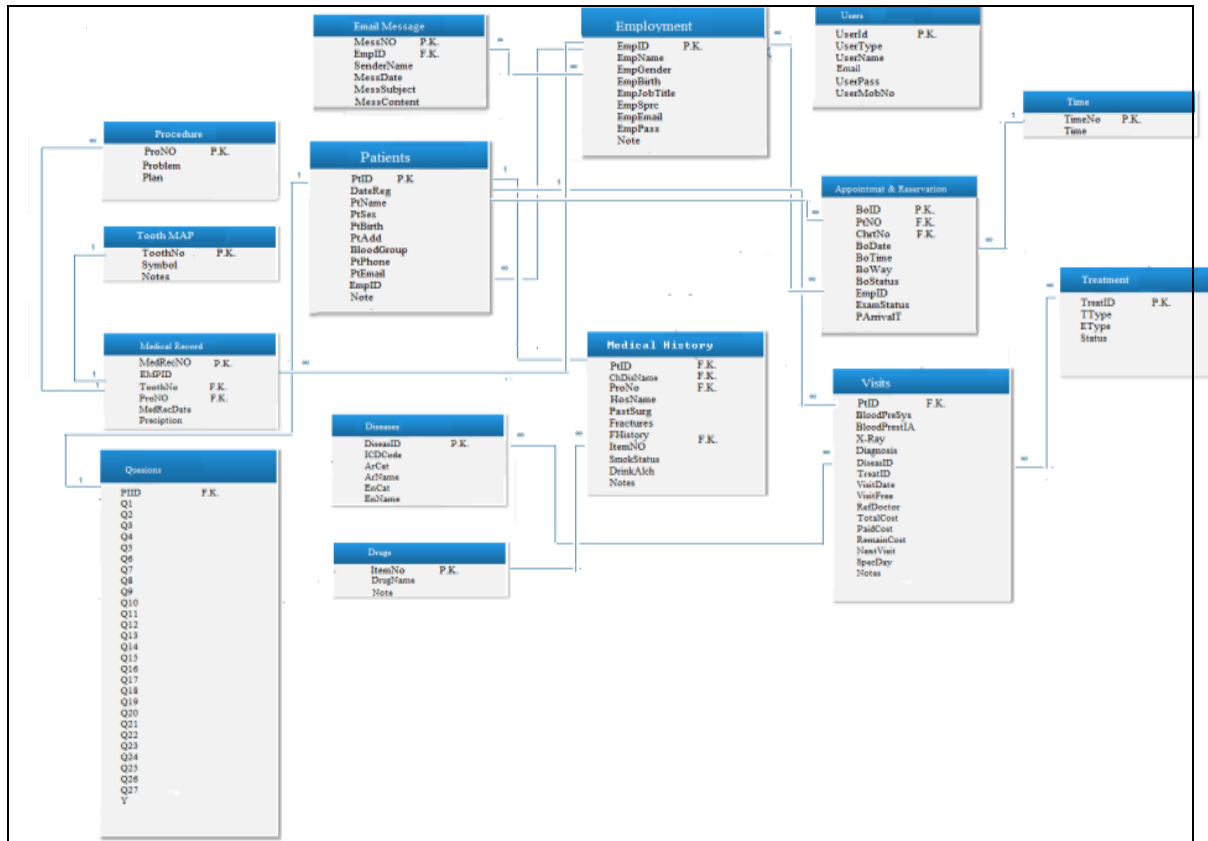


Figure3. Relational Database

To take advantage of the volume of available data and the above-mentioned databases, an has been created, in line with modern technology in the use of databases, which can be linked to other systems.

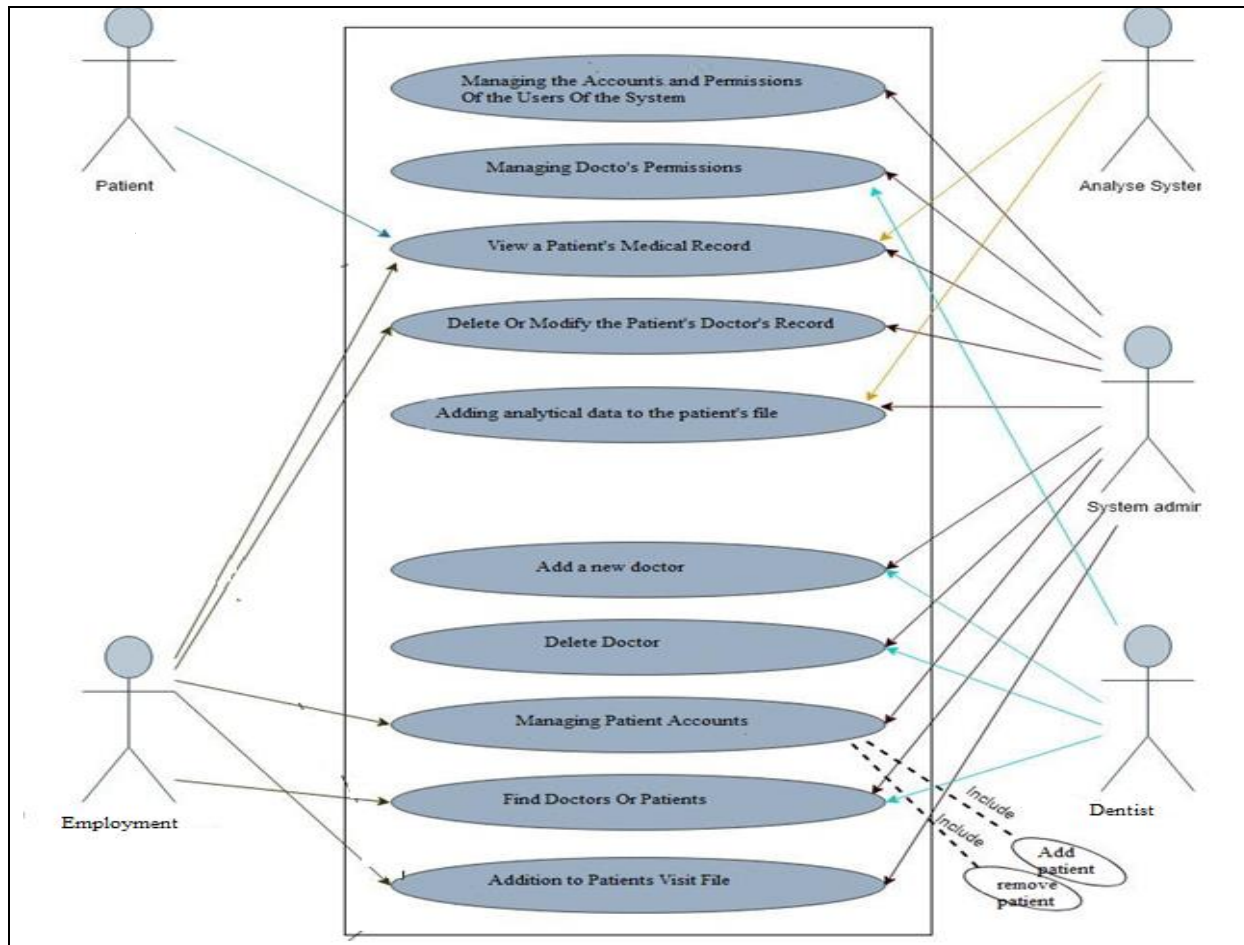


Figure4. analyze system(User Case)

When logging in, and in order to be ensure about the protection of information, the user is allowed to log into the system with his name, password and doctor ID number.

The system, not only doesn't allow its users to access the account of others and see their private information, but also restricts the content of the screens according to the user permission.

The (PHP) language ensures protection by rejecting repeated attempts to log in, NOSQL Injection, and activating all authentication functions to ensure the correct entry.

Some features of the system are Adding, Viewing, Modifying, Deleting, And Searching.

The doctor or his assistant are allowed to add everything new to the patient's visit profile, starting from the status of his booking - new, confirmed, postponed, canceled - and the required data on the visit schedule, new patient mean new file open, View the patient's medical record by entering his number , modify or delete the patient's medical record , Allow users to inquire about doctors or patients by number, full name, or username of the doctor or patient.

3.2 CHAID Algorithm

Table 1. Model Summary Of CHAID methode

Specifications	Dependent Variable	Y
	Independent Variables	$X_1 - X_{27}$
	Validation	none
	Maximum Tree Depth	3
	Minimum Cases in Parent Node	100
	Minimum Cases in Child Node	50

Results	Independent Variables Included	X_1, X_7, X_{27}
	Number of Nodes	7
	Number of Terminal Nodes	4
	Depth	3

Tree diagram in Figure 5 show, the most significant independent variable is X_{27} : “Possibility of revisiting the clinic”,

X_{27} at $\alpha=0.001$: ($\chi^2 = 165.221, df = 2, p_{value} = 0.000$). As the first steep, it splits the sample of (407) responses, into 2 groups containing different groups of X_{27} presented as node 1 & 2. The first node, included (215) respondents from the variable X_{27} which coded (3: disagree), while the second one is terminal node included (92) respondents from the variable X_{27} , which coded (1: agree, and 2: neutral) within tree's second level, one statistically significant variable Adequate working hours (X_7) is identified at $\alpha=0.05$, ($\chi^2 = 14.853, df = 2, p_{value} = 0.002$), which in turn leads us to the third and fourth node. Node3, included (150) respondents from the variable X_7 which coded (3: disagree), while Node4, included (50) respondents from the variable X_7 which coded (1: agree, & 2: neutral).

Within tree's third level(final) :

Gender: X_1 , it is significant for splitting of Nodes5 and Nodes6 at $\alpha=0.05$, $\chi^2 = 6.253, df = 1, p_{value} = 0.012$

Generally, the leaf tree frame, (fixed as 4, 5 & 6) pertain to (3: disagree with recommend this dental clinic to others), and one (marked as 2) pertain to (2: indifferent to recommend this dental clinic to others).

In fact, the track from the root to the leaf nodes produce some rules for classifying reviewers' opinions (in one of the variable-specific categories, for example, the rule in Node6: Who does not want to visit the dental clinic again, and the working hours are not suitable for him, 89.6% would not advise anyone else to visit this clinic, and the other rules derived can be explained by a similar tactic.

To finish the process of classification, all its performance have been assessed. Our findings suggest that if the reviewers' opinions in terms of the 3 indep.var. are known, the hazard of inaccurately classified -based on entire sample- is 17.9%, with std. Error is 0.02.

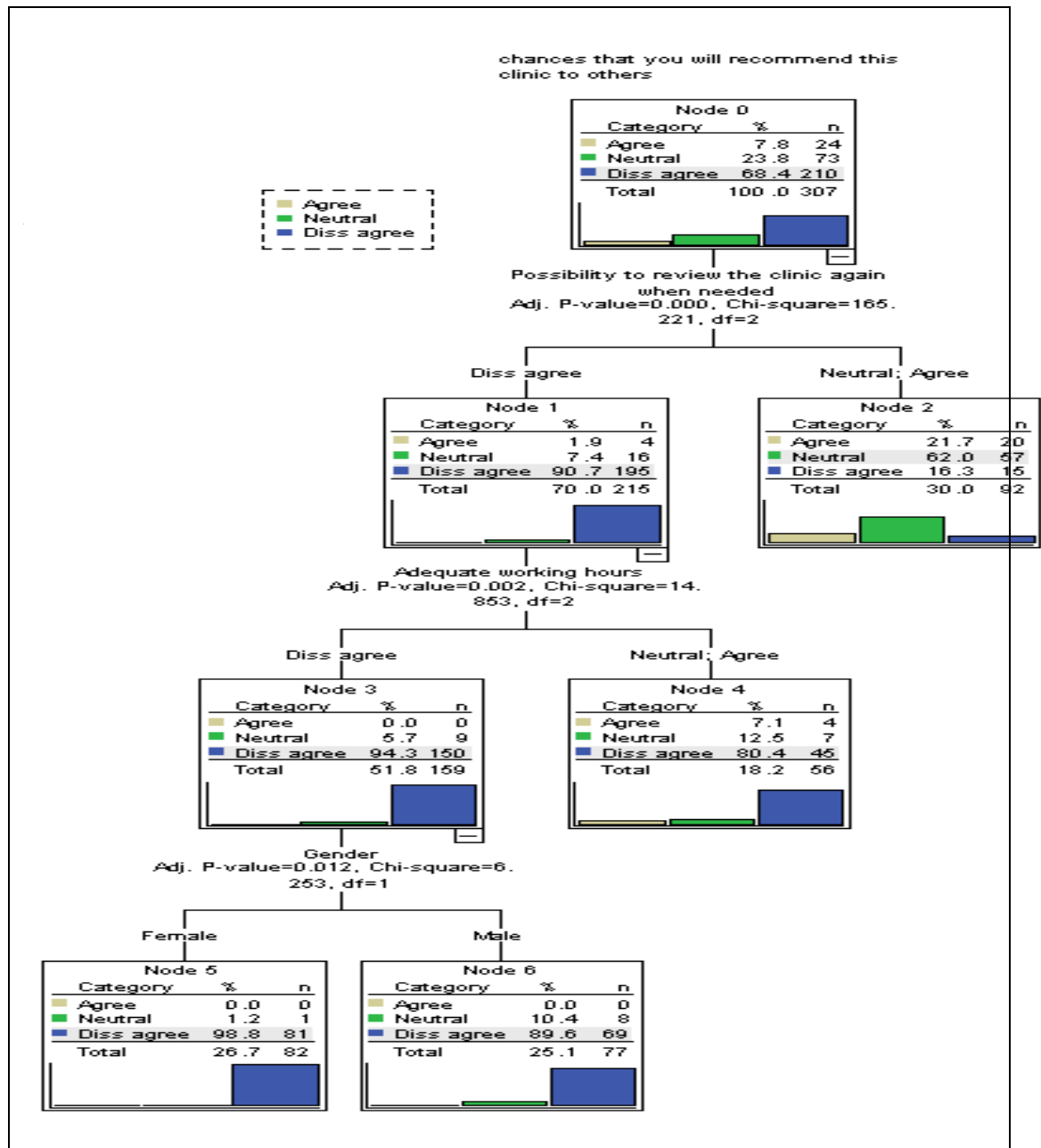


Figure5. Decision tree analysis with CHAID model.

Table 2. presents the classification CHAID

Reviewers' Opinions		Predicted			Correctly Classified
		Agree	Neutral	Diss. agree	
Observed	1:Agree	0	20	4	0.0 %
	2:Neutral	0	57	16	78.1 %
	3:Diss-agree	0	15	195	92.9 %
	% Over all	0.0	30.0	70.0	82.1 %

In accordance with the table 2 , It can be said that in general the accuracy of the model is 82.1%, the model accurately ranked (252) out of (297) in the sample under discuss. Significant differences can be observed in the classification accuracy, according to the categories of the variable.

3.3 Multinomial Logistic Regression (MLR) Algorithm

The(MLR) model's estimation and testing steeps is "The chances that you will recommend this clinic to others".

Independent categorical variables (27) were selected for inclusion in the multivariable logistic regression model. As shown in Table 3, the χ^2 test for the last model, the 2 - Log Likelihood for the full model (86.835) less than it is for the null model (491.546), the likelihood ratio represents the unexplained variance in the outcome variable.

The Likelihood Ratio chi-square test which is a test of goodness-of-fit, for model predicts, $\chi^2 (106) = 404.710$, $p < 0.001$,

Table 3. Model Fitting Information

Model	Model Fitting Criteria	Likelihood Ratio Tests		
	-2 Log Likelihood	Chi-Square	df	Sig.
Intercept Only	491.546			
Final	86.835	404.710	106	.000

the resp. var. explained by the predictors indep.var., 73.2% of the variance in dep. variables (the proportion of variance) according to "Cox and Snell R^2 " value, 91.7 % according to " Nagelkerke R^2 " value, and 82.3% according to "McFadden R^2 " value.

Table 4 illustrates the likelihood ratio test, As the results shown, it can be seen that relationship between some of the independent variables ($X_{27}, X_{26}, X_{24}, X_{21}$ respectively) and the dependent variable is a statistically significant

Table 4. Evaluate the relationship between variables and the dependent variable

Effect	Model Fitting Criteria	Likelihood Ratio Tests		
	2 Log Likelihood of Reduced Model	Chi-Square	DF	Sig.
<u>Intercept</u>	86.835	.000	0	.
X ₁	88.918	2.082	2	.353
X ₂	90.194	3.358	6	.763
X ₃	90.223	3.387	2	.184
X ₄	94.973	8.138	4	.087
X ₅	92.836	6.001	4	.199
X ₆	88.825	1.990	4	.738
X ₇	88.648	1.813	4	.770
X ₈	87.794	.959	4	.916
X ₉	87.979	1.143	4	.887
X ₁₀	86.845	.009	4	1.000
X ₁₁	88.213	1.378	4	.848
X ₁₂	89.333	2.497	4	.645
X ₁₃	94.873	8.038	4	.090
X ₁₄	90.868	4.033	4	.402
X ₁₅	88.836	2.001	4	.736
X ₁₆	88.023	1.188	4	.880
X ₁₇	91.994	5.159	4	.271
X ₁₈	88.067	1.232	4	.873
X ₁₉	88.015	1.179	4	.881
X ₂₀	89.694	2.859	4	.582
X ₂₁	96.904	10.068	4	.039
X ₂₂	92.380	5.545	4	.236
X ₂₃	88.697	1.862	4	.761
X ₂₄	96.790	9.955	4	.041
X ₂₅	86.933	.098	4	.999
X ₂₆	101.653	14.817	4	.005
X ₂₇	394.129	307.294	4	.000

Correct classification rates for the MLR model as shown in Table 5 , It indicate that the accuracy of the model is 95.4, and the expected values according to the dep. variable (7.8, 22.5, 69.7) % isn't significantly different from that in the main data (100.0, 87.7, 97.6) %.

Table5. classification rates for the MLR model

Observed	Predicted			Correctly Classified
	Agree	Neutral	Disagree	
1:Agree	24	0	0	100.0%
2:Neutral	0	64	9	87.7%
3:Diss-agree	0	5	205	97.6%
% Over all	7.8%	22.5%	69.7%	95.4%

3.4 Cluster Analysis

As shown in table 6, although the lowest "BIC coefficient" is for 7 clusters, according , the optimal No. of clusters is two, because the lowest value of the Schwarz's Bayesian Criterion as well as the largest proportion of space is for two clusters

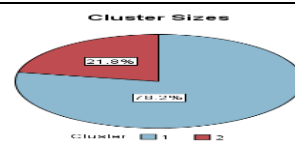
Table 6.Cluster Distribution

Number of Clusters	Schwarz's Bayesian Criterion (BIC)	BIC Change	Ratio of BIC Change	Ratio of Distance Measures
1	13879.447			
2	12679.278	-1200.170	1.000	2.198
3	12304.983	-374.295	.312	1.579
4	12183.328	-121.654	.101	1.117
5	12107.391	-75.937	.063	1.239
6	12106.766	-.625	.001	1.382
7	12193.355	86.589	-.072	1.052
8	12291.273	97.917	-.082	1.070
9	12403.394	112.122	-.093	1.130
10	12538.898	135.504	-.113	1.065

The clusters distribution is shown in Table 7

Table 7. Cluster Distribution

Cluster	N		% of Combined	% of Total
	1	2		
1	240		78.2%	78.2%
2		67	21.8%	21.8%
Combined	307		100.0%	100.0%
Total	307		100.0%	100.0%



From cluster quality in Figure 6 show the value of average silhouette is 0.358

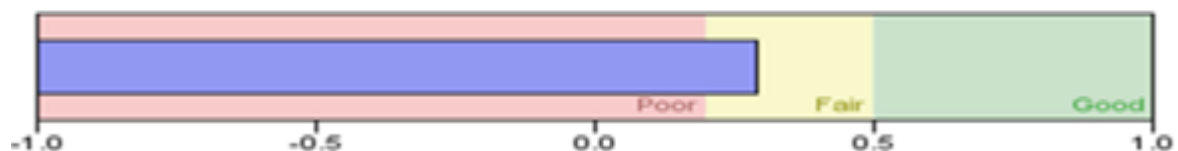


Figure6. silhott measure of cohesion separation

As our interest is to know the important variables that affect the opinion of reviewers to visit the dental clinic during the Covid-19 pandemic, Figure 7 show that X_{27} , X_{21} then X_{26} , X_7 , X_{24} , X_{13} , X_{17} are the most contribute to differentiating the first cluster and X_{27} , X_{24} , X_{21} , then X_{13} , X_{17} , X_1 differentiate the second

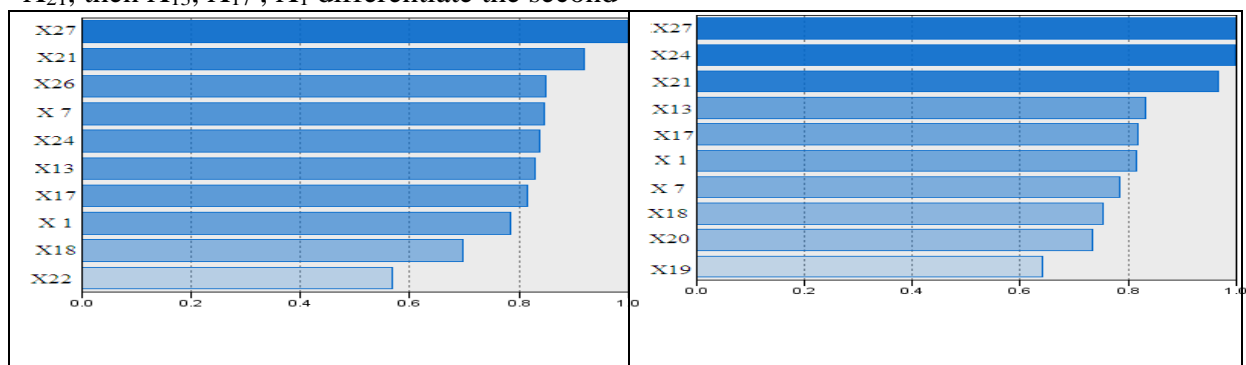


Figure7. Variables Importance for Clusters one & cluster 2

4. Conclusion

In accordance with CHAID Algorithm, In general the model accuracy is very good. Although the differences can be observed in the classification accuracy, the our data the variable X₂₇: Possibility of revisiting the clinic has the biggest potential to classify observations

In accordance with Multinomial Logistic Regression Algorithm (MLR), The change value of Model Fitting Criteria for the final model and the null model indicate better fit, and the test of goodness-of-fit indicates significant model predicts. From Cox and Snell R² value, Nagelkerke R² value, McFadden R² value, the predicted model was able to explain the variance in the conviction of individuals well. There is a statistically significant relationship between: (X₂₁: Comprehensive examinations and treatment), (X₂₄: Collaboration and teamwork demonstrated by the dentist's team), (X₂₆: Your trust in the dentist), (X₂₇: Possibility to review the clinic again when needed) and the dependent variable (y: Chances that you will recommend this clinic to others). The correct classification rates for the MLR model are highly valued, on other hand, there is no significant different between the expected values of the dep. variables and the main data.

In accordance with 2-steeps cluster algorithm indicate that The optimal number of clusters is two, with size 78.2% and 21.8% respectively. From silhouette measure, the cluster quality is fair. The categorical variables which contribute the most of differentiating for each two cluster are: (X₂₇: Possibility to review the clinic again when needed) ,(X₂₄: Collaboration and teamwork demonstrated by the dentist's team) and (X₂₁: Comprehensive examinations and treatment).

Reference:

- [1] Carmen Llena; Gonzalo Clemente and Leopoldo Forner,2010,” Parental Satisfaction with Children’s Primary Dental Care in Valencia, Spain”, Primary Dental Care 2011 ; 17(4):25-30, DOI:[10.1308/135576111794065739](https://doi.org/10.1308/135576111794065739)
- [2]Fabrício P. A. ; Fabrício Pelizer Almeida ; Moisés Keniel Guilherme de Lima ; Demóstenes Coutinho Gomes ; Esther Ferreira de Souza,2020, “Logistic Regression Models and Classification Tree for Deaths and Recovered Patients Records of Covid-19 in the State of Minas Gerais, Brazil”, IJAERS, Vol-7, Issue-10,OCT.(2020), ISSN: 2349-6495(P) | 2456-1908(O), <https://dx.doi.org/10.22161/ijaers.710.16>
- [3] Anirban Ray ; Debjani Sen Gupta ; Jayasree Sar Choudhury ; Pramit Ghosh , “Resilience of Healthcare Providers during COVID-19 Pandemic: A Rapid Assessment using Digital Platform”, Journal of Clinical and Diagnostic Research.2022 Dec, Vol-16(12): VC01-VC07 DOI: [10.7860/JCDR/2022/53497.17198](https://doi.org/10.7860/JCDR/2022/53497.17198)
- [4] Farhad Sheybani; 2019, “Predicting the Individuals’ job satisfaction and determining the factors affecting it using the CHAID Decision Tree Data Mining Algorithm, Case Study: the National Opinion Research Center of the United States.”, EJERS, European Journal of Engineering Research and Science, Vol. 4, No. 3, March 2019, DOI: <http://dx.doi.org/10.24018/ejers.2019.4.3.1169>
- [5] Maryli F. Rosas; Shaneth C. Ambat; Alejandro D. Magnaye; John Renbert F. Rosas, 2019, “Classification and Regression Decision Tree: A Mining Technique for Students’ Insights on the University Services with Text Analysis”, 9th IEEE Annual Ubiquitous Computing, Electronics & Mobile Communication Conference (UEMCON) , DOI: [10.1109/UEMCON44053.2018](https://doi.org/10.1109/UEMCON44053.2018)

- [6] Dimitrios Papakyriakou & Ioannis S. Barbounakis, “Data Mining Methods: A Review”, International Journal of Computer Application, Volume 183, No.48, 2022,5-19. DOI: [10.5120/ijca2022921884](https://doi.org/10.5120/ijca2022921884)
- [7] Kun Gao; Hassan Ali Khan; Wenwen Qu, 2022, “Clustering with Missing Features: A Density-Based Approach”, Song-Kyoo (Amang) Kim and Chan Yeob Yeun, 14(1),60, 2022, <https://doi.org/10.3390/sym14010060>
- [8] Gaurav Gosavi; Gajanan Gawde, 2022, “Prediction Techniques for Data mining”, National Conference on Emerging Trends in Computer Engineering and Technology.
- [9] Kwame Boakye Agyapong; Dr. J.B Hayfron-Acquah; Dr. Michael Asante,2016, “An Overview of Data Mining Models(Descriptive and Predictive)”, International Journal of Software & Hardware Research in Engineering, Vol. 4 ,Issu. 5, ISSN-2347-4890.
- [10] Sudhir M. Gorade; Ankit Deo; Preetesh Purohit ,2017, “A Study of Some Data Mining Classification Techniques”, International Research Journal of Engineering and Technology (IRJET), , e-ISSN: 2395 -0056 , p-ISSN: 2395-0072 Vol. 04 Iss. 04.,
- [11] Himani Sharma ; Sunil Kumar,2013, “A Survey on Decision Tree Algorithms of Classification in Data Mining”, International Journal of Science and Research (IJSR), ISSN (Online): 2319-7064, Index Copernicus Value (2013): 6.14 | Impact Factor (2015): 6.391.
- [12] Bahzas Taha Jijo; Adnan Mohsin Abdulazeez; 2021,Classification Based on Decision Tree Algorithm for Machine Learning, [Journal of Applied Science and Technology Trends](https://doi.org/10.38094/jastt20165) 2(01):20-28, DOI:[10.38094/jastt20165](https://doi.org/10.38094/jastt20165)
- [13] Naim Monjezi, 2021,The Application Of the CART and CHAID Algorithms insugar Beet Yield Prediction ,Basrah J.Agric.Sci.,34(1):1-13
- [14] Murat Gunduz ; Ibrahim AL-Ajji,2021, “Employment of CHAID and CRT decision tree algorithms to develop bid/no-bid decision-making models for contractors” , Engineering, Construction and Architectural Management, ISSN: 0969-9988, <https://www.emerald.com/insight/0969-9988>
- [15] Etik Zukhronah; Yuliana Susanti; Hasih Pratiwi; Respatiwan and Sri sulistijowati H. ,2021, “Decision tree technique for classifying cassava production”, AIP Conference Proceedings : Vol. 2021, Iss. 1. [10.1063/1.5062777](https://doi.org/10.1063/1.5062777), <https://doi.org/10.1063/1.5062777>.
- [16] Andrew Gelman; Jennifer Hill; Aki Vehtar; 2022, “Regression and Other Stories” ,Andrew Gelman, Jennifer Hill, and Aki Vehtari, ch. 13,pp217-237
- [17] Tomasz Rymarczyk; Edward Kozłowski; Grzegorz Kłosowski; Konrad Niderla, 2019: “Logistic Regression for Machine Learning in Process Tomography”, Sensors 19(15), 3400, <https://doi.org/10.3390/s19153400>.
- [18] Andrés Villanueva Manjarres ; Luis Gabriel Moreno Sandoval ; Martha Salinas , “Data Mining techniques applied in educational environments: Literature review”; Digital Education ; Number 33; 2023
- [19] Sixiang Jia ; Haochen Mou ; Yiteng Wu ; Wenting Lin ; Yajing Zeng ; Yiwen Chen ; Yayu Chen ; Qi Zhang ; Wei Wang ; Chao Feng and Shudong Xia,2022: “A Simple Logistic Regression Model for Predicting the Likelihood of Recurrence of Atrial Fibrillation Within 1 Year After Initial Radio-Frequency Catheter Ablation Therapy”, Frontiers in Cardiovascular Medicine , <https://doi.org/10.3389/fcvm.2021.819341>
- [20] Daniela Şchiopu; “Applying TwoStep Cluster Analysis for Identifying Bank Customers’ Profile”, Seria Ştiinţe Economic, Vol. LXII, No. 3, 2010, pp66-75.

Microbial contamination of mobile phones: A study of bacterial prevalence

Alaa L.abdullah- Director General of Education Baghdad-Third Rusafa

Hawraa kadhim falhi - Al Kindi Hospital

Dr.Hadi hussein abbas - Al kindi hospital

alaalaebi@gmail.com

<https://scholar.google.com/citations?user=jTyypxUAAAJ&hl=ar&authuser=1>

Microbial contamination of mobile phones: A study of bacterial prevalence

Alaa L.abdullah- Director General of Education Baghdad-Third Rusafa

Hawraa kadhim falhi - Al Kindi Hospital

Dr.Hadi hussein abbas - Al kindi hospital

alaalaebi@gmail.com

<https://scholar.google.com/citations?user=jTyypxUAAAAJ&hl=ar&authuser=1>

Abstract

Because mobile phone use is so widespread (it was estimated in 2011 that there were around five billion mobile phone users), public concerns about the possible health effects of mobile phones receive a lot of coverage in the media. Because so many people use mobile phones, medical researchers are concerned that any associated health risks, even small ones, could cause significant public health problems. It is important to understand the risks and possible effects of mobile phone use, and make up your own mind about how you use your mobile phone.

A total of (10) (84 %) out of 12 physicians consented to participate in the study , with 2 (16 %) refusing to participate ,bacteria isolated from doctor mobile phone were, staphylococcus spp. was the predominant bacteria, found at 100% prevalence, on both the upper and lower surfaces of the doctor personal mobile phones ,15 % pseudomonas spp. and 5% Klebsiella spp.

Seventeen (90%) out of 19 laboratory workers consented to participate in the research study , while 2 refused (10 %),the prevalence of bacterial isolate from personal mobile phones were , 100% staphylococcus spp was the dominant bacteria on both the upper and lower surfaces of the personal mobile phones of laboratory workers, 67% E.coli , 19.2 % klebsiella spp. and 22 % pseudomonas spp.

A total of 14 (88 %) out of 16 hospital nurses consented to participate in the research study ,with 2 (13 %) refusing to participate, the prevalence of bacterial isolate from personal mobile phones were, 100% staphylococcus spp was the dominant bacteria on both the upper and lower surfaces of the personal mobile

phones of laboratory workers., 34.5 % E.coli , 50 % klebsiella spp. and 11.5 % pseudomonas spp.

A total of 9 (90 %) out of 10 patient accompany consented to participate in the research study ,with 1 (10 %) refusing to participate, the prevalence of bacterial isolate from personal mobile phones were, 100% staphylococcus spp was the dominant bacteria on both the upper and lower surfaces of the personal mobile phones of patient accompany, 9.1 % klebsiella spp.,18.2% pseudomonas spp. and 9.1 % streptococcus spp.

A total of 11 (84 %) out of 14 hospital administration consented to participate in the research study ,with 4 (16 %) refusing to participate, the prevalence of bacterial isolate from personal mobile phones were , 100% staphylococcus spp was the dominant bacteria on both the upper and lower surfaces of the personal mobile phones of hospital administration, 9.1 % klebsiella spp., 18.2 % pseudomonas spp. and 9.1 % streptococcus spp.

Introduction

The global system for mobile telecommunication was established in 1982 in Europe with a view of providing an improved communications network in many countries, mobile phones outnumber landline telephones since most adults and many children now own mobile phones. At present, Asia has the fastest growth rate of mobile phone subscribers in the world. Today, mobile phones have become one of the most indispensable accessories of professional and social life with advancement in telecommunication, mobile phones are used for internet browsing, text messaging, ticket booking, listening music, GPS, and many applications. The vast majority of mobile phones are hand-held Because of the advancement and benefits of the mobile phone, the utility level because high and it is easy to overlook it's hazard to health.

This constant handling of the phone by different users exposes it to an array of microorganisms, and makes it a good carrier for microbes, especially those associated with the skin resulting in the spread of different microorganisms

from user to user. Although they are usually stored in bags or pockets, mobile phones are handled frequently and held very close to the mouth, and exposed frequently to the face. However, the mobile phones are used routinely all daylong but not cleaned properly. All mobile phones under consideration were infected by several microbes, most of which belongs to natural flora of the human body as well as airborne fungi.

A study reported that many species of commonly found bacteria's such as *Staphylococcus aureus*, *Staphylococcus epidermidis*, *Pseudomonas aeruginosa*, *Neisseria sicca*, *Micrococcus luteus*, *Proteus mirabilis*, were identified on mobile phone surface. This indicates the necessity to maintain the mobile phones at adequate level of cleanliness. It was reported that a mobile phone can harbor more microorganisms than a man's lavatory seat, the sole of a shoe or the door handle.

Contamination of mobile phones can be through sources such as human skin or handbag, phone pouch, bags, pockets, environment and food particles. These sources are links through which microorganisms colonize the phone, thus causing diseases that range from mild to chronic. Although, microorganisms isolated so far by health researchers are mostly normal flora of the source of contamination, they may serve as mobile reservoirs for infections, allowing the transportation of the contaminated bacteria to many different clinical environments further, sharing of mobile phones between people may directly facilitate the spread of potential pathogenic bacteria to the community.

The potential of mobile phones as vectors to nosocomial infection has been studied before mobile phones were found to carry microorganisms because count of bacteria increases at high temperature and our phones are ideal breeding sites for these microbes as they are kept warm and snug in our pockets and handbags. The important factors of contamination are the personal hygiene

level, location, frequency of usage, duration of usage of the phone and possible number of users. Mobile phones may get contaminated by bacteria (such as *Escherichia coli*, *Pseudomonas aeruginosa* and *Klebsiella*), which cause hospital infections, and may serve as a vehicle for the spread of nosocomial pathogens. Since the same phone is used both inside and outside of the hospital, the phone if contaminated plays a major role in the spread of hospital infection bacteria to the community at large. Type of microorganism that occupies the hand phones the most according to studies are the Coagulase negative *Staphylococcus*, followed by *Staphylococcus aureus*, thirdly *E. coli*, followed by other microorganisms like *Klebsiella pneumoniae*, and *P. aeruginosa*. The frequent use of mobile phone can lead to nosocomial disease which is caused by bacteria like *Staphylococcus aureus*, *Pseudomonas*, there are various diseases associated with the mobile phone contamination. Some of the diseases are mobile phone dermatitis, in which people who spend long time on their mobile phone develop an allergic reaction to the phone's nickel surface.

The problem was identified in several published case reports patients with unexplained rashes on their face and ear. Closer investigation revealed that the reaction was caused by nickel in the mobile phone handsets where it is often found in the casing or buttons, particularly in the most fashionable models. Beside this mobile phone affects sperm motility, which an experiment conducted to exposure of human sperm to a mobile phone for 5 minutes significantly decreased sperm motility then in another study the exposure of mobile phone during pregnancy and after birth increased fetal and neonatal heart rate and decreased with increasing gestational age.

Exposure to mobile phone on average 34 minutes per day was associated with decreased nocturnal concentration of hormone melatonin in adults. Mobile phones have become an integral and indispensable part of daily life. Mobile phones are increasingly becoming an important means of communication. The

vast majority of mobile phones are hand-held. Combination of constant handling with the heat generated by the phones creates a prime breeding ground for many microorganisms that are normally found on the skin. Mobile phones have also been reported to be a reservoir for microorganisms.

It has been reported that a mobile phone can harbor more microorganisms than a man's lavatory seat, the sole of a shoe or the door handle. Although, microorganisms isolated so far by health researchers are mostly normal flora of the source of contamination, they may serve as mobile reservoirs of infection, allowing the transportation of the contaminating bacteria to many different clinical environments. Further, sharing of mobile phones between people may directly facilitate the spread of potentially pathogenic bacteria to the community.

The potential of mobile phones as vectors to nosocomial infection has been studied before. These studies reported that the most commonly found bacterial isolate was Coagulase Negative Staphylococcus (CONS) as a part of normal skin flora. Among Health Care Workers (HCWs), it has been reported that medical devices like thermometers, stethoscopes and non-medical devices like computer keyboards, faucet, ballpoint pens, files, books and mobile phone have an important role in the transmission and spread of microorganisms. Bacterial flora on mobile phones of faculty members may vary in composition, number and antibiotic sensitivity, to that found on mobile phones of non-faculty members.

This is probably the first study in Saudi Arabia that attempts to study the bacterial flora present on the mobile phones of faculty members and personnel, and to compare it with that found on mobile phones of personnel in terms of composition, number and antibiotic sensitivity. In spite of all the advantages gained from the cell phones, the health hazard it might pose to its users should

not be over looked. Cell phones come in close contact with the body such as face, ears, lips and hands during usage and serve as a ready surface for colonization of pathogenic as well as non-pathogenic microorganisms. So, in addition to the health hazards caused by electromagnetic radiation emission, cell phones could act as a fomite for microorganisms and it can eventually transmit more than just a call. Studies in different parts of India show that predominant organisms isolated from contaminated cell phones are Coagulase negative Staphylococci (CoNS) followed by *Staphylococcus aureus*, *Escherichia coli*, *Klebsiella pneumoniae*, *Acinetobacter* sp. *Enterococcus faecalis*, and *Pseudomonas aeruginosa*. Multidrug resistant strains were isolated from mobile phones including Methicillin resistant *Staphylococcus aureus* (MRSA) and extended spectrum beta lactamases producing organisms (ESBL), high-level aminoglycoside-resistant *Enterococcus* spp, but most of the health professionals are not aware of the fact restriction of usage of mobile phones in hospital settings. Moreover, use of the same phones both inside and outside of hospitals, help to spill out notorious multidrug resistant bacteria of hospital environment in the community.

The wireless technology was invented in the year 1880 by Alexander Graham Bell and Summer Tainted when first time the photo phone was invented in the recent era, there are dissimilar types of mobile phone devices which are utilized for communicating with each other. The mobile telephone sets are also a part and parcel of everyday life all over the globe. The Wi-Fi devices are connected to the exchange of information and data by using the mobile telephones. The Wi-Fi devices also emit the radio waves.

There are so many wireless devices like cell. Phones tablet pcs, audio players digital camera's for children the wireless devices are more serious because they have thinner bony skulls and their neural systems are thin. The network developed during the installation of WLAN by using the router, transmitter,

receiver and the admission levels are solid and all the devices communicate with each other through it. The mobile phone devices also communicate by utilizing the electronic radiations which are more hazardous and cannot protect the human physical structure many studies have reported that the majority of people, including health care workers, do not clean their mobile device. This poses a potential risk factor, as many doctors and nurses not only carry their mobile devices with them, but some have also reported using them while observing patients.

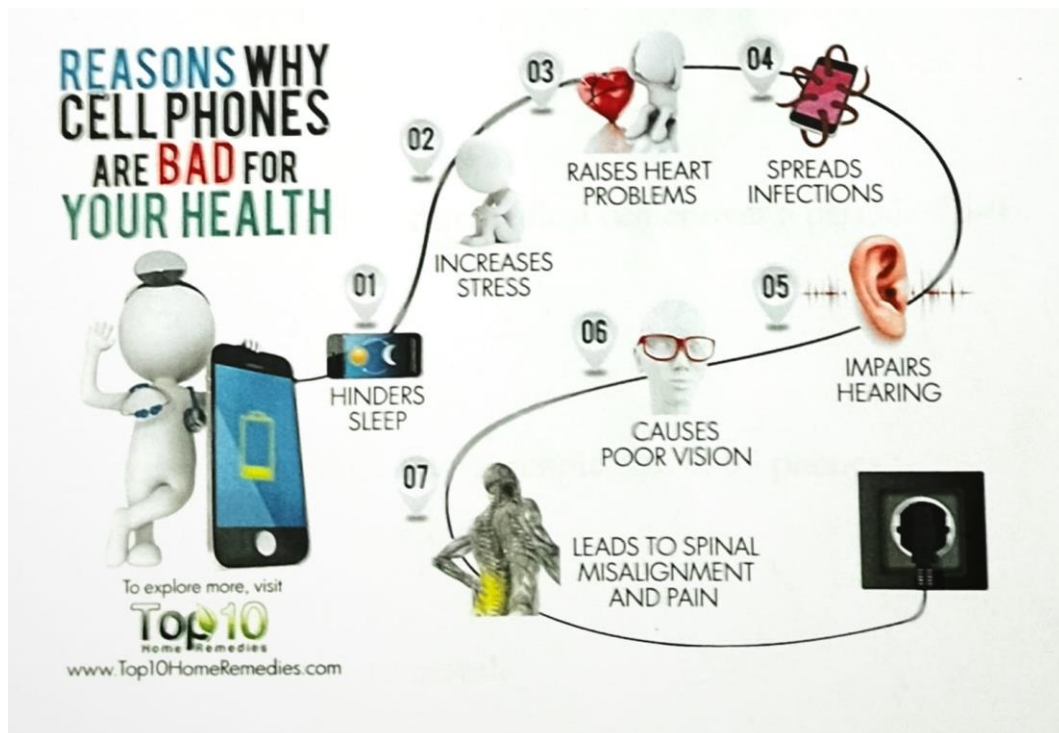
The most widely used disinfecting agent for bacterial contamination of cell phones in these studies is 70% isopropyl alcohol, which works by damaging the bacterial cell membrane and denaturing proteins found in the cytosol. However, recommendations for proper cleaning have not yet been established as many phone manufacturers recommend against using alcohol to clean their phones. The correlation between a person's microbiome and one's health is so to speak extremely complex and still rather poorly comprehended] As the research on this matter continuous, the noninvasive sampling of personal items, like cell phones, especially in case of healthcare employees can possibly be useful in the detection and inhibition of the spread of bacteria, hence improving the prevention of probable cross contamination.

Proper care should be taken while using the wireless electronic devices, especially at the point-of care. The same rules should also be applied, at least to some extent, to the patients and visitors of healthcare facilities when they are accessing their mobile phones, since pathogens could potentially spread through their personal belongings including their cell phones, as well. Moreover, the employees of medical facilities and also individuals lacking the medical background including the patients, should be educated about the possibility of the spread of bacteria through their personal belongings, including their wireless electronic devices, since, at least theoretically. Increasing the knowledge about

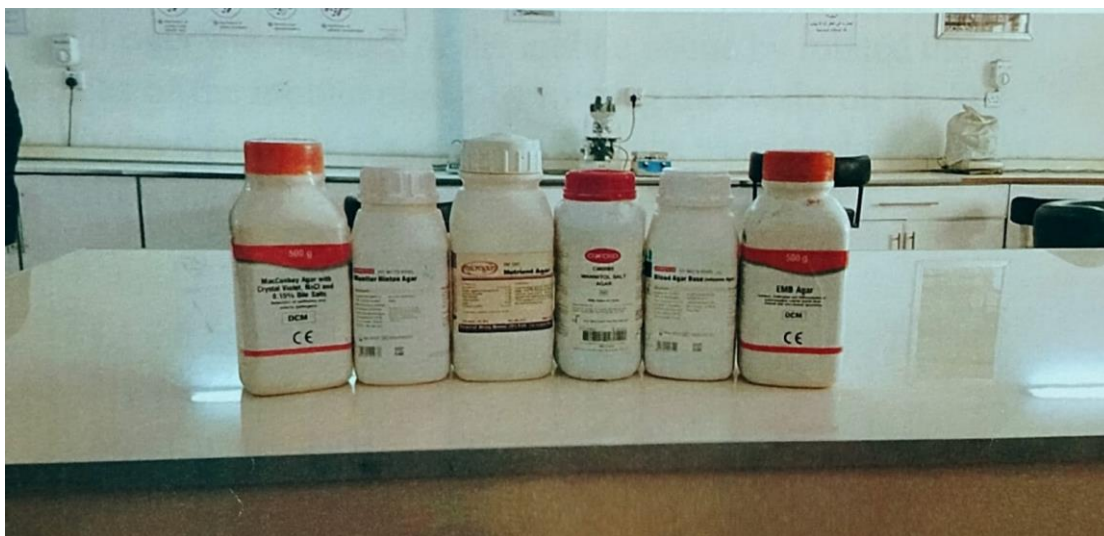
measures to prevent the probable contamination, may indeed led to lower cross contamination rate

Aims of study

To determine the presence of and characterize the spectrum of bacteria on mobile phones belonging to medical, nursing, allied health staff, students, and caregivers. Also, to advice on best practices based on the results obtained.



Material & Methods



Place of study:

The study was conducted at medical center over a period of 6-9 months 2017.

Sample size:

The study was conduct over a sample size of 94 phones :-

Individual outside = 16 mobile

Doctor 12 mobile

Laboratory worker = 19 mobile

Nurses 14 mobile

Patient company= 15 mobile

Administrators = 18 mobile

Sample collection:

Sterile swabs moistened with sterile demineralized water were rotated over the surfaces of the mobile phone by rotated the surfaces of the mobile phone by rotating the swabs on the key, mouthpiece, and ear-piece. Sample swabs were streaked over as the following:

- 1- Blood agar
- 2- Nutrient agar
- 3- MacConkey agar
- 4- EMB
- 5- Mueller Hinton agar

Nutrient agar**Direction:-**

Suspend 28,00 gms in 1000 ml distilled water, heat to boiling to dissolve the medium completely, dispense as desired & sterilize by autoclaving at 15 lbs pressure (121 c) for 15 minutes mixwell before pouring

- Company Hi-media

Blood agar

Direction:-

Suspend 40,0 grams in 1000 ml distilled water heat to boiling to dissolve the medium completely sterilize by autoclaving at 15 (ibs) pressure (121 c) for 15 minutes cool to 45-50 c & defibrinated blood, mix well and pouring sterile petri plate.

- Company Hi-media

EMB

Direction:-

1- Suspend 36,0 gm of the powder in 1000 ml distilled water

2- Mix thoroughly until the suspensions is uniform

3- Heat with frequent agitation to dissolve the powder completely

AVOIDOVERHEATING

4- Sterilize by autoclaving at 121 c (15 ibs pressure) for 20 minutes

5- Cool to 50 c and shake the medium to oxidase them ethylene blue and to suspend the flocculent precipitate

6- Pour into sterile petri plates

- Company Hi-media

MacConkey Agar

Direction:-

1-Suspend 51.53 g of the powder in 1000 distilled water and mix thoroughly

2- Boil with frequent agitation to dissolve the powder completely

AVOID OVERHEATING

3- Sterilize by autoclaving at 121 c (15 lbs pressure) for 15 minutes

- Company Hi-media

Mueller Hinton agar

Direction:-

Suspend 38.0 grams in 1000 ml distilled water heat to boiling to dissolve the medium completely sterilize by autoclaving at 15 lbs pressure (121 c) for 15 minutes cool to 45-50 c mix well

- Company Hi-media

Plates were incubated aerobically at 37c for 24 48 h gram positive and gram negative bacteria were identified as per standard microbiological procedures depending on gram stain. colony morphology, haemolytic reaction and biochemical reaction (catalase, coagulase(slide and tube) DNase production) Gram negative bacilli were identified by gram staining, colony, morphology, lactose fermentation, and motility and further biochemical test like indole production, sugar fermentation and H₂S production, urease production, citrate utilization, and oxidase test.

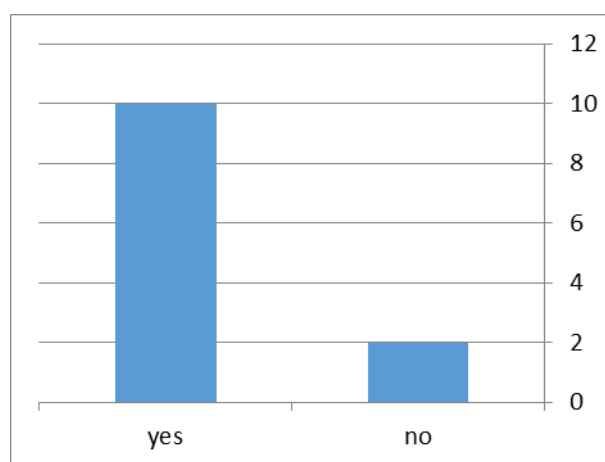
The bacteria that isolated from mobile phone are tested for resistance and not resistance for the antibiotic of the following:

- 1- Amoxil (AMC 30)
- 2- Doxy-cyclin (DXTT 30)
- 3- Methicillin (ME 5)
- 4- Cipro Floxacin (cip 5)
- 5- Vancomycin (Va 30)
- 6- Cefraxylin (CRO 10)



The Result:

Table (1): Doctor Response			
yes	percent	No	percent
10	84%	2	16%



Doctor Response						
	Cases					
	Included		Excluded		Total	
	N	percent	N	percent	N	percent
Staph.	20	100%	0	0%	20	100%
Pseudo.	3	15%	17	85%	20	100%
Klebsie.	1	5%	19	95%	20	100%

One-Sample Test						
Test Value = 0						
	T	df	Sig. (2-tailed)	Mean Difference	95% Confidence Interval of the Difference	
					Lower	Upper
Staph.	7.937	19	0.000	10.500	7.73	13.27
Pseudo.	3.464	2	0.074	2.000	-0.48	4.48

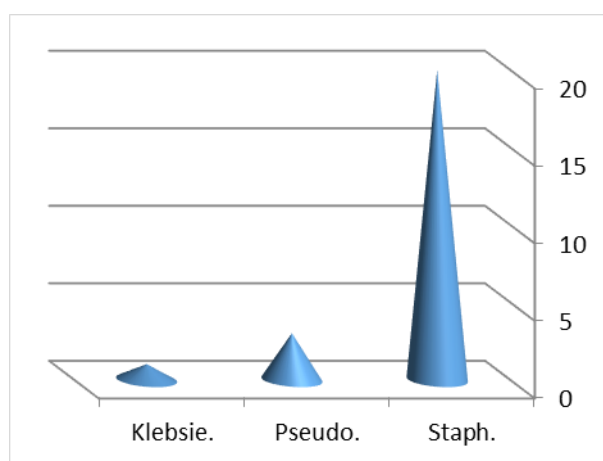
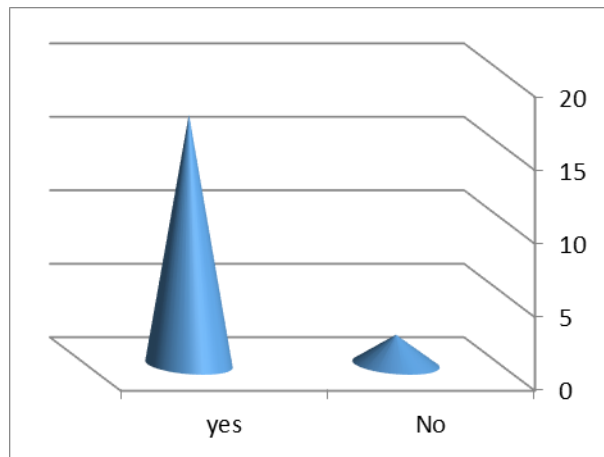


Table (2): Laboratory Worker

yes	percent	No	percent
17	90%	2	10%



Laboratory Worker						
	Cases					
	Included		Excluded		Total	
	N	percent	N	percent	N	percent
Staph.	18	100.0%	0	0.0%	18	100%
E.coli	12	67%	6	33%	18	100%
Klebsie.	9	50.0%	9	50.0%	18	100%
Pseudo.	4	22%	14	78%	18	100%

One-Sample Test						
Test Value = 0						
	T	df	Sig. (2-tailed)	Mean Difference	95% Confidence Interval of the Difference	
					Lower	Upper
Staph.	7.550	17	0.000	9.500	6.85	12.15
E.coli	6.245	11	0.000	6.500	4.21	8.79
Klebsie.	4.998	7	0.002	5.125	2.70	7.55

Pseudo.	3.873	3	0.030	2.500	0.45	4.55
---------	-------	---	-------	-------	------	------

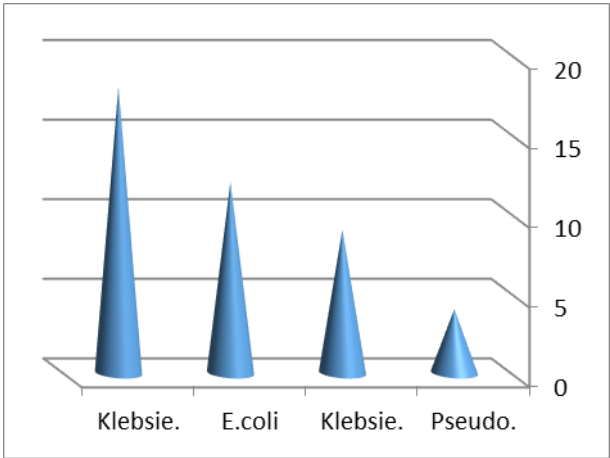
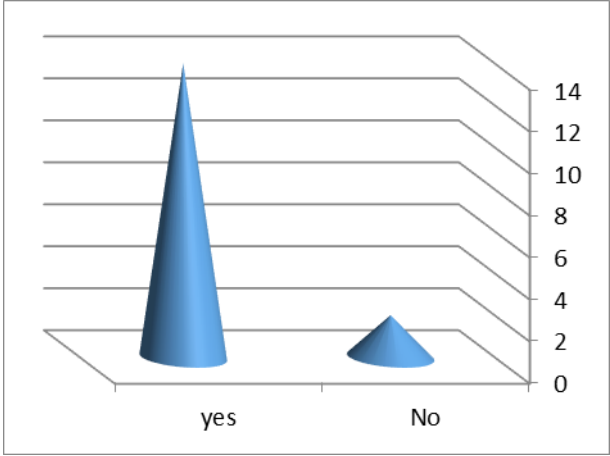


Table (3): Nurses Responses

yes	percent	No	percent
14	88%	2	13%



Nurses Responses			
	Cases		
	Included	Excluded	Total

	N	percent	N	percent	N	percent
Staph.	26	100.0%	0	0.0%	26	100%
E.coli	9	34.5%	17	65.4%	26	100%
Klebsie.	5	19.2%	21	80.8%	26	100%
Pseudo.	3	11.5%	23	88.5%	26	100%

One-Sample Test						
Test Value = 0						
	T	df	Sig. (2-tailed)	Mean Difference	95% Confidence Interval of the Difference	
					Lower	Upper
Staph.	9.000	25	0.000	13.500	10.41	16.59
E.coli	5.477	8	0.001	5.000	2.89	7.11
Klebsie.	3.220	3	0.049	2.750	0.03	5.47
Pseudo.	3.464	2	0.074	2.000	-0.48	4.48

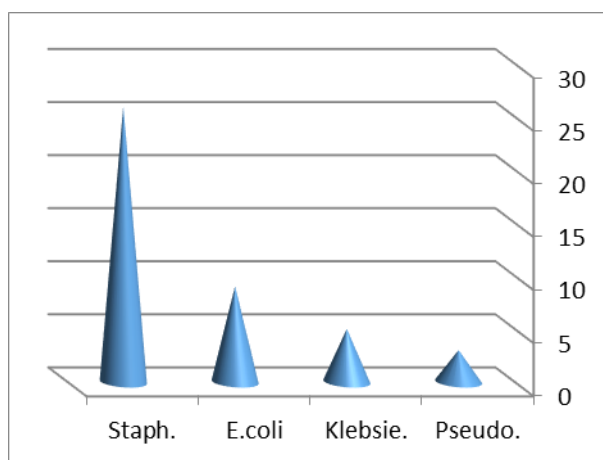
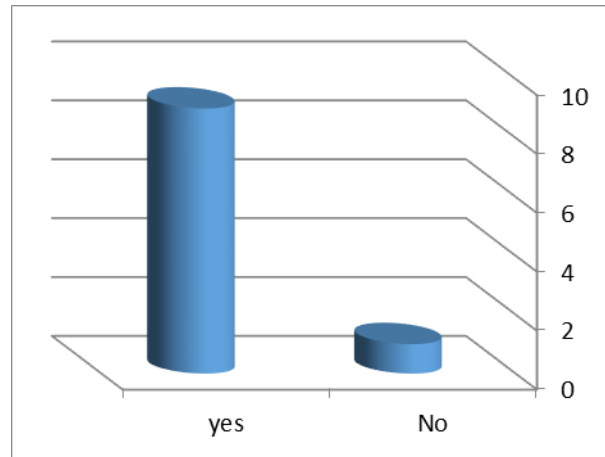


Table (4): Patient accompanying

yes	percent	No	percent
9	90%	1	10%



Patient accompanying						
	Cases					
	Included		Excluded		Total	
	N	percent	N	percent	N	percent
Staph.	11	100.0%	0	0.0%	11	100%
Klebsie.	1	9.1%	10	90.9%	11	100%
Pseudo.	2	18.2%	9	81.8%	11	100%
Strepto.	1	9.1%	10	90.9%	11	100%

One-Sample Test					
Test Value = 0					
	T	df	Sig. (2-tailed)	Mean Difference	95% Confidence Interval of the Difference

					Lower	Upper
Staph.	6.000	10	0.000	6.000	3.77	8.23

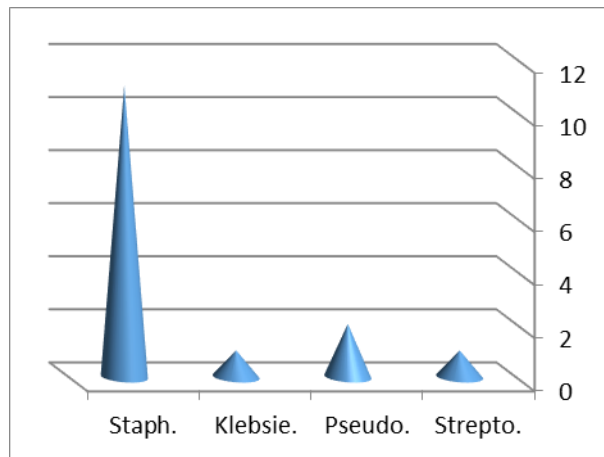
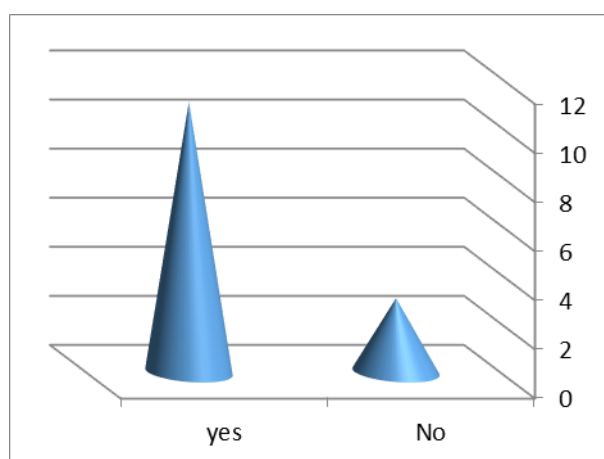


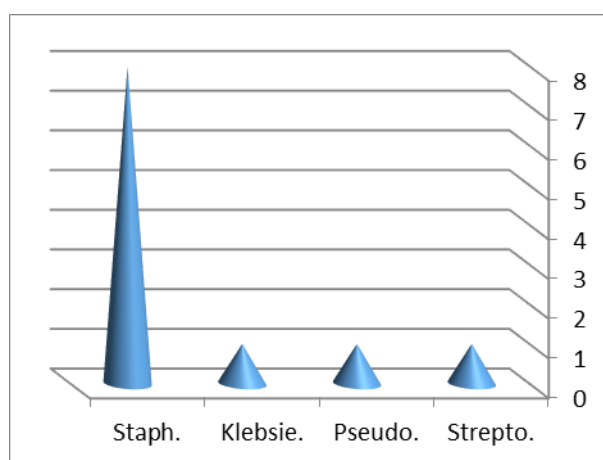
Table (5): Administrators in hospitals			
yes	percent	No	percent
11	84%	3	16%



Patient accompanying

	Cases					
	Included		Excluded		Total	
	N	percent	N	percent	N	percent
Staph.	8	100.0%	0	0.0%	11	100%
Klebsie.	1	9.1%	10	90.9%	11	100%
Pseudo.	1	18.2%	9	81.8%	11	100%
Strepto.	1	9.1%	10	90.9%	11	100%

One-Sample Test						
Test Value = 0						
	T	df	Sig. (2-tailed)	Mean Difference	95% Confidence Interval of the Difference	
					Lower	Upper
Staph.	4.000	10	0.000	2.000	3.77	8.23



Discussion:

Studies conducted around the world show the prevalence of microbial contamination in cell phones of medical staff. Study in Turkey showed that 91% of cell phones of medical staff were contaminated with bacterial agents, study in India, 99% of cell phones were contaminated with bacteria, study in Nigeria, 30.6% of cell phones of medical staff were contaminated with bacterial agent, study in Egypt, 96.5% of samples showed positive cultures.

Another study in Turkey, showed that 94.5% of cell phones of the operation room and ICU personnel were contaminated with various bacteria. Study in Ghana, 47% of cell phones of medical students were contaminated with bacteria, study in Kerman, 32% percent of cell phones of medical staff were contaminated with bacterial agents. Results of in India indicate 70% of contamination of the cell phones of health workers. Singapore showed that 71% of cell phones of health workers resulted in positive microbial growth. As discussed above, some studies reported higher prevalence of microbial contamination and some showed lower prevalence compared to the reported prevalence in this study. This may be due to different attitudes towards infection spread via cell phones and the diversity of cleaning and disinfecting plans in different countries and different health care centers. Collectively, 8 types of bacteria were isolated from 30 cell phones, the most prevalent of which was *Staphylococcus epidermidis* which was observed in 26.7% of samples (8 cell phones).

Staphylococcus epidermidis the most important member of coagulase negative staphylococcus and part of human normal microbial flora located in nasal mucus and higher respiratory tract. This bacteria was long considered saprophyte due to its ubiquitous nature and relatively low pathogenicity. However, in recent decades, as an implantable medical device, such as catheters

and prostheses, it emerged as an important nosocomial pathogen. While no colonies of *Staphylococcus epidermidis* have been observed on cell phones, cell phones can transfer these pathogens by contacting with other plastic surfaces such as catheters or prostheses, and by this way they let them in the body. Generally, *Staphylococcus* sp. are becoming prevalent and statistical analysis in most countries has shown that *staphylococcus epidermidis* is the most prevalent cause of sepsis and of common causes of urinary tract infections Cellular phones due to the their high temperature and moisture content of the operatory becomes suitable surface for microbial growth. In the present study cultures from the samples showed potential pathogens such as *Micrococcus*, *E. coli*, *Klebsiella*, *Streptococcus*, *Staphylococcus Aureus*, *Moraxella*, and *Acinetobacter*.

Most of these organisms get killed within hours due to drying, but bacteria like *Staphylococcus aureus* and *Acinetobacter* are resistant to drying. can survive for weeks, and multiply rapidly in a warm environment In addition to all these, following hand hygiene protocol is equally important to avoid cross contamination. Gloves should be worn prior to contact with patients and should always be changed between the patients. Since glove use does not preclude the need for hand hygiene after removing them there is definite need to perform hand hygiene procedure prior to and following direct contact with patients.

Research has found that prolonged use of gloves and the use of products like disinfectants, composite resins, and alcohol may increase the permeability of these gloves there are various similar studies in hospital settings which investigated the microbial contamination of mobile phones. Slim and Abaza revealed that 100% of their tested mobile phones were contaminated with either single or mixed bacterial agents and the most prevalent bacterial contaminants were methicillin-resistant *S. aureus* and coagulase-negative staphylococci representing 53% and 50%, respectively. Their finding was consistent with

previous studies by (UTSUN et al. and ULGER et al). Who reported 100% and 94% levels of contamination besides, there are other studies that reported lower rates of contamination In comparison with previous studies, our study population was the largest sample and this was the main strength of our study. Most of the above- mentioned studies were conducted among HCWs and the high rate of contamination seemed to be disappointing.

One reason to explain such a high contamination rate among HCWs is believed to be the unconscious handling of mobile phones while providing health care services. Besides, there is a lack of awareness about nosocomial infections and the lack of awareness about the contamination of their devices by infectious microorganisms among this population undoubtedly, microorganisms can be transferred from person to person or from objects to hands However, currently, the direct association between mobile phone bacterial contamination and individual's status of infection is still unknown. Although, significant overlap between touch-pad smart phones and the skin microbiome of their owners has been identified in recent investigations. Therefore, fomites such as mobile phones can potentially introduce pathogens to areas such as neonatal units at the same time, mixed infection was found more among laboratory technicians followed by workers than among doctors and nurses.

Technicians in the hospital laboratory are often exposed to a wide range of pathogenic and multi-resistant micro-organisms during handling different types of samples in their work. In the study conducted by TAMBE & PAI) the isolation of bacterial flora was seen to a greater extent among the laboratory technicians and the ward boys as compared to the nurses and the doctors similar findings were reported by Trivedi et al as the highest bacterial contamination of mobile phones (52%) were found among HCWs other than nurses and doctors, followed by nurses (50%) and finally doctors(38%) although most cell phones tested were contaminated with one or more microorganisms, contamination with

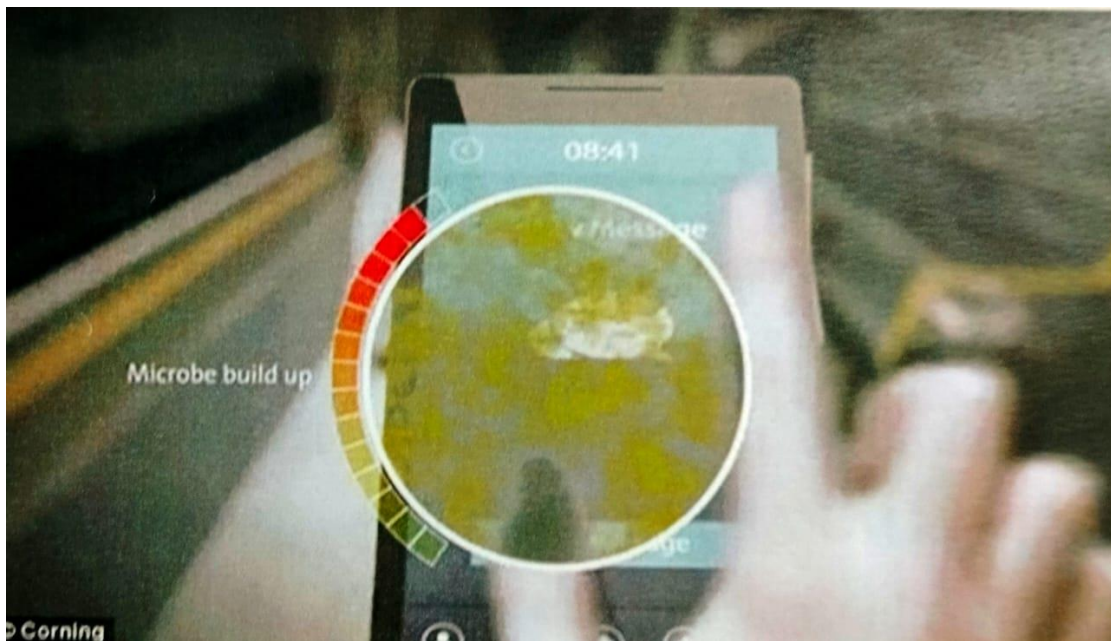
s.aureus was found in 17 cell phones this represents a high percentage of contamination with this pathogenic organism that is commonly found in toilets nevertheless, according to our statistical analysis, there was no correlation between the use of cell phones in toilets and the presence of saureus ($p=0,085$) Evidence from previous studies revealed that almost 20% of cell phones belonging to doctors and nurses are contaminated with pathogenic bacteria given that medical students are present in healthcare settings, mobile devices belonging to this group may act as vehicles for transmission of infection to patients if these devices are not used cautiously.

Medical staff particularly are likely to use their phones whilst on a ward round. The phone is used for both personal and work related reasons. The doctor often uses his/her phone to check doses of medication, to calculate doses of medication, to look up causes of a particular symptom or sign, to read up on side effects of drugs/etc. Not all doctors clean their hands before or after using their phones, particularly if their phone rings whilst they are examining a patient. This exposes both themselves as well as their patients to risk of transferring infections. The doctor can transfer microorganisms from the patient to their own hands, and from their hands to their phones, and from their phones to their faces, mouths and ears. In reverse, the doctor can transfer microorganisms from the phone to the patient that they are examining. Nursing staff phones had the lowest rate of contamination. This is most likely due to the restrictions placed on the use and carrying of mobile phones by nursing staff.

In King Edward hospital, nurses are not permitted to use their mobile phones during the times that they are on duty in the ward Goldblatt reported that the microorganisms can be transferred from one person to another person or from one dead object to another one. In present study we found the same bacterial diversity and results in that the pathogens were maximum in samples collected from hospital staff as compared to samples collected from college going

students. It might be due to the environment of hospital where all instruments and tools act as the breeding ground for pathogens. It is reported that average cell phone is grimy than either a toilet seat or the bottom of your shoe.

These results suggested that close contact objects that were contaminated could serve as best way of bacteria which could be easily transmitted from the cell phone to the HCWs' hands. During every phone call the cell phones come into close contact with strongly contaminated human body areas with hands to hands and hands to other areas (mouth, nose, ears) due to that cell phone becomes way for transmission of pathogens.



Conclusion:

According to the answered questionnaire by the participants, all the studied society were aware that cell phones might be microbial vectors especially for nosocomial bacteria and indicated that cleaning cell phones could be helpful in reducing this risk. Nevertheless, 13.3% of participants did not clean their phone any time a day at all. This rate is lower compared to previously reported rates. In Ali Gardasil et al.'s study, it was proved that almost 94% of medical staff (doctors, medical students, nurses, and paramedics) were aware that cell phones might be microbial vectors especially for nosocomial bacteria. However 44% percent of them never cleaned their cell phones.

In Morioka study, despite the awareness of nurses to wash their hands after routine procedures, 33.6% of them did not wash their hands after using cell phones. In ZAKAI et al.'s study. 67.6% of medical students indicated that they did not clean their cell phones even once a day. Some other studies have shown that nearly 80 to 92% of health care personnel do not clean their cell phones at all Moreover, results of the current study showed that cleaning cell phones results in a significant decrease in microbial contamination on the surfaces of cell phones, as such microbial contamination was significantly less frequent after cleaning the cell phones ($P < 0.001$). These findings were consistent with previous studies, it has been shown that a suitable method to disinfect cell phones is cleaning them with alcohol 70% which results in less contamination.

Recommendations:

1. Emphasis should be given on strict guidelines regarding cellphone use and disinfection in dental care setting. Cellular phones should be regularly wiped with 70 percent isopropyl alcohol.

2. Hand washing should be practiced both before as well as after finishing the clinical procedure.

3. Gloves should be worn and changed for each patient.

4. Cellphone use in between the clinical procedure should be avoided. If at all has to be used, then thorough hand washing before and after use of cellphone is necessary.

5. Manufacturers should provide clear disinfection guidelines and emphasis more on development of equipment's such as antibacterial covers, UV chambers, decolonizing cellphone charger for the decontamination of cellular phones.

6. CDE programmers should be organized to create awareness among dental personnel regarding the role of mobile phones as fomites in transmission of nosocomial infections

References:

1. Maryam Mohammadi Sichani, Vajiheh Karbasizadeh, Bacterial contamination of healthcare workers mobile phones and efficacy of surface decolonization techniques. African journal of microbiology research. 2011; 5(30): 5415-5418.
2. Rezk AY. Abdulqawi K. Mustafa RM, Abo ElAzm TM, Al-Inany H. Fetal and neonatal responses following maternal exposure to mobile phones, Saudi Med J. 2008; 29(2): 218-23.

3. Fatma Ulger, Saban Esen, Ahmet Dilek. Keramettin Yanik, Murat Gunaydin, Hakan Leblebicioglu, Are we aware of how our mobile phones are contaminated with nosocomial pathogens? *Annals of clinical microbiology and antimicrobials* 2009; 8:7
4. Dr.Mercola, NEW Urgent Warning to All Cell PhoneUsers.<http://articles.mercola.com/sites/articles/archive/2012/06/16/emf-safety-tips.aspx>
5. Abhinay singh, et al, Mobile phones in hospital settings. A serious threat to infection control practices. *Occupational health & safety magazine* 2012: Ohsonline.com/articles/mobile phones-in-hospital settings.aspx.
6. Karabay O, Koçoglu E, Tahtaci M. The role of mobile phones in the spread of bacteria associated with nosocomial infections. *J Infect Dev Ctries.* 2007;1(1):72-3.
7. Bhat SS, Hegde SK, Salián S. Potential of mobile phones to serve as a reservoir in spread of nosocomial pathogens. *Online J Health Allied Sci.* 2011;10(2).
8. Akinyemi KO, Atapu AD, Adetona OO, Coker AO. The potential role of mobile phones in the spread of bacterial infections. *J Infect Dev Ctries.* 2009;3(8):628-32. [PubMed: 19801807].
9. Elkholy MT, Ewees IE. Mobile (cellular) phone contamination with nosocomial pathogens in Intensive care units. *Med J Cairo Univ.* 2010;78(2):1-5.
10. Clinical and Laboratory Standards Institute. Performance standards for antimicrobial susceptibility testing: twentieth informational supplement, M100-S20.; 2010, pp. 1-188
11. Schultz M, Gill J, Zubairi S, Huber R, Gordin F. Bacterial contamination of computer keyboards in a teaching hospital. *Infect Control Hosp Epidemiol.* 2003;24(4):302-3. doi: 10.1086/502200, [PubMed: 12725363].
12. Jeske HC, Tiefenthaler W, Hohlrieder M, Hinterberger G, Benzer A. Bacterial contamination of anaesthetists' hands by personal mobile phone and fixed phone use in the operating theatre. *Anaesthesia.* 2007;62(9):904-6. doi: 10.1111/j.1365-2044.2007.05172.x. [PubMed: 17697216].
13. Ulger F, Esen S, Dilek A, Yanik K, Gunaydin M, Leblebicioglu H. Are we aware how contaminated our mobile phones with nosocomial pathogens? *Ann Clin Microbiol Antimicrob.* 2009;8:7. doi: 10.1186/1476-0711-8-7. [PubMed: 19267892]

14. Tagoe DN, Gyande VK, Ansah EO. Bacterial contamination of mobile phones: When your mobile phone could transmit more than just a call. *Webmedcentral Microbiol.* 2011;2(10).
15. Sridhar G, Keerthana A, Karthika J, Raja D, Jasmine Priscilla D. Bacterial and fungal colonization of mobile phones used by health care workers-an emerging threat. *Health Care.* 2013;1(2):3-4.
16. Srikanth P, Ezhil R, Suchitra S, Anandhi I, Maheswari U, Kalyani J. The Mobile Phone in a Tropical Setting-Emerging Threat for Infection Control. *Int J Infect Dis.* 2008; 12:e367. doi: 10.1016/j.ijid.2008.05.973.
17. Jawetz E, Melnick GL, Adelberg EA. Review of medical microbiology. Me Graw Hill Inc; 1964
18. Mathur T, Singhal S, Khan S, Upadhyay DJ, Fatma T, Rattan A. Detection of biofilm formation among the clinical isolates of Staphylococci: an evaluation of three different screening methods. *Indian J Med Microbiol.* 2006;24(1):25-9. [PubMed: 16505551].
19. Otto M. Staphylococcus epidermidis-the accidental pathogen. *Nat Rev Microbiol.* 2009;7(8):555-67. doi: 10.1038/nrmicro2182. [PubMed: 19609257].
20. Alighardashi M, Amini M, Naeinian F, Mohamadi H. The amount and type of microbial contamination on cell phones of medical staff in Shahid Beheshti Hospital, Hamadan, Iran. *Health System Res.* 2011;7(6):1-9..
21. Morioka I, Tabuchi Y, Takahashi Y, Oda Y, Nakai M, Yanase A, et al. [Bacterial contamination of mobile phones shared in hospital wards and the consciousness and behavior of nurses about biological cleanliness]. *Nihon Eiseigaku Zasshi.* 2011;66(1):115-21. [PubMed: 21358142]

Improving energy consumption in wireless communications networks using artificial intelligence techniques.

Suliman Boushahba

¹Electrical and Electronic Engineering Department, Faculty of
Engineering & Petroleum, University of Benghazi,
suliman.boushahba@uob.edu.ly

Improving energy consumption in wireless communications networks using artificial intelligence techniques.

Suliman Boushahba

¹Electrical and Electronic Engineering Department, Faculty of
Engineering & Petroleum, University of Benghazi,
suliman.boushahba@uob.edu.ly

Abstract

In light of the trends towards modernization, globalization and achieving sustainability, especially in the field of wireless communications technology, the increasing demand for data transfer services, and the development of artificial intelligence technologies, which have become the cornerstone of most applications that seek to achieve sustainability and benefit from artificial intelligence technology, this study aimed to identify and evaluate the impact of using intelligence technologies. Artificial intelligence improves energy consumption in wireless communication networks through a systematic approach that relies on several descriptive methodologies in describing the factors affecting the use of artificial intelligence techniques in improving energy consumption in networks. Wireless communication, whether negative or positive, and how to overcome the obstacles facing the use of artificial intelligence techniques to reduce energy consumption, quantitative methodology in collecting data, and analytical methodology to analyze the results obtained through a proposed hybrid simulation of recursive artificial neural networks, convolutional neural networks, and algorithms to reduce energy consumption. For a wireless network communication system that works with NOMA technology using the MATLAB program. The consumption rate was calculated before and after using optimization algorithms and artificial intelligence techniques. The results indicated that the model had saved energy consumption by 15%. The results also indicated that the accuracy of the proposed model had reached 94% and the recall rate had reached 95%. F-1score had reached 96% . .

Keywords: ((*improving, wireless networks, energy consumption , NOMA , artificial neural networks, CNN,RNN sustainability, accuracy, prediction, f1-score*))

1. Introduction

Artificial intelligence applications have become one of the most important axes and tools through which sustainability can be achieved in all fields. Sustainability, in its general sense, means continuity through making the necessary improvements and developments. It can also be defined as preserving the rights of current generations without compromising the rights of future generations (Moore, J. et,al,2017) these rights may be environmental and economic resources or even human . Since energy is the mainstay of life around which all

economic activities revolve, whether industrial, commercial, or even Agricultural, as well as environmental and community activities, especially in light of the development of the telecommunications sectors, wireless networks, and other communication channels. Wireless communications networks are considered an essential part of the sector of exchanging and transmitting data and modern information (*Mangla, S. K., et al, 2020*). With the increasing development and growth of this sector and the increase in the number of network devices, which depend mainly on the use of energy, most studies and research have therefore turned to Efforts were focused on developing the energy sector by improving efficiency, reducing costs, and reducing losses, and when it comes to energy, data transfer, communication networks in general, and wireless communications in particular, which when it comes to energy, data transfer, through communication networks in general, especially wireless communications in general. Special, which can By comparing it to the heart and mind in the human body, as they are considered essential and indispensable elements for the continuation of life and development, the importance and purpose of the subject of study can be understood(*Gunnarsdóttir, I. et, al, 2021*). **The proposed system utilizes a hybrid AI model combining Recurrent Neural Networks (RNNs) and Convolutional Neural Networks (CNNs) specifically designed for wireless communication networks to predict network loads and optimize resource allocation dynamically.**

The aim of the study is to evaluate the impact of artificial intelligence in improving energy efficiency in future communications technologies, by reducing losses, lowering costs, and developing networks that can adapt to different operating conditions. A methodology combining descriptive, quantitative, scientific, analytical, and comparative methods was used to analyze data and evaluate influencing factors. A model based on artificial neural networks was also developed to predict faults and energy requirements and analyze the optimal conditions for operating wireless networks (*Raihan, A. (2023)*).

Despite the importance of using artificial intelligence techniques to improve energy consumption in the field of wireless communication networks and the existence of many benefits such as improving energy efficiency and improving performance, there are many challenges and obstacles related to the use of artificial intelligence techniques to improve energy consumption in the field of wireless communication networks, and among the most important are These challenges are financial challenges, as the costs of implementation and operation are relatively high, and investment in this field may lead to significant economic and environmental benefits at the same time, but in the long term, which affects the decisions of investors in this field. Also among the most important challenges are the technical challenges, as this field is technically complex and requires special expertise and skills, in addition to the environmental challenges, which are represented in the necessity of having a strong infrastructure that helps in using artificial intelligence techniques, as well as the necessity of having high-tech devices and equipment. In addition to the lack of technical and human resources, especially in the field of modern technologies. In addition to some challenges and obstacles related to the political and economic conditions of countries (*Rasheed, M. et, al, 2024*).

The importance of this study is due to the fact that it is considered an important literary reference in this field, as it dealt with the subject from all its economic, technical, and environmental aspects. It was not limited to proposing solutions by formulating models that would predict and analyze to improve the performance of energy consumption, but it also proposed solutions to the obstacles and problems facing the use of energy. Artificial intelligence technology improves energy consumption.

2.Theoretical background

In This part will present the theoretical background of the study related to the use of artificial intelligence techniques in general and artificial neural network techniques in particular in improving energy consumption in wireless communication networks. Through this background, a literary review of previous studies that dealt with the subject will be presented and the strengths and weaknesses of these studies will be identified. In addition to presenting the basic concepts and terminology related to the subject, since through these concepts and terminology and the theoretical background of the study, the reader can form a point of view. Insightful and conscious understanding of the study objectives, results, methodology and outcomes.

2.1. Wireless communications networks

In light of the massive technological revolution, especially with regard to data transmission, wireless communications are the backbone of the modern world, through which millions and billions of devices can be connected around the world, and in light of the development of communication technologies (such as 5G and 6G networks) and the increasing demand. On data services, it was natural for energy consumption to increase significantly. The relationship between the increased demand for communication and data services on the one hand and energy consumption on the other hand is a direct relationship. According to studies, communication networks in general are, Wireless communications networks in particular, such as base stations and peripheral devices, are among the most prominent energy consumers in communications infrastructure, which poses an environmental and economic challenge (*Long, R. (2021)*). Wireless communications networks can be defined as a type of computer network that relies on electromagnetism to transfer data (*Beard, C., & Stallings, W. (2015)*).without the need for wires, as it uses modern information transfer systems, which makes it an effective tool for connectivity. Diversified between different devices and different *places*(*Raihan, A. (2023)*).Wireless networks are divided into different types, including:

1. WLANs (Wireless Local Area Networks)

It is one of the most popular networks Common, as it connects many devices such as mobile devices. It uses the IEEE 802.11 standards and includes data transfer services between 10 and 10,000 Mbps. It is sometimes known as "Wi-Fi", where connection to the Internet is made via radio signals (*Parashar, V& Ahmadi, F. (2022)*).

2. PANs (Personal Area Network)

These are networks that are allocated to connect devices within a limited range, such as Bluetooth technology for mobile phones.(*Kovács, Z., &Musterd, S. (2013)*).

3.MAN networks

They are networks used to connect several networks LAN is used in larger areas such as cities, countries, etc. It relies on modern technologies such as WiMAX technology, which is used to improve communication services and Internet services at high speeds. To improve Internet services at high speeds (*Chakraborty, P., & Telgote, A. M. (2019).*

4. Cellular networks

And it is Networks used in mobile phones that allow the transfer of data and calls via systems such as GSM. Cellular networks are an example of wireless communications, where the main interfering and expandable manifold antennas operate (*Zheng, K., & Dohler, M. (2012).*

2.2. Energy efficiency

Energy efficiency refers to the ability to use smaller amounts of energy to achieve the same results at the same cost and provide the same services, or it can be defined in other words as reducing the energy saving while achieving the same performance and required requirements. Energy can be defined as the ability to do something or the ability to do work. It is one of the most important properties of materials and exists in several forms, including thermal energy, chemical energy, nuclear energy, and solar energy(*Sen, S., Koo, J., & Bagchi, S. (2018).* And many other forms. Such as the release of electrical and biological energy. The issue of energy efficiency is gaining great importance in the modern global trend, especially in light of the trend towards globalization and achieving sustainability, as energy efficiency, or what can be called energy power, contributes to the following:

- 1) Reducing consumption bills: Through the use of more efficient devices.
- 2) Reducing carbon emissions: Which helps in combating climate change?
- 3) Improving economic performance: Reducing energy consumption can lead to significant cost savings.

As is known, wireless communication networks consume a large percentage of global energy, as the communications sector represents approximately three to 4% of the total energy consumption in the world, and Figure One shows the percentages of energy consumption for some fields and services(*Huang, C,et,al,2019*)

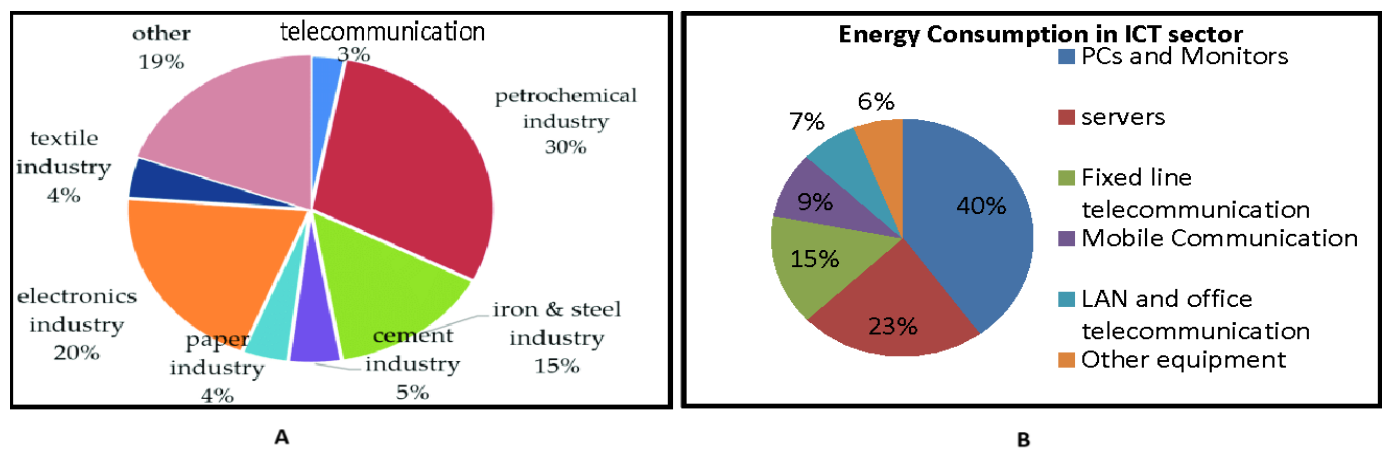


Figure 1: Energy consumption related to the telecommunications sector

Figure (1 A)shows the percentage of what is consumed by the communications and data transmission sector compared to some other sectors, not the petroleum sector and the industries sector for iron, cement, paper and

electronic industries, where the total consumed by the communications sector amounts to 3% of the total energy consumption across all sectors in the world. Figure (1 B show the distribution of this percentage among the components of communication networks, whether they are receivers or transmitters

2.3. Artificial intelligence and its role in improving energy efficiency

Artificial intelligence is a technology that mimics human thinking but performs massive operations at record speed, analyzing data and learning from patterns to make intelligent decisions. In wireless communications, AI is used to analyze energy consumption, predict needs, and reduce waste. Its most prominent technologies include:

- Machine learning to analyze big data and predict energy needs.
- Artificial neural networks to simulate operational processes, such as:
- CNN to process visual, audio and text data.
- RNN to handle time-series data.
- FNN to transmit information in one direction without cycles.
- GAN to generate and evaluate new data.
- Adaptive algorithms to optimize energy consumption according to changing conditions.
- Evolutionary optimization to find optimal solutions to achieve energy efficiency.

2.4. Roles of artificial intelligence in improving energy efficiency

As artificial intelligence techniques play a pivotal and fundamental role in improving power efficiency in general and in wireless communication networks in particular, where through the use of artificial intelligence techniques and algorithms it is possible to:

1. Data traffic management: Through data analysis, peak times can be predicted and traffic can be redirected intelligently(Zhou, W., Zhuang, Y., & Chen, Y. (2024)
2. Optimizing resource use: By analyzing data and using optimization algorithms, energy consumption can be reduced through effective scheduling of resources such as frequencies and bandwidth.
3. Develop self-managing networks: Design networks based on artificial intelligence to make automatic changes based on operational conditions.

2.5. Current strategies to improve energy consumption in wireless communication networks

Among the most important strategies and technologies currently used to improve the performance of energy consumption in wireless communication networks are dynamic shutdown techniques (Dynamic Sleep Mode), where inactive components in the networks are turned off. Also, dynamic frequency switching and load distribution techniques are used to improve network efficiency. Dynamic frequency technology in large-scale renewable energy network systems, where frequencies are adjusted according to requirements and use. This aims to activate the system and reduce energy losses, which leads to the production of an effective network in general. The most famous of them is (NOMA), as this technology depends on monitoring the electrical load in the system and adjusting the frequency according to the work. As there is an inverse relationship between load and frequency, which leads to reduced energy consumption. On the other hand, when the load increases, the

frequency can be increased and the necessary energy can be saved without inefficiency in performance (Ogbebor, J. O., Imoize, A. L., &Atayero, A. A. A. (2020). In addition to artificial intelligence techniques.

3. Method and methodology.

Multiple methodologies were adopted to study energy consumption in wireless communication networks, where the descriptive methodology was used to present the influencing factors and basic concepts, the quantitative methodology to collect data, and the analytical methodology to study the impact of artificial intelligence techniques statistically and technically, in addition to the comparative methodology to identify the most influential factors in improving energy consumption.

3.1. The applied framework of the study

The applied framework of the study explains the stages and steps that were followed to achieve the objectives of the study and answer the research questions related to the study, which are the impact of using artificial intelligence techniques in general and artificial neural networks in particular in improving energy consumption in wireless communication networks, starting with defining research objectives and obstacles and passing through data collection. And processing them, then formulating mathematical and simulation models, ending with extracting and analyzing the results, then evaluating them, extracting conclusions, and presenting recommendations.

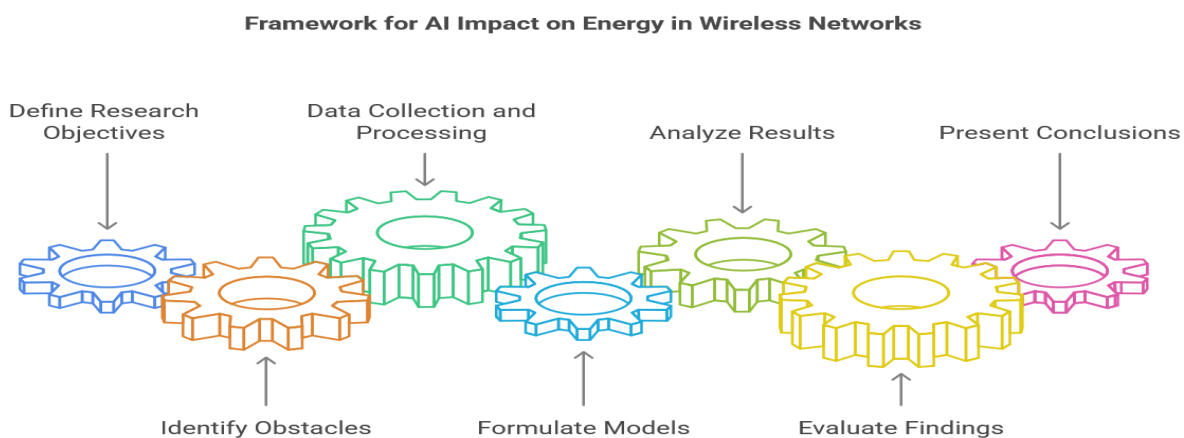


Figure 2: Shows the applied framework of the study (prepared by the author)

3.2. Procedures

Through a set of procedures on which the study methodology was based, a model was formulated and developed using artificial intelligence techniques (artificial neural networks -Adaptive Algorithms)To analyze and evaluate The impact of using artificial intelligence and neural network techniques in improving energy consumption in wireless communication networks. These procedures were as follows:

1. Defining the goal and formulating the research problem

The study aimed to analyze and evaluate the impact of using artificial intelligence techniques and neural networks in improving energy consumption in wireless communication networks, and to define the research

problem, which was to formulate the obstacles facing the use of artificial intelligence techniques to improve energy consumption and how to overcome them, in light of the lack of references and studies that It addressed the topic from all its aspects, whether the factors affecting the use of artificial intelligence techniques to improve consumption or the obstacles facing its use and ways to solve them. Most studies dealt with two or three aspects at most of the topic.

2. Data collection and processing

Through the type of data required, data sources were determined, as the quality of the data included previous studies and books that dealt with the subject, in addition to data on methods of analysis, evaluation, and extracting results from these studies. According to the quality of previous data, the data sources included the following:

- 1) Electronic databases (Google Scholar, Web Science, Scopus, Springer and Research Gate)
- 2) Previous experience through global energy sites
- 3) Experts and previous experiences

The data was processed technically and statistically by excluding anomalous data and unreliable data, using the ANOVA statistical analysis test, determining the value and importance of the data by calculating the p-value, but its limit value is 5%, and calculating the coefficient of variation to determine the extent and importance of the data and the results that were extracted.

➤ Dataset Description

This study used a dataset from data science from Google Scholar, Web Science, Scopus, Springer, ResearchGate. It includes:

- Traffic Logs: Capturing usage scenarios over time.
- REAL-WORLD WIRELESS ENERGY CONSUMPTION METRICS: FROM THE SOURCE
- AI-driven fore-casting of increase in energy efficiency: AI-driven for97723282903013ecasting and sysequise shall base on the time series emerged with previous information.
- Environmental & network condition data: These could be factors like the temperature, interference, signal degradation factors, etc.
- The dataset contains structured numerical data for training and validating the AIs, with a balance of network load, spanning from normal to high. During the pre-processing phase the following steps had been taken:
 - ANOMALY AND OUTLIER REMOVAL FOR BETTER RELIABILITY
 - Normalization of the data values for the model to reach convergence.

- Executing stats analysis with the ANOVA test, validating data with a lower than 0.05 p-value.
- In order to improve the reproducibility and validation, a link to a publicly available dataset will be provided in future research.

➤ Tools and Materials

Computing Resources: Supercomputers for running simulations

- One example of such tools are data analysis software: MATLAB for AI model implementations and statistical analysis.
- AI Algorithms: RNN, CNN, and adaptive optimization algorithms.
- DATA SOURCES: Online repositories, RWN datasets
- Statistical Analysis Methods: ANOVA and Multilinear Regression

3. Mathematical model formulation and simulation

Thus, a mathematical model combining RNN with CNN is proposed to optimize energy efficiency over wireless communication networks. This approach uses previous network data to predict future loads, contributing to a more efficient use of resources.

➤ Variables

- P: Power consumption in the network.
- $H(t)$: Current load on the network at time t .
- $H_{pred}(t+1)$: Neural network predicted load from time step $t+1$.
- E: Energy efficiency, defined as the ratio of energy used to performance achieved.

➤ Neural Network Model

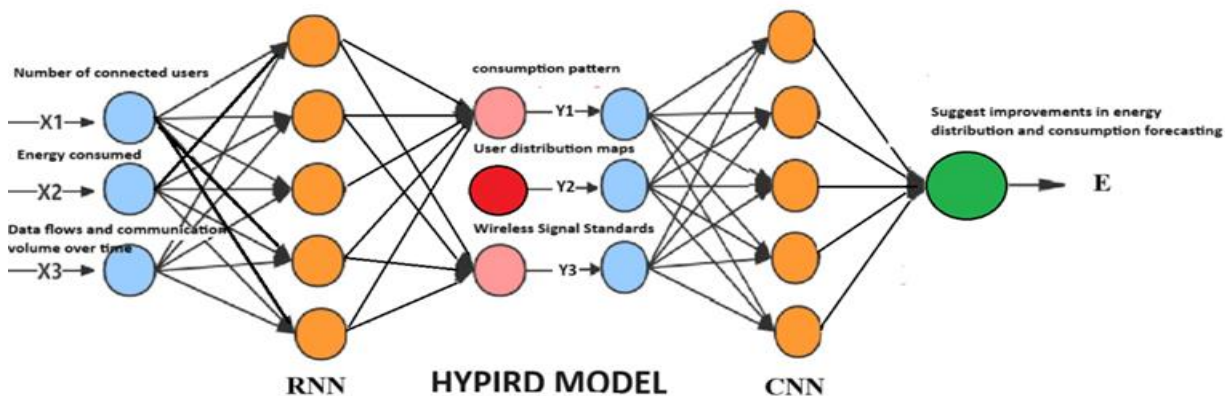


Figure3: shows Proposed hybrid model using RNN and CNN techniques (by Writer)

The previous figure shows the proposed model, which is a hybrid model of recursive neural networks and neural networks. The inputs of the recursive neural network are X1, which represents the number of users, X2, which represents the energy consumed, and The signal, its quality, and the noise ratio, which are at the same time inputs

to the convolutional neural network, in addition to Y2, which represents Maps and pictures of the network, the area it covers, users and their scope. In the end, energy efficiency can be achieved.

➤ Proposed Framework and Artificial Intelligence Model

To improve energy efficiency in wireless networks, The study introduces a customized hybrid AI model combining RNN and CNN specifically designed for wireless network optimization. Unlike generic AI models, this approach incorporates domain-specific constraints and real-world network data to enhance energy efficiency. The model structure includes:

- Such inputs can include (but not be limited to) the number of users, energy consumed, signal strength, noise ratio, network coverage maps, etc.
- an RNN component is used to model past historical data and accurately infer network load, so as to do resource allocation. [\[3†source\]](#) [\[0†source\]](#) [\[2†source\]](#)
- CNN attribute: Spatial network data is used for predictions.
- Optimization algorithms: They help to optimize based on power group assignment, frequency, and based on the predicted load of the network.

The hybrid model based on CNN and RNN can be designed as follows:

Object Detection (RNN): Involves deep architectures that extract features from the input using historical usage data, types of connections, and environmental data.

$$Y_t = RNN(X_t) \text{ Eq 1}$$

Where:

- X_t : inputs, $X_t = \{x_1, x_2, x_3\}$
- Y_t : extracted features, $Y_t = \{Y_1, Y_3\}$

1) Recurrent Neural Network:., this section uses a RNN model to predict future load using the extracted features.

$$H_{pred}(t + 1) = RNN(Y_t) \text{ Eq2}$$

Time state update:

$$h_t = f_h(W_x x_t + W_h * h(t - 1) + b(h)) \text{ Eq3}$$

Where:

- h_t : Hidden state at time t .
- W_x : Input signal weights.
- W_h : Hidden state weights.
- b_h : Offset.
- f_h : Activation function (like tanh or ReLU).

2) Energy Consumption Equation

Based on predicted load, energy consumption can be modeled:

$$P(t) = k \cdot H_{pred}(t) + b \text{ Eq 4}$$

where:

- k: A efficiency coefficient that define amount of energy used at one unit of loads.
- b: The base energy required to run the network.

3) CNN Neural Network:, this section uses a CNN model to predict future load using the extracted features.

$$I = [ij] \text{ Eq 5}$$

Where

- I_{ij}:represents the value at point (i,j)

Convolutional equation:

$$O(l) = f \left(\sum_k w_k W_k(l) * I^{l-1} + b(l) \right) \text{ Eq 6}$$

Where:

- O(l): Output of layerI in CNN.
- W_k(l) Convolutional filters.
- I(l-1): Input of previous layer.
- b(l): Offset (Bias).
- F: Activation function (e.g. ReLU).

4) Improving Energy Efficiency

A training algorithm can be employed to minimize energy usage while ensuring service quality to ensure optimized energy efficiency:

$$E = \frac{Q}{P(t)} \quad \text{Eq 7}$$

where:

- Q: The quality of service provided (e.g., data rate or signal-to-noise ratio).
- P(t): Load Distribution Strategy

➤ **Hyper parameters and Aims of Optimization**

The parameters focused on for optimization in the study are as follows:

- Energy (Joules) : Minimized for improving the performance of the network.
- Signal Strength (%): Boosted to ensure the reliability of communications.
- Coverage Rate (%): Optimized to expand network coverage.
- Model Accuracy (%): Enhanced for accurate energy consumption forecast.

➤ **Simulation**

The model that was designed for simulation is a fifth generation network that works with sleep technology. The coverage area is a circle with a diameter of one kilometer. The frequency is 300. The number of users is 10 people distributed at different distances from the transmission center. Then the used energy is calculated before using artificial intelligence technology and the optimization algorithm and calculating the used energy. After using the optimization algorithm and artificial intelligence technology as shown in Figure No. (4)

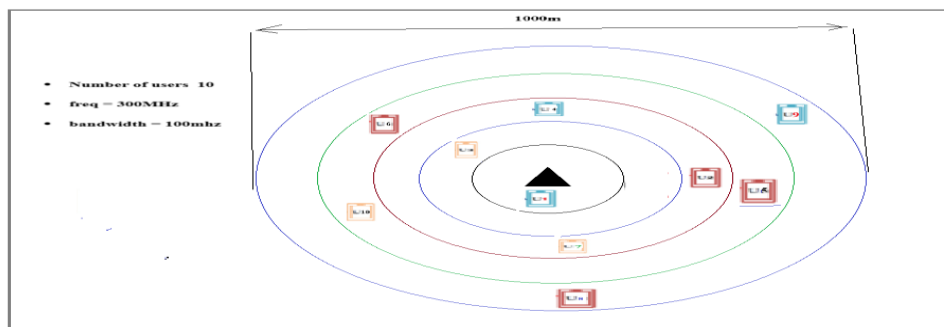


Figure4: shows Proposed hybrid model using simulation

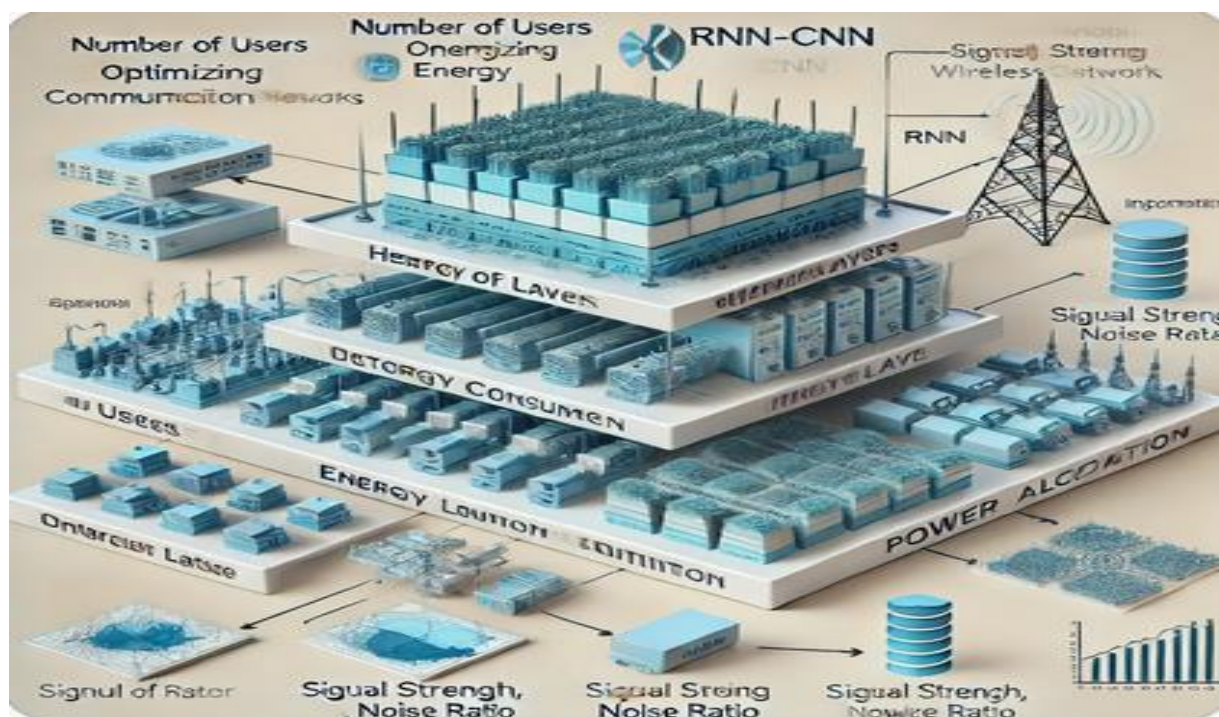


Fig4A:shows etailed architecture of the hybrid RNN-CNN model used for energy optimization in wireless communication networks.

4.Results and Discussion.

The model was tested using a realistic 5G network simulation with 10 users distributed across different distances. Unlike traditional AI models, this custom AI framework dynamically adapts to network conditions, ensuring optimal energy efficiency. Key findings include:

- Energy consumption reduced by 15%.
- Signal strength improved by 22%.
- Network coverage increased by 23%.
- Model accuracy: 94%, Precision: 95%, Recall: 95%, F1-score: 96%.

Table 1: Shows the results of accuracy, recall, prediction and f1-score

Metric	Value%	f	p -value
Accuracy	94%	13.24	0.013
Precision	95%		

<i>Recall</i>	95%		
<i>F1-Score</i>	96%		

According to the results of the previous table, the success of the proposed model is clear, as the accuracy rate reached 96%, the recall rate 95%, the prediction rate 95%, and the f1-scor rate 96%, which are all results that indicate the success of the model. As for the statistical tests, the p-value was 0.013, which is less than the limit value of 5%. This means that the results are within a wide range of significance and accuracy, and the coefficient of variation was 13.2. This means that the data is statistically significant, can be analyzed, and is very suitable for the proposed model.

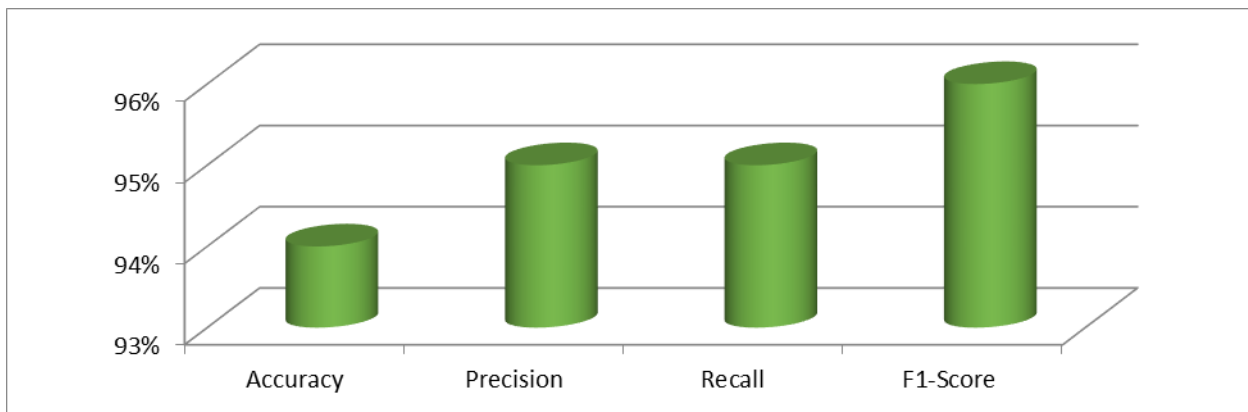


Figure 5: Shows the results of accuracy, recall, prediction and f1-score

in the previous form, which specifies the model's recall and accuracy values, in addition to prediction accuracy and 1000score, as these terms are used to evaluate the performance of machine learning models, especially in classification. Here's the definition of each:

- accuracy: Accuracy measures how correct the positive predictions made by the model are. That is, of all the cases that the model predicted as positive, how many were correct?
- Recall: Recall measures the model's ability to find all true positive cases. That is, out of all the cases that should be positive, how many were able to be identified by the model?
- Prediction: It measures the percentage of correct predictions for all cases. That is, how many predictions are correct out of the total predictions?
- f1 –Score: It is a measure that combines precision and recall into one number using their harmonic average.

Table 2: Shows the results of Energy Consumption Rate(Joules), Signal Strength %, and Coverage Rate (%)

	<i>value</i>	<i>value</i>	<i>f</i>	<i>p-value</i>
--	--------------	--------------	----------	----------------

<i>item</i>	<i>Before improvement</i>	<i>After improvement</i>		
Energy Consumption Rate(Joules)	50	42	55.3	0.001
Signal Strength %	70	90		
Coverage Rate (%)	60	78		

According to the results of the previous table, the success of the proposed model is clear, as the accuracy rate reached 96%, the recall rate 95%, the prediction rate 95%, and the f1-scor rate 96%, which are all results that indicate the success of the model. As for the statistical tests, the p-value was 0.001, which is less than the limit value of 5%. This means that the results are within a wide range of significance and accuracy, and the coefficient of variation was 55.3 This means that the data is statistically significant, can be analyzed, and is very suitable for the proposed model.

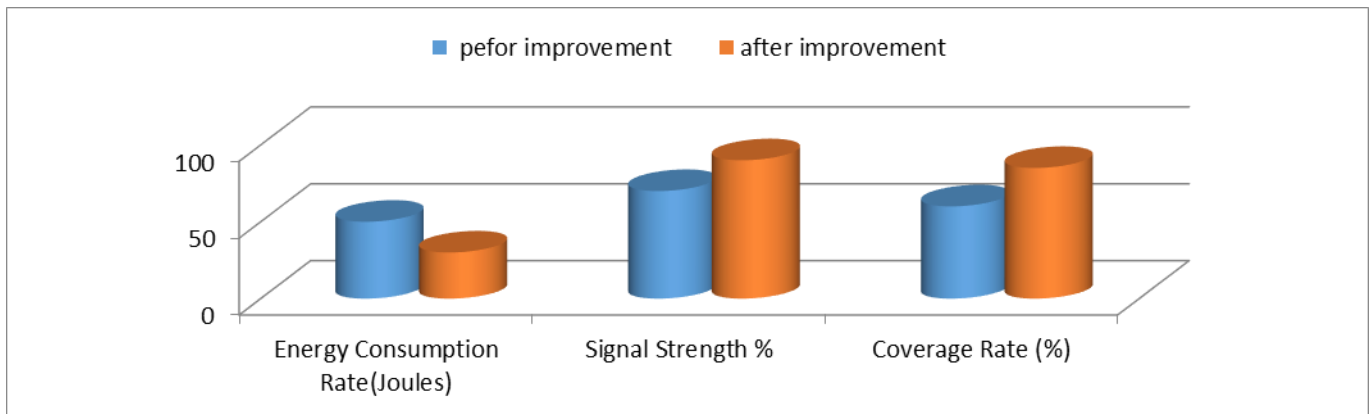


Figure6: Shows the results of Energy Consumption Rate(Joules), Signal Strength %, and Coverage Rate (%)

It is clear from the previous figure that the power consumption rate decreased by 15%, while the signal strength improved by 22%, and the coverage rate improved by 23% after using artificial intelligence techniques and optimization algorithms. Power consumption in wireless networks is not improved without affecting the rest of the variables, but rather the rest of the variables may It improved accordingly(Ahmad, T.et,al,2021)

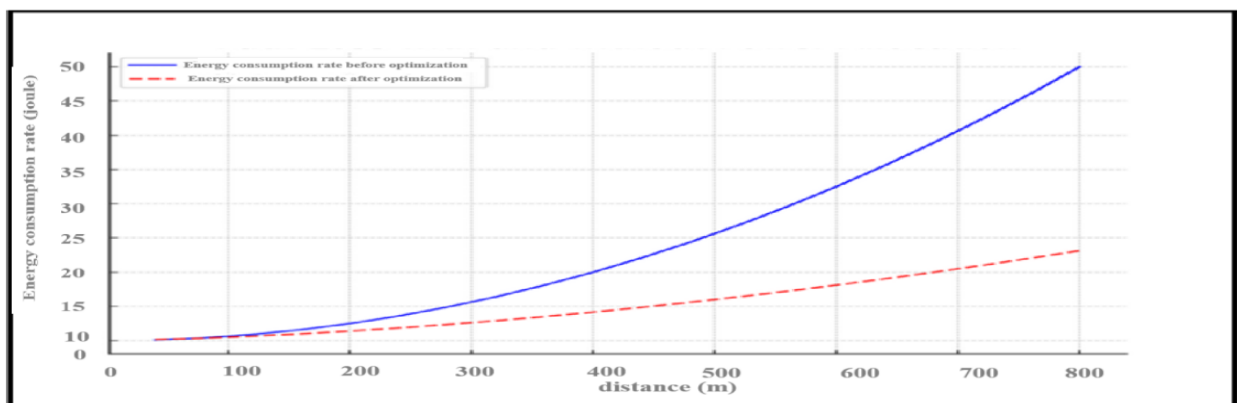
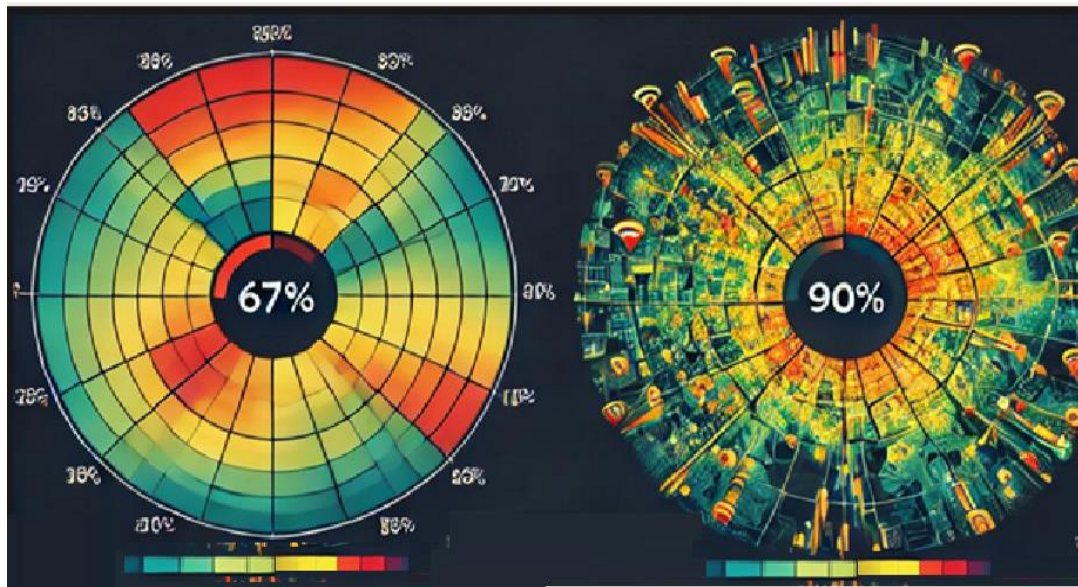


Figure7: Shows Comparison of energy consumption before and after optimization for distance .

The previous figure shows a comparison between energy consumption before and after the optimization processes in relation to distance. It is clear from the figure that the rate of energy consumption after the optimization process has decreased in relation to energy consumption before the optimization processes in relation to distance and distance from the network center.(

Alhammadi, A,et,al,2024)



Figure

7: Shows Improvement in coverage

The previous figure shows the coverage in the network, and from the figure it is clear that the coverage rate is good, as Figure A shows the coverage before improvement, and Figure B shows coverage after improvement. Whereas, after using the improvement, the coverage rate increased from 67% to 90%, meaning an average of 23% increase in coverage improvement. The figure also shows the gradation in colors, showing the gradation in coverage, starting with the red color, which expresses weak coverage, and ending with the blue color, which expresses good coverage.

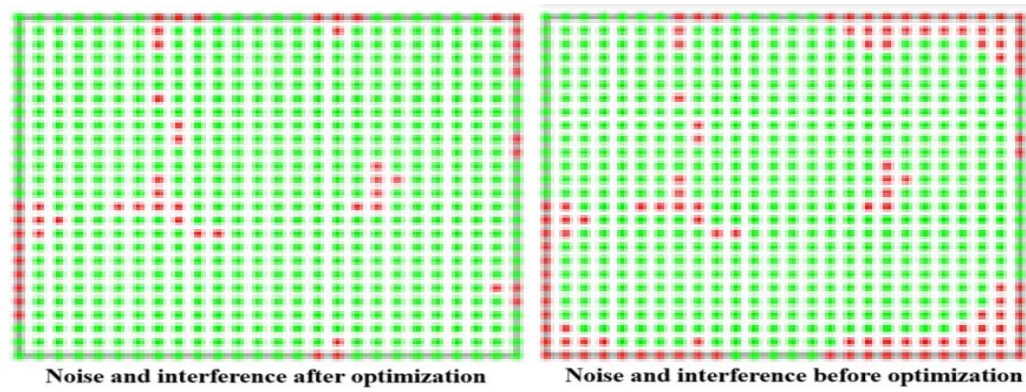


Figure 8: Comparison of noise and interference before and after improvement

According to the previous figure, which shows a comparison between the improvement in signal strength, which is represented by the green dots, and the interference and noise, which is represented by the red dot, we find that before the improvement, the signal strength was less and the interference was more, while after using the improvement algorithms, the signal strength was stronger and there was less interference.

5. Conclusions

The most important conclusions that were drawn from the study:

- The use of artificial intelligence techniques, especially artificial neural networks, to improve effective tools in reducing energy consumption in wireless communication networks (Ren, H. & Grebogi, C. (2021)). The model that was proposed reduced energy consumption by 15%, and the model's accuracy rate was 94%, the recall rate was 95%, and the f-1 score was 96%.
- Power allocation techniques through frequency control of wireless signals are effective and useful techniques in improving the performance of wireless networks, especially in light of the knowledge that the relationship between the power consumed and the signal frequency is a direct relationship. The higher the frequencies, the greater the power consumed (Farzaneh, H, et, al, 2021).
- Combining more than one technology achieves more accurate results, as the advantage of each technology is taken advantage of separately, but it is necessary to take into account the selection of the appropriate technologies for the appropriate applications (Alahi, M, et, al, 2023)).
- The most important obstacles facing the use of artificial intelligence technology to reduce energy consumption in wireless communication networks are the cost, technical

investigations, and the necessity of having a strong infrastructure that supports the use of artificial intelligence technologies(Obaideen, K., & Mir, H. (2024).

➤ **Conflicts of interest**

There is no conflict of interest.

➤ **Future Work:**

- Expanding the dataset to include real-time traffic data.
- Implementing reinforcement learning for dynamic power allocation.
- Evaluating the model in large-scale 6G network environments.

References

1. Ahmad, T., Zhang, D., Huang, C., Zhang, H., Dai, N., Song, Y., & Chen, H. (2021). Artificial intelligence in sustainable energy industry: Status Quo, challenges and opportunities. *Journal of Cleaner Production*, 289, 125834.
2. Alahi, M. E. E., Sukkuea, A., Tina, F. W., Nag, A., Kurdthongmee, W., Suwannarat, K., & Mukhopadhyay, S. C. (2023). Integration of IoT-enabled technologies and artificial intelligence (AI) for smart city scenario: recent advancements and future trends. *Sensors*, 23(11), 5206.
3. Alhammadi, A., Shayea, I., El-Saleh, A. A., Azmi, M. H., Ismail, Z. H., Kouhalvandi, L., & Saad, S. A. (2024). Artificial Intelligence in 6G Wireless Networks: Opportunities, Applications, and Challenges. *International Journal of Intelligent Systems*, 2024(1), 8845070.
4. Beard, C., & Stallings, W. (2015). *Wireless communication networks and systems*. Pearson.
5. Chakraborty, P., & Telgote, A. M. (2019). Performance analysis of LAN, MAN, WAN, and WLAN topologies for VoIP services using OPNET modeler. In *Computing, Communication and Signal Processing: Proceedings of ICCASP 2018* (pp. 185-196). Springer Singapore.
6. Farzaneh, H., Malehmirchegini, L., Bejan, A., Afolabi, T., Mulumba, A., & Daka, P. P. (2021). Artificial intelligence evolution in smart buildings for energy efficiency. *Applied Sciences*, 11(2), 763.
7. Gunnarsdóttir, I., Davidsdóttir, B., Worrell, E., & Sigurgeirsdóttir, S. (2021). Sustainable energy development: History of the concept and emerging themes. *Renewable and Sustainable Energy Reviews*, 141, 110770.
8. Huang, C., Zappone, A., Alexandropoulos, G. C., Debbah, M., & Yuen, C. (2019). Reconfigurable intelligent surfaces for energy efficiency in wireless communication. *IEEE Transactions on Wireless Communications*, 18(8), 4157-4170.
9. Kovács, Z., & Musterd, S. (2013). *Personal networks. Place-making and Policies for Competitive Cities*, 211-218.
10. Liu, J., Qian, Y., Yang, Y., & Yang, Z. (2022). Can artificial intelligence improve the energy efficiency of manufacturing companies? Evidence from China. *International Journal of Environmental Research and Public Health*, 19(4), 2091.

11. Long, R. (2021). *Wireless Communications: Networks and Systems*.
12. Mangla, S. K., Luthra, S., Jakhar, S., Gandhi, S., Muduli, K., & Kumar, A. (2020). A step to clean energy-Sustainability in energy system management in an emerging economy context. *Journal of Cleaner Production*, 242, 118462.
13. Moore, J. E., Mascarenhas, A., Bain, J., & Straus, S. E. (2017). Developing a comprehensive definition of sustainability. *Implementation Science*, 12, 1-8.
14. Obaideen, K., Albasha, L., Iqbal, U., & Mir, H. (2024). Wireless power transfer: Applications, challenges, barriers, and the role of AI in achieving sustainable development goals-A bibliometric analysis. *Energy Strategy Reviews*, 53, 101376.
15. Parashar, V., Kashyap, R., Rizwan, A., Karras, D. A., Altamirano, G. C., Dixit, E., & Ahmadi, F. (2022). Aggregation-Based Dynamic Channel Bonding to Maximise the Performance of Wireless Local Area Networks (WLAN). *Wireless Communications and Mobile Computing*, 2022(1), 4464447.
16. Raihan, A. (2023). An overview of the implications of artificial intelligence (AI) in sixth generation (6G) communication network. *Research Briefs on Information and Communication Technology Evolution*, 9, 120-146.
17. Rasheed, M. Q., Yuhuan, Z., Ahmed, Z., Haseeb, A., & Saud, S. (2024). Information communication technology, economic growth, natural resources, and renewable energy production: Evaluating the asymmetric and symmetric impacts of artificial intelligence in robotics and innovative economies. *Journal of Cleaner Production*, 447, 141466.
18. Sen, S., Koo, J., & Bagchi, S. (2018). TRIFECTA: Security, energy efficiency, and communication capacity comparison for wireless IoT devices. *IEEE Internet Computing*, 22(1), 74-81.
19. Truong, N. S., Ngo, N. T., & Pham, A. D. (2021). Forecasting Time-Series Energy Data in Buildings Using an Additive Artificial Intelligence Model for Improving Energy Efficiency. *Computational Intelligence and Neuroscience*, 2021(1), 6028573.
20. Zheng, K., Hu, F., Wang, W., Xiang, W., & Dohler, M. (2012). Radio resource allocation in LTE-advanced cellular networks with M2M communications. *IEEE Communications Magazine*, 50(7), 184-192.
21. Zhou, W., Zhuang, Y., & Chen, Y. (2024). How does artificial intelligence affect pollutant emissions by improving energy efficiency and developing green technology. *Energy Economics*, 131, 107355.

**comparison of using or not among laparoscopic cholecystectomy
patients with non-00complicated gallbladder disease in large
hospital**

SALEEM ENAD SALEEM HASHEESH

comparison of using or not among laparoscopic cholecystectomy patients with non-complicated gallbladder disease in large hospital

SALEEM ENAD SALEEM HASHEESH

Abstract

Laparoscopic cholecystectomy provides a safe and effective treatment for patients with gallstones as it reduces post-operative pain with almost negligible scar, short hospital stay and earlier return to work. The study compared drain insertion post laparoscopic cholecystectomy in matter of post-operative pain, port site infection, hospital stay and post-operative collection. 100 patients were included in this study, 70 were females (70%) and 30 were males (30%). The study revealed that there is significant reduction in postoperative pain in patients without drain than in those with drain. Moreover regarding postoperative wound infection it was also lower in patient with no drain. There were also statistically significant reduction in postoperative hospital stay in patients without drain. Furthermore, the results found that postoperative intraabdominal collection was significantly lower in patients with drain in first 24 hours, while after that there were no significant difference regarding intraabdominal collection.

Key words: *Laparoscopic cholecystectomy, Gall Bladder, Hospital*

الملخص العربي

يوفر استئصال المرارة بالمنظار علاجاً آمناً وفعالاً للمرضى الذين يعانون من حصوات المرارة لأنه يقلل من آلام ما بعد الجراحة مع ندبات قليلة جداً، وإقامة قصيرة في المستشفى والعودة إلى العمل مبكراً.

تستخدم المصارف الوقائية في جراحة البطن على نطاق واسع إما للكشف عن المضاعفات مبكراً، مثل نزيف ما بعد الجراحة أو تسرب الصفراء، أو لتصريف التجمعات التي قد تكون سامة، مثل

الصفراء. ومع ذلك، فإن البيانات القائمة على الأدلة لا تدعم استخدام الصرف الوقائي في غالبية جراحات البطن.

لا تزال حصوات المرارة من أكثر الحالات شيوعاً بالعيادات الخارجية الجراحية. أثبت استئصال المرارة بالمنظار، بعد ظهوره في عام 1987، نفسه بسرعة باعتباره العلاج القياسي الذهبي لحصوات المرارة. في عام 1913 تم وصف استئصال المرارة بدون تصريف، ومنذ ذلك الحين تم تقسيم الجراحين سواء كانوا سيستخدمونها أم لا في حالات غير معقدة. يواصل معظم الجراحين استخدام التصريف الروتيني خوفاً من تسرب أو نزيف الصفراء. تحدث مثل هذه المضاعفات دائماً على الرغم من وضع التصريف. لذا فإن هناك حاجة للدراسة، سواء لوضع الصرف أم لا، ونتائجها.

من بين 100 مريضاً شملتهم هذه الدراسة ، كان 70 من الإناث (70%) و 30 من الذكور (30%)، مع نسبة الإناث إلى الذكور 3.1:1 تقريباً. تم توزيع المرضى بشكل عشوائي على مجموعتين: المجموعة الأولى (أ) خضعوا لعملية استئصال المرارة بالمنظار مع إدخال التصريف، وتتكون هذه المجموعة من 50 مريضاً، 12 منهم من الذكور (24%) و 38 من الإناث (76%) بينما خضعت المجموعة الثانية (ب) أيضاً لاستئصال المرارة بالمنظار ولكن بدون إدخال تصريف وتتكون هذه المجموعة من 50 مريضاً، 18 ذكور (36%) و 32 إناث (64%).

تشمل دراستنا المرضى الذين يعانون من التهاب حصوي مراري مزمن والذي يشار إليه في استئصال المرارة بالمنظار الاختياري.

❖ فيما يتعلق بألم ما بعد الجراحة:

كان أعلى في المرضى في المجموعة أ (مع الصرف) منه في المجموعة ب (بدون صرف) ، وكان ذلك ذا دلالة إحصائية (قيمة P أقل من 0.05).

❖ فيما يتعلق التهاب أماكن دخول المنظار الجراحي:

تمت متابعة جميع المرضى المشمولين في هذه الدراسة بعد الجراحة لعدوى أماكن دخول المنظار الجراحي (حتى اليوم السابع من إزالة الغرز) ووجدنا أن حدوث عدوى في أماكن دخول

المنظار الجراحي كان أعلى في المجموعة أ (مع الصرف) في الموقع حيث تم إدخال الصرف ، وكانت ذات دلالة إحصائية (قيمة P أقل من 0.05).

❖ فيما يتعلق الإقامة في المستشفى بعد الجراحة:

كانت الإقامة في المستشفى أقل بكثير في المرضى الذين ليس لديهم تصريف (المجموعة ب) حيث تم خروج 42 مريضاً (84%) في نفس يوم العملية من المستشفى وهو ذو دلالة إحصائية (قيمة P أقل من 0.05).

❖ فيما يتعلق بالتجمعات ما بعد الجراحة:

تابعنا التجمعات ما بعد الجراحة في المجموعتين في اليوم الأول والثاني والثالث وتبين أن التجمعات في اليوم الأول بعد العملية كانت أقل في المجموعة أ (مع استنزاف)، حيث 80% من المرضى لم يطوروا تجمعات بالبطن، بينما طور 16% من المرضى تجمعات أقل من 50 مل، بينما طور 4% من المرضى تجمعات 50-100 مل.

في حين أن المجموعة ب (بدون تصريف) 16% من المرضى لم يطوروا تجمعات بالبطن، بينما طور 76% من المرضى تجمعات أقل من 50 مل، بينما طور 8% من المرضى تجمعات 50-100 مل.

وكان ذلك ذا دلالة إحصائية في اليوم الأول بعد الجراحة (قيمة P أقل من 0.05) ، بينما لم تكن ذات دلالة في الـ 72 ساعة التالية.

Introduction

Laparoscopic cholecystectomy has largely replaced open cholecystectomy because of shorter hospital stay, faster recovery, and lower overall morbidity. Unfortunately, however, the morbidity due to bile duct injury has increased with the advent of the laparoscopic approach (**Henry et al., 2011**).

Laparoscopic cholecystectomy provides a safe and effective treatment for patients with gallstones as it reduces post-operative pain with almost negligible scar, short hospital stay and earlier return to work (**El-Labban et al., 2012**).

Routine drainage of abdominal cavity after surgery has been of great controversy. Nevertheless, the policy of routine abdominal drainage is increasingly questioned. Many surgeons believe that routine drainage after surgery may prevent postoperative intrabdominal infection. The goal of this study is to assess the role of drains in laparoscopic cholecystectomy (**Park et al., 2015**).

Laparoscopic cholecystectomy is the main treatment of symptomatic gallstones. Routine drainage after laparoscopic cholecystectomy is an issue of great debate (**El-Labban et al., 2012**).

Gallstones are still one of the most common conditions in surgical outpatient department. Laparoscopic cholecystectomy, after its advent in 1987, rapidly established itself as the gold standard treatment of gallstones. In 1913 cholecystectomy without drainage was described, and since then surgeons were divided whether to use it or not in uncomplicated cases. Most surgeons continue to use routine drain for the fear of bile leakage or bleeding. Such complications invariably occurred inspite of sub hepatic drainage. So, there arises a need for study, whether to put drain or not, and its consequences (**Gadhvi et al., 2018**).

Prophylactic drains in abdominal surgery are widely used either to detect complications early, such as postoperative hemorrhage or bile leakage, or to drain collections which may be toxic, as bile. However, evidence-based data do not support the use of prophylactic drainage in the majority of abdominal procedures (*Picchio et al., 2014*).

Aim of the Work

Our study is to assess whether to put a drain or not in uncomplicated laparoscopic cholecystectomy.

Review of Literature

Anatomy of the Biliary Tree and the Gall Bladder

1. Gall bladder:

The Gall bladder acts as a reservoir for bile located under surface of the liver at the confluence of the right and left halves of the liver. It is separated from the hepatic parenchyma by a cystic plate, which is constituted of connective tissue applied to the Glisson capsule (*Schulick, 2012*).

The Gall bladder may be deeply imbedded into the liver or occasionally presents on a mesenteric attachment, but usually lays in a Gall bladder fossa (*Schulick, 2012*).

The Gall bladder varies in size and consists of a fundus, a body, and an infundibulum. The tip of the fundus usually reaches the free edge of the liver and is closely applied to the cystic plate. The infundibulum of the gallbladder makes an angle with the body and may obscure the common hepatic duct, constituting a danger point during cholecystectomy (*Schulick, 2012*).

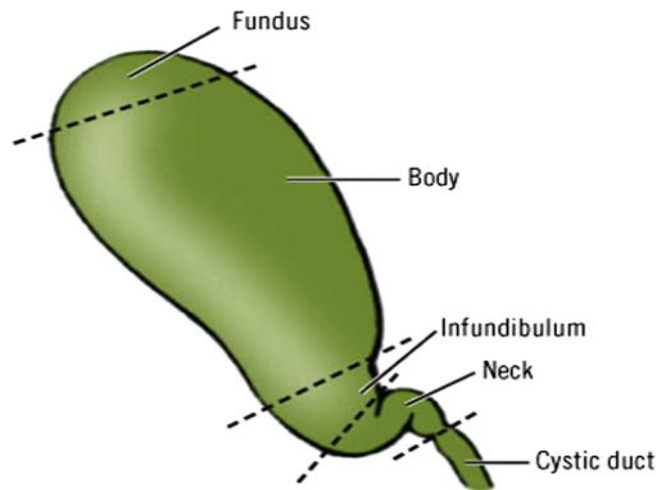


Figure 1: The Gallbladder parts

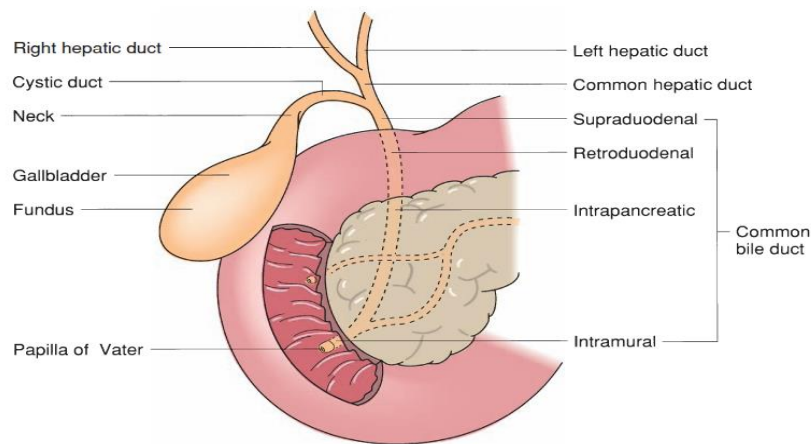


Figure 2: Anatomy of the Extrahepatic Biliary Tree

2. Cystic Duct and artery & Calot's triangle:

The cystic duct exits the gallbladder and joins the common hepatic duct to form the common bile duct at an acute angle. The length and course of the cystic duct can be variable. It may be short or absent and have a high union with the hepatic duct, or it may be long and running parallel to, behind, or spiralling around to the common hepatic duct, sometimes as far distally as at the duodenum. Variations of the cystic duct and its point of union with the common hepatic duct are surgically important and misidentification can lead to bile duct injuries [Figure 3] (***Schwartz's Principles of Surgery, 2019***).

The cystic duct arises from the infundibulum of the gallbladder and extends to join the common hepatic duct. The lumen measures between (1-3) mm in diameter, and its length varies depending on the type of union with the common hepatic duct.

Arterial blood reaches the Gall bladder via the cystic artery, which usually originates from the right hepatic artery. There are several known variations in the origin and course of the cystic artery.

The venous drainage of the gallbladder is directly into the liver parenchyma or into the common bile duct plexus (**Schulick, 2012**).

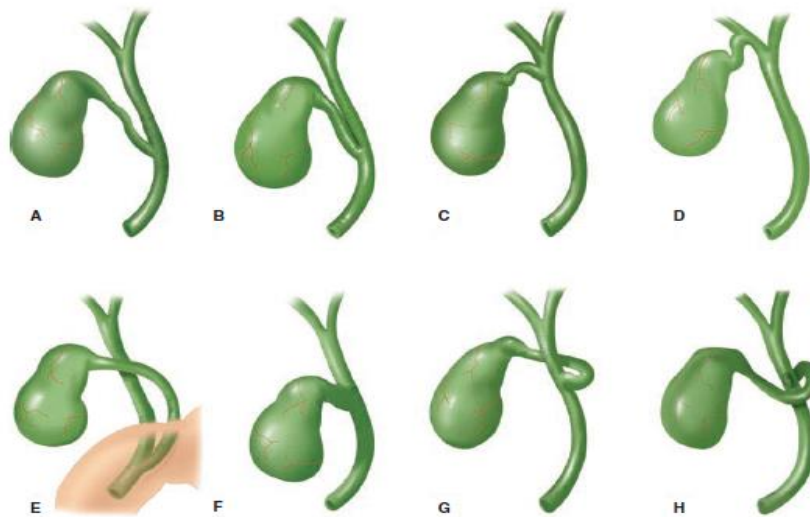


Figure 3: Variations of the cystic duct anatomy. **A.** Low junction between the cystic duct and common hepatic duct. **B.** Cystic duct adherent to the common hepatic duct. **C.** High junction between the cystic and the common hepatic duct. **D.** Cystic duct drains into right hepatic duct. **E.** Long cystic duct that joins common hepatic duct behind the duodenum. **F.** Absence of cystic duct. **G.** Cystic duct crosses posterior to common hepatic duct and joins it anteriorly. **H.** Cystic duct courses anterior to common hepatic duct and joins it posteriorly (**Schwartz's Principles of Surgery, 2019**).

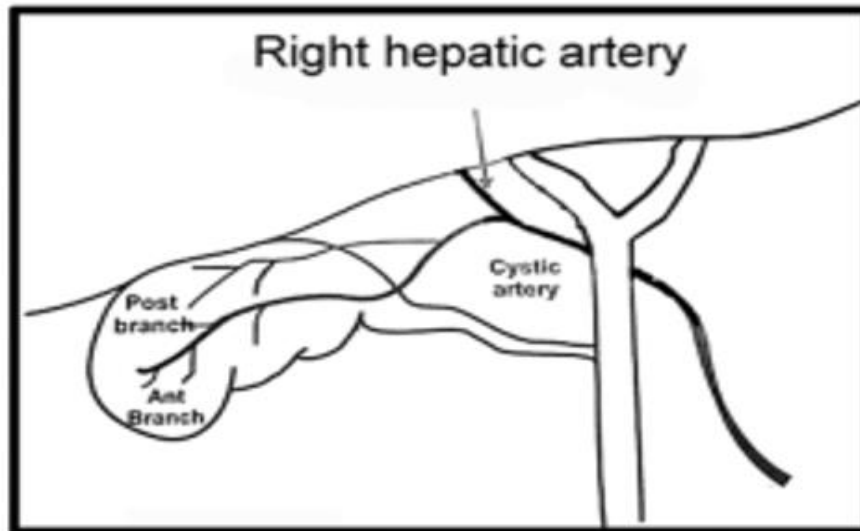


Figure 4: Anterior and posterior branches of the cystic artery

The right hepatic artery courses behind the common hepatic duct normally, before entering the liver but in almost 25% it may be anterior. A tortuous right hepatic artery is not uncommon, making a “Caterpillar turn” or “Moynihan’s hump” before giving off a short cystic artery. This situation makes the right hepatic artery more prone to injury in cholecystectomy and should be suspected if an unusually large cystic artery is seen [Figure 5] (*O’Rourke, 2018*).

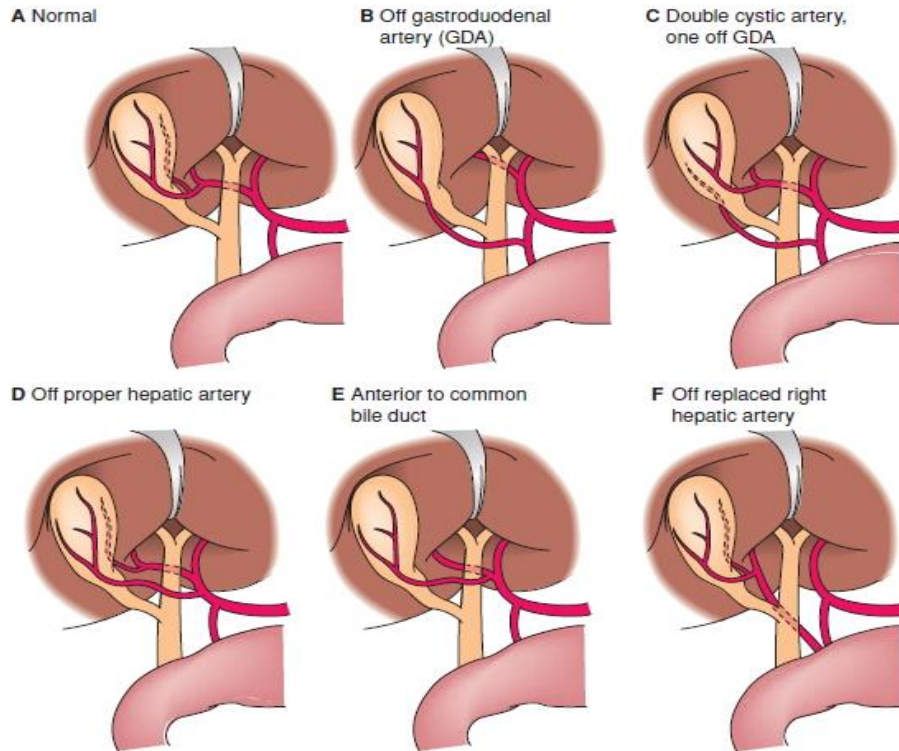


Figure 5: Variations of Cystic artery

However, a double cystic duct is extremely rare and poses a challenge for surgeons during an operation. Diagnosis of this condition can only be confirmed during laparoscopic cholecystectomy (*Shabanali et al., 2014*).

3. The Accessory and aberrant ducts

There are a large number of accessory ducts [Fig. 6] described. However, the those most likely to be encountered during a cholecystectomy are the draining parts of the right lobe (*Choudhury, 2014*).

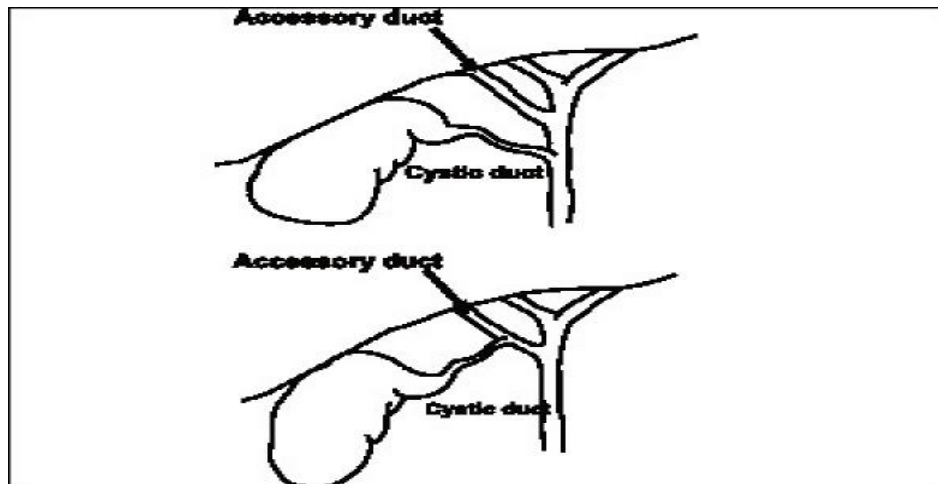


Figure 6: Accessory and aberrant ducts

Duct of Luschka (DL) is an accessory bile duct (ABD) that exits liver (usually the segment V) and joins the right hepatic or common hepatic ducts, although there is debate whether this eponymous nomenclature is precise and correct. There is also debate regarding the definition and the incidence of this variation, as it can range from 1% to 50%.

It is also defined by some authors as any duct along the gallbladder fossa between it and the liver, others define it as a small bile duct from segment V of the liver that traverses the gallbladder fossa and joins the CHD” (*Goke et al., 2018*).

4. Calot’s triangle:

The triangle of Calot is a bounded by the cystic duct, the common hepatic duct, and the cystic artery. It was described by Jean-Francois Calot in his 1890. “Calot’s” triangle has become ensconced in the surgical vernacular. However, the term is not anatomically precise as it is commonly used. It isn’t consistently present, since it is defined by the location of the cystic artery which can be entirely outside of this region. Though Hepatocystic triangle is preferred terminology considering this anatomical area (*Asbun et al., 2020*).

It is a cysto-hepatic triangle bounded by the hepatic duct medially, the cystic duct and neck of the gall bladder inferiorly and the inferior surface of the liver superiorly (**Schulick, 2012**).

In this triangle runs the cystic artery, often the right hepatic artery, rarely a bile duct and also contains the cystic lymph node. Hence this triangle has a greatly important area of dissection during cholecystectomy. The apex of the triangle is the most critical area (cysto-hepatic angle) as the cystic artery passes (**Schulick, 2012**).

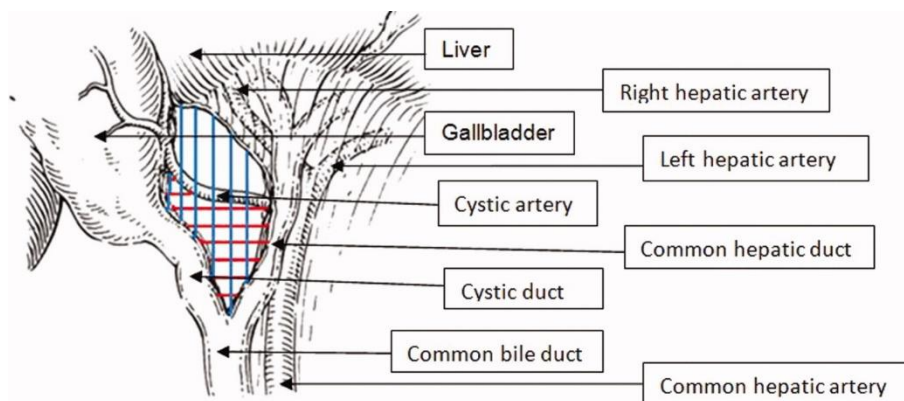


Figure 7: Calot's triangle (**Abdalla et al., 2013**).

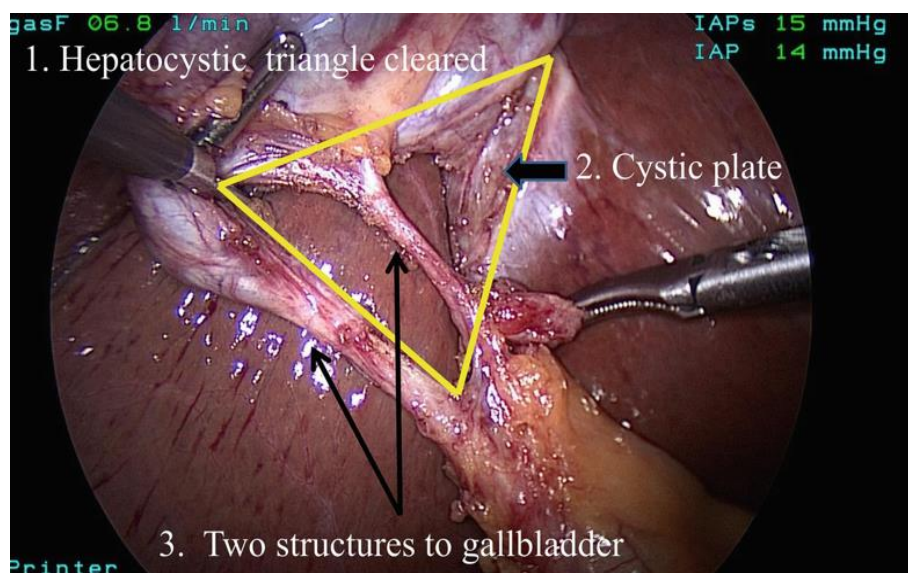


Figure 8: hepato-cystic triangle (**Asbun et al., 2020**).

5. Common Bile Duct:

The cystic and common hepatic ducts join to form the common bile duct. The common bile duct is approximately 8 to 10 cm in length and 0.4 to 0.8 cm in diameter. The common bile duct can be divided into three anatomic segments: supraduodenal, retroduodenal, and intrapancreatic **(Schulick, 2012)**.

The supraduodenal segment resides in the hepatoduodenal ligament lateral to the hepatic artery and anterior to the portal vein; the course of the retroduodenal segment is posterior to the first portion of the duodenum, anterior to the inferior vena cava, and lateral to the portal vein. The pancreatic portion of the duct lies within a tunnel or groove on the posterior aspect of the pancreas. The common bile duct then enters the medial wall of the duodenum, courses tangentially through the submucosal layer for 1 to 2 cm, and terminates in the major papilla in the second portion of the duodenum. The distal portion of the duct is encircled by smooth muscle that forms the sphincter of Oddi **(Schulick, 2012)**.

The common bile duct usually joins the pancreatic duct to form a common channel before entering the duodenum at the ampulla of Vater. Some patients will have an accessory pancreatic duct emptying into the duodenum. The blood supply of the common bile duct is segmental in nature and consists of branches from the cystic, hepatic, and gastroduodenal arteries. These meet to form collateral vessels that run in the 3 and 9 o'clock positions. The venous drainage forms a plexus on the anterior surface of the common bile duct **(Schulick, 2012)**.

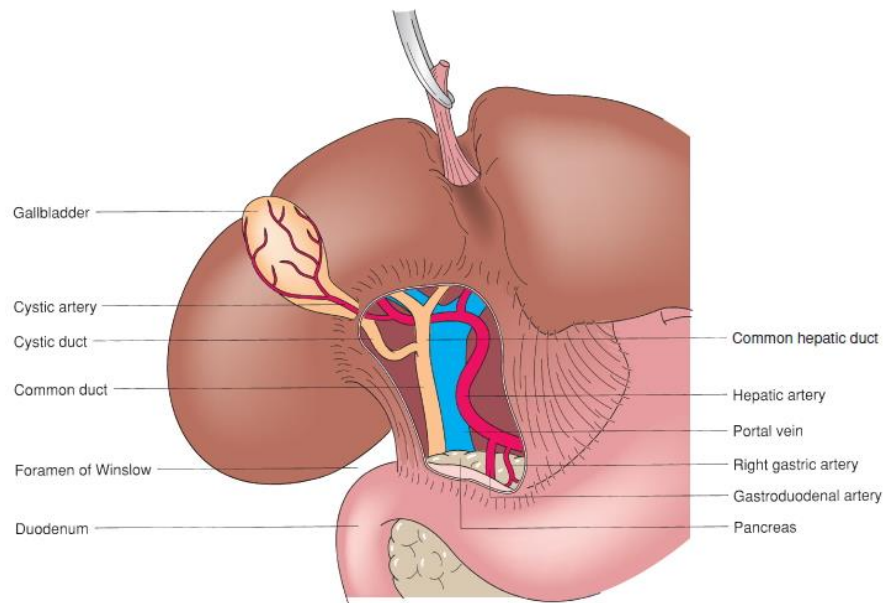


Figure 9: Relationship of structures within the hepatoduodenal ligament

Nerve supply of the biliary tract:

Parasympathetic fibers, mainly from the hepatic branch of the anterior vagal trunk, stimulate contraction of the gall bladder and relax the ampullary sphincter. Sympathetic fibres from the coeliac ganglia, which inhibit contraction. Afferent fibres including those subserving pain from the gall bladder may: run with right sided sympathetic fiber and reach spinal cord segments, (T7-9) and this explains radiation of the pain to the back in the infrascapular region or run into the right phrenic nerve (C3-5) and this explains the occasional referral of pain to the right shoulder region (McMinn, 2000).

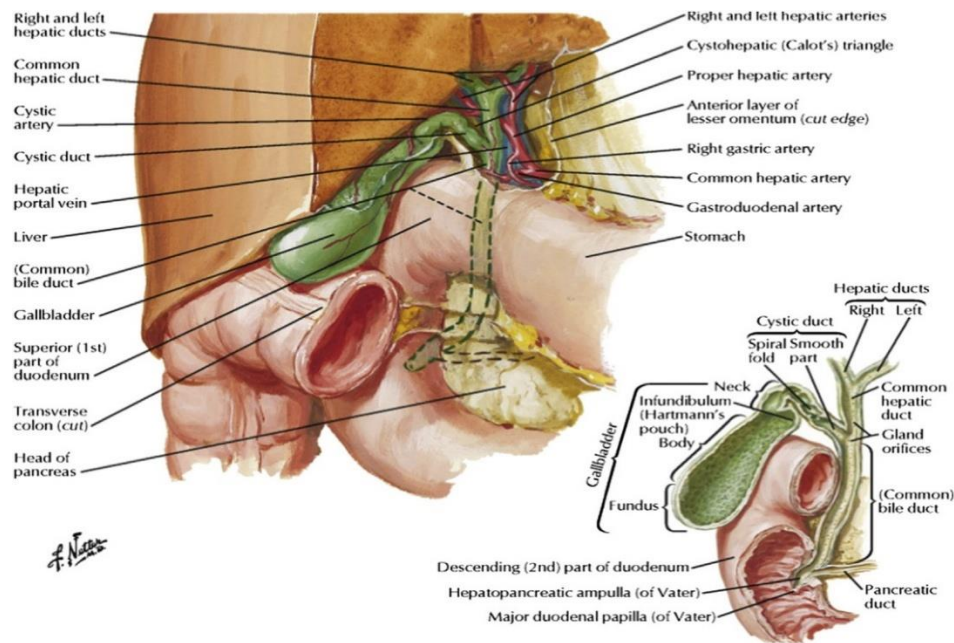


Figure 10: Classic view of extrahepatic biliary ducts

5. Anatomical Variations of the Biliary Tract

Extrahepatic Biliary Atresia

Congenital biliary atresia is the most serious malformation of the biliary tract. A short segment, an entire duct, or the whole system may be atretic; the atretic duct may be hypoplastic, stenosed, or reduced to a fibrous band that is easily overlooked by the surgeon.

Hepatic biliary duct atresias may be divided into three groups:

First group:

Patent proximal hepatic ducts and occluded distal ducts. Patency may occur in any portion of the right or left hepatic duct as it emerges from the liver. This atresia is called "correctable" (*Francoeur et al., 2003*).

Second group:

Occluded proximal ducts. No portion of the emerging hepatic duct is patent. This atresia is called "noncorrectable" (*Francoeur et al., 2003*).

Third group:

Includes the presence of intrahepatic atresia. In this form of atresia, the extrahepatic ducts may be present or absent. The mechanism of intrahepatic atresia remains obscure and the condition is as yet non correctable. It requires early liver transplantation (*Francoeur et al., 2003*).

There are morphological variations and abnormalities in more than 33% of gall bladders such as duplication. Sites of potential malformations of the extrahepatic biliary tract and common bile duct (*John et al., 2004*).

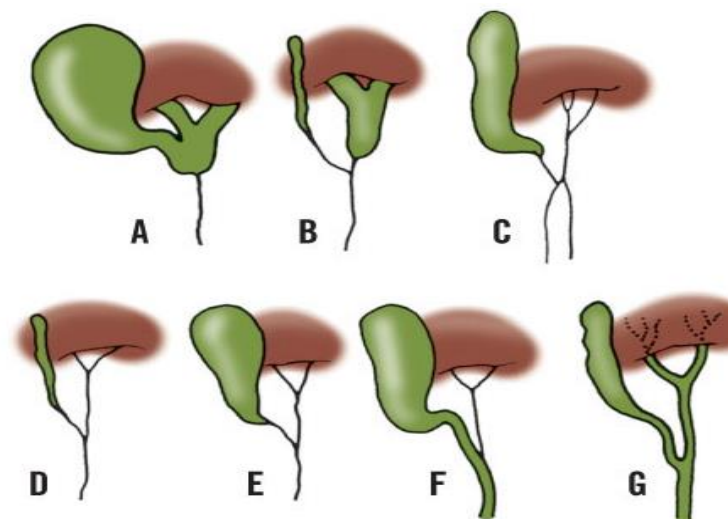


Figure 11: Different types of Biliary Atresia

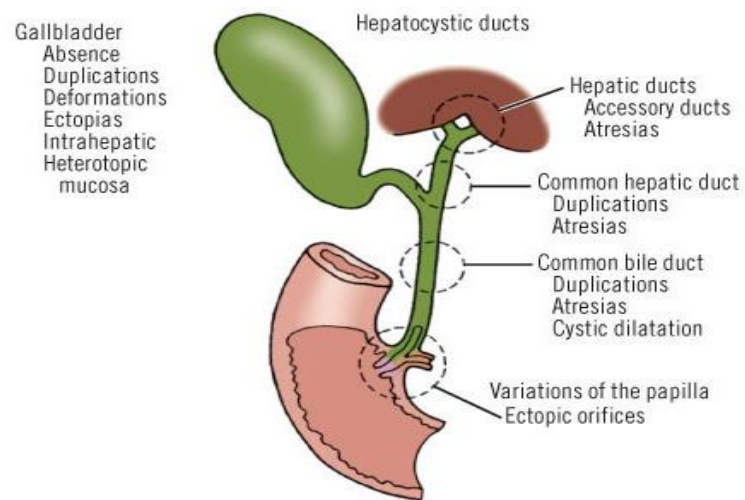


Figure 12: Sites of potential biliary tract malformations

Anomalies of Gall Bladder

1. Absence of Gall bladder

Occasionally the gallbladder (and usually the cystic duct as well) is absent or vestigial. The absence must be confirmed by ruling out an intrahepatic gallbladder or a left-sided Gall bladder (*John et al., 2004*).

2. Multiple Gall bladder

The first human double Gall bladder was found by autopsy in 1674, the first such anomaly to be recorded from observation of a living patient was in 1911, multiple gall bladders form a continuous spectrum of malformations, from an externally normal organ with an internal longitudinal septum to the most widely separated accessory gallbladders. For practical purposes, the anomalies can be categorized into six basic types. Three types belong to the split primordium group and three belong to the accessory gallbladder group (*John et al., 2004*).

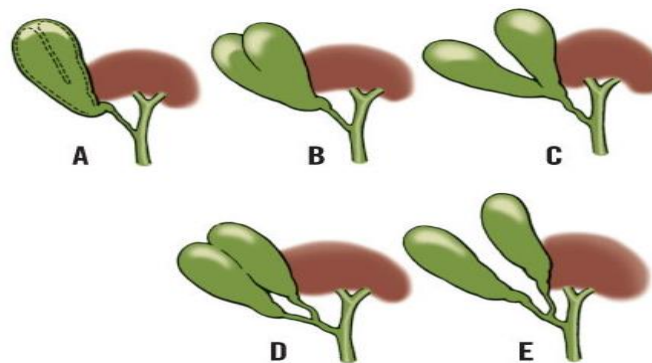


Figure 13: Different types of multiple Gall bladders

3. Left sided Gall bladder

Rarely, a Gall bladder is found on the inferior surface of the left lobe of the liver. In such cases, the cystic duct enters the common bile duct from the left. There is no associated functional disorder. Ultrasonography should detect this anomaly, but the radiologist must be alert (*John et al., 2004*).

4. Intrahepatic Gall bladder

Intrahepatic Gall bladder is submerged in the liver and gives the appearance of absence of the gallbladder. CT scan or ultrasonography may provide its only evidence. A high percentage of occurrences of Gall bladder stones are associated with this anomaly (*John et al., 2004*).

5. Mobile Gall bladder

Mobile Gall bladder is attached to the liver by a mesentery. Such a gallbladder is susceptible to torsion and strangulation. Otherwise, it causes no symptoms (*John et al., 2004*).

Physiology of the Gallbladder

Gallbladder considered a part of the extrahepatic biliary system where the bile stored and concentrated. Bile originally formed in the liver. Then to the common hepatic duct through intrahepatic ducts. Then through the cystic duct to be stored in the gallbladder. When the food in the stomach & duodenum stimulates gallbladder to empty, it contracts and empties the concentrated bile back through the cystic duct, down the common bile duct, into the second portion of the duodenum through the ampulla Vater. Opening and closing of the sphincter of Oddi at the ampulla Vater controls the bile flow (***Jones et al., 2020***).

Gallbladder epithelium plays role in concentrating bile, which contains channels transport sodium chloride actively. The typical capacity of the gallbladder is 30 mL but it can distend up to 300 mL of fluid. The wall of the gallbladder is composed of the visceral peritoneum (on areas not in direct contact with the liver), subserosa, muscularis mucosa, lamina propria, and columnar epithelium (***Keplinger et al., 2014***).

Patient Positioning

In North American positioning, the patient is lying spine and the surgeon is positioned on the patient's left side. In European positioning, the patient is in low stirrups and the surgeon is on the patient's left or between the patient's legs.

With North American positioning, the camera operator usually stands on the patient's left and to the left of the surgeon, while the assistant stands on the patient's right. The video monitor is positioned on the patient's right above the level of the costal margin. If a second monitor is available, it should be positioned on the patient's left, to the right of the surgeon, where the assistant can have an unobstructed and comfortable view. Exposure can be improved by tilting the patient in the reverse Trendelenburg position and rotating the table with the patient's right side up. Gravity pulls the duodenum, the colon, and the omentum away from the gallbladder, thereby increasing the working space available in the upper abdomen.

The OR table should allow easy access for a fluoroscopic C arm, to facilitate intraoperative cholangiography. The table cover should be radiolucent (*Souba et al., 2005*).

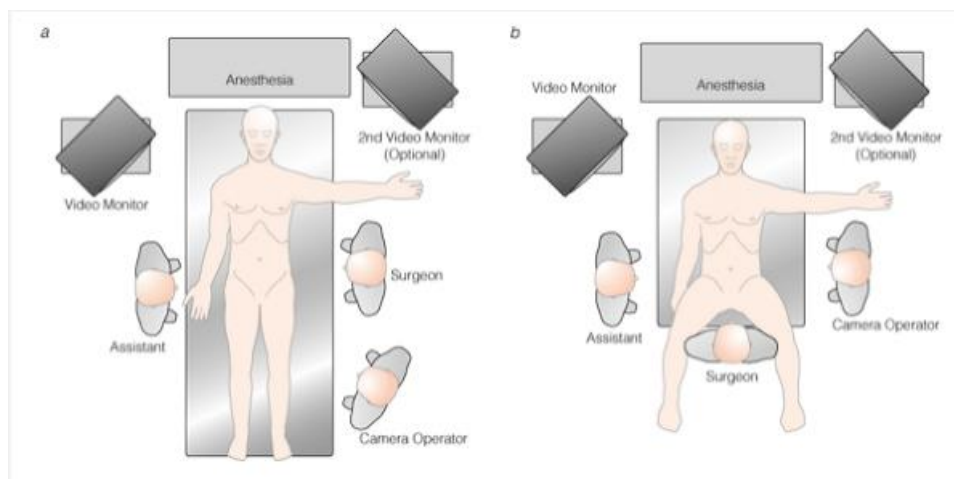


Figure 14: Setup for Laparoscopic Cholecystectomy

Technique

Patients undergoing laparoscopic cholecystectomy are prepared and draped in a similar fashion to open cholecystectomy. Conversion to an open operation is necessary in up to 3% of patients undergoing elective cholecystectomy and up to 25% of patients undergoing laparoscopic cholecystectomy for acute cholecystitis.

Either an open or closed technique can be used to establish a pneumoperitoneum. With the open technique, a small incision is made at the umbilicus, and a blunt cannula (Hasson cannula) is inserted into the peritoneal cavity and anchored to the fascia.

An 11-mm trocar is inserted through the supraumbilical incision once a pneumoperitoneum is established. A 30-degree laparoscope is then inserted through the umbilical port, and an examination of the peritoneal cavity is performed. An 11-mm operating port is placed subxiphoid, and two additional 5-mm trocars are positioned subcostally in the right upper quadrant in the midclavicular line and in right iliac region in anterior axillary line.

The two 5-mm ports are used for grasping the gallbladder and exposing the gallbladder and cystic duct. The infundibulum and retract it laterally to further expose the triangle of Calot. Traction on the fundus should be upward toward the patient's head, and traction on the Hartmann pouch laterally to the right.

This combination “dis-aligns” the common duct and cystic duct so that they appear as distinct structures. Incorrect traction aligns the ducts so that they appear as a continuous structure (**Henry et al., 2011**).

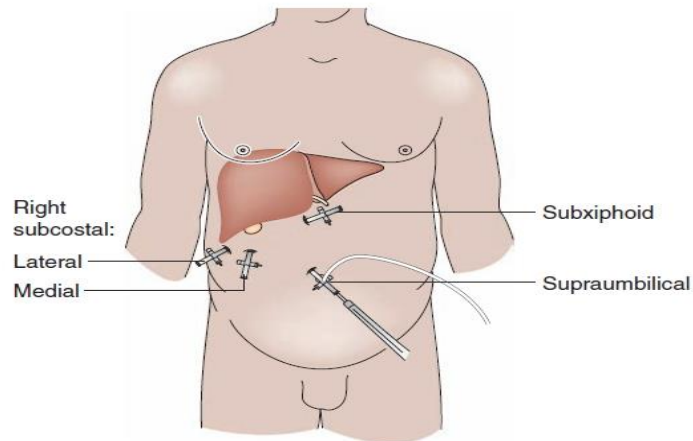


Figure 15: Port sites

Elective laparoscopic cholecystectomy can be safely performed as an outpatient procedure. Among patients selected for outpatient management, 77% to 97% of patients can be successfully discharged the same day. Factors contributing to overnight admission include uncontrolled pain, nausea and vomiting, operative duration greater than 60 minutes, and cases completed late in the day (**Henry et al., 2011**).

Routine operative cholangiography has been advocated to avoid ductal injury. However, opinion on the subject is sharply divided. Biliary injuries occur less frequently in the hands of surgeons who perform operative cholangiography routinely. However, in about 50% of ductal injuries, a cholangiogram fails to prevent the injury although abnormal anatomy is present (i.e., cholangiograms are often incorrectly interpreted) (**Henry et al., 2011**).

The indications for intraoperative cholangiography, when it is performed selectively, are known choledocholithiasis, a history of jaundice, a history of pancreatitis, a large cystic duct and small gallstones, any abnormality in preoperative liver function tests, and dilated biliary ducts on preoperative sonography. Provided these indications are carefully followed, selective cholangiography may be as effective in detecting clinically relevant stones as routine cholangiography.

Serious complications of laparoscopic cholecystectomy are rare, the mortality rate being less than 0.3%. As cholecystectomy rates have risen, however, the total number of deaths has not decreased (**Henry et al., 2011**).

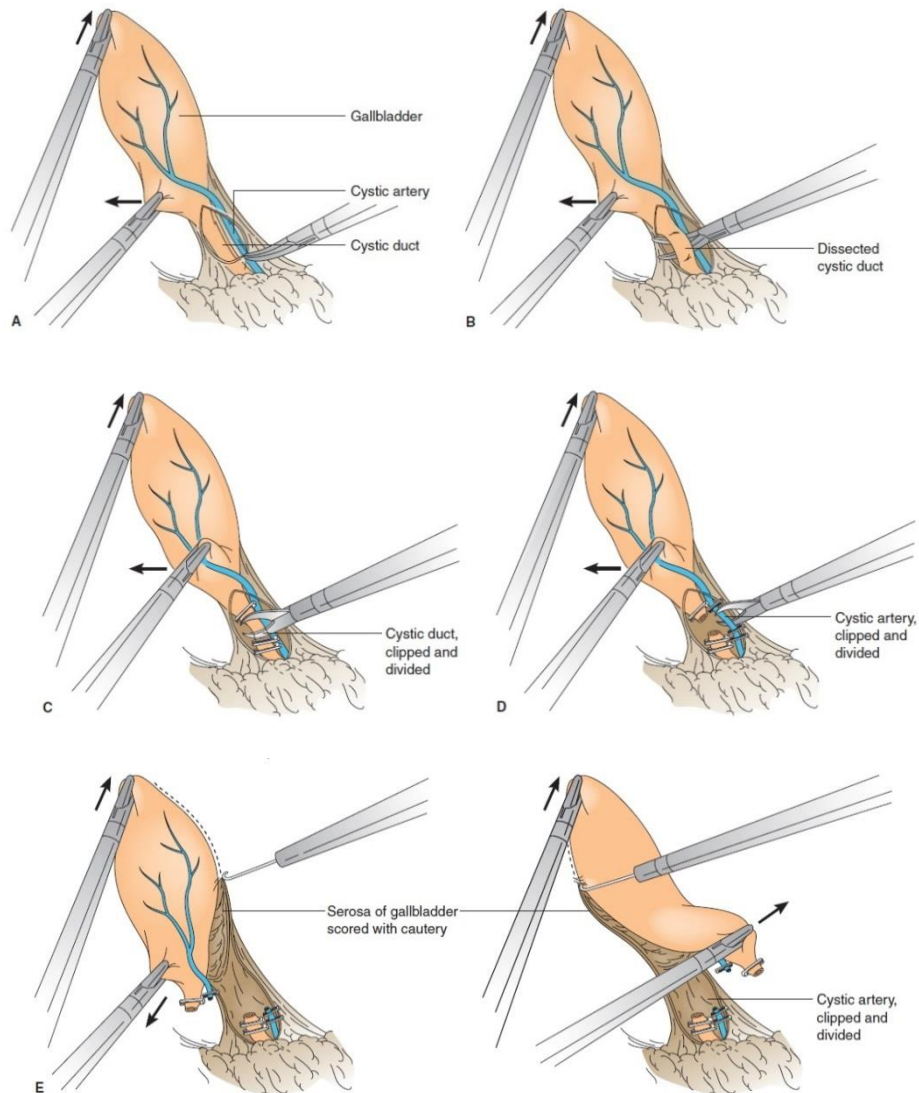


Figure 16: Operative steps

However its important to visualize the *critical view of safety* in order to try to prevent complications of biliary tree injury either CBD or Common Hepatic Ducts injury.

Critical View of Safety

Anatomy is important when performing laparoscopic cholecystectomy. The concept of the critical view of safety (CVS) was originated by Strasberg et al in 1995 (**Hori et al., 2016**).

The triangle of Calot is cleared of fat and fibrous tissue. Only two structures are connected to the lower end of the Gall bladder once this is done, and the lowest part of the gall bladder attachment to the liver bed has been exposed. The latter is an important step, equivalent in the open technique to taking the gallbladder off the liver bed. It is not necessary to expose the common bile duct. Once the critical view is attained, cystic structures may be occluded, as they have been conclusively identified. Failure to achieve the critical view is an indication for conversion or, possibly, cholangiography to define ductal anatomy. It is the author's opinion that there is considerable danger in relying simply on the appearance of the "cystic duct" — Gall bladder junction, as this may be deceiving, especially in the presence of severe inflammation (**Strasberg et al., 2002**).

Surgeon should be positively identify cystic duct and cystic artery (CA) before cutting or clipping them. Calot's triangle must be dissected well. Gall bladder lower end should be dissected off the liver bed, and the bottom of the liver should be visible. It is not necessary to directly confirm the CHD and CBD. Hence, only two structures should be seen to enter the GB. Positive identification of the CD and CA as they join the GB infundibulum is required before these structures can be divided (**Hori et al., 2016**).

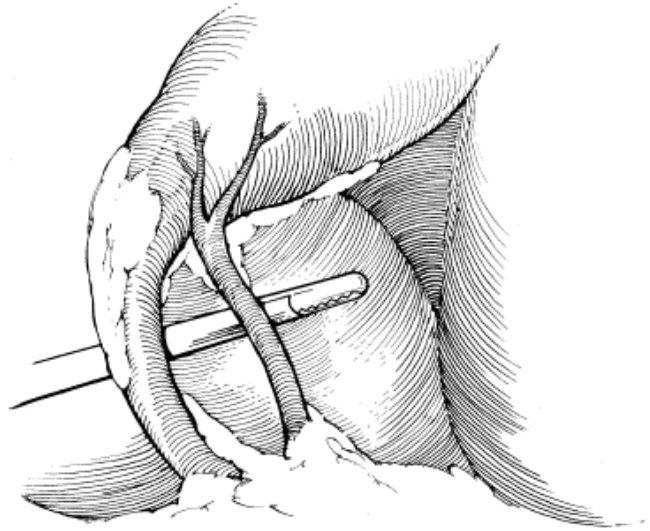


Figure 17: The Critical view of Safety

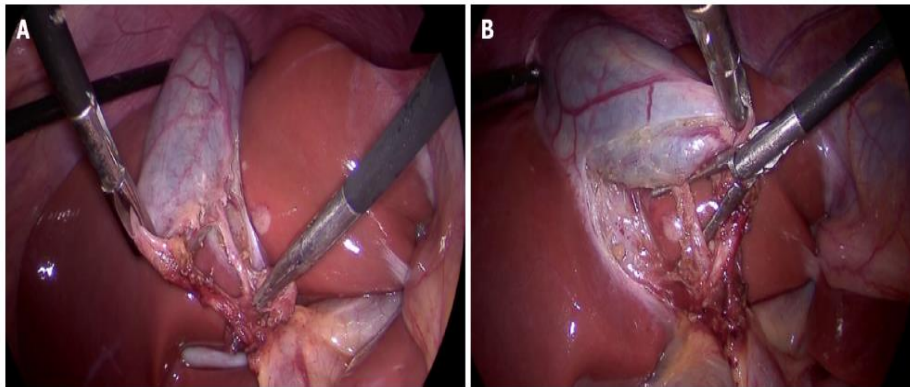


Figure 18: [A &B] Critical view of safety with all three components: (1) Fibrofatty tissue has been cleared from the hepatocystic triangle; (2) Lower part of the cystic plate has been clearly exposed; and (3) Only two tubular structures are seen entering the gallbladder. A: Anterior view; B: Posterior view (inverted hepatocystic triangle).

Complications of Laparoscopic Cholecystectomy

Laparoscopic cholecystectomy (LC) remains an extremely safe procedure with a mortality rate of (0.22-0.4%). Major morbidity occurs in approximately 5% of patients (*Steiner et al., 2004*).

Complications include the following:

1. Trocar/Veress needle injury:

Intestinal injury may occur during establishment of abdominal access, adhesiolysis, or dissection of the gallbladder off of the duodenum or colon. An injury to the bowel should be repaired with careful 1- or 2-layer suture closure. The incidence of injury to viscera or vessels from a Hasson trocar or Veress needle is similar (in the range of 0.2%) (**Ahmad et al., 2019**).

A recent systematic review showed that an open-entry technique is associated with a significant reduction in failed entry when compared to a closed-entry technique, with no difference in the incidence of visceral or vascular injury (**Ahmad et al., 2019**).

Significant benefits were noted with the use of a direct-entry technique when compared to the Veress Needle. The use of the Veress Needle was associated with an increased incidence of failed entry, extraperitoneal insufflation and omental injury; direct-trocar entry is therefore a safer closed-entry technique (**Ahmad et al., 2019**).

2. Haemorrhage:

Large-vessel vascular injury usually occurs at the time of initial abdominal access. These may be lethal complications. Development of a retroperitoneal hematoma or hypotension should be treated immediately by conversion to laparotomy.

The most obvious danger is that of hemorrhage from the many large blood vessels lying anterior to the biliary tree. Such vessels are inconstant in number and location. The posterior superior pancreaticoduodenal artery, anterior to the retroduodenal portion of the common bile duct, is the vessel most frequently encountered (**Steiner et al., 2004**).

All the vessels listed in Table (1) are subject to possible injury.

Table 1: Segments of the Biliary tract and frequency of arteries lying anterior to them

Segment	Artery Anterior	Percent Frequency
Right and left hepatic ducts	Right hepatic artery	12-15
	Cystic artery	<5
Common hepatic duct	Cystic artery	15-24
	Right hepatic artery	11-19
	Common hepatic artery	<5
Supraduodenal common bile duct	Anterior artery to CBD	50
	Posterosuperior pancreaticoduodenal artery	12.5
	Gastroduodenal artery	5.7-20*
	Right gastric artery	<5
	Common hepatic artery	<5
	Cystic artery	<5
	Right hepatic artery	<5
Retroduodenal common bile duct	Posterosuperior pancreaticoduodenal artery	76-87.5
	Supraduodenal artery	11.4

(John et al., 2004)

The following list of variations in the cystic artery may help one avoid common pitfalls:

- The cystic artery usually arises from the right hepatic artery (A).
- Dual cystic arteries, one arising from each of the hepatic arteries (B)
- Cystic artery arising from the common hepatic artery (C)
- Cystic artery arising from the gastroduodenal artery (D)
- Cystic artery arising from an anterior right hepatic artery (E)
- A single cystic artery arising from the left hepatic artery (F).

(Strasberg, 2011)

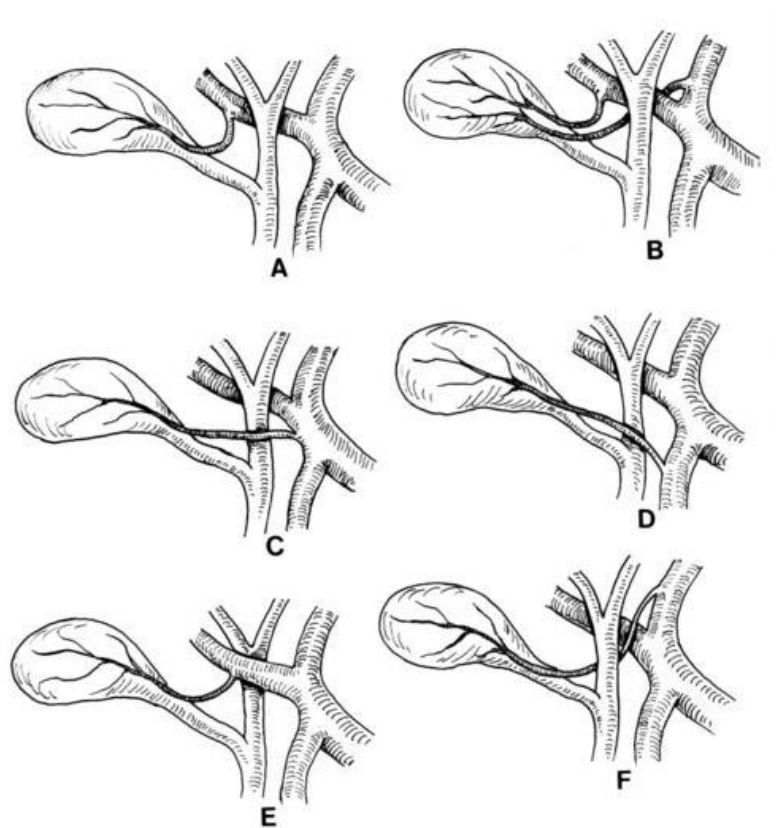


Figure 19: Anatomic variations of the blood supply for the Gall bladder

Injury to the portal vein or the inferior vena cava is a serious complication. These vessels must, of course, be repaired at once (*Tchirkow et al., 2002*).

Excessive bleeding in the region of the triangle of Calot should not be treated laparoscopically. Attempts at blind clipping or cauterizing significant bleeding usually leads to worsening haemorrhage or hepatic artery injury. If, and only if, a bleeding site can be definitely identified and the locations of both the hepatic artery and common bile duct (CBD) are known, bleeding may be controlled with electrocautery or clips (*Tchirkow et al., 2002*).

Management of Haemorrhage:

Prevention of arterial bleeding begins by dissecting the artery carefully and completely before clipping and by inspecting the clips to ensure that they are placed completely across the artery without incorporating

additional tissue (e.g., a posterior cystic artery or right hepatic artery). When arterial bleeding is encountered, it is essential to maintain adequate exposure and to avoid blind application of hemostatic clips or cauterization. The laparoscope should be withdrawn slightly so that the lens is not spattered with blood. The surgeon should then pass an atraumatic grasping forceps through a port other than the operating port and attempt to grasp the bleeding vessel. An additional trocar may have to be inserted for simultaneous suction-irrigation. Once proximal control is obtained, the operative field should be suctioned and irrigated to improve exposure. Hemostatic clips are then applied under direct vision; in addition, a sponge may be introduced to apply pressure to the bleeding vessel. Conversion to open cholecystectomy is indicated whenever bleeding cannot be promptly controlled laparoscopically (**Strasberg, 2011**).

Bleeding from veins of the Gall bladder bed or from veins of the common bile duct is a minor complication which can usually be controlled by fulguration of the bleeding site using a spatulated electrocautery wand for this purpose (**Strasberg, 2011**).

If a larger intrahepatic sinus has been entered, hemostatic agents (eg, microfibrillar collagen) can be placed laparoscopically in the liver bed, and pressure can be held with a clamp.. The argon plasma coagulator (APC) can be an excellent tool for severe Gall bladder fossa oozing that is not responsive to simple electro-cautery (**Strasberg, 2011**).

A second vascular complication of biliary surgery is ischemia to the liver from unintended ligation of the right hepatic artery or an accessory or replacing aberrant right hepatic artery. Interference with the blood supply of the common bile duct may result in ischemia and stricture. Other surgeons feel that the blood supply is good and that collateral circulation will prevent local ischemia (**Strasberg, 2011**).

3. Post cholecystectomy syndrome:

This refers to a set of abdominal symptoms that occur with a frequency of up to 40% after cholecystectomy. Symptoms are often vague and include dyspepsia, flatulence, bloating, right upper quadrant pain, and epigastric pain.

The most common causes of this syndrome are dietary indiscretion, retained CBD stones, inflammation of the cystic duct remnant, and sphincter of Oddi dysfunction (**Zhou et al., 2003**).

4. Bile ducts injury or stricture:

The most dreaded complication of LC is injury to the common bile or common hepatic duct. The estimated incidence of bile duct injury in cholecystectomies performed laparoscopically varies from 0.3-2.7%), In contrast; biliary tract injuries were noted to occur in 0.25-0.5% of open cholecystectomies (**McMahon et al., 2004**).

A major risk factor for bile duct injury is the experience of the surgeon, other risk factors are the presence of aberrant biliary tree anatomy and the presence of local acute or chronic inflammatory (**Lien et al., 2007**).

Data suggest that the incidence of bile duct injury during open cholecystectomy is 1 in 500 to 1,000 cases), The incidence of bile duct injury during laparoscopic cholecystectomy is clearly higher. Although a wide range in the incidence of injury can be found in reported series, the most accurate data most likely come from surveys encompassing thousands of patients. These reports reflect the results from a large number of surgeons in both community and teaching hospitals. The results of such series suggest an incidence of bile duct (**Bertrand et al., 2003**).

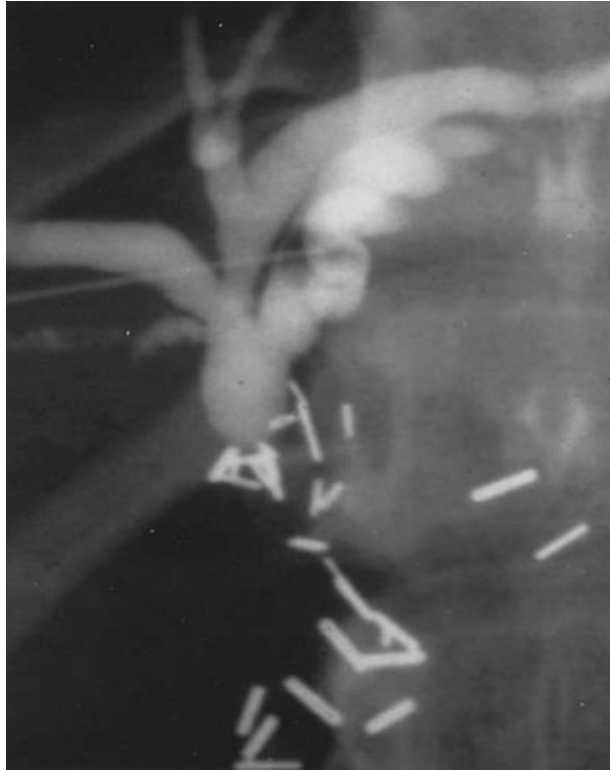


Figure 20: Percutaneous transhepatic cholangiogram in a patient with a bile duct stricture secondary to iatrogenic injury during cholecystectomy

Patients and Methods

This study was done to compare whether patients with intraabdominal drain following uncomplicated laparoscopic cholecystectomy are associated with more complications and hospital stay than those without intraabdominal drain.

Patients' population:

This study is a case series of 100 patients who underwent laparoscopic cholecystectomy.

We didn't include patients who had:

1. Been operated for laparoscopic cholecystectomy other than cholelithiasis.
2. All patient contraindicated to laparoscopic surgery.
3. Emergency operations were excluded.
4. Acute cholecystitis, empyema GB, mucocele of GB.
5. Patient with bleeding tendency (preoperative increase in INR or thrombocytopenia).
6. Patient with chronic liver or kidney diseases.
7. Intraoperative bleeding OR inadequate hemeostasis.
8. Patients can be excluded based on operator's judgement.

The included patients presented to the General Surgery Department at Rafidia Surgical Hospital .

Clinically all the patients were presented to undergo laparoscopic cholecystectomy operation and post-operative follow up for incidence of drain site pain, drain site infection, postoperative collection & hospital stay,

Laboratory and radiological investigations were carried out in order to detect any intra-abdominal collection.

Type of Patients:

This was a prospective study that included 100 patients with cholelithiasis who were twenty to sixty five years old and from both sexes attending to the hospital. The patients were randomly allocated into two groups each included 50 patients, first group (Group A) underwent laparoscopic cholecystectomy and we put intra-abdominal drain, the second group (Group B) underwent laparoscopic cholecystectomy without intra-abdominal drain.

Study procedure:

All patients were subjected to preoperative, operative, and postoperative assessment:

1. **Preoperative:** the preoperative assessment included full history taking, clinical examination, which included general examination of the chest, heart, and abdomen.

Patients were prepared for surgery, by explaining to them what is the procedure, its risks and benefits.

2. **Operative:** the operations were performed on the patients under general anesthesia and in supine position.
3. **Postoperative:** patients were followed up weekly for 2 to 3 weeks. Early postoperative follow-up included evaluation of postoperative pain, hospital stay and port site infection.

Patients' evaluation:

Clinical examination:

- Complete history taking.

- Detailed general and local physical examination.
- Operative details were all reviewed.

Laboratory investigations:

- 1- Full blood count.
- 2- Coagulation profile.
- 3- AST.
- 4- ALT.
- 5- Alkaline phosphatase.
- 6- Direct bilirubin.
- 7- Total bilirubin.

Statistical Analysis

Data were collected, revised, coded and entered to the Statistical Package for Social Science (IBM SPSS) version 23. The quantitative data were presented as mean, standard deviations and ranges when their distribution found parametric. Also qualitative variables were presented as numbers and percentages.

The comparison between groups regarding qualitative data was done by using ***Chi-square test***.

The comparison between two independent groups with quantitative data and parametric distribution were done by using ***Independent t-test***

The confidence interval was set to 95% and the margin of error accepted was set to 5%. So, the p-value was considered significant as the following:

P-value > 0.05: Non significant (NS)

P-value < 0.05: Significant (S)

P-value < 0.01: Highly significant (HS)

Results

Among the 100 patients with chronic calcular cholecystitis included in this study 70 were females (70%) and 30 were males (30%).

The 100 patients were randomly distributed into two equal groups (50 patients each): Group A underwent laparoscopic cholecystectomy and we put intra-abdominal drain and, while Group B underwent laparoscopic cholecystectomy but we didn't insert intra-abdominal drain.

Patients' age ranged from 20 to 65.

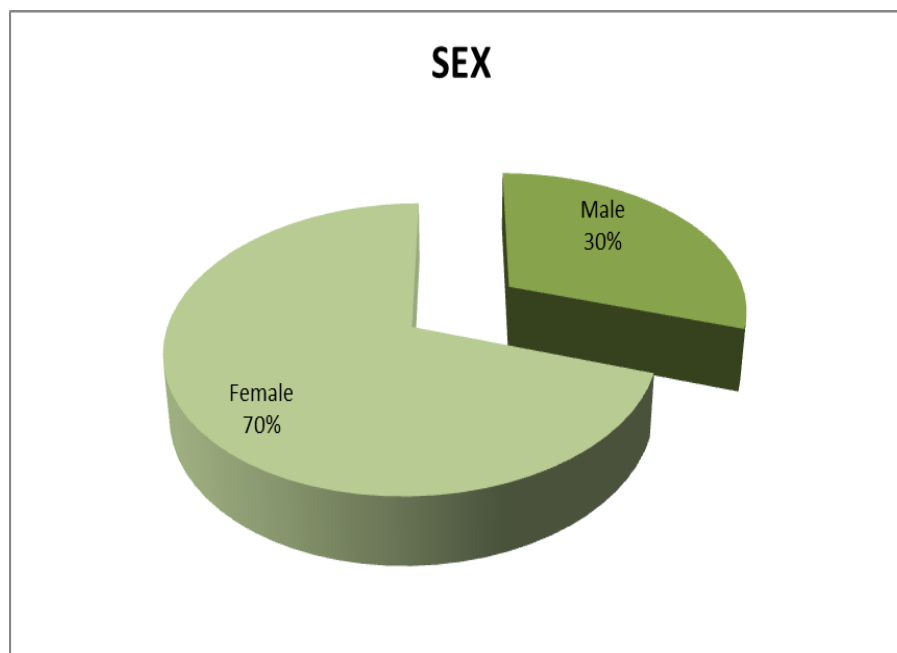


Figure 21: Sex distribution

➤ **Analysis of postoperative pain at drain/port site:**

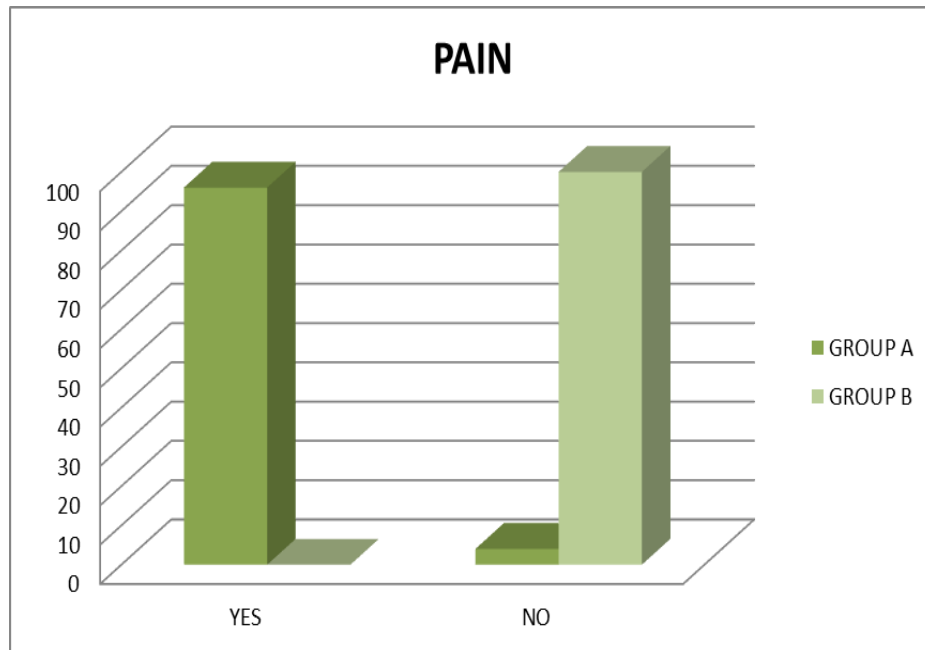


Figure 22: Analysis of postoperative pain at drain/port site

The incidence of postoperative pain at port site where drain was inserted was more in patients in group A (96%), while patients without drain (group B) experienced no or minimal postoperative pain (0% approximately). (P value 0.000 which is highly significant).

➤ **Analysis of postoperative infection at port/drain site:**

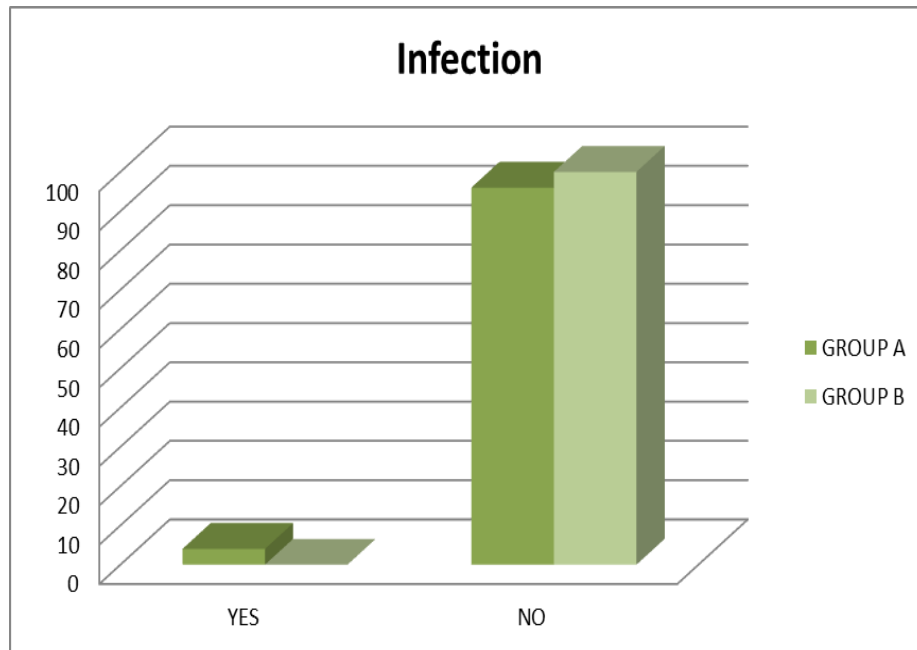


Figure 23: Analysis of postoperative infection at port/drain site

Also the incidence of postoperative drain site infection is higher in patients in Group A (drain from the port site) 4%, (P value 0.000). While in group B (patients with no drain) almost no patient experienced port site infection.

➤ **Analysis of post operative hospital stay:**

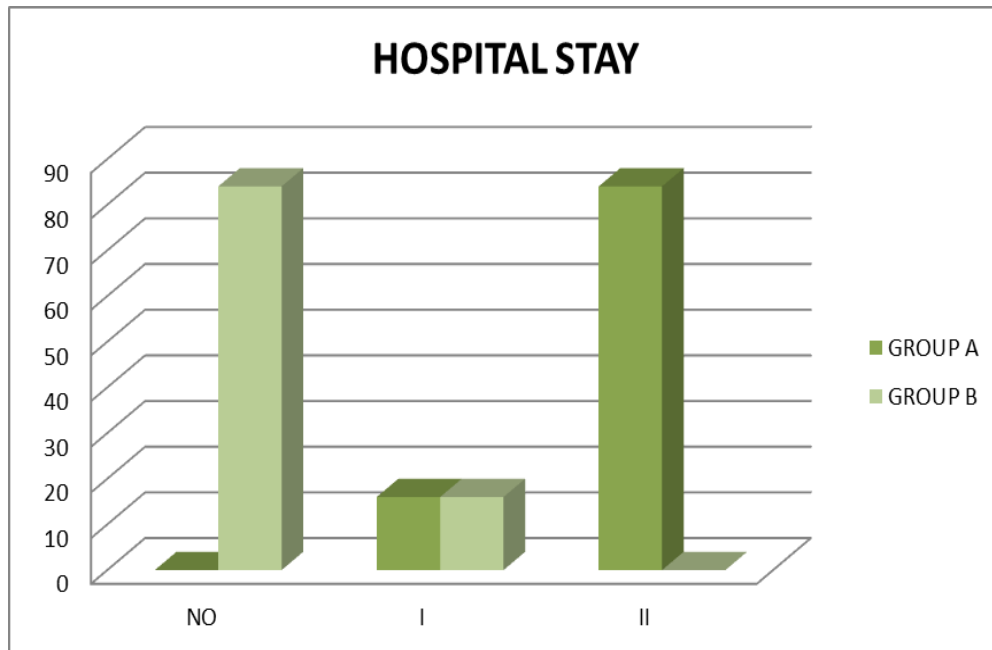


Figure 24: Analysis of post operative hospital stay

Regarding hospital stay, majority of patients with drain (group A) required hospital stay for almost 2 days (16% of patients discharged in day 1 postoperatively while 84% of patients discharged on day 2 post-operative), while those without drain (group B) 84% of patients discharged at the same day, while 16% discharged day 1 postoperative).

➤ **Analysis of postoperative collection:**

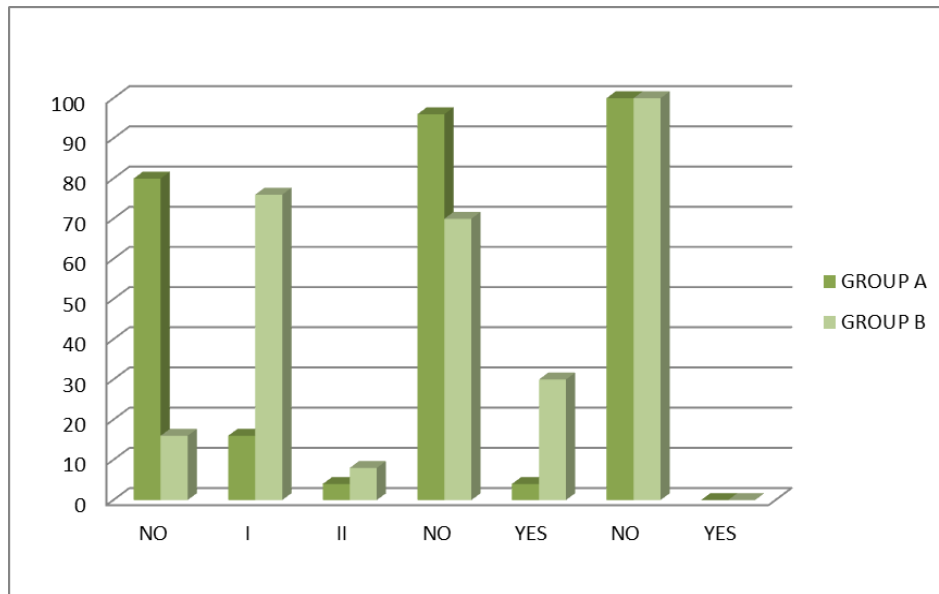


Figure 25: Analysis of postoperative collection

Regarding post-operative intrabdominal collection, we followed up patients using ultrasound on day 1, day 2 and day 3 postoperative (POD1, POD2, POD3), (**No** collection, **I** collection < 50 ml, **II** collection 50-100 ml).

This revealed intra-abdominal fluid collection POD1 was lower in drain group (Group A) than in non-drain group (Group B).

POD 1 the collection was lower in group A, 80% of patients developed no collection, while 16% of patients developed collection < 50 ml, while 4% of patients developed collection from 50-100ml, while those in group B, 16% of patients developed no collection, while 76% developed collection <50 ml, while 8% of patients developed collection 50-100 ml.

POD2 only 4% of patients those in group A (with drain) developed minimal collection that disappeared on next day. Group B (without drain)30% of patients developed minimal collection that disappeared on next day.

Table 2: Comparison between two groups regarding age, sex, pain, infection, hospital stay and collection postoperative day 1, 2, 3

		Group A	Group B	Test value	P- value	Sig.
		No.= 50	No.= 50			
Age	Mean±SD	37.80 ± 10.32	34.28 ± 9.33	1.266•	0.212	NS
	Range	22 – 63	20 – 53			
Sex	Males	12 (24.0%)	18 (36.0%)	0.000*	1.000	NS
	Females	38 (76.0%)	32 (64.0%)			
Pain	No	2 (4.0%)	50 (100.0%)	46.154*	0.000	HS
	Yes	48 (96.0%)	0 (0.0%)			
Infection	No	48 (96.0%)	50 (100.0%)	46.154*	0.000	HS
	Yes	2 (4.0%)	0 (0.0%)			
Hospital stay	No	0 (0.0%)	21 (84.0%)	42.000*	0.000	HS
	I	4 (16.0%)	4 (16.0%)			
	II	21 (84.0%)	0 (0.0%)			
POD1	No	40 (80.0%)	8 (16.0%)	38.789*	0.000	HS

	I	8 (16.0%)	38 (76.0%)			
	II	2 (4.0%)	4 (8.0%)			
POD2	No	48 (96.0%)	35 (70.0%)	2.083*	0.149	NS
	Yes	2 (4.0%)	15 (30.0%)			
POD3	No	50 (100.0%)	50 (100.0%)	-	-	-
	Yes	0 (0.0%)	0 (0.0%)			

P-value >0.05: Non significant (NS); P-value <0.05: Significant (S); P-value< 0.01: highly significant (HS)

*:Chi-square test; •: Independent t-test

Discussion

Laparoscopic cholecystectomy has largely replaced open cholecystectomy because of shorter hospital stay, faster recovery, and lower overall morbidity. However, the morbidity due to bile duct injury has increased with the advent of the laparoscopic approach (**Henry et al., 2011**).

Prevention of intra-abdominal collections after laparoscopic cholecystectomy is our main concern. Post cholecystectomy collection in the sub-hepatic space is usually absorbed whether a drain is used or not.

Intraperitoneal collection of blood may cause postoperative pyrexia, prolong the hospital stay, and increase the incidence of wound infection, while the presence of bile in the peritoneal cavity produces peritoneal irritation.

Only some clinically significant abdominal collections may need intervention. The drain may also give false sense of security as it may get blocked and later patients present with complications.

Our study revealed that less post-operative port site pain, infection and hospital stay in group B (without drain) in comparison with group A (with drain) and those results were statistically significant ($P\text{-value} < 0.01$).

Regarding post cholecystectomy free intra-abdominal collection, it was less evident by ultrasound in group A (with drain) rather than group B (without drain) in first 24 hours. Although the results were statistically significant in the first 24 hours, the difference became insignificant on subsequent ultrasound after 72hrs. ($p\text{-value} < 0.01$ in day 1 postoperative, $P\text{-value} > 0.05$ in day 2 postoperative).

Our results are similar to the result conducted by El-Labban et al. regarding postoperative hospital stay and abdominal collection, while his results were opposite to our study regarding port site infection, pain were there no statistical difference (**EL-Labban et al., 2012**).

Opposite results were obtained by Ishikawa et al in their randomized study which include 295 patients where Group A (with drain) include 145 patients and Group B (without drain) include 150 patient, where he stated that no significant difference between the two groups with respect to postoperative complication rate, while regarding postoperative hospital stay the results were similar to our study (**Ishikawa et al., 2011**).

This is in support with results by Georgiou C as he included 116 patients, where 63 patient in drained group (YD) and 53 in non-drained group (ND) in regard postoperative pain, hospital stay as he stated that the proportion of patients staying in hospital for >2 days was higher in the YD group: 28.6% of the patients versus 13.2% in the ND group ($P = .05$).

As for Subhepatic fluid was more often observed in the YD group (47% versus 34% in the ND), but the difference was not statistically significant (**Georgiou et al., 2011**).

Our results were also consistent with those reported by Yang et al, who reported that the abdominal drain group displayed significantly higher pain scores (MD: 1.07; 95% CI: 0.69–1.46; $P < .001$), abdominal drain prolonged the duration of postoperative hospital stay (MD: 0.47 day; 95% CI: 0.14–0.80; $P = .005$). Wound infection was found to be associated with the use of abdominal drains (RR: 1.97; 95% CI: 1.11–3.47; $P = .02$) (**Yang et al., 2020**).

Similarly, our result is supported by results of the study by Sharma et al who found that postoperative pain was higher in the group A (with drain) than in Group B (without drain), also the proportion of the patients staying in the hospital for more than two days was higher in group A (with drain), 14 (46.66%) and 8 (26.66%) in group B (without drain) ($p < 0.05$) while there was no statistical difference in the rate of wound infections (**Sharma et al., 2016**).

Summary

Laparoscopic cholecystectomy provides a safe and effective treatment for patients with gallstones as it reduces post-operative pain with almost negligible scar, short hospital stay and earlier return to work.

Prophylactic drains in abdominal surgery are widely used either to detect complications early, such as postoperative hemorrhage or bile leakage, or to drain collections which may be toxic, as bile. However, evidence-based data do not support the use of prophylactic drainage in the majority of abdominal procedures.

Gallstones are still one of the most common conditions in surgical outpatient department. Laparoscopic cholecystectomy, after its advent in 1987, rapidly established itself as the gold standard treatment of gallstones. In 1913 cholecystectomy without drainage was described, and since then surgeons were divided whether to use it or not in uncomplicated cases. Most surgeons continue to use routine drain for the fear of bile leakage or bleeding. Such complications invariably occurred in spite of sub hepatic drainage. So, there arises a need for study, whether to put drain or not, and its consequences.

Among the 100 patients included in this study, 70 were females (70%) and 30 were males (30%), with female to male ratio 3.1: 1 approximately. The 100 were randomly distributed into two groups: Group A patients underwent laparoscopic cholecystectomy with drain insertion and this group composed of 50 patients 12 were males (24%) and 38 were females (76%). While Group B also underwent laparoscopic cholecystectomy but without drain insertion and this group composed of 50 patients, 18 males (36%) and 32 females (64%)

In our study we include patients with chronic calculous cholecystitis which is indicated for elective laparoscopic cholecystectomy.

Regarding the Postoperative Pain:

It was higher in patients in Group A (with drain) than in Group B (without drain), and that was statistically significant (P value less than 0.05).

Regarding Port Site Infection:

All patients included in this study were followed post-operative for port site infection (till day 7 time of stitch removal) and we found the incidence of port site infection was higher in Group A (with drain) at site where the drain was inserted, and that was statistically significant (P value less than 0.05).

Regarding postoperative hospital stay:

Hospital stay was much less in patients without drain (Group B) as 42 patient (84%) were discharged at the same day of operation which is statistically significant (P value less than 0.05).

Regarding postoperative collection:

We followed up postoperative collection in the two groups in day1, 2 and 3 and revealed that, POD 1 the collection was lower in Group A (with drain), 80% of patients developed no collection, while 16% of patients developed collection < 50 ml, while 4% developed collection 50-100 ml, while those in Group B (without drain) 8% of patient developed no collection, while 76% of patients developed < 50 ml, while 8% of patients developed 50-100 ml.

And that was statistically significant in day1 postoperative (P value less than 0.05), while it was non-significant in the following 72 hours.

Conclusion

Uncomplicated gall stone diseases can be treated by laparoscopic cholecystectomy without need for drain with reasonable safety by an experienced surgeon. With no usage of drain, it is significantly advantageous in terms of post-operative pain, use of analgesics, infection and hospital stay.

In our study we compare drain insertion post laparoscopic cholecystectomy in matter of post-operative pain, port site infection, hospital stay and post-operative collection.

It revealed that there is significant reduction in postoperative pain in patients without drain than in those with drain.

Moreover regarding postoperative wound infection it was also lower in patient with no drain.

There were also statistically significant reduction in postoperative hospital stay in patients without drain.

Furthermore, postoperative intrabdominal collection is significantly lower in patients with drain in first 24 hours, while after that there were no significant difference regarding intrabdominal collection.

References

- Abdalla, S., Pierre, S. and Ellis, H., 2013.** Calot's triangle. *Clinical anatomy*, 26(4), pp.493-501.
- Ahmad, G., Baker, J., Finnerty, J., Phillips, K. and Watson, A., 2019.** Laparoscopic entry techniques. *Cochrane Database of Systematic Reviews*, (1).
- Asbun, H.J., Shah, M.M., Ceppa, E.P. and Auyang, E.D. eds., 2020.** *The SAGES Manual of Biliary Surgery*. Springer.
- Bertrand, C., 2003.** Prevalence of bile duct injury following cholecystectomy. *Acta Chirurgica Belgica*, 103(2), pp.143-150.
- Choudhury, P., 2014.** Relevant biliary anatomy during cholecystectomy. *Journal of Evolution of Medical and Dental Sciences*, 3(35), pp.9332-9343.
- El-Labban, G., Hokkam, E., El-Labban, M., Saber, A., Heissam, K. and El-Kammash, S., 2012.** Laparoscopic elective cholecystectomy with and without drain: A controlled randomised trial. *Journal of minimal access surgery*, 8(3), p.90.
- Francoeur, J.R., Wiseman, K., Buczkowski, A.K., Chung, S.W. and Scudamore, C.H., 2003.** Surgeons' anonymous response after bile duct injury during cholecystectomy. *The American journal of surgery*, 185(5), pp.468-475.
- Gadhvi, U.I., Bhimani, D.A., Waghela, J. and Rajgor, D.K., 2018.** A comparative study of laparoscopic cholecystectomy with and without abdominal drain. *International Journal of Research in Medical Sciences*, 6(11), p.3639.
- Georgiou, C., Demetriou, N., Palaris, T., Theodosopoulos, T., Katsouyanni, K. and Polymeneas, G., 2011.** Is the routine use of drainage after elective laparoscopic cholecystectomy justified? A randomized trial. *Journal of Laparoendoscopic & Advanced Surgical Techniques*, 21(2), pp.119-123.
- Goke, K., de Oliveira Leite, T.F. and Chagas, C.A.A., 2018.** The accessory bile duct and the duct of Luschka. *Acta Scientiae Anatomica*, 1(1), pp.17-20.

- Henry AP, Steven AA, and Attila N. 2011.** Calcuolos biliary disease, Greenfield chapter 60, 2011.
- Hori, T., Oike, F., Furuyama, H., Machimoto, T., Kadokawa, Y., Hata, T., Kato, S., Yasukawa, D., Aisu, Y., Sasaki, M. and Kimura, Y., 2016.** Protocol for laparoscopic cholecystectomy: Is it rocket science?. World Journal of Gastroenterology, 22(47), p.10287.
- Ishikawa, K., Matsumata, T., Kishihara, F., Fukuyama, Y., Masuda, H. and Kitano, S., 2011.** Laparoscopic cholecystectomy with and without abdominal prophylactic drainage. Digestive endoscopy, 23(2), pp.153-156.
- John ES, Gene LC, Thomas AW, Roger SF, Andrew NK, Lee JS, Panajiotis NS, Petros SM, 2004.** Skandalakis Surgical Anatomy, Chapter 20.
- Jones MW, Deppen JG.** Physiology, Gallbladder. [Updated 2019 Jan 17]. In: StatPearls [Internet]. Treasure Island (FL): StatPearls Publishing; 2020 Jan-. Available from: <https://www.ncbi.nlm.nih.gov/books/NBK482488/>
- Keplinger, K.M. and Bloomston, M., 2014.** Anatomy and embryology of the biliary tract. Surgical Clinics, 94(2), pp.203-217.
- Lien, H.H., Huang, C.C., Liu, J.S., Shi, M.Y., Chen, D.F., Wang, N.Y., Tai, F.C. and Huang, C.S., 2007.** System approach to prevent common bile duct injury and enhance performance of laparoscopic cholecystectomy. Surgical Laparoscopy Endoscopy & Percutaneous Techniques, 17(3), pp.164-170.
- McMahon, A.J., Fullarton, G., Baxter, J.N. and O'dwyer, P.J., 2004.** Bile duct injury and bile leakage in laparoscopic cholecystectomy. British journal of surgery, 82(3), pp.307-313.
- McMinn, R.M., 2000.** Last's anatomy-regional and applied. London: Churchill Livingstone, 2000.
- O'Rourke TR. 2018.** Operative Anatomy and Surgical Landmarks of the Biliary System. InThe Management of Gallstone Disease 2018 (pp. 1-19). Springer, Cham.

- Park, J.S., Kim, J.H., Kim, J.K. and Yoon, D.S., 2015.** The role of abdominal drainage to prevent of intra-abdominal complications after laparoscopic cholecystectomy for acute cholecystitis: prospective randomized trial. *Surgical endoscopy*, 29(2), pp.453-457.
- Picchio, M., Lucarelli, P., Di Filippo, A., De Angelis, F., Stipa, F. and Spaziani, E., 2014.** Meta-analysis of drainage versus no drainage after laparoscopic cholecystectomy. *JSLs: Journal of the Society of Laparoendoscopic Surgeons*, 18(4).
- Schulick, R.D., 2012.** Hepatobiliary anatomy. In *Greenfield's Surgery: Scientific Principles and Practice: Fifth Edition* (pp. 873-887). Wolters Kluwer Health Adis (ESP).
- Schwartz's Principles of Surgery, 2019.** 11th edition (2019) pages: 1394,1395,1396,1397, 1412,1413.
- Shabanali, A., Reza, D.M., Khadijeh, A., Maryam, B. and Reza, A., 2014.** Double cystic duct. *International Journal of Anatomy and Research*, 2, pp.601-604.
- Sharma, A. and Gupta, S.N., 2016.** Drainage versus no drainage after elective laparoscopic cholecystectomy. *Kathmandu Univ Med J (KUMJ)*, 14(53), pp.69-72.
- Souba, W.W., Pink, M.P., Jurkovich, G.J., Kaiser, L.R., Pearce, W.H., Pemberton, J.H. and Soper, N.J., 2001.** *ACS Surgery: Principles & Practice*, 2005. WebMD.
- Steiner CA, Bass EB, Talamini MA, Pitt HA, Steinberg EP. 2004.** Surgical rates and operative mortality for open and laparoscopic cholecystectomy in Maryland. *N Engl J Med*; 330(6):403-408
- Strasberg, S.M. and Helton, W.S., 2011.** An analytical review of vasculobiliary injury in laparoscopic and open cholecystectomy. *Hpb*, 13(1), pp.1-14.
- Strasberg, S.M., 2002.** Avoidance of biliary injury during laparoscopic cholecystectomy. *Journal of hepato-biliary-pancreatic surgery*, 9(5), pp.543-547.

- Yang, J., Liu, Y., Yan, P., Tian, H., Jing, W., Si, M.,... & Guo, T. (2020).** Comparison of laparoscopic cholecystectomy with and without abdominal drainage in patients with non-complicated benign gallbladder disease: A protocol for systematic review and meta-analysis. *Medicine*, 99(20), e20070.
- Zhou, P.H., Liu, F.L., Yao, L.Q. and Qin, X., 2003.** Endoscopic diagnosis and treatment of post-cholecystectomy syndrome. *Hepatobiliary & pancreatic diseases international: HBPD INT*, 2(1), pp.117-120.

**Neutrosophic Hybrid Weibull Inverse Weibull distribution:
Mathematical Properties with simulation
and Neutrosophic Real Data Application**

Kamal N. Abdullah¹, Mundher A. Khaleel²

^{1,1} Mathematics Departments, College of Computer Science and Mathematics, Tikrit University, Iraq

^{1,2} Mathematics Departments, College of Computer Science and Mathematics, Tikrit University, Iraq

^{1,1} kn230022pcm@st.tu.edu.iq ^{1,2} mun880088@tu.edu.iq

Neutrosophic Hybrid Weibull Inverse Weibull distribution: Mathematical Properties with simulation and Neutrosophic Real Data Application

Kamal N. Abdullah¹, Mundher A. Khaleel²

^{1,1} Mathematics Departments, College of Computer Science and Mathematics, Tikrit University, Iraq

^{1,2} Mathematics Departments, College of Computer Science and Mathematics, Tikrit University, Iraq

^{1,1} kn230022pcm@st.tu.edu.iq ^{1,2} mun880088@tu.edu.iq

Abstract:

This study is concerned with finding a statistical distribution that deals with a Neutrosophic random variable and Neutrosophic parameters called Neutrosophic Hybrid Weibull Inverse Weibull (NHWIW) distribution. The basic functions of proposed distribution are found, as well as many statistical properties of distribution with an estimation of the model parameters in three different techniques, with a Monte Carlo simulation to determine the estimation efficiency of NHWIW distribution, with a comparison with three measures to determine the best method for estimation. A practical application is also conducted on two types of Neutrosophic real data, the first represented by mortality data for children under five years of age, and the second is COVID-19 in Netherlands for thirty days, where the analysis efficiency of the NHWIW distribution is determined by comparing it with six other distributions using 4 information criteria and 4 statistical measures, which showed the efficiency and flexibility of NHWIW distribution.

Keywords: HWG-family, Neutrosophic data, Bias, Cramér-von Mises, and flexibility.

1. Introduction:

Probability distributions are a fundamental tool in statistical modeling used to describe and analyze various phenomena in many fields. One of the most prominent methods recently developed to expand the scope of basic distributions is the T-X method, which provides a flexible framework for creating new distributions with improved mathematical properties, making them more accurate in representing real-world data. The method is based on forming a family of complex distributions using transformation functions, which contributes to enhancing the flexibility and ability to deal with complex properties, such as heterogeneous or asymmetrically distributed data [1]. Examples of this method include: BIIIEE-X family [2], NOGEE-G family [3], WEE-X Family [4], OLG family [5], NGOF-G Family [6], EOIW-G Family [7], GOM-G family [8], and HOE-Φ family [9]. This study based on HWG family which has a CDF function by form [10]:

$$F_{HWG}(x, a, b, \zeta) = 1 - e^{(-a[-\mathcal{G}(x; \varepsilon) \log(1 - \mathcal{G}(x; \varepsilon))]^b)}, \quad x \geq 0, a, b > 0 \quad (1)$$

And PDF function by form:

$$f_{HWG}(x, a, b, \zeta) = ab \mathcal{g}(x; \varepsilon) \left[\frac{\mathcal{G}(x; \varepsilon)}{1 - \mathcal{G}(x; \varepsilon)} - \log(1 - \mathcal{G}(x; \varepsilon)) \right] \times [-\mathcal{G}(x; \varepsilon) \log(1 - \mathcal{G}(x; \varepsilon))]^{b-1} e^{(-a[-\mathcal{G}(x; \varepsilon) \log(1 - \mathcal{G}(x; \varepsilon))]^b)} \quad (2)$$

Where $\mathcal{G}(x; \varepsilon)$, and $\mathcal{g}(x; \varepsilon)$ are CDF and PDF functions for any baseline distribution and $a, b \geq 0$ are shapes parameters for HWG family.

On other hand, the Neutrosophic logic (N.L) is a recent development in the field of fuzzy and uncertain data analysis. This logic aims to address ambiguity and uncertainty in data by introducing three main dimensions: Truth (T), falsehood (F), and indeterminacy (I). this framework provides an effective way to model data that cannot be conclusively characterized using traditional methods. There

are two types of N.L: the traditional method, in which the data is divided into three parts and then dealt with by using, for example, the triangular function, in which the peaks represent the T values and the troughs represent F values and what is in between represents I values, or trapezoidal function in the same manner. As for the second method, which depends on the values of intervals and contains all parts of N.L, which called the direct method, and it's the method used in forming the proposed distribution.

Focuses on finding a statistical distribution that deals with a Neutrosophic variables and parameters. The main gap is the lack of previous research that integrates Neutrosophic data with complex distributions such as a distribution based on a hybrid family of Weibull distribution and a hybrid integral limit. Existing studies often focus on traditional data or on specific distributions without considering Neutrosophic data of an uncertain or ambiguous nature. The aim of the study is to develop a " Neutrosophic Hybrid Weibull Inverse Weibull" and test its efficiency and flexibility on real Neutrosophic data using multiple estimation methods, and compare with other distributions to determine the efficiency and flexibility in dealing with Neutrosophic data.

2. Neutrosophic Hybrid Weibull Inverse Weibull (NHWIW) distribution

Let X be a random variable, then the CDF and PDF functions for Inverse Weibull distribution has a forms [11]:

$$G(x; q, p) = e^{-qx^{-p}}, \quad q, p, x > 0 \quad (3)$$

$$g(x; q, p) = qp x^{-(p+1)} e^{-qx^{-p}}, \quad q, p, x > 0 \quad (4)$$

Where q, p are shape parameters for Inverse Weibull distribution.

To get the CDF function for Hybrid Weibull Inverse Weibull we combine equation (1) with equation (3) by form:

$$F(x) = 1 - e^{-a[-e^{-qx^{-p}} \cdot \log(1 - e^{-qx^{-p}})]^b}, \quad x, a, b, q, p > 0 \quad (5)$$

The PDF function for Hybrid Weibull Inverse Weibull (HWIW) we combine equation (2) with equation (3) and (4) to get it by form:

$$f(x) = ab qp x^{-(p+1)} e^{-qx^{-p}} \left[\frac{e^{-qx^{-p}}}{1 - e^{-qx^{-p}}} - \log(1 - e^{-qx^{-p}}) \right] \\ \times [-e^{-qx^{-p}} \cdot \log(1 - e^{-qx^{-p}})]^{b-1} e^{-a[-e^{-qx^{-p}} \cdot \log(1 - e^{-qx^{-p}})]^b} \quad (6)$$

In order to integrate the HWIW distribution with N.L, the random variable and parameters of HWIW distribution are converted to Neutrosophic random variable and Neutrosophic parameters as follows:

Let $X_N = d + tI$, $tI \in [X_L, X_U]$, where X_L, X_U are lower and upper values of the neutrosophic random variable having determined part d and indeterminate part tI , $tI \in [I_L, I_U]$. Note that the NHWIW distribution reduces to classical HWIW distribution when $X_L = X_U$. The neutrosophic cumulative density function (NCDF) of NHWIW has a Neutrosophic shape parameters $a_N \in [a_L, a_U]$, $b_N \in [b_L, b_U]$, $q_N \in [q_L, q_U]$, and $p_N \in [p_L, p_U]$, has the form:

$$F(x_N) = 1 - e^{-a_N \left[-e^{-q_N x_N^{p_N}} \cdot \log(1 - e^{-q_N x_N^{p_N}}) \right]^{b_N}}, \quad x_N, a_N, b_N, q_N, p_N > 0 \quad (7)$$

To obtain the nature of NCDF, the function is plotted with different intervals of parameters and in 2-dimentional and 3-dimensional forms as follows:

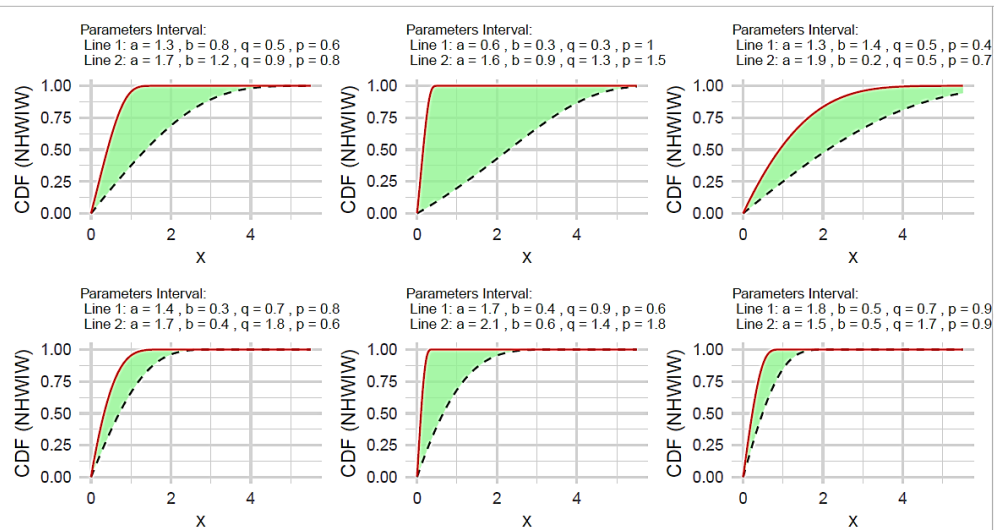


Figure 1. plot of NCDF for NHWIW distribution

And the probability density function (NCDF) of NHWIW has a form:

$$f(x_N) = q_N p_N x_N^{-(p_N+1)} e^{-q_N x_N^{-p_N}} \left[\frac{e^{-q_N x_N^{-p_N}}}{1 - e^{-q_N x_N^{-p_N}}} - \log(1 - e^{-q_N x_N^{-p_N}}) \right] \quad (8)$$

$$\times \left[-e^{-q_N x_N^{-p_N}} \cdot \log(1 - e^{-q_N x_N^{-p_N}}) \right]^{b_N-1} e^{\left(-a_N \left[-e^{-q_N x_N^{-p_N}} \cdot \log(1 - e^{-q_N x_N^{-p_N}}) \right]^{b_N} \right)}$$

To obtain the nature of NCDF, the function is plotted with different intervals of parameters and in 2-dimentional and 3-dimensional forms as follows:

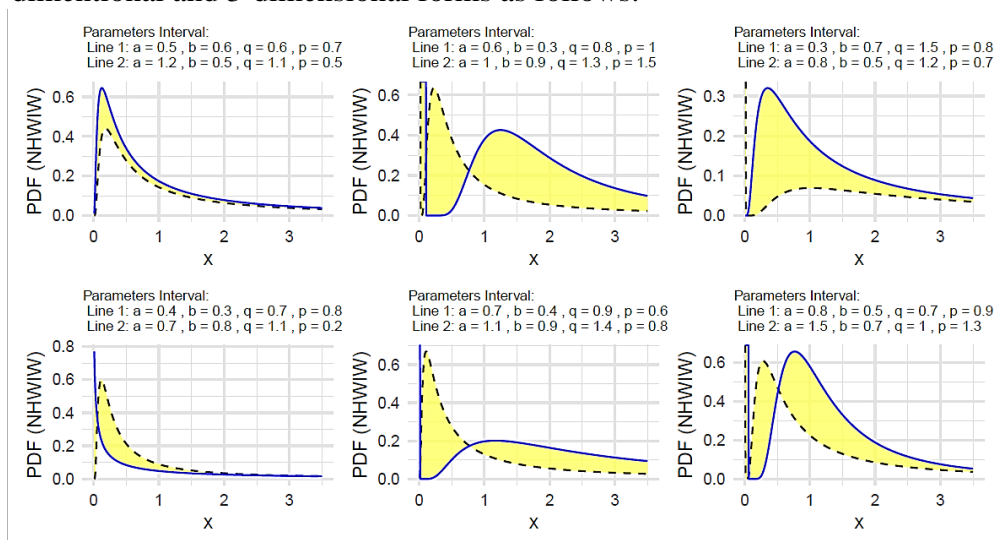


Figure 2. plot of NPDF for NHWIW distribution

While the survival function for NHWIW distribution given by formula [12]:

$$S(x_N) = e^{\left(-a_N \left[-e^{-q_N x_N^{-p_N}} \log(1 - e^{-q_N x_N^{-p_N}})\right]^{b_N}\right)} \quad (9)$$

And the hazard function has a formula:

$$h(x_N) = \frac{q_N p_N x_N^{-(p_N+1)} e^{-q_N x_N^{-p_N}} \left[\frac{e^{-q_N x_N^{-p_N}}}{1 - e^{-q_N x_N^{-p_N}}} - \log(1 - e^{-q_N x_N^{-p_N}}) \right]}{\left[-e^{-q_N x_N^{-p_N}} \log(1 - e^{-q_N x_N^{-p_N}}) \right]^{1-b_N}} \quad (10)$$

3. Properties for NHWIW distribution

In this section we will prove some statistical properties for NHWIW distribution, and show what changing of classical IW distribution.

3.1 NCDF and NPDF expansion

Due to the difficulty of NCDF and NPDF functions in equations (7) and (8) respectively, these functions are simplified in order to simplify the proof of NHWIW distribution properties. This is done using binomial expansion, the exponential function expansion, and the logarithm expansion. Therefore, the simplified NCDF function is obtained as follows:

$$F(x_N) = 1 - \psi \left(e^{-q_N x_N^{-p_N}} \right)^{j+2ib_N} \quad (11)$$

Where $\psi = \sum_{i=j=0}^{\infty} \frac{(-1)^{i+ib_N+j}}{i!} a_N^i d_{ib_N,j}$, and $d_{ib_N,j} = j^{-1} \sum_{m=1}^j \frac{m(ib_N+1)-j}{m+1}$ for $j \geq 0$ and $d_{ib_N,0} = 1$

By same way we can expansion NPDF function to get a form:

$$f(x_N) = M x_N^{-(p_N+1)} e^{-(2ib_N+2b_N+j+k)q_N x_N^{-p_N}} - N x_N^{-(p_N+1)} e^{-(2ib_N+2b_N+j+z)q_N x_N^{-p_N}} \quad (12)$$

Where $M = \sum_{i=j=k=0}^{\infty} \frac{(-1)^{i+ib_N+b_N-1+j+k}}{i!} a_N^{i+1} d_{ib_N+b_N-1,j} b_N q_N p_N$

And $N = \sum_{i=j=z=0}^{\infty} \frac{(-1)^{i+ib_N+b_N-1+j}}{i!} a_N^{i+1} d_{ib_N+b_N-1,j} d_{1,z} b_N q_N p_N$

As $d_{1,z} = z^{-1} \sum_{m=1}^j \frac{2m-j}{m+1}$ for $z \geq 0$ and $d_{1,0} = 1$ and

$d_{ib_N+b_N-1,j} = j^{-1} \sum_{m=1}^j \frac{m(ib_N+b_N)-j}{m+1}$ for $j \geq 0$ and $d_{ib_N+b_N-1,0} = 1$

3.2 Moment

Let X_N be any Neutrosophic random variable, then the n^{th} moment for NHWIW distribution is given by form [13], [14], [15], [16]

$$\mu_n = E(x_N^n)_{NHWIW} = \int_{-\infty}^{\infty} x_N^n f(x_N) dx_N \quad (13)$$

By putting equation (12) in equation (13) we have got a form:

$$\mu_n = M \int_0^{\infty} x_N^{n-(p_N+1)} e^{-(2ib_N+2b_N+j+k)q_N x_N^{-p_N}} - N \int_0^{\infty} x_N^{n-(p_N+1)} e^{-(2ib_N+2b_N+j+z)q_N x_N^{-p_N}} dx_N$$

To get a final form:

$$\mu_n = \frac{\Gamma\left(\frac{n-p_N}{p_N}\right)}{p_N q_N \frac{n-p_N}{p_N}} \left[\frac{M}{(2ib_N+2b_N+j+k) \frac{n-p_N}{p_N}} - \frac{N}{(2ib_N+2b_N+j+z) \frac{n-p_N}{p_N}} \right] \quad (14)$$

The first four moments are found by substituting the value of n and as follows:

$$\mu_1 = \frac{\Gamma(\frac{1-p_N}{p_N})}{p_N q_N \frac{1-p_N}{p_N}} \left[\frac{M}{(2ib_N+2b_N+j+k) \frac{1-p_N}{p_N}} - \frac{N}{(2ib_N+2b_N+j+z) \frac{1-p_N}{p_N}} \right] \quad (15)$$

$$\mu_2 = \frac{\Gamma(\frac{2-p_N}{p_N})}{p_N q_N \frac{2-p_N}{p_N}} \left[\frac{M}{(2ib_N+2b_N+j+k) \frac{2-p_N}{p_N}} - \frac{N}{(2ib_N+2b_N+j+z) \frac{2-p_N}{p_N}} \right] \quad (16)$$

$$\mu_3 = \frac{\Gamma(\frac{3-p_N}{p_N})}{p_N q_N \frac{3-p_N}{p_N}} \left[\frac{M}{(2ib_N+2b_N+j+k) \frac{3-p_N}{p_N}} - \frac{N}{(2ib_N+2b_N+j+z) \frac{3-p_N}{p_N}} \right] \quad (17)$$

$$\mu_4 = \frac{\Gamma(\frac{4-p_N}{p_N})}{p_N q_N \frac{4-p_N}{p_N}} \left[\frac{M}{(2ib_N+2b_N+j+k) \frac{4-p_N}{p_N}} - \frac{N}{(2ib_N+2b_N+j+z) \frac{4-p_N}{p_N}} \right] \quad (18)$$

From it, we can obtain the skewness and Kurtosis of NHWIW distribution respectively as follows [16]:

$$SK_{NHWIW} = \frac{\frac{\Gamma(\frac{3-p_N}{p_N})}{p_N q_N \frac{3-p_N}{p_N}} \left[\frac{M}{(2ib_N+2b_N+j+k) \frac{3-p_N}{p_N}} - \frac{N}{(2ib_N+2b_N+j+z) \frac{3-p_N}{p_N}} \right]}{\left(\frac{\Gamma(\frac{2-p_N}{p_N})}{p_N q_N \frac{2-p_N}{p_N}} \left[\frac{M}{(2ib_N+2b_N+j+k) \frac{2-p_N}{p_N}} - \frac{N}{(2ib_N+2b_N+j+z) \frac{2-p_N}{p_N}} \right] \right)^{\frac{3}{2}}} \quad (19)$$

$$KU_{NHWIW} = \frac{\frac{\Gamma(\frac{4-p_N}{p_N})}{p_N q_N \frac{4-p_N}{p_N}} \left[\frac{M}{(2ib_N+2b_N+j+k) \frac{4-p_N}{p_N}} - \frac{N}{(2ib_N+2b_N+j+z) \frac{4-p_N}{p_N}} \right]}{\left(\frac{\Gamma(\frac{2-p_N}{p_N})}{p_N q_N \frac{2-p_N}{p_N}} \left[\frac{M}{(2ib_N+2b_N+j+k) \frac{2-p_N}{p_N}} - \frac{N}{(2ib_N+2b_N+j+z) \frac{2-p_N}{p_N}} \right] \right)^2} - 3 \quad (20)$$

To know the change in the moments of NHWIW distribution with change in intervals of Neutrosophic parameters, table 1 shows a set of moments with variance, skewness, and Kurtosis as follows:

Table.1 some intervals of moments for NHWIW

a_N	b_N	q_N	p_N	$\hat{\mu}_{1N}$	$\hat{\mu}_{2N}$	$\hat{\mu}_{3N}$	$\hat{\mu}_{4N}$	σ_N^2	S_N	K_N
[1.8,2.8]	[1.6,2.6]	[1.4,2.4]	[1.1,2.1]	[2.146064, 2.857927]	[4.723157, 10.57421]	[10.64869, 52.02946]	[24.5692,3 54.4007]	[0.117566, 2.406463]	[1.037403, 1.513134]	[1.101352, 3.169558]
			[1.2,2.2]	[2.0717, 2.593549]	[4.391856, 8.343002]	[9.518114, 33.94803]	[21.06914, 179.7407]	[0.099915, 1.616506]	[1.034139, 1.408741]	[1.092322, 2.58227]
		[1.6,2.6]	[1.3,2.3]	[2.077192, 2.651157]	[4.406707, 8.434903]	[9.540035, 32.68622]	[21.05919, 157.4864]	[0.09198,1 .40627]	[1.031285, 1.334273]	[1.084459, 2.213517]

			[1.4,2.4]	[2.014016, 2.458261]	[4.135742, 7.066473]	[8.652692, 24.02667]	[18.43118, 98.13544]	[0.079482, 1.023426]	[1.028777, 1.279056]	[1.077572, 1.965262]
			[1.5,2.5]	[2.047589, 2.552581]	[4.257436, 7.198049]	[8.983496, 22.42205]	[19.22557, 77.17473]	[0.064815, 0.682379]	[1.022641, 1.161056]	[1.060677, 1.489517]
				[1.991347, 2.400354]	[4.022199, 6.28886]	[8.235853, 17.98276]	[17.08652, 56.13042]	[0.056736, 0.527161]	[1.020971, 1.140246]	[1.056152, 1.419235]
			[1.7,2.7]	[1.966076, 2.347823]	[3.916789, 5.956809]	[7.902665, 16.33094]	[16.14081, 48.38371]	[0.051334, 0.444536]	[1.019479, 1.123287]	[1.052119, 1.363552]
				[1.894836, 2.153215]	[3.634783, 5.001715]	[7.055468, 12.54589]	[13.85253, 34.02125]	[0.04438, 0.36538]	[1.018141, 1.121561]	[1.048509, 1.359917]
			[1.8,2.8]							
			[1.9,2.9]							

Table 1 presents the different values of statistical moments (mean, variance, skewness, kurtosis) for the NHWIW distribution with changes in the upper and lower boundary parameters of the unspecified variables. The values show that the moments of the distribution change significantly when the boundaries are modified. Skewness and kurtosis are used to assess the shape of the distribution. The mean expresses the expected center of the distribution and changes with the variation of the ambiguous parameters. The variance. High values indicate that the distribution can handle disparate and scattered data, while it indicates the level of concentration in the values. Low values indicate that the distribution can handle data with a wide range. Low values indicate that the distribution is balanced, which enhances its suitability to realistic data.

3.3 Moment Generating Function

Let X_N be any Neutrosophic random variable, then the Moment Generating Function (MGF) for NHWIW distribution is given by form [17] , [18] :

$$M_x(t) = E(e^{tx}) = \int_{-\infty}^{\infty} e^{tx} f(x_N) dx$$

From equation (14) and using exponential expansion we get a final form:

$$M_x(t) = \sum_{r=0}^{\infty} \frac{t^r}{r!} \left[\frac{\Gamma(\frac{n-p_N}{PN})}{p_N q_N \frac{n-p_N}{PN}} \left[\frac{M}{(2ib_N + 2b_N + j + k) \frac{n-p_N}{PN}} - \frac{N}{(2ib_N + 2b_N + j + z) \frac{n-p_N}{PN}} \right] \right] \quad (21)$$

3.4 Quantile function of NHWIW distribution

The Quantile function has a major role in application of Monte Carlo simulation and represents the inverse of NCDF function $Q(u) = F^{-1}(u)$ [19], which is obtained for the NHWIW distribution as follows:

$$Q(u) = \left[\frac{\log \left[\frac{\Theta}{\Theta + W_{-1}(\Theta) e^{\Theta}} \right]}{q_N} \right]^{\frac{-1}{b_N}}, \Theta = \left[\frac{-\log(1-u)}{a_N} \right]^{\frac{1}{b_N}} \quad (22)$$

Table 2 expresses a set of intervals of the Quintile function values of NHWIW for different intervals as follow:

Table 2: Quintile function values of NHWIW for different intervals

s_N	(a_N, b_N, q_N, p_N)				
	[0.4, 0.8],[1.1, 1.9] [0.4, 1.4],[1.2, 1.7]	[0.6, 1.6],[1, 1.5] [0.4, 1.4],[1, 1.5]	[0.5,1.5],[1.1,1.6] [0.51.5],[1.1,1.6]	[1.2,1.7],[1,1.5] [0.8,1.8],[1.2,1.7]	[1.1,1.7],[1.9,1.9] [0.7,1.7],[1.5,2]
0.1	[0.5880204,1.50829]	[0.407121, 1.194348]	[0.622559, 1.33252]	[0.669702, 3.3304]	[0.9420654, 3.28916]
0.2	[0.8511505,1.75326]	[0.6020268, 1.40746]	[0.898051, 1.54565]	[0.86103, 1.38635]	[1.1027903, 1.56190]
0.3	[1.1616532, 1.95887]	[0.8308531, 1.59006]	[1.214072, 1.72384]	[1.047516, 1.5928]	[1.2370894, 1.68682]
0.4	[1.5748618, 2.15671]	[1.1324191, 1.76916]	[1.621220, 1.89484]	[1.253187, 1.7644]	[1.3657090, 1.80121]
0.5	[2.1794962, 2.36248]	[1.5680264, 1.95911]	[2.07237, 2.194616]	[1.499006, 1.9283]	[1.4988826, 1.91481]
0.6	[2.590992, 3.165274]	[2.174631, 2.267291]	[2.26927, 3.086756]	[1.816802, 2.0979]	[1.6459544, 2.03529]
0.7	[2.863979, 5.033473]	[2.43857, 3.5705340]	[2.50435, 4.680039]	[2.270645, 2.2853]	[1.8204959, 2.17226]
0.8	[3.226530, 9.576866]	[2.800418, 6.695981]	[2.816750, 8.25737]	[2.50855, 3.02963]	[2.0505678, 2.34410]
0.9	[3.821119, 28.62166]	[3.423055, 19.87242]	[3.33042, 21.51546]	[2.80425, 4.80523]	[2.4236659, 2.60524]

Table 2 presents the values of the quantile function for the NHWIW distribution for different probability intervals. The different values reflect changes in the range of the data distribution based on the probability. Narrower intervals show greater accuracy in representing the data, while wider intervals reflect greater flexibility. Small values indicate the distribution's ability to provide accurate boundaries for the intervals.

3.5 Renyi entropy

The Renyi entropy is given by form [20], [21] :

$$I_R(c)_{NHWIW} = \frac{1}{1-c} \log \int_0^\infty f(x_N)^c dx$$

$$I_R(c)_{NHWIW} = \frac{1}{1-c} \log \int_0^\infty (Mx_N^{-(p_N+1)} e^{-(2ib_N+2b_N+j+k)q_Nx_N^{-p_N}} - Nx_N^{-(p_N+1)} e^{-(2ib_N+2b_N+j+z)q_Nx_N^{-p_N}})^c dx$$

Then the final form:

$$II_R(c)_{NHWIW} = \frac{1}{1-c} \log \left[R \cdot \Gamma \left(\frac{1-c(p_N+1)}{p_N} \right) \right]$$

$$R = \sum_{n=0}^c (-1)^n \binom{c}{n} M^{c-n} N^n \frac{1}{p_N q^{\frac{-c(p_N+1)}{p_N} + \frac{1}{p_N} (2icb_N + 2cb_N + cj + ck - nk + nz)} \frac{-c(p_N+1)}{p_N} + \frac{1}{p_N}} \quad (23)$$

4. Estimation

4.1 maximum likelihood estimation

The NHWIW distribution parameters are determine using maximum likelihood estimation approach. For sample $x_{N1}, x_{N2}, \dots, x_{Nm}$ the random sample [22], [23], [24], [25], [26] The NHWIW distribution NPDF is followed:

$$L(\theta_N, x_{N_i}) = \prod_{i=1}^m q_N p_N x_{N_i}^{-(p_N+1)} e^{-q_N x_{N_i}^{-p_N}} \left[\frac{e^{-q_N x_{N_i}^{-p_N}}}{1 - e^{-q_N x_{N_i}^{-p_N}}} - \log \left(1 - e^{-q_N x_{N_i}^{-p_N}} \right) \right]$$

$$\times \left[-e^{-q_N x_{N_i}^{-p_N}} \cdot \log \left(1 - e^{-q_N x_{N_i}^{-p_N}} \right) \right]^{b_N-1} e^{\left(-a_N \left[-e^{-q_N x_{N_i}^{-p_N}} \cdot \log \left(1 - e^{-q_N x_{N_i}^{-p_N}} \right) \right]^{b_N} \right)}$$

we compute the log- likelihood:

$$\begin{aligned}
L = & m \log(q_N) + m \log(p_N) - (p_N - 1) \sum_{i=1}^m \log(x_{N_i}) - \sum_{i=1}^m q_N x_{N_i}^{-p_N} \\
& + \sum_{i=1}^m \log \left[\frac{e^{-q_N x_{N_i}^{-p_N}}}{1 - e^{-q_N x_{N_i}^{-p_N}}} - \log \left(1 - e^{-q_N x_{N_i}^{-p_N}} \right) \right] \\
& + (b_N - 1) \sum_{i=1}^m \log \left[-e^{-q_N x_{N_i}^{-p_N}} \cdot \log \left(1 - e^{-q_N x_{N_i}^{-p_N}} \right) \right] \\
& - a_N \sum_{i=1}^m \left[-e^{-q_N x_{N_i}^{-p_N}} \cdot \log \left(1 - e^{-q_N x_{N_i}^{-p_N}} \right) \right]^{b_N}
\end{aligned} \tag{24}$$

4.2 Least square estimation

The following formula can be used to estimate a parameters using the Least square estimation (LSE) method [27], [28]:

$$\varphi(\theta_N) = \sum_{i=1}^m \left[1 - e^{\left(-a_N \left[-e^{-q_N x_{N_i}^{-p_N}} \cdot \log \left(1 - e^{-q_N x_{N_i}^{-p_N}} \right) \right]^{b_N} \right) - \frac{1}{n+1}} \right]^2 \tag{25}$$

4.3 Weighted Least square estimation

The following formula can be used to estimate a parameters using the Weighted Least square estimation (WLSE) method [29]:

$$W(\theta_N) = \sum_{i=1}^m \frac{(n+1)^2 (n+2)}{i(n-i+1)} \left[1 - e^{\left(-a_N \left[-e^{-q_N x_{N_i}^{-p_N}} \cdot \log \left(1 - e^{-q_N x_{N_i}^{-p_N}} \right) \right]^{b_N} \right) - \frac{i}{n+1}} \right]^2 \tag{26}$$

Estimates of the parameters for the three previously described methods may be obtained by finding the partial derivative of four parameters and setting it to zero. Computer technologies such as the R language are used since it is difficult to find these values in numerical solutions.

5. Simulation

To demonstrate the efficiency of the estimation of NHWIW distribution, a Monte Carlo simulation is conducted for the three methods presented in a fourth section, where the sizes of generated samples were relied upon at $n=50, 100, 150$, and 200 , to 1000 with the calculation of the values of mean square error (MSE), and its root (RMSE) [30], and the calculation of the bias in the estimated parameters, where Table 3 shows the simulation values as follows:

Table 3 : Monte Carlo simulations conducted for the NHWIW

$r_N = [0.4, 1.4], \quad u_N = [0.5, 1.5], \quad b_N = [0.7, 1.7], \quad c_N = [0.8, 1.8]$					
N	Est.	Ess. Par.	MLE	LSE	WLSE
50	Mean	\widehat{a}_N	[2.71415, 3.8807]	[1.81833, 2.2308]	[2.18454, 2.62480]
		\widehat{b}_N	[2.14886, 3.4619]	[2.00585, 2.14894]	[2.28999, 2.41772]
		\widehat{q}_N	[1.98333, 2.030004]	[1.68494, 2.65528]	[1.49501, 2.36023]
		\widehat{p}_N	[1.78887, 2.01288]	[1.74966, 2.63342]	[1.46794, 2.40224]
	MSE	\widehat{a}_N	[22.2105, 25.1223]	[1.40892, 1.91622]	[2.77863, 3.67925]
		\widehat{b}_N	[2.20026, 5.72680]	[0.44948, 1.0952]	[0.98082, 1.91795]
		\widehat{q}_N	[3.88680, 5.14601]	[0.96725, 2.38973]	[1.04593, 2.03972]
		\widehat{p}_N	[1.26702, 2.03484]	[0.96801, 1.11202]	[0.64689, 0.95739]
	RMSE	\widehat{a}_N	[4.7128, 5.01222]	[1.18698, 1.38427]	[1.66692, 1.91813]
		\widehat{b}_N	[1.48332, 2.3930]	[0.67043, 1.04654]	[0.99036, 1.38490]
		\widehat{q}_N	[1.97149, 2.26848]	[0.98348, 1.54587]	[1.02270, 1.42818]
		\widehat{p}_N	[1.12562, 1.42648]	[0.98387, 1.05452]	[0.80430, 0.97846]
	Bias	\widehat{a}_N	[1.314151, 1.9807]	[0.33082, 0.41833]	[0.72480, 0.78454]
		\widehat{b}_N	[0.64886, 1.4619]	[0.14894, 0.50585]	[0.41772, 0.78999]
		\widehat{q}_N	[0.26999, 0.28333]	[0.015057, 0.35528]	[0.06023, 0.20498]
		\widehat{p}_N	[0.01112, 0.48711]	[0.05033, 0.13342]	[0.33205, 0.09775]
100	Mean	\widehat{a}_N	[2.31534, 3.4201]	[1.85065, 2.25892]	[1.96960, 2.52434]
		\widehat{b}_N	[1.6431, 2.78082]	[1.95885, 2.19012]	[1.95962, 2.37243]
		\widehat{q}_N	[2.04081, 2.10196]	[1.54758, 2.51858]	[1.44971, 2.36524]
		\widehat{p}_N	[1.80824, 2.09797]	[1.62019, 2.56520]	[1.48308, 2.427468]
	MSE	\widehat{a}_N	[6.10985, 16.8563]	[1.28531, 1.92259]	[1.61472, 2.84221]
		\widehat{b}_N	[0.52321, 2.10325]	[0.42942, 0.75540]	[0.67244, 0.73143]
		\widehat{q}_N	[1.90643, 2.19297]	[0.51869, 1.71932]	[0.362008, 1.65003]
		\widehat{p}_N	[0.70767, 0.72883]	[0.52677, 0.82273]	[0.32772, 0.84436]
	RMSE	\widehat{a}_N	[2.47181, 4.10565]	[1.13371, 1.38657]	[1.27071, 1.68588]
		\widehat{b}_N	[0.72333, 1.45026]	[0.65530, 0.86914]	[0.82002, 0.85523]

		\widehat{q}_N	[1.38073, 1.48086]	[0.72020, 1.31123]	[0.60167, 1.28453]
		\widehat{p}_N	[0.84123, 0.85372]	[0.72579, 0.90704]	[0.57247, 0.91889]
	Bias	\widehat{a}_N	[0.91534, 1.52011]	[0.35892, 0.45065]	[0.56960, 0.62434]
		\widehat{b}_N	[0.14319, 0.78082]	[0.19012, 0.45885]	[0.37243, 0.45962]
		\widehat{q}_N	[0.25918, 0.40196]	[0.15241, 0.21858]	[0.06524, 0.25028]
		\widehat{p}_N	[0.00824, 0.40202]	[0.065207, 0.17980]	[0.07253, 0.31691]
150	Mean	\widehat{a}_N	[2.39295, 2.59663]	[1.69799, 2.28928]	[1.84874, 2.51742]
		\widehat{b}_N	[1.48475, 2.38927]	[1.84251, 2.22170]	[1.82141, 2.36527]
		\widehat{q}_N	[2.32242, 2.26305]	[1.56125, 2.38488]	[1.55411, 2.22098]
		\widehat{p}_N	[1.83872, 2.33146]	[1.62906, 2.47499]	[1.61889, 2.31876]
	MSE	\widehat{a}_N	[5.19190, 6.34498]	[0.76663, 1.61336]	[1.38675, 2.57476]
		\widehat{b}_N	[0.36447, 0.76441]	[0.41032, 0.45602]	[0.17093, 0.63993]
		\widehat{q}_N	[1.85714, 2.85060]	[0.39942, 0.41032]	[0.39838, 1.05506]
		\widehat{p}_N	[0.30307, 0.49069]	[0.29310, 1.01496]	[0.40961, 0.52287]
	RMSE	\widehat{a}_N	[2.27857, 2.51892]	[0.87557, 1.27018]	[0.27180, 1.60460]
		\widehat{b}_N	[0.60371, 0.8743]	[0.64056, 0.67529]	[0.63118, 0.79996]
		\widehat{q}_N	[1.36277, 1.68837]	[0.63200, 1.00745]	[0.64001, 1.02716]
		\widehat{p}_N	[0.55052, 0.70049]	[0.54139, 0.75893]	[0.52135, 0.72310]
	Bias	\widehat{a}_N	[0.69663, 0.99295]	[0.38928, 1.17760]	[0.44874, 0.61742]
		\widehat{b}_N	[0.015245, 0.38927]	[0.22170, 0.29799]	[0.32141, 0.36527]
		\widehat{q}_N	[0.036943, 0.62242]	[0.08488, 0.34251]	[0.07901, 0.14588]
		\widehat{p}_N	[0.03872, 0.16853]	[0.025003, 0.13874]	[0.18110, 0.18123]
200	Mean	\widehat{a}_N	[2.56066, 2.69271]	[1.65731, 2.22683]	[1.74361, 2.39868]
		\widehat{b}_N	[1.428845, 2.33717]	[1.77586, 2.16486]	[1.70362, 2.29352]
		\widehat{q}_N	[2.19764, 2.30402]	[1.61052, 2.37936]	[1.65621, 2.25097]
		\widehat{p}_N	[1.77657, 2.30401]	[1.68037, 2.492011]	[1.66439, 2.36508]
	MSE	\widehat{a}_N	[6.98059, 8.23299]	[0.73184, 1.36073]	[0.941745, 2.21622]
		\widehat{b}_N	[0.25652, 0.56396]	[0.31173, 0.35832]	[0.28724, 0.46309]
		\widehat{q}_N	[1.12979, 2.25599]	[0.351277, 0.86185]	[0.39563, 1.00733]

		\widehat{p}_N	[0.15658, 0.33635]	[0.29343, 0.49330]	[0.19297, 0.43221]
	RMSE	\widehat{a}_N	[2.64208, 2.86931]	[0.85547, 1.16650]	[0.97043, 1.48869]
		\widehat{b}_N	[0.506478, 0.75097]	[0.55833, 0.59860]	[0.53595, 0.68050]
		\widehat{q}_N	[1.06291, 1.50199]	[0.59268, 0.92836]	[0.62899, 1.00366]
		\widehat{p}_N	[0.39571, 0.57996]	[0.54169, 0.70235]	[0.43929, 0.65742]
	Bias	\widehat{a}_N	[0.79271, 1.16066]	[0.25731, 0.32683]	[0.34361, 0.49868]
		\widehat{b}_N	[0.071154, 0.33717]	[0.16486, 0.27586]	[0.20362, 0.29352]
		\widehat{q}_N	[0.10235, 0.60402]	[0.07936, 0.08947]	[0.043784, 0.04902]
		\widehat{p}_N	[0.023423, 0.19598]	[0.00798, 0.11962]	[0.13491, 0.13560]

Table 3 shows the lowest MSE and RMSE values for the MLE method, indicating that it is the most accurate. Bias is low in all methods, reflecting the quality of the estimates. MLE (Maximum Likelihood Estimation) showed superior performance, especially with large sample sizes, making it the best fit for the distribution. LSE and WLSE perform well with small sample sizes but are less accurate as the size increases.

6. Application

To demonstrate the extent of the quality of the distribution and its efficiency in practical applications, the practical aspect is an important aspect to show this, as in this part a practical applications is conducted on real neutrosophic data that is used [31], with a comparison of the results obtained between the proposed distribution and six other distribution represented by:

- Neutrosophic beta inverse Wiebull (NBeIW)
- Neutrosophic Kumaraswamy inverse Wiebull (NKuIW)
- Neutrosophic Exponented generalized inverse Wiebull (NEGIW)
- Neutrosophic log-Gamma inverse Wiebull (NLGamIW)
- Neutrosophic Gompertz inverse Wiebull (NGoIW)
- Neutrosophic inverse Wiebull (NIW)

This comparison required the use of four information criteria, which are (AIC [19], CAIC [32], [33], HQIC [34], [35], , and BIC [36]) in addition to four statistical measures, which are (Kolmogorov-Smirnov (KS), Anderson-Darling (A), Cramér-von Mises (W), and p-value [37], [38]).

Data set-1

The first represented by mortality data for children under five years of age [31].

Var	N	Mean	SD	Median	Trimmed	Mad	Min	Max	Range	SK	KU	Se
1	26	[15.76, 16.76]	[7.27, 7.37]	[14.21, 15.32]	[15.22, 16.26]	[7.87, 8.27]	[6.81, 7.98]	[31.53, 31.81]	[23.83, 24.72]	0.56	[-0.96, -0.93]	[1.43, 1.45]

The results of the criteria for the distributions were displayed in Table 4, while Table 5 expressed the value of the statistical measures, while Table 6 displayed the values of the estimated parameters for each distribution.

Table 4. results of the criteria for the distributions

Dist.	-2L	AIC	CAIC	BIC	HQIC
Hwiw	[85.40969, 85.5326]	[178.8194, 179.06]	[180.7241, 180.97]	[183.851, 184.097]	[180.268, 180.514]
BeIW	[86.0416, 87.6206]	[180.089, 183.302]	[181.994, 185.207]	[185.122, 188.334]	[181.538, 184.751]
KuIW	[86.1110, 86.5381]	[180.234, 181.085]	[182.139, 182.990]	[185.267, 186.118]	[181.683, 182.535]

EGIW	[86.2713,86.31197]	[180.564,180.649]	[182.469,182.554]	[185.597,185.681]	[182.014,182.098]
LGamIW	[85.63031,85.8919]	[179.260,179.785]	[181.165,181.690]	[184.293,184.818]	[180.709,181.235]
GoIW	[87.0561, 87.2476]	[182.112, 182.495]	[184.017, 184.400]	[187.144, 187.527]	[183.561, 183.944]
IW	[96.1148, 104.916]	[196.24, 213.9324]	[196.761, 214.454]	[198.756, 216.448]	[196.9645, 214.65]

From Table 4, NHWIW achieved the lowest values for most of the criteria, indicating its high fit to the data. The IW distribution was the least efficient due to its high values, as low values of the criteria enhance the stability of the distribution when comparing models with different complexities .

Table 5. value of the statistical measures

Dist.	W	A	K-S	p-value
HWIW	[0.03774283,0.0473640]	[0.313303,0.341763]	[0.103911, 0.106321]	[0.900544,0.9142441]
BeIW	[0.04349193,0.0582771]	[0.3464307,0.40208]	[0.088246, 0.119375]	[0.8107124,0.9765447]
KuIW	[0.04234476,0.0551776]	[0.341253,0.386771]	[0.081400, 0.094516]	[0.9572919,0.9896749]
EGIW	[0.04774075,0.0614708]	[0.370513,0.420625]	[0.082911, 0.090155]	[0.9714649,0.9874063]
LGamIW	[9.373411,9.426508]	[52.44084, 52.46839]	[0.9483765, 0.94545]	5.551115e-16
GoIW	[0.0627775,0.06469447]	[0.461921, 0.464890]	[0.12449, 0.1460138]	[0.5858848,0.7699224]
IW	[0.04225913,0.0575322]	[0.339643,0.397695]	[0.227421, 0.364774]	[0.001313552,0.1155558]

Table 5 shows that NHWIW achieved the highest p-value and lowest W and A values, reflecting its high fit to the data. Other distributions showed poorer performance compared to NHWIW .

Table 6. Estimator value interval for parameters by MLE

Dist.	\hat{a}_N	\hat{b}_N	\hat{q}_N	\hat{p}_N
HWIW	[0.013462, 0.0280360]	[3.3452479,3.5492839]	[7.5562016, 12.242277]	[1.918304,1.948398]
BeIW	[5.941547,6.880572]	[3.479567, 3.568686]	[6.136480,7.531162]	[0.966692,1.129877]
KuIW	[5.85491, 5.858095]	[4.048258,4.141243]	[6.026946, 6.382458]	[1.111050,1.119379]
EGIW	[3.8376168, 4.5794689]	[6.6182216, 7.6331922]	[7.205414,7.2723604]	[0.789913,0.848330]
LGamIW	[7.337486, 8.415236]	[5.380997, 6.665243]	[7.4194373, 8.495675]	[1.17855,1.194137]
GoIW	[0.006215729,0.00781413]	[1.4543039, 1.4894439]	[1.9634420,1.9943284]	[1.486703,1.493761]
IW	---	---	[6.1610960,13.242297]	[0.8713852,1.14196]

Table 6 shows the estimated intervals of the main parameters of the NHWIW distribution compared to other distributions (such as BeIW, KuIW, etc.) using the maximum likelihood estimation (MLE) method for the first dataset. The NHWIW distribution showed narrow intervals of the parameters, indicating the stability of the estimates, while other distributions such as BeIW and KuIW showed greater variation in the intervals of the parameters, which may indicate their poor efficiency compared to NHWIW.

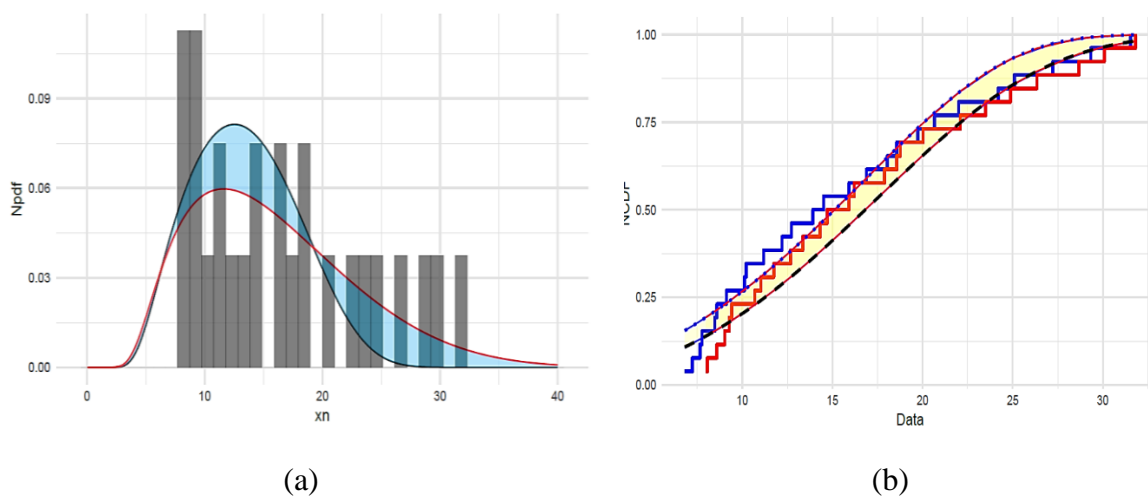


Figure 3: (a) Fitting pdfs NHWIW with histogram data set, (b) Empirical Fitted CDFs NHWIW with data set

Figure 3 (a) shows how well the probability density function (PDF) of the NHWIW distribution matches the actual data for the first set. The distribution shows a strong fit with the structural distribution of the data, with the curve following the shape of the experimental data. This indicates the ability of NHWIW to accurately and flexibly represent real data. Figure 3 (b) shows the empirical CDF compared with the theoretical CDF. The strong fit between the distributions reflects the efficiency of NHWIW in representing the cumulative probability of the data.

Data set-2

The second is COVID-19 in Netherlands for thirty days [39]

Var	N	Mean	SD	Median	Trimmed	Mad	Min	Max	Range	SK	KU	Se
1	30	[6.14, 6.36]	[3.51, 3.56]	[5.37, 5.64]	[5.79, 6]	[2.72, 2.85]	[1.27, 1.34]	[14.92, 15.66]	[13.64, 14.33]	[0.8, 0.82]	[-0.18, 0.03]	[0.64, 0.65]

Table 7. results of the criteria for the distributions

Dist.	-2L	AIC	CAIC	BIC	HQIC
HWIW	[76.43589, 77.09943]	[160.8718, 162.1989]	[162.4718, 163.7989]	[166.4766, 167.8036]	[162.6648, 163.9919]
BeIW	[76.48142, 77.32048]	[160.9628, 162.641]	[162.5628, 164.241]	[166.5676, 168.2457]	[162.7559, 164.434]
KuIW	[76.59179, 77.27442]	[161.1836, 162.5488]	[162.7836, 164.1488]	[166.7884, 168.1536]	[162.9766, 164.3419]
EGIW	[78.25885, 79.37512]	[164.5248, 166.7519]	[166.1248, 168.3519]	[170.1296, 172.3567]	[166.3179, 168.545]
LGamIW	[76.56406, 77.31349]	[161.1281, 162.627]	[162.7281, 164.227]	[166.7329, 168.2318]	[162.9211, 164.42]
GoIW	[77.94244, 79.25779]	[163.9185, 166.5239]	[165.5185, 168.1239]	[169.5233, 172.1287]	[165.7115, 168.3169]
IW	[80.90795, 81.86503]	[165.8159, 167.7301]	[166.2603, 168.1745]	[168.6183, 170.5325]	[166.7124, 168.6266]

Table 7 compares NHWIW with other distributions using informative criteria such as AIC, BIC, CAIC, and HQIC for the second dataset. NHWIW distribution had the lowest values for all criteria compared to other distributions. Other distributions, such as IW and GoIW, showed high values, indicating their poor performance in fitting the data.

Table 8. value of the statistical measures

Dist.	W	A	K-S	p-value
HWIW	[0.0233792, 0.0241559]	[0.1664448, 0.1756536]	[0.070432, 0.0770078]	[0.9881955, 0.99588]
BeIW	[0.02499, 0.02863132]	[0.185047, 0.2137449]	[0.08221554, 0.085797]	[0.96637, 0.977128]
KuIW	[0.0217852, 0.0257614]	[0.1728076, 0.1938708]	[0.0685944, 0.076441]	[0.9891058, 0.9971004]
EGIW	[0.0612384, 0.082723]	[0.4535322, 0.57210]	[0.1106459, 0.114588]	[0.784162, 0.8173854]
LGamIW	[9.976712, 10.01212]	[60.25735, 60.30363]	[0.9854649, 0.987072]	1.221245e-15
GoIW	[0.0474965, 0.0719870]	[0.3674051, 0.5081394]	[0.0990987, 0.105585]	[0.8571036, 0.9018158]
IW	[0.1411036, 0.1590753]	[0.940501, 1.032139]	[0.1517456, 0.153257]	[0.4380138, 0.4503734]

Table 8 NHWIW had the highest p-value and the lowest values for W, A, and K-S, indicating that this distribution is superior to other distributions and provides an excellent fit to the data and there is no evidence to reject the hypothesis of the distribution. Distributions such as IW showed high values for the criteria, reflecting their poor representation of the data.

Table 9. Estimator value interval for parameters by MLE

Dist.	\hat{a}_N	\hat{b}_N	\hat{q}_N	\hat{p}_N
Hwiw	[5.837801, 6.1923656]	[4.02133, 4.2564547]	[0.8979603, 0.91083]	[0.3596752, 0.37002]
BeIW	[0.326699, 0.5555232]	[23.3992253, 26.28143]	[13.330017, 19.726555]	[0.642861, 0.746774]
KuIW	[3.5882782, 9.1795205]	[65.592337, 74.372615]	[1.0179446, 2.7114185]	[0.421744, 0.426545]
EGIW	[4.458458, 5.3694787]	[2.5368242, 2.864744]	[3.8798198, 4.1462443]	[0.652446, 0.696044]
LGamIW	[0.4306123, 0.5999024]	[21.714107, 25.562351]	[12.796964, 15.607732]	[0.624186, 0.698871]
GoIW	[7.8853573, 8.9050606]	[0.9466685, 1.2100697]	[7.3119639, 8.3552368]	[0.706303, 0.712820]
IW	---	---	[7.869781, 8.576315]	[1.553003, 1.564124]

Table 9 NHIW distribution showed more accurate and stable estimation intervals compared to other distributions. Distributions such as GoIW and BeIW showed wide variations in estimates.

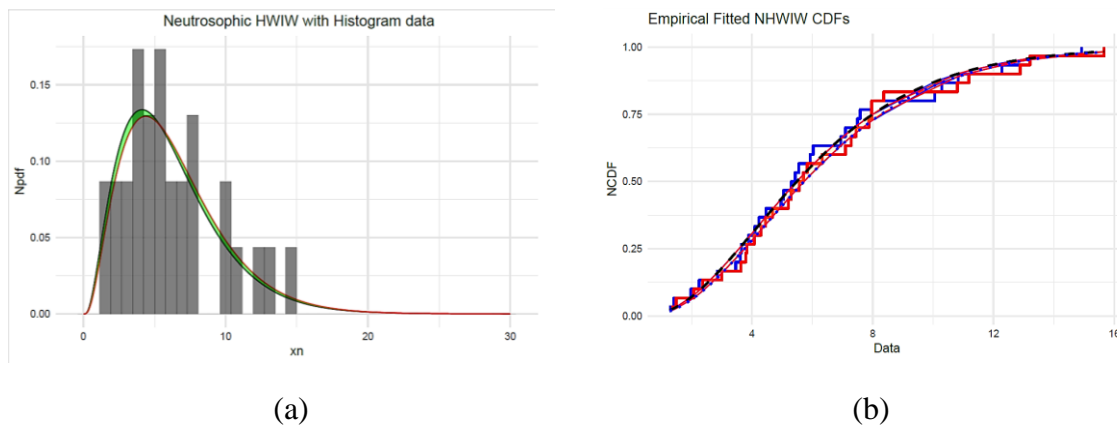


Figure 4: (a) Fitting pdfs NHIW with histogram data set2, (b) Empirical Fitted CDFs NHIW with data set2

Figure 4 (a) shows how well the PDF of the NHIW distribution fits the real data of the second group (COVID-19 data). The curve shows that NHIW captures the main characteristics of the data. The good fit indicates the flexibility of the distribution in dealing with different types of data. Figure 4 (b) compares the empirical CDF with the theoretical NHIW CDF for the second group of data. The close fit between the two curves reflects the accuracy of NHIW in predicting the cumulative probabilities of the data. This enhances the reliability of the distribution and its relevance to real-world data such as COVID-19.

Conclusion

The NHIW distribution showed high efficiency in representing real data compared to 6 other distributions. NHIW outperformed in information criteria (AIC, BIC, CAIC, HQIC) and statistical criteria (K-S, W, A, p-value). The distribution has great flexibility that enables it to adapt to uncertain or ambiguous data using neutrosophic parameters. The maximum likelihood method (MLE) was the most accurate in estimating the parameters, indicating the stability of the model. Simulations proved that NHIW provides accurate estimates even with small or medium sample sizes. The distribution is suitable for representing real data such as under-five mortality and COVID-19 data in the Netherlands. NHIW showed high agreement with experimental data as shown in the figures. NHIW represents an important step in applying neutrosophic logic in statistical modeling and bridges the research gap in integrating ambiguous data with complex mathematical distributions.

References

- [1] A. Alzaatreh, C. Lee and F. Famoye, "A new method for generating families of continuous distributions," *Metron*, p. 63–79, 71 2013.
- [2] S. Hussain, M. U. Hassan, M. S. Rashid and R. Ahmed, "Families of Extended Exponentiated Generalized Distributions and Applications of Medical Data Using Burr III Extended Exponentiated Weibull Distribution,"

Mathematics, p. 3090, 14 11 2023.

- [3] A. B. Odeyale, S. U. Gulumbe, U. Umar and K. O. Aremu, "New New Odd Generalized Exponentiated Exponential-G Family of Distributions," *UMYU Scientifica*, pp. 56-64, 4 2 2023.
- [4] S. Hussain, M. U. Hassan, M. S. Rashid and R. Ahmed, "Families of Extended Exponentiated Generalized Distributions and Applications of Medical Data Using Burr III Extended Exponentiated Weibull Distribution," *Mathematics*, p. 3090, 14 11 2023.
- [5] N. A. Noori, A. A. Khalaf and M. A. Khaleel, "A New Generalized Family of Odd Lomax-G Distributions Properties and Applications," *Advances in the Theory of Nonlinear Analysis and Its Application*, pp. 1-16, 4 7 2023.
- [6] I. A. Sadiq, S. I. Doguwa, A. Yahaya and J. Garba, "New Generalized Odd Fréchet-G (NGOF-G) Family of Distribution with Statistical Properties and Applications," *UMYU Scientifica*, pp. 100-107, 3 2 2023.
- [7] Y. Y. Abdelall, A. S. Hassan and E. M. Almetwally, "A new extention of the odd inverse Weibull-G family of distributions: Bayesian and non-Bayesian estimation with engineering applications," *Computational Journal of Mathematical and Statistical Sciences*, pp. 359-388, 2 3 2024.
- [8] A. I. Ishaq, U. Panitanarak, A. A. Alfred, A. A. Suleiman and H. Daud, "The Generalized Odd Maxwell-Kumaraswamy Distribution: Its Properties and Applications," *Contemporary Mathematics*, pp. 711-742, 2024.
- [9] G. A. Mahdi, M. A. Khaleel, A. M. Gemeay, M. Nagy, A. H. Mansi, M. M. Hossain and E. Hussam, "A new hybrid odd exponential- Φ family: Properties and applications," *AIP Advances*, 4 14 2024.
- [10] N. A. Noori and M. A. khaleel, "Estimation and Some Statistical Properties of the hybrid Weibull Inverse Burr Type X Distribution with Application to Cancer Patient Data," *Iraqi Statisticians Journal*, pp. 8-29, 2 1 2024.
- [11] N. A. Noori, A. A. Khalaf and M. A. Khaleel, "A new expansion of the Inverse Weibull Distribution: Properties with Applications," *Iraqi Statisticians Journal*, pp. 52-62, 1 1 2024.
- [12] N. A. Noori, "Exploring the Properties, Simulation, and Applications of the Odd Burr XII Gompertz Distribution," *Advances in the Theory of Nonlinear Analysis and Its Application*, pp. 60-75, 4 7 2023.
- [13] A. L. Solomon Sarpong and S. Nasiru, "Odd Chen-G family of distributions," *Annals of Data Science*, pp. 369-391, 2 9 2022.
- [14] M. M. Alanaz and Z. Y. Algamal, "Neutrosophic exponentiated inverse Rayleigh distribution: Properties and Applications," *International Journal of Neutrosophic Science*, pp. 36-43, 4 21 2023.
- [15] M. M. Alanaz, M. Y. Mustafa and Z. Y. Algamal, "Neutrosophic Lindley distribution with application for Alloying Metal Melting Point," *International Journal of Neutrosophic Science*, pp. 65-71, 4 21 2023.
- [16] A. A. Khalaf, M. Q. Ibrahim and N. A. Noori, "[0,1]Truncated Exponentiated Exponential Burr type X Distribution with Applications," *Iraqi Journal of Science*, pp. 4428-4440, 8 65 2024.
- [17] H. J. Gómez, K. I. Santoro, I. B. Chamorro, O. Venegas, D. I. Gallardo and H. W. Gómez, "A Family of Truncated Positive Distributions," *Mathematics*, p. 4431, 21 11 2023.
- [18] A. A. Khalaf and M. khaleel, "The New Strange Generalized Rayleigh Family: Characteristics and Applications to COVID-19 Data," *Iraqi Journal For Computer Science and Mathematics*, vol. 5, no. 3, pp. 92-107, 2024.
- [19] M. A. Khaleel, P. E. Oguntunde, J. N. Al Abbasi, N. A. Ibrahim and M. H. AbuJarad, "The Marshall-Olkin Topp Leone-G family of distributions: A family for generalizing probability models," *Scientific African*, p. e00470, 8 2020.
- [20] K. H. Al-Habib, M. A. Khaleel and H. Al-Mofleh, "A new family of truncated nadarajah-haghighi-g properties with real data applications," *Tikrit Journal of Administrative and Economic Sciences*, p. 2, 61 19 2023.
- [21] L. Handique, M. A. ul Haq and C. Subrata, "Generalized Modified exponential-G family of distributions: its properties and applications," *International Journal of Mathematics and Statistics*, pp. 1-17, 1 21 2020.
- [22] A. Z. Afify, H. Yousof and S. Nadarajah, "The beta transmuted-H family for lifetime data," *Statistics and its Interface*, pp. 505-520, 3 10 2017.
- [23] F. Chipepa, B. O. Oluyede and B. Makubate, "A New Generalized Family of Odd Lindley-G Distributions With Application," *International Journal of Statistics and Probability*, pp. 1-23, 6 8 2019.
- [24] F. A. Bhatti, G. G. Hamedani, M. C. Korkmaz, G. M. Cordeiro, H. M. Yousof and M. Ahmad, "On Burr III Marshal Olkin family: development, properties, characterizations and applications," *Journal of Statistical Distributions and Applications*, pp. 1-21, 6 2019.
- [25] K. H. Habib, M. A. Khaleel, H. Al-Mofleh, P. E. Oguntunde and S. J. Adeyeye, "Parameters Estimation for the [0, 1] Truncated Nadarajah Haghighi Rayleigh Distribution," *Scientific African*, p. e02105, 2024.
- [26] J. Farrukh, M. A. Nasir, M. H. Tahir and N. H. Montazeri, "The odd Burr-III family of distributions," *Journal of Statistics Applications and Probability*, pp. 105-122, 1 6 2017.
- [27] N. S. Khalaf, A. Hameed, K. Moudher, M. A. Khaleel and Z. M. Abdullah, "the Topp Leone flexible Weibull distribution: an extension of the flexible Weibull distribution," *International Journal of Nonlinear Analysis and*

Applications, pp. 2999-3010, 1 13 2022.

- [28] A. Khaoula, N. Seddik-Ameur, A. A. Abd El-Baset and M. A. Khaleel, "The Topp-Leone Extended Exponential Distribution: Estimation Methods and Applications," *Pakistan Journal of Statistics and Operation Research*, pp. 817-836, 4 18 2022.
- [29] H. Sharqa , M. Ahsan-ul-Haq, J. Zafar and M. A. Khaleel, "Unit Xgamma Distribution: Its Properties, Estimation and Application: Unit-Xgamma Distribution," *Proceedings of the Pakistan Academy of Sciences: A. Physical and Computational Sciences*, pp. 15-28, 1 59 2022.
- [30] S. Naz, L. A. Al-Essa, H. S. Bakouch and C. Chesneau, "A transmuted modified power-generated family of distributions with practice on submodels in insurance and reliability," *Symmetry* , p. 1458, 7 15 2023.
- [31] Z. Khan, M. M. A. Almazah, O. H. Odhah and H. M. Alshanbari, "Generalized Pareto Model: Properties and Applications in Neutrosophic Data Modeling," *Mathematical Problems in Engineering*, p. 3686968, 1 2022.
- [32] M. M. Rahman, A. M. Gemeay, M. A. I. Khan, M. A. Meraou, M. E. Bakr, A. H. Muse, E. Hussam and O. S. Balogun, "A new modified cubic transmuted-G family of distributions: Properties and different methods of estimation with applications to real-life data," *AIP Advances*, p. 095025, 9 13 2023.
- [33] P. E. Oguntunde, M. A. Khaleel, H. I. Okagbue and O. A. Odetunmbi, " the Topp–Leone Lomax (TLLo) distribution with applications to airborne communication transceiver dataset," *Wireless Personal Communications*, pp. 349-360, 2019.
- [34] G. M. Cordeiro, M. Alizadeh, T. G. Ramires and E. M. M. Ortega, "The generalized odd half-Cauchy family of distributions: Properties and applications," *Communications in Statistics-Theory and Methods*, pp. 5685-5705, 11 46 2017.
- [35] S. Abid and R. Abdulrazak, "[0, 1] truncated Frechet-Weibull and Frechet distributions," *International Journal of Research in Industrial Engineering*, pp. 106-135, 1 7 2018.
- [36] M. Aboraya, "A new one-parameter G family of compound distributions: copulas, statistical properties and applications," *Statistics, Optimization & Information Computing*, forthcoming, p. 942–962, 9 2021.
- [37] O. E. Al-Saqal, Z. A. Hadied and Z. Y. Algamal, "Modeling bladder cancer survival function based on neutrosophic inverse Gompertz distribution," *International Journal of Neutrosophic Science*, pp. 75-5, 1 25 2025.
- [38] N. A. Noori, A. A. Khalaf and M. A. Khaleel, "A new expansion of the Inverse Weibull Distribution: Properties with Applications," *Iraqi Statisticians Journal*, pp. 52-62, 1 1 2024.
- [39] H. M. Almongy, E. M. Almetwally, H. M. Aljohani, A. S. Alghamdi and E. H. Hafez, "A new extended Rayleigh distribution with applications of COVID-19 data," *Results in Physics*, p. 104012, 23 2021.

A Comprehensive of Derivative-Free Optimization (DFO) Methods : A Review

¹Marwan S. Jameel

²Ahmed Farooq Qasim

³Zeiad Yahya Ali Allawee

¹Collage of Environmental Science, University of Mosul, Mosul, Iraq.

²College of Computer Science and Mathematics, University of Mosul, Mosul, Iraq.

³College of Physical Education and Sports Sciences, University of Mosul, Iraq.

¹maran.jameel@omosul.edu.iq

²ahmednumerical@uomosul.edu.iq

³zead77@uomosul.edu.iq

A Comprehensive of Derivative-Free Optimization (DFO) Methods : A Review

Marwan S. Jameel¹, Ahmed Farooq Qasim², Zeiad Yahya Ali Allawee³

¹maran.jameel@omosl.edu.iq

¹Collage of Environmental Science, University of Mosul, Mosul, Iraq.

²ahmednumerical@uomosul.edu.iq

²College of Computer Science and Mathematics, University of Mosul, Mosul, Iraq.

³zead77@uomosul.edu.iq

³College of Physical Education and Sports Sciences, University of Mosul, Iraq.

Abstract: In recent times, computational efficiency has witnessed a tremendous development, making it a vital element in many sectors such as applied sciences, medicine, industry, technology, and mathematics in general. However, these techniques face significant challenges related to the ability to apply them effectively and safely. Although there is much research on numerical optimization methods in mathematics, there is a lack of directions that combine these studies and clarify the common trends between them. This review aims to provide a comprehensive analysis of recent studies related to the applications of numerical optimization methods in solving unrestricted optimization problems and nonlinear equations of different shapes and classifications, specifically the derivative-free optimization (DFO) method, focusing on the challenges facing researchers in applying and dealing with them, the opportunities available for the future, and ways to expand them. Derivative-Free Optimization (DFO) refers to a set of optimization techniques used when derivatives of the objective function are not available or are unreliable. This can occur in various practical scenarios, such as when dealing with noisy measurements, complex simulations, or black-box functions where the mathematical form of the objective is not explicitly known.

Keyword: Derivative-Free Optimization Methods, optimization problems, Direct numerical methods.

المخلص: شهدت الكفاءة الحسابية في الآونة الأخيرة تطوراً هائلاً، مما جعلها عنصراً حيوياً في العديد من القطاعات مثل العلوم التطبيقية والطب والصناعة والتكنولوجيا والرياضيات بشكل عام. ومع ذلك، تواجه هذه التقنيات تحديات كبيرة تتعلق بالقدرة على تطبيقها بشكل فعال وآمن. على الرغم من وجود الكثير من الأبحاث حول طرق التحسين العددي في الرياضيات، إلا أن هناك نقصاً في الاتجاهات التي تجمع بين هذه الدراسات وتوضح الاتجاهات المشتركة بينها. تهدف هذه المراجعة إلى تقديم تحليل شامل للدراسات الحديثة المتعلقة بتطبيقات طرق التحسين العددي في حل مشاكل التحسين غير المقيدة والمعادلات غير الخطية ذات الأشكال والتصنيفات المختلفة، وتحديدًا طريقة التحسين الخالي من المشتقات (DFO)، مع التركيز على التحديات التي يواجهها الباحثون في تطبيقها والتعامل معها، والفرص المتاحة للمستقبل، وسبل توسيعها. يشير التحسين الخالي من المشتقات (DFO) إلى مجموعة من تقنيات التحسين المستخدمة عندما لا تكون مشتقات دالة الهدف متاحة أو غير موثوقة. يمكن أن يحدث هذا في سيناريوهات عملية مختلفة، مثل عند التعامل مع القياسات الصاخبة، أو المحاكاة المعقدة، أو وظائف الصندوق الأسود حيث لا يُعرف الشكل الرياضي للهدف صراحةً.

الكلمات المفتاحية: طرق التحسين الخالية من المشتقات، مشاكل التحسين، الطرق العددية المباشرة.

1. General Overview of Derivative-Free Optimization (DFO)

Derivative-Free Optimization (DFO) refers to the process of improving candidate solutions for problems where derivatives, either analytical or automatic, are not accessible, unreliable, too expensive to obtain, or their errors are too large to be useful. DFO methods have remained, for a number of decades, one of the most evolved and

effective subfields of derivative-free methodology. This is primarily due to the great abundance of practical scenarios where no analytical gradient of the function to be minimized is available. Applications where DFO is particularly necessary are numerous, including cases where computational simulations are used to represent complex physical phenomena described by partial differential equations or in cases of other systems where, for example, the system is represented by a table of data and, in fact, an analytical expression describing the system itself cannot be provided. Additionally, occasionally, even if an analytical gradient is known to exist, its computation, as well as storing it, may not be feasible or advantageous, particularly when the problem dimension is large. (Ploskas & Sahinidis, 2022)(Royer et al.2024)(Kim et al., 2021)(Ma et al.2021)(Phan et al.2022)(Jarry-Bolduc, 2023)(Beyhaghi et al.2020)(Larson & Menickelly, 2024)(Zhao et al.2021)(Stripinis et al.2024)

There are many situations where problems occur where we cannot provide an analytical expression for gradients. For example, in parameter estimation and the related fields of identification and calibration, the complicated, multi-dimensional, black-box, noisy, possibly discrete computer experiments that give us the values of the fitness objective to be minimized are generally obtained by running some sophisticated simulator, often written in some compiled digital library and then called directly from the optimization code. This is usually required if the simulator irresponsibly destroys the numerical evidence of its constraints. In the presence of such real-world scenarios, which unfortunately are still numerous due to the increased exploitation of simulations in various disciplines such as engineering, finance, artificial intelligence, and parallel and distributed systems, DFO techniques and numerous algorithms are seen as a vital and necessary application.

1.1. Definition and Importance of DFO in Optimization Problems

Derivative-Free Optimization (DFO) is an approach to identifying a point that minimizes an objective function within a suitable search space when there is no information about the first-order or higher-order derivative, such as gradient, Hessian, etc. DFO enables us to solve optimization problems when

- (i) The function to be minimized is computationally expensive to evaluate, and
- (ii) The derivatives are intractable to compute.

Because of this, DFO has been widely studied and applied in various fields, including but not limited to machine learning, engineering design, parameter estimation, and optimization in simulation. The main difference between DFO problems and classical optimization is that gradients cannot be used to steer the search. Unlike derivative-based optimization approaches, DFO iteratively refines the candidate solutions using the objective function value without using derivative information. From a design perspective, the derivative-free optimization (DFO) problem corresponds to a scenario that combines interval analysis with a black box and the box uncertainty set. Collections of competing DFO methods have been proposed and compared on various DFO datasets. Generally, DFO methods perform poorly on DFO datasets compared to their derivative-based counterparts. DFO algorithms often converge to the estimated optimum of functions that have high, irregular variability. As limited as DFO may be in terms of identifying global solutions, the method is appreciated because it finds a solution to problems where the existing state of the art cannot, whereas, in practice, gradient-based optimization is used in most local problems. It has been suggested that perhaps DFO is finding feasible solutions in NLP instances where first-order optimization based on derivatives fails. Among the abundance of DFO approaches, there is no single criterion for identifying all situations where each performs best. It is a problem-dependent selection of methods that becomes important for solving DFO problems during applications. In general, to show where DFO stands in the optimization world, some identification and comparison of the most competitive approaches are necessary (Begin et al. 2010)(Rao, 2019).

2. Historical Development and Evolution of DFO Techniques

Derivative-Free Optimization (DFO) techniques have a rich history spanning several decades and have experienced continual evolution to become one of the most active, burgeoning areas in optimization research. This section provides a historical perspective of how DFO techniques evolved over time and is divided into seven subsections. We provide an overview of techniques, when the earliest work was published, and how these ideas have evolved. The review structure and content are selected to offer a visual of DFO's historical evolution(Chen et al. 2012).

Research techniques used today in mathematical models for optimization problems can be traced back to numerous milestones in theoretical developments and applications; the advances listed above had a significant impact on the development of DFO techniques. Most recently, the rapid evolution of computation on everything from personal computers to super machines has had significant implications in this field of research. Initially, DFO techniques were developed for solving non-smooth optimization problems, but it wasn't long until researchers also began applying DFOs to computationally difficult smooth problems(Mukherjee et al. 2024).

The field of optimization has always been driven by applications. The explosion of applications due to rapid technological changes has expanded the portfolio of optimization challenges to include computationally difficult real-world problems—problems that are hard to solve using classical optimization techniques. As indicated above, the very nature of these problems inspired the creation of DFO methods as a separate discipline in optimization research, rather than the strategy of last resort. These elements from a historical perspective highlight the interplay between theoretical advances and the real-world need for improved optimization strategies, changes in computation, and applications(Liu, 2024).

2.1. Early Approaches and Milestones in DFO Research

In this paper, we provide an in-depth overview of optimization methods based on derivatives. Our focus is on modern derivative-free optimization (DFO), which has substantially advanced within the last decade. We argue that despite the rise of derivative-based methods and the fact that it is possible to easily compute first-order derivatives for many applications, DFO has its right to exist and keeps capturing the attention of research and development communities(SANTOS,2021).

Derivative-free optimization (DFO) has often been formulated based on the approach to derivative-based optimization. The idea of DFO can be found in the rational description of direct search methods. Direct search (DS) refers to optimization methods that do not rely on first- or second-order derivatives of the objective function. Although the name direct search came about long before derivative-based methods, DS has been studied independently until a stronger connection to continuous optimization could be made. The start of the modern era can be found in 1961 with pioneering work on the simple good terminating (SGT) method for managing constraint violations. The approach was later advanced and subsequently generalized to allow for control of memory and computational effort. At around the same time, principal axes search (PAS) was intensively studied and can be interpreted as a variant of the method for the extreme case of having one evaluation point, commonly called the zero-n neighbor method. Notice that redundancy in the number of evaluations is the mother of pure DFO optimization(Ploskas, 2022).

Convergence analysis of the zero-n principal axes search and its stochastic variant was completed during early 1961, while correspondences with Kuhn were mentioned in 1963. During this time of rapid growth, many world-class facilities emerged, ensuring progress was being made simultaneously across countries. Possible reasons for the close release dates of derivative-free methods are:

- (i) The original game-theoretical paradigm while working on more intensive work on cooperative games; and

- (ii) Continued work along the lines of potential competition and potential reduction direct search method.

After two decades of direct search research, the field moved away from and then back to optimal, combinatorial, numerical, and analytical methods.

Zero-n based derivative-free optimization, such as the close of computerization, automated problem transformation, automated analysis, automated design, and distributed algorithms, is a reflection of continuous mathematical work being done in association with the extensive proliferation. While zero-n methods resolved algorithmic issues such as quality of initialization and stopping tolerances with very few evaluations, the gain from these methods may seem small. Yet, this is the allure of pure technology: it drives constant algorithmic contributions. Initially, DFO was introduced to handle problems where the availability of the derivatives was a major challenge. Since then, a body of research has emerged which indicated that optimization with gradients was easier than before with the use of modern solvers that provide gradients (Royar, 2016).

3. Fundamental Concepts in DFO

The aim of this section is to give the readers some fundamental concepts for understanding all the methodologies seen in the literature, and some motivation about the reasons why we do not use derivatives to optimize in general. Derivative-free optimization (DFO) is a class of mathematical optimization strategies where the optimization algorithm does not depend on the gradient or the Hessian of the problem to be solved. These methodologies arose to cover some optimization problems that gradient-based optimizers are not capable of solving. The use of the DFO approach, instead of the well-studied advantage of derivative-based ones, is mainly due to the absence of a closed-form expression. Hence, computing or approximating the gradient relies on specific designs or numerical calculations that would not always be possible within the methods of DBO.

At first glance, the absence of the gradient might sound like a restriction on the use of dimensionality reduction strategies. However, this is not actually the case: the objective function may not give the same results as its true value, leading to a lack of smoothness in the behavior of the surfaces. These problems are denoted as volcano functions or barndoor functions, and they represent particular cases of optimization where the design of the corresponding algorithm is considered a difficult pursuit. Roughly, there are two main effects when the gradient information is not available: the manifold of solutions is wider, and therefore some optimality conditions need to relax the convergence rate; and the convergence *ceteris paribus* strongly depends on the initial algorithm configuration.

The lack of (inferable) smoothness in the objective functions also implies the need to design sampling strategies (when the input dimension is relatively high, these strategies may not do exhaustive grid searches) and accurate queries of the objective function that must ensure robust convergence due to the aforementioned behavior of the parameter of interest; such strategies are supported by the classification of the function found in cases where solutions are perturbed. Even more, due to the possible lack of regularities, the ultimate goal pursued is to introduce convergence speculative algorithms in a broad sense. The aim is to demonstrate that the solutions are "practically" optimal, since the convergence rate reducing the value of the function to the minimum is indeed one of the most chimerical pursuits in DFO and its domain of applications: optimization without derivatives (Scheinberg, 2000) (Custódio et al., 2017) (Hare & Macklem, 2013).

3.1. Derivative-Free vs. Derivative-Based Optimization

In many respects, the growth in popularity of DFO can be attributed to exploring fundamental differences and similarities with derivative-based methods. One of the primary ideas to communicate is that derivative-based methods have the upper hand whenever derivative information is available because this information is exploitable and makes optimization tasks easier. In practice, derivatives reduce search space, speed up convergence of methods, and empower problem-specific techniques by providing invaluable insights. This holds

for unconstrained as well as constrained optimization. The speed-up of methods and insights of derivative information become even more pronounced in smooth optimization, a notion commonly used when discussing gradient-based optimization techniques. This sustainability for exploiting the derivative information in smooth optimization is interlinked with relatively high-frequency methods as convergence angles are small in the neighborhood of minima.

Unfortunately, though unconstrained optimization problems frequently have 'easy' search landscapes, using second- and higher-order information provides faster, more efficient, and superior algorithms. These ideas are the cornerstone of gradient- and/or Hessian-based derivative-free methods in smooth optimization. However, there is also a body of evidence that makes a case for derivative-free methods having computational efficiency. In conclusion, using derivative-based optimization when derivatives are not available is counterproductive and cannot be used as an alternative in practice. Furthermore, rarely encountered or discontinuous objective functions require specific algorithm design that is tailored to DFO. Additionally, using derivative-based optimization when derivatives are available is an added computational overhead when repeatedly using DFO in high-resolution studies (Körkel et al., 2005) (Larson et al., 2019).

4. Classification of DFO Methods

DFO methods can be divided into two primary categories: direct search methods and model-based methods. However, the number of techniques and ideas behind DFO is quite diverse and rich. Hopefully, in the future, some options from direct search techniques will be combined with the model-based ones. In this chapter, the following classification and the main principles behind these methods will be presented.

- **Direct Search Methods:**
 - Nelder-Mead Method: A popular method that uses a simplex of $n+1$ points in n -dimensional space to iteratively update the simplex by reflecting, expanding, and contracting.
 - Pattern Search: An approach that systematically explores the space by using a pattern or a set of directions to guide the search.
- **Surrogate-Based Methods:**
 - Kriging (Gaussian Process) Regression: A statistical technique that builds a surrogate model of the objective function based on a sample of function evaluations. It helps in making predictions and guiding the search.
 - Radial Basis Function (RBF) Interpolation: Constructs a surrogate model by fitting a radial basis function to the sampled data.
- **Evolutionary Algorithms:**
 - Genetic Algorithms: Population-based methods that mimic natural selection processes, using operations like crossover and mutation to explore the search space.
 - Differential Evolution: A type of evolutionary algorithm that uses differences between randomly selected pairs of solutions to guide the search.
- **Stochastic Methods:**
 - Simulated Annealing: A probabilistic technique inspired by the annealing process in metallurgy, which explores the search space by probabilistically accepting worse solutions to escape local optima.
- **Response Surface Methods:**
 - Central Composite Designs (CCD): A technique used to build a second-order polynomial approximation of the objective function based on sampled data.
 - Box-Behnken Designs: A method for constructing response surface models that provides a balance between the number of runs and the quality of the model.

Lastly, in terms of selecting methods, not only classification based on what is done in techniques can be helpful. It can show the idea behind the method and be a hint when the techniques have been successful. If we have some

conditions on the problem, we can consider using this piece of information to apply the appropriate scheme. Choosing a different method than suggested does not preclude successful results; it was observed on some benchmarks. However, considering these options can be a good starting point. The first classification mentioned above provides such information because it can show successful ways of solving an optimization scheme. The presented classifications can also give some prompts as to the nature of the methods and aid in deciding what is the correct category to choose from.

According to the division used in the previous chapter, the current section presents a complete classification of derivative-free optimization methods. Given the computational properties of the problem, a choice may be made between these methods when trying to solve a particular problem. All the presented methods omit the analyzer calculation or add randomization to work efficiently. In each case, it is not possible to take advantage of the optimizer or the objective function (Custódio et al., 2017) (Audet & Hare, 2020) (Ma et al., 2021).

4.1. Direct Search Methods

Direct search methods traverse the feasible search space by performing simulations or experiments at a limited number of sampling points, selected in a systematic pattern. The major characteristic of direct search is that it does not use gradients. In each iteration, the position of the sampling points is determined without using any gradient information. The design of the next points is generally based on the 'appearance' of the points so far. The type of pattern generated in this way, together with the objective function, determines whether the search advances or moves, i.e., the search direction. Direct search methods can be classified into complete direct search methods, incomplete direct search methods, and compact direct search methods, depending on how and when the sampling points are generated and evaluated. The use of a mating strategy between feasible and infeasible points, especially in functions with a high proportion of constraints, reduces considerably unnecessary exploration in infeasible regions and discarding good potential regions due to the usage of non-feasible points.

Direct search methods have several advantages. From a practical point of view, they are very simple and can be easily implemented. They do not require the calculation of derivatives. In the context of DFO, if the calculation of first-order gradients is cheap, methods that combine the use of direct search methods along with the computation of the gradients can be used. On the other hand, they also have some limitations and difficulties. For instance, direct search methods use a systematic search pattern that is not scalable in high dimensions. A potential solution is the use of patterns that do not span the entire size of the search space. Moreover, the convergence of direct search methods is still an open question. Many researchers have looked for a combining strategy with local and global search. Some heuristics and genuinely technical modifications have been proposed to improve and generalize the idea of a direct search method (Kramer et al., 2011) (Larson et al., 2019).

4.2. Model-Based Methods

The central idea of model-based methods is the construction of an approximation using samples to represent the original function. By considering a certain number of data points, the surrogate model is then induced to fill the gap between those data. Accordingly, a model of the objective function is shaped, stressing particularly those areas where the surrogate function model is uncertain. By processing this model, decision-making is more informed, resulting in refinement of the final solution. Model-based DFAs often combine exploration with exploitation. The former points to further seeking of a solution by attempting to gain more information about uncertain evaluations and leading to an enhancement of the trust in the surrogate model. Moreover, regarding the exploitation point, the surrogate function is employed for the actual optimization strategy.

There are various DFO model-based techniques, e.g., methods stemming from Taylor expansions or utilizing spline approximations. Popular models applied in various fields primarily include polynomial regression for their ease of use and incorporation of standard majorization/minorization or radial basis functions as well as Gaussian

processes as more powerful tools ensuring suitable model representations. Within the DFO community, attention has mainly been given to Gaussian processes. The exploitation of a model-based approach can often lead to a potentially faster convergence rate than using model-free methods. Moreover, a good surrogate model allows heightened efficiency in terms of exploration, particularly in better exploiting the space. However, the exploration is significantly dependent on uncertainties characterized by the surrogate model. An additional strength of those methods is the capability of performing variable fixing to explore less promising regions. Some candidates have been proposed to address variables at an optimal level in the case of multi-fidelity solutions. Despite the promising and versatile features of Gaussian process surrogates, many issues concerning computational costs, hyper-parameter adjustment, and updating strategies still hinder their applications. Much effort has been poured into overcoming these issues. Model-based techniques have often proved effective in practical scenarios. For instance, improving scaling factors for simulations with incomplete physical parameter knowledge was properly handled by a combination of multi-fidelity co-kriging, chaotic map, genetic algorithm, and artificial neural networks. Some key components, when categorized under EDA, help to predict wind drift-tail mixing by employing a self-organizing map or neural network(Hutter et al., 2011)(Kumar & Levine, 2020)(Eisenhower et al., 2012).

5. Key Components of DFO Algorithms

5.1. Exploration vs. Exploitation Strategies

Exploration strategies refer to methods in which the focus is on sampling different or diverse regions of the search space. This is, in general, useful to understand the behavior of the objective function for distinct regions of the domain. On the other hand, exploitation strategies focus on the exploitation of the solutions that led to good results in the past by mainly concentrating on a small region in the proximity of the current best solution.

The efficiency of optimization algorithms is influenced by the right or wrong amount of exploration and exploitation behavior. By solely performing exploitation, one may end up in local optima or miss the global optimum. In contrast, overwhelming exploration may lead to slow convergence rates and result in inefficient algorithmic behavior. A range of techniques have been proposed that contain both explorative and exploitative properties aiming at offering a compromise for good overall algorithmic performance.

Adaptive methods dynamically change the focus during the course of the algorithm based on feedback received. For instance, one well-known adaptive method is based on the concept of using a mesh as a local search heuristic in combination with a local model of the objective function that is minimized without the need to evaluate the objective function in the whole mesh. Some of the state-of-the-art algorithms adopt this strategy, guiding the global search by adaptively, based on past histories, performing either exploration or exploitation behavior(Al-Rifaie, 2021).

6. Applications and Case Studies of DFO

The various applications and case studies of DFO as a state-of-the-art optimization metaheuristic technique to solve real-world optimization problems are demonstrated. Its applications show a broad range of problem sizes due to its computational efficiency. The use of DFO demonstrates a convergence to nearly optimum solutions and presents itself as an adaptive and more robust method for various engineering, finance, and artificial intelligence-based problems. The engineering applications include a robust design optimization of a vehicle's side impact structure, oil pipeline batch arrangement optimized using DFO, and DFO used in aero-optical phase characterized by means of an experimental weapon bay. The applications of DFO in financial and economic studies include European general economic problems, American option pricing, and performance response surfaces for European test problems. Various studies and case studies in artificial intelligence include the autonomous learning capability and searching for the global minimum. Each case study serves a unique way to

show the versatility of DFO. Thus, for a particular application, once the three top appropriate DFO methods are identified, choosing one of them strongly depends on the level of importance of requirements and challenges of a case study. The computational requirement of a case study will necessitate a user to choose a suitable DFO algorithm among the three extracted best DFO algorithms. The amount of computational resource can be estimated by the number of iterations provided processing time is held constant. How to properly evaluate the computational cost when finite differences are used as a search engine, the simplicity of the used DFO algorithms, and finally, the nature of the evaluated objective function in a case study are discussed. The future use cases of DFO applications include density-based clustering application, genetic regulation, industrial DFO applications, neural network training, pharmacokinetic multi-compartment model calibration, and UAV path planning. These applications were extracted from different scientific studies including trajectory optimization. This is because a common problem across these DFO applications is the need to handle multivariate, multimodal, non-continuous, discontinuous functions, noisy functions, one-shot function evaluations, non-smooth, non-convex, or differentiable functions. The use case applications of DFO show that DFO can be employed in various studies regardless of the applied discipline (Audet & Hare, 2020).

6.1. Engineering Design Optimization

Derivative-Free Optimization (DFO) has been investigated and applied as a solution to various design optimization challenges since the 1990s. Engineering design problems are often complex, with a high, non-differentiable design space dimensionality and thus suffer from a lack of either closed-form expressions or analytical gradients of the objective function, making DFO a feasible alternative to traditional derivative-based optimization methods. It can be employed to optimize the design parameters of the system to yield an enhanced steady-state value of the objective function by exploiting computational tool capabilities, such as emulators developed using model-based reasoning techniques or simulation engines for developing metamodels using computational fluid dynamics. The potential of DFO methods to address issues of nonlinearity, multimodality, high dimensionality, etc., has been demonstrated in a variety of formalized test problems.

DFO methods have been successfully demonstrated in a variety of engineering optimization scenarios. This includes the design and control of wind and solar renewable energy systems to track reference signals issued by the grid operator, voltage and reactive power control in distribution systems, optimal control strategies, such as scheduling and heat integration for the process industry, optimal keystroke level and cognitive workload assessment in human-machine systems, controller tuning utilizing multidisciplinary design optimization, retrofit design of subsea compressors, liner end geometry design in solid rocket motors, and optimization of an internal combustion engine. The design in these problems is undertaken in high dimensionality design spaces in transient and/or steady-state operational modes.

An engineering problem is different from a mathematical optimization problem due to the presence of constraints and/or computational challenges. Constraints could be applied to represent physical laws such as mass conservation, energy balance, and momentum, which could be violated if the suggested design change is considered unrealistic. Additionally, due to the significant computational time, the power system operators may utilize approximated modes of the power system model to work in cases of policy analysis and operational planning. However, when simulator fidelity is needed for real-time operations, operator-driven control scheme evaluations, and regulatory compliance checking, execution of computationally expensive simulations is considered essential. Also called NP-Hard computing, these problems cannot be solved by evaluating all possible evaluations. Therefore, randomized local search methods are essential to tackling such problems. Additionally, global search optimization is necessary in the case of multimodal design spaces, as previously briefed. Identifying small regions around local minima can be performed by hill-climbing methods, allowing the searcher to explore regions around the found local minimum. Additionally, increased time will render the numerical

search inexpensive as the region around the local minima is identified. However, the use of local search algorithms may help ensure a suboptimal solution is not missed under such conditions.

7. Challenges and Limitations in DFO

Recent research demonstrates that DFO is inherently challenging in many aspects. It is hard to theoretically guarantee the global convergence and the evaluation efficiency for minimizing non-convex and possibly poorly conditioned functions. Many DFO methods encounter local minimizers or fail to converge to minimizers for some non-convex problems. The number of function evaluations required for satisfying precision typically poses a curse of dimensionality in high-dimensional search spaces since both the number of evaluations grows prohibitively with the increasing dimensionality and the volume of the search region grows exponentially with the increasing dimensionality. Some negative scaling results and numerical observations also indicate that the level of noise, the strength of randomness, and the amount of sampling could have a significant impact on the performance of DFO algorithms. It is challenging to evaluate these factors in a real-world optimization scenario since real-world objective functions are typically non-challenging to different degrees, i.e., they do not possess a uniform blend of all negative features.

Much current research on DFO aims to address these challenges. It investigates various solutions from perspectives such as algorithm designs, variable and space transformations, function-prior learning, surrogates, upper-confidence bounding, and sampling, as well as hyper-parameter settings. Specifically, given a finite budget for evaluating the black-box objective function, many new methods aim to alleviate the curse of dimensionality by more efficiently navigating sampling in the search space, more accurately inferring objective function behaviors, or more precisely evaluating and updating the acquired information. However, different methods seek different trade-offs between evaluation efficiency and model accuracy because it is challenging to jointly benefit from both aspects. More precisely, the purely global search approach is efficient for evaluation but has the limitation of ignoring sampling accuracy, whereas the pure exploitation approach will deal with the latter but not the former. Emerging convergences illustrate that acquiring the right balance between evaluation budget and model accuracy is of significant interest in the development of nonlinear optimization approaches.

Although the state-of-the-art DFO methods have made considerable advances, research in this area encounters some challenges that need to be thoroughly researched and addressed. Several frequently encountered pitfalls in practice have been observed. Several black-box objective functions are expensive and even intractable to evaluate. It is indicated that the performance of inexpensive DFO algorithms would degrade, particularly for the optimization of black-box functions that either present a considerable amount of randomness or accumulate significant noise during evaluations. A reasonable adjustment arising from the cost evaluation for noisy and random functions has been suggested via adjustments in the log budget. Non-convergence may be observed in this situation. One important route for future research is to focus on narrowly escaping from local minima traps either analytically or numerically. Several practical problems for which this is often observed remain to be identified by the research community. It was observed by a few observers that algorithms often employ ill-advised explorations while failing to escape from the local minima traps. The DFO research community should acknowledge that many formulations may encounter such pitfalls and recognize them as important challenges by acknowledging these constraints or limitations. Even if they may be bridged by advancing the methods involved in combining global sampling and global search, significant efforts have to be utilized to obtain competitive solutions. Given the highly non-trivial significance of these pitfalls to the design of trust region methods, significant breakthroughs could mark significant future contributions at the level of DFO technology (Cartis et al., 2019).

7.1. Convergence Rates and Scalability Issues

In this section, we offer insights into the challenges associated with obtaining improvements in the convergence rates of DFO methods. We also analyze the impact of increasing the considered dimensionality on performance in deep search methods and multi-objective optimizers.

Convergence has long been a measure of the performance of optimization algorithms. Good convergence refers to the ability to quickly find a high-quality solution, combined with confidence in the reliability of that solution. Determining the exact convergence rate for DFO methods is non-trivial due to the interdependency between methods and test problems, though such convergence can be classified by how reliable the method is, in terms of state or probability of convergence, and how rapidly the method is expected to reach the optimum. Although the structure of a problem can impact the convergence rate of a DFO method, a low convergence rate can enable other techniques, thereby avoiding premature convergence.

In higher dimensions or larger systems, feasible search areas become more likely to exist, indicating slow convergence or convergence to a sub-optimal solution. Increasing the dimensionality of search problems also increases the computational cost for individual function evaluations, broadening the definition of dimensionality to include 'effective dimensions.' This is important in multi-objective problems in which a true definition of dimensionality could involve not only the number of objectives and parameters but also the number and nature of the constraints. The implications for the scalability of this limited notion of dimensionality are reduced to the increased function evaluations, leading to an increase in computational budget time on system performance. Techniques that adaptively sample based on past performance or smartly explore the entire design space show promise. As for convergence in complicated problems, iterative optimization may have to be used. Without verified filters, stagnation criteria should be fixed or adapted, with additional heuristics to facilitate further exploration (Jamieson et al., 2012) (Cartis et al., 2019) (Larson et al., 2019).

8. Recent Advances and Future Directions in DFO

During the past few years, significant research on DFO has been conducted. The advances in computational techniques have made it possible to solve complex problems in real-time, thus challenging DFO methods to be more robust, efficient, and adaptive to changes in the searching environments. Recent studies proposed DFO methodologies for specialized workings and changed the classical optimization techniques to derive more powerful algorithms in different application areas. To fulfill the need for efficient algorithms, an integration of machine learning into DFO methods has been used in the aerodynamics, flight mechanics, and multiobjective optimization fields. On the other hand, several metaheuristic techniques have inspired researchers to develop algorithms that imitate the behavior of certain logic. A recent study treated the global optimization problem using a base optimizer based on natural laws. Researchers aimed to propose a novel optimizer in the DFO algorithm family, which belongs to the class of crossing mechanisms in animal locomotion systems.

Four-legged animal mode: Develops a four-legged animal locomotion system. In the mathematical framework, the hexapod functions as a multi-variable global optimizer that searches the function landscape. To our knowledge, the integration of both strategies to identify the set of Pareto optimal solutions in multimodal optimization has never been conducted before. A survey on multi-swarm techniques is also used in the computation model of the DFO algorithm. In undertaking these models for the DFO algorithm, inspired solutions of animal behavior are considered to be promising futuristic work. DFO algorithms that mimic the behavior of animals, social organisms, and other natural inspirations have gained increasing attention. Nowadays, it becomes attractive to mimic a hybrid of the derivation-free and mutation-based evolution strategy in DFO adaptations, i.e., a combination of the swarm-based, mutation-based, and so on in DFO adaptations.

All constants in the elementary operations should influence the optimization technique differently in the process of exploring and exploiting the mathematical space; modification of these constants may impact the optimization technique differently. Devising a new strategy is a very challenging task in nature. A future research challenge in

developing DFO is the ongoing need for enhancements in light of their many applications. Real-time environments, data-driven modeling, robust and fast characterizations, huge signals or characteristics, and physical behaviors impose many boundaries that necessitate the design of an accurate and efficient DFO method. In principle, there exists no such DFO method that is inherently faster than all the others in every aspect of optimization. Since the human-inspired optimization strategies continuously and tirelessly follow the improvements in at least a specific aspect of the optimization process, every newly proposed DFO technique should be compared not only with its recent ancestors but also with the more classic ones anew. Therefore, the meaningful construction of corresponding benchmarks largely depends upon evolving applications. There is absolutely no fixed set of test functions that can be universally classified as the representative test problems for all natural scenarios. The construction of an efficient DFO method, therefore, inherently necessitates exposure to the needs and demands of continuously evolving practical applications (Young et al., 2021)(Custódio et al., 2017)(Roberts, 2019).

8.1. Metaheuristic Integration in DFO

Metaheuristic integration within DFO is widely considered in terms of how it improves optimization outcomes. Metaheuristics are population-based algorithms in nature and work closely with the DFO algorithm to add the ingredients of search (exploration and exploitation) to the black-box optimization algorithm. Those algorithms that improve the characteristics of exploration within the search space are called exploratory optimization methods. They improve the current design points and automatically select them as a center for more local high-resolution designs. Slightly adjustable, the method used in both exploration and exploitation generates optimal solutions.

During the initial development of the DFO algorithm, metaheuristics played an initial fusion process or standalone procedure. Over the last few years, there have been many strategies that make DFO amalgamate metaheuristics as useful, adaptive, more robust, and domain-independent. There are different levels of integration, which point out our continuum starting from independent evolution and ending with completely iterated DFO. The most integrated and popular fields with metaheuristics are local search methods, genetic algorithms, simulated annealing methods, and particle swarm optimization methods. Adaptive hybrid methods are introduced as a modern era integration of DFO nowadays. The integrated process of variable metric methods with genetic algorithms, ant colony optimization methods, and so on reflects good applications of DFO that are used in current real-world problems. Together with this, there are many other integration problems to solve real-world issues, leading to some challenging domains as well in optimizing the DFO. This includes optimal population size selection, good combinations of parameters, balancing the domain between exploration and exploitation, and diversification. Recent theoretical advice reported that they have shown potential to improve black-box optimization of DFO. This is now a kernel idea of research to find the best combination and a single way to tweak the experts' knobs and switches. The world is exploring more than many optimization approaches with DFO in the optimum DFO solution (Ploskas & Sahinidis, 2022)(Gray & Fowler, 2011).

References:

- 1- Ploskas, N. & Sahinidis, N. V. (2022). Review and comparison of algorithms and software for mixed-integer derivative-free optimization. *Journal of Global Optimization*. [springer.com](https://www.springer.com)
- 2- Royer, C. W., Sohab, O., & Vicente, L. N. (2024). Full-low evaluation methods for bound and linearly constrained derivative-free optimization. *Computational Optimization and Applications*, 1-37. [PDF]
- 3- Kim, B., Cai, H. Q., McKenzie, D., & Yin, W. (2021). Curvature-aware derivative-free optimization. *arXiv preprint arXiv:2109.13391*. [PDF]
- 4- Ma, K., Sahinidis, N. V., Rajagopalan, S., Amaran, S., & Bury, S. J. (2021). Decomposition in derivative-free optimization. *Journal of Global Optimization*, 81(2), 269-292. [HTML]

- 5- Phan, D. T., Liu, H., & Nguyen, L. M. (2022). StepDIRECT-A Derivative-Free Optimization Method for Stepwise Functions. In Proceedings of the 2022 SIAM International Conference on Data Mining (SDM) (pp. 477-485). Society for Industrial and Applied Mathematics. [siam.org](https://www.siam.org)
- 6- Jarry-Bolduc, G. (2023). Numerical analysis for derivative-free optimization. [ubc.ca](https://www.ubc.ca)
- 7- Beyhaghi, P., Alimo, R., & Bewley, T. (2020). A derivative-free optimization algorithm for the efficient minimization of functions obtained via statistical averaging. *Computational Optimization and Applications*, 76(1), 1-31. [PDF]
- 8- Larson, J. & Menickelly, M. (2024). Structure-aware methods for expensive derivative-free nonsmooth composite optimization. *Mathematical Programming Computation*. [PDF]
- 9- Zhao, F., Grossmann, I. E., García- Muñoz, S., & Stamatis, S. D. (2021). Flexibility index of black- box models with parameter uncertainty through derivative- free optimization. *AIChE Journal*, 67(5), e17189. [academia.edu](https://www.academia.edu)
- 10- Stripinis, L., Kūdela, J., & Paulavičius, R. (2024). Benchmarking derivative-free global optimization algorithms under limited dimensions and large evaluation budgets. *IEEE Transactions on Evolutionary Computation*. [HTML]
- 11- Begin, T., Baynat, B., Sourd, F., & Brandwajn, A. (2010). A DFO technique to calibrate queueing models. *Computers & Operations Research*, 37(2), 273-281.
- 12- Rao, S. S. (2019). *Engineering optimization: theory and practice*. John Wiley & Sons.
- 13- Chen, C., Jin, L., Gao, G., Weber, D., Vink, J. C., Hohl, D. F., ... & Pirmez, C. (2012, June). Assisted history matching using three derivative-free optimization algorithms. In *SPE Europec featured at EAGE Conference and Exhibition?* (pp. SPE-154112). SPE.
- 14- Mukherjee, G., Mallik, B. B., Kar, R., & Chaudhary, A. (Eds.). (2024). *Advances on Mathematical Modeling and Optimization with Its Applications*. CRC Press.
- 15- Liu, J., Sarker, R., Elsayed, S., Essam, D., & Siswanto, N. (2024). Large-scale evolutionary optimization: A review and comparative study. *Swarm and Evolutionary Computation*, 101466.
- 16- Ploskas, N., & Sahinidis, N. V. (2022). Review and comparison of algorithms and software for mixed-integer derivative-free optimization. *Journal of Global Optimization*, 82(3), 433-462.
- 17- SANTOS, N. A. C. (2021). CONTRIBUTIONS IN GLOBAL DERIVATIVE-FREE OPTIMIZATION TO THE DEVELOPMENT OF AN INTEGRATED TOOLBOX OF SOLVERS.
- 18- Royer, C. (2016). *Derivative-free optimization methods based on probabilistic and deterministic properties: complexity analysis and numerical relevance* (Doctoral dissertation, Université Paul Sabatier-Toulouse III).
- 19- Hare, W., & Macklem, M. (2013). Derivative-free optimization methods for finite minimax problems. *Optimization Methods and Software*, 28(2), 300-312.
- 20- Custódio, A. L., Scheinberg, K., & Nunes Vicente, L. (2017). Methodologies and software for derivative-free optimization. *Advances and trends in optimization with engineering applications*, 495-506.
- 21- Scheinberg, K. (2000). *Derivative free optimization method*. Department Computing and Software, McMaster University.
- 22- Gray, G. A., & Fowler, K. R. (2011). Traditional and hybrid derivative-free optimization approaches for black box functions. In *Computational Optimization, Methods and Algorithms* (pp. 125-151). Berlin, Heidelberg: Springer Berlin Heidelberg.
- 23- Young, D., Haney, W., & Cremaschi, S. (2021). Derivative-free optimization of combinatorial problems—A case study in colorectal cancer screening. *Computers & Chemical Engineering*, 145, 107193.
- 24- Roberts, L. (2019). *Derivative-free algorithms for nonlinear optimisation problems* (Doctoral dissertation, University of Oxford.).

- 25- Larson, J., Menickelly, M., & Wild, S. M. (2019). Derivative-free optimization methods. *Acta Numerica*, 28, 287-404.
- 26- Jamieson, K. G., Nowak, R., & Recht, B. (2012). Query complexity of derivative-free optimization. *Advances in Neural Information Processing Systems*, 25.
- 27- Cartis, C., Fiala, J., Marteau, B., & Roberts, L. (2019). Improving the flexibility and robustness of model-based derivative-free optimization solvers. *ACM Transactions on Mathematical Software (TOMS)*, 45(3), 1-41.
- 28- Körkel, S., Qu, H., Rücker, G., & Sager, S. (2005, June). Derivative based vs. derivative free optimization methods for nonlinear optimum experimental design. In *Current Trends in High Performance Computing and Its Applications: Proceedings of the International Conference on High Performance Computing and Applications*, August 8–10, 2004, Shanghai, PR China (pp. 339-344). Berlin, Heidelberg: Springer Berlin Heidelberg.
- 29- Audet, C., & Hare, W. (2020). Model-based methods in derivative-free nonsmooth optimization (pp. 655-691). Springer International Publishing.
- 30- Ma, K., Sahinidis, N. V., Rajagopalan, S., Amaran, S., & Bury, S. J. (2021). Decomposition in derivative-free optimization. *Journal of Global Optimization*, 81(2), 269-292.
- 31- Eisenhower, B., O'Neill, Z., Narayanan, S., Fonoberov, V. A., & Mezić, I. (2012). A methodology for meta-model based optimization in building energy models. *Energy and Buildings*, 47, 292-301.
- 32- Kumar, A., & Levine, S. (2020). Model inversion networks for model-based optimization. *Advances in neural information processing systems*, 33, 5126-5137.
- 33- Hutter, F., Hoos, H. H., & Leyton-Brown, K. (2011). Sequential model-based optimization for general algorithm configuration. In *Learning and Intelligent Optimization: 5th International Conference, LION 5*, Rome, Italy, January 17-21, 2011. Selected Papers 5 (pp. 507-523). Springer Berlin Heidelberg.
- 34- Al-Rifaie, M. M. (2021). Exploration and exploitation zones in a minimalist swarm optimiser. *Entropy*, 23(8), 977.
- 35- Audet, C., & Hare, W. (2020). Model-based methods in derivative-free nonsmooth optimization (pp. 655-691). Springer International Publishing.
- 36- Cartis, C., Fiala, J., Marteau, B., & Roberts, L. (2019). Improving the flexibility and robustness of model-based derivative-free optimization solvers. *ACM Transactions on Mathematical Software (TOMS)*, 45(3), 1-41.
- 37- Gratton, S., Laloyaux, P., & Sartenaer, A. (2014). Derivative- free optimization for large- scale nonlinear data assimilation problems. *Quarterly Journal of the Royal Meteorological Society*, 140(680), 943-957.
- 38- Cartis, C., Ferguson, T., & Roberts, L. (2020). Scalable derivative-free optimization for nonlinear least-squares problems. *arXiv preprint arXiv:2007.13243*.
- 39- Hare, W. L. (2010). Using derivative free optimization for constrained parameter selection in a home and community care forecasting model. In *International perspectives on operations research and health care*, Proceedings of the 34th meeting of the EURO working group on operational research applied to health sciences (pp. 61-73).
- 40- Shi, H. J. M., Xuan, M. Q., Oztoprak, F., & Nocedal, J. (2021). On the numerical performance of derivative-free optimization methods based on finite-difference approximations. *arXiv preprint arXiv:2102.09762*.
- 41- Martínez, J. M., & Sobral, F. N. C. (2013). Constrained derivative-free optimization on thin domains. *Journal of Global Optimization*, 56(3), 1217-1232.
- 42- van de Berg, D., Shah, N., & del Rio-Chanona, E. A. (2024). Hierarchical planning-scheduling-control—Optimality surrogates and derivative-free optimization. *Computers & Chemical Engineering*, 108726.
- 43- Berahas, A. S., Sohab, O., & Vicente, L. N. (2023). Full-low evaluation methods for derivative-free optimization. *Optimization Methods and Software*, 38(2), 386-411.

Runge-Kutta Method to generate Tree- Graph

¹Saleh Jasim Mohammad

² Awni M.Gaftan

^{1,2}Tikrit University

pcm@st.tu.edu.iq²⁴Sj2300

²Awny Muhammed@tu.edu.iq

Runge-Kutta Method to generate Tree- Graph

Saleh Jasim Mohammad

Awni M.Gaftan

Tikrit University

Tikrit University

Sj230024pcm@st.tu.edu.iq

Awny.Muhammed@tu.edu.iq

Abstract :

In this paper we introduced some of Runge-Kutta methods to solve (ODE)

In which application, application we using the results of Runge-Kutta method to obtain the (Tree-graph) then this trees are using generate trees .

Where each node in the tree represents the calculated numerical values of the equation at each step. The method is also applied to an electrical containing a resistor (R), a capacitor (C),and an inductor (L), where the voltage damping equation is solved numerically and compared analytical solution .The research concludes that tree representations provide a clear view of the numerical evolution ,making them useful in other fields such as dynamic systems analysis.

Key words : Runge-Kutta method,Electrical Circuit Equation, Tree structure , Differential equations, Numerical Analysis ,dynamical system.

1- Introduction :

Many researchers are using Runge-Kutta methods to solve many problems in Physic ,Chemical ,Engineering, and other Sciences .In (2012)Delin Tan and Zheng Chen are introduces a general formula of Fourth-order Runge -kutta method [8] .

Gerald and Wheatley (2004)discussed the wide application of numerical analysis ,including Runge -Kutta methods, in solving engineering problems[1]. Smith and Griffiths (1986) Adressed the usu of Runge -Kutta methods for solving initial value problems-in ordinary differential equations [3] . Ogata, K. (2009). *utilizzed the Runge -Kutta method to find the numerical solution*[4]. Zill (2008) *applied the method to solve deferential equations with modeling application* [5]. Kreyszig (2011) *provided a comprehensive explanation of Runge -Kutta method advanced engineering mathematics* [7] Prentice Hall Bashir M.S. and Mohammed M.S.(2008) are used Runge-Kutta methods of higher order to solving stiff systems [9] .

In (2009),Dawood S. used Runge-Kutta method to find the numerical solution for $(C_2 \setminus C_1 \setminus 2 \setminus 3)$ System [10].

Bratislar T. in(2004) is used the Runge-Kutta method to solving flow problems , which the governing equation is ordinary differential equation (ODE).[11]and the classic refreence by Kreyszig

(2011) which provides a solid background in engineering mathematics and numerical solution techniques [15].

Theoretical part :

2- ALGORITHM RUNGE-KUTTA METHOD OF FOURTH ORDER

Now, we introduce the algorithm of Runge-Kutta method and we use the results to obtain Tree-graph .

2.1 Algorithm Inputs :

- A function $f(x,y)$ representing the differential equation $y' = f(x,y)$
- Initial values x_0 and y_0
- Step size h , which determines the increment in each iteration
- Number of steps N , specifying how many iterations to perform .

Execution steps:

2.2 Determine the computation points:

The range between x_0 and x_N is divided into equally spaced points $x_1 = x_0 + h, x_2 = x_0 + 2h, \dots, x_N = x_0 + Nh$

2.3 Compute the four intermediate values k_1, k_2, k_3 and k_4

For $n = 0, 1, \dots, N-1$ do:

$$k_1 = hf(x_n, y_n)$$

$$k_2 = hf(x_n + \frac{1}{2}h, y_n + \frac{1}{2}k_1)$$

$$k_3 = hf(x_n + \frac{1}{2}h, y_n + \frac{1}{2}k_2)$$

$$k_4 = hf(x_n + h, y_n + k_3)$$

$$x_{n+1} = x_n + h$$

$$y_{n+1} = y_n + \frac{1}{6}(k_1 + 2k_2 + 2k_3 + k_4)$$

2.4 Construct the Tree Representation :

a - Each node stores (x_n, y_n) , and links between nodes represent the computational steps .

b - The root represents the initial conditions, and each level corresponds to the

Numerical solution at sub subsequent steps .

OUTPUT :

a - $x_n + 1, y_n + 1$

b -The tree structure representing the numerical evolution of $(x-n, y-n)$.

End

Stop

End

3- Particular Part :

In this section we applying the Runge-Kutta method to solve the electrical-circuit and we obtain the Tree-graph .

Consider the circuit of figure 2.2 containing a capacitor of C for Example : using the Runge-Kutta method with Kutta's constants

ads , a resister of R ohms , and an inductance of L Henries .

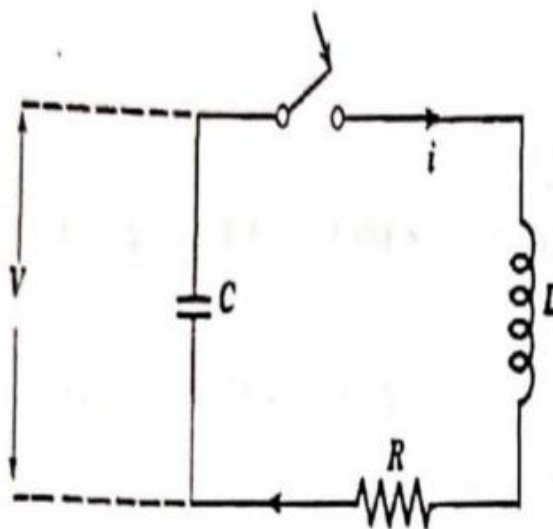


figure 3.1 Electrical circuit .

Assume that the capacitor is initially charged to a voltage V_0 , and that suddenly the switch is closed at time $t=0$. show that the ordinary differential equation describing V , the damped oscillation of voltage across the capacitor is given as a function of time by

$$LC \frac{d^2 V}{dt^2} + RC \frac{dV}{dt} + V = 0, \quad 3.2$$

Subject to the initial conditions

$$V(0) = V_0$$

$$3.3$$

$$\frac{dV}{dt}(0) = 0$$

$$\text{Let } \bar{\alpha}^2 = \frac{1}{LC} - \frac{R^2}{4L^2} \quad 3.4$$

$$\alpha = \sqrt{|\bar{\alpha}^2|}$$

And show that the following analytical solutions satisfy (3.2) with conditions (3.3):

For $\bar{\alpha}^2 > 0$ (the under-damped or oscillatory case) :

$$V = \frac{V_0 \exp\left(-\frac{Rt}{2L}\right) \cos\left(\alpha t - \tan^{-1}\left(\frac{R}{2L\alpha}\right)\right)}{\alpha\sqrt{CL}} \quad 3.5$$

For $\bar{\alpha}^2 = 0$ (the critically -damped case):

$$V = v_0 \exp\left(-\frac{Rt}{2L}\right) \left(1 + \frac{Rt}{2L}\right) \quad 3.6$$

For $\bar{\alpha}^2 < 0$ (the over-

damped case):

$$V = V_0 \exp\left(-\frac{Rt}{2L}\right) \left[\left(\frac{1}{2} + \frac{R}{4L\alpha}\right) \exp(\alpha t) + \left(\frac{1}{2} - \frac{R}{4L\alpha}\right) \exp(-\alpha t) \right] \quad 3.7$$

Write a test program that calls on RUNGE to solve the differential equation (3.2) with initial conditions (3.3) and then compares the numerical solution with the value of the appropriate analytical solution . For test purposes ,consider the following cases :

$$V_0 = 100 \text{ volts}$$

$$C = 2 \times 10^{-6} \text{ farads}$$

$$L = 0.5 \text{ henries}$$

$$R = 100 \text{ ohms}$$

$$h = 0.00001, 0.0001, 0.001, 0.002, 0.005, 0.01 \text{ .}$$

Method of Solution

The fourth-order Runge-Kutta algorithm for the one-step integration of a single first-order equation with one appropriate initial condition

$$y_{ji} = y_j(x_i) \quad , \quad j = 1, 2, \dots, n$$

The initial conditions for the zeroth step $y_{j0} = 1, 2, 3, \dots, n$ will usually be known exactly. There after, the initial conditions for the i th step will be approximations to the true initial conditions $y_j(x_i)$, $j = 1, 2, \dots, n$, since they will result from applications of Runge-Kutta method on the $(i - 1)$ th interval. For a system of n equations, the one-step integration across the i th interval may be described by:

$$y_{ji+1} = y_{ji} + h\phi_j = y_{ji} + h(k_{j1} + 2k_{j2} + 2k_{j3} + k_{j4})/6 \quad 3.8a$$

$$k_{j1} = f_j(x_i + y_1, y_{2i}, \dots, y_{ni}) \quad 3.8b$$

$$y_{ji}^* = y_{ji} + \frac{1}{2} h k_{j1} \quad 3.8c$$

$$k_{j2} = f_j(x_i + \frac{1}{2} h, y_{1i}^*, y_{2i}^*, \dots, y_{ni}^*) \quad 3.8d$$

$$\bar{y}_{ji} = y_{ji} + \frac{1}{2} h k_{j2} \quad 3.8e$$

$$k_{j3} = f_j(x_i + \frac{1}{2} h, \bar{y}_{1i}, \bar{y}_{2i}, \dots, \bar{y}_{ni}) \quad 3.8f$$

$$\bar{y}_{ji}^* = y_{ji} + h k_{j3} \quad 3.8g$$

$$k_{j4} = f_j(x_i + h, \bar{y}_{1i}^*, \bar{y}_{2i}^*, \dots, \bar{y}_{ni}^*) \quad 3.8h$$

The relationships in (3.8) are applied in parallel at each point in the algorithm for all n equations, that is, for $j = 1, 2, 3, \dots, n$

Let four vectors of length at least n be denoted by the names Y , \bar{Y} , F and ϕ . Before carrying out the Runge-Kutta integration for the i th step, the following variables must be initialized: $x \leftarrow x_j$, value of the independent variable.

$h \leftarrow h$, step size for integration across the i th step, $x_{i+1} \rightarrow x_i$.

$n \leftarrow n$, number of first-order differential equations.

$Y_j \leftarrow y_{ji}$, $j = 1, 2, \dots, n$ solution values for the n equations at x_i .

Then (3.8) may be described by a five-pass procedure.

Pass 1

1. Calculate the values f_j , $j = 1, 2, \dots, n$ using the current x and Y_j values.

These are equivalent to the values k_{j1} , $j = 1, 2, \dots, n$, of (3.8b)

$$F_j \leftarrow f_j(x, Y_1, Y_2, \dots, Y_n) = k_{j1} = f_j(x_i, y_{1i}, y_{2i}, \dots, y_{ni}, j = 1, 2, \dots, n) \quad (3.9)$$

Pass 2

2- Save the current values Y_j , $j = 1, 2, \dots, n$ in another vector of equal length \bar{Y} . This assigns the solution values at the beginning of the i th step to the vector \bar{Y} .

$$\bar{Y}_j \leftarrow Y_j = y_{ji}, j = 1, 2, \dots, n \quad (3.10)$$

3- Begin accumulation of the values ϕ_j , $j = 1, 2, \dots, n$, in (3.8a)

$$\phi_j \leftarrow F_j = k_{ji}, j = 1, 2, 3, \dots, n. \quad (3.11)$$

4- Compute the value $y_{ji}^*, j = 1, 2, \dots, n$, in (6.3.8c) and assign them to

Elements of the vector Y .

$$Y_j \leftarrow \bar{Y}_j + \frac{h}{2} F_j = y_{ji}^* = y_{ji} + \frac{h}{2} k_{j1}, j = 1, 2, \dots, n. \quad (3.12)$$

5- Increment x to the value needed in (3.8d)

$$x \leftarrow x + \frac{h}{2} = x_i + \frac{h}{2}. \quad (3.13)$$

6- Calculate the values $f_j, j = 1, 2, \dots, n$ using the current x and Y_j values. These

Are equivalent to the values $k_{j2}, j = 1, 2, \dots, n$, of (3.8d)

$$F_j \leftarrow f_j(x, Y_1, Y_2, \dots, Y_n) = k_{j2} = f_j\left(x_i + \frac{h}{2}, y_{1i}^*, y_{2i}^*, \dots, y_{ni}^*\right), j = 1, 2, \dots, n \quad (3.14)$$

Pass 3

7- Add the contribution of k_{j2} to $\phi_j, j = 1, 2, \dots, n$ in (3.8a)

$$\phi_j \leftarrow \phi_j + 2F_j = k_{j1} + 2k_{j2}. \quad (3.15)$$

8- compute the values $\bar{y}_{ji}, j = 1, 2, \dots, n$, in (3.8e) and assign them to elements of the vector Y .

$$Y_j \leftarrow Y_j + \frac{h}{2} F_j = \bar{y}_{ji} = y_{ji} + \frac{h}{2} k_{j2}, j = 1, 2, 3, \dots, n. \quad (3.16)$$

9- calculate the values $f_j, j = 1, 2, 3, \dots, n$ using the current x and Y_j values. These are equivalent to the values $k_{j3}, j = 1, 2, 3, \dots, n$, of (3.8f).

$$\begin{aligned} F_j &\leftarrow f_j(x, Y_1, Y_2, \dots, Y_n) = K_{j3} \\ &= f_j\left(x_i + \frac{h}{2}, \bar{y}_{1i}, \bar{y}_{2i}, \dots, \bar{y}_{ni}\right), j = 1, 2, \dots, n. \end{aligned} \quad (3.17)$$

Pass 4

10- Add the contribution of k_{j3} to $\Phi_j, j = 1, 2, \dots, n$ in (3.8a)

$$\Phi_j \leftarrow \Phi_j + 2F_j = k_{j1} + 2k_{j2} + 2k_{j3}, j = 1, 2, \dots, n. \quad (3.18)$$

11- compute the values $\bar{y}_{ji}^*, j = 1, 2, \dots, n$ in (6.3.8g) and assign them to elements of the vector Y .

$$Y_j \leftarrow \bar{Y}_j + hF_j = \bar{y}_{ji}^* = y_{ji} + hk_{j3}, j = 1, 2, \dots, n. \quad (3.19)$$

12- Increment x to the value needed in (6.3.8h).

$$x \leftarrow x + \frac{h}{2} = x_i + h = x_{i+1}. \quad (3.20)$$

13- Calculate the values $f_j, j = 1, 2, \dots, n$ using the current x and Y , values. These are equivalent to the values $k_{j4}, j = 1, 2, \dots, n$ of (3.8h)

$$F_j \leftarrow f_j(x, Y_1, Y_2, \dots, Y_n) = k_{j4} \\ = f_j(x, h, \bar{y}_1^*, \bar{y}_2^*, \dots, \bar{y}_n^*) \quad , j = 1, 2, \dots, n \quad . \quad (3.21)$$

Pass 5

14- Complete the evaluation of $\Phi_j, j = 1, 2, \dots, n$ in (3.8a) .

$$\Phi_j \leftarrow (\phi_j + F_j) / 6 = (k_{j1} + 2k_{j2} + 2k_{j3} + k_{j4}) / 6 \quad . \quad (3.22)$$

15- Compute the values $y_{j,i+1}, j = 1, 2, \dots, n$ in (3.8a) and assign them to

Elements of the Y vector .

$$Y_j \leftarrow Y_j + h\phi_j = y_{ji} + h\phi_j, j = 1, 2, \dots, n \quad . \quad (3.23)$$

As a consequence of the procedure described by (3.9) to (3.23), h and n remain unchanged, and x and the vector Y contain :

$$x = x_{i+1}, \text{ value of the independent variable } Y_j = y_{j,i+1} \quad , j = 1, 2, \dots, n$$

Solution values for the n equations at x_{i+1} .

All initial values have been assigned for the next integration step, from

x_{i+1} to x_{i+2} , The step size, h , may be changed if desired. The five – pass

Procedure of (6.3.9) to (6.3.23) may be repeated for the next step .

Note that the parts of the procedure given by (6.3.9), (6.3.14), (6.3.17) and

(6.3.21) are identical ,

$$F_j \leftarrow f_j(x, Y_1, Y_2, \dots, Y_n), j = 1, 2, \dots, n \quad . \quad (3.24)$$

And are the only ones that refer directly to the n differential equations ,

$f_j, j = 1, 2, \dots, n$ of (3.1) . Therefore, it is possible to write a general

-purpose function called RUNGE that implements all parts of the procedure out-

Lined, except for initialization of n, x, h and $Y_j, j = 1, 2, \dots, n$, and step (3.9), (3.14), (3.17) and (3.21). The calling program will then contain all information about the specific system of differential equation, and be responsible for printing result, changing the step size, terminating the integration process, and evaluating the F_j when needed. The five passes of the algorithm can be handled by five different calls upon RUNGE, as shown schematically in Fig.3.2 Let a step counter, m , preset to 0, be maintained by the function RUNGE, and let the value returned by RUNGE signal the calling program to indicate whether the $F_j, j = 1, 2, \dots, n$ of (3.24) are to be computed (following the first four passes

for not (when integration across one step is completed following the fifth pass). Let the value returned be 1 when the F_j are to be evaluated and 0 when one complete integration step is completed. The main program used to test the function RUNGE solves the second-order ordinary differential equation (6.3.2) subject to initial conditions (3.3). Since the charge q on a capacitor is related to the capacitance C and voltage V , by: $q = CV$. (3.25)

The current i , into the capacitor is given by:

$$i = \dot{q} = -C \frac{dv}{dt} \quad (3.26)$$

The voltage V , across a resistor and inductance in series is given by :

$$V = L \frac{di}{dt} + Ri \quad (3.27)$$

Then, from (6.3.26) and (6.3.27), the voltage across the capacitor as a function of time is given by (3.2),

$$\frac{d^2v}{dt^2} = -\frac{R}{L} \frac{dv}{dt} - \frac{1}{LC} V \quad (3.28)$$

The initial conditions are :

$$V(0) = V_0, \quad \frac{dV}{dt}(0) = 0 \quad (3.29)$$

Differentiation of the three proposed solution, (3.5), (3.6) and (3.7), and substitution into (3.28), shows that, for the given value of $\bar{\alpha}^2$, each satisfies (3.28) and initial condition (3.29).

The second-order equation (3.28) must be rewritten as a system of two first-order equations. Let :

$$Y_1 = V$$

$$Y_2 = \frac{dV}{dt}, \quad (3.30)$$

$$X = t.$$

Then

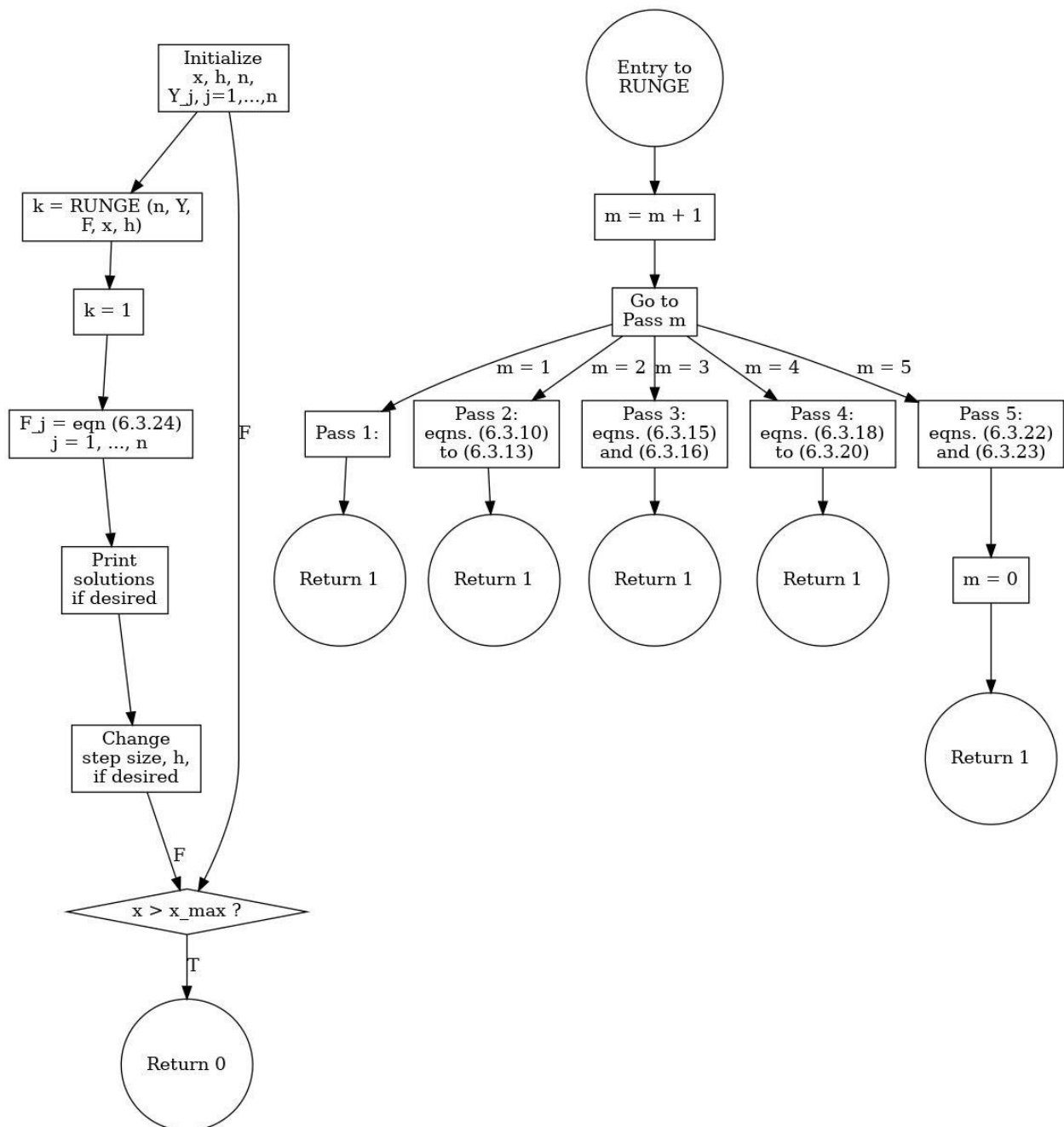
$$F_1 = \frac{dY_1}{dx} = \frac{dY}{dt} = Y_2.$$

$$F_2 = \frac{dY_2}{dx} = \frac{d^2V}{dt^2} = -\frac{R}{L} \frac{dV}{dt} - \frac{1}{LC} V = -\frac{R}{L} Y_2 - \frac{1}{LC} Y_1. \quad (3.31)$$

The initial conditions of (3.29) are

$$Y_{1,0} = V_0$$

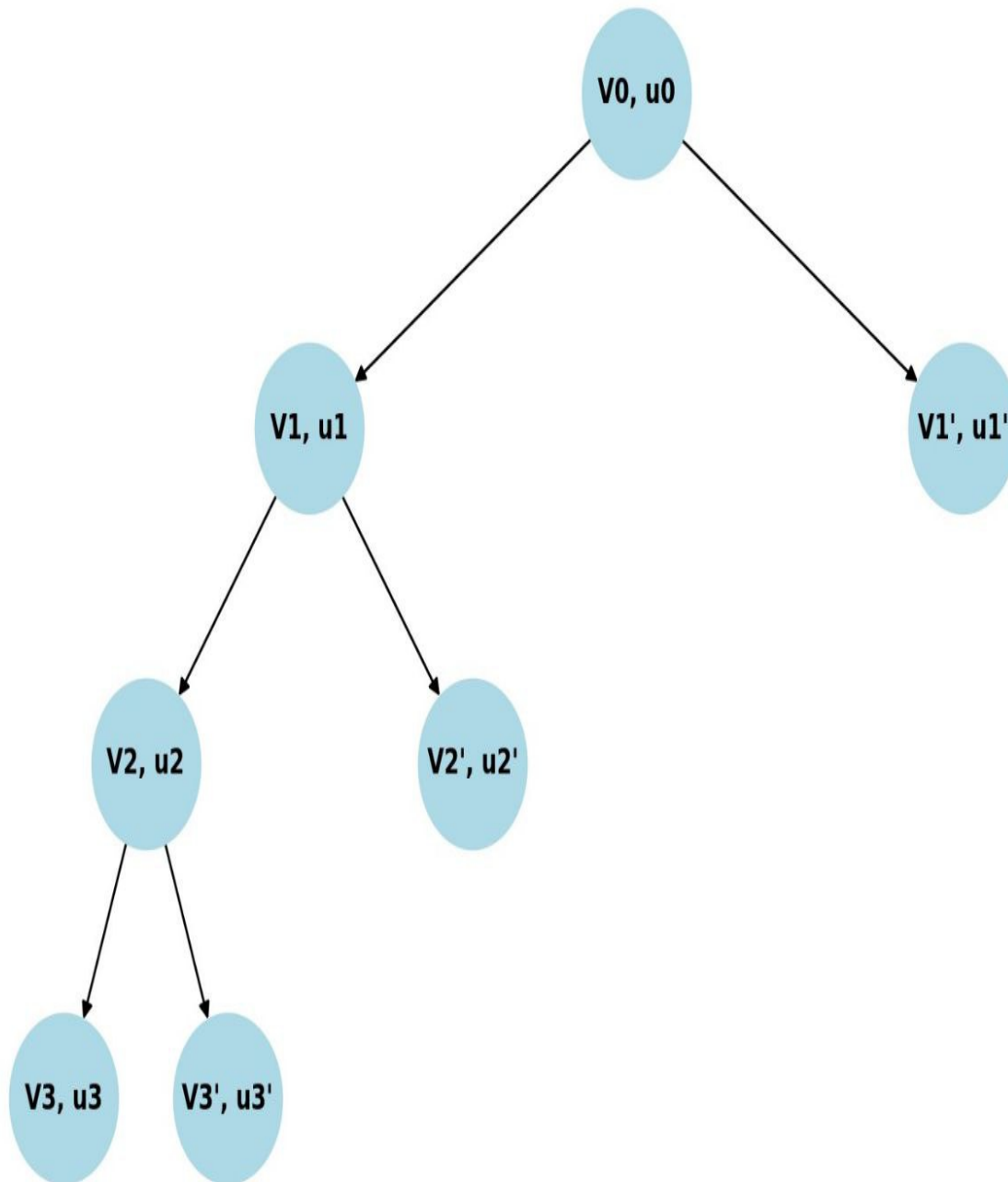
$$Y_{2,0} = 0. \quad (3.32)$$



The Tree of calculation values via Runge-kutta

Represent the calculation of the time values of voltage and current using the Runge-Kutta. Each node represents the value V_n and $U_n = \frac{dv}{dt}$ at a certain step, and the frika is an expression of the relationships between these values.

Tree Representation of Runge-Kutta Solution for Electrical Circuit



Explanation of the drawing

1- Nodes : Each node represents the value of voltage V and current $U = \frac{dv}{dt}$ at a certain step.

2- The root represents the initial values(v_0, u_0) .

- 3- Grills : An expression of the calculated values at the different ascending steps
- 4- using the method Runge-Kutta fourth .
- 5- Edges : The strip of values between each other , where each bit becomes anew risk in the numerical load .

Conclusion

- 1- The Runge-Kutta Fourth-order method provides a highly accurate numerical solution for RLC circuit differential equations .
- 2- Tree-based representations help visualize computational dependencies and provide a structured way to understand numerical evolution.
- 3- This approach can be applied to broader fields such as control systems ,dynamic analysis ,and applied physics .

References

- 1- Gerald, C. F., & Wheatley, P. O. (2004). *Applied numerical analysis* (7th ed.). Addison Wesley.
- DelinChapra, S. C., & Canale, R. P. (2010). *Numerical methods for engineers* (6th ed.). McGraw-Hill.
- 2- Kiusalaas, J. (2005). *Numerical methods in engineering with MATLAB*. Cambridge University Press.
- 3- Smith, H. T., & Griffiths, D. F. (1986). *Numerical solution of ordinary differential equations: Initial value problems*. Oxford University Press.
- 4- Ogata, K. (2009). *Modern control engineering* (5th ed.). Prentice Hall.
- 5- Zill, D. G. (2008). *A first course in differential equations with modeling applications* (8th ed.). Brooks/Cole.
- 6- Butcher, J. C. (2016). *Numerical methods for ordinary differential equations* (3rd ed.). John Wiley & Sons.
- 7- Kreyszig, E. (2011). *Advanced engineering mathematics* (10th ed.). John Wiley & Sons.
- Tan and Zheng Chen.(2012),A General Formula of Fourth-Order Runge-Kutta Method .
- 8- Tan,Z.,and Chen,Z.(2012).A general formula of fourth-order Runge-kutta method.
- 9- Bashir ,M.S. and Mohammed,M.S. (2008).Higher-Order Runge-kutta Methods for Solving Stiff Systems .
- 10- Dawood.S.(2009).Numerical solution of $(C\backslash C\backslash 2\backslash 3)$ System Using Runge-Kutta Method .
- 11- Bratislar,T.(2004).Application of Runge-Kutta Method in Solving Flow Problems Governed by ordinary Differential Equations (ODEs) .
- 12- Butcher,J.C.(2008).Numerical Methods for Ordinary Differential Equations .John Wiley and Sons .
- 13- Press ,W.H.,Teukolsky ,S.A.,Vetterling ,W.T.,and Flannery ,B.P.(2007).Numerical Recipes:The Art of Scientific Computing .Cambridge University Press.
- 14- Hairer,E.,Norsett ,S.P.,and Wanner,G.(1993).Solving Ordinary Differential Equations I:Nos tiff Problems .Springer .
- 15- Kreyszig,E.(2011).Advanced Engineering Mathematics (10th ed.).Wiley .